

2 (mix)

NASA CR-112243

FINAL REPORT

A STUDY OF THE DYNAMICS OF ROTATING
SPACE STATIONS WITH ELASTICALLY
CONNECTED COUNTERWEIGHT AND
ATTACHED FLEXIBLE APPENDAGES

Volume I Theory

By

Fred Austin, Joel Markowitz, Stephen Goldenberg,
and George A. Zetkov

Prepared under Contract No. NAS 1-10973
Grumman Aerospace Corporation
Bethpage, New York 11714

for

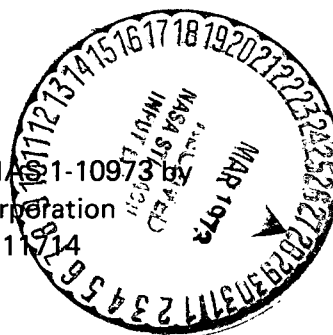
NATIONAL AERONAUTICS AND SPACE ADMINISTRATION

March 1973

(NASA-CR-112243) A STUDY OF THE
DYNAMICS OF ROTATING SPACE STATIONS WITH
ELASTICALLY CONNECTED COUNTERWEIGHT AND
ATTACHED FLEXIBLE (Grumman Aerospace
Corp.) 391 p HC \$21.75 CSCL 20K

G3/23 65557
Unclass

N73-19672



FINAL REPORT

A STUDY OF THE DYNAMICS OF ROTATING
SPACE STATIONS WITH ELASTICALLY
CONNECTED COUNTERWEIGHT AND
ATTACHED FLEXIBLE APPENDAGES

Volume I Theory

By

Fred Austin, Joel Markowitz, Stephen Goldenberg,
and George A. Zetkov

Prepared under Contract No. NAS 1-10973 by
Grumman Aerospace Corporation
Bethpage, New York 11714

for

NATIONAL AERONAUTICS AND SPACE ADMINISTRATION

March 1973

TABLE OF CONTENTS

<u>Section</u>	<u>Page</u>
1.0 INTRODUCTION AND SUMMARY	1-1
1.1 Study Objectives and a Sample Configuration	1-1
1.2 Organization of the Study and Mathematical-Model Idealization	1-2
2.0 CONCLUSIONS	2-1
3.0 PHASE I -- DEVELOPMENT OF THE MODAL-SYNTHESIS PROCEDURE . .	3-1
3.1 Introduction	3-1
3.2 Selection of Subroutine Modes	3-5
3.3 Theory	3-8
3.3.1 Transformation From Local to Global Coordinates for a Typical Substructure	3-11
3.3.2 Substructure Coupling	3-19
3.4 Numerical Results	3-35
4.0 PHASE II -- DEVELOPMENT OF THE EQUATIONS OF MOTION FOR THE DYNAMIC SIMULATION	4-1
4.1 Assumptions Used in the Formulation	4-15
4.1.1 Laboratory and Counterweight Structure	4-15
4.1.2 Connecting Structure	4-15
4.1.3 Structural Coordinate Systems	4-16
4.1.4 Fluid	4-16
4.1.5 Moving Point Masses	4-17
4.2 Development of the Equations of Motion in Vector Form	4-19
4.2.1 Structural Mass on Laboratory	4-22
4.2.2 Fluid Motion in the Laboratory	4-22
4.2.2.1 Through Pipe	4-25

Preceding page blank

TABLE OF CONTENTS (Continued)

<u>Section</u>	<u>Page</u>
4.2.2.2 Reservoir Nominally Emptying (for $V > 0$)	4-30
4.2.2.3 Reservoir Nominally Filling (for $V > 0$)	4-36
4.2.3 Moving Point Mass on Laboratory	4-37
4.2.4 Structural Mass on Counterweight	4-44
4.2.5 Subsidiary Relations	4-45
4.2.5.1 Angular Momentum About Point O	4-45
4.2.5.2 Kinetic Energy	4-46
4.2.5.3 Location of Space-Station Center of Mass	4-48
4.3 Matrix Form of Equations of Motion	4-49
4.3.1 Inertia Matrix for Reservoir Fluid	4-49
4.3.2 Coordinate Systems and Conversion of Dynamic Equations to Matrix Form	4-51
4.3.3 Combined Equations of Motion for Entire System	4-58
4.3.4 Modal-Constraint Reduction Procedure	4-59
4.3.5 Adjustment of Input Data	4-64
4.4 Structural Forces	4-66
4.4.1 Laboratory and Counterweight Structure	4-66
4.4.2 Connecting Structure	4-68
4.4.2.1 Circular Beam	4-70
4.4.2.2 Cable Truss	4-72
4.5 Structural Loads	4-73
4.6 Computation Procedure	4-74
5.0 CONTROL SYSTEMS	5-1
5.1 Introduction	5-1

TABLE OF CONTENTS (Continued)

<u>Section</u>	<u>Page</u>
5.1.1 Rigid-Body Control-Systems Development Program	5-1
5.1.2 Operation of Control Systems on Flexible Idealization.	5-3
5.2 Reaction Jet Configuration in Rigid-Vehicle Simulation .	5-4
5.3 Service Routines used by Main Command and Control Routines	5-6
5.3.1 Command Routine POSCOM (Position Command)	5-6
5.3.2 Command Routine VELCOM (Velocity Command)	5-6
5.3.3 Control Routine POSCTR (Position Control)	5-6
5.3.4 Control Routine VELCTR (Velocity Control)	5-11
5.4 Main Command and Control Routines.	5-11
5.4.1 Activation of Commands and Controls	5-11
5.4.2 Counterweight Position Control.	5-11
5.4.3 Elevator Position Control	5-13
5.4.4 Wobble Damping.	5-13
5.4.4.1 Gimbal Angle Command	5-13
5.4.4.2 Gimbal Angle Control	5-14
5.4.4.3 Analysis of Gimbal Angle Control System. .	5-17
5.4.4.4 Gimbal Angle Rate Control System	5-18
5.4.4.5 Analysis of Gimbal Angle Rate Control System	5-20
5.4.5 Mass Balance Control.	5-20
5.4.5.1 Mass Balance Control on Rigid- Vehicle Idealization	5-21
5.4.5.2 Mass Balance Control on Flexible- Vehicle Idealization	5-21
5.5 Demonstration Runs on Rigid-Vehicle Idealization	5-23
5.5.1 Attitude Control.	5-25
5.5.2 Spin Rate Hold During Counterweight Deployment	5-28

TABLE OF CONTENTS (Continued)

<u>Section</u>	<u>Page</u>
5.5.3 Spin Up	5-31
5.5.4 Mass Balance	5-32
5.5.5 Wobble Damping	5-38
5.5.6 Simultaneous Mass Balancing and Wobble Damping	5-42
5.6 Conclusions Based on Rigid-Body Demonstration Runs . .	5-42
6.0 NUMERICAL RESULTS DEMONSTRATING THE COMPUTER PORGRAMS . . .	6-1
6.1 Testing of the Programs	6-1
6.2 Demonstration Runs.	6-4
6.2.1 Attitude Control	6-4
6.2.2 Deployment with Spin-Rate Hold	6-7
6.2.3 Spin Up	6-13
6.2.4 Quiescent State	6-13
6.2.5 Wobble Control	6-19
6.2.6 Elevator Motion with Balance Mass Control. . . .	6-25
6.2.7 Fluid Pumped through Laboratory.	6-27
7.0 CONCEPTS FOR A SCALE MODEL	7-1
7.1 Introduction.	7-1
7.2 Suspension-System Design.	7-2
7.2.1 The Gimbaled Supports.	7-5
7.2.2 Proportional Mechanism	7-5
7.2.3 Main Yoke.	7-7
7.2.4 Horizontal Freedom of Space Station Mass Center. .	7-9
7.2.5 Weight-Balancing Mechanism	7-9
7.3 Spurious Effects.	7-11

TABLE OF CONTENTS (Continued)

<u>Appendix</u>		<u>Page</u>
A.	Fluid Motion Derivatives	A-1
B.	Relations Required to Convert The Equations of Motion from Vector to Matrix Form	B-1
	B1. Coordinate Transformations and Angular Velocities.	B-1
	B2. Cross Products	B-4
	B3. Useful Identities	B-4
C.	Phase II Computation Procedure and Summary of Equations. .	C-1
D.	Reduction of the Size of the Numerical-Integration Problem.	D-1
	D1. Nonrotating Elastic Structure	D-1
	D1.1 The Lagrangian Form	D-1
	D1.2 The Constraint Reduction Method	D-2
	D1.3 The Modal Reduction Method.	D-4
	D2. Rotating Space Station.	D-8
E.	Initial Alignment of Rigid-Body Axes	E-1
	E1. Laboratory.	E-1
	E2. Counterweight	E-4
F.	Physical Properties of Space Station Model Used to Demonstrate the Computer Programs.	F-1
	F1. Laboratory and Counterweight	F-1
	F2. Connecting Structure.	F-19
G.	Connecting-Structure Subroutine Computation Procedure and Summary of Equations	G-1
	G1. Circular Beam	G-2
	G2. Cable Truss	G-6
H.	Computation Procedure for Control-System Subroutines	H-1

TABLE OF CONTENTS (Continued)

<u>Appendix</u>		<u>Page</u>
H1.	Command Routine POSCOM (Position Command)	H-6
H2.	Command Routine VELCOM (Velocity Command)	H-12
H3.	Command Routine CWCMD (Counterweight Command)	H-14
H4.	Command Routine ELCOM (Elevator Command)	H-16
H5.	Command Routine MUCOM (Commands Position of Moving Masses)	H-17
H6.	Command Routine SPNCOM (Spin Command)	H-18
H7.	Command Routine PMPCOM (Pump Command)	H-20
H8.	Control Routine POSCTR (Position Control)	H-21
H9.	Control Routine VELCTR (Velocity Control)	H-23
H10.	Control Routine ATTCTR (Attitude Control)	H-25
H11.	Control Routine SPNCTR (Spin Control)	H-30
H12.	Control Routine WBLCTR (Wobble Control)	H-32
H13.	Control Routine BMCTR (Balance Mass Control)	H-39
I.	Synthesized Modes of the Laboratory.	I-1
J.	Data for Demonstration Runs.	J-1
K.	Data for Rigid-Body Runs Using Control-Systems Development Program	K-1

FOREWORD

This report is submitted to the NASA Langley Research Center in partial fulfillment of Contract NAS 1-10973. This contract involves the formulation of a mathematical model for predicting the dynamic behavior of a class of rotating flexible space-station configurations, and the preparation of associated computer programs.

Volume I contains the development of the required theoretical techniques, and Volume II is a computer-program user's manual.

Dr. Robert W. Fralich of the NASA Langley Research Center is the Technical Monitor. Dr. Fred Austin of the Grumman Aerospace Corporation is the Project Engineer.

The principal contributors to this investigation and their areas of responsibility are listed below:

Dr. F. Austin	Derivation of Equations of Motion for Dynamic Simulation. Development of Concepts for Model. Modification of Control Systems to Operate on Flexible Vehicle
Dr. J. Markowitz	Derivation of Structural Load Equations and Development of Computation Procedure
Mr. S. Goldenberg	Development of Modal Coupling Procedure
Mr. G. Zetkov	Development of Control Systems and Associated Computer Subroutines
Mr. E. Lowe	Development of Computer Programs

The authors gratefully acknowledge Mr. A. Schloth's useful contributions which include computing modes and numerical check work. The technical comments provided by Dr. R. Fralich and Messrs. E. Lerner, J. Smedfjeld, M. Mantus, and H. Berman are appreciated.

1.0 INTRODUCTION AND SUMMARY

1.1 STUDY OBJECTIVES AND A SAMPLE CONFIGURATION

The overall objectives of this study are as follows:

- Develop the theoretical techniques required to determine the dynamic behavior of a realistically modeled rotating space station
- Provide the Langley Research Center with a versatile computer program that is operational in the LRC computer facility
- Present practical concepts for experimental verification of the analytical results

The specific objectives of the program involve the development of a mathematical model capable of simulating the three-dimensional dynamic behavior of a rotating flexible space station. This model and its associated computer program includes the following features:

- A flexible Laboratory with attached flexible appendages
- A flexible Counterweight with attached flexible appendages
- A flexible connecting structure whose characteristics allow for the mathematical treatment of deployment and retraction
- Moving point masses in the Laboratory for the simulation of crew or cargo motion, a mass-balancing system, etc.
- Fluid in motion on the Laboratory for the simulation of a fluid-type mass-balancing system, disturbances due to fluid transfer in the cooling system, etc.
- Provisions for control systems
- Provisions for general external disturbances on any portion of the Laboratory or the Counterweight

One example of a configuration that can be studied using the mathematical model developed herein is shown in Figure 1.1. The Laboratory is constructed of a core module and several appendages including two solar panels. All of these modules including the core module are flexible. The Counterweight is also composed of several flexible modules. In addition, there is a flexible Connecting Structure which is capable of deployment and retraction. As indicated, fluid in motion is present in the pipe which terminates at a reservoir at each end. Several moving point masses represent crew members, an elevator, and a mass-balancing system. Control systems (not shown) control deployment, spin rate, mass balancing, wobble and (when the system is not rotating) attitude.

1.2 ORGANIZATION OF THE STUDY AND MATHEMATICAL-MODEL IDEALIZATION

Both the analysis and the computer program have been organized into two phases. In Phase I (Modal Synthesis), the modal properties of each Laboratory substructure (core module, appendage, solar panel, etc.) are coupled to derive the non-rotating modal properties of the entire Laboratory. The Counterweight modes are similarly synthesized. Each coupled structure (Laboratory or Counterweight) may be comprised of up to 17 substructures (five core modules and twelve appendages as shown schematically in Figure 3.1). The vibration modes of the various substructures are supplied to the computer program as input data and they do not have to have physical motions in a common coordinate system. One limitation is that appendages cannot be connected to other appendages. Detailed information on the idealization used for the Phase I study is presented in Section 3.0.

The modal properties of both the Laboratory and the Counterweight are automatically transferred from the Phase I to the Phase II computer program. Alternatively, if the user already has vibration modes for the entire Laboratory or the Counterweight, he may supply these directly to the Phase II computer program and use these modes to complete the study. There are no physical restrictions (such as interconnected appendages) on modes which are supplied to Phase II directly by the user.

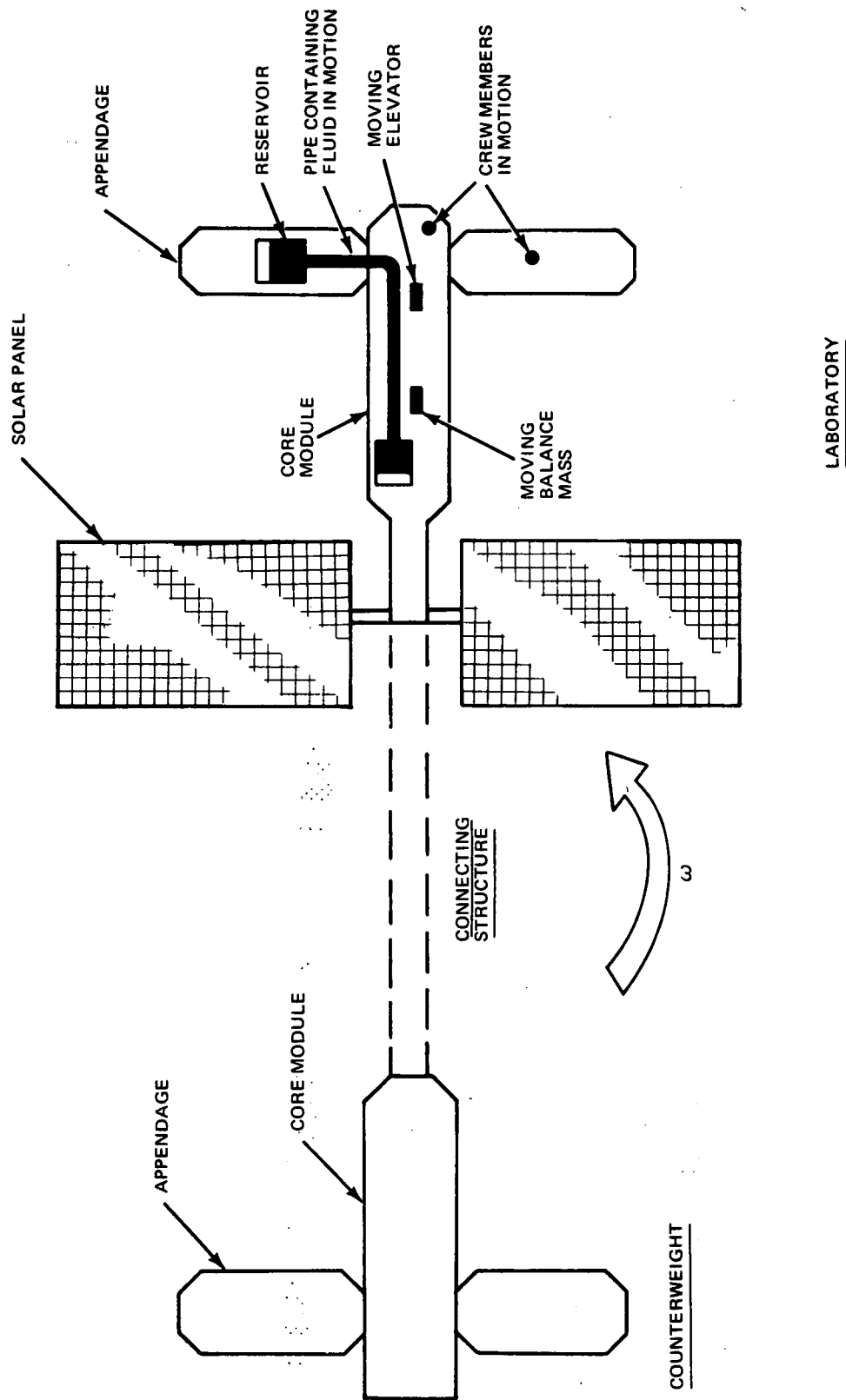


Fig. 1.1 One Example of a Space Station that Can be Studied Using the General Mathematical Model

In the Phase II study, the equations of motion were written for an idealized vehicle which has the following properties (see Figure 4.1):

- An arbitrary number of structural masses (including rotatory inertias) on the Laboratory and on the Counterweight
- A massless flexible connecting structure; the length may be varied as a function of time
- Damping in all structures
- An arbitrary number of moving point masses on the Laboratory which travel along its deformed shape
- A fluid system consisting of an incompressible fluid confined within two reservoirs and a connecting pipe; this system may be located anywhere within the Laboratory
- Forces and torques which may be applied to any structural mass

Detailed information on this idealization is presented in Sections 4.0 and 4.1.

Whereas the equations of motion are written for a general vehicle, certain restrictions were imposed as a result of available computer facilities; for example, the number of masses on the Laboratory is limited to 100, and the number of masses on the Counterweight is similarly restricted. These restrictions are listed in Volume II, the Computer Program User's Manual.

The Newton and Euler equations were written for each mass point in vector form. Then the system of equations was transformed to a system of Lagrange equations with quasi coordinates (i.e., angular-velocity components were among the coordinates used). This technique combines the simplicity of the vector derivation with the advantages of the Lagrange approach, such as the ability to handle constraints automatically.

The user may conduct a series of increasingly complex dynamic studies by making use of the constraint options which are available in the program. These include automatic rigidizing of the Laboratory, the Counterweight, or the entire Space Station. While the Connecting Structure has no elastic deformation in the last option, it still can deploy and retract. Other features designed to assist the analyst include optional print-out of the total system kinetic energy, angular momentum in inertial coordinates, and center-of-mass position.

In order to provide additional versatility, several items are modeled in subroutines so that they may be easily replaced by the user. Examples are:

- The structural properties of the Connecting Structure
- The motion commands
- The control systems

The connecting-structure subroutine supplied with the computer program contains a model of a tubular beam described in Section 4.4.2. This beam is built-in at each end; however, it is capable of deployment and retraction.

Motion-command subroutines command the sequence and history of such controlled events as crew or elevator motion, spin speed, and deployment. The subroutines provided contain a set of functions which are based on a sequence of constant accelerations.

Four control subroutines are provided. These model systems control the attitude of the non-spinning vehicle, the spin speed, position of the Space Station center of mass (mass balancing), and wobble damping. Jets are employed to accomplish the attitude and spin-speed control functions; center-of-mass control is accomplished by moving a balance mass, and wobble damping is accomplished by using a control-moment gyroscope. The control systems were designed for a rigid space-station model (which can deploy and retract) and were then modified for operation on the Phase II flexible-body computer program.

Concepts are presented in Section 7 for an experimental model which can be used to verify the major analytical results. This model is capable of deployment and retraction maneuvers and can be fitted with a scaled set of control systems.

2.0 CONCLUSIONS

The analysis and computer programs summarized in the previous section provide the capability to perform comprehensive dynamic analyses of a large class of rotating and non-rotating flexible space stations. The modes of a Laboratory and Counterweight can be synthesized in the Phase I program using, as input data, the modes of the component modules. A structure consisting of up to 17 modules may be treated.

Time histories of dynamic behavior of a Space Station consisting primarily of a Laboratory and a Counterweight with any shape and mass distribution may be investigated by using the Phase II computer program. The Connecting Structure and control systems may be changed by replacing subroutines. Moving masses and a fluid system may be located anywhere on the Laboratory. Demonstration runs were made using a complex idealization of a realistic Space Station. Mass motion, fluid motion, and all control systems operated properly. These demonstrations verify the practicality of a very general computer program for investigating the time history motions of flexible satellites. This program is a powerful tool for the design of complex rotating and non-rotating spacecraft.

One of the control systems developed for demonstration purposes sensed mass shifts due to a moving elevator and automatically moved a balance mass to maintain the balance of the rotating Space Station. This unique type of control system has not been applied previously. Attitude control, deployment, spin up, and wobble control maneuvers were also successfully demonstrated. The program may be used to investigate sequential or simultaneous controlled maneuvers in a single run.

Concepts were developed for constructing an operational scale model of the rotating Space Station. A complete set of controls may be mounted on this model to study controlled maneuvers including deployment and retraction. This model should be far superior to any existing space station model.

3.0 PHASE I — DEVELOPMENT OF THE MODAL-SYNTHESIS PROCEDURE

3.1 INTRODUCTION

The flexibility characteristics of the Laboratory and Counterweight are represented in the analysis by their non-rotating free-free modes of vibration. These modes are synthesized from the mass and modal properties of the individual modules which make up the Laboratory and Counterweight.

To provide the versatility for analyzing a wide variety of configurations, the synthesis procedure is developed for the general seventeen-body idealization shown in Figure 3.1. The user will have the capability of eliminating selected bodies from this most general arrangement. In this way many configurations having a lesser number of flexible bodies may be studied. The most general configuration was selected so that any combination of five modules could be synthesized; in addition, a configuration with one core module and ten appendages can be studied. For example, Figure 3.2A illustrates a structure with three core modules and two appendages. Notice that Module 16 was moved from its core-module position in Figure 3.1 and is now considered an appendage. To obtain the configuration of Figure 3.2B, Module 11 must be considered an appendage.

A computer program was prepared to carry out the synthesis procedure developed herein. This program is described in Section 2 of Volume II, the User's Manual.

Although free-free modes are required for Phase II, the program may also be used to synthesize the cantilever modes of the structure if it is held at any point in Module 1.

One feature of the synthesis procedure is that the substructure modal matrices may be supplied in coordinate systems that are not parallel to the coordinate system in which the result, the coupled modes, are obtained. Accordingly, modules need not be in the same plane. In fact they may be skewed at any angle in space.

Another feature of the procedure is that the user is permitted to supply constrained substructure modes. These are modes which were obtained for idealizations where constraints were employed; for example, in a beam analysis axial extension may have been neglected. Constraints may be handled by two different methods. In the first, the user supplies modes

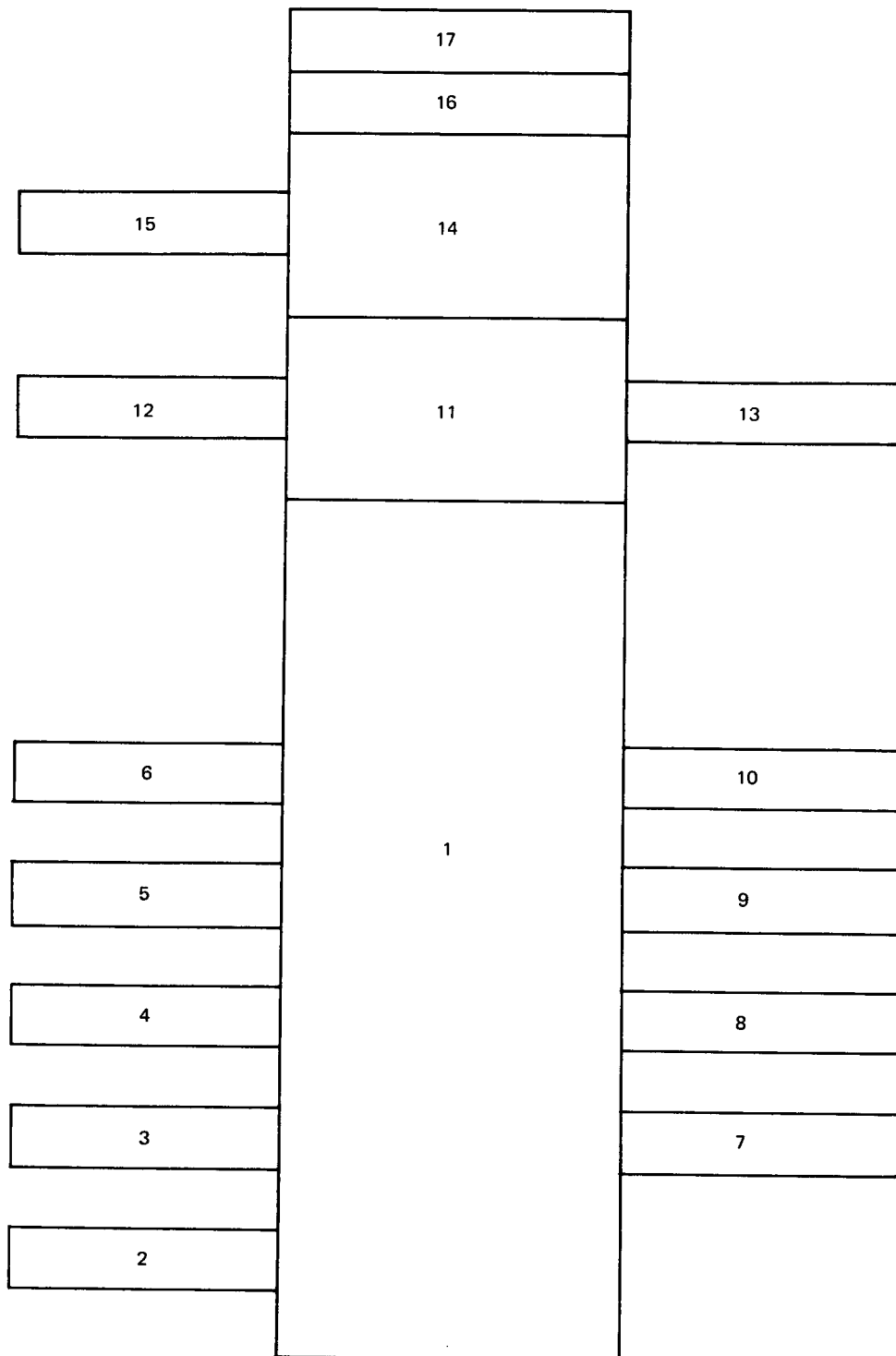
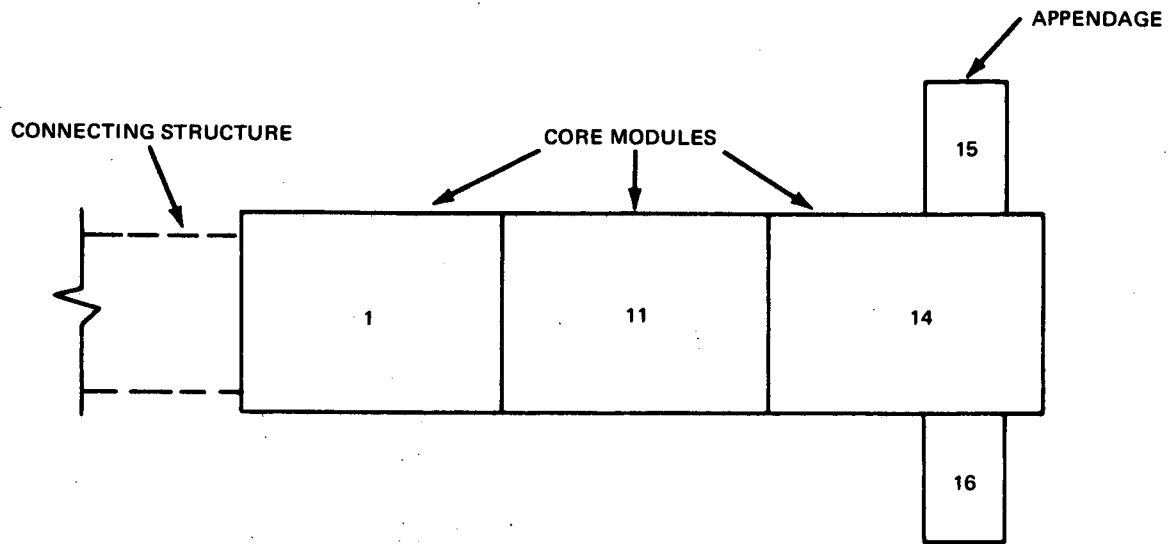
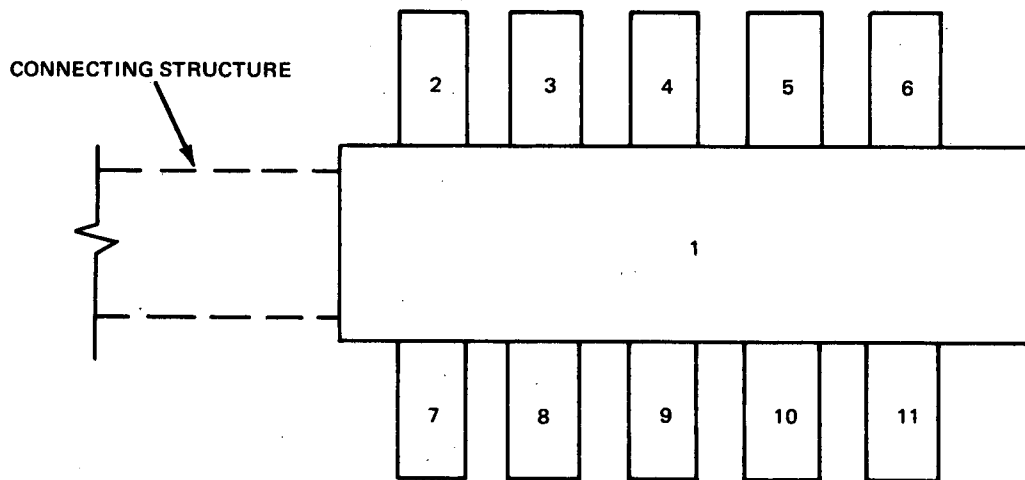


Fig. 3.1 General 17-Module Configuration for Modal Synthesis



(A) THREE CORE MODULES WITH TWO APPENDAGES



(B) ONE CORE MODULE WITH 10 APPENDAGES

Fig. 3.2 Examples of Manned-Laboratory and Counterweight Configurations That May be Synthesized

containing six rectangular coordinates for each mass point; however, constrained coordinates are either related by equations of constraint or may be zero. By the second method, the user may supply modes containing less than six coordinates to describe the motion of each mass point; however, he must either identify which if any of the six coordinates are zero or he must supply constraint relations which transform the supplied coordinates to the six rectangular coordinates. As described in a footnote in Section 3.3, only certain types of constraint relations may be supplied. This feature was limited by the available computer storage space.

Capability is not provided to automatically synthesize structures where appendages are interconnected; however, the user may bypass the Phase I computer program and supply the normal modes and modal masses of any Laboratory and/or Counterweight to Phase II. In this way, any Laboratory or Counterweight with linear elastic properties may be employed in the Space-Station study.

3.2 SELECTION OF SUBSTRUCTURE MODES

It is assumed that the normal modes of vibration of each of the substructures have been determined from conventional lumped-parameter vibration-analysis procedures. Thus, we assume that we have available, at the outset, the natural frequencies, mode shapes, generalized masses, and discrete mass matrices associated with each flexible body. As indicated in Figure 3.3, if free-free modes of the coupled structure are desired, then the free-free modes of Module 1 must be supplied; if the cantilevered modes of the coupled structure are desired, then the cantilever modes of Module 1 must be supplied. When obtaining cantilever modes, Module 1 must be fixed at the same point as the total structure. In either case, cantilevered modes are used for all other modules. It is assumed that all modes are orthogonal and that the junction surface between bodies has no deformation. Substructure mode shapes may be computed in any convenient coordinate system, since the program will transform all mode shapes into a common rectangular coordinate system prior to synthesis.

As with any synthesis technique, the procedures discussed here will yield an exact representation of the coupled system if all of the substructure modes are used. In practice, however, each substructure is approximately represented by its lower-frequency modes. Thus the synthesized modes are approximate, with the lower-frequency modes generally being most accurate. How well the synthesis procedure works is dependent on how many modes are used to represent the substructures, and how accurately these substructure modes represent the motions of the coupled structure.

The analyst can exercise some control over the accuracy of the synthesis through the judicious selection of the substructure modes to be used. Another means of improving accuracy is to use so-called "mass-loaded" modes. This means that the mass and inertia properties of all influencing substructures are included in the preliminary idealization used for obtaining the modes of a core module. For example, referring to Figure 3.3, the modes of Module 1 would be calculated with Module 2 through 17 attached as rigid masses, those of 11 with 12 through 17 attached, those of 14 with 15, 16, and 17 attached, and those of 16 with 17 attached. The modes obtained in this manner are closer to those of the coupled system than modes computed

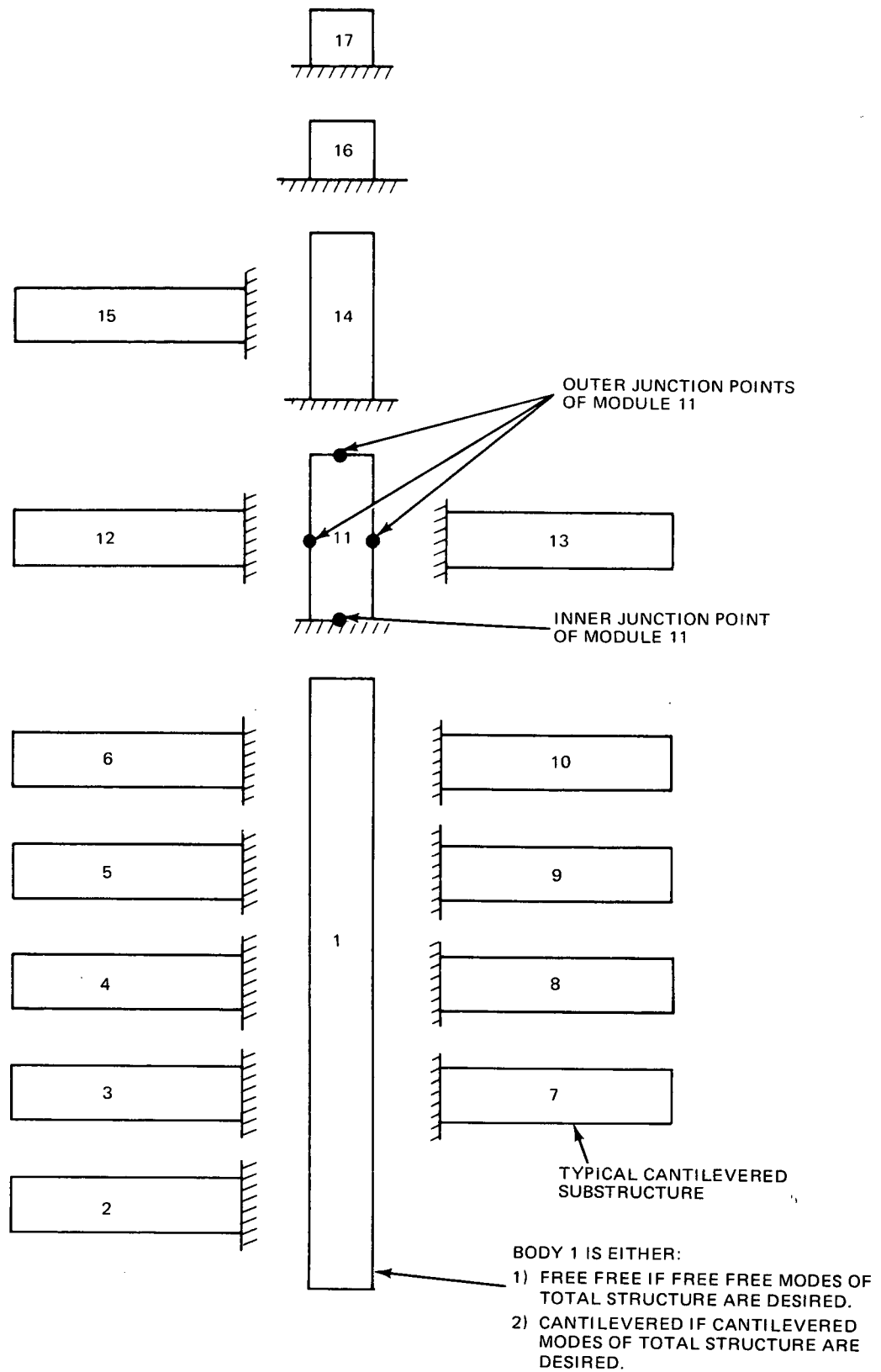


Fig. 3.3 Arrangement of Substructures for Modal Synthesis

without mass-loading, and thus produce consistently better results when used in the synthesis procedure. Since these modes are used only to represent the deformations of the substructure during synthesis, the real (unloaded) masses are used in the synthesis-problem mass matrix.

Modes obtained from substructures which are idealized with no mass at their outer junction points (see Figure 3.3) yield particularly poor results unless the mass-loading technique is employed. This is due to the fact that mode shapes, calculated with zero mass at an outer junction point, cannot represent the severe changes in the elastic deformation pattern induced by the loads and torques which are applied by the attached substructures.

3.3 THEORY

The analytical procedure presented in this section may be used to compute the modal data (natural frequencies, modal masses and mode shapes) of a structure, given the modal data and physical mass matrices of the substructures which make up the total structure. The following symbols are used in this section.

$[A_{i, j}]$	The $6n \times 6$ matrix giving the rigid-body displacements of each mass point in the i^{th} substructure due to the motion of its attachment point with substructure j
$^{(k)} [A_{i, j}]$	The 6×6 partition of $[A_{i, j}]$ which contains the rows corresponding to motions of the attachment point joining substructures i and k
$^{(i)} [a]$	The 6×6 matrix relating $\{u\}^{(i)}$ to $\{u\}_j^*$
a	A point on the $+z$ axis (see Figure 3-4)
$[B]$	Transformation from $\{\xi\}$ to $\{q\}$
b	A point in the first quadrant of the x, z plane, not on the z axis (see Figure 3-4)
$\bar{I}, \bar{J}, \bar{K}$	Unit vectors in the X, Y, Z directions (see Figure 3-4)
$\bar{i}, \bar{j}, \bar{k}$	Unit vectors in the x, y, z directions (see Figure 3-4)
$[k_X]$	Stiffness matrix for the coupled structure in the global coordinate system
$[k_y]$	Stiffness matrix for the coupled structure in the coordinate system in which the substructure modes are supplied
$[k_\xi]$	Stiffness matrix for the coupled structure in the $\{\xi\}$ coordinate system
$^{(i)} [m_X]$	The $6n \times 6n$ physical mass matrix in the global coordinate system for the i^{th} substructure
$^{(i)} [m_x]$	The $6n \times 6n$ physical mass matrix in the local coordinate system for the i^{th} substructure

$[m_X]$	Block-diagonal matrix containing all of the $[m_X^{(i)}]$'s
$[m_\xi]$	Mass matrix in the $\{\xi\}$ coordinate system
$[M_i \omega_i^2]$	Diagonal matrix of modal stiffness for the i^{th} substructure
n	The number of mass points in a substructure
0	Origin of the local and global coordinate systems (see Figure 3-4)
$\{q_{i,j}\}$	The $6n \times 1$ vector of displacements in the global coordinate system of mass points in the i^{th} substructure relative to the attachment point with substructure j
$\{q_{i,0}\}$	The $6n \times 1$ vector of absolute displacements in the global coordinate system of mass points in the i^{th} substructure
$\{q_{i,j}^{(k)}\}$	The 6×1 partition of $\{q_{i,j}\}$ which contains the motions of the attachment point joining substructures i and k
$\{q_X^{(i)}\}$	The $6n \times 1$ vector of physical displacements in the global coordinate system for the i^{th} substructure
$\{q_x^{(i)}\}$	The $6n \times 1$ vector of physical displacements in the local coordinate system for the i^{th} substructure
$\{q_y^{(i)}\}$	The vector of physical displacements of the i^{th} substructure in the coordinate system in which the substructure modes are supplied
$\{q_X\}$	Vector containing absolute displacements of all substructures in the global coordinate system
$\{\bar{q}_X\}$	Contains displacement vectors of all substructures relative to the supports shown in Figure 3-3 in the global coordinate system
$[T^{(i)}]$	Constraint matrix for the i^{th} substructure
T	Kinetic energy

$\{U\}_{i, j}$	The $6n \times 1$ vector of rigid-body displacements in the global coordinate system of mass points in the i^{th} substructure due to displacements of the attachment point with the j^{th} substructure
$\begin{pmatrix} i \\ \{u\} \end{pmatrix}$	The 6×1 vector of rigid-body displacements of the i^{th} mass point due to attachment point motion
$\{u\}_j^*$	The 6×1 vector of attachment point displacement in the global coordinate system
\bar{V}_{0i}	A vector from point "0" to point "i"
\bar{V}_N	A vector normal to the x, z plane
$\{V\}$	A 3×1 vector in the global coordinate system
$\{v\}$	A 3×1 vector in the local coordinate system
V	Potential energy
X, Y, Z	Global coordinate system (see Figure 3-4)
X_i, Y_i, Z_i	Coordinates of point i in the global coordinate system
x, y, z	Local coordinate system (see Figure 3-4)
x_i, y_i, z_i	Coordinates of point i in the local coordinate system
α_{ij}	Elements of the 3×3 transformation matrix, $[\alpha]$, relating local to global coordinates
$\begin{pmatrix} i \\ [\beta] \end{pmatrix}$	$6n \times 6n$ coordinate transformation matrix from local to global axes for the i^{th} substructure
$\begin{pmatrix} i \\ [\gamma] \end{pmatrix}$	Transformation from the coordinates in which the substructure modes are supplied to global coordinate system
$\{\xi_i\}$	Vector of modal displacements for substructure i
$\{\xi\}$	Vector containing the substructure modal displacements for all substructures
$[\phi_i], \begin{pmatrix} i \\ [\phi_X] \end{pmatrix}$	Matrix of mode shapes for substructure i in the global coordinate system

$\begin{pmatrix} j \\ \phi_i \end{pmatrix}$	Partition of $[\phi_i]$ containing the rows corresponding to motions of the attachment point joining substructures i and j
$\{\phi\}_i$	i^{th} eigenvector of the coupled system in the global coordinate system
$\begin{pmatrix} i \\ \phi_x \end{pmatrix}$	Matrix of mode shapes in the local coordinate system for the i^{th} substructure
$\begin{pmatrix} i \\ \phi_y \end{pmatrix}$	Matrix of mode shapes as supplied for the i^{th} substructure
$\{\phi_\xi\}_i$	i^{th} eigenvector of the coupled system in the $\{\xi\}$ coordinate system
Ω_i	i^{th} circular frequency of the coupled system

It should be noted that the local and global coordinate systems have their origins at the base (attachment point) of the module being considered.

3.3.1 Transformation From Local to Global Coordinates for a Typical Substructure

Since the mode shapes and mass matrices of the substructures are in their own individual "local" coordinate systems, they must be transformed into a common "global" coordinate system prior to coupling. The required transformation matrices are generated from user-specified information which will now be described. The local coordinate system for a typical module is translated as indicated in Figure 3.4. Then, for each module, the user specifies:

- the X, Y, Z coordinates of any point "a" on the positive z axes
- the X, Y, Z coordinates of any point "b" in the first quadrant of the x, z plane (but not on the z axes)

Point a, of course, fixes the direction of the z axes; however, the x, y axes may be any axes in the plane perpendicular to z. Point b fixes the location of the x, z plane and therefore of the x and y axes.

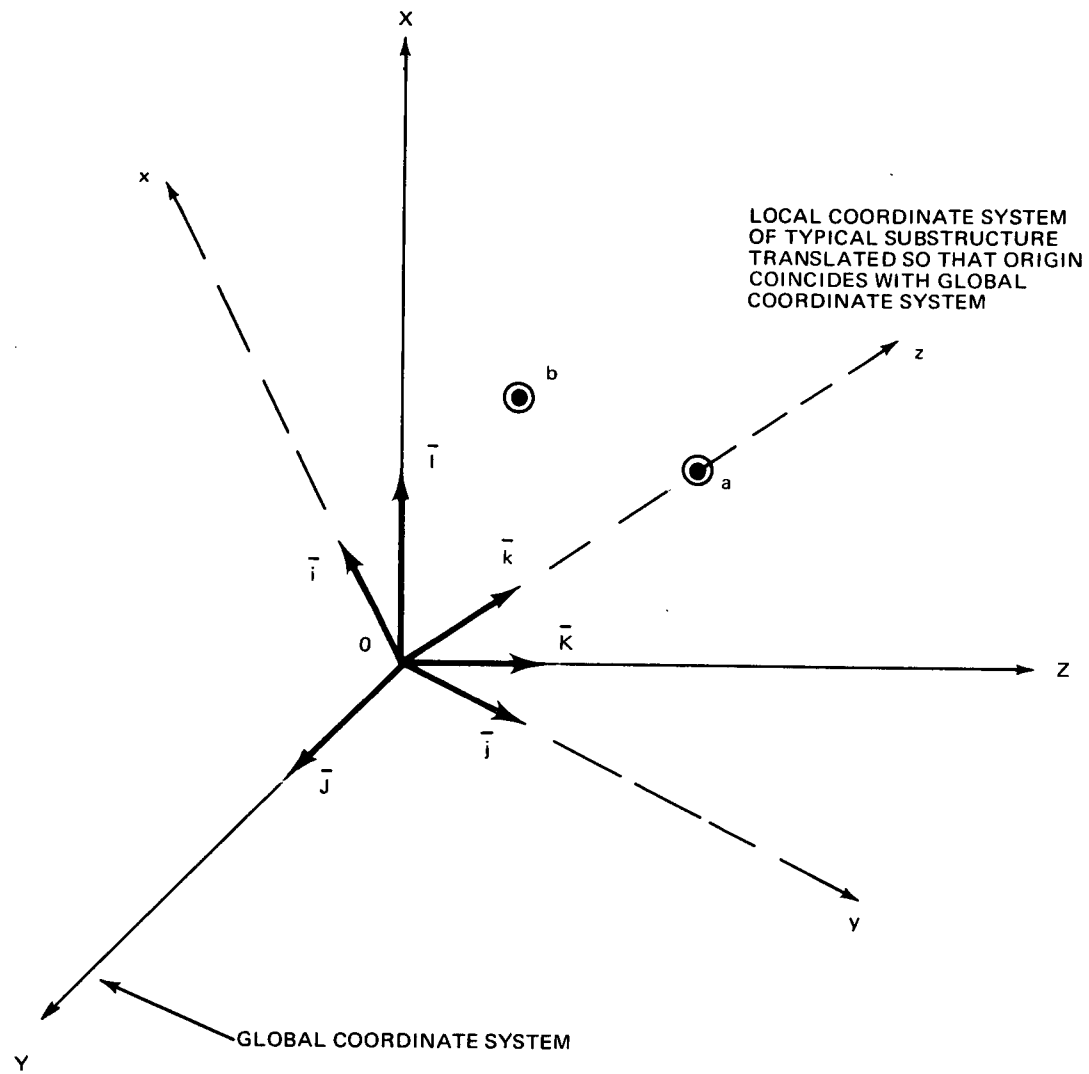


Fig. 3.4 Local and Global Coordinate Axes

The following operations are employed to generate the transformation matrix from the X, Y, Z to the x, y, z coordinate system. The vector from point "O" to point "a" may be written:

$$\bar{V}_{Oa} = \bar{I} X_a + \bar{J} Y_a + \bar{K} Z_a = \bar{I} \alpha_{31}^* + \bar{J} \alpha_{32}^* + \bar{K} \alpha_{33}^* \quad (3.1)$$

Since \bar{V}_{Oa} lies along the +z axis, the unit vector \bar{k} may be obtained by normalizing \bar{V}_{Oa} to a unit length.

$$\bar{k} = \bar{I} \alpha_{31} + \bar{J} \alpha_{32} + \bar{K} \alpha_{33} \quad (3.2)$$

where

$$\alpha_{ij} = \alpha_{ij}^* / C_k$$

and

$$C_k = \sqrt{\alpha_{31}^{*2} + \alpha_{32}^{*2} + \alpha_{33}^{*2}}$$

A vector normal to the x, z plane may be constructed by taking the cross product of \bar{V}_{Oa} and \bar{V}_{Ob} .

$$\begin{aligned} \bar{V}_N &= \bar{V}_{Oa} \times \bar{V}_{Ob} \\ &= \bar{I} (Y_a Z_b - Y_b Z_a) + \bar{J} (X_b Z_a - X_a Z_b) + \bar{K} (X_a Y_b - X_b Y_a) \\ &= \bar{I} \alpha_{21}^* + \bar{J} \alpha_{22}^* + \bar{K} \alpha_{23}^* \end{aligned} \quad (3.3)$$

Since \bar{V}_N lies along the + y axis, the unit vector \bar{j} may be obtained by normalizing \bar{V}_N to a unit length.

$$\bar{j} = \bar{I} \alpha_{21} + \bar{J} \alpha_{22} + \bar{K} \alpha_{23} \quad (3.4)$$

where

$$\alpha_{ij} = \alpha_{ij}^* / C_j$$

and

$$C_j = \sqrt{\alpha_{21}^{*2} + \alpha_{22}^{*2} + \alpha_{23}^{*2}}$$

A unit vector along the x axis may be constructed by taking the cross product of \bar{j} with \bar{k} .

$$\bar{i} = \bar{j} \times \bar{k}$$

$$= \bar{I} (\alpha_{33} \alpha_{22} - \alpha_{32} \alpha_{23}) + \bar{J} (\alpha_{31} \alpha_{23} - \alpha_{33} \alpha_{21}) + \bar{K} (\alpha_{32} \alpha_{21} - \alpha_{31} \alpha_{22})$$

$$= \bar{I} \alpha_{11} + \bar{J} \alpha_{12} + \bar{K} \alpha_{13} \quad (3.5)$$

The transformation matrix between local and global coordinates may be written by combining Equations (3.2), (3.4) and (3.5),

$$\begin{Bmatrix} \bar{i} \\ \bar{j} \\ \bar{k} \end{Bmatrix} = \begin{bmatrix} \alpha_{11} & \alpha_{12} & \alpha_{13} \\ \alpha_{21} & \alpha_{22} & \alpha_{23} \\ \alpha_{31} & \alpha_{32} & \alpha_{33} \end{bmatrix} \begin{Bmatrix} \bar{I} \\ \bar{J} \\ \bar{K} \end{Bmatrix} \quad (3.6)$$

or

C

$$\{U\} = [\alpha] \{V\} \quad (3.7)$$

where

$$\alpha_{31} = X_a / c_K ; \quad \alpha_{32} = Y_a / c_K ; \quad \alpha_{33} = Z_a / c_K$$

$$c_K = \sqrt{X_a^2 + Y_a^2 + Z_a^2}$$

$$\alpha_{21}^* = Y_a Z_b - Y_b Z_a ; \quad \alpha_{22}^* = X_b Z_a - X_a Z_b ; \quad \alpha_{23}^* = X_a Y_b - X_b Y_a$$

$$\alpha_{21} = \alpha_{21}^* / c_J ; \quad \alpha_{22} = \alpha_{22}^* / c_J ; \quad \alpha_{23} = \alpha_{23}^* / c_J$$

$$c_J = \sqrt{\alpha_{21}^{*2} + \alpha_{22}^{*2} + \alpha_{23}^{*2}}$$

$$\alpha_{11} = \alpha_{33} \alpha_{22} - \alpha_{32} \alpha_{23} ; \quad \alpha_{12} = \alpha_{31} \alpha_{23} - \alpha_{33} \alpha_{21}$$

$$\alpha_{13} = \alpha_{32} \alpha_{21} - \alpha_{31} \alpha_{22}$$

Since Equation (3.7) is an orthogonal transformation, the inverse transformation, may be written

$$\{V\} = [\alpha]^T \{U\} \quad (3.8)$$

Equation (3.8) is the desired result which will now be used to transform the mass point locations from the local to the global coordinate system.

$$\begin{Bmatrix} X_i \\ Y_i \\ Z_i \end{Bmatrix} = [\alpha]^T \begin{Bmatrix} x_i \\ y_i \\ z_i \end{Bmatrix} \quad (\text{For } i = 1, 2, \dots, n) \quad (3.9)$$

These global mass point locations will be required in the coupling analysis.

From Equation (3.7), the transformation between displacements in the local and global coordinate systems for the i^{th} substructure may be written as

$$\begin{Bmatrix} q_x^{(i)} \end{Bmatrix} = \begin{Bmatrix} \beta^{(i)} \end{Bmatrix} \begin{Bmatrix} q_x^{(i)} \end{Bmatrix} \quad (3.10)$$

where

$$\begin{Bmatrix} \beta^{(i)} \end{Bmatrix} = \begin{bmatrix} [\alpha] & & & \\ & [\alpha] & & \\ & & \ddots & \\ & & & [\alpha] \end{bmatrix}$$

is a square matrix of order $6n$, and the displacement vectors are made up of the three translations and three rotations at each mass point.

A physical mass matrix, $[m_x^{(i)}]$, is supplied for each substructure. These matrices are in the local coordinate system and are defined as if there were six degrees-of-freedom at every mass point. They may be transformed into the global coordinate system using $[\beta^{(i)}]$. The kinetic energy of the i^{th} substructure is

$$T = \frac{1}{2} \{ \dot{q}_x^{(i)} \}^T [m_x^{(i)}] \{ \dot{q}_x^{(i)} \} \quad (3.11)$$

or, making use of Equation (3.10)

$$T = \frac{1}{2} \{ \dot{q}_x^{(i)} \} [\beta^{(i)}]^T [m_x^{(i)}] [\beta^{(i)}] \{ \dot{q}_x^{(i)} \} \quad (3.12)$$

Therefore the mass matrix in the global coordinate system is

$$[m_x^{(i)}] = [\beta^{(i)}]^T [m_x^{(i)}] [\beta^{(i)}] \quad (3.13)$$

A matrix of mode shapes, $[\phi_y^{(i)}]$, is to be supplied for each substructure. For the user's convenience, it will not be necessary to supply modes with six degrees of freedom at each mass point. In addition, to accommodate a wide variety of substructure idealizations, it will not be necessary for all of these degrees of freedom to be parallel to the local coordinate system. For example, the mode shapes for a plate may include only the three degrees-of-freedom at a point which represent out of plane motion. In addition, the plate may not be parallel to the local coordinate system established by the rest of the substructure. These constraints are due to the idealization employed in calculating substructure modes.

Before the transformation to global coordinates can be made, the mode shapes are first transformed into the local coordinate system which has six degrees-of-freedom at a point by use of the constraint matrix,

$^{(i)} [T]$. This matrix is defined by the following transformation from displacements $\{q_y^{(i)}\}$ in the user's coordinates to displacements $\{q_x^{(i)}\}$ in the local rectangular coordinate system:

$$\{q_x^{(i)}\} = [T^{(i)}]^T \{q_y^{(i)}\} \quad (3.14a)$$

Thus,

$$[\Phi_x^{(i)}] = [T^{(i)}]^T [\Phi_y^{(i)}] \quad (3.14b)$$

$^{(i)} [T]$ is generally obtained from kinematic considerations. If the constrained coordinates are parallel to the local coordinate axes, the $^{(i)} [T]$ matrix is simply an identity matrix of order $6n$, with those rows deleted which correspond to degrees-of-freedom not present in $[\phi_y^{(i)}]$.

In this case the program will automatically generate the $^{(i)} [T]$ matrix; however if the constraints are not parallel to the local axes, the $^{(i)} [T]$ matrix describing the constraint must be supplied by the user.*

* In order to utilize less computer core storage space $^{(i)} [T]$ is limited in form to matrices which are block diagonal with sub-constraint matrices for each mass point on the main diagonal. This restriction limits the type of constraints that can be considered with this procedure to cases where the coordinates of a mass point are related. While the computer program has been restricted as described, the theory presented herein is more general and can handle constraints which relate coordinates of different mass points.

The transformation to global coordinates may now be made.

$$\left\{ \begin{matrix} (i) \\ q_x \end{matrix} \right\} = \left[\begin{matrix} (i) \\ \gamma \end{matrix} \right] \left\{ \begin{matrix} (i) \\ q_y \end{matrix} \right\} \quad (3.15a)$$

and

$$\left[\begin{matrix} (i) \\ \phi_x \end{matrix} \right] = \left[\begin{matrix} (i) \\ \gamma \end{matrix} \right] \left[\begin{matrix} (i) \\ \phi_y \end{matrix} \right] \quad (3.15b)$$

where

$$\left[\begin{matrix} (i) \\ \gamma \end{matrix} \right] = \left[\begin{matrix} (i) \\ \beta \end{matrix} \right]^T \left[\begin{matrix} (i) \\ \tau \end{matrix} \right]^T$$

3.3.2 Substructure Coupling

Now that the substructure mode shapes and mass matrices have been transformed into the global coordinate system, the coupling procedure may be developed.

The equation giving the rigid-body displacements of the i^{th} mass point of a substructure due to motions of its attachment point with substructure j may be written as

$$\left\{ \begin{matrix} (i) \\ \mu \end{matrix} \right\} = \left[\begin{matrix} (i) \\ a \end{matrix} \right] \left\{ \begin{matrix} \mu \end{matrix} \right\}_j^*$$

or, referring to Figure 3.5,

$$\left\{ \begin{matrix} (i) \\ \mu_x \\ (i) \\ \mu_y \\ (i) \\ \mu_z \\ (i) \\ \theta_x \\ (i) \\ \theta_y \\ (i) \\ \theta_z \end{matrix} \right\} = \left[\begin{array}{ccc|ccc} 1 & & & & & \\ & 1 & & & & \\ & & 1 & & & \\ \hline & & & -z_i & z_i & -y_i \\ & & & y_i & -x_i & x_i \\ \hline & & & 1 & & \\ & & & & 1 & \\ & & & & & 1 \end{array} \right] \left\{ \begin{matrix} \mu_x^* \\ \mu_y^* \\ \mu_z^* \\ \theta_x^* \\ \theta_y^* \\ \theta_z^* \end{matrix} \right\}_j \quad (3.16)$$

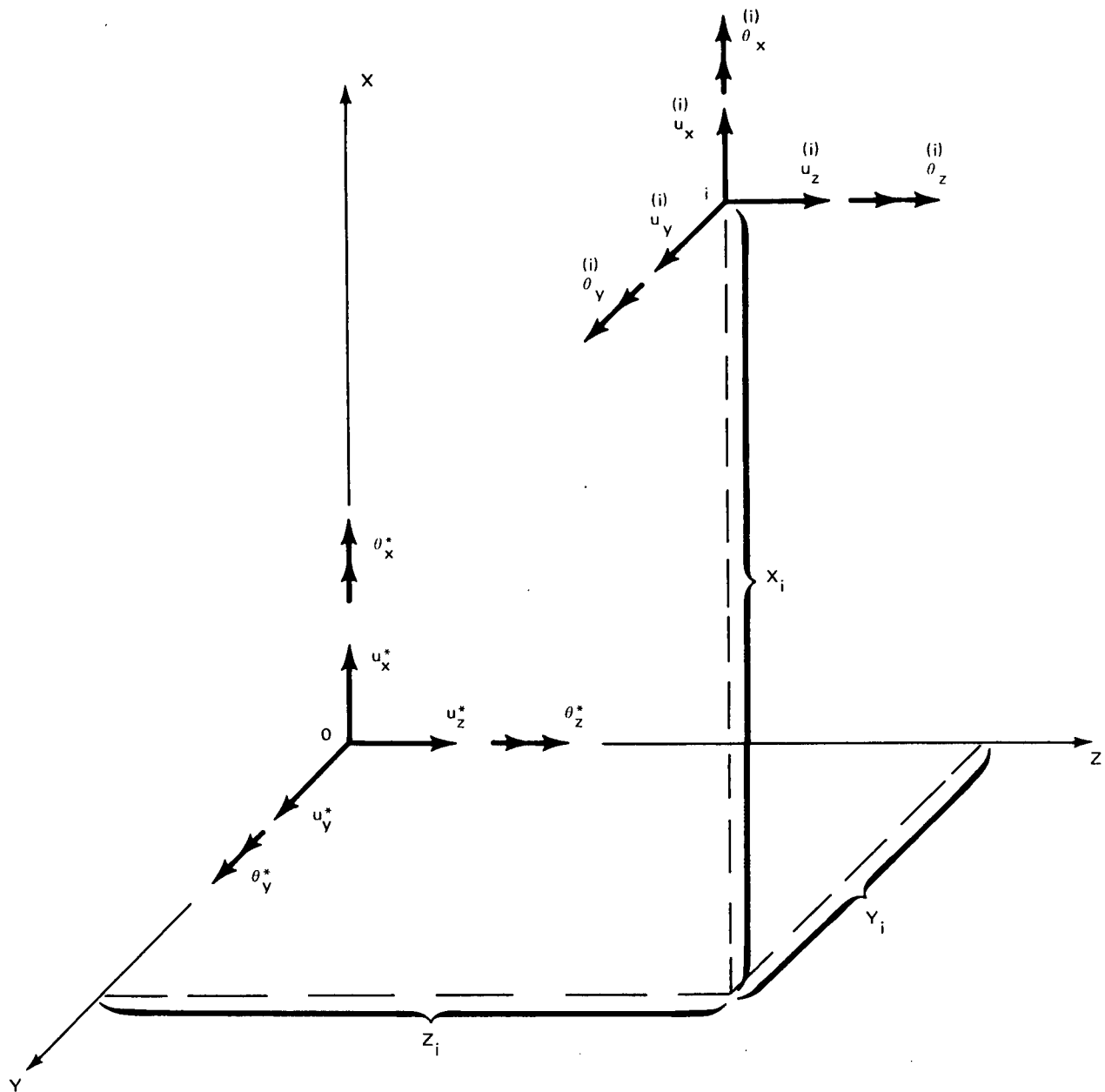


Fig. 3.5 Mass Point Displacements Due To Attachment Point Motions

and the displacements for all of the mass points in the module are,

$$\begin{Bmatrix} u^{(1)} \\ u^{(2)} \\ u \\ \vdots \\ u^{(n)} \end{Bmatrix} = \begin{bmatrix} a^{(1)} \\ a^{(2)} \\ a \\ \vdots \\ a^{(n)} \end{bmatrix} \{u\}_j^*$$

or, for the entire i^{th} substructure,

$$\{U_{i,j}\} = [A_{i,j}] \{u\}_j^* \quad (3.17)$$

To obtain the absolute displacements of the i^{th} substructure, the elastic displacement of the i^{th} substructure relative to the j^{th} substructure must be added to $\{U_{i,j}\}$. The result is

$$\{q_{i,0}\} = \{q_{i,j}\} + \{U_{i,j}\} \quad (3.18)$$

Making use of Equation (3.17), this becomes

$$\{q_{i,0}\} = \{q_{i,j}\} + [A_{i,j}] \{q_{j,0}^{(i)}\} \quad (3.19)$$

Applying Equation (3.19) to Substructures 2 through 11 of Figure 3.3 yields:

$$\{q_{i,0}\} = \{q_{i,1}\} + [A_{i,1}] \{q_{1,0}^{(i)}\} \quad \text{For } i=2,3,\dots,11 \quad (3.20)$$

Applying Equation (3.19) to Substructures 12, 13, and 14, and making use of Equation (3.20) (with $i = 11$), yields:

$$\{q_{12,0}\} = \{q_{12,11}\} + [A_{12,11}]\{q_{11,1}^{(12)}\} + [A_{12,1}]\{q_{1,0}^{(11)}\} \quad (3.21)$$

where:

$$[A_{12,1}] = [A_{12,11}][A_{11,1}^{(12)}]$$

$$\{q_{13,0}\} = \{q_{13,11}\} + [A_{13,11}]\{q_{11,1}^{(13)}\} + [A_{13,1}]\{q_{1,0}^{(11)}\} \quad (3.22)$$

where:

$$[A_{13,1}] = [A_{13,11}][A_{11,1}^{(13)}]$$

$$\{q_{14,0}\} = \{q_{14,11}\} + [A_{14,11}]\{q_{11,1}^{(14)}\} + [A_{14,1}]\{q_{1,0}^{(11)}\} \quad (3.23)$$

where:

$$[A_{14,1}] = [A_{14,11}][A_{11,1}^{(14)}]$$

Applying Equation (3.19) to Substructures 15 and 16, and making use of Equation (3.23), yields:

$$\begin{aligned} \{q_{15,0}\} = & \{q_{15,14}\} + [A_{15,14}]\{q_{14,11}^{(15)}\} + [A_{15,11}]\{q_{11,1}^{(14)}\} \\ & + [A_{15,1}]\{q_{1,0}^{(11)}\} \end{aligned} \quad (3.24)$$

where:

$$[A_{15,11}] = [A_{15,14}] [A_{14,11}^{(15)}]$$

$$[A_{15,1}] = [A_{15,14}] [A_{14,11}^{(15)}] [A_{11,1}^{(14)}]$$

$$\begin{aligned} \{q_{16,0}\} = \{q_{16,14}\} + [A_{16,14}] \{q_{14,11}^{(16)}\} + [A_{16,11}] \{q_{11,1}^{(14)}\} \\ + [A_{16,1}] \{q_{1,0}^{(11)}\} \end{aligned} \quad (3.25)$$

where:

$$[A_{16,11}] = [A_{16,14}] [A_{14,11}^{(16)}]$$

$$[A_{16,1}] = [A_{16,14}] [A_{14,11}^{(16)}] [A_{11,1}^{(14)}]$$

The application of Equations (3.19) and (3.25) to Substructure 17, yields:

$$\begin{aligned} \{q_{17,0}\} = \{q_{17,16}\} + [A_{17,16}] \{q_{16,14}^{(17)}\} + [A_{17,14}] \{q_{14,11}^{(16)}\} \\ + [A_{17,11}] \{q_{11,1}^{(14)}\} + [A_{17,1}] \{q_{1,0}^{(11)}\} \end{aligned} \quad (3.26)$$

where:

$$[A_{17,14}] = [A_{17,16}] [A_{16,14}^{(17)}]$$

$$[A_{17,11}] = [A_{17,16}] [A_{16,14}^{(17)}] [A_{14,11}^{(16)}]$$

$$[A_{17,1}] = [A_{17,16}] [A_{16,14}^{(17)}] [A_{14,11}^{(16)}] [A_{11,1}^{(14)}]$$

The physical displacements may be written in terms of substructure modal displacements by making the substitution

$$[q_{1,1}] = [\phi_1] \{\xi_1\} \quad (3.27)$$

where the $[\phi_X^{(i)}]$ of Equation (3.15b) has been renamed $[\phi_i]$ to simplify the notation. The mode shapes for Substructure 1, $[\phi_1]$, are free-free since the absolute displacement, $\{q_{1,0}\}$ is required. Those of Substructures 2 through 17, $[\phi_2] \dots [\phi_{17}]$, are computed with the substructures constrained at their junction points as shown in Figure 3.2, since motion relative to these junction points is required. Thus,

$$[q_{1,0}] = [\phi_1] \{\xi_1\} \quad (3.28)$$

and, making use of Equation (3.27), Equations (3.20) through (3.26) become:

$$\{q_{1,0}\} = [\phi_1] \{\xi_1\} + [A_{1,1}] [\phi_1^{(1)}] \{\xi_1\} \quad (\text{For } i = 2, 3, \dots, 11) \quad (3.29)$$

$$\{q_{12,0}\} = [\phi_{12}] \{\xi_{12}\} + [A_{12,11}] [\phi_{11}^{(12)}] \{\xi_{11}\} + [A_{12,1}] [\phi_1^{(11)}] \{\xi_1\} \quad (3.30)$$

$$\{q_{13,0}\} = [\phi_{13}] \{\xi_{13}\} + [A_{13,11}] [\phi_{11}^{(13)}] \{\xi_{11}\} + [A_{13,1}] [\phi_1^{(11)}] \{\xi_1\} \quad (3.31)$$

$$\{q_{14,0}\} = [\phi_{14}] \{\xi_{14}\} + [A_{14,11}] [\phi_{11}^{(14)}] \{\xi_{11}\} + [A_{14,1}] [\phi_1^{(11)}] \{\xi_1\} \quad (3.32)$$

$$\{q_{15,0}\} = [\phi_{15}]\{\xi_{15}\} + [A_{15,14}][\phi_{14}^{(15)}]\{\xi_{14}\} + [A_{15,11}][\phi_{11}^{(14)}]\{\xi_{11}\} \\ + [A_{15,1}][\phi_1^{(11)}]\{\xi_1\} \quad (3.33)$$

$$\{q_{16,0}\} = [\phi_{16}]\{\xi_{16}\} + [A_{16,14}][\phi_{14}^{(16)}]\{\xi_{14}\} + [A_{16,11}][\phi_{11}^{(14)}]\{\xi_{11}\} \\ + [A_{16,1}][\phi_1^{(11)}]\{\xi_1\} \quad (3.34)$$

$$\{q_{17,0}\} = [\phi_{17}]\{\xi_{17}\} + [A_{17,16}][\phi_{16}^{(17)}]\{\xi_{16}\} + [A_{17,14}][\phi_{14}^{(16)}]\{\xi_{14}\} \\ + [A_{17,11}][\phi_{11}^{(14)}]\{\xi_{11}\} + [A_{17,1}][\phi_1^{(11)}]\{\xi_1\} \quad (3.35)$$

Equations (3.25) through (3.32) may be written, in matrix notation, as:

$$\{q_x\} = [B]\{\xi\} \quad (3.36)$$

or

$$\begin{bmatrix} q_{1,0} \\ q_{2,0} \\ q_{3,0} \\ q_{4,0} \\ q_{5,0} \\ q_{6,0} \\ q_{7,0} \\ q_{8,0} \\ q_{9,0} \\ q_{10,0} \\ q_{11,0} \\ q_{12,0} \\ q_{13,0} \\ q_{14,0} \\ q_{15,0} \\ q_{16,0} \\ q_{17,0} \end{bmatrix} = \begin{bmatrix} B_{1,1} & & & & & & & & & & & & & & & & \\ & B_{2,1} & B_{2,2} & & & & & & & & & & & & & & & \\ & B_{3,1} & & B_{3,3} & & & & & & & & & & & & & & \\ & B_{4,1} & & & B_{4,4} & & & & & & & & & & & & & \\ & B_{5,1} & & & & B_{5,5} & & & & & & & & & & & & \\ & B_{6,1} & & & & & B_{6,6} & & & & & & & & & & & \\ & B_{7,1} & & & & & & B_{7,7} & & & & & & & & & & \\ & B_{8,1} & & & & & & & B_{8,8} & & & & & & & & & \\ & B_{9,1} & & & & & & & & B_{9,9} & & & & & & & & \\ & B_{10,1} & & & & & & & & & B_{10,10} & & & & & & & \\ & B_{11,1} & & & & & & & & & & B_{11,11} & & & & & & \\ & B_{12,1} & & & & & & & & & & & B_{12,12} & & & & & \\ & B_{13,1} & & & & & & & & & & & & B_{13,13} & & & & \\ & B_{14,1} & & & & & & & & & & & & & B_{14,14} & & & \\ & B_{15,1} & & & & & & & & & & & & & & B_{15,15} & & \\ & B_{16,1} & & & & & & & & & & & & & & & B_{16,16} & \\ & B_{17,1} & & & & & & & & & & & & & & & & B_{17,17} \end{bmatrix} \begin{bmatrix} \xi_1 \\ \xi_2 \\ \xi_3 \\ \xi_4 \\ \xi_5 \\ \xi_6 \\ \xi_7 \\ \xi_8 \\ \xi_9 \\ \xi_{10} \\ \xi_{11} \\ \xi_{12} \\ \xi_{13} \\ \xi_{14} \\ \xi_{15} \\ \xi_{16} \\ \xi_{17} \end{bmatrix}$$

where:

$$\begin{aligned} [B_{\lambda,\lambda}] &= [\phi_\lambda] \quad \lambda = 1, 2, \dots, 17 & [B_{\lambda,\lambda}] &= [A_{\lambda,\lambda}] [\phi_\lambda^{(\lambda)}] \quad \lambda = 12, 13, 14 & [B_{16,14}] &= [A_{16,14}] [\phi_{14}^{(16)}] \\ [B_{\lambda,1}] &= [A_{\lambda,1}] [\phi_1^{(\lambda)}] \quad \lambda = 2, 3, \dots, 11 & [B_{\lambda,11}] &= [A_{\lambda,11}] [\phi_{11}^{(\lambda)}] \quad \lambda = 15, 16, 17 & [B_{17,14}] &= [A_{17,14}] [\phi_{14}^{(17)}] \\ [B_{\lambda,1}] &= [A_{\lambda,1}] [\phi_1^{(\lambda)}] \quad \lambda = 12, 13, \dots, 17 & [B_{15,14}] &= [A_{15,14}] [\phi_{14}^{(15)}] & [B_{17,16}] &= [A_{17,16}] [\phi_{16}^{(17)}] \end{aligned}$$

The mass matrix may now be transformed to the $\{\xi\}$ coordinate system. The kinetic energy of the coupled system is,

$$T = \frac{1}{2} \{\dot{q}_x\}^T [m_x] \{\dot{q}_x\} \quad (3.37)$$

where

$$[m_x] = \begin{bmatrix} m_x^{(1)} & & \\ & m_x^{(2)} & \\ & & \ddots \\ & & & m_x^{(n)} \end{bmatrix}$$

or, making use of Equation (3.36)

$$T = \frac{1}{2} \{\dot{\xi}\}^T [B]^T [m_x] [B] \{\dot{\xi}\} \quad (3.38)$$

Therefore the mass matrix in the $\{\xi\}$ coordinate system may be written as

$$[m_\xi] = [B]^T [m_x] [B] \quad (3.39)$$

or, performing the indicated matrix multiplications in partitioned form:

$$[m_E] = \begin{bmatrix} M_{1,1} & M_{1,2} & M_{1,3} & M_{1,4} & M_{1,5} & M_{1,6} & M_{1,7} & M_{1,8} & M_{1,9} & M_{1,10} & M_{1,11} & M_{1,12} & M_{1,13} & M_{1,14} & M_{1,15} & M_{1,16} & M_{1,17} \\ M_{1,2}^T & M_{2,2} & & & & & & & & & & & & & & & \\ M_{1,3}^T & & M_{3,3} & & & & & & & & & & & & & & \\ M_{1,4}^T & & & M_{4,4} & & & & & & & & & & & & & \\ M_{1,5}^T & & & & M_{5,5} & & & & & & & & & & & & \\ M_{1,6}^T & & & & & M_{6,6} & & & & & & & & & & & \\ M_{1,7}^T & & & & & & M_{7,7} & & & & & & & & & & \\ M_{1,8}^T & & & & & & & M_{8,8} & & & & & & & & & \\ M_{1,9}^T & & & & & & & & M_{9,9} & & & & & & & & \\ M_{1,10}^T & & & & & & & & & M_{10,10} & & & & & & & \\ M_{1,11}^T & & & & & & & & & & M_{11,11} & M_{11,12} & M_{11,13} & M_{11,14} & M_{11,15} & M_{11,16} & M_{11,17} \\ M_{1,12}^T & & & & & & & & & & M_{11,12}^T & M_{12,12} & & & & & \\ M_{1,13}^T & & & & & & & & & & M_{11,13}^T & & M_{13,13} & & & & \\ M_{1,14}^T & & & & & & & & & & M_{11,14}^T & & & M_{14,14} & M_{14,15} & M_{14,16} & M_{14,17} \\ M_{1,15}^T & & & & & & & & & & M_{11,15}^T & & & M_{14,15}^T & M_{15,15} & & \\ M_{1,16}^T & & & & & & & & & & M_{11,16}^T & & & M_{14,16}^T & & M_{16,16} & M_{16,17} \\ M_{1,17}^T & & & & & & & & & & M_{11,17}^T & & & M_{14,17}^T & & M_{16,17}^T & M_{17,17} \end{bmatrix}$$

✓

where

$$M_{1,1} = \sum_{\lambda=1}^{17} B_{\lambda,1}^T m_x^{(1)} B_{\lambda,1}$$

$$M_{\lambda,\lambda} = B_{\lambda,\lambda}^T m_x^{(1)} B_{\lambda,\lambda} \quad (\text{For } \lambda = 2, 3, \dots, 10)$$

$$M_{11,11} = \sum_{\lambda=11}^{17} B_{\lambda,11}^T m_x^{(1)} B_{\lambda,11} ; \quad M_{11,12} = B_{12,11}^T m_x^{(12)} B_{12,12}$$

$$M_{11,13} = B_{13,11}^T m_x^{(13)} B_{13,13} ; \quad M_{11,14} = \sum_{\lambda=14}^{17} B_{\lambda,11}^T m_x^{(1)} B_{\lambda,14}$$

$$M_{11,15} = B_{15,11}^T m_x^{(15)} B_{15,15} ; \quad M_{11,16} = B_{16,11}^T m_x^{(16)} B_{16,16} + B_{17,11}^T m_x^{(17)} B_{17,16}$$

$$M_{11,17} = B_{17,11}^T m_x^{(17)} B_{17,17}$$

$$M_{12,12} = B_{12,12}^T m_x^{(12)} B_{12,12}$$

$$M_{13,13} = B_{13,13}^T m_x^{(13)} B_{13,13}$$

$$M_{14,14} = \sum_{\lambda=14}^{17} B_{\lambda,14}^T m_x^{(1)} B_{\lambda,14} ; \quad M_{14,15} = B_{15,14}^T m_x^{(15)} B_{15,15}$$

$$M_{14,16} = B_{16,14}^T m_x^{(16)} B_{16,16} + B_{17,14}^T m_x^{(17)} B_{17,16} ; \quad M_{14,17} = B_{17,14}^T m_x^{(17)} B_{17,17}$$

$$M_{15,15} = B_{15,15}^T m_x^{(15)} B_{15,15}$$

$$M_{16,16} = B_{16,16}^T m_x^{(16)} B_{16,16} + B_{17,16}^T m_x^{(17)} B_{17,16} ; \quad M_{16,17} = B_{17,16}^T m_x^{(17)} B_{17,17}$$

$$M_{17,17} = B_{17,17}^T m_x^{(17)} B_{17,17}$$

$$M_{\lambda,\lambda} = B_{\lambda,\lambda}^T m_x^{(1)} B_{\lambda,\lambda} \quad (\text{For } \lambda = 2, 3, \dots, 10, 12, 13, 15, 17)$$

$$M_{1,11} = \sum_{\lambda=11}^{17} B_{\lambda,1}^T m_x^{(1)} B_{\lambda,11}$$

$$M_{1,14} = \sum_{\lambda=14}^{17} B_{\lambda,1}^T m_x^{(1)} B_{\lambda,14}$$

$$M_{1,16} = B_{16,1}^T m_x^{(16)} B_{16,16} + B_{17,1}^T m_x^{(17)} B_{17,16}$$

It should be noted that, since $[B_{ii}]$ is $[\phi_i]$, $[M_{22}]$ through $[M_{10,10}]$, $[M_{12,12}]$, $[M_{13,13}]$, and $[M_{15,15}]$ are the diagonal modal mass matrices for the respective structures.

The stiffness matrix will now be transformed into the $\{\xi\}$ coordinate system. Making use of Equations (3.15a) and (3.15b), we may write

$$\begin{Bmatrix} q_x^{(1)} \\ q_x^{(2)} \\ \vdots \\ q_x^{(n)} \end{Bmatrix} = \begin{bmatrix} \gamma^{(1)} & & \\ & \gamma^{(2)} & \\ & & \ddots \\ & & & \gamma^{(n)} \end{bmatrix} \begin{Bmatrix} q_y^{(1)} \\ q_y^{(2)} \\ \vdots \\ q_y^{(n)} \end{Bmatrix}$$

or $\{\bar{q}_x\} = [\gamma] \{q_y\}$ (3.40a)

and

$$\begin{bmatrix} \phi_x^{(1)} \\ \phi_x^{(2)} \\ \vdots \\ \phi_x^{(n)} \end{bmatrix} = \begin{bmatrix} \gamma^{(1)} & & \\ & \gamma^{(2)} & \\ & & \ddots \\ & & & \gamma^{(n)} \end{bmatrix} \begin{bmatrix} \phi_y^{(1)} \\ \phi_y^{(2)} \\ \vdots \\ \phi_y^{(n)} \end{bmatrix}$$

or $[\dot{\phi}_x] = [\gamma] [\dot{\phi}_y]$ (3.40b)

The potential energy may be written as

$$V = \frac{1}{2} \{ \bar{q}_x \}^T [K_x] \{ \bar{q}_x \} \quad (3.41)$$

or, making use of Equation (3.40a)

$$V = \frac{1}{2} \{ q_y \}^T [\gamma]^T [K_x] [\gamma] \{ q_y \} \quad (3.42)$$

Therefore the stiffness matrix in the "y" coordinate system is

$$[K_y] = [\gamma]^T [K_x] [\gamma] \quad (3.43)$$

Making use of Equation (3.27), we may write,

$$\{ \bar{q}_x \} = [\phi_x] \{ \xi \} \quad (3.44)$$

and, substituting this into Equation (3.41)

$$V = \frac{1}{2} \{ \xi \}^T [\phi_x]^T [K_x] [\phi_x] \{ \xi \} \quad (3.45)$$

Therefore, the stiffness matrix in the $\{\xi\}$ coordinate system is

$$[K_\xi] = [\phi_x]^T [K_x] [\phi_x] \quad (3.46a)$$

Substituting $[\phi_x]$ from Equation (3.40b) into Equation (3-46a) yields

$$[K_\xi] = [\phi_y]^T [\gamma]^T [K_x] [\gamma] [\phi_y] \quad (3-46b)$$

or, making use of Equation (3.43)

$$[K_\xi] = [\phi_y]^T [K_y] [\phi_y] \quad (3.47)$$

Therefore the stiffness matrix in the $\{\xi\}$ coordinate system is the diagonal matrix

$$[K_\xi] = \begin{bmatrix} [M_1 \omega_1^2] & & \\ & [M_2 \omega_2^2] & \\ & & \ddots \\ & & & [M_{17} \omega_{17}^2] \end{bmatrix} \quad (3.48)$$

made up of the modal stiffness matrices of the individual modules. It should be noted that for modules not present, the rows and columns corresponding to those modules are omitted in $[m_\xi]$ and $[k_\xi]$, and the matrices are reduced in size accordingly.

The eigenvalue problem for the coupled system may be written as

$$[k_{\xi}] \{\Phi_{\xi}\}_i = \Omega_i^2 [m_{\xi}] \{\Phi_{\xi}\}_i \quad (3.49)$$

where $[k_{\xi}]$ is given by Equation (3.48), and $[m_{\xi}]$ is given by Equation (3.39). The eigenvectors are transformed into the global coordinate system by

$$\{\Phi\} = [B] \{\Phi_{\xi}\} \quad (3.50)$$

Whenever Substructure 1 is represented by one or more rigid-body modes, the stiffness matrix of Equation (3.49) will be singular, since it will contain zeros on the diagonal corresponding to these rigid-body modes. This presents a problem for some eigenvalue algorithms. The singularity may, however, be easily removed by reducing the order of the problem as will be shown. Assuming that the rigid body modes are the first modes of module number 1, Equation (3.49) may be partitioned into

$$\begin{bmatrix} 0 & | & 0 \\ \hline 0 & | & k_{ee} \end{bmatrix} \begin{Bmatrix} \Phi_r \\ \hline \Phi_e \end{Bmatrix} = \Omega^2 \begin{bmatrix} m_{rr} & | & m_{re} \\ \hline m_{re}^T & | & m_{ee} \end{bmatrix} \begin{Bmatrix} \Phi_r \\ \hline \Phi_e \end{Bmatrix} \quad (3.51)$$

where the zeros in $[k_{\xi}]$ occur since this matrix is diagonal, and the first diagonal terms are known to vanish. For the elastic modes ($\Omega^2 \neq 0$), the upper partition of Equation (3.51) may be solved for $\{\Phi_r\}$ in terms of $\{\Phi_e\}$ after cancelling Ω^2 . The result is

$$\{\Phi_r\} = -[m_{rr}]^{-1} [m_{re}] \{\Phi_e\} \quad (\text{For } \Omega^2 \neq 0) \quad (3.52)$$

while the lower partition yields

$$[K_{ee}]\{\Phi_e\} = \Omega^2([m_{re}]^T\{\Phi_r\} + [m_{ee}]\{\Phi_e\}) \quad (3.53)$$

(For $\Omega^2 \neq 0$)

Combining Equations (3.52) and (3.53) yields

$$[K_{ee}]\{\Phi_e\} = \Omega^2([m_{ee}] - [m_{re}]^T[m_{rr}]^{-1}[m_{re}])\{\Phi_e\} \quad (3.54)$$

(For $\Omega^2 \neq 0$)

The eigenvalue problem of Equation (3.54) has a nonsingular stiffness matrix. Solution of this eigenvalue problem will yield the elastic frequencies and mode shapes of the system. The mode shapes may be transformed by

$$\{\Phi_F\} = \begin{Bmatrix} \Phi_r \\ \Phi_e \end{Bmatrix} = \begin{bmatrix} -m_{rr}^{-1}m_{re} \\ I \end{bmatrix} \{\Phi_e\} \quad (3.55)$$

3.4 NUMERICAL RESULTS

A computer program has been written to perform the calculations described in the previous section. This program is described in the User's Manual, Volume II. Various problems including five, nine, and ten-module configurations have been run to check the program and the synthesis technique itself. These problems test virtually every part of the program. Results for the five-module problem are presented in this section.*

Figure 3.6 shows the five module free-free problem, consisting of modules number 1 through 5 of Figure 3.1. All modules lie in the X-Z plane and are idealized as beams, connected at the centerline of Module 1. All twenty-five mass points have six degrees of freedom, except for mass points 8 and 9 which do not have a degree-of-freedom in the "X" direction. This is due to the fact that the two members connecting mass point 8 with mass points 7 and 9 are rigid in the "X" direction, and therefore mass points 8 and 9 are constrained to move with mass point 7 in that direction. The detailed physical properties of the core module and the four appended modules are presented in Appendix F. Mass points 2 and 5 do not appear in the appendix. These points are massless and are centered between the two surrounding points.

The eigenvalue problem for the five module structure of Figure 3.6 was solved in the following four ways:

- Direct Solution:

To provide a basis for comparison, the problem was first formulated as if it were a single structure with 148 degrees of freedom. The modes and frequencies were then computed using Grumman's COMAP matrix package.

- Synthesis No. 1:

In Synthesis No. 1, the 20 lower-frequency modes of Module 1, and the 10 lower-frequency modes of Modules 2 through 5 were used. Thus, a total of 60 modes in all were used. These modes were conventional modes rather than the mass-loaded modes discussed in Section 3.2

* Phase I results for the Laboratory configuration (which was used in the demonstration of the Phase II computer program described in Section 6) are presented in Appendix I. Input data and results for the nine-module configuration are presented in Appendices A1 and A2 of Volume II, respectively.

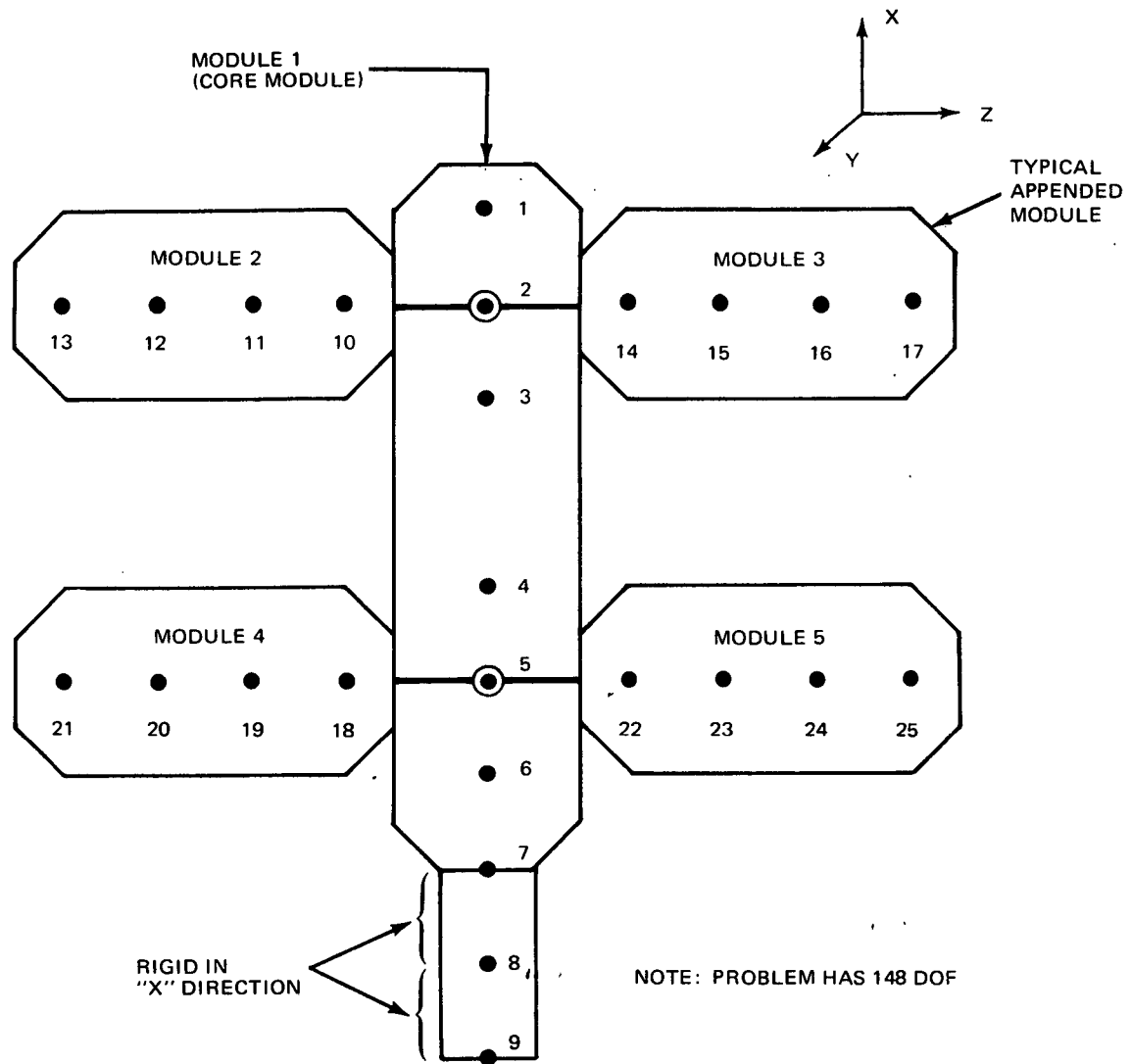


Fig. 3.6 5-Module Check Problem

- Synthesis No. 2:

The same modes were used as in Synthesis No. 1 for the appendages (Modules 2 through 5); however, the 20 mass-loaded modes were used for Module 1.

- Synthesis No. 3:

The same modes were used as in Synthesis No. 2, however an additional 10 mass-loaded modes were used to represent Module 1. The total number of modes for all modules is therefore 70.

The frequencies obtained in each of the above runs are presented in Table 3.1. Comparison of the results of Synthesis No. 1 with those of the direct solution shows them to be poor. The first frequency is off by 5%, the fifth is off by 20%, and only a very few frequencies are considered acceptable. Synthesis No. 2 results are a considerable improvement on those of Synthesis No. 1. The first five frequencies agree with the direct solution to four significant figures, and the first seventeen frequencies are accurate within 1%. This demonstrates the advantages which may be gained through the use of mass loading.

The first 36 frequencies of Synthesis No. 3 are in agreement with those of the direct solution to within 1%. The great improvement in accuracy over Synthesis No. 2 is due to the judicious selection of the additional ten modes employed in the synthesis. Since most of the first 36 modes of the coupled structure involve elastic motion of module number 1, with Modules 2 through 5 moving rigidly or in their lowest modes, the use of the additional modes for module number 1 was a logical choice. In general the analyst should use more modes to represent the more flexible modules. A further improvement could have been made by using selected substructure modes, rather than the ten, twenty or thirty lowest frequency modes.

TABLE 3-1 FREQUENCY COMPARISON FOR THE
FIVE MODULE CHECK PROBLEM

MODE NO.	FREQUENCY - RADIAN/SEC			
	DIRECT SOLUTION	SYNTHESIS NO. 1 (60 modes)	SYNTHESIS NO. 2 (60 modes, mass loading)	SYNTHESIS NO. 3 (70 modes, mass loading)
1	13.67	14.35	13.67	13.67
2	14.02	14.58	14.02	14.02
3	18.37	18.48	18.38	18.38
4	20.54	28.53	20.54	20.54
5	27.76	33.18	27.76	27.76
6	48.54	49.45	48.55	48.54
7	49.86	52.46	49.96	49.87
8	56.64	62.34	56.64	56.64
9	63.76	65.19	64.10	63.77
10	68.72	69.26	69.06	68.78
11	71.79	73.49	72.89	71.79
12	84.78	86.01	85.87	84.80
13	97.95	103.4	98.17	97.99
14	106.6	107.4	106.6	106.6
15	109.5	122.7	109.5	109.5
16	125.4	138.0	125.7	125.4
17	125.6	146.9	127.8	125.6
18	134.0	170.5	142.6	134.1
19	139.8	170.6	170.6	139.9
20	141.8	171.8	173.1	141.9
21	147.2	172.9	173.2	147.2
22	170.1	173.7	176.9	170.6
23	172.8	208.7	215.8	172.8
24	172.9	215.8	215.8	173.2
25	173.9	215.8	236.7	173.9
26	174.4	230.2	236.7	174.4
27	176.8	232.0	238.6	176.9
28	178.7	236.6	256.4	178.7
29	180.3	236.6	264.2	180.3
30	212.1	243.7	273.6	212.3
31	215.8	255.6	288.5	215.8
32	215.8	268.6	357.4	215.8
33	225.5	357.2	359.0	225.5
34	226.1	358.7	361.7	226.1
35	236.6	359.6	365.1	236.6
36	236.6	384.4	383.5	236.6

4.0 PHASE II -- DEVELOPMENT OF THE EQUATIONS OF MOTION FOR THE DYNAMIC SIMULATION

The symbols used in Section 4 are identified below.

<u>SCALAR OR VECTOR FORM</u>	<u>MATRIX FORM</u>	
A		pipe cross-sectional area; also origin of \underline{X} axes
\bar{A}		origin of \underline{Y} axes
A_i		cm of m_i
A_i^R		area of reservoir in m_i
\sim		(subscript); Connecting Structure connects to $\underline{a}^{\text{th}}$ Counterweight mass $\bar{m}_{\sim a}$
B_a		cm of \bar{m}_a
b_i		inside radius of reservoir on m_i
	$[C_M], [\bar{C}_M]$	modal damping matrices for Laboratory and Counterweight, respectively
\vec{D}_k^j	$\{D_k^j\}$	vector from m_k to $\mu_j^{(3)}$
\vec{d}_k^j	$\{d_k^j\}$	same as $\{D_k^j\}$ assuming there is no structural deformation
E, \bar{E}		points on Laboratory and Counterweight, respectively, to which connecting structure attaches
\hat{e}_p		unit vector along $\vec{u} \times \vec{du}$

SCALAR OR
VECTOR FORM

MATRIX
FORM

\hat{e}_i^R	$\{e_i^R\}$	unit vector along centerline of reservoir in $m_i^{(1)}$ directed from base of reservoir toward reservoir-pipe
\hat{e}_t^i	$\{e_i\}$	unit vector tangential to pipe centerline along nominal direction of fluid velocity ⁽¹⁾
\hat{e}_i^B	$\{e_i^B\}$	$\{e_i\}$ for pipe section on m_i which is connected to reservoir on m_i . $\{e_i^B\}$ is always directed outward from control volume ⁽¹⁾
\vec{F}_i, \vec{F}_a	$\{f_i\}, \{\bar{f}_a\}$	resultant force on m_i and \bar{m}_a , respectively ⁽³⁾⁽⁴⁾
	$\{f\}, \{\bar{f}\}$	structural force on point in m_ℓ , or \bar{m}_ℓ , respectively ⁽³⁾⁽⁴⁾
$\vec{F}_i^m, \vec{F}_i^f, \vec{F}_i^\mu$	$\{F_i^m\}, \{F_i^f\}, \{F_i^\mu\}$	see Equations (4.5), (4.6) and accompanying discussion ⁽³⁾
	$\{f_c^i\}, \{\bar{f}_c^a\}$	control force on m_i or \bar{m}_a , respectively ⁽¹⁾⁽²⁾
	$\{f_M\}, \{\bar{f}_M\}$	stiffness and damping in modal coordinates for Laboratory and Counterweight, respectively
	$\{f_s^i\}, \{\bar{f}_s^a\}$	supplementary force on m_i or \bar{m}_a , respectively ⁽¹⁾⁽²⁾
	$\{f_E^*\}$	resultant force applied by Laboratory on on Connecting Structure at point E; vector is expressed in \bar{z} axes.
	$\{f_\ell^i\}, \{\bar{f}_\ell^a\}$	structural force on point in m_ℓ , or \bar{m}_ℓ , respectively. ⁽³⁾⁽⁴⁾

SCALAR OR
VECTOR FORM

MATRIX
FORM

\vec{G}_i	$\{G_i\}$	see Equations (4.26) and (4.27) for the pipe and Equations (4.46) and (4.47) for the reservoir ⁽¹⁾
	$\{G_i^P\}$	$\{G_i\}$ for pipe section of i^{th} mass containing a reservoir
	$\{H_i\}$	$[\Gamma(u_i)] \{e_i\}$
h_i, h_{i_0}		height of fluid in reservoir on m_i ; h_{i_0} is initial value of h_i
\vec{I}_i	$[I_i]$	moment of inertia dyadic (matrix) of m_i about A_i ⁽¹⁾
\vec{I}_a	$[\bar{I}_a]$	moment of inertia dyadic (matrix) of \bar{m}_a about B_a ⁽²⁾
\vec{I}_i^f	$[I_i^f]$	moment of inertia dyadic (matrix) of fluid in m_i about A_i ⁽¹⁾
\vec{I}_i^R, \vec{I}_i^P	$[I_i^R], [I_i^P]$	portions of \vec{I}_i^f for reservoir and reservoir-pipe, respectively
\tilde{i}		(subscript); Connecting Structure connects to \tilde{i}^{th} Laboratory mass $m_{\tilde{i}}$
\vec{J}_i	$[J_i]$	moment of inertia of pipe cross-sectional area about A_i ⁽¹⁾
\vec{J}_i^B	$[J_i^B]$	\vec{J}_i at reservoir=pipe intersection with control surface
k^*		subscript denoting the structural mass m_{k^*} that is nearest to the moving point mass under consideration

SCALAR OR
VECTOR FORM

MATRIX
FORM

	$\{L\}$	angular momentum of Space Station expressed in \underline{Z} axes
	$[L_i]$	moment of inertia matrix of fluid in reservoir on m_i about principal center of mass axes of fluid; number 3 axis is along \hat{e}_i^R
\vec{L}_i	$\{L_i\}$	angular momentum of m_i and any point masses and fluid associated with m_i about 0; matrix form is expressed in \underline{Z} axes
$\vec{L}_i^P, \vec{L}_i^R, \vec{L}_i^\mu$	$\{L_i^P\}, \{L_i^R\}, \{L_i^\mu\}$	contributions to \vec{L}_i of fluid in through pipe on m_i , in reservoir including reservoir-pipe on m_i , and moving masses associated with m_i , respectively
\vec{L}_a	$\{\bar{L}_a\}$	angular momentum of \bar{m}_a about 0; matrix form is expressed in \underline{Z} axes
	$\ell, \bar{\ell}'$	index number of mass point on Laboratory or Counterweight, respectively, at which structural loads are required
$\vec{\ell}, \vec{\ell}_0$	$\{\ell\}, \{\ell_0\}$	Connecting Structure vector from E to E expressed in \underline{Z} axes; subscript o indicates undeformed value
	$[M], [\bar{M}]$	mass matrix for Laboratory (not including fluid or moving point masses) or Counterweight, respectively ^{(3), (4)}
M		total mass of Space Station including fluid and moving point masses
m_i, \bar{m}_a		i^{th} structural mass of Laboratory or a^{th} structural mass of Counterweight, respectively

SCALAR OR
VECTOR FORM

MATRIX
FORM

m_i^f

mass of fluid on m_i

m_i^R, m_i^P

for case of reservoir, contribution to m_i^f of reservoir and reservoir-pipe, respectively

n, \bar{n}

number of structural masses on Laboratory or Counterweight, respectively

0

origin of \underline{z} axes which are fixed in space

$\{P_z\}$

axial tension in Connecting Structure due to centrifugal force. Vector is expressed in \underline{z} axes

$[Q]$

matrix used in obtaining generalized forces (see Section 4.3.4)

Q

mass flow rate of fluid

$\vec{q}_i, \vec{\bar{q}}_a$

$\{q_i\}, \{\bar{q}_a\}$

deflection of A_i and B_a , respectively⁽³⁾⁽⁴⁾

$\{q\}, \{\bar{q}\}$

vector containing all displacements and rotations of Laboratory and Counterweight, respectively

\vec{R}

$\{R\}$

vector from 0 to A (see Figure 4.1)⁽³⁾

$\{\bar{R}\}, \{R_0\}$

vector from A to \bar{A} (see Figure 4.1); subscript 0 indicates value when Space Station is undeformed⁽⁴⁾

$\{\Delta\bar{R}\}$

$\{\bar{R}\} - \{R_0\}$

\vec{R}_c

$\{Z_{CM}\}$

vector from 0 to Space Station cm; matrix form is expressed in \underline{z} axes

$\vec{R}_i, \vec{\bar{R}}_a$

$\{R_i\}, \{\bar{R}_a\}$

vector from 0 to A_i or B_a , respectively⁽³⁾⁽⁴⁾

SCALAR OR VECTOR FORM	MATRIX FORM	
\vec{r}_i	$\{r_i\}$	vector from A to A_i ⁽³⁾
\vec{r}_a	$\{\bar{r}_a\}$	vector from \bar{A} to B_a ⁽⁴⁾
	$[S \quad (\quad)]$	transformation from Euler angles to angular velocities (see Appendix B)
\vec{S}_i	$\{S_i\}$	first moment of mass of fluid in through pipe on m_i about A_i ⁽¹⁾
\vec{S}_i^P, \vec{S}_i^R	$\{S_i^P\}, \{S_i^R\}$	contribution to \vec{S}_i of reservoir-pipe and reservoir, respectively
\vec{s}	$\{s\}$	vector from origin of \tilde{X}^i axes to E ⁽¹⁾
$\vec{\bar{s}}$	$\{\bar{s}\}$	vector from origin of \tilde{Y}^a axes to \bar{E} ⁽²⁾
\vec{T}_i, \vec{T}_a	$\{\tau_i\}, \{\bar{\tau}_a\}$	resultant torque on m_i and \bar{m}_a , respectively ⁽¹⁾⁽²⁾
$\vec{T}_i^m, \vec{T}_i^f, \vec{T}_i^\mu$	$\{T_i^m\}, \{T_i^f\}, \{T_i^\mu\}$	see Equations (4.7), (4.8) and accompanying discussion ⁽¹⁾
t		time
	$\{t_{\ell'}\}, \{\bar{t}_{\ell'}\}$	coordinates of point in $m_{\ell'}$, or $\bar{m}_{\ell'}$, respectively, at which structural loads are computed. Vector is expressed in $\tilde{X}^{\ell'}$ or $\tilde{Y}^{\ell'}$ axes, respectively
\vec{U}_j	$\{U_j\}$	vector from A to μ_j if Laboratory were undeformed ⁽³⁾
\vec{u}	$\{u\}$	vector to centerline of fluid container ⁽¹⁾
$\vec{u}_i^B, \vec{u}_i^R, \vec{u}_i^C$	$\{u_i^B\}, \{u_i^R\}, \{u_i^C\}$	see Figure 4.6 ⁽¹⁾

SCALAR OR
VECTOR FORM

MATRIX
FORM

V		velocity of fluid in pipe
\vec{v}_j	$\{v_j\}$	elastic deflection of moving point mass μ_j (3)
\tilde{W}^i		principal cm axes of fluid in reservoir
\vec{W}_j	$\{W_j\}$	vector from A to μ_j (3)
\tilde{X}		mean or "rigid-body" axes moving with average motion of Laboratory
\tilde{X}^i		body axes in m_i with origin at A_i ; when $i = \underline{i}$, $m_{\underline{i}}$ contains Connecting Structure attachment point (E)
	$\{\dot{x}\}$	see Equation (4.104)
\tilde{Y}		mean or "rigid body" axes moving with average motion of Counterweight
\tilde{Y}^a		body axes in \bar{m}_a with origin at B_a ; when $a = \underline{a}$, $\bar{m}_{\underline{a}}$ contains Connecting Structure attachment point (\bar{E})
	$\{\tilde{Y}^{a'}\}_{\text{a}}, \{\tilde{Y}^{a'}\}_{\text{b}}$	see Section 4.4.2
\tilde{Z}		inertial coordinate system
$\bar{\tilde{Z}}$		coordinate system on $\bar{m}_{\underline{a}}$ (with origin at \bar{E}) used for expressing structural loads applied by Connecting Structure
	$\{\beta\}$	Euler angles locating $\bar{\tilde{Z}}$ axes relative to \tilde{Y}^a axes (5)

SCALAR OR
VECTOR FORM

MATRIX
FORM

	$[\Gamma()]$	matrix form of cross-product operator (see Appendix B)
γ		ratio of modal damping to critical modal damping for beam Connecting Structure
	$\{\gamma\}$	Euler angles locating \tilde{X} axes ⁽⁵⁾ with respect to \tilde{Z} axes ⁽⁵⁾
$\Delta()$		nominal outlet value of () minus nominal inlet value for through pipe
	$\{\delta\}$	$\{\ell\} - \{\ell_o\}$, deflection of Connecting Structure
	$\{\zeta_i\}$	Euler angles locating \tilde{W}^i axes relative to \tilde{X}^i axes ⁽⁵⁾
	$\{\eta\}$	Euler angles locating \tilde{Y} axes with respect to \tilde{X} axes ⁽⁵⁾
	$\{\eta_o\}$	$[\pi \ 0 \ 0]^T$
	$\{\eta^*\}$	$\{\eta\} - \{\eta_o\}$
$\vec{\theta}_i, \vec{\theta}_a$	$\{\theta_i\}, \{\bar{\theta}_a\}$	elastic rotation of m_i or \bar{m}_a , respec- tively (3), (4)
κ		kinetic energy of Space Station
$\kappa_i, \bar{\kappa}_a$		kinetic energy of all mass associated with m_i (including structural mass, fluid, and moving point masses) or \bar{m}_a , respectively
	$[\kappa], [\bar{\kappa}]$	modal stiffness matrices for Laboratory or Counterweight, respectively
	$[\Lambda]$	mass matrix for Space Station
	$[\Lambda_R]$	reduced mass matrix after modal- constraint reduction

SCALAR OR
VECTOR FORM

MATRIX
FORM

λ_k^j

weighting coefficient proportional to the influence of m_k on the motion of μ_j (see Equation (4.65))

$[\mu], [\bar{\mu}]$

modal mass matrix for Laboratory and Counterweight, respectively

μ_j

mass of j^{th} moving point mass

$\{\xi\}, \{\bar{\xi}\}$

modal coordinates for Laboratory and Counterweight, respectively

$\{\dot{\xi}_T\}, \{\bar{\xi}_T\}$

see Equation (4.108)

Π_k^j

see Equation (4.64)

$[\Pi()]$

coordinate transformation where name of Euler-angle set is inserted in ()⁽⁵⁾

$\Pi_{ij}()$

i, j^{th} element of $[\Pi()]$

ρ

mass density of fluid

$\sum_{m_k}^{\mu_j}$

sum over all m_k 's influencing the motion of μ_j

$\{\tau_c^i\}, \{\bar{\tau}_c^a\}$

control torque on m_i or \bar{m}_a about A_i or B_a , respectively⁽¹⁾⁽²⁾

$\{\tau_\ell^i\}, \{\bar{\tau}_\ell^i\}$

structural torque on point in m_ℓ , or \bar{m}_ℓ^i , respectively⁽³⁾⁽⁴⁾

SCALAR OR
VECTOR FORM

MATRIX
FORM

	$\{\tau_s^i\}, \{\tau_s^a\}$	torque of supplementary forces on m_i or \bar{m}_a about A_i or B_a , respectively ^{(1), (2)}
	$\{\tau_E^*\}$	resultant torque applied by Laboratory on Connecting Structure at point E; vector is expressed in \bar{z} axes
U		fluid control volume
	$[\Phi], [\bar{\Phi}]$	modal matrices for Laboratory and Counterweight ^{(3), (4)}
	$[\phi], [\bar{\phi}]$	see Equations (4.109), (4.110), and (4.112)
	$\{\phi^*\}$	Euler angles expressing deformation of Connecting Structure (m_i relative to \bar{z} axes) ⁽⁵⁾
ω	$\{\omega^X\}$	angular velocity of \bar{X} axes ⁽³⁾
	$\{\omega^Y\}$	angular velocity of \bar{Y} axes ⁽⁴⁾
ω_i, ω_a	$\{\omega^{X^i}\}, \{\omega^{Y^a}\}$	angular velocity of \bar{X}^i or \bar{Y}^a axes, respectively ^{(1), (2)}
	$[1], [1_r]$	identity matrix or $r \times r$ identity matrix, respectively
$\begin{pmatrix} \cdot \\ \rightarrow \end{pmatrix}$		derivative of vector measured in rotating \bar{X} axes
$\begin{pmatrix} o \\ \rightarrow \end{pmatrix}$		derivative of vector measured in body axes (\bar{X}^i or \bar{Y}^a axes)
$\begin{pmatrix} \cdot \\ s \end{pmatrix}$		derivative of vector measured in inertially fixed (spatial) coordinate system

Footnotes for Symbols

- (1) The matrix form is expressed in the \tilde{X}^i axes for the symbol pertaining to the Laboratory
- (2) The matrix form is expressed in the \tilde{Y}^a axes for the symbol pertaining to the Counterweight
- (3) The matrix form is expressed in the \tilde{X} axes for the symbol pertaining to the Laboratory
- (4) The matrix form is expressed in the \tilde{Y} axes for the symbol pertaining to the Counterweight
- (5) See Appendix B for order of rotations

Figure 4.1 illustrates the general idealized configuration considered herein. The equations of motion are written for an arbitrary number* of lumped masses on both the Laboratory and the Counterweight and the position and orientation of these masses is also arbitrary. The rotatory inertia of these structural mass points is included.

At the user's option, fluid in motion may or may not be present on the Laboratory. If fluid is present, any two Laboratory structural masses may be specified as containing reservoirs, one nominally emptying and the other nominally filling. As illustrated in Figure 4.2A, a pipe which connects these reservoirs passes through a number of user-designated intermediate masses. (Only two intermediate masses are shown in the diagram for the sake of illustration.) The pipe section which passes through a particular mass is called a through pipe; the pipe segment on a mass which is connected to a reservoir is called a reservoir pipe.

The Laboratory also contains an arbitrary number of moving mass points which represent elevators, crew motion, etc. The rotatory inertia of these masses is neglected since they are assumed to be small relative to the Laboratory. All moving masses move relative to the Laboratory along paths prescribed by the user. The deformation of these paths due to structural vibration is included in the analysis.

The Counterweight does not contain fluids or moving masses.

* For numerical limitations in the computer program see Section 3.5 of Volume II

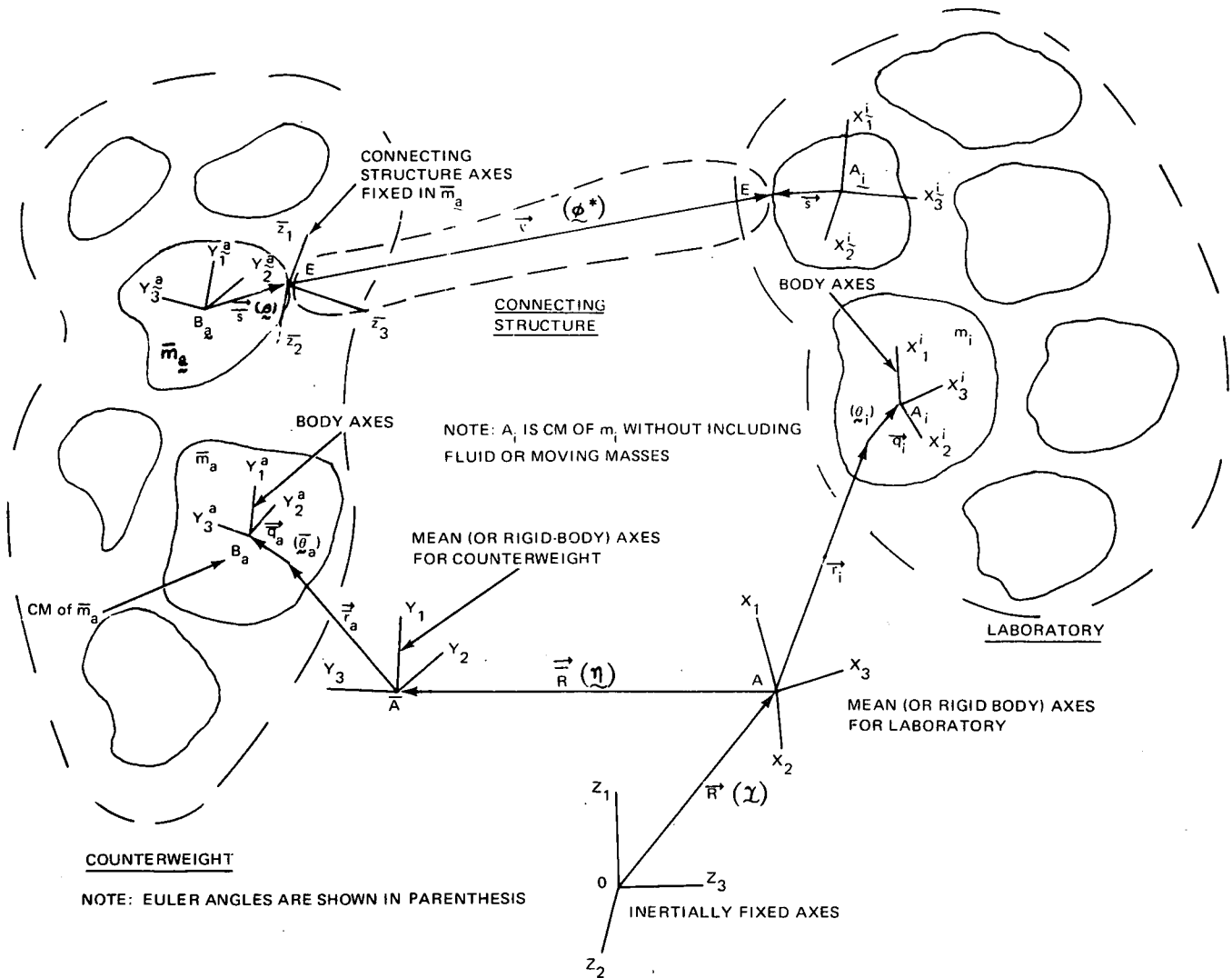
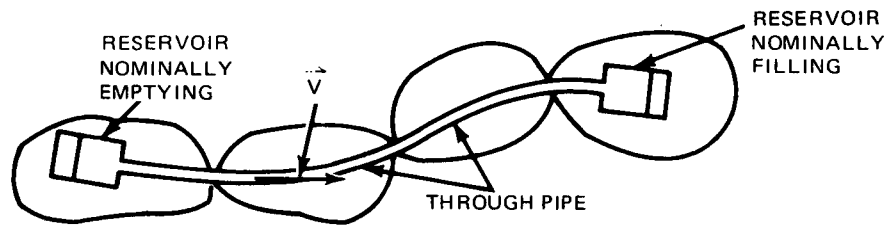
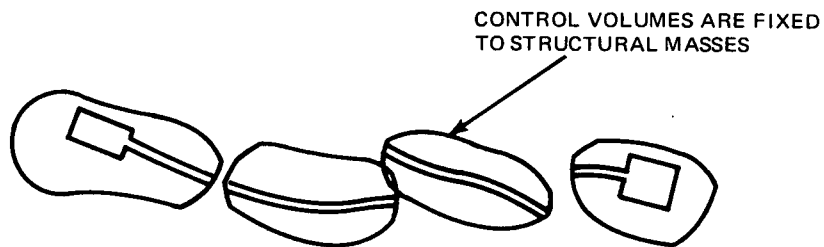


Fig. 4.1 Idealization and Coordinate Systems

Note: Only two intermediate masses containing through pipes are shown; however, the analysis was done for an arbitrary number of masses



(A) Undeformed System



(B) Deformed System

Fig. 4.2 Fluid Control-Volume Idealization Used for Computing Rates of Change of Linear and Angular Momenta

4.1 ASSUMPTIONS USED IN THE FORMULATION

For reference, a list of the assumptions used in the formulation is presented below:

4.1.1 Laboratory and Counterweight Structure

- Elastic motion within the Laboratory and Counterweight is assumed small and is linearized. However, the large rigid-body portion of the motion of these structures is not linearized; neither is the elastic motion of the Laboratory relative to the Counterweight
- Elastic motion of the Laboratory and the Counterweight is, in general, represented by a truncated number of non-rotating mode shapes of each body. The modes are assumed to be orthogonal; therefore equal-frequency mode shapes must be orthogonalized before use
- Damping is assumed to be a percentage of the non-rotating critical damping in each mode. The user may specify different percentages for each mode

4.1.2 Connecting Structure

The structural properties of the connecting structure are coded in a subroutine so that the user may easily replace the connecting structure. The subroutine supplied for program demonstration purposes contains a math model of a tubular beam with the following properties:

- Linear structural properties
- The stiffening effects of tension due to centrifugal force are included
- The beam length is variable to simulate Counterweight deployment and retraction. The undeformed beam length is a variable function of time which is specified by a user-supplied subroutine. The subroutine supplied with this report is described in Section 5

4.1.3 Structural Coordinate Systems (See Figure 4.1)*

In the Phase II computations the local coordinate systems \tilde{X}^i that are fixed in structural masses m_i in the Laboratory, the rigid-body coordinates \tilde{X} for the Laboratory, the local coordinate systems \tilde{Y}^a that are fixed in structural masses \bar{m}_a in the Counterweight, and the rigid-body coordinates \tilde{Y} for the Counterweight are assumed to be parallel when the entire Space Station is undeformed; however, for convenience, the Y_2 and Y_2^a axes are in the negative X_2 and X_2^a directions, respectively, and the Y_3 and Y_3^a axes are in the negative X_3 and X_3^a directions, respectively. These assumptions do not limit the generality of the program since the user can always set up the problem using coordinate systems that are oriented as described above. In fact, the user can supply input data into the Phase I (Modal-Synthesis) program in terms of coordinates that are not parallel, and Phase I can be used to automatically supply results to Phase II in terms of coordinates that are in the required directions.

4.1.4 Fluid

- Fluid flow in both the pipe and the reservoir is uniform; i.e., the cross-sectional velocity profile is a straight line rather than a parabola or more complex shape. A bladder or piston is assumed to confine the fluid within each reservoir so that (1) sloshing does not occur and (2) the fluid height within the reservoir is a well-defined quantity
- The fluid is incompressible
- For the purpose of computing the rate of change of linear and angular momentum of the fluid, it is assumed that each control volume has the rigid-body motion of the associated mass point, and the control volumes touch at the boundary points when there is no deformation. This approximation gives rise to the inconsistency that the pipe is discontinuous when the Laboratory is undeformed (see Figure 4.2B). However, for the purpose of computing the structural loads contributed by the pipe, the pipe is assumed to deform.

 * See Sections 4.2 and 4.3.2 for additional discussions of these coordinate systems during deformation.

These effects are included in the stiffness and damping matrices

- A structural mass cannot contain more than one through pipe nor can it contain both a through pipe and a reservoir
- Fluid velocity as a function of time is specified by a subroutine which may be easily replaced by the user. The curve shown in Figure 5.5 has been coded in the subroutine provided under this contract. This curve is discussed in Section 5.3.2
- The pipe is assumed to always be full. If a reservoir empties, the fluid velocity is set to zero and the specified velocity function is disregarded
- The pipe is assumed to be of constant area
- Each reservoir is a right circular cylinder, and the pipe axis is tangent to the cylinder axes at the reservoir entrance

4.1.5 Moving Point Masses

- Rotatory inertia is neglected
- The motion is a user-specified function of time which is coded in a subroutine so that it may be easily changed. The function shown in Figures 5.3 and 5.4 has been programmed in the subroutine provided under this contract. This function is discussed in Section 5.3.1.
- Since the mass moves along the elastic structure, the portion of its motion due to deformation has been estimated and added to the pre-specified rigid-body motion. When the moving mass is located between structural masses its motion is obtained as the weighted average of up to sixteen surrounding masses. The average is weighted so that as the moving mass approaches a structural mass mode point, its position and velocity approach that of the structural mass. The closer the distance to the structural mass,

the more the motion of that mass is counted in the averaging process. The details are described in Section 4.2.3

- The acceleration terms in the equations for the moving point masses are always evaluated late in time by one numerical-integration time step. At $t = 0$, these terms are set to zero. As discussed in Section 4.3.2, this approximation results in a considerable savings in computer core storage space.

4.2 DEVELOPMENT OF THE EQUATIONS OF MOTION IN VECTOR FORM

The coordinate systems used and the vectors which locate these coordinate systems are illustrated in Figure 4.1. The \underline{Z} coordinates (with axes Z_1 , Z_2 , and Z_3) are a set of inertially fixed axes with their origin located at any convenient point in space. The \underline{X} coordinates are the mean, or "rigid-body" axes of the Laboratory and move with the average motion of the laboratory as it flexes and moves through space. The position of these axes will be more accurately defined in Section 4.3.4. Similarly, the \underline{Y} axes are the mean axes for the Counterweight. Each structural mass m_i in the Laboratory has its cm at A_i , and A_i is also the origin of the body coordinates \underline{X}^i which are fixed in m_i . The corresponding terms used for a typical Counterweight mass point \bar{m}_a are B_a and \underline{Y}^a , respectively.

For clarity, a portion of Figure 4.1 is shown in Figure 4.3, and some additional detail has been included. From the geometry of this figure, for a mass located on the Laboratory,

$$\vec{R}_i = \vec{R} + \vec{r}_i + \vec{q}_i \quad (4.1)$$

If ordinary dotted derivatives are measured in the \underline{X} coordinate system which rotates at $\vec{\omega}$ and dotted derivatives used with the superscript "s" denote derivatives measured in an inertial or "spatial" coordinate system,

$$\dot{\vec{r}}_i = \ddot{\vec{r}}_i = 0 \quad (4.2)$$

$$\dot{\vec{R}}_i^s = \dot{\vec{R}} + \dot{\vec{q}}_i + \vec{\omega} \times \vec{R}_i ; \quad \dot{\vec{R}}_i = \dot{\vec{R}} + \dot{\vec{q}}_i \quad (4.3)$$

$$\ddot{\vec{R}}_i^s = \ddot{\vec{R}} + \ddot{\vec{q}}_i + 2\vec{\omega} \times \dot{\vec{R}}_i + \vec{\omega} \times (\vec{\omega} \times \vec{R}_i) + \dot{\vec{\omega}} \times \vec{R}_i \quad (4.4)$$

In writing Equations (4.3) and (4.4) we have anticipated that the components of \vec{R} will be projected along the rotating \underline{X} axes.

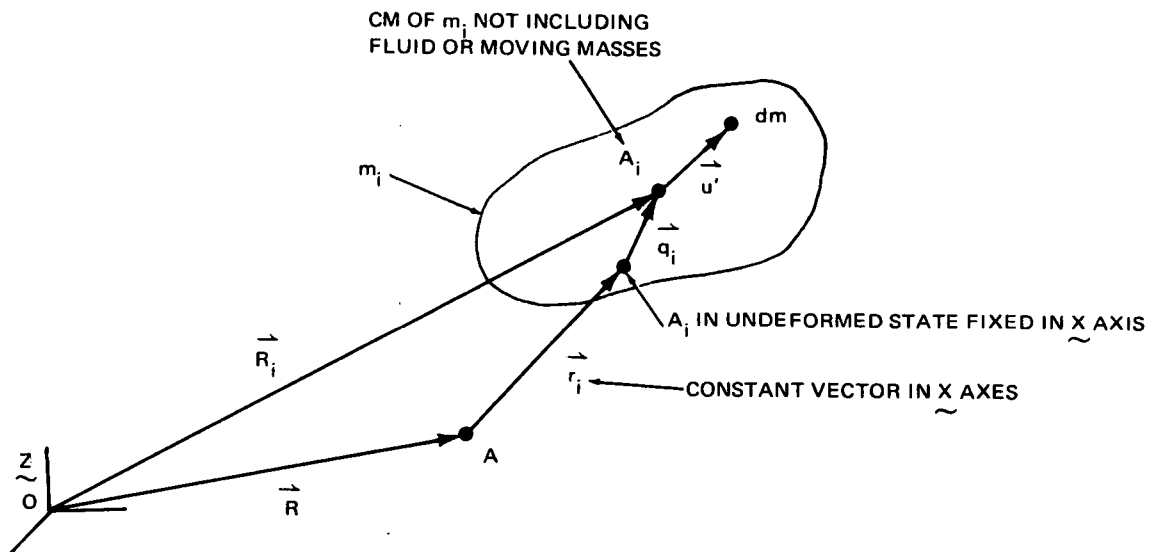


Fig. 4.3 Typical Mass on the Laboratory

The resultant force on m_i is

$$\vec{F}_i = \frac{d}{dt} \left(\int_{S_Y} (\ddot{\vec{R}}_i^s + \ddot{\vec{u}}'^s) dm \right)_S \quad (4.5)$$

where the " S_Y " indicates that the integration and differentiation applies to the fixed system of mass particles located on m_i at time t , and the subscript " S " indicates that the derivative is measured in an inertial coordinate system. Equation (4.5) is broken up as follows:

$$\vec{F}_i = \vec{F}_i^m + \vec{F}_i^f + \vec{F}_i^u \quad (4.6)$$

where \vec{F}_i^m denotes the contribution of the rigid structural mass m_i to the right side of Equation (4.5), \vec{F}_i^f denotes the contribution of the fluid on m_i , and \vec{F}_i^u denotes the contribution of the moving point masses associated with m_i .

The equation for the torque about point A_i is treated similarly. Again referring to Figure 4.3:

$$\vec{T}_i = \int_{S_Y} \vec{u}' \times (\ddot{\vec{R}}_i^s + \ddot{\vec{u}}'^s) dm$$

or

$$\vec{T}_i = \left(\int_{S_Y} \vec{u}' dm \right) \times \ddot{\vec{R}}_i^s + \frac{d}{dt} \left(\int_{S_Y} \vec{u}' \times \ddot{\vec{u}}'^s dm \right)_S \quad (4.7)$$

The terms on the right side of Equation (4.7) are broken up into their contributions due to rigid mass, fluid, and moving point-masses as follows:

$$\vec{T}_i = \vec{T}_i^m + \vec{T}_i^f + \vec{T}_i^u \quad (4.8)$$

The various contributions in Equation (4.6) and (4.8) will be computed separately in the subsections which follow and will be combined in Section 4.3 where the equations are converted to matrix form.

4.2.1 Structural Mass on Laboratory

Evaluation of the right sides of Equations (4.5) and (4.7) for the rigid mass m_i is straightforward. The results are

$$\vec{F}_i^m = m_i \ddot{\vec{R}}_i \quad (4.9)$$

and

$$\vec{T}_i^m = \vec{I}_i \cdot \ddot{\vec{\omega}}_i + \vec{\omega}_i \times \vec{I}_i \cdot \vec{\omega}_i \quad (4.10)$$

where the circle indicates a derivative which is measured in the \tilde{x}^i coordinate system.

4.2.2 Fluid Motion in the Laboratory

When evaluating the derivatives in Equations (4.5) and (4.7) for the fluid, the effect of mass transfer through the boundary of m_i must be accounted for. A suitable expression for accomplishing this is derived in Appendix A and the result is summarized below. As indicated in Appendix A the control volume for the fluid associated with m_i is assumed to be fixed relative to m_i . This assumption is discussed in Section 4.1.3. Consider any vector quantity \vec{Q} that is a quantity per unit mass of the fluid. For example \vec{Q} may be the linear momentum of a particle of mass dm . The total contribution of \vec{Q} to the mass present within the control volume at a fixed time is

$$\vec{G} = \int_{s_V} \vec{Q} dm = \int_{s_V} \vec{Q} \rho dV \quad (4.11)$$

As time varies, the boundary of this system of particles changes so that it will no longer coincide with the control-volume boundary. The problem of differentiating Equation (4.11) is complicated by the fact that the control volume moves in space since it is located on a spinning, vibrating space station. It is shown in Appendix A that the inertial derivative of \vec{G} is

$$\left(\frac{d\vec{G}}{dt}\right)_S = \frac{d}{dt} \left(\int_{cv} \vec{Q} \rho dV \right)_S + \oint_{cs} \vec{Q} \rho \vec{V} \cdot d\vec{A} \quad (4.12)$$

where cv indicates that the integral is computed over the time-varying quantity of fluid present within the control volume, cs designates the control surface, or control-volume boundary, \vec{V} is the velocity of fluid relative to the control surface measured in rotating axis fixed relative to the control volume, and $d\vec{A}$ is the differential control-surface area multiplied by the outward unit-normal vector. The last integral in Equation (4.12) is the contribution, to the derivative, of fluid passing through the control volume.

Equations (4.11) and (4.12) are now used to evaluate the contribution of the fluid to the derivative on the right side of Equation (4.5). Setting $dm = \rho dV$, the result is

$$\vec{F}_i^s = \frac{d}{dt} \left(\int_{cv} (\vec{R}_i^s + \vec{u}'^s) \rho dV \right)_S + \oint_{cs} (\vec{R}_i^s + \vec{u}'^s) \rho \vec{V} \cdot d\vec{A} \quad (4.13)$$

where

$$\vec{u}'^s = \vec{V} + \vec{\omega}_i \times \vec{u}' \quad (4.14)$$

Equation (4.14) is substituted into Equation (4.13), and the integration is partially carried through. In performing this step, it is noted that the control surface is pierced at most twice (case of a through pipe) or only once (case of a reservoir). Also, the flow is assumed incompressible (so that ρ is constant) and uniform (so that \vec{V} is constant over the pipe cross-sectional area). In addition

$$\int_{\text{Boundary}} \vec{u}' (\vec{V} \cdot d\vec{A}) = \vec{u} VA$$

where \vec{u} is the value of \vec{u}' at the cg of A (that is, at the point where the pipe centerline intersects the boundary) and A is cross-sectional area of the pipe. The result of the above manipulations is

$$\begin{aligned} \vec{F}_i^s = & \frac{d}{dt} \left(m_i^f \vec{R}_i^s + \int_{cv} \vec{v} \rho dV + \vec{\omega}_i \times \vec{S}_i \right)_s \\ & + \vec{R}_i^s \Delta Q + V \Delta (Q \hat{e}_t^i) + \vec{\omega}_i \times \Delta (Q \vec{u}_i) \end{aligned} \quad (4.15)$$

where m_i^f is the total mass of the fluid in m_i , Δ indicates the change in the quantity from the nominal pipe inlet (inlet with $V > 0$) to the nominal pipe outlet*, and Q is the mass flow rate, i.e.,

$$Q = \rho V A; \quad \dot{Q} = \rho \dot{V} A \quad (4.16)$$

and

$$\vec{S}_i = \int_{cv} \vec{u}' \rho dV \quad (4.17)$$

Next, Equation (4.11) and (4.12) are applied to evaluate the derivative on the right side of Equation (4.7) for the case of the fluid. Similar manipulations to those employed in obtaining Equation (4.15) yield

$$\begin{aligned} \vec{T}_i^s = & \vec{S}_i \times \ddot{\vec{R}}_i^s + \frac{d}{dt} \left(\int_{cv} \vec{u}' \times \vec{v} dm + \int_{cv} \vec{u}' \times (\vec{\omega}_i \times \vec{u}') dm \right)_s \\ & + \oint_{cs} \vec{u}' \times \vec{v} \rho \vec{v} \cdot d\vec{A} + \oint_{cs} \vec{u}' \times (\vec{\omega}_i \times \vec{u}') \rho \vec{v} \cdot d\vec{A} \end{aligned} \quad (4.18)$$

In the following sections, Equations (4.15) and (4.18) will be evaluated for the three possible cases (see Figure 4.2A): a mass containing a through pipe, a mass containing an emptying reservoir, and a mass containing a filling reservoir.

* E.g., $\Delta Q = Q_{out} - Q_{in}$. For the case of a mass containing a reservoir which is nominally emptying Q_{in} would be set to zero since there is no inlet pipe piercing the associated control volume.

4.2.2.1 Through Pipe

Equations (4.15) and (4.18) are evaluated for the case a mass containing a through pipe. The following assumptions are employed:

- The pipe has a constant cross section
- The fluid is incompressible
- \vec{V} is uniform over the pipe cross section

Using the notation illustrated in Figure 4.4, the terms in Equation (4.15) are evaluated as follows:

$$\int_{CV} \vec{V} \rho dV = V \int_{CV} \hat{e}_t \rho A ds = \rho V A \int_{CV} d\vec{u} = Q \Delta \vec{u}_i \quad (4.19)$$

where s is the arc length of the pipe centerline. Since the fluid is incompressible and the pipe is always full, the flow out is equal to the flow in and $\Delta Q = 0$. Using this fact and Equation (4.19), Equation (4.15) yields

$$\begin{aligned} \vec{F}_i^P = \vec{F}_i^f = m_i^f \ddot{\vec{R}}_i^s - \vec{S}_i \times \ddot{\vec{\omega}}_i + \dot{Q} \Delta \vec{u}_i + 2Q \vec{\omega}_i \times \Delta \vec{u}_i \\ + \vec{\omega}_i \times (\vec{\omega}_i \times \vec{S}_i) + VQ \Delta \hat{e}_t^i \end{aligned} \quad (4.20)$$

where \vec{F}_i^f has been renamed \vec{F}_i^P to denote that Equation (4.20) represents \vec{F}_i^f for the case of a through pipe.

\vec{S}_i is a constant vector defined by Equation (4.17) which expresses the first moment of mass of the fluid in the through pipe. It is computed in terms of its components along the \underline{X}^i axes by multiplying the mass of the fluid in the through pipe by the vector from A_i to the cm of this fluid, or, alternatively,

$$\vec{S}_i = \rho \int_s \int_A \vec{u}' dA ds = \rho A \int_s \vec{u} ds^* \quad (4.21)$$

where the fact has been used that the centerline of the pipe is also the locus of the cross-sectional area c.g.; i.e.,

$$\int_A \vec{u}' dA = \vec{u} A \quad (4.22)$$

* This expression involves an approximation if the control surface intersects the end of the pipe obliquely; however, the inaccuracy is very small for the usual case where the inner diameter is small compared with the pipe length.

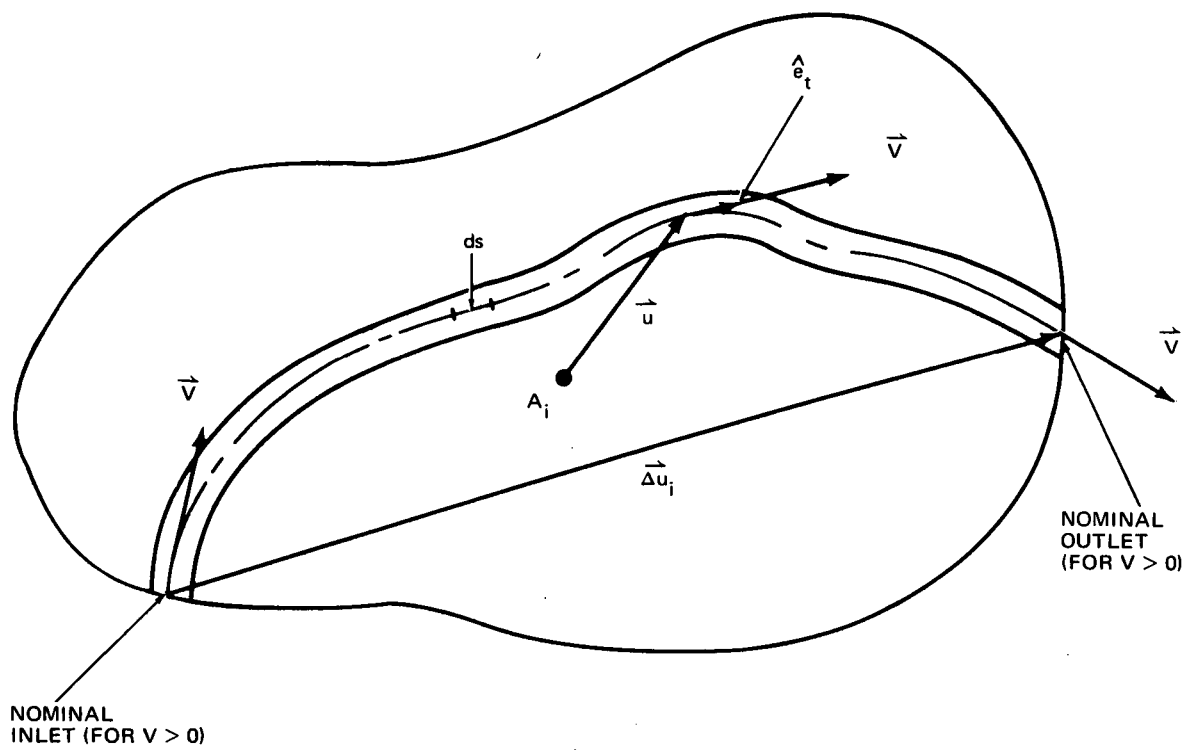


Fig. 4.4 Mass Containing a Through Pipe

Now \vec{u} is expressed in terms of its components along the \tilde{X}^i axes ($\vec{u} = X_1^i \hat{e}_1^i + X_2^i \hat{e}_2^i + X_3^i \hat{e}_3^i$), so that Equation (4.17) yields

$$\vec{S}_i = S_1^i \hat{e}_1^i + S_2^i \hat{e}_2^i + S_3^i \hat{e}_3^i \quad (4.23)$$

where

$$S_j^i \equiv \rho A \int_{\text{pipe } i} X_j^i ds = \int_{\text{pipe } i} X_j^i dm \quad (4.24)$$

Next the terms in the torque equation, Equation (4.18), are evaluated. Using Equation (4.22),

$$\begin{aligned} \int_{CV} \vec{u}' \times \vec{V} dm &= \int_{CV} \vec{u}' \times \vec{V} \rho dV = \rho V \int_s \int_A \vec{u}' \times \hat{e}_t dA ds \\ &= \rho V \int_s \left(\int_A \vec{u}' dA \right) \times \hat{e}_t ds = \rho V A \int_{\text{nominal inlet}}^{\text{nominal outlet}} \vec{u} \times d\vec{u} \end{aligned}$$

or, using Equation (4.16)

$$\int_{CV} \vec{u}' \times \vec{V} dm = Q \int_{\text{nominal inlet}}^{\text{nominal outlet}} \vec{u} \times d\vec{u} = Q \vec{G}_i \quad (4.25)$$

where

$$\vec{G}_i \equiv \int_{\text{nominal inlet}}^{\text{nominal outlet}} \vec{u} \times d\vec{u} \quad (4.26)$$

\vec{G}_i is a constant which is a characteristic of the fluid in the through pipe. It can be evaluated either by expanding \vec{u} into components or by noting, from Figure 4.5, that \vec{G}_i is the following function of the area A_p swept out by \vec{u} :

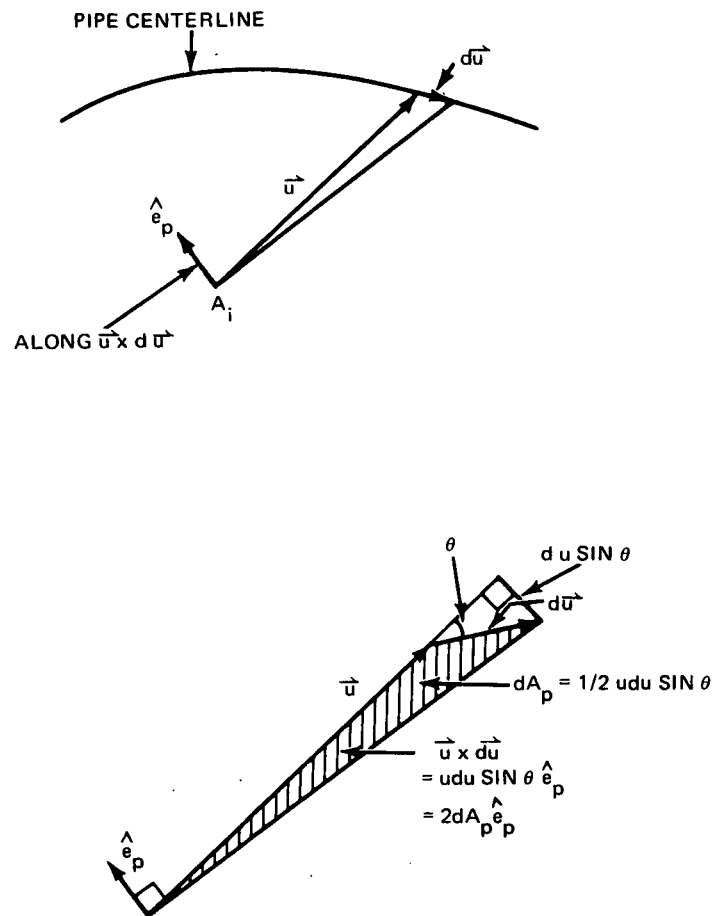


Fig. 4.5 Expression Required for the Evaluation of \vec{G}_i

$$\vec{G}_i = 2 \int_{\substack{\text{nominal} \\ \text{outlet}}}^{\substack{\text{nominal} \\ \text{inlet}}} \hat{e}_p dA_p \quad (4.27)$$

where \hat{e}_p is the unit normal vector which is perpendicular to the plane of \vec{u} and $d\vec{u}$ and directed along $\vec{u} \times d\vec{u}$. When the surface swept out by \vec{u} is a plane, \hat{e}_p is constant and the evaluation of Equation (4.27) is particularly simple.

The next integral to be evaluated in Equation (4.18) is

$$\int_{cv} \vec{u}' \times (\vec{\omega}_i \times \vec{u}') dm = \vec{I}_i^* \cdot \vec{\omega}_i \quad (4.28)$$

where \vec{I}_i^* is the moment of inertia dyadic of the fluid about point A_i .

The next integrals needed are

$$\begin{aligned} \oint_{cs} \vec{u}' \times \vec{V} \rho \vec{V} \cdot d\vec{A} &= \rho V \int_{\substack{cs \\ out}} \vec{u}' \times \hat{e}_t dA - \rho V \int_{cs} \vec{u}' \times \hat{e}_t dA \\ &= \rho V \Delta (\vec{u} \times \hat{e}_t) = Q V \Delta (\vec{u}_i \times \hat{e}_t^i) \end{aligned} \quad (4.29)$$

and

$$\oint_{cs} \vec{u}' \times (\vec{\omega}_i \times \vec{u}') \rho \vec{V} \cdot d\vec{A} = \Delta \left[\rho V \int_{cs} \vec{u}' \times (\vec{\omega}_i \times \vec{u}') dA_n \right]$$

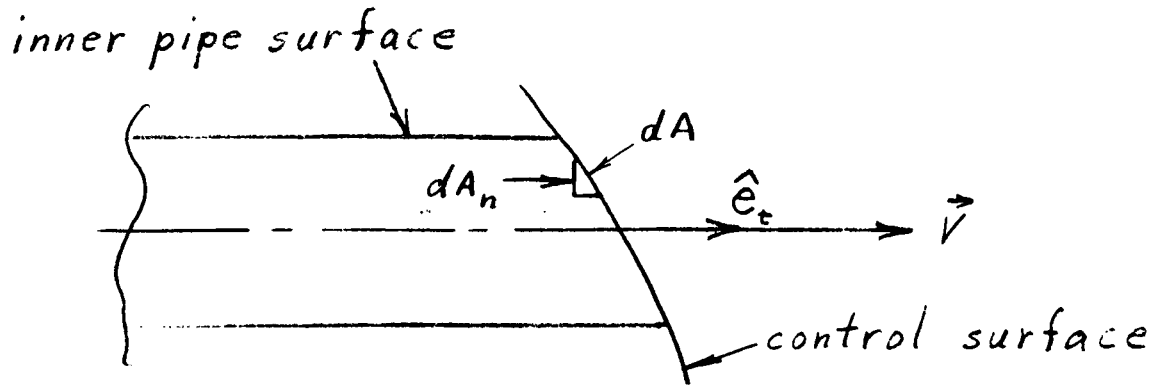
where $dA_n = \hat{e}_t \cdot d\vec{A}$. The above equation is expressed as follows:

$$\oint_{cs} \vec{u}' \times (\vec{\omega}_i \times \vec{u}') \rho \vec{V} \cdot d\vec{A} = \rho V (\Delta \vec{J}_i^*) \cdot \vec{\omega}_i \quad (4.30)$$

where

$$\vec{J}_i^* = \int_{cs} (\vec{u}'^2 \vec{E} - \vec{u}' \vec{u}') dA_n \quad (4.31)$$

In Equation (4.31), \vec{E} is the unit dyadic. \vec{J}_i^* is the moment of inertia dyadic of the control surface area component which is projected perpendicular to \vec{V} as indicated in the sketch below.



Equations (4.25), (4.28), (4.29) and (4.30) are now substituted into the torque relation, Equation (4.18), and the indicated differentiation is performed. The result is:

$$\begin{aligned} \vec{T}_i^P = \vec{T}_i^f = \vec{S}_i \times \ddot{\vec{R}}_i^s + \vec{I}_i^f \cdot \ddot{\vec{\omega}}_i + \vec{\omega}_i \times (Q \vec{G}_i + \vec{I}_i^f \cdot \vec{\omega}_i) \\ + \rho V (\Delta \vec{J}_i) \cdot \vec{\omega}_i + \dot{Q} \vec{G}_i + Q V \Delta (\vec{u}_i \times \hat{e}_t^i) \end{aligned} \quad (4.32)$$

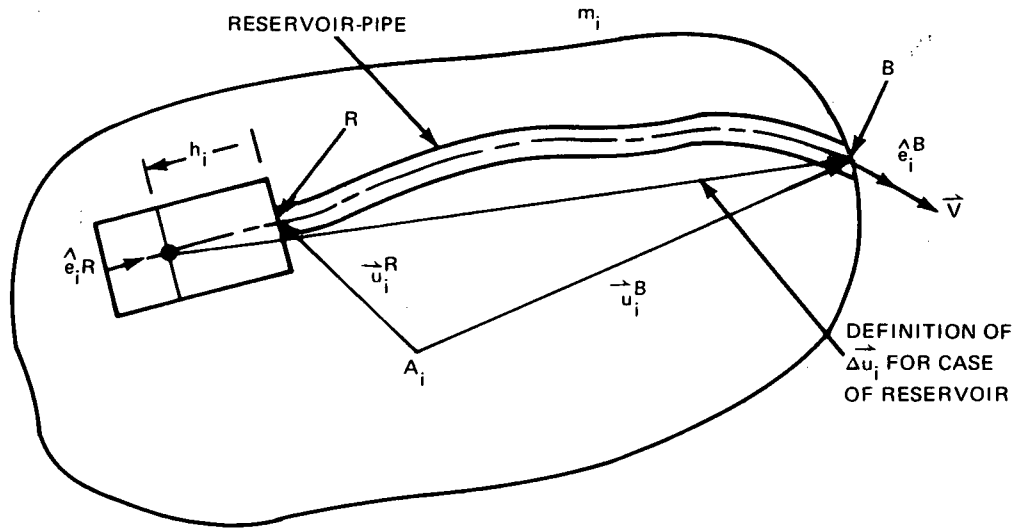
where \vec{T}_i^P denotes the value of \vec{T}_i^f for the case of a through pipe.

4.2.2.2 Reservoir Nominally Emptying (For $V > 0$)

The derivations of this section will be done for the reservoir which is nominally emptying (for $V > 0$). The results for the reservoir which is nominally filling will be obtained from the final expressions by replacing V with $-V$. The reservoir (shown nominally emptying) is illustrated in Figure 4.6. It is assumed to be cylindrical with radius b_i and to have a bladder or piston which confines the fluid so that the fluid height h_i is a well-defined quantity.

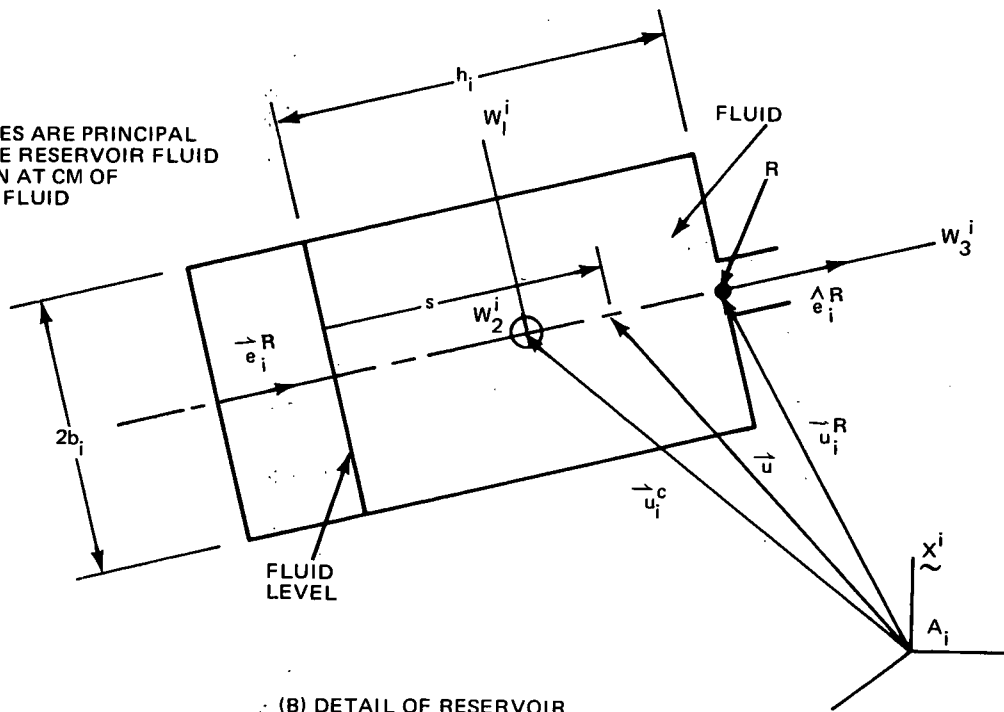
The terms required for Equation (4.15) are now evaluated. Proceeding as in Equation (4.19)

$$\int_{CV} \vec{V} \rho dV = Q \Delta \vec{u}_i \quad (4.33)$$



(A) RESERVOIR WITH ASSOCIATED PIPE SECTION

NOTE: W AXES ARE PRINCIPAL AXES OF THE RESERVOIR FLUID WITH ORIGIN AT CM OF RESERVOIR FLUID



(B) DETAIL OF RESERVOIR

Fig. 4.6 Structural Mass Containing a Reservoir

where $\Delta \vec{u}_i$ is the time-varying vector illustrated in Figure 4.6A for the case of the reservoir. To compute $\Delta \vec{u}_i$, the flow rate in the reservoir is equated to the flow rate in the pipe; thus

$$Q = \rho V A = \rho V_i^R A_i^R$$

where V_i^R and A_i^R are the reservoir-fluid's velocity and the reservoir cross-sectional area, respectively. From the above expression

$$V_i^R = - \frac{dh_i}{dt} = V \frac{A}{A_i^R} \quad (4.34)$$

Integrating,

$$h_i = h_{i_0} - \frac{A}{A_i^R} \int_0^t V dt \quad (4.35)$$

where h_{i_0} is the initial fluid height. The velocity of the fluid in the pipe, V , is a function of time which is specified by the user in a subroutine. If either reservoir empties, it is assumed that the pump shuts off; thus, the subroutine providing V is disregarded, and V is set to zero. For this reason the case of a partially empty pipe is not considered. From the geometry of Figure 4.6,

$$\Delta \vec{u}_i = \vec{u}_i^B - \vec{u}_i^R + h_i \hat{e}_i^R \quad (4.36)$$

$\Delta \vec{u}_i$ is now expressed in terms of input data, $(\vec{u}_i^B, \vec{u}_i^R, \text{ and } \hat{e}_i^R)$ and the quantity h_i which the computer evaluates by using Equation (4.35). \vec{S}_i is written in terms of the constant portion \vec{S}_i^P for the fluid in the pipe section shown in Figure 4.6, and the variable portion \vec{S}_i^R for the reservoir as follows:

$$\vec{S}_i = \vec{S}_i^P + \vec{S}_i^R \quad (4.37)$$

\vec{S}_i^P is evaluated in accordance with Equations (4.23) and (4.24) for the fluid in the pipe section, and, proceeding as in Equation (4.21),

$$\vec{S}_i^R = A_i^R \rho \int_0^{h_i} \vec{u} ds$$

From Figure 4.6B, $\vec{u} = \vec{u}_i^R - (h_i - s) \vec{e}_i^R$. This quantity is substituted into the above equation; and the integration is carried out. The result is

$$\vec{S}_i = \vec{S}_i^P + m_i^R (\vec{u}_i^R - \frac{1}{2} h_i \vec{e}_i^R) \quad (4.38)$$

where m_i^R is the mass of the fluid in the reservoir; i.e.,

$$m_i^R = A_i^R \rho h_i \quad (4.39)$$

For future reference, it is noted that the total fluid mass on m_i is

$$m_i^f = m_i^P + m_i^R \quad (4.40)$$

where m_i^P is the mass of fluid in the pipe. Equation (4.33) is now substituted into Equation (4.15), and the differentiation is carried out. The result is

$$\begin{aligned} \vec{F}_i^R = \vec{F}_i^f = & m_i^f \ddot{\vec{R}}_i + \dot{m}_i^f \dot{\vec{R}}_i + \dot{Q} \Delta \vec{u}_i + Q \Delta \dot{\vec{u}}_i \\ & + Q \vec{\omega}_i \times \Delta \vec{u}_i + \dot{\vec{\omega}}_i \times \vec{S}_i + \vec{\omega}_i \times \dot{\vec{S}}_i + \vec{\omega}_i \times (\vec{\omega}_i \times \vec{S}_i) \\ & + Q \ddot{\vec{R}}_i + Q V \dot{\vec{e}}_i^R + Q \vec{\omega}_i \times \vec{u}_i^R \end{aligned}$$

where \vec{F}_i^R has been used to denote \vec{F}_i^f for the case of a reservoir. Some of the terms appearing in the above equation are evaluated as follows:

$$\dot{m}_i^f = -Q \quad (4.41)$$

Using Equations (4.36) and (4.34),

$$\Delta \vec{u}_i^o = -V \frac{A}{A_i^R} \hat{e}_i^R \quad (4.42)$$

Equations (4.38), (4.39), (4.34) and (4.16) yield,

$$\vec{S}_i^o = -Q(\vec{u}_i^R - h_i \hat{e}_i^R) \quad (4.43)$$

Equations (4.41) to (4.43) and (4.36) are substituted into the above relation for \vec{F}_i^R and the result is

$$\begin{aligned} \vec{F}_i^R = \vec{F}_i^f = m_i^f \ddot{\vec{R}}_i^s - \vec{S}_i^o \times \vec{\omega}_i^o + Q \Delta \vec{u}_i^o \\ + QV(\hat{e}_i^s - \frac{A}{A_i^R} \hat{e}_i^R) + 2Q\vec{\omega}_i^o \times \Delta \vec{u}_i^o \\ + \vec{\omega}_i^o \times (\vec{\omega}_i^o \times \vec{S}_i^o) \end{aligned} \quad (4.44)$$

where the terms required in Equation (4.44) are computed using Equations (4.36), (4.35), (4.38), (4.39) and (4.40).

Next, the terms in the torque equation, Equation (4.18) will be developed for the reservoir which is nominally emptying. By proceeding in the manner used to obtain Equation (4.25), we obtain

$$\int_{cv} \vec{u}' \times \vec{V} dm = Q \vec{G}_i \quad (4.45)$$

where (with R representing the reservoir and P the pipe section shown in Figure 4.6)

$$\vec{G}_i = \vec{G}_i^R + \vec{G}_i^P \quad (4.46)$$

with

$$\vec{G}_i^R \equiv \int_R \vec{u} \times d\vec{u}, \quad \vec{G}_i^P \equiv \int_P \vec{u} \times d\vec{u} \quad (4.47)$$

\vec{G}_i^P is a constant characteristic of the reservoir pipe which may be computed by applying Equation (4.27) for the pipe section and then supplied as input data; however \vec{G}_i^R is a variable requiring further evaluation. Expressing \vec{u} in accordance with Figure 4.6B, Equation (4.47) yields

$$\vec{G}_i^R = \int_R [\vec{u}_i^R - (h_i - s) \hat{e}_i^R] \times \hat{e}_i^R ds = \int_R \vec{u}_i^R \times \hat{e}_i^R ds$$

or

$$\vec{G}_i^R = \vec{u}_i^R \times \hat{e}_i^R h_i \quad (4.48)$$

The next term is

$$\int_{c_v} \vec{u}' \times (\vec{\omega}_i \times \vec{u}') dm = \vec{I}_i^f \cdot \vec{\omega}_i \quad (4.49)$$

where

$$\vec{I}_i^f \equiv \vec{I}_i^R + \vec{I}_i^P \quad (4.50)$$

The fluid moment of inertia dyadic \vec{I}_i^P is input data; however the value for the reservoir \vec{I}_i^R is a variable which requires further evaluation. This is more conveniently done using matrix forms and therefore will be done later in Section 4.3.1. The next integrals required are

$$\oint_{cs} \vec{u}' \times \vec{r} \rho \vec{r} \cdot d\vec{A} = \rho V \int_{out} \vec{u}' \times \hat{e}_t dA = \rho V \vec{u}_i^B \times \hat{e}_i^B \quad (4.51)$$

and

$$\oint_{cs} \vec{u}' \times (\vec{\omega}_i \times \vec{u}') \rho \vec{r} \cdot d\vec{A} = \rho V \vec{J}_i^B \cdot \vec{\omega}_i \quad (4.52)$$

where \vec{J}_i^B is the value of \vec{J}_i given by Equation (4.31) at the pipe outlet (point B of Figure 4.6A). Substitution of Equations (4.45), (4.49), (4.51), and (4.52) into Equation (4.18) and carrying out the differentiation yields

$$\begin{aligned}\vec{T}_i^R = \vec{T}_i^f = \vec{S}_i \times \ddot{\vec{R}}_i^s + \dot{Q} \vec{G}_i + Q \vec{G}_i^o + \vec{I}_i^f \cdot \vec{\omega}_i + \vec{I}_i^f \cdot \vec{\omega}_i^o \\ + \vec{\omega}_i \times (Q \vec{G}_i + \vec{I}_i^f \cdot \vec{\omega}_i) + QV \vec{u}_i^B \times \hat{e}_i^B + \rho V \vec{J}_i^B \cdot \vec{\omega}_i\end{aligned}$$

Equations (4.46), (4.48) and (4.34) yield

$$\vec{G}_i^R = -V \frac{A}{A_i^R} \vec{u}_i^R \times \hat{e}_i^R$$

Therefore

$$\begin{aligned}\vec{T}_i^R = \vec{T}_i^f = \vec{S}_i \times \ddot{\vec{R}}_i^s + \vec{I}_i^f \cdot \vec{\omega}_i + (\vec{I}_i^R + \rho V \vec{J}_i^B) \cdot \vec{\omega}_i \\ + \vec{\omega}_i \times (\vec{I}_i^f \cdot \vec{\omega}_i + Q \vec{G}_i) + \dot{Q} \vec{G}_i \\ + QV (\vec{u}_i^B \times \hat{e}_i^B - \frac{A}{A_i^R} \vec{u}_i^R \times \hat{e}_i^R)\end{aligned}\quad (4.53)$$

As was the case with \vec{I}_i^R , the required expression for \vec{J}_i^R will also be developed in Section 4.3.1.

4.2.2.3 Reservoir Nominally Filling (For $V > 0$)

The required relationships are obtained from the results of the previous section, Equations (4.44) and (4.53) where the subsidiary relations which define required terms are Equations (4.35), (4.36), (4.38), (4.39), (4.40), (4.46), (4.47), (4.48) and (4.50). To obtain the results for the reservoir which is nominally filling, V , Q , and \dot{Q} are replaced by $-V$, $-Q$, and $-\dot{Q}$, respectively, wherever they appear in these equations. When the equations are converted to matrix form, in Section 4.3.1, this is accomplished by placing a parameter k_i in front of V , Q and \dot{Q} in the reservoir equations and setting $k_i = +1$ for the case where the reservoir is nominally emptying and $k_i = -1$ for the case where the reservoir is nominally filling.

4.2.3 Moving Point Mass on Laboratory

Moving point masses on the Laboratory may be used to represent crew motion, elevators, balance masses, etc. The motion of a typical mass μ_j is composed of a pre-specified function of time $\vec{U}_j(t)$ relative to the Laboratory and a component \vec{v}_j due to elastic deflection (see Figure 4.7). The vector to μ_j from the cm A_k of the k^{th} Laboratory structural mass m_k is \vec{d}_k^j when the laboratory is undeformed and \vec{D}_k^j when the deformations are considered. From the geometry of Figure 4.7,

$$\vec{R}^{\mu_j} = \vec{R} + \vec{W}_j \quad (4.54)$$

$$\dot{\vec{R}}^{\mu_j} = \dot{\vec{R}} + \dot{\vec{W}}_j + \vec{\omega} \times \vec{W}_j \quad (4.55)$$

$$\ddot{\vec{R}}^{\mu_j} = \ddot{\vec{R}} + \ddot{\vec{W}}_j + 2\vec{\omega} \times \dot{\vec{W}}_j + \vec{\omega} \times (\vec{\omega} \times \vec{W}_j) + \dot{\vec{\omega}} \times \vec{W}_j \quad (4.56)$$

where

$$\vec{W}_j = \vec{U}_j(t) + \vec{v}_j \quad (4.57)$$

$$\dot{\vec{W}}_j = \dot{\vec{U}}_j(t) + \dot{\vec{v}}_j \quad (4.58)$$

$$\ddot{\vec{W}}_j = \ddot{\vec{U}}_j(t) + \ddot{\vec{v}}_j \quad (4.59)$$

$$\vec{d}_k^j = \vec{U}_j(t) - \vec{r}_k \quad (4.60)$$

Since \vec{r}_k is constant in the \tilde{X} coordinate system,

$$\dot{\vec{d}}_k^j = \dot{\vec{U}}_j(t) \quad (4.61)$$

$$\ddot{\vec{d}}_k^j = \ddot{\vec{U}}_j(t) \quad (4.62)$$

In order to rigorously express the structural loads on each μ_j , it would be necessary to derive stiffness and damping matrices that are

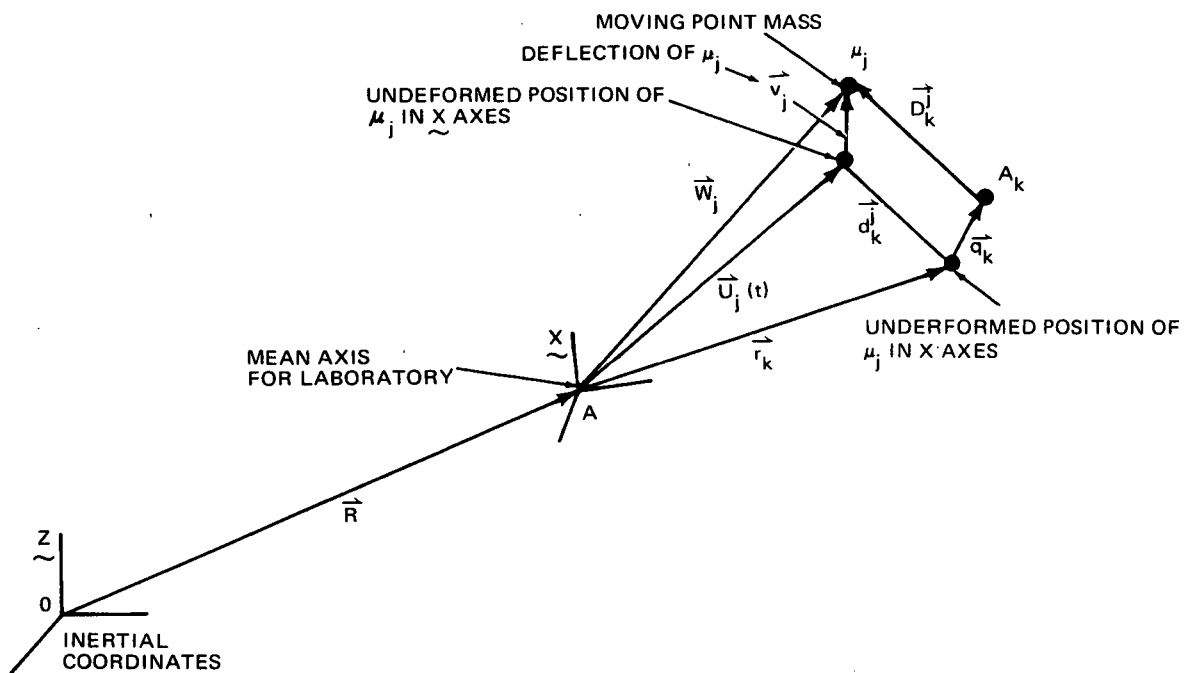


Fig. 4.7 Position of Moving Point Mass on Laboratory

functions of the variable positions of each μ_j . In addition, as a moving mass approaches a structural mass, certain coefficients in these matrices would approach infinity. For example, if the deflection of each m_k were held at zero, the load applied to μ_j that is needed to produce a unit deflection of μ_j would approach infinity as μ_j approached any m_i . This load is a diagonal term in the stiffness matrix. For these reasons, the following simplifications are introduced in the determination of the elastic motion of the moving masses. First, the elastic deflection \vec{v}_j and its derivatives $\dot{\vec{v}}_j$ and $\ddot{\vec{v}}_j$ are computed as if μ_j were moving on a rigid structural mass m_k which is near μ_j . Different values of \vec{v}_j , $\dot{\vec{v}}_j$, and $\ddot{\vec{v}}_j$ can be obtained depending on which neighboring structural mass m_k is used, and the values used in this analysis will be a weighted average of the respective \vec{v}_j 's, $\dot{\vec{v}}_j$'s, and $\ddot{\vec{v}}_j$'s obtained above. Then, using these average values, the dynamic terms, the contribution to the right sides of Equations (4.5) and (4.7), are computed and added to the dynamic terms for the nearest structural mass. In this way the inertia forces applied by the moving masses to the structure are approximately accounted for.

To obtain the required averages, first assume that μ_j moves along a single rigid mass m_k (or its imaginary extension). Since m_k is rigid, referring to Figure 4.7, within linear terms $\vec{D}_k^j = \vec{d}_k^j + \vec{\theta}_k \times \vec{d}_k^j$, where $\vec{\theta}_k$ is the angular deflection of m_k relative to the \underline{X} axes. Then, from the geometry of Figure 4.7,

$$\vec{v}_j = \vec{q}_k + \vec{\theta}_k \times \vec{d}_k^j$$

Differentiating and substituting Equations (4.61) and (4.62) yields

$$\dot{\vec{v}}_j = \dot{\vec{q}}_k + \dot{\vec{\theta}}_k \times \vec{d}_k^j + \vec{\theta}_k \times \dot{\vec{U}}_j$$

and

$$\ddot{\vec{v}}_j = \ddot{\vec{q}}_k + \ddot{\vec{\theta}}_k \times \vec{d}_k^j + 2\dot{\vec{\theta}}_k \times \dot{\vec{U}}_j + \vec{\theta}_k \times \ddot{\vec{U}}_j$$

Next, instead of assuming that μ_j moves along a single mass, it is desired to include the influence of many of the surrounding structural masses. Weighting functions λ_k^j (which will later be defined precisely) are introduced for this purpose. It is assumed that \vec{v}_j , $\dot{\vec{v}}_j$, and $\ddot{\vec{v}}_j$ are given by the following weighted sum of the above values which were obtained by considering only a single mass:

$$\left. \begin{aligned} \vec{v}_j &= \sum_{m_k} \mu_j \lambda_k^j (\vec{q}_k + \vec{\theta}_k \times \vec{d}_k^j) \\ \dot{\vec{v}}_j &= \sum_{m_k} \mu_j \lambda_k^j (\dot{\vec{q}}_k + \dot{\vec{\theta}}_k \times \vec{d}_k^j + \vec{\theta}_k \times \dot{\vec{v}}_j) \\ \ddot{\vec{v}}_j &= \sum_{m_k} \mu_j \lambda_k^j (\ddot{\vec{q}}_k + \ddot{\vec{\theta}}_k \times \vec{d}_k^j + 2 \dot{\vec{\theta}}_k \times \dot{\vec{v}}_j + \vec{\theta}_k \times \ddot{\vec{v}}_j) \end{aligned} \right\} \quad (4.63)$$

where $\sum_{m_k}^{\mu_j}$ denotes the sum over all structural masses m_k that influence

the motion of μ_j . In practice, these m_k 's are selected by the program user. As time progresses, and μ_j moves into different regions, the user may specify different set of m_k 's.

A formula for the λ_k^j 's will now be specified such that the λ_k^j 's obey the following properties:

$$(a) \quad \lambda_k^j > 0$$

$$(b) \quad \sum_{m_k}^{\mu_j} \lambda_k^j = 1$$

$$(c) \quad \lambda_k^j \rightarrow 0 \quad \text{whenever any } d_\ell^j \rightarrow 0 \quad (\ell \neq k) \quad \text{where } d_\ell^j = |d_\ell^j|$$

$$(d) \quad \frac{\partial \lambda_k^j}{\partial U_{jr}} \rightarrow 0 \quad \text{whenever any } d_\ell^j \rightarrow 0 \quad \text{for all } j, k, \text{ and } \ell \text{ and any } X\text{-axis component } U_{jr} \text{ of } \vec{U}_j \quad (\vec{U}_j = U_{j1} \hat{e}_1 + U_{j2} \hat{e}_2 + U_{j3} \hat{e}_3)$$

Properties (a) and (b) were selected so that the total motion \vec{v}_j given by Equation (4.63) is the sum of the percentages of the rigid-body motion of all the m_k 's; i.e., property (a) states that each percentage must be positive, and property (b) states that the total of all of the percentages is 100%.

Property (c) guarantees that \vec{v}_j , $\dot{\vec{v}}_j$, and $\ddot{\vec{v}}_j$ approach the rigid-body values associated with m_k whenever μ_j approaches any m_k . This follows from the fact that in addition to $\lambda_k^j \rightarrow 0$ ($k \neq \ell$), by property (b) $\lambda_\ell^j \rightarrow 1$. Since the λ_k^j 's which will be selected are continuous well-behaved functions of \vec{U}_j , the closer μ_j is to any m_k , the more influence m_k will have on the motion of μ_j .

Property (d) assures the following: If the deformations \vec{q}_k and $\vec{\theta}_k$ of all m_k 's were held fixed, and μ_j were moved towards the cm A_k of an m_k , then, in addition to the deflection, the tangent of the path of μ_j , as defined by Equation (4.63), should approximate the tangent of the true path under the prescribed structural deformations. This requires that as μ_j moves toward the cm of a particular m_k , say m_ℓ , the contributions to the differential vector tangent to the approximate and exact paths must approach each other; i.e.,

$$\frac{\partial \vec{v}_j}{\partial U_{jr}} (\vec{U}_j + \vec{v}_j) dU_{jr} \rightarrow \frac{\partial}{\partial U_{jr}} (\vec{U}_{jr} + \vec{q}_\ell + \vec{\theta}_\ell \times \vec{d}_\ell^j) dU_{jr} \quad \text{as } d_\ell^j \rightarrow 0 \quad (r = 1, 2, 3)$$

where $\vec{U}_{jr} + \vec{q}_\ell + \vec{\theta}_\ell \times \vec{d}_\ell^j$ is the path of μ_j as if μ_j moved on the rigid body m_ℓ . This relation will be true if

$$\frac{\partial \vec{v}_j}{\partial U_{jr}} \rightarrow \frac{\partial}{\partial U_{jr}} (\vec{q}_\ell + \vec{\theta}_\ell \times \vec{d}_\ell^j) \quad \text{as } d_\ell^j \rightarrow 0 \quad (r = 1, 2, 3)$$

Property (d) guarantees the above relation, since Equation (4.63) yields

$$\frac{\partial \vec{v}_j}{\partial U_{jr}} = \sum_{m_k} \mu_j \lambda_k^j \frac{\partial (\vec{q}_k + \vec{\theta}_k \times \vec{d}_k^j)}{\partial U_{jr}} + \sum_{m_k} \mu_j \frac{\partial \lambda_k^j}{\partial U_{jr}} (\vec{q}_k + \vec{\theta}_k \times \vec{d}_k^j) \quad (r = 1, 2, 3)$$

and when $d_\ell^j \rightarrow 0$, $\lambda_\ell^j \rightarrow 1$, $\lambda_k^j \rightarrow 0$ for $k \neq \ell$, and $\partial \lambda_k^j / \partial U_{jr} \rightarrow 0$ for all k ; thus, $\partial \vec{v}_j / \partial U_{jr}$ approaches the rigid-body value as required.

Functions for λ_k^j which have the desired properties (a-d) are now constructed as follows. First we form

$$\prod_k^j = \prod_{\substack{m_\ell \\ \ell \neq k}} \mu_j (d_\ell^j)^2 \quad (4.64)$$

where the Π on the right denotes the product of the $(d_\ell^j)^2$ for all masses m_ℓ that influence the motion of μ_j ; however $(d_k^j)^2$ is excluded from this product. π_k^j already has properties (a) and (c). In order to guarantee property (b), we define λ_k^j such that

$$\lambda_k^j \equiv \frac{\pi_k^j}{\sum_{m_i} \mu_i \pi_i^j} \quad \text{for more than one } m_k; \quad \lambda_k^j \equiv 1 \quad \text{for one } m_i. \quad (4.65)$$

Property (d) can be verified by differentiation. The reason for squaring (d_ℓ^j) 's in Equation (4.64) was to arrive at λ_k^j 's that would satisfy Property (d). Using only the first power of the d_i^j 's would however satisfy Properties (a-c).

One inconsistency in the approximations used in Equation (4.63) is that since the λ_k^j 's are variables, $\dot{\vec{v}}_j$ and $\ddot{\vec{v}}_j$ cannot be obtained exactly by differentiating \vec{v}_j and $\dot{\vec{v}}_j$, respectively. However, because of property (d), the differentiated and defined values do approach each other whenever μ_j approaches any m_k .

The rate of change of linear momentum of μ_j may now be computed as

$$\vec{F}_{k*}^{\mu_j} = \mu_j \cdot \ddot{\vec{R}}^{\mu_j} \quad (4.66)$$

where $\ddot{\vec{R}}^{\mu_j}$ is given by Equation (4.56) with \vec{W}_j and its derivatives given by Equations (4.57) to (4.59), using Equations (4.63) to (4.65). The subscript k^* has the following meaning. In the matrix computation scheme described in Section 4.3.2, $\vec{F}_{k*}^{\mu_j}$ is determined for each μ_j , and the result contributes to the dynamic terms (Equation (4.5)) for the nearest influencing m_i . It is this value of i that is denoted by k^* . For simplicity, the nearest influencing m_i (m_{k*}) is actually determined for the underformed vehicle; i.e., the m_i with the smallest d_i^j (or equivalently the largest π_i^j) is considered to be nearest. In this process of adding $\vec{F}_{k*}^{\mu_j}$ into Equation (4.5), more than one μ_j may contribute towards a particular \vec{F}_i , and the total of these contributions is the \vec{F}_i^μ of Equation (4.6).

Referring to Figure 4.7, the contribution of μ_j to the dynamic terms on the right side of the torque equation, Equation (4.7), is

$$\vec{T}_{k*}^{\mu_j} = \mu_j \cdot \vec{D}_{k*}^j \times \ddot{\vec{R}}^{\mu_j} \quad (4.67)$$

where

$$\vec{D}_{k*}^{\mu_j} = \vec{W}_j - \vec{r}_{k*} - \vec{g}_{k*} \quad (4.68)$$

and \vec{R}^{μ_j} is determined by using the same equations as were used for obtaining Equation (4.66). As was the case for \vec{F}_i^{μ} , more than one μ_j may contribute towards \vec{T}_i , and the total of these contributions is the \vec{T}_i^{μ} of Equation (4.8).

4.2.4 Structural Mass on Counterweight

For the counterweight, Newton's equation and Euler's equation are written for each mass point in a straightforward manner. Taking the a^{th} counterweight mass point as typical,

$$\vec{F}_a = \bar{m}_a \ddot{\vec{R}}_a^s \quad (4.69)$$

where \vec{R}_a is the vector from point O to point B_a in Figure 4.1. The Euler equation is

$$\vec{T}_a = \vec{I}_a \cdot \overset{\circ}{\vec{\omega}}_a + \vec{\omega}_a \times \vec{I}_a \cdot \vec{\omega}_a \quad (4.70)$$

where the circle indicates that the derivative is measured in the \tilde{Y}^a coordinate system. From the geometry of Figure 4.1,

$$\vec{R}_a = \vec{R} + \vec{\bar{R}} + \vec{r}_a + \vec{q}_a \quad (4.71)$$

Expressions for the derivatives of \vec{R}_a , for use in Equation (4.69), are expressed in the proper coordinate system, and the results have been incorporated into the relations of Appendix C where the equations are presented in matrix form.

4.2.5 Subsidiary Relations

The program will, on command, print the angular momentum vector about point 0 (the origin of the inertial reference axes Z), the total-system kinetic energy, and the location of the total-system center of mass. These quantities are developed below.

4.2.5.1 Angular Momentum About Point 0

Referring to Figure 4.3, the angular momentum associated with a typical mass m_i on the Laboratory is

$$\vec{L}_i = \int_{cv} (\vec{R}_i + \vec{u}') \times (\dot{\vec{R}}_i^s + \dot{\vec{u}}'^s) dm \quad (4.72)$$

or

$$\vec{L}_i = \vec{L}_i^m + \vec{L}_i^f + \vec{L}_i^\mu \quad (4.73)$$

where the superscripts m, f, and μ denote the contributions to the right side of Equation (4.72) of the structural mass m_i , the fluid on m_i , and the moving point masses associated with m_i , respectively.

For a rigid mass point on the Laboratory, Equation (4.72) provides the classical result:

$$\vec{L}_i^m = \vec{I}_i \cdot \vec{\omega}_i + m_i \vec{R}_i \times \dot{\vec{R}}_i^s \quad (4.74)$$

For the fluid on m_i , Equation (4.14) is substituted into Equation (4.72) and the indicated multiplication is carried out. After substituting Equation (4.17), the result is

$$\begin{aligned} \vec{L}_i^f = & m_i^f \vec{R}_i \times \dot{\vec{R}}_i^s + \vec{R}_i \times \int_{cv} \vec{V} dm + \vec{R}_i \times (\vec{\omega}_i \times \vec{S}_i) \\ & + \vec{S}_i \times \dot{\vec{R}}_i^s + \int_{cv} \vec{u}' \times \vec{V} dm + \int_{cv} \vec{u}' \times (\vec{\omega}_i \times \vec{u}') dm \end{aligned} \quad (4.75)$$

For the case of a through pipe, Equations (4.19), (4.25), and (4.28) are substituted into Equation (4.75) and the result is

$$\begin{aligned} \vec{L}_i^f = & m_i^f \vec{R}_i \times \dot{\vec{R}}_i^s + k_i Q \vec{R}_i \times \Delta \vec{u}_i + \vec{R}_i \times (\vec{\omega}_i \times \vec{S}_i) \\ & + \vec{S}_i \times \dot{\vec{R}}_i^s + k_i Q \vec{G}_i + \vec{I}_i^f \cdot \vec{\omega}_i \end{aligned} \quad (4.76)$$

where $k_i = +1$ and the parameters in the above relation are given by the equations of Section 4.2.2.1.

For the case of a reservoir which is nominally emptying Equations (4.33), (4.45), and (4.49) are substituted into Equation (4.75). Again, Equation (4.76) with $k_i = +1$ is obtained; however for this case the parameters m_i^f , $\vec{\Delta u}_i$, \vec{S}_i , \vec{G}_i , and \vec{I}_i^f are defined by the relations of Section 4.2.2.2.

For the case of a reservoir which is nominally filling, Equation (4.76) is once again obtained except that k_i must now be set to -1. The equations for the parameters are identical to those for the emptying reservoir given in Section 4.2.2.2.

For a moving point mass μ_j , the angular momentum about point 0 is

$$\vec{L}^{\mu_j} = \mu_j \vec{R}^{\mu_j} \times \dot{\vec{R}}^{\mu_j} \quad (4.77)$$

where \vec{R}^{μ_j} and $\dot{\vec{R}}^{\mu_j}$ are computed using the relations of Section 4.2.3.

For a structural mass \bar{m}_a on the Counterweight, the angular momentum about point 0 is

$$\vec{L}_a = \vec{I}_a \cdot \vec{\omega}_a + \bar{m}_a \vec{R}_a \times \dot{\vec{R}}_a \quad (4.78)$$

In the program, the contributions of each structural mass on the Laboratory and the Counterweight, of all fluid, and all moving point masses are totaled to arrive at the system angular momentum \vec{L} about point 0. In practice, it is never necessary to compute \vec{L}_i^u since the \vec{L}^{μ_j} 's are totaled separately.

4.2.5.2 Kinetic Energy

The kinetic energy of a structural mass on the Laboratory is

$$K_i^m = \frac{1}{2} \vec{\omega}_i \cdot \vec{I}_i \cdot \vec{\omega}_i + \frac{1}{2} m_i \dot{\vec{R}}_i^2 \quad (4.79)$$

Referring to Figure 4.3, the kinetic energy of the fluid present on m_i is

$$K_i^f = \frac{1}{2} \int_{CV} (\dot{\vec{R}}_i + \vec{u}')^2 dm$$

where the second power is used to indicate the dot product of the vector

with itself. Substitution of Equation (4.14) and subsequent use of Equation (4.17) yields

$$K_i^f = \frac{1}{2} m_i^f \dot{\vec{R}}_i^2 + \dot{\vec{R}}_i \cdot \left(\int_{CV} \vec{V} dm + \vec{\omega}_i \times \vec{S}_i \right) + \frac{1}{2} \int_{CV} V^2 dm \\ + \frac{1}{2} \vec{\omega}_i \cdot \int_{CV} \vec{u}' \times (\vec{\omega}_i \times \vec{u}') dm + \vec{\omega}_i \cdot \int_{CV} \vec{u}' \times \vec{V} dm \quad (4.80)$$

For the case of the through pipe, Equations (4.19), (4.25), and (4.28) are substituted into Equation (4.80), and the result is

$$K_i^p = K_i^f = \frac{1}{2} m_i^f (\dot{\vec{R}}_i^2 + V^2) + \frac{1}{2} \vec{\omega}_i \cdot \vec{I}_i^f \cdot \vec{\omega}_i \\ + Q \vec{\omega}_i \cdot \vec{G}_i + \dot{\vec{R}}_i \cdot (\vec{\omega}_i \times \vec{S}_i + Q \Delta \vec{u}_i) \quad (4.81a)$$

where the parameters of the above relation are given by the equations of Section 4.2.2.1.

For the case of a reservoir which is nominally emptying, Equations (4.33), (4.34), (4.45), and (4.49) are substituted into Equation (4.80), and the result is

$$K_i^R = K_i^f = \frac{1}{2} m_i^f \dot{\vec{R}}_i^2 + \frac{1}{2} \left[m_i^p + m_i^R \left(\frac{A}{A_i^R} \right)^2 \right] V^2 \\ + \frac{1}{2} \vec{\omega}_i \cdot \vec{I}_i^f \cdot \vec{\omega}_i + k_i Q \vec{\omega}_i \cdot \vec{G}_i + \dot{\vec{R}}_i \cdot (\vec{\omega}_i \times \vec{S}_i + k_i Q \Delta \vec{u}_i) \quad (4.81b)$$

where $k_i = +1$ and the parameters of the above relation are given by the equations of Section 4.2.2.2.

For the case of a reservoir which is nominally filling, Equation (4.81b) is again obtained; however, k_i must be set to -1.

The kinetic energy of a typical moving point mass is simply

$$K^{\mu_j} = \frac{1}{2} \mu_j (\dot{\vec{R}}^{\mu_j})^2 \quad (4.82)$$

where the relations of Section 4.2.3 are to be used in obtaining $\dot{\vec{R}}^{\mu_j}$.

The kinetic energy of a structural mass on the Counterweight is

$$\bar{K}_a = \frac{1}{2} \vec{\omega}_a \cdot \vec{I}_a \cdot \vec{\omega}_a + \frac{1}{2} \bar{m}_a (\dot{\vec{R}}_a)^2 \quad (4.83)$$

In the program, the contributions of each structural mass on the Laboratory and the Counterweight, of all fluid, and all moving point masses are totalled to arrive at the system kinetic energy K.

4.2.5.3 Location of Space-Station Center of Mass

The location of the Space-Station center of mass is

$$\vec{R}_c = \frac{1}{M} \int \vec{R} dm \quad (4.84)$$

where \vec{R}_c and \vec{R} are measured from point O, the origin of the \underline{Z} axis. The evaluation of the contributions to Equation (4.84) of the various masses is straightforward and the results are summarized in the table below:

Contribution to $\vec{R} dm$	
Type of Mass	Contribution
Structural Mass on Laboratory (m_i)	$m_i \vec{R}_i$
Fluid on m_i	$m_i^f \vec{R}_i + \vec{S}_i$
Moving Point Mass	$\mu_j \vec{R} \mu_j$
Structural Mass on Counterweight	$\bar{m}_a \vec{R}_a$

The total contribution for all masses on the Space Station is computed in accordance with the above table. In the program these contributions are totalled for use in the matrix form of Equation (4.84).

4.3 MATRIX FORM OF EQUATIONS OF MOTION

The equations of motion developed in Section 4.2 will be converted to matrix form so that they can be programmed. To facilitate this conversion task, a special notation has been developed which is presented in Appendix B. In addition, some helpful identities were used, and these are also presented in Appendix B.

4.3.1 Inertia Matrix for Reservoir Fluid

Before the equations of motion are converted, it is necessary to develop expressions for the moment of inertia of the fluid present in a reservoir \vec{I}_i^R and its derivative in the \tilde{X}^i axes \vec{I}_i^R . These expressions are developed at this point, because the matrix identities developed in Appendix B greatly facilitate this work. As shown in Figure 4.6, the \tilde{W}^i axes are the principal axes for the reservoir fluid with their origin at the fluid center of mass. \tilde{W}_3^i is along the symmetry axis of the cylinder. Let the moment-of-inertia matrix about the \tilde{W}^i axes be $[L_i]$. Then $[L_i]$ is diagonal, and its diagonal elements are

$$\left. \begin{aligned} L_{11}^i &= L_{22}^i = m_i^R \left(\frac{1}{4} b_i^2 + \frac{1}{12} h_i^2 \right) \\ L_{33}^i &= \frac{1}{2} m_i^R b_i^2 \end{aligned} \right\} \quad (4.85)$$

By using Equation (B18), the moment of inertia matrix of the reservoir fluid about the \tilde{X}^i axes is

$$[I_i^R] = [\Pi(\zeta_i)]^T [L_i] [\Pi(\zeta_i)] - m_i^R [\Gamma(u_i^c)]^2 \quad (4.86)$$

where ζ_i is the set of Euler angles orienting the \tilde{W}^i axes with respect to the \tilde{X}^i axes,* and from Figure 4.6,

$$\{u_i^c\} = \{u_i^R\} - \frac{h_i}{2} [\Pi(\zeta_i)]^T \{e_3\} \quad (4.87)$$

with $\{e_3\} = [0 \ 0 \ 1]^T$, and with $\{u_i^c\}$ and $\{u_i^R\}$ expressed in the \tilde{X}^i axes. The elements of the matrix $[I_i^R]$ are the required components of the dyadic \vec{I}_i^R expressed in the \tilde{X}^i axes.

To obtain $\frac{d}{dt} \vec{I}_i^R$, Equation (4.86) is differentiated and the result is

* Since the reservoir is cylindrical with the \tilde{W}_3^i axes along the cylinder axis (see Figure 4.6), ζ_{i3} is arbitrary. For simplicity it is taken as zero. $[\Pi(\zeta_i)]$ may then be computed as a function of \hat{e}_i^R (see Step 16 of Appendix C).

$$[\dot{I}_i^R] = [\pi(\zeta_i)]^T [\dot{L}_i] [\pi(\zeta_i)] + k_i Q [\Gamma(u_i^c)]^2 - m_i^R [\Gamma(\dot{u}_i^c)] [\Gamma(u_i^c)] - m_i^R [\Gamma(u_i^c)] [\Gamma(\dot{u}_i^c)] \quad (4.88)$$

where $k_i = +1$ for the case of the reservoir which is nominally emptying and -1 for the reservoir which is nominally filling, and $[\dot{L}_i]$ and $\{\dot{u}_i^C\}$ are obtained below. $[\dot{L}_i]$ is diagonal, and the diagonal elements are obtained by differentiating Equations (4.85) and substituting Equations (4.39), (4.41), (4.34), and (4.16) into the results. This yields

$$\left. \begin{aligned} \dot{L}_{11}^i &= \dot{L}_{22}^i = -\frac{1}{4} k_i Q (b_i^2 + h_i^2) \\ \dot{L}_{33}^i &= -\frac{1}{2} k_i Q b_i^2 \end{aligned} \right\} \quad (4.88a)$$

Differentiating Equation (4.87), and substituting Equation (4.34) into the result yields

$$\{\dot{u}_i^c\} = \frac{1}{2} k_i V \frac{A}{A_i^R} [\pi(\zeta_i)]^T \{e_3\} \quad (4.89)$$

4.3.2 Coordinate Systems and Conversion of Dynamic Equations to Matrix Form

The coordinate systems used were discussed to some extent in Section 4.2 and are shown in Figure 4.1. When there is no deformation of any sort, each \tilde{X}^i coordinate system is parallel to the \tilde{X} coordinates and each \tilde{Y}^a coordinate system is parallel to the \tilde{Y} coordinates. In the undeformed state the Y_2 and Y_3 axes are in the minus X_2 and X_3 directions, respectively. In general, when the system is deformed, the Euler angle sets orienting the coordinate systems are as follows:

$$\begin{aligned} \tilde{X} \text{ with respect to } \tilde{Z} &: \gamma \\ \tilde{X}^i \text{ with respect to } \tilde{X} &: \theta_i \text{ (linear)} \\ \tilde{Y} \text{ with respect to } \tilde{X} &: \eta \\ \tilde{Y}^a \text{ with respect to } \tilde{Y} &: \bar{\theta}_a \text{ (linear)} \end{aligned}$$

These Euler-angle sets are indicated in parentheses on Figure 4.1 next to the vectors separating the origins of the corresponding coordinate systems. The order of rotation for a typical Euler angle set is described in Appendix B.

The matrix form of the vectors used in Figure 4.1 contains the components of the vectors projected onto the coordinate systems indicated below:

<u>Matrix Form</u>	<u>Coordinate System</u>
$\{R\}, \{r_i\} \{q_i\}$	\tilde{X}
$\{\bar{R}\}, \{\bar{r}_a\}, \{\bar{q}_a\}$	\tilde{Y}

As indicated above, the notation used for the matrix form is usually similar to that which was used for the vector form. For the complete correspondence of notation see the symbol list at the beginning of Section 4. Henceforth, the three Euler angle components will be written in the vector braces (e.g., $\gamma = \{\gamma\}$).

The elastic deformations of $\{q_i\}$ and $\{\theta_i\}$ of the Laboratory, and $\{\bar{q}_a\}$ and $\{\bar{\theta}_a\}$ of the Counterweight will be linearized; however large deformations of the Connecting Structure are permitted. Accordingly, the variations in $\{\bar{R}\}$ and $\{\eta\}$ could be large, and these variations are not linearized. However, these quantities are usually composed of a large nominal value and a much smaller variation as indicated below:

$$\left. \begin{aligned} \{\bar{R}\} &= \{\bar{R}_0\} + \{\Delta \bar{R}\} \\ \{\eta\} &= \pi \{e_1\} + \{\eta^*\} \end{aligned} \right\} \quad (4.90)$$

where $\{e_1\} = [1 \ 0 \ 0]^T$.

The vector equations of motion of Section 4.2 are now converted into matrix form using the relation of Appendix B. There is one matrix force equation and one matrix torque equation, (a total of six equivalent scalar equations), for each of the n structural masses on the Laboratory and for each of the \bar{n} structural masses on the Counterweight. In addition to the $6(n + \bar{n})$ variables $\{q_i\}$, $\{\theta_i\}$ ($i=1, \dots, n$) and $\{\bar{q}_a\}$, $\{\bar{\theta}_a\}$

($a = 1, \dots, \bar{n}$) , the 12 variables $\{R\}$, $\{V\}$, $\{\Delta\bar{R}\}$, and $\{\pi^*\}$ will appear in the equations; therefore there will be 12 more variables than equations of motion. However, there are 12 conditions yet to be specified; viz, the relations that locate the mean axes \underline{X} and \underline{Y} . The force equation for each Laboratory mass m_i is written in the \underline{X} coordinate system, and the force equation for each Counterweight mass \bar{m}_a is written in the \underline{Y} coordinate system. However, the torque equations are written in the local coordinate systems \underline{X}^i and \underline{Y}^a for m_i and \bar{m}_a , respectively. The matrix equations corresponding to the vector equations of Section 4.2 are listed below, and a discussion of the details concerning these equations will follow.

Structural Mass on Laboratory

$$\text{Newton: } [\lambda_1^i] \{\ddot{r}\} + [\lambda_2^i] \{\ddot{v}\} + [\lambda_3^i] \{\dot{\omega}^x\} + \{\delta_1^i\} = \{F_i^m\} \quad (4.91)$$

$$\text{Euler: } [\lambda_3^i] \{\dot{\omega}^x\} + [\lambda_4^i] \{\ddot{\theta}_2\} + \{\delta_2^i\} = \{T_i^m\} \quad (4.92)$$

Through Pipe

$$\text{Newton: } [\lambda_5^i] \{\ddot{r}\} + [\lambda_6^i] \{\ddot{v}\} + [\lambda_7^i] \{\dot{\omega}^x\} + [\lambda_8^i] \{\ddot{\theta}_2\} + \{\delta_3^i\} = \{F_i^p\} \quad (4.93)$$

$$\text{Euler: } [\lambda_8^i] \{\ddot{r}\} + [\lambda_9^i] \{\ddot{v}\} + [\lambda_{10}^i] \{\dot{\omega}^x\} + [\lambda_{11}^i] \{\ddot{\theta}_2\} + \{\delta_4^i\} = \{T_i^p\} \quad (4.94)$$

Reservoir : Emptying ($k = 1$) or Filling ($k = -1$)

$$\text{Newton: } [\lambda_{11}^i] \{\ddot{r}\} + [\lambda_{12}^i] \{\ddot{v}\} + [\lambda_{13}^i] \{\dot{\omega}^x\} + [\lambda_{14}^i] \{\ddot{\theta}_2\} + \{\delta_5^i\} = \{F_i^R\} \quad (4.95)$$

$$\text{Euler: } [\lambda_{14}^i] \{\ddot{r}\} + [\lambda_{15}^i] \{\ddot{v}\} + [\lambda_{16}^i] \{\dot{\omega}^x\} + [\lambda_{17}^i] \{\ddot{\theta}_2\} + \{\delta_6^i\} = \{T_i^R\} \quad (4.96)$$

Moving Point Mass

$$\begin{aligned} \text{Newton: } [(\alpha 1)^i] \{\ddot{R}\} + [(\alpha 1)^i] \{\ddot{\rho}_{k*}\} + [(\alpha 3)^i] \{\dot{\omega}^x\} + [(\alpha 4)^i] \{\ddot{\theta}_{k*}\} \\ + \{\delta(1)^i\} = \{F_{k*}^{\mu}\} \end{aligned} \quad (4.97)$$

$$\begin{aligned} \text{Euler: } [(\alpha 5)^i] \{\ddot{R}\} + [(\alpha 5)^i] \{\ddot{\rho}_{k*}\} + [(\alpha 7)^i] \{\dot{\omega}^x\} + [(\alpha 8)^i] \{\ddot{\theta}_{k*}\} \\ + \{\delta(2)^i\} = \{T_{k*}^{\mu}\} \end{aligned} \quad (4.98)$$

Structural Mass on Counterweight

$$\begin{aligned} \text{Newton: } [\lambda_{17}^a] \{\ddot{r}\} + [\lambda_{18}^a] \{\dot{\omega}^x\} + [\lambda_{19}^a] \{\ddot{\Delta\bar{r}}\} + [\lambda_{20}^a] \{\ddot{\rho}_0\} \\ + [\lambda_{21}^a] \{\dot{\omega}^y\} + \{\delta_7^a\} + [\lambda_{22}^a] \{\ddot{\rho}_0\} = \{F_a^c\} \end{aligned} \quad (4.99)$$

$$\text{Euler: } [\Lambda_{21}^e] \{\dot{\omega}\} + [\Lambda_{22}^e] \{\ddot{\theta}\} + \{\mathcal{F}_2^e\} = \{\bar{T}_2\} \quad (4.100)$$

In the above equations the force equations have been labeled "Newton" and the torque equations have been labeled "Euler." The coefficients and lower derivative terms are defined in the tables of Appendix C. Various secondary computations are also required to obtain terms which appear in the definition of these matrices and to obtain related information such as kinetic energy, Table 4.1 serves as a guide to the conversion of the equations from vector to matrix form, and a similar guide to the secondary equations is presented in Table 4.2. In addition, various geometrical and kinematical relations are required and are listed in Appendix C. These relations are easily derived by application of the equations of Appendix B to the geometry indicated in Figure 4.1. In addition, Appendix C includes other relations which will be derived in future sections, for example, the equations required to transform the initial conditions from a form which is convenient for the program user, to the form required for computation.

For the following reasons, additional approximations were made in the derivation of Equations (4.97) and (4.98). When Equations (4.91-4.100) are combined as indicated by Equations (4.6) and (4.8), to obtain the equations of motion for the system, the acceleration-coefficient matrix would be relatively sparse (i.e., contain mostly zeros) if no moving point masses were present. However, since the elastic motion of the moving point masses can be influenced by the motion of any structural mass on the Laboratory, the moving point masses can cause nonzero terms to appear in the acceleration coefficients associated with every Laboratory variable. The sparseness of the acceleration-coefficient matrix is however very useful in saving computer storage space since space must only be reserved for non-zero blocks in this matrix. Because elastic motion of the moving point masses has only been approximately evaluated, it was decided that it was worthwhile to make a further approximation to conserve the sparseness of the acceleration-coefficient matrix. At first, all acceleration terms attributable to moving masses were written on the right side of the equations of motion and evaluated one time-step back; however, this caused numerical-integration instabilities, and this technique was therefore abandoned.

Instead, second derivative terms associated with the $\{\ddot{q}_k\}$'s and $\{\ddot{\theta}_k\}$'s were evaluated only at the mass point m_{k*} which is nearest to μ_j and λ_{k*}^j was set to 1. These acceleration terms were previously averaged over all m_k 's which influenced μ_j . The lower-derivative acceleration terms (coriolis and centrifugal) are still averaged. This approximation maintains the sparseness of the acceleration-coefficient matrix, and accordingly makes possible the saving of considerable computer-storage space.

The loads appearing on the right side of Equations (4.91-4.100) are accumulated and projected onto the proper coordinate system in Equations (37-39) of Appendix C. These include loads applied to the Counterweight by the Connecting Structure $\{f_E^*\}$ and $\{\tau_E^*\}^{(1)}$; loads applied by the control-system actuators $\{f_C^i\}$, $\{\tau_C^i\}$, $\{\bar{f}_C^a\}$, and $\{\bar{\tau}_C^a\}^{(2)}$; and supplementary loads $\{f_s^i\}$, $\{\tau_s^i\}$, $\{\bar{f}_s^a\}$ and $\{\bar{\tau}_s^a\}$. These supplementary loads may represent any excitation which the user may desire, to incorporate (for example, environmental disturbances). They are currently set to zero; however to incorporate supplementary loads, the user would program the appropriate load functions in a subroutine. Structural loads which are internal to the Laboratory or Counterweight are included later in modal-coordinate form.⁽³⁾

- - - - -
- (1) These loads are discussed in Section 4.4.2.
 - (2) These loads are discussed in Section 5.
 - (3) These loads are discussed in Section 4.4.1.

Equation Number	
Matrix Form	Vector Form
<u>Structural Mass on Laboratory</u>	
4.91	4.9
4.92	4.10
<u>Through Pipe</u>	
4.93	4.20
4.94	4.32
<u>Reservoir</u>	
4.95	4.44 ⁽¹⁾
4.96	4.53 ⁽¹⁾
<u>Moving Point Mass</u>	
4.97	4.66
4.98	4.67
<u>Structural Mass on Counterweight</u>	
4.99	4.69
4.100	4.70

(1) Vector equations are for a reservoir which is nominally emptying. See Section 4.2.2.3 to adjust for a reservoir which is nominally filling.

Table 4.1 Guide to the Conversion of the Main Equations from Vector to Matrix Form

Table 4.2 Guide to the Conversion of the Secondary
Equations From Vector to Matrix Form

Vector or Scalar Symbol	Equation Number	
	Appendix C	Section 4
<u>Structural Mass on Laboratory</u>		
\vec{L}_i^m	A18	4.74
κ_i^m	A19	4.79
<u>Through Pipe</u>		
Q, \dot{Q}	5a, 5b	4.16
S_i	input data	4.21, or 4.23 and 4.24
G_i	input data	4.26 and 4.27
\vec{U}_i	input data	4.31
$\vec{L}_i^P = \vec{L}_i^f$	A22	4.76
κ_i^P	A23	4.81a
<u>Reservoir</u>		
h_i	7	4.35 ⁽¹⁾
$\vec{u}_i^B, \vec{u}_i^R, \vec{e}_i^R$	} input data	
\vec{S}_i^P, \vec{I}_i^P		
\vec{S}_i		
m_i^R, m_i^f	12	4.38
$\Delta \vec{u}_i$	9, 10	4.39, 4.40
G_i^P	11	4.36
\vec{G}_i	input data	4.47
\vec{I}_i^f	13	4.46 with 4.48
\vec{L}_i^R	16 with 14 and 15	4.50 with 4.86 using 4.85 and 4.87
κ_i^R	A20	same as 4.76
\vec{I}_i^R	A21	4.81b
\vec{I}_i^R	19 with 17 and 18	4.88 with 4.88a and 4.89
<u>Moving Point Masses</u>		
\vec{d}_k^j	20	4.60
\vec{W}_j	23a	4.57 with 4.63
\vec{W}_j	23b	4.58 with 4.63
TABLE CONTINUED ON NEXT PAGE		

(1) This equation is for a reservoir which is nominally emptying. See Section 4.2.2.3 to adjust for a reservoir which is nominally filling.

Vector or Scalar Symbol	Equation Number	
	Appendix C	Section 4
	<u>Moving Point Masses (Continued)</u>	
\vec{L}^{u_i}	A24	4.77
\vec{K}^{u_j}	A25	4.82
	<u>Structural Mass on Counterweight</u>	
\vec{L}_a	A26	4.78
\vec{K}_a	A27	4.83

Table 4.2 (Continued) Guide to the Conversion of the Secondary Equations from Vector to Matrix Form

4.3.3 Combined Equations of Motion for Entire System

Equations (4.91) - (4.100) are combined in accordance with the scheme indicated by Equations (4.6) and (4.8) to obtain the equations of motion for the entire system. The result is of the form

$$[\Lambda]\{\ddot{x}\} = \{f\} + \{\sigma\} \quad (4.101)$$

where $[\Lambda]$ is the mass matrix, $\{\ddot{x}\}$ represents the acceleration terms, $\{f\}$ is the force vector (containing both forces and torques), and $\{\sigma\}$ contains the lower derivative dynamic terms. Specifically, $[\Lambda]$ is given by Equation (36) of Appendix C, $\{f\}$ contains the indicated 3-element vectors,

$$\{f\} = \begin{Bmatrix} \vdots \\ f_1 \\ \vdots \\ f_2 \\ \vdots \\ f_3 \\ \vdots \\ f_4 \\ \vdots \\ f_5 \\ \vdots \\ f_6 \\ \vdots \end{Bmatrix} = \begin{Bmatrix} f_L \\ \vdots \\ f_c \end{Bmatrix} \quad (4.102)$$

the lower-derivative terms are

$$\{\sigma\} = \begin{Bmatrix} \vdots \\ \nabla_1^a \\ \vdots \\ \nabla_2^a \\ \vdots \\ \nabla_3^a \\ \vdots \\ \nabla_4^a \\ \vdots \\ \nabla_5^a \\ \vdots \end{Bmatrix} \quad (4.103)$$

and $\{\dot{x}\}$ is defined as follows:

$$\{\dot{x}\} = \begin{Bmatrix} \dot{R} \\ \omega^x \\ \vdots \\ \dot{\theta} \\ \Delta \dot{R} \\ \omega^y \\ \vdots \\ \dot{\varphi} \end{Bmatrix} \quad (4.104)$$

where $\{q\}$ and $\{\bar{q}\}$ are the elastic coordinate vectors of the Laboratory and Counterweight, respectively; viz.

$$\{q\} = \begin{Bmatrix} q_1 \\ \theta_1 \\ \vdots \\ q_n \\ \theta_n \end{Bmatrix} ; \quad \{\bar{q}\} = \begin{Bmatrix} \bar{q}_1 \\ \bar{\theta}_1 \\ \vdots \\ \bar{q}_n \\ \bar{\theta}_n \end{Bmatrix} \quad (4.105)$$

4.3.4 Modal-Constraint Reduction Procedure

In order to accommodate detailed elements such as solar panels, many structural masses are needed in the idealization. Thus, Equations (4.101) are quite large in size, and the solutions are likely to contain high-frequency contributions. Direct solution would therefore require a very small numerical-integration step size, and, in addition, large matrices would have to be inverted. To make matters worse, the physical time for maneuvers such as deployment and spin-up is very large relative to the short periods of vibration associated with elastic motion. In order to reduce the size of the equations in an automatic and orderly way, thereby alleviating these problems, two basic methods will be used: viz, the modal-reduction method and the constraint-reduction method. These closely related methods are explained in Appendix D, and the procedure to be used is summarized below.

First, $\{\delta\pi^X\}$ is defined as the vector containing the three virtual differential rotations about each axis of the \underline{X} coordinate system. $\{\pi^X\}$ is known as the quasi coordinate corresponding to $\{\omega^X\}$; $\{\delta\pi^Y\}$ is similarly defined for the \underline{Y} coordinate system. Then the virtual work is computed and placed in the form given by Equation (D24). In this way, the $[Q]$ matrix is obtained. The procedure is greatly simplified by varying only one virtual displacement at a time, computing the corresponding work, and then adding the results.

The final result of the virtual work computation is the matrix $[Q]$ which is presented in Appendix C as Equation (45) (where the required terms are defined by Equations (44) and (45a - 45c)).

If modes are used for the reduction, the Laboratory and Counterweight elastic coordinates are represented as follows:

$$\{\bar{q}\} = [\bar{\Phi}] \{\bar{x}\}, \quad \{\bar{\dot{q}}\} = [\bar{\Phi}] \{\bar{\dot{x}}\} \quad (4.106)$$

where $[\bar{\Phi}]$ and $[\bar{\Phi}]$ contain the elastic free-free modes of the Laboratory and Counterweight, respectively; i.e., the rigid-body modes are removed. At first it was planned to fix the \underline{X} and \underline{Y} coordinate system in a key mass of the Laboratory and Counterweight, respectively, and to use cantilever modes in $[\bar{\Phi}]$ and $[\bar{\Phi}]$ which would be obtained by fixing the key masses. In addition to the modal coordinates, the physical coordinates of these key masses would be employed. It was then, however, determined that high-frequency components could be present in the numerical integration solution. These high frequencies are associated with the motion of the key masses which is described by use of physical coordinates. For this reason it was decided to use the more involved procedure of employing free-free modes.

The number of masses used in the Laboratory and Counterweight are n and \bar{n} , respectively, and the respective number of modes are p and \bar{p} ; therefore the dimensions of $[\bar{\Phi}]$ and $[\bar{\Phi}]$ are $n \times p$ and $\bar{n} \times \bar{p}$, respectively. The coordinates are now related to a reduced set of coordinates by employing the following modal-constraint relations:

$$\{\delta x\} = [\bar{\Phi}] \{\delta \bar{x}_T\}, \quad \{\dot{\bar{x}}\} = [\bar{\Phi}] \{\dot{\bar{x}}_T\} \quad (4.107)$$

where

$$\{\delta \bar{x}_T\} = \begin{Bmatrix} \delta R \\ \delta \pi^X \\ \delta \bar{x} \\ \delta(\Delta \bar{R}) \\ \delta \pi^Y \\ \delta \bar{y} \end{Bmatrix}, \quad \{\dot{\bar{x}}_T\} = \begin{Bmatrix} \dot{R} \\ \omega^X \\ \dot{\bar{x}} \\ \Delta \dot{\bar{R}} \\ \omega^Y \\ \dot{\bar{y}} \end{Bmatrix} \quad (4.108)$$

and $[\phi]$ is an appropriate constraint matrix that relates the coordinates $\{\delta x\}$ to the reduced coordinates $\{\delta \xi_T\}$. When the modes given by Equation (4.106) are used to represent the Laboratory and Counterweight and when the Connecting Structure is flexible, $[\phi]$ has the following value:

$$[\phi] = \begin{bmatrix} \overset{6}{[I_6]} & \overset{p}{|} & \overset{6}{|} & \overset{\bar{p}}{|} \\ \hline & \overset{6n}{[\Phi]} & & \\ \hline & & \overset{6}{[I_6]} & \\ \hline & & & \overset{6\bar{n}}{[\bar{\Phi}]} \end{bmatrix} \quad \begin{matrix} \text{dimensions} \\ \swarrow \\ 6 \\ 6n \\ 6 \\ 6\bar{n} \end{matrix} \quad (4.109)$$

where $[I_6]$ is the 6 x 6 identity matrix. Equation (4.107) now has the effect of substituting modal coordinates for the elastic motion while duplicating the rigid-body coordinates. $[\phi]$ always contains $12 + 6(n + \bar{n})$ rows; however the number of columns used depends on the constraints. If all structures are flexible, $[\phi]$ contains $12 + p + \bar{p}$ modes. The main constraints which the user may select and the corresponding forms of the $[\phi]$ matrices and the $\{\xi_T\}$ vectors are indicated below:

A. Rigid Laboratory

This constraint may be used in combination with the rigid Counterweight. Equation (4.109) is applicable; however p , which is the width of $[\Phi]$ and the height of $\{\xi\}$ shrinks to zero. I.e.,

$$[\phi] = \begin{bmatrix} \overset{6}{[I_6]} & \overset{6}{|} & \overset{\bar{p}}{|} \\ \hline & & \\ \hline & \overset{6}{[I_6]} & \\ \hline & & \overset{6\bar{n}}{[\bar{\Phi}]} \end{bmatrix} \quad \begin{matrix} 6 \\ 6n \\ 6 \\ 6\bar{n} \end{matrix} \quad (4.110)$$

rigid
Laboratory

$$\{\ddot{\xi}_T\} = \left\{ \begin{array}{c} \dot{R} \\ \omega^x \\ \Delta \dot{R} \\ \omega^y \end{array} \right\} \quad \begin{array}{l} \text{rigid} \\ \text{Laboratory} \end{array} \quad (4.111)$$

B. Rigid Counterweight

Equation (4.109) is applicable; however \bar{p} which is the width of $[\bar{\phi}]$ and the height of $\{\bar{\xi}\}$ shrinks to zero.

C. Rigid Vehicle

The Laboratory, the Counterweight, and the Connecting Structure are rigid, i.e., there is no elastic motion, however the Connecting Structure is still capable of extension and retraction. For this case,

$$[\phi] = \left[\begin{array}{c|c|c|c} \overset{6}{[1_6]} & & & \overset{6}{6} \\ \hline 0 & & & \overset{6n+3}{6n+3} \\ \hline 0 \mid [\pi(\eta_0)] & & & \overset{3}{3} \\ \hline 0 & & & \overset{6n}{6n} \end{array} \right] \quad \begin{array}{l} \text{rigid} \\ \text{vehicle} \end{array} \quad (4.112)$$

$$\{\dot{\xi}_T\} = \begin{Bmatrix} \dot{R} \\ \omega^x \end{Bmatrix} \quad \begin{array}{l} \text{rigid} \\ \text{vehicle} \end{array} \quad (4.113)$$

In addition to the above constraints, the program user may include other constraints by supplying modes which obey these constraints in $\{\Phi\}$ and $\{\bar{\Phi}\}$. For example, elastic motion in a particular direction could be eliminated by this method.

The final steps are to form the reduced mass matrix:

$$[\Lambda_R] \equiv [\Phi]^T [Q] [\Lambda] [\Phi] \quad (4.114)$$

and the reduced right-side vector:

$$\{\nabla_R\} \equiv [\Phi]^T [Q] (\{f\} + \{c\}) \quad (4.115)$$

In Equation (4.115), it is not necessary to include the forces of constraint in $\{f\}$. Finally the desired reduced equations of motion are formed as follows:

$$[\Lambda_R] \{\ddot{\xi}_T\} = \{\nabla_R\} \quad (4.116)$$

Equation (4.116) is solved for $\{\ddot{\xi}_T\}$, and $\{\ddot{\xi}_T\}$ and then integrated once.* Some of the components of the result, namely $\{\dot{R}\}$, $\{\dot{\xi}\}$, $\{\dot{\Delta R}\}$, and $\{\dot{\xi}\}$, may be integrated again to obtain the displacements; however, auxiliary expressions are needed to obtain $\{\dot{\gamma}\}$ and $\{\dot{\eta}^*\}$ from $\{w^X\}$ and $\{w^Y\}$ in order to determine the Euler angles by integration. Suitable relationships were derived using the theory of Appendix B, and the results are Equations (A17) of Appendix C.

* $[\Lambda_R]$ is a symmetric matrix. This fact can be advantageously used, since more rapid solution schemes are available for symmetric matrices; also, less storage is required for $[\Lambda_R]$.

Initially, values of $\{\xi\}$, $\{\dot{\xi}\}$, $\{\bar{\xi}\}$, and $\{\dot{\bar{\xi}}\}$ must be obtained from the corresponding values of $\{q\}$, $\{\dot{q}\}$, $\{\bar{q}\}$, and $\{\dot{\bar{q}}\}$. Equations (4.106) cannot be inverted since the modal matrices are not square; however, a method of obtaining the modal coordinates which provides a best fit approximation, in a certain sense, to Equations (4.106) is established in Appendix D, and the results are Equations (D30) to (D33).

4.3.5 Adjustment of Input Data

In accordance with Equation (4.106) the elastic free-free modes of the Laboratory and the Counterweight are used to represent the elastic motion of the respective structures. It is well known that the linear and angular momentum of each mode shape vanishes. Since the elastic coordinates $\{q_i\}$ and $\{\theta_i\}$ are a linear combination of the modes, it follows that the linear and angular momentum of the elastic coordinates must also vanish; i.e., for the Laboratory

$$\sum_{i=1}^n m_i \{q_i\} = 0 \quad (4.117)$$

$$\sum_{i=1}^n ([I_i] \{\theta_i\} + m_i [r(r_i)] \{q_i\}) = 0 \quad (4.118)$$

The analagous relationships for the Counterweight may be obtained by simply placing a bar over each symbol of Equations (4.117) and (4.118). Equations (4.117) and (4.118) indicate that the flexible-body coordinates $\{q\}$ are a dependent set of coordinates. This fact was already used in the previous section. A physical interpretation of these equations is that they serve to locate the mean or "rigid-body" axes (\underline{X} axes) relative to the Laboratory. For example, using Equation (4.117), the distance from the origin of the \underline{X} axes to the cm of the Laboratory structure* is

$$\frac{1}{M_L} \sum_{i=1}^n m_i (\{r_i\} + \{q_i\}) = \frac{1}{M_L} \sum_{i=1}^n m_i \{r_i\}$$

* The structure referred to does not include the moving masses or fluids.

where M_L is the total Laboratory mass. This distance is seen to be a constant; therefore Equation (4.117) serves to locate the origin of the \underline{X} axes relative to the deformed structure. Similarly, Equation (4.118) serves to fix the angular position of the \underline{X} axes relative to the structure. The details of the computation of the angular position are provided in Appendix E since it will be seen that this computation is needed at $t = 0$.

The set of initial conditions $\{q\}$ and $\{\dot{q}\}$ should actually obey Equations (4.117), (4.118) and their derivatives; however, in order to avoid burdening the user, it is permissible to supply input data relative to any coordinate system \underline{X}' which is near \underline{X} . The computer program will automatically determine the location of the \underline{X} axes and will compute the initial conditions relative to the \underline{X} axes. The new initial conditions satisfy Equations (4.117), (4.118) and their derivatives, and are suitable for initializing the numerical-integration procedure. The derivation for this step is presented in Appendix E, and the results have been incorporated into the computation procedure presented in Appendix C.

The procedure described in the above paragraph is also carried out for the counterweight.

4.4. STRUCTURAL FORCES

4.4.1. Laboratory and Counterweight Structure

From Equations (4.115) and (4.116), the reduced set of Equations of motion are

$$[\Lambda_R] \{\ddot{\xi}_T\} = [\phi]^T [\varphi] (\{f_{int}\} + \{f_{ext}\} + \{\sigma\}) \quad (4.119)$$

where $\{f\}$ has been written as the sum of the forces applied by the Laboratory and Counterweight structures $\{f_{int}\}$ (not including forces applied by the Connecting Structure) and the balance of the forces $\{f_{ext}\}$ which includes the external forces and forces applied by the connecting structure. From Equation (D25a) of Appendix D, it is clear that

$$\{f_{int}\}_{gen} = [\phi]^T [\varphi] \{f_{int}\} \quad (4.120)$$

$$\{f_{ext}\}_{gen} = [\phi]^T [\varphi] \{f_{ext}\} \quad (4.121)$$

where $\{f_{int}\}_{gen}$ and $\{f_{ext}\}_{gen}$ are the contributions of $\{f_{int}\}$ and $\{f_{ext}\}$ to the generalized forces associated with $\{\xi_T\}$. $\{f_{int}\}$ is next partitioned into forces applied to the Laboratory and forces applied to the Counterweight as follows:

$$\{f_{int}\} = \begin{Bmatrix} f_{int_L} \\ f_{int_C} \end{Bmatrix} \quad (4.122)$$

Substitution of Equation (45) of Appendix C and Equations (4.109) and (4.122) into Equation (4.120) yields the following equation which applies when all structures are flexible:

$$\{f_{int}\}_{gen} = \begin{Bmatrix} 0 \\ [\Phi]^T [\varphi_L] \{f_{int_L}\} \\ 0 \\ [\bar{\Phi}]^T [\varphi_C] \{f_{int_C}\} \end{Bmatrix} \quad \begin{matrix} \text{all structures} \\ \text{flexible} \end{matrix} \quad (4.123)$$

where the zeros were obtained by realizing that these terms are the generalized forces corresponding to $\{R\}$, $\{\gamma\}$, $\{\Delta\bar{R}\}$ and $\{\eta^*\}$; i.e., the generalized forces corresponding to $\{R\}$ and $\{\Delta\bar{R}\}$ are the resultant forces on the entire Space Station and Counterweight, respectively; the generalized force corresponding to γ is the resultant torque of all forces applied to the entire Space Station about point O on Figure 4.1; and the generalized force corresponding to η^* is the resultant torque of all forces applied to the Counterweight about point A in Figure 4.1. Clearly, the contributions to these generalized forces of all structural forces within the Laboratory and the Counterweight must vanish since these forces are internal to the structure.

The Laboratory and Counterweight structural forces are next expressed in terms of their stiffness and damping matrices;

$$\{f_{int_L}\} = -[K]\{\xi\} - [C]\{\dot{\xi}\} = -[K][\Phi]\{\xi\} - [C][\Phi]\{\dot{\xi}\}$$

$$\{f_{int_C}\} = -[\bar{K}]\{\bar{\xi}\} - [\bar{C}]\{\dot{\bar{\xi}}\} = -[\bar{K}][\bar{\Phi}]\{\bar{\xi}\} - [\bar{C}][\bar{\Phi}]\{\dot{\bar{\xi}}\}$$

These equations are substituted into Equation (4.123), and the result is linearized yielding

$$\{F_M\} \equiv \{f_{int}\}_{gen} = \begin{Bmatrix} 0 \\ f_M \\ 0 \\ \bar{f}_M \end{Bmatrix} \quad \begin{matrix} \text{all structures} \\ \text{flexible} \end{matrix} \quad (4.124)$$

where $\{f_{\text{int}}\}_{\text{gen}}$ has been renamed $\{F_M\}$ for convenience, the zeros in Equation (4.124) are 1×6 zero vectors, and

$$\{f_M\} = -[K]\{\xi\} - [C_M]\{\dot{\xi}\} \quad (4.125)$$

$$\{\bar{f}_M\} = -[\bar{K}]\{\bar{\xi}\} - [\bar{C}_M]\{\dot{\bar{\xi}}\} \quad (4.126)$$

In Equation (4.125), $[K]$ and $[C_M]$ are the diagonal modal stiffness and modal damping matrices for the Laboratory, and $[\bar{K}]$ and $[\bar{C}_M]$ are the corresponding matrices for the Counterweight. Provision has been made to input to the program a percentage of critical damping for each mode.

Finally, Equation (4.119) may be expressed as

$$[\Lambda_R]\{\ddot{\xi}_T\} = [\phi]^T[\phi]\{\nabla\} + \{F_M\} \quad (4.127)$$

where

$$\{\nabla\} \equiv \{f_{\text{ext}}\} + \{\sigma\} \quad (4.128)$$

4.4.2. Connecting Structure

The forces and moments applied to the Connecting Structure by the Laboratory are computed in a separate subroutine and then supplied to the main program where, on the basis of equilibrium of the massless Connecting Structure, the corresponding forces and moments applied to the Laboratory and Counterweight are computed. The object of performing the basic structural calculations in a subroutine is to enable the user to study any type of structure desired; that is, the subroutine may contain the usual type of stiffness and damping matrices or any other set of equations (linear or nonlinear) which relates the structural forces and moments to structural displacements and velocities. The computation procedure is outlined below (Refer to Figure 4.1):

- (1) First, the main program must be supplied with the following geometrical information:
 - (a) The specific Laboratory and Counterweight masses (the i th and a th, respectively) to which the structure is connected.
 - (b) Vectors $\{s\}$ and $\{\bar{s}\}$ expressed in X^i and Y^a , respectively (see Figure 4.1) which specify the exact location of the connection points (E and \bar{E}) in the aforementioned masses.*
 - (c) Data specifying the orientation of the structural reference system \bar{z} relative to the associated body system Y^a in the Counterweight mass \bar{m}_a (\bar{z} is fixed in \bar{m}_a). This reference system is the system in which the forces and moments are to be computed in the structural subroutine. The orientation of the \bar{z} axes is specified in the same manner as discussed in Section 2.3.1 of Volume II; i.e., by specifying the vectors $\{Y^{a'}\}_{\odot}$ and $\{Y^{a'}\}_{\oplus}$ in the $Y^{a'}$ coordinate system which is parallel to the Y^a coordinate system but has its origin at \bar{E} . These vectors locate point \odot which is any point on the positive \bar{z}_3 axis and point \oplus which is any point in the first quadrant of the $\bar{z}_1\bar{z}_3$ plane.
- (2) If the vehicle is deploying or retracting, the main program must call on the deployment subroutine for information regarding the deployment; that is, the subroutine must supply vector $\{\ell_o\}$ and its derivatives $\{\dot{\ell}_o\}$ and $\{\ddot{\ell}_o\}$, where $\{\ell_o\}$ is the vector (projected onto \bar{z}) from \bar{E} to E in the undeformed vehicle.
- (3) The main program then computes the displacement and velocity of point E in the \bar{z} system. The angular displacement and rate of system z relative to \bar{z} are also computed; system z is fixed in Laboratory node i and is parallel to \bar{z} when the vehicle is undeformed.

* In the case of a cable truss, for which there are a number of connection points, vectors $\{s\}$ and $\{\bar{s}\}$ are still needed to locate points E and \bar{E} for use in the deployment computations. The cable attachment points themselves are specified by vectors $\{s_j\}$ (in the Laboratory) and $\{\bar{s}_j\}$ (in the Counterweight) where $j = 1, 2, \dots$ number of cables.

- (4) The structural subroutine then computes the forces and moments applied to the Connecting Structure by the Laboratory at point E.
- (5) Then, on the basis of equilibrium of the massless Connecting Structure, the main program computes the forces and moments applied to the Counterweight at \bar{E} .

The theory for two types of structures has been developed. The structures are i) a circular beam of constant cross-section, and ii) a cable truss. The subroutine provided with the program is applicable for the circular beam.

4.4.2.1. Circular Beam

For the purposes of illustration, a structural subroutine is supplied with the program. The structure is a beam of constant circular cross-section. For simplicity, the deployment feature is idealized by simply assuming that the beam becomes longer as the Counterweight deploys; however its elastic properties per unit length remain constant. In addition to the usual beam stiffness matrix, an incremental beam stiffness matrix is included to account for the stiffening effect due to the action of the centrifugal forces. Structural damping was based upon modal damping which was obtained as follows:

- (1) The vehicle was idealized as two rigid masses connected by the aforementioned beam, as shown in Figure 4.8. Note that the axis of the beam passes through the two mass centers. Each mass was assigned typical mass properties. The inertial properties were assumed to be the same in each of the two transverse bending planes; otherwise, different modes would occur in the two planes and different physical damping coefficients would result for motion in these planes.
- (2) The elastic bending, torsion, and axial modes of the vehicle were obtained. Modal mass, stiffness and (critical) damping matrices were computed.

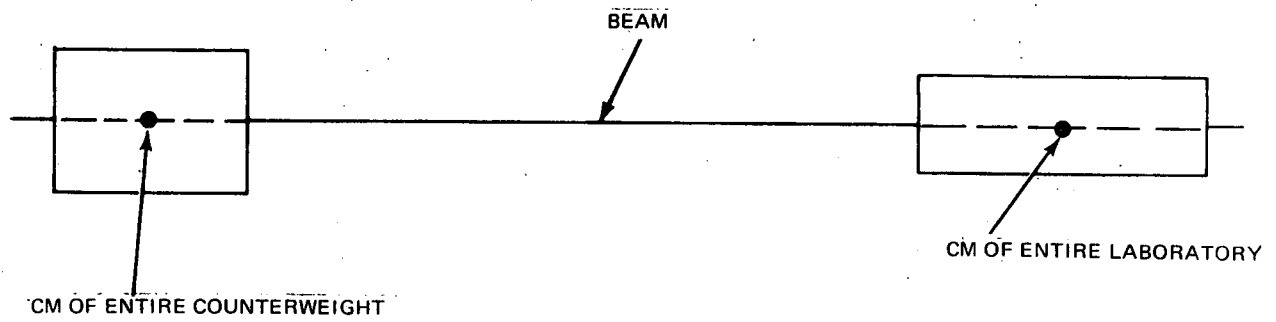


Fig. 4.8 Idealization Used to Determine Damping Matrix of Connecting Structure

- (3) Structural damping of the beam was assumed to be some fraction γ , of critical modal damping; different values of γ were used for the torsional, axial, and bending modes. The modal damping was then transformed back to physical coordinates. The resulting damping is a function of the undeformed length ℓ_0 of the Connecting Structure.

As the length ℓ_0 of the beam approaches zero during a retraction maneuver, the beam stiffness coefficients approach infinity. Actually, the flexibility of the end supports and the Laboratory-Counterweight docking hatch prevents infinite coefficients from occurring; however these detailed flexibility effects are not modeled in the subroutine provided. Instead, in order to retain reasonable structural flexibility for small ℓ_0 , the stiffness coefficients are computed using a minimum length $\ell_{0\min}$ whenever $\ell_0 < \ell_{0\min}$. $\ell_{0\min}$ is input data.

4.4.2.2 Cable Truss

The second type of Connecting Structure is a cable truss which may contain up to 16 cables, all of which may have different stiffness and damping properties. It is assumed that all cables are connected to the same mass at each end (i.e., the i^{th} Laboratory mass and the a^{th} Counterweight mass, respectively). Furthermore, it is assumed that the undeformed cable lengths are such that all cables are taut when the vehicle is in an undeformed configuration. However, cables may go slack when the vehicle deforms. The tensile force in each cable acts along the cable and is taken to be proportional to the stretch and stretch rate of the cable. Finally, all the individual cable forces are replaced by a single resultant force passing through point E and a resultant moment about point E.

4.5 STRUCTURAL LOADS

The facility is provided to compute structural loads at the junction points between modules (see Figure 3.1) or at any other point where the structure (Laboratory or Counterweight) can be separated into two free bodies. This is accomplished on a structure by separating the structure at the load-computation point and considering one portion of the structure as a free body. The load applied by the free body is then computed by taking the resultant of all of the inertia and applied loads on the free body. Since Connecting-Structure loads are included in the equations as external loads, the remaining portion of the Laboratory (or Counterweight) may also be used as the free body. Of course, results which are opposite in sign would then be obtained. The index numbers of all mass points in the free body must be supplied as input data in addition to the coordinate vector $\{t_{\ell},\}$ ($\{\bar{t}_{\bar{\ell}},\}$ on the Counterweight) to the the load-computation point. $\{t_{\ell},\}$ is stated in the local \tilde{X}^{ℓ} coordinate system which is fixed in m_{ℓ} , the mass containing the load-computation point. $\{\bar{t}_{\bar{\ell}},\}$ is defined similarly for the case of a load-computation point in the Counterweight. The forces $\{f'_{\ell},\}$ and torques $\{\tau'_{\ell},\}$ for the Laboratory are expressed in the \tilde{X} axes, and the forces $\{\bar{f}_{\bar{\ell}},\}$ and torques $\{\bar{\tau}'_{\bar{\ell}},\}$ for the Counterweight are expressed in the \tilde{Y} axes.

The equations required for the structural-load computations are listed in Appendix C. To reduce the complexity of the computation procedure, the structural-load computations use second derivatives that are evaluated at the previous numerical-integration cycle. In the Runge-Kutta numerical integration scheme used, the program cycles through each time point twice, and the integrated variables are improved in accuracy only slightly during the second pass. Consequently, the use of second derivatives evaluated during the previous cycle is a reasonable approximate procedure; however, the computation can not be performed at $t=0$.

C

4.6 COMPUTATION PROCEDURE

A summary of all of the required equations for computation and a step by step computation procedure is presented in Appendix C. The Phase II computer program was based on this Appendix.

Summaries of all of the required equations for the Connecting-Structure subroutines and corresponding computation procedures are presented in Appendix G.

5.0 CONTROL SYSTEMS

5.1 INTRODUCTION

The control systems were first developed on a rigid idealization of the Space Station and were then tested on a flexible idealization. The rigid model was capable of deployment and retraction. This section includes a discussion of the development and performance of the control systems on the rigid model. Sample rigid-body computer runs are included. Certain modifications were required to the control-system subroutines for proper operation on the flexible-vehicle idealization, and these modifications are also described in this section. Flexible-vehicle time-history results are presented in Section 6. The detailed computation procedure used in the rigid-body and flexible-body versions of the control-system subroutines is presented in Appendix H.

The control systems synthesized for the program are: vehicle attitude control (Space Station is not spinning), vehicle spin rate control, Counterweight position control, moving mass (elevator, etc.) position control, vehicle wobble damping, vehicle center-of-mass position control, fluid velocity (pump) control. The Counterweight, moving mass (except the balance mass), and fluid velocity control systems are assumed to be perfect; i.e., the controlled variables are set equal to their commanded values.

5.1.1 Rigid-Body Control-Systems Development Program

A rigid-body computer program was first prepared to develop the control systems. In this program, the Space Station consists of two rigid bodies, the Laboratory and the Counterweight, which are normally rigidly attached to each other. As shown in Figure 5.1, the origin of a set of axes X_1 , X_2 , and X_3 is located at the Laboratory center of mass with axis X_1 parallel to the nominal Space Station spin axis and axis X_3 along the long axis of the Laboratory. The origin of a set of axes Y_1 , Y_2 , and Y_3 is located at the Counterweight center of mass. The Counterweight can be moved relative to the Laboratory along a line parallel to Laboratory axis 3. The Counterweight attitude relative to the Laboratory is fixed by any preselected set of three Euler angles.

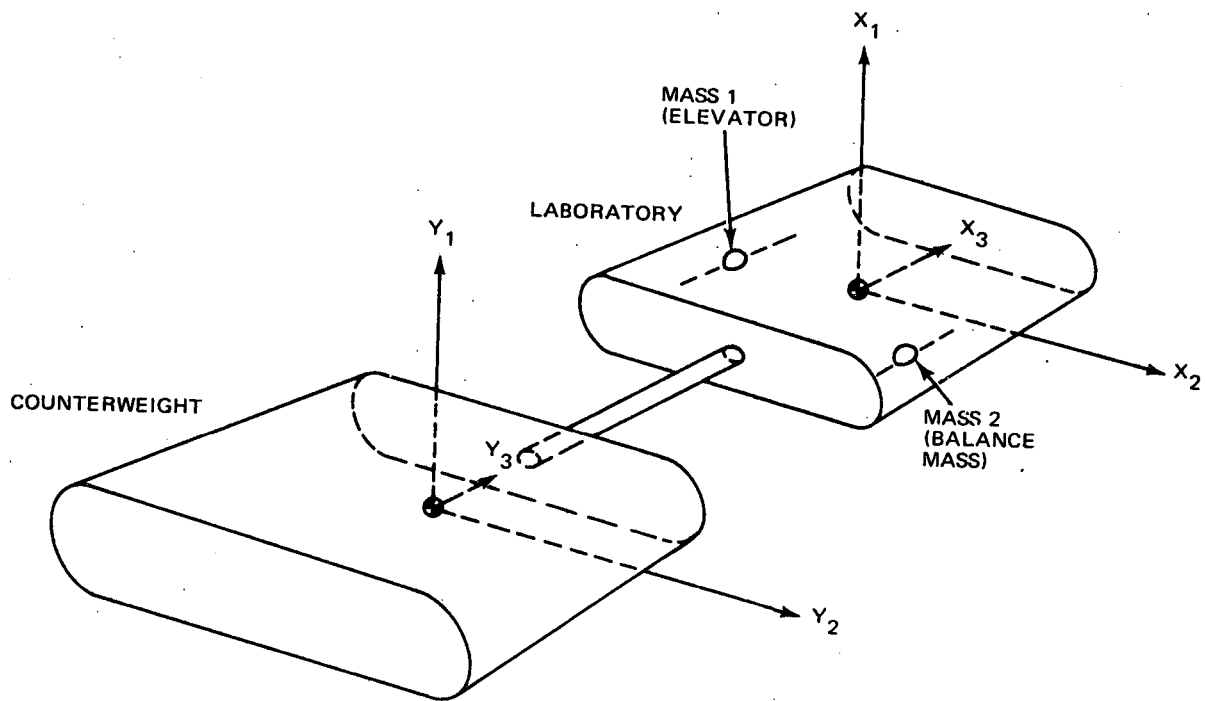


Fig. 5.1 Rigid Body Space Station Configuration Used for Development of Control Systems

There are 2 point masses, numbers 1 and 2, which can travel inside the Laboratory along a line parallel to Laboratory axis 3. Mass 1 represents an elevator. Mass 2 represents a balance mass, used to balance mass 1.

The rigid-body equations are written so that the Space Station motion includes the effects of the positions and motions of the Counterweight and 2 masses, given the positions and motions of the Counterweight and 2 masses relative to the Laboratory. The mass decrease in the jet fuel tanks resulting from reaction jet operation is not simulated. The effects of the CMG on the motions of the Space Station are computed, given the relative positions and motions of the CMG.

Thus, only the Space Station moves "freely" (subject to initial conditions and the time histories of its external forces and moments). The rigid-body equations were derived based on the implicit assumption that the motion of the Counterweight relative to the Laboratory, as well as the motions of the two masses, and the CMG would be prescribed as a function of time or vehicle state. To more nearly perfectly assess the performance of the control systems, the motions of the Laboratory, Counterweight, 2 masses, and CMG would have to be solved simultaneously.

The approach used in the program to deal with the limitations is the following. In the cases of the Counterweight, elevator, and balance mass, the commanded accelerations relative to the Laboratory are assumed to be obtained. In the case of the CMG, the computation of the CMG gimbal angle acceleration is slightly in error, because at each instant of time, this acceleration is computed using as an input the Laboratory angular acceleration, computed one iteration previously (instead of using the Laboratory angular acceleration computed presently). When the inertia of the CMG is extremely small relative to the inertia of the Space Station - as it is in this case - the error is extremely small.

5.1.2 Operation of Control Systems on Flexible Idealization

After checkout on the rigid idealization, the control systems were added to the flexible idealization described in Section 4. Wherever the input to a control subroutine required the motion measured at the sensor, the flexible-

body motion of the mass point containing the sensor was used so that the vibration of the sensor support was included. Similarly, the loads applied by the actuators were applied to the mass point where the actuator was attached, and the actuator moved with this mass point; thus, the vibration of the actuator was included. Aside from the balance-mass control system, all control systems operated on the flexible idealization with either no or minor modification. The balance-mass control system required major modification.

5.2 REACTION JET CONFIGURATION IN RIGID-VEHICLE SIMULATION*

The reaction jet configuration on the Laboratory is shown in Figure 5.2. In some cases, two jets are used in parallel (for positive torque: 1 and 3, 6 and 7; for negative torque: 14 and 15, 9 and 11). This was done to obtain sufficient control authority for the spin axis during Counterweight deployment, without using jets of different sizes.

The jets are located out of the plane of the solar panels and modules. The jet configuration represents only a first step toward optimization on the basis of weight, reliability, plume impingement, wiring, maintainability, etc. Jets 1 to 16 were simulated in the computer program. Jets 17 to 20 were not simulated because they were put on primarily for translation.

The jets mounted on the Counterweight are arranged in the same configuration as the jet configuration on the Laboratory. Jets 1 to 16 were mounted on the Counterweight, but not used for control.

Table 5.1 below shows the jet combinations to achieve desired torques without translation:

Table 5.1 Jet Combinations to Achieve Torques Without Translation

Torque About Axis	Jet Combination
+1	13, 10; 1 or 3 or (1 and 3), 6 or 7 or (6 and 7)
-1	2, 5; 14 or 15 or (14 and 15), 9 or 11 or (9 and 11)
+2	4, 12; 20, 18
-2	16, 8; 17, 19
+3	14 or 15 or (14 and 15), 1 or 3 or (1 and 3), 10, 5
-3	13, 2; 9 or 11 or (9 and 11), 6 or 7 or (6 and 7)

*The jet configuration used on the flexible idealization omitted jets 17-20 (see Section 6.0).

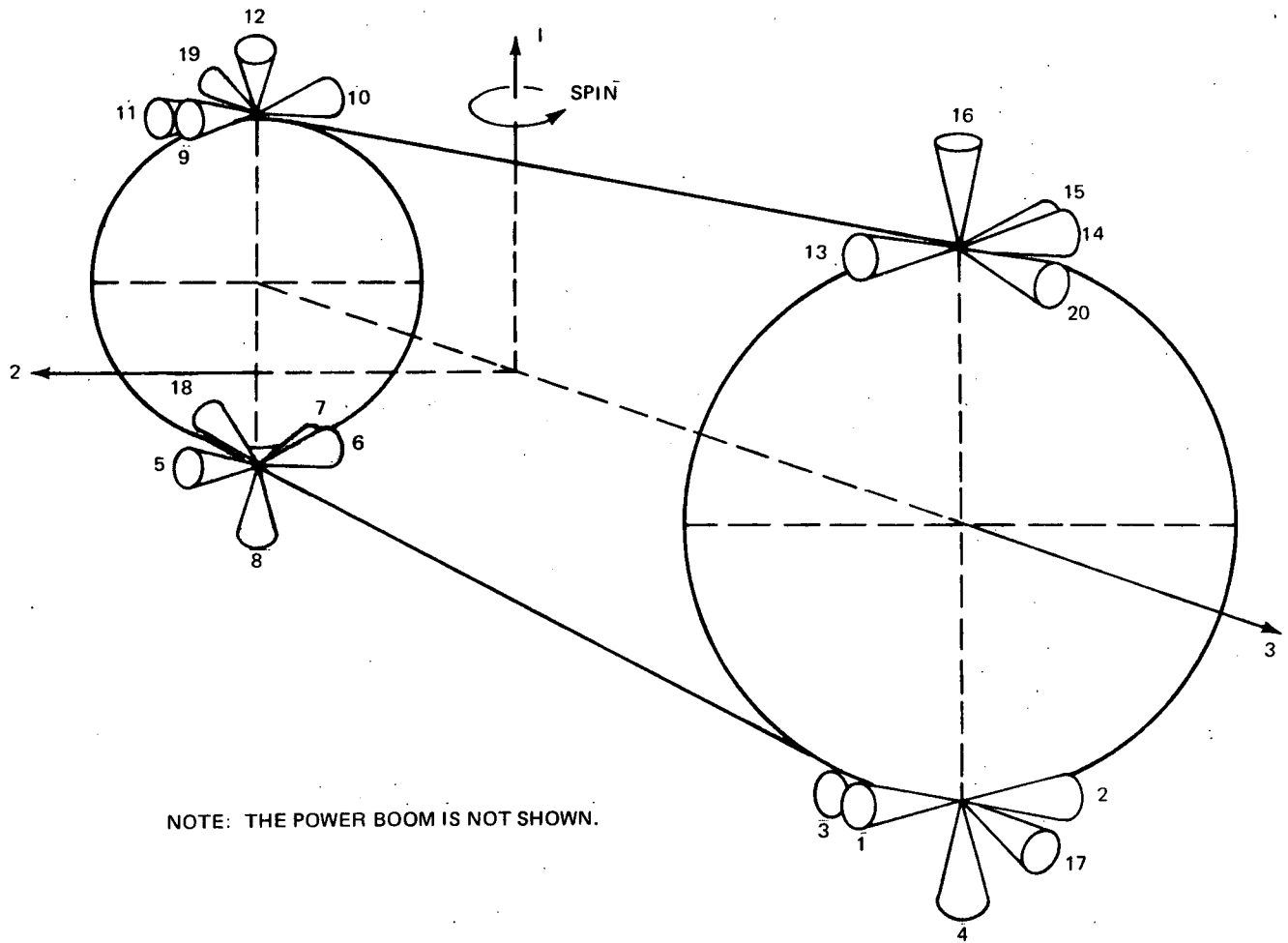


Fig. 5.2 Jet Configuration on Laboratory Core Module in Rigid-Vehicle Simulation

5.3 SERVICE ROUTINES USED BY MAIN COMMAND AND CONTROL ROUTINES

Several service routines are used by one or more of the main command or control routines. These service routines are first described in this section.

5.3.1 Command Routine POSCOM (Position Command)

Routine POSCOM was devised for commanding a change in the location of some element. This routine is used for commanding changes in the locations of the Counterweight, elevator, and other moving rigid masses (except the balance mass) relative to the Laboratory. There are three possible acceleration levels: A positive constant, zero, and a negative constant. The element is accelerated until a specified maximum velocity is achieved or the time for decelerating has been reached. The case in which the specified maximum velocity is reached and maintained for a time interval is shown in Figure 5.3. The case in which the specified maximum velocity is not reached is shown in Figure 5.4.

For the case of moving rigid masses, this routine is used to command the motion of the mass along each of the three Laboratory axes.

5.3.2 Command Routine VELCOM (Velocity Command)

Routine VELCOM is designed to command a change in the rate of some element. This program is used for commanding changes in the spin rate of the Space Station and in the fluid flow rate in the piping system. There are three possible acceleration levels: a positive constant, zero, and a negative constant. The element is accelerated until the desired rate is achieved. Figure 5.5 shows the development of the rate command.

5.3.3 Control Routine POSCTR (Position Control)

Routine POSCTR was devised for controlling the position of some element. This routine is used for controlling the attitude of the non-rotating Space Station. The position control policy is shown in Figure 5.6. The symbols e and \dot{e} designate error and error rate, respectively. The switching curves are either parabolic or straight lines. In the upper right shaded region, a constant negative control torque or force is applied; in the unshaded region, no control torque or force is applied; in the lower left shaded region, a constant positive control torque or force is applied.

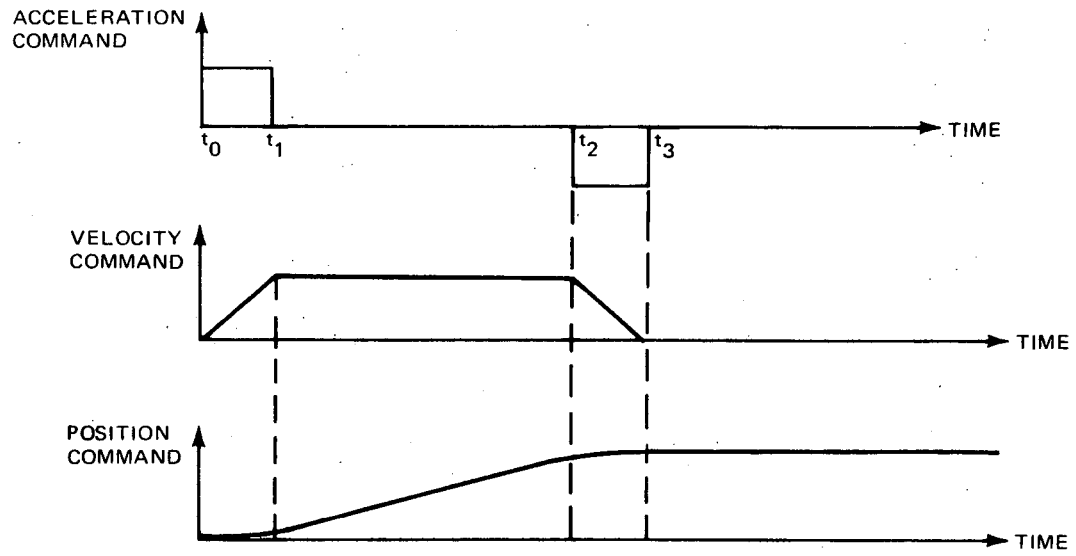


Fig. 5.3 Development of Position Command For Case in Which Velocity Command Achieves Velocity Command Limit

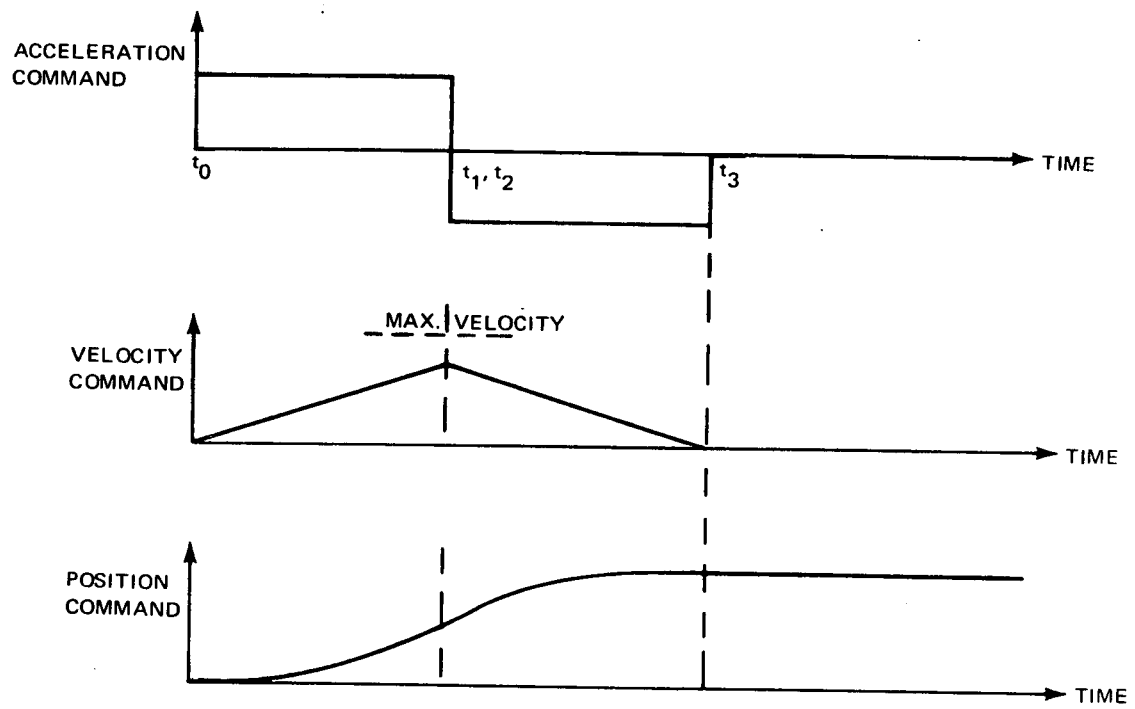


Fig. 5.4 Development of Position Command for Case in Which Velocity Command is Always Less Than Velocity Command Limit

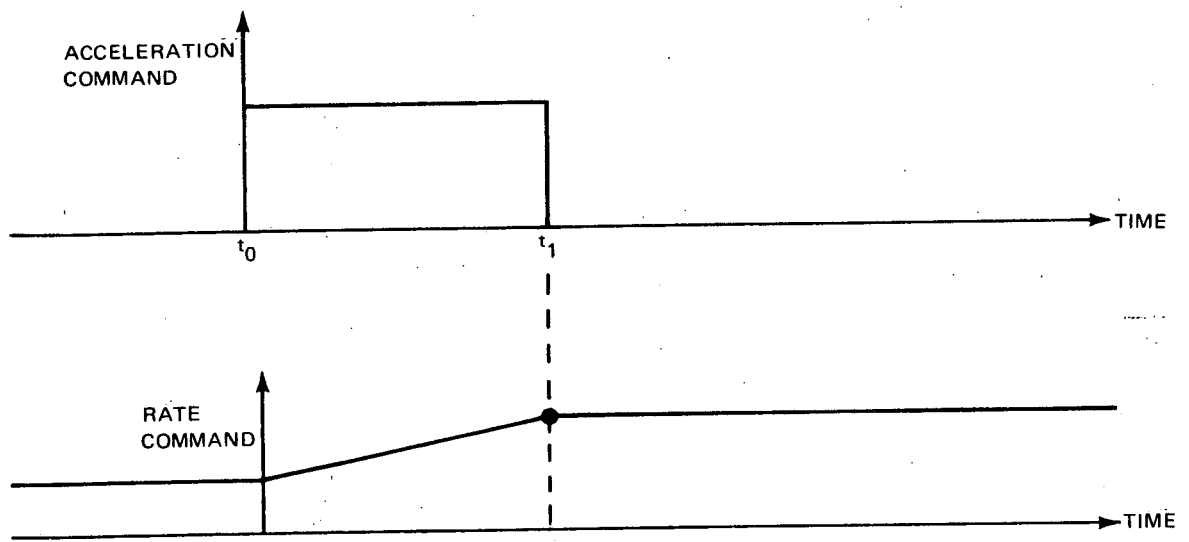


Figure 2-4 Development of Rate Command

Fig. 5.5 Development of Rate Command

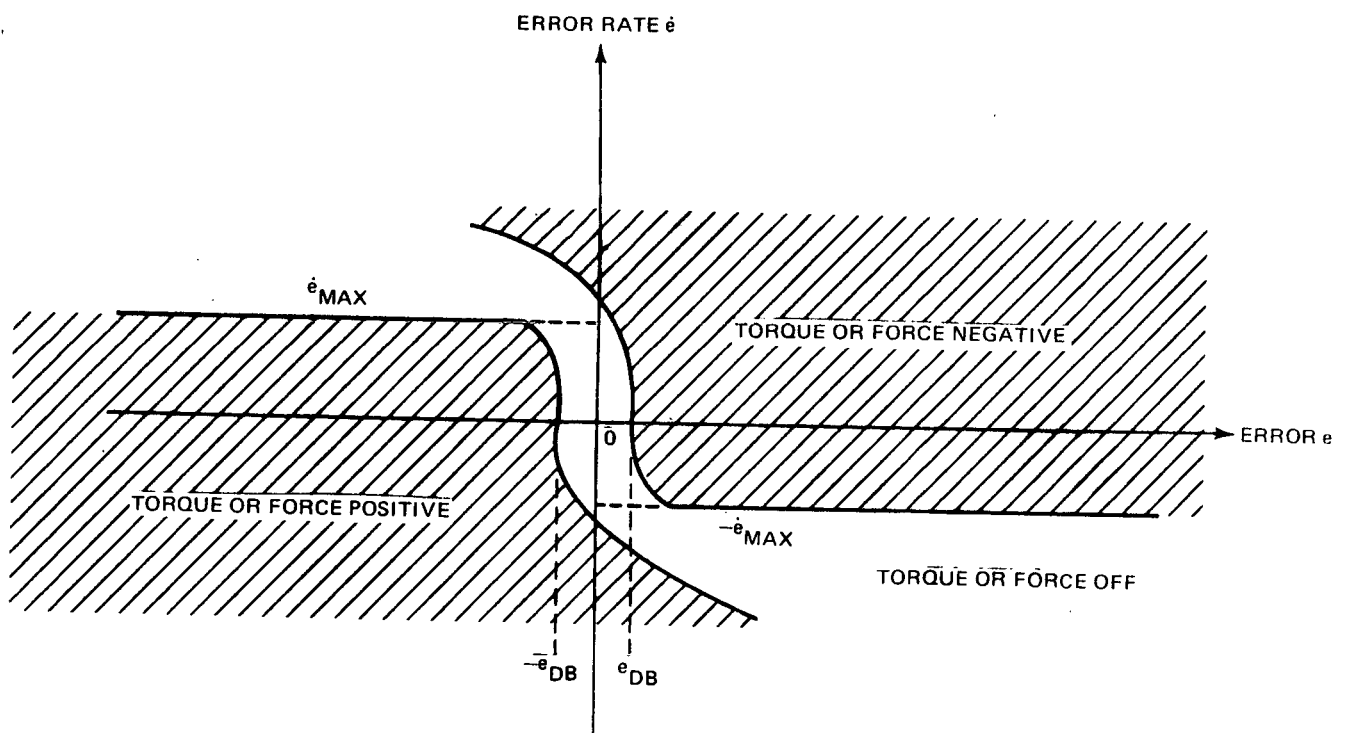


Fig. 5.6 Position Control

5.3.4 Control Routine VELCTR (Velocity Control)

Routine VELCTR was devised for controlling the velocity of some element. This routine is used for controlling the Space Station spin rate and the balance mass velocity.* The velocity control policy is shown in Figure 5.7. The symbol \dot{e} designates rate error. The error region is the line \dot{e} . Starting with $\dot{e} = 0$ and the control torque or force = 0, then, as \dot{e} is increased positively, the control remains = 0 until $\dot{e} = \dot{e}_{DB}$, when negative control is applied. For $\dot{e} > \dot{e}_{DB}$, negative control is still applied. As \dot{e} drops off so that $0 < \dot{e} < \dot{e}_{DB}$, negative control remains on. When $\dot{e} = 0$, control is turned off. The operation in the left-half plane is exactly the same, except that positive -- instead of negative -- control is applied.

5.4 MAIN COMMAND AND CONTROL ROUTINES

5.4.1 Activation of Commands and Controls

The commands for the Counterweight and elevator positions and the Space Station spin rate are computed every time point. Updating can occur at any time under any conditions in each or any combination of these commands. There are no restrictions on the commands.

The controls for the Counterweight and elevator positions are computed at every time point under any conditions. Space Station zero-g attitude control is activated only when the spin rate command is equal to zero. Space Station spin rate control is activated only when the spin rate command is not equal to zero. Wobble damping is activated only when the magnitude of the spin rate command is equal to 0.02 rad/sec or larger. Balance mass control is activated only when the Counterweight velocity is zero and the magnitude of the spin rate command is greater than a minimum angular velocity which is specified as input data (.4 rad/sec was used in all numerical work in this report).

5.4.2 Counterweight Position Control

The Counterweight acceleration, velocity, and position relative to the Laboratory are equated to the command Counterweight acceleration, velocity, and position, respectively.

 *VELCTR is used to control the balance mass velocity in the rigid-body idealization only. As described later, the balance mass control system required revision to operate properly on the flexible idealization, and the revised law does not utilize the VELCTR routine.

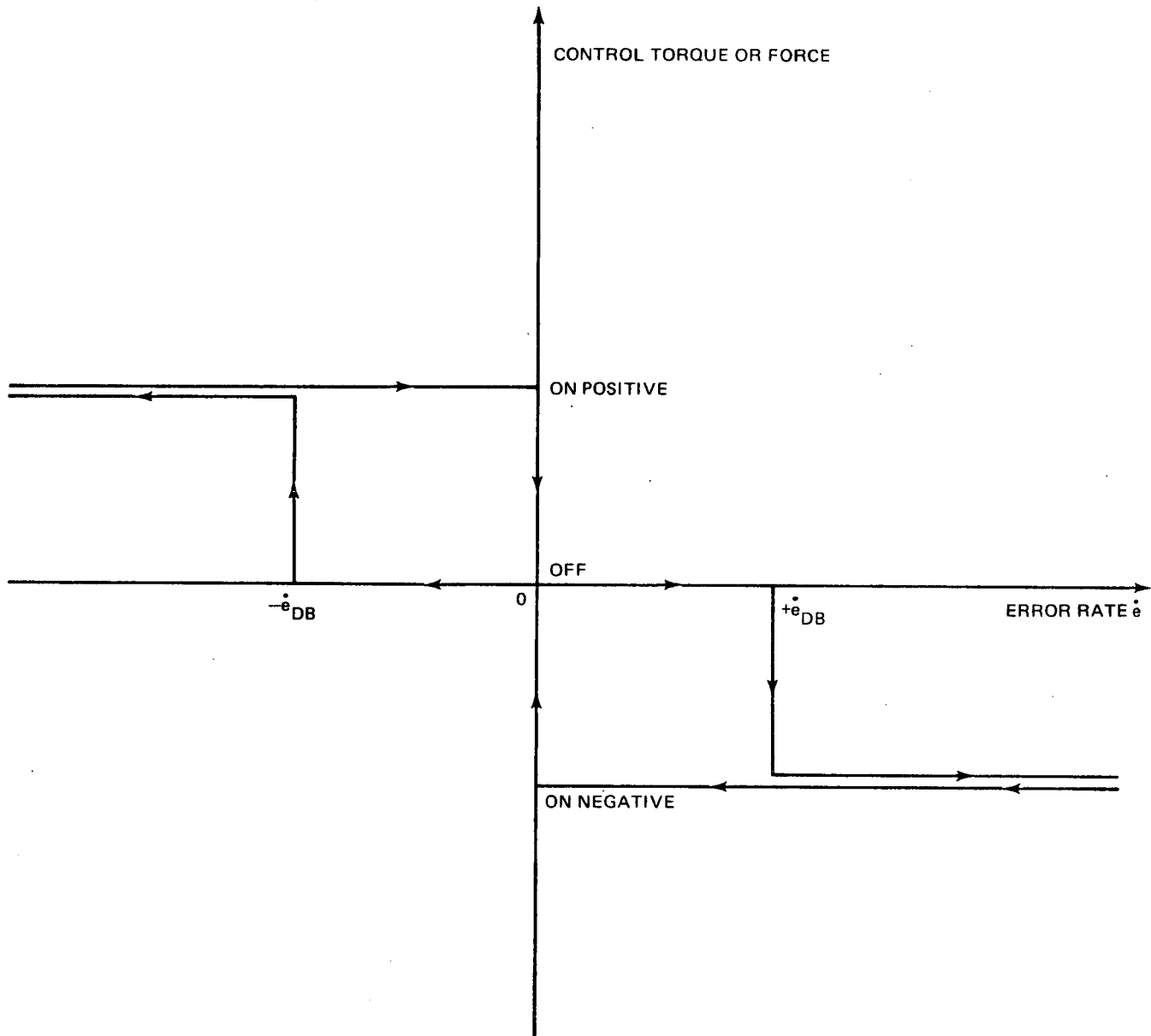


Fig. 5.7 Velocity Control

5.4.3 Elevator Position Control

The elevator acceleration, velocity, and position relative to the Laboratory are equated to the commanded elevator acceleration, velocity, and position, respectively.

5.4.4 Wobble Damping

Wobble damping of the Space Station is achieved by use of a single-gimbal control moment gyro (CMG). The CMG gimbal axis is parallel to the Space Station spin axis. The gimbal angle is measured positive counterclockwise relative to Laboratory axis 3 in the rigid-vehicle notation. The CMG momentum vector is located in the vehicle transverse plane at an angle 90° less than the gimbal angle. The angle of the Space Station angular rate vector component in the transverse plane is measured positive counterclockwise from Laboratory axis 2.

5.4.4.1 Gimbal Angle Command

The gimbal angle command law used is the highly effective 90° h-lag law. In this law, the CMG angular momentum vector is commanded to lag the Space Station angular velocity component in the transverse plane by 90° . For a discussion of the development and effectiveness of this law see the literature. (1)(2)

When the magnitude of the following quantity (which may be regarded as a measure of the wobble),

$$e_3 = 10 \left(\frac{1}{2} \left(M_{11}(2,2)\omega_2^2 + \frac{(M_{11}(1,1) - M_{11}(3,3)) M_{11}(3,3)\omega_3^2}{(M_{11}(1,1) - M_{11}(2,2))} \right) \right) \quad (5.1)$$

mom
CMG ω_1

-
- (1) Zetkov, G., Berman, H., Austin, F., Lidin, S., Markowitz, J., et al, "Study of Control Moment Gyroscope Applications to Space Base Wobble Damping and Attitude Control Systems," Grumman Aerospace Guidance and Control Rep. GCR-70-4, September 1970, prepared by Grumman Aerospace Corporation and Sperry Flight Systems Division.
- (2) Austin, F., and Berman, H., "Simple Approximations for Optimum Wobble Damping of Rotating Satellites Using a CMG," AIAA Journal, Vol. 10, No. 9, September 1972, pp 1160-1164.

D

where

$$\begin{aligned} M_{II} &\triangleq \text{vehicle moment of inertia} \\ \omega &\triangleq \text{vehicle angular velocity} \\ \text{mom}_{CMG} &\triangleq \text{momentum of CMG} \end{aligned}$$

becomes larger than 0.001 (0.01 in the flexible-vehicle idealization), the CMG is applied continuously to reduce wobble. The gimbal angle commanded is the angle of the transverse angular velocity vector minus 90° . When the magnitude of the quantity e_3 becomes less than 0.0001 (0.001 in the flexible-vehicle idealization), the CMG is commanded to apply zero control torque. That is, the gimbal is commanded to rotate negatively at a rate magnitude equal to the magnitude of the Laboratory spin rate. The limits on e_3 were lowered in the final routine supplied with the flexible-body program, because the command to apply zero torque would not occur during the flexible-body runs with the higher limits. The reason for this is that the flexible-system residual vibration influences ω_2 and ω_3 in Equation (5.1).

5.4.4.2 Gimbal Angle Control

A block diagram of the gimbal angle control system is shown in Figure 5.8. The difference err_g between the commanded and actual gimbal angle is processed in the shortest path logic unit to compute the shortest route to drive the gimbal angle towards the commanded gimbal angle. For example, referring to Figure 5.9, the desired gimbal angle rotates positively for the configuration under investigation in which the Space Station spin axis inertia is larger than either of the transverse inertias. In the case shown, it is faster to rotate the gimbal clockwise (negatively) than to rotate counterclockwise (positively). The error, $\beta_{DES} - \beta$, however, is positive; without the shortest path logic unit, the gimbal would be driven counterclockwise along the longer route.

The output signal of the shortest path logic is multiplied by the gain K_T . The result is passed through the lead-lag filter $(1 + as)/s$. The output of the filter is added to the computed signal tq_{PASS} . The computed signal tq_{PASS} is used to compensate for the torque on the Laboratory resulting from the interaction of the CMG moment of momentum with the Laboratory transverse angular rates. This torque on the Laboratory is shown at point A of Figure 5.8.

Fig. 5.8 CMG Gimbal Angle Control System

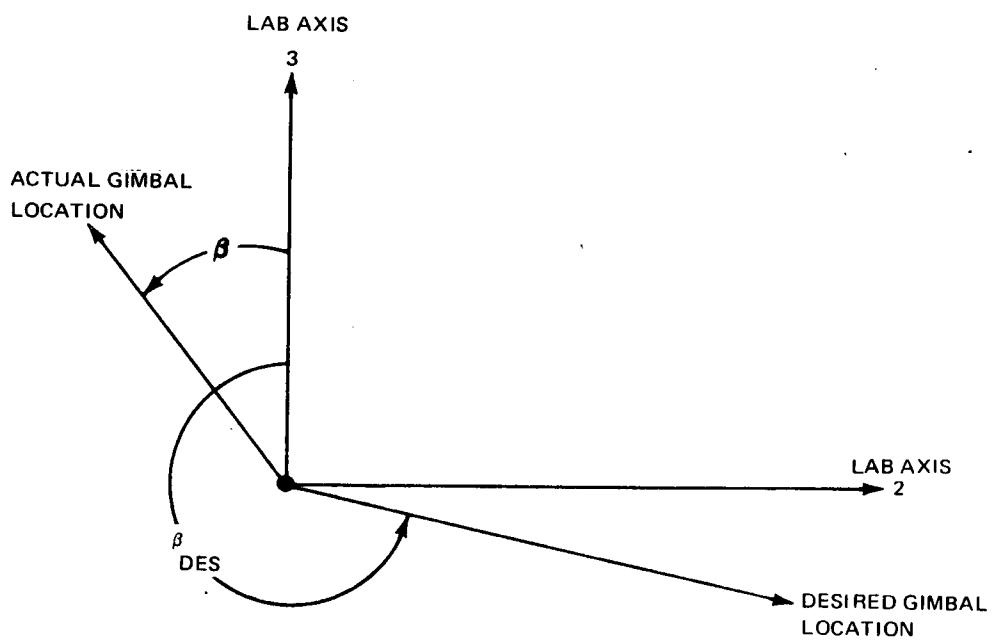
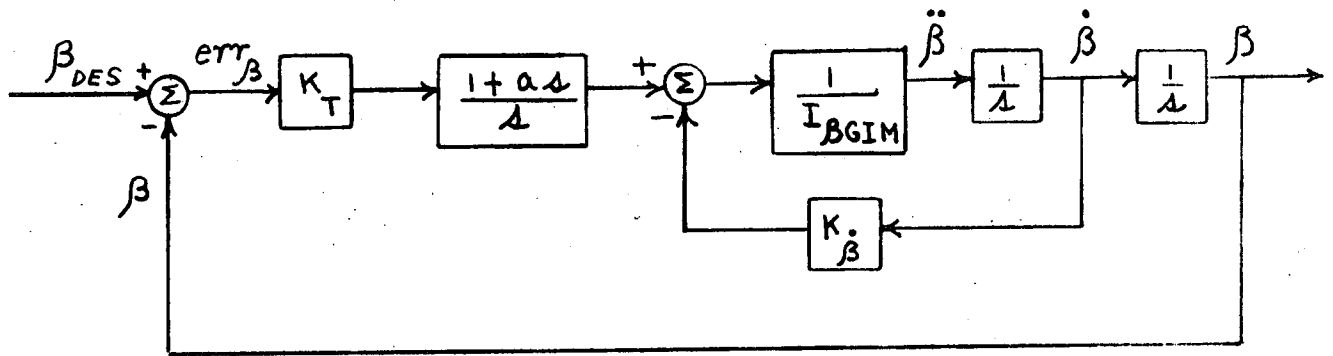


Fig. 5.9 Case When Quicker Path for CMG Gimbal is Opposite from that Indicated by Error, ($\beta_{DES} - \beta$)

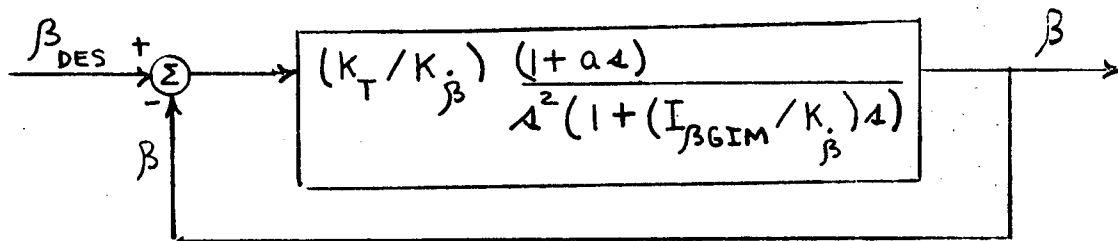
Motor torque saturation is simulated by the limiter. Electromotive feedback in the motor is modeled by the signal tq_{FDBK} , which is proportional to gimbal rate. The total torque on the gimbal tq_{GIM} is divided by the gimbal plus transverse wheel inertia $I_{\beta GIM}$ to obtain the gimbal acceleration relative to space, $\ddot{\beta}_p + \dot{\omega}_1$. The gimbal acceleration relative to the Laboratory is obtained by subtracting out the Laboratory acceleration $\dot{\omega}_1$ (one iteration ago). The gimbal acceleration is then integrated twice to obtain the gimbal angle.

5.4.4.3 Analysis of Gimbal Angle Control System

The basic gimbal angle control system is shown in the figure below. The shortest path logic unit, the torquer saturation, the subtraction of $\dot{\omega}_1$ from $\ddot{\beta}_p$, the disturbance torque tq_{PASS} , and the compensation signal for tq_{PASS} are omitted in this figure.



Replacing the inner loop with $\left[1/K_{\dot{\beta}}\right] \left[1/(1 + (I_{\beta GIM}/K_{\dot{\beta}})s)\right]$ and simplifying, the diagram reduces to that shown below.



The parameters are set as follows:

$$K_{\dot{\beta}} = 2 I_{\beta \text{GIM}}$$

$$a = 10 I_{\beta \text{GIM}} / K_{\dot{\beta}}$$

Also $K_T = 0.15 [K_{\dot{\beta}}^3 / I_{\beta \text{GIM}}^2]$

$$t_{q \text{ LIM}} = K_{\dot{\beta}}$$

The frequencies are as follows and, using the above equations for the parameters, the frequencies have the indicated numerical values:

inner loop: $\omega = K_{\dot{\beta}} / I_{\beta \text{GIM}} = 2 \text{ rad/sec}$

compensation filter: $\omega = 1/a = K_{\dot{\beta}} / 10 I_{\beta \text{GIM}} = .2 \text{ rad/sec}$

overall system: $\omega \cong \sqrt{1.5} K_{\dot{\beta}} / I_{\beta \text{GIM}} = 2.45 \text{ rad/sec}$

5.4.4.4 Gimbal Angle Rate Control System

To apply zero control torque to the Space Station, a switch is made from gimbal angle to gimbal angle rate control, and the gimbal angle rate commanded is the negative of the spin rate. A block diagram of the gimbal angle rate control system is shown in Figure 5.10. The difference $\text{err}_{\dot{\beta}}$ between the commanded and actual gimbal angle rate is multiplied by K_T . The result is passed through the filter $(1 + as)/s$. The output of the filter err_{LL} is integrated to generate err_{LLI} . The computed signal $t_{q \text{ PASS}}$, which is subtracted from err_{LLI} , is used to compensate for the torque on the Laboratory resulting from the interaction of the CMG moment of momentum with the Laboratory transverse angular rates (this torque is shown at point A of Figure 5.10).

Motor torque saturation is simulated by the limiter. Electromotive feedback in the motor is modeled by the signal $t_{q \text{ FDBK}}$, which is proportional to gimbal rate. The total torque on the gimbal $t_{q \text{ GIM}}$ is divided by the gimbal inertia $I_{\beta \text{GIM}}$ to obtain the gimbal acceleration relative to space, $\ddot{\theta}_P + \dot{\omega}_1$. The gimbal acceleration relative to the Laboratory is obtained by subtracting out the Laboratory acceleration $\dot{\omega}_1$ (one iteration ago). The gimbal acceleration is then integrated once to obtain the gimbal angle rate.

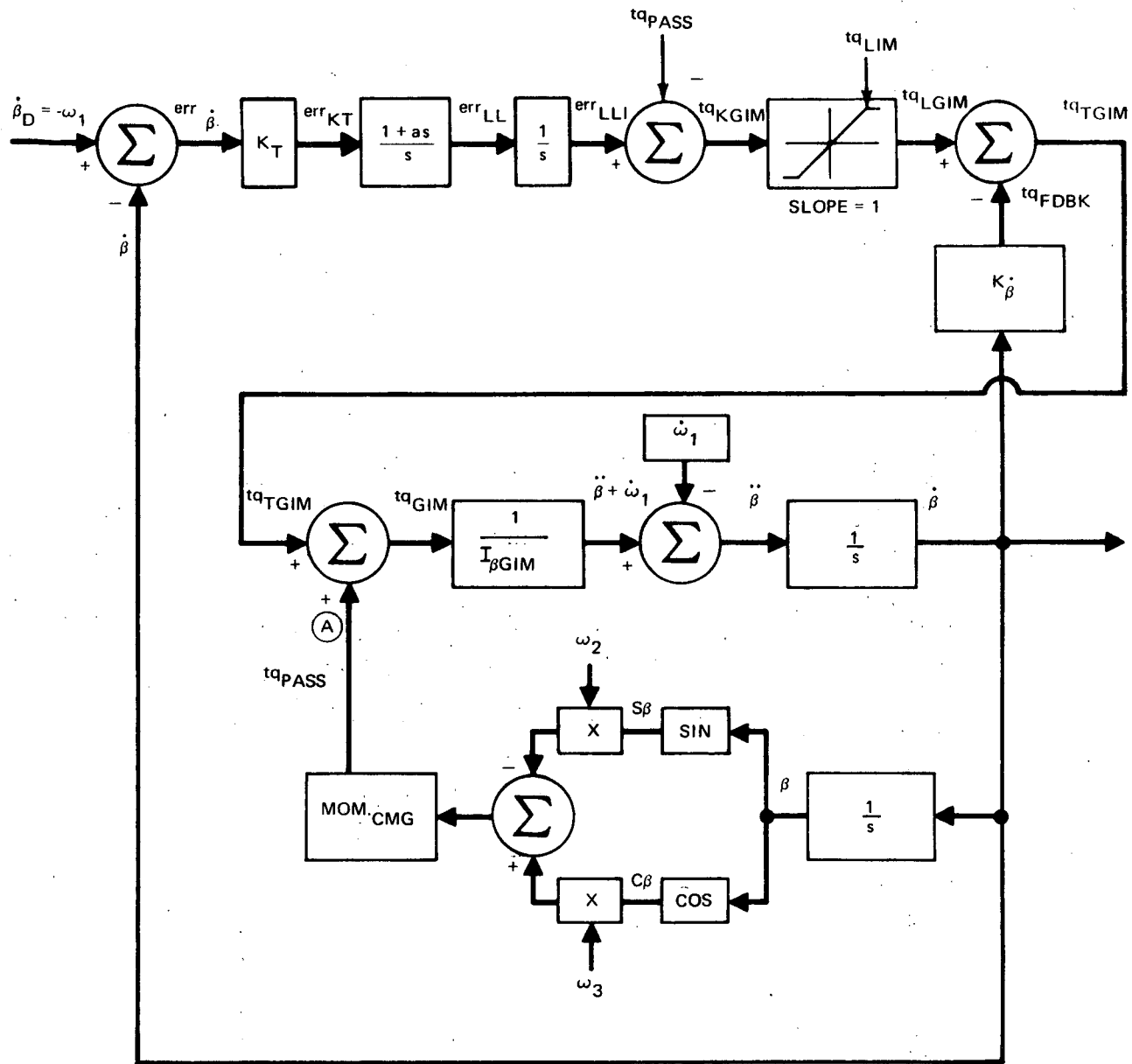
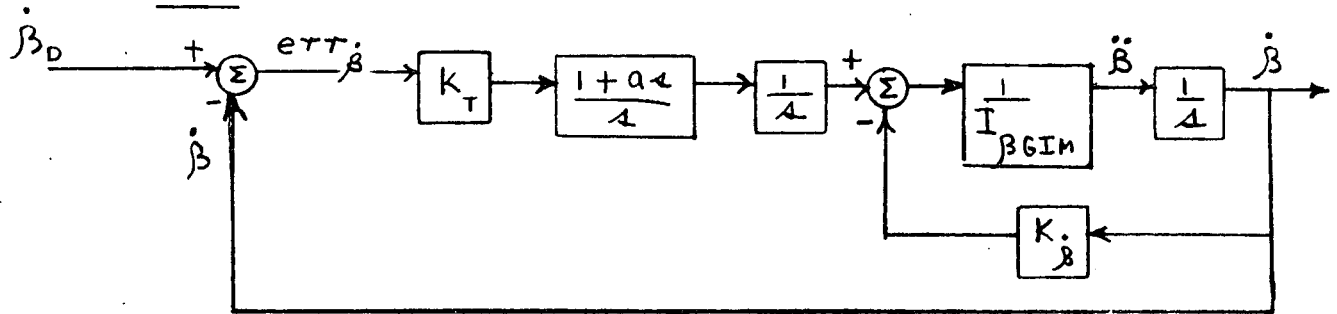


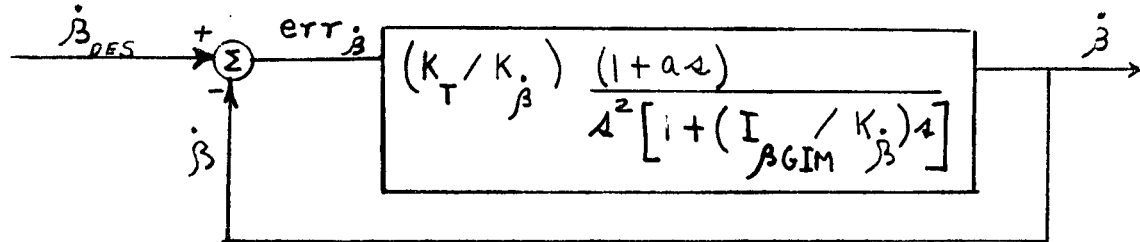
Fig. 5.10 CMG Gimbal Angle Rate Control System

5.4.4.5 Analysis of Gimbal Angle Rate Control

The basic gimbal angle rate control system is shown below.



Replacing the inner loop with $\left(\frac{1}{K_{\dot{\beta}}}\right) \left(\frac{1}{1 + \left(\frac{1}{I_{\beta GIM} K_{\dot{\beta}}}\right)s}\right)$ and simplifying, the diagram reduces to that shown below.



This diagram is the same as that in Section 5.4.4.3 for gimbal angle control. Thus, the dynamics of gimbal angle rate control are the same as those of gimbal angle control. The formulas for the parameters $K_{\dot{\beta}}$, a , and K_T and the frequencies $\omega_{\text{inner loop}}$, ω_{filter} , and ω_{overall} given in the section on gimbal angle control apply also to gimbal angle rate control. When $I_{\beta GIM}$, $K_{\dot{\beta}}$, t_{q_LIM} , mom_{CMG} , and K_T are inserted as input data and the parameter a is computed in the subroutine WBLCTR, these values are suitable for both gimbal angle and angle-rate control.

5.4.5 Mass Balance Control

The balance mass control system designed for the rigid-vehicle idealization required modification to operate properly on the flexible-vehicle idealization. First, the rigid-vehicle control system will be discussed; then, the required modifications for operation on the flexible-vehicle will be described.

5.4.5.1 Mass Balance Control on Rigid-Vehicle Idealization

The location of the Space Station center of mass is maintained at a desired point by use of a balance mass. As the location of the elevator (mass number 1) inside the Laboratory is changed, the location of the balance mass is automatically changed to compensate for the displacement of the elevator. The removal of mass from the Laboratory and its deposit into the elevator is not simulated. The position of the elevator is assumed known. The weight of the loaded elevator is estimated, the estimate being approximately the geometric mean between the weights of the unloaded and maximum-loaded elevator. A block diagram of the center of mass position control system is shown in Figure 5.11.

The center of mass position command is formed by summing the mass-distance moments of the Counterweight, elevator, and balance mass and dividing by the total station mass, thus

$$\{X^{CMND}\} = \frac{1}{M} \left(M_B \{X^B\}_{EXTENDED} + m_1 \{X^{(1)}\}_{NOM} + m_2 \{X^{(2)}\}_{NOM} \right) \quad (5.2)$$

The position of the accelerometer sensor $\{X^{SENS}\}$ is compared with the Space Station center of mass position command $\{X^{CMND}\}$, the difference being used to compute the acceleration commanded to be sensed by the accelerometer along Laboratory axis 3, $\ddot{X}^{CMND}(3)$. The commanded and sensed accelerations are compared, resulting in the error $err_{\ddot{X}}$, which in turn is multiplied by the fixed gain K_{eXSE} to obtain the balance mass velocity command \dot{X}_{23C} along Laboratory axis 3. The commanded and actual velocities of the balance mass are compared, and the difference $e_{\dot{X}23}$ is processed in the subroutine VELCTR to obtain the commanded acceleration of the balance mass along Laboratory axis 3. The actual acceleration of the balance mass is assumed to be equal to the commanded acceleration. The acceleration is integrated twice to obtain the position of the balance mass, which in turn is an input into the computation of the actual position of the Space Station center of mass, $\{X^C\}$. This position $\{X^C\}$ and the accelerometer location $\{X^{SENS}\}$ affect the value of the accelerometer measurement $\ddot{X}_{SENS}(3)$ along Laboratory axis 3.

5.4.5.2 Mass Balance Control on Flexible-Vehicle Idealization

When the control system described in Section 5.4.5.1 was operated on the flexible-vehicle idealization, a limit-cycle vibration of the Laboratory was

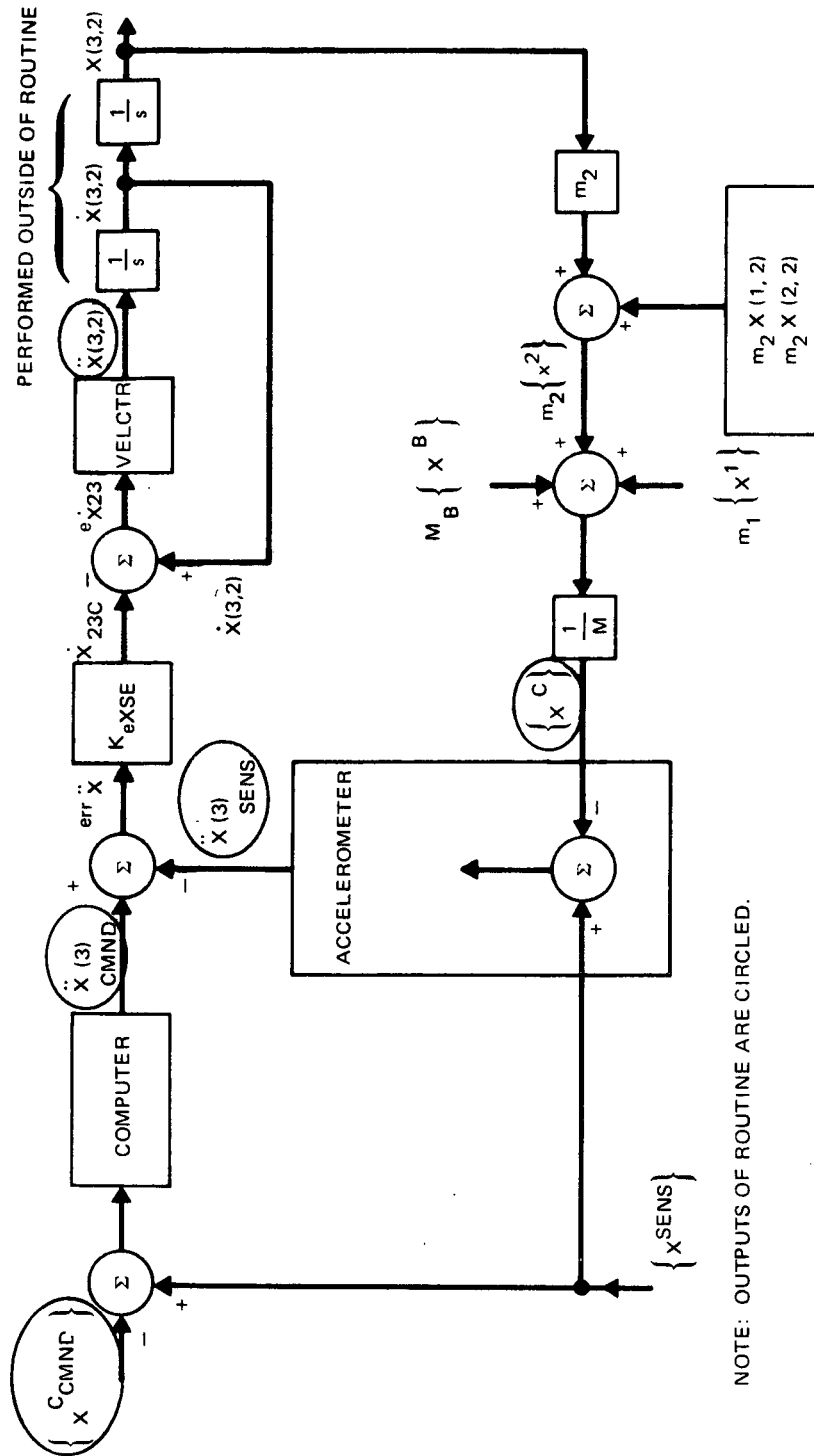


Fig. 5.11 Space Station Center of Mass Position Control System for Rigid Vehicle Idealization

induced (see Section 6.2.6). This caused the balance mass to chatter at a relatively high structural frequency. Its long term motion appeared to be either neutrally stable or slightly unstable. At any rate, it did not balance the elevator motion. For this reason, and also because many of the rigid-vehicle dynamics relations were deleted from the control law, the control system was modified extensively.

The control system for the flexible vehicle idealization is shown in Figure 5.12. The acceleration commanded at the accelerometer in the 3 direction $\ddot{x}^{CMND}(3)$ is generated in a similar way as in the rigid-body program. The sensed angular velocity, angular acceleration, and the commanded distance from the center of mass to the accelerometer are fed into a computer which computes $\ddot{x}^{CMND}(3)$ by using an equation which assumes the Space Station is rigid and in balance. The commanded distance from the center of mass to the accelerometer is a constant and is input data to the program. This distance includes the elastic stretching of the vehicle due to centrifugal forces. The commanded and sensed accelerations are subtracted to form $err_{\ddot{x}}$ which may be filtered to form e_{FILT} . This filtering was used before any other modifications were made; however, it was not helpful in achieving proper control. The filter remains in the program although it was bypassed in the demonstration runs by setting $\tau_{BAL} = 0$. The balance mass acceleration is assumed to be given by the following relation:

$$\ddot{x}^{(i)}(3, 2) = -K_{DESE} \dot{x}^{(i)}(3, 2) + K_{eXSE} e_{FILT} \quad (5.3)$$

This relation provides a smooth build-up of acceleration. It replaces the on-off VELCTR policy which was used in the rigid-vehicle mass balance control law. As seen in Section 6.2.6, the revised control law operated properly on the flexible-vehicle idealization.

5.5 DEMONSTRATION RUNS ON RIGID-VEHICLE IDEALIZATION

Six types of runs were established to demonstrate the operation of the Space Station control systems: (1) zero-g attitude control, (2) spin rate hold during Counterweight deployment, (3) spin-up, (4) Space Station center of mass position control during elevator operation, (5) wobble damping, and

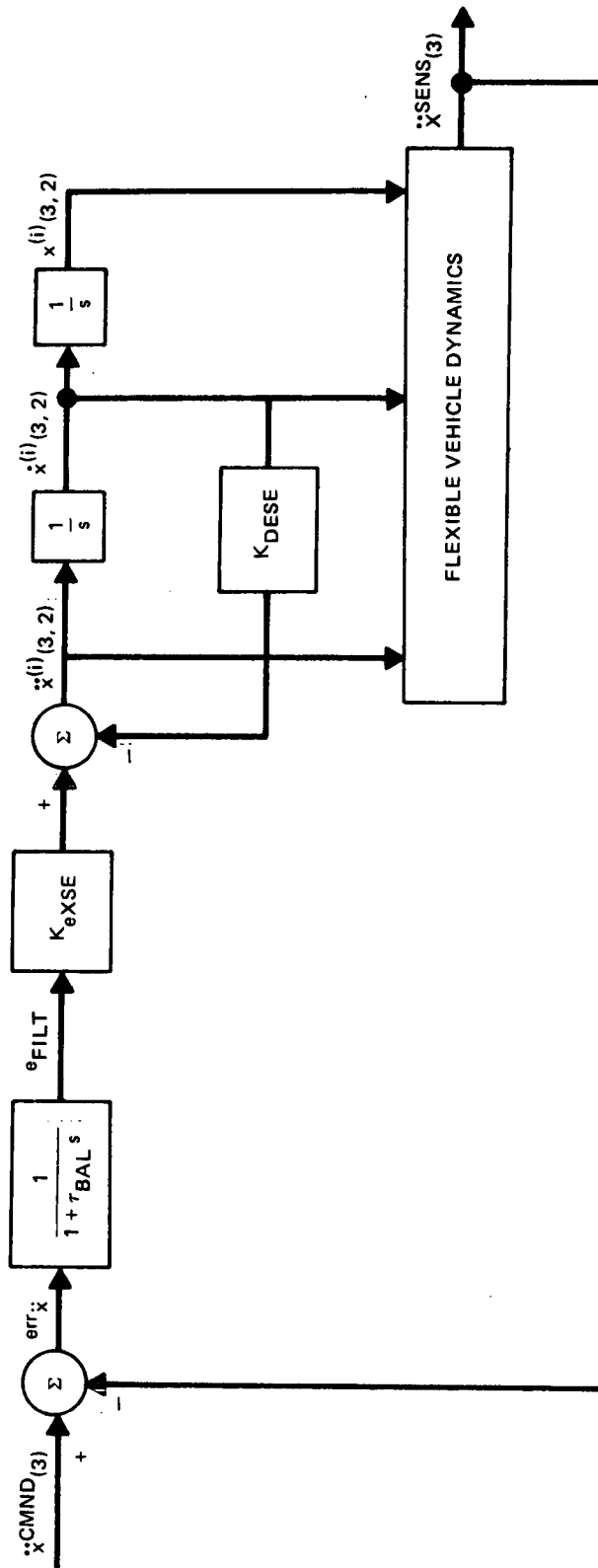


Fig. 5.12 Space-Station Center-of-Mass Position Control System for Flexible Vehicle Idealization

(6) simultaneous center of mass position control and wobble control. The Space Station parameter values used in each type of run were the same. The input data for all runs is tabulated in Appendix K.

5.5.1 Attitude Control

Run 10

Run 10 demonstrates attitude control. Initial errors in attitude were used to test for convergence to the desired state of zero Euler angles.

Description of Run 10

As shown in plots 1 to 3 of Run 10, Figure 5.13, there is an error of $0.0175 \text{ rad } (1^\circ)$ in all 3 Euler angles at time = 0. These errors are reduced to values near 0 in approximately minimum time. Error reduction is faster about axis 2 than about axis 1, because (1) the inertia of $14.104651 \times 10^6 \text{ kg} \cdot \text{m}^2$ about axis 2 is less than the inertia of $17.7912 \times 10^6 \text{ kg} \cdot \text{m}^2$ about axis 1 and (2) the average moment arm for axes 1 and 2 is the same, 4.572 m (15 feet). Error reduction about axis 3 is faster than about axes 1 and 2, because--even though the average moment arm of 1.8288 m (6 feet) for axis 3 is less than the average moment arm of 4.572 m (15 feet) for axes 1 and 2 -- the inertia of $3.820159 \times 10^6 \text{ kg} \cdot \text{m}^2$ about axis 3 is much less than the inertias of 17.7912×10^6 and $14.104691 \times 10^6 \text{ kg} \cdot \text{m}^2$ about axes 1 and 2, respectively. From the printout (not shown), the errors in the Euler angles at time = 100 seconds are $+0.1505 \times 10^{-3}$, 0.1510×10^{-3} , and -0.1283×10^{-3} radian about axes 1, 2, and 3, respectively.

As shown in plots 4 to 6, Figure 5.14, torques are applied by the 222.4 N (50 pound) thrust jets (2 jets for each polarity, 4 jets for each of 3 axes) to reduce the Euler angle errors to tolerable levels. Considering axis 1 at time = 0, $\theta_1 = 0.01745 \text{ rad}$ and $\dot{\theta}_1 = 0$; thus, the operating point in the phase plane of Figure 5.6 is located in the right shaded region on the line + e, to the right of $+e_{\theta DB} = 0.0001745 \text{ rad}$; thus, negative torque is commanded. Referring to Plot 4 of Figure 5.14, the torque initially is negative as called for. Between time = 0 and 12.3 sec, the trajectory of the operating point in the phase plane of Figure 5.6 is downward and to the left until it meets the curved parabolic portion of the switching curve (note: in this case, the parabolic switching boundaries are flattened relative to those shown). From time = 12.3 to 12.5 sec, no torque is applied; and from time = 12.5 to 25.75 sec, positive torque is applied. With time, the duration times of torque application decrease, while the duration times for coast increase, until stable limit cycle operation is achieved.

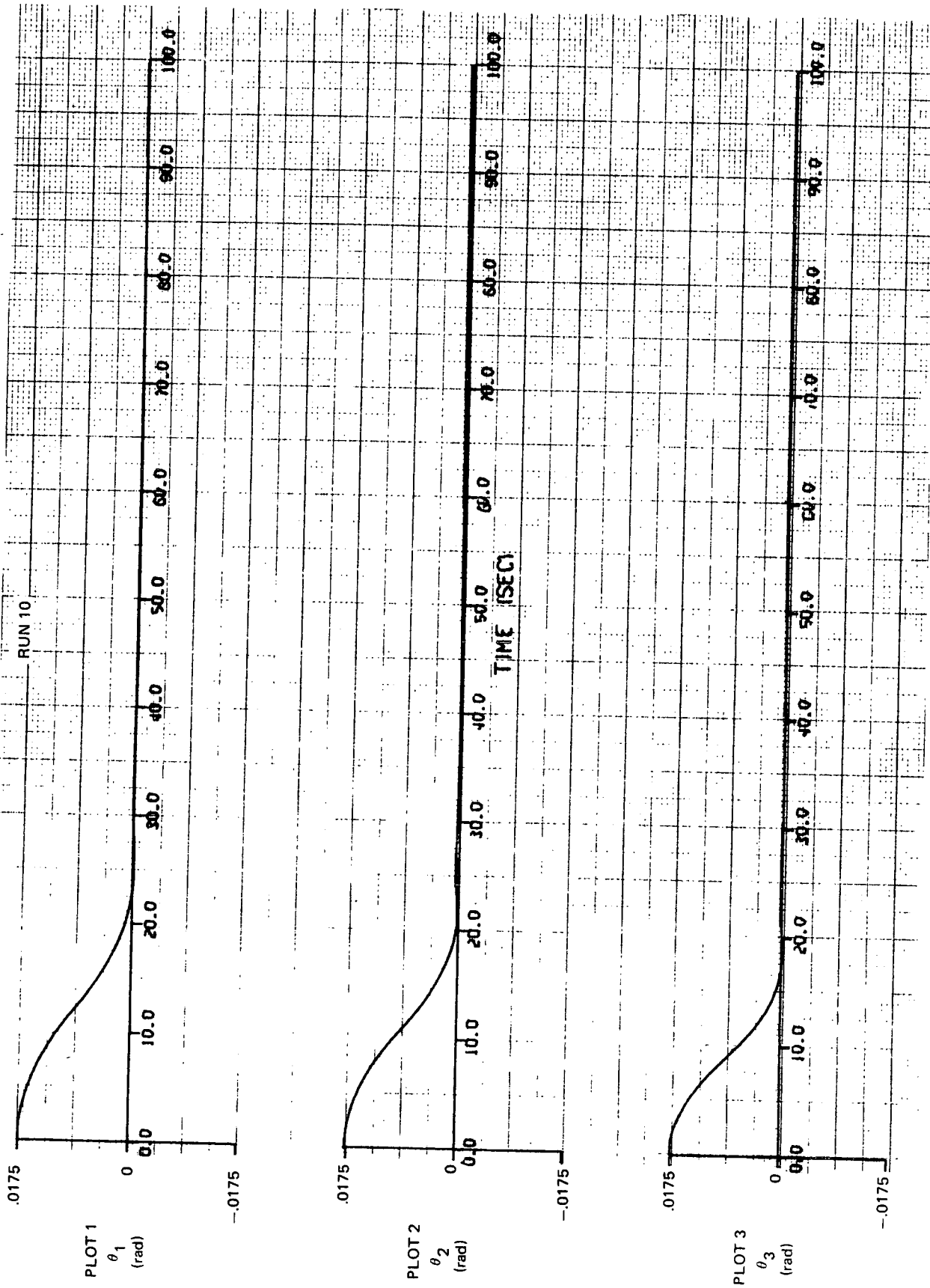


Fig. 5.13 Attitude Control: Errors in Euler Angles

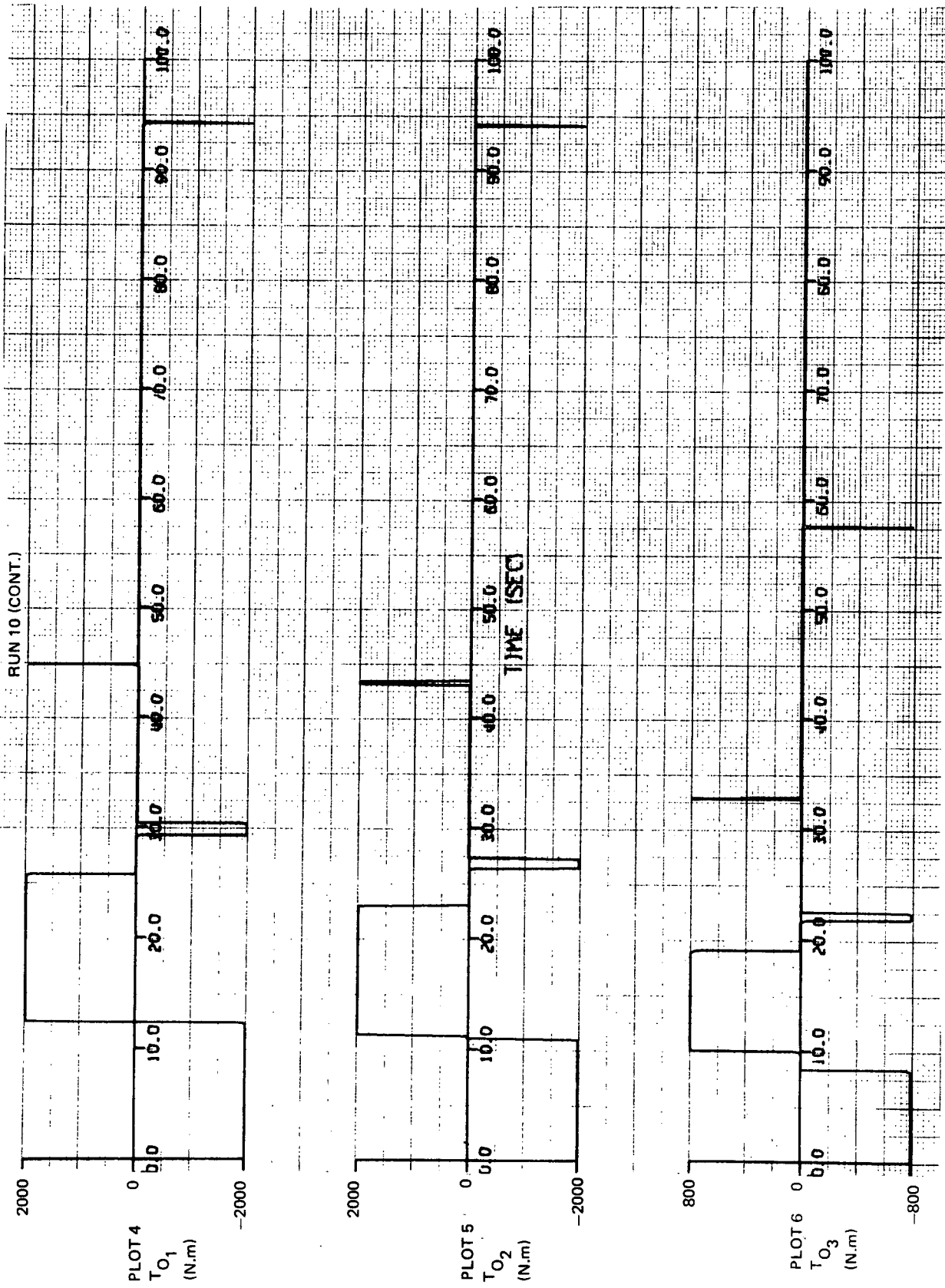


Fig. 5.14 Attitude Control: Control Torques Applied to Vehicle by Jets

5.5.2 Spin Rate Hold During Counterweight Deployment

Run 21

Run 21 demonstrates the control of the Counterweight as it is moved from its retracted to its deployed position and the control of spin rate while the Counterweight is in motion. The initial spin rate is 0.2 RPM. Five seconds after the run begins, the deployment of the Counterweight begins. The complete deployment is simulated.

Description of Run 21

As shown in Run 21, Plot 1, of Figure 5.15, the acceleration of the Counterweight relative to Laboratory axis 3 is -30.48 mm/sec^2 (-0.1 ft/sec^2) from time = 5 to 7 seconds and $+30.48 \text{ mm/sec}^2$ from time = 667 to 669 sec. Plot 2 shows the Counterweight velocity along Laboratory axis 3 increasing negatively to -60.96 mm/sec from time = 5 to 7 seconds, constant at -60.96 mm/sec from time = 7 to 667 seconds, and going to zero from time = 667 to 669 seconds. Plot 3 shows the Counterweight position along Laboratory axis 3 at -23.99 m from time = 0 to 5 seconds, increasing negatively from -23.99 to -66.81 m from time = 5 to 669 seconds, and essentially constant at -66.81 m from time = 669 to 800 seconds.

Plot 4 of Figure 5.16 shows the spin rate error at 0 from time = 0 to 5 seconds. Limit cycling occurs from time = 5 to 712 seconds. The cycle consists of the spin rate first increasing negatively to -0.00021 rad/sec (equals the deadband) as a result of the Counterweight motion and then going to zero as a result of the combined effect of the Counterweight motion and jet control torque. From time = 712 to 800 seconds, the spin rate error increases negatively at a low rate ($7.4 \times 10^{-8} \text{ rad/sec}^2$) as the result of a small residual creepage of the Counterweight ($1.9 \times 10^{-4} \text{ m/sec}$). Plot 5 shows the spin acceleration equals 0 from time = 0 to 5 seconds, increases negatively to $-0.000067 \text{ rad/sec}^2$ as the Counterweight accelerates, is constant at $-0.000067 \text{ rad/sec}^2$ as the Counterweight travels at constant velocity, and then jumps to $+0.000158 \text{ rad/sec}^2$ as a result of the combined effect of the jet control torque and Counterweight motion. Subsequently, the spin acceleration oscillates between two values: the positive value corresponding to the combined effect of the jet control torque and constant

RUN 21

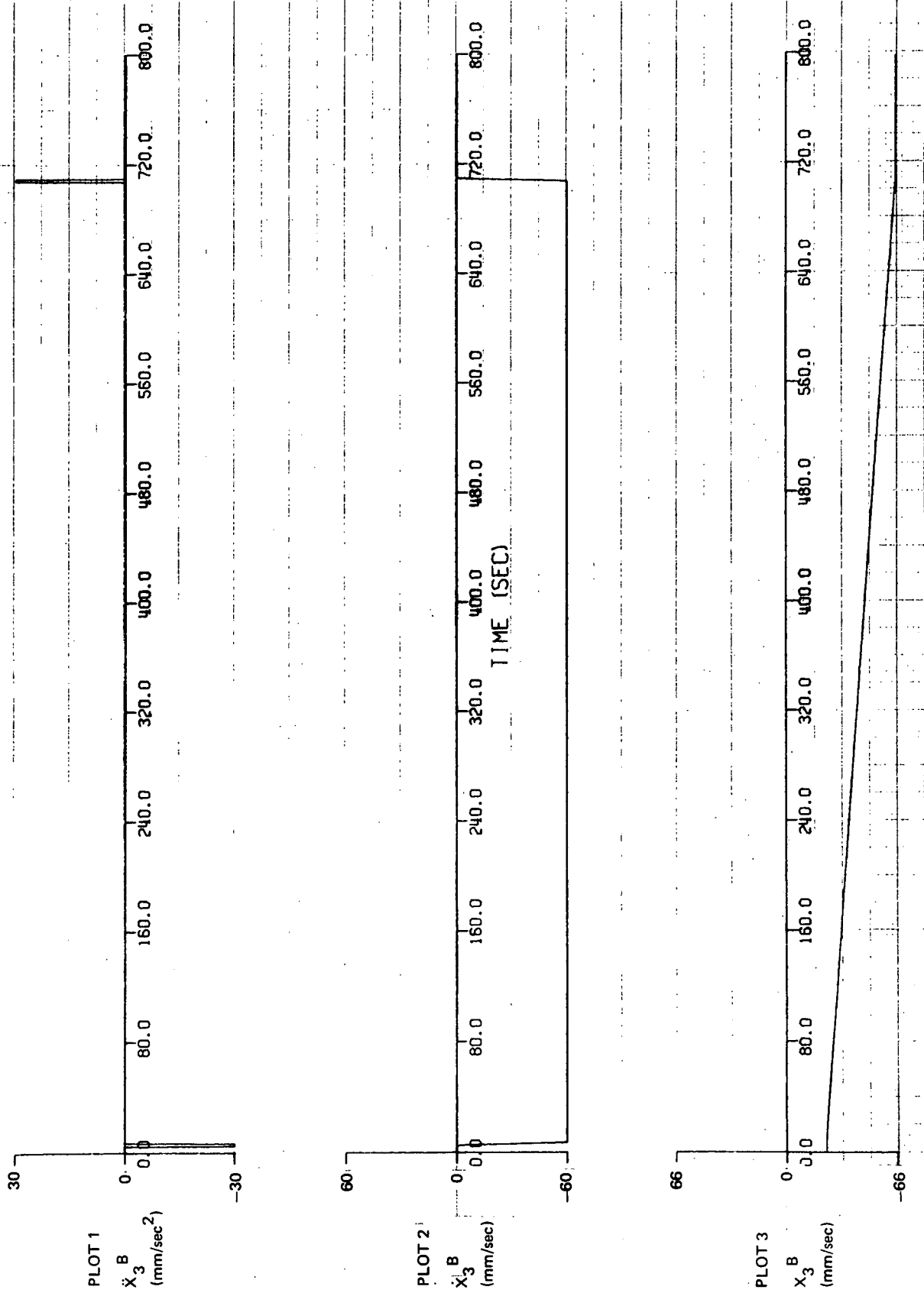


Fig. 5.15 Counterweight Deployment: Counterweight Acceleration, Velocity, and Position Relative to Laboratory

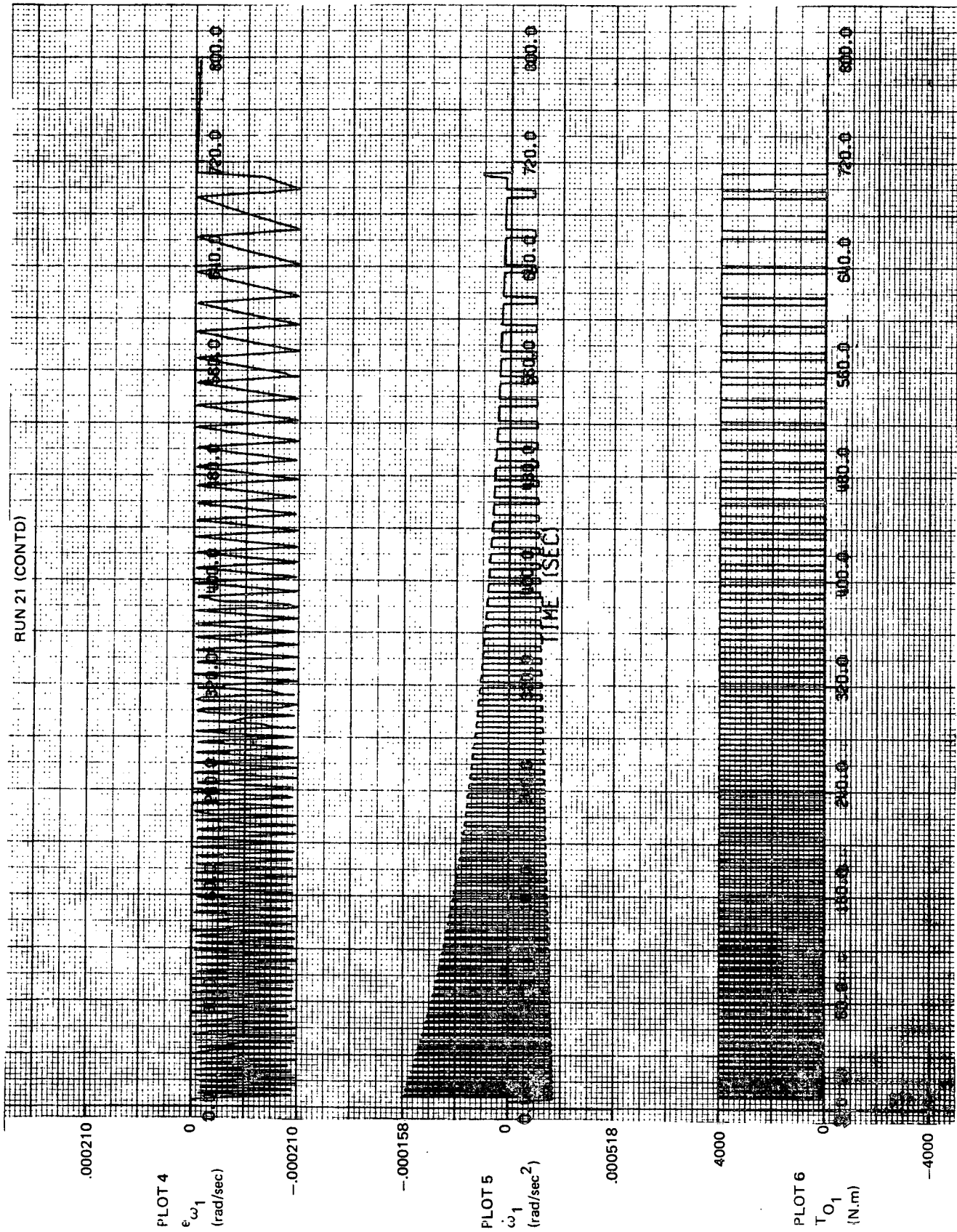


Fig. 5.16 Counterweight Deployment: Spin Rate Error, Spin Acceleration, and Control Torque Applied to Vehicle by Jets

Counterweight velocity and the negative value corresponding to the effect of the constant Counterweight velocity. As the inertia of the Space Station increases, both the spin deceleration resulting from constant Counterweight velocity and the spin acceleration resulting from the applied jet control torque decrease in magnitude. Thus, both the high and low values of the oscillation decrease in magnitude with time. From time = 708 to 710 seconds, the spin acceleration increases from 0.0000079 to 0.000044 rad/sec², as the counterweight decelerates to a stop. From time = 710 to 712 seconds, the jet control torque continues to be applied until the spin rate error is nulled, at which point the jet control torque is removed, and the spin acceleration essentially remains at zero. The period of each cycle gradually increases, because the magnitude of spin acceleration decreases both on the positive and negative side while the spin rate dead band remains constant. Plot 6 shows the jet control torque oscillating between the two levels 0 and 4067 N · m from time = 5 to 712 seconds. The jets turn on each time that the magnitude of the spin rate error becomes equal to the spin rate error dead band and turns off each time that the spin rate error has been reduced to zero.

5.5.3 Spin-Up

In these demonstration runs it was decided to investigate whether the Space Station could be controlled with all control-system components located only on the Laboratory. Accordingly, the moment arm between the spin jets was only 9.144 m. As a result, using four 222.4 N (50 pound) jets, it would take over five hours of real time to complete the spin-up maneuver. The first 50 seconds of the spin-up maneuver was simulated, and the control system operated properly. This run is not included herein. Instead, the following run is included which demonstrates a complete spin-up maneuver. The jet thrusts were increased by a factor of 100 in order to complete the run using an economical amount of computer time.

Run 31

Run 31 demonstrates the control of Space Station spin rate, as the spin rate is commanded to be increased from 0.2 RPM to 4 RPM. During the spin-up, the Counterweight is fully deployed at -66.81 m. By increasing the thrust level of each jet by a factor of 100 over the value of 222.4 N, each jet had in Run 21, the complete spin-up is simulated, but at a jet level 100 times more than desired.

Description of Run 31

As shown in Run 31, Plot 1 on Figure 5.17, the spin acceleration command is 0 from time = 0 to 5 seconds, $0.00427 \text{ rad/sec}^2$ from time = 5 to 98 seconds (100 times larger than in Run 30), and 0 thereafter. Plot 2 shows the spin rate command initially at 0.02094 rad/sec ; from time = 5 to 98 seconds, it climbs steadily toward 0.4189 rad/sec . The spin rate command then remains constant at 0.4189 rad/sec . Plot 3 shows the spin rate following the spin rate command of Plot 2.

The spin rate error (spin rate minus the spin rate command) is given in Plot 4 of Figure 5.18. From time = 5 to 5.05 seconds, the spin rate error grows negatively to -0.0002 rad/sec (the spin rate error dead band is 0.0002094). The error then immediately backs off to -0.00016 rad/sec . The back-off is physically impossible; this irregularity results from an error in integrating $\dot{\omega}_1$. That is, the 4-point Adams formula is used, without reverting to starting formulas. From time = 5.05 to 98 seconds, the error grows very slowly from -0.00016 to -0.00019 rad/sec . At time = 98 seconds, the spin rate command stops climbing. During the next 0.05 seconds, the jets remain on until the spin rate error is zeroed. Plot 5 shows the spin acceleration = 0 from time = 0 to 5.05 seconds. At time = 5.05 seconds, it jumps to $+0.00427 \text{ rad/sec}^2$, because the spin rate error exceeds its dead band and the jet control torque shown in Plot 6 is applied. From time = 5.05 to 98 seconds, the spin acceleration = $0.00427 \text{ rad/sec}^2$ as the jets remain on to increase the spin rate as commanded. At time = 98 seconds, the spin acceleration drops to zero, because the spin rate command has stopped climbing and the spin rate error has been nulled. Plot 6 shows the jet control torque. Its level of $406.7 \text{ kN} \cdot \text{m}$ is 100 times the nominal value of $4.067 \text{ kN} \cdot \text{m}$.

The printout data showed that the CMG gimbal angle rate at time = 0 is equal to the negative of the spin rate, i.e., -0.02094 rad/sec , and as the spin rate is increased from $+0.02094$ to $+0.4189 \text{ rad/sec}$, the gimbal angle rate goes from -0.02094 to -0.4189 rad/sec .

5.5.4 Mass Balance

Run 40

Run 40 demonstrates the control of the Space Station center of mass location, with the station spin rate at 4 RPM and initial wobble at zero. The

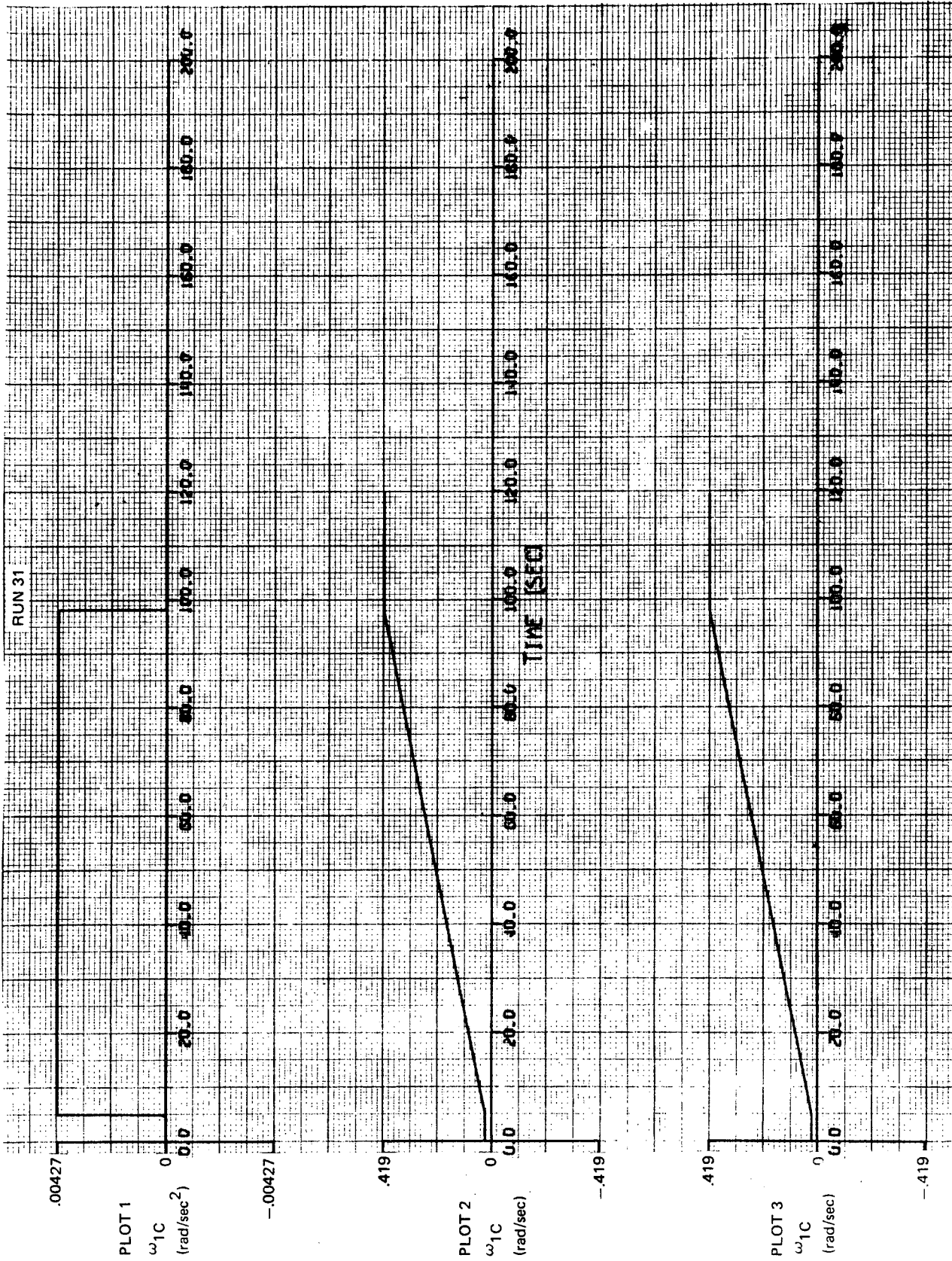


Fig. 5.17 Spin-Up: Spin Acceleration Command, Spin Rate Command, and Spin Rate

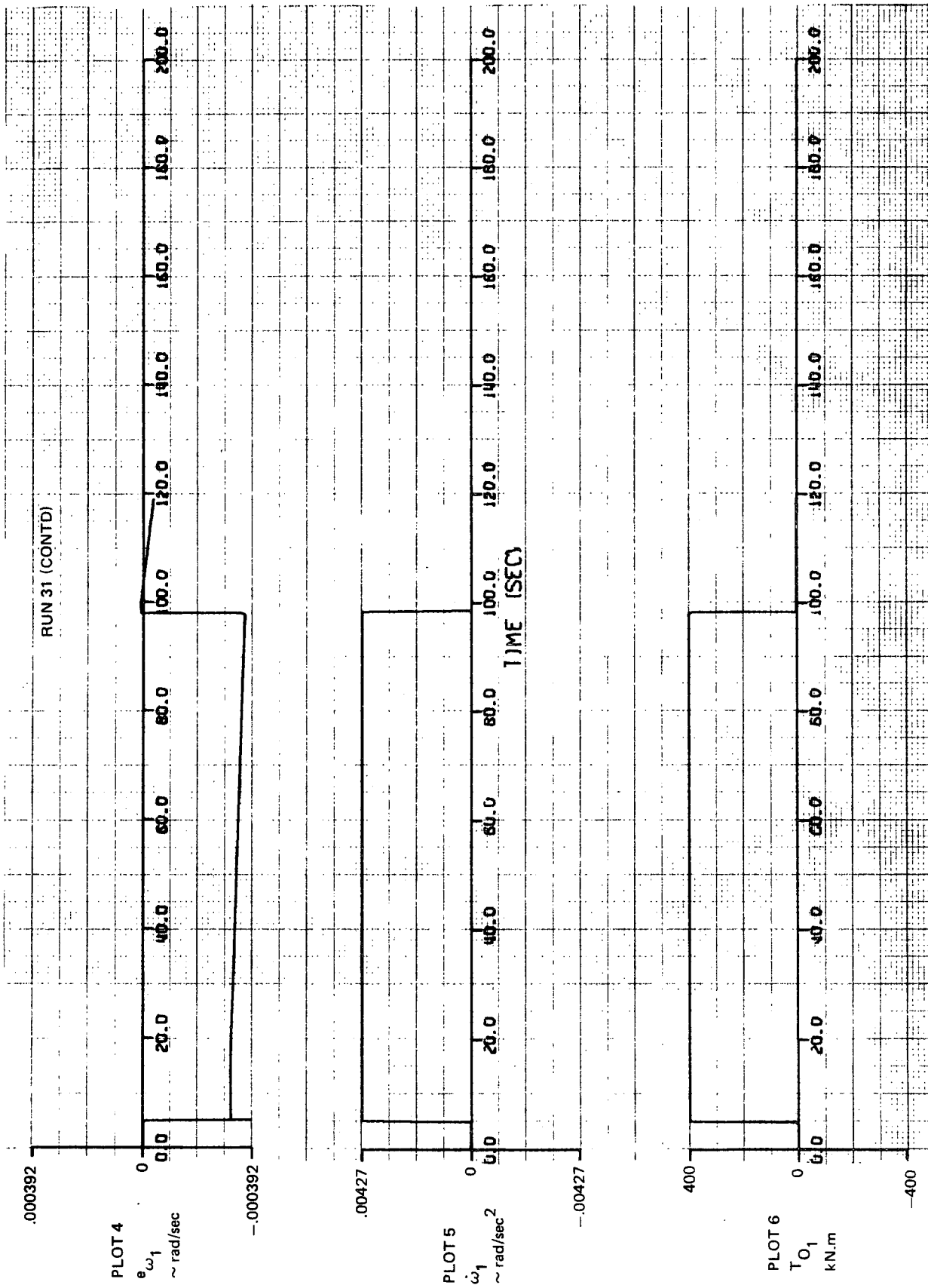


Fig. 5.18 Spin-Up: Spin Rate Error, Spin Acceleration, and Control Torque Applied to Vehicle by Jets

Counterweight location is fixed at its fully deployed position, -66.81 m. Initially, the location of the Space Station center of mass is at its desired position. Beginning at time = 5 seconds, the elevator is moved from 0 to 1.524 m (5 feet).

Description of Run 40

Mass balancing is shown in Run 40, Figures 5.19 and 5.20. Plot 1 shows the Space Station center of mass position command along Laboratory axis 3 to be constant at -26.912 m (exact value from the printout). Plot 2 shows the actual Space Station center of mass location along Laboratory axis 3 to be -26.9 m (the printout indicated that this location fluctuates by no more than ± 0.015 from -26.912 m during the run). Plot 3 shows that the sensor acceleration command for the accelerometer located at 4.654 m along Laboratory axis 3 is approximately -5.55 m/sec^2 or $-0.57g$ (it fluctuates between -5.557 and -5.517 m/sec^2 during the run). The acceleration commanded minus acceleration sensed, as given in Plot 4, shows the error jumping to $+0.001 \text{ m/sec}^2$ at time = 5 seconds when the elevator begins its motion. This error reverses polarity at time = 6.3 seconds and reaches a peak negative value of -0.0036 m/sec^2 at time = 12 seconds. At time = 20.6 seconds, a steady limit cycle is achieved with the maximum magnitude of error being 0.0002 m/sec^2 , or $1.87 \times 10^{-5}g$; thus a sensitive accelerometer is required.* The jumps in the error occur when there is a discontinuity in the acceleration of the elevator, as may be deduced by comparing Plot 6, elevator position, with Plot 4. The jump occurs in the accelerometer signal as a result of the jump in the acceleration of the elevator. The jump in the error signal could be softened by filtering the accelerometer output; one hypothetical result of inserting the filter is: the balance mass, shown in Plot 5, would, beginning at time = 5 sec, move in the wrong direction by a lesser amount than that shown. Plot 6 shows the elevator at 0 m until time = 5 seconds, when it begins to increase toward 1.524 m as commanded. At time = 19.25 seconds, the new desired location of 1.524 m has been reached. The elevator position then remains constant. The position of the balance mass shown in Plot 5 is 0 m initially and at time = 5 seconds starts driving in the wrong direction to a peak value of $+0.12$ m before

*An alternative is to increase the velocity error dead band. Successful balancing was achieved with the dead band increased from $.3 \text{ mm/sec}$ to 5 mm/sec . This eliminated the limit cycling entirely; however, the balance mass no longer responded to small elevator motions.

RUN 40

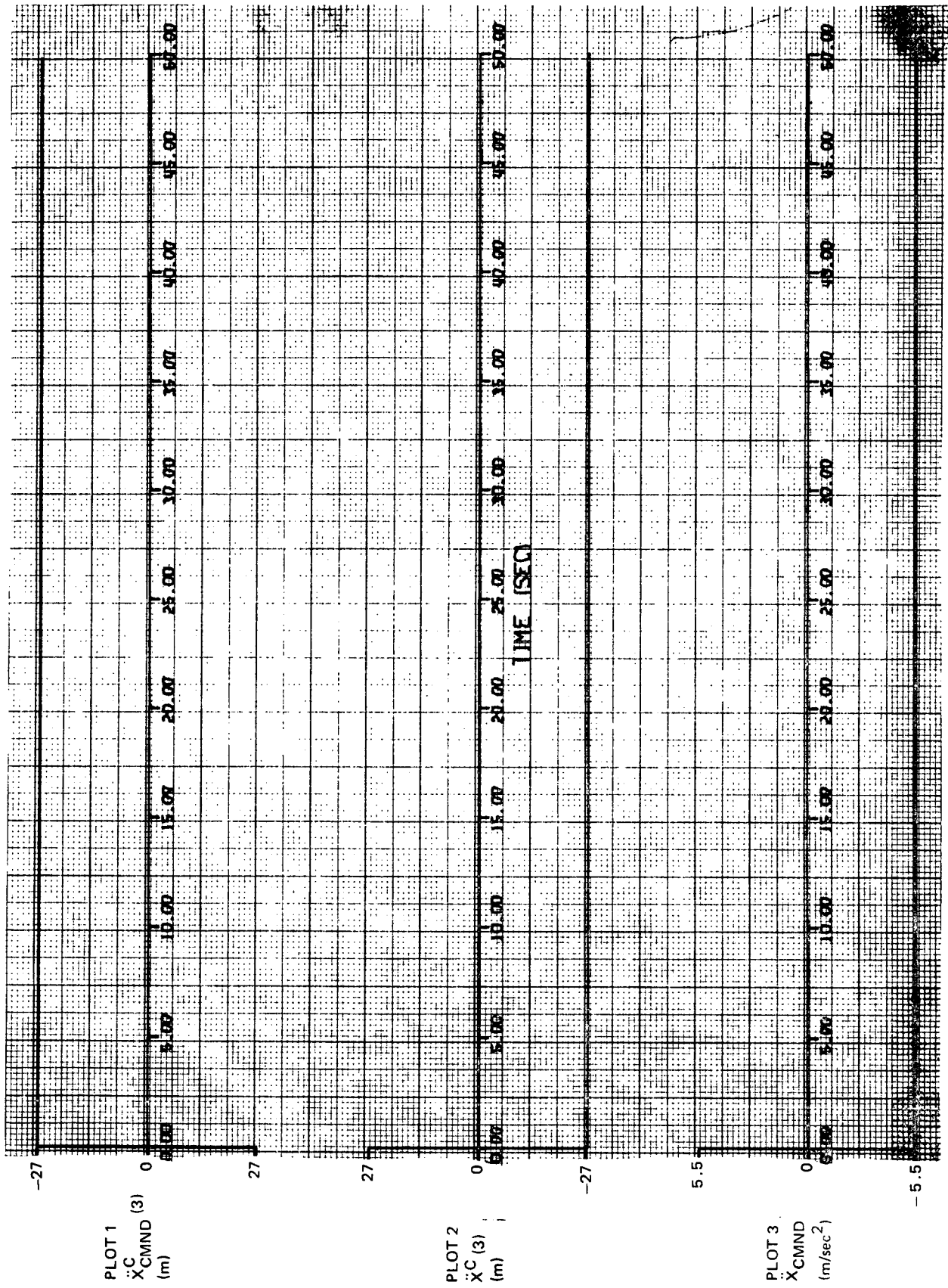


Fig. 5.19 Mass Balancing: CM Location Command, CM Location, and Sensor Acceleration Command

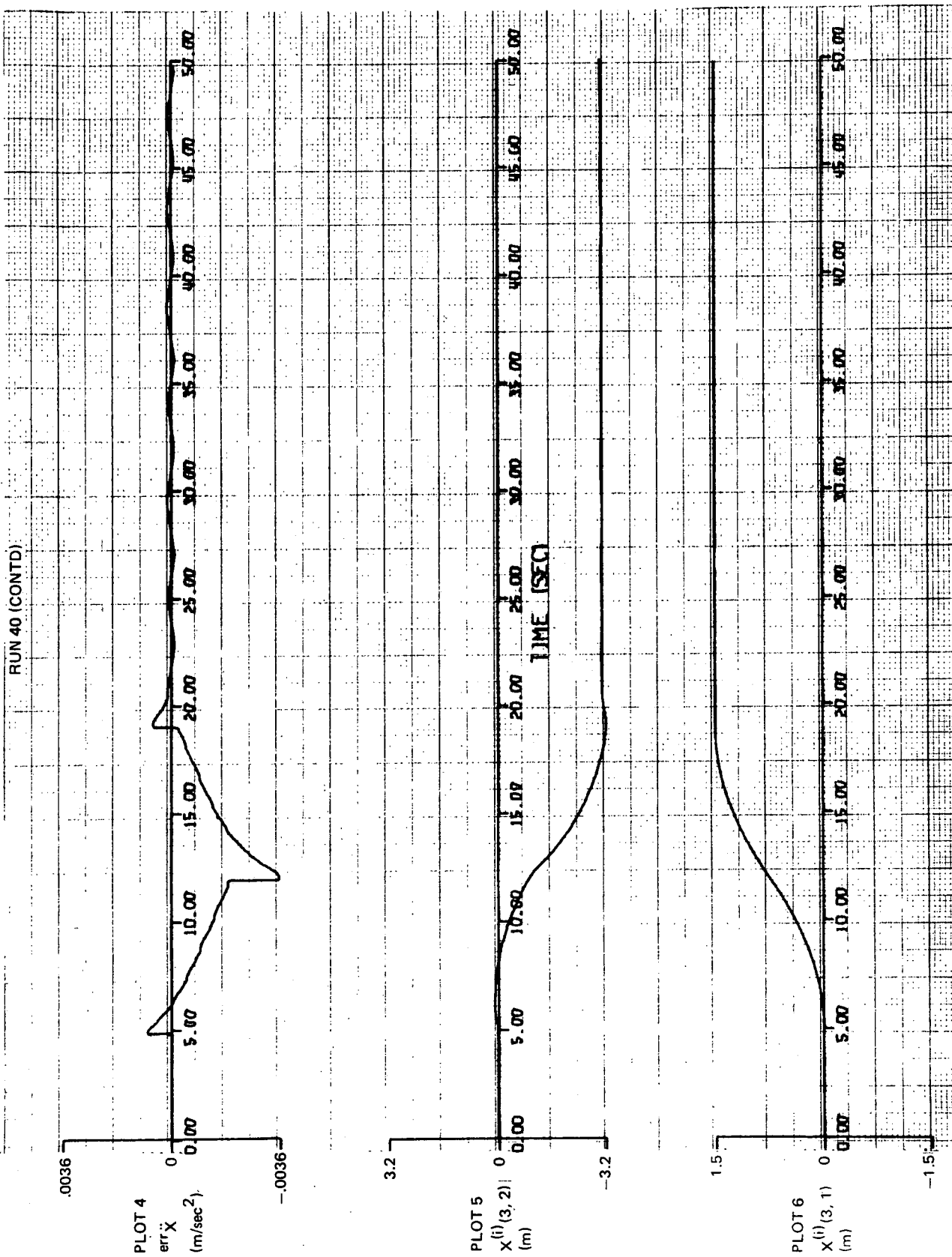


Fig. 5.20 Mass Balancing: Acceleration Commanded Minus Acceleration Sensed, and Positions of Balance Mass and Elevator

it moves toward negative values. At time = 20 seconds, the position of the balance mass has stabilized and from this time point on, remains between -3.018 and -3.078 m or ± 0.030 m from the required location of -3.048 m. The balance mass has generally moved in the opposite direction from that of the elevator and twice the distance, as it should since the balance mass of 2268 kg (5000 pounds) is half the elevator mass of 4536 kg. The estimate for the elevator mass used in the control system is 2268 kg.

5.5.5 Wobble Damping

Run 50

Run 50 demonstrates control of the Space Station wobble, for a Station spin rate of 4 RPM, an initial angular rate about Laboratory axis 2 of 0.001 rad/sec, and an initial angular rate about Laboratory axis 3 of zero. With the Counterweight fully deployed at -66.81 m, the elevator and balance mass each weighing 2268 kg and each located at the Laboratory center of mass, the Space Station inertias are 95.33×10^6 , 91.64×10^6 , and 3.821×10^6 kg · m² about axes 1, 2, and 3, respectively. The CMG is initially set to give no control torque. The initial gimbal angle is zero and initial gimbal angle rate is equal to the negative of the spin rate.

Description of Run 50

At time zero, the CMG is in the "off" mode (control is not being applied) and the wobble state, as measured by the quantity

$$5 \left[I_2 \omega_2^2 + \left((I_1 - I_3) I_3 \omega_3^2 / (I_1 - I_2) \right) \right] / (\text{mom}_{\text{CMG}}) \omega_1$$

is larger than the high threshold value 0.001. In this case, control is turned on and applied until the wobble state is reduced to the low threshold value 0.0001, at which point control is turned off; i.e., the gimbal angle is commanded to rotate clockwise at the negative of the spin rate. At this point, gimbal angle control is switched to gimbal angle rate control. When in the gimbal angle rate control mode, the gimbal angle command remains constant; this occurs at time = 40.75 seconds.

As shown in Run 50, plots 1 and 2 of Figure 5.21, the angular rates about the transverse Laboratory axes 2 and 3 oscillate with a decreasing magnitude. At time = 41 seconds, the angular rates ω_2 and $\omega_3 = +0.467 \times 10^{-5}$ and

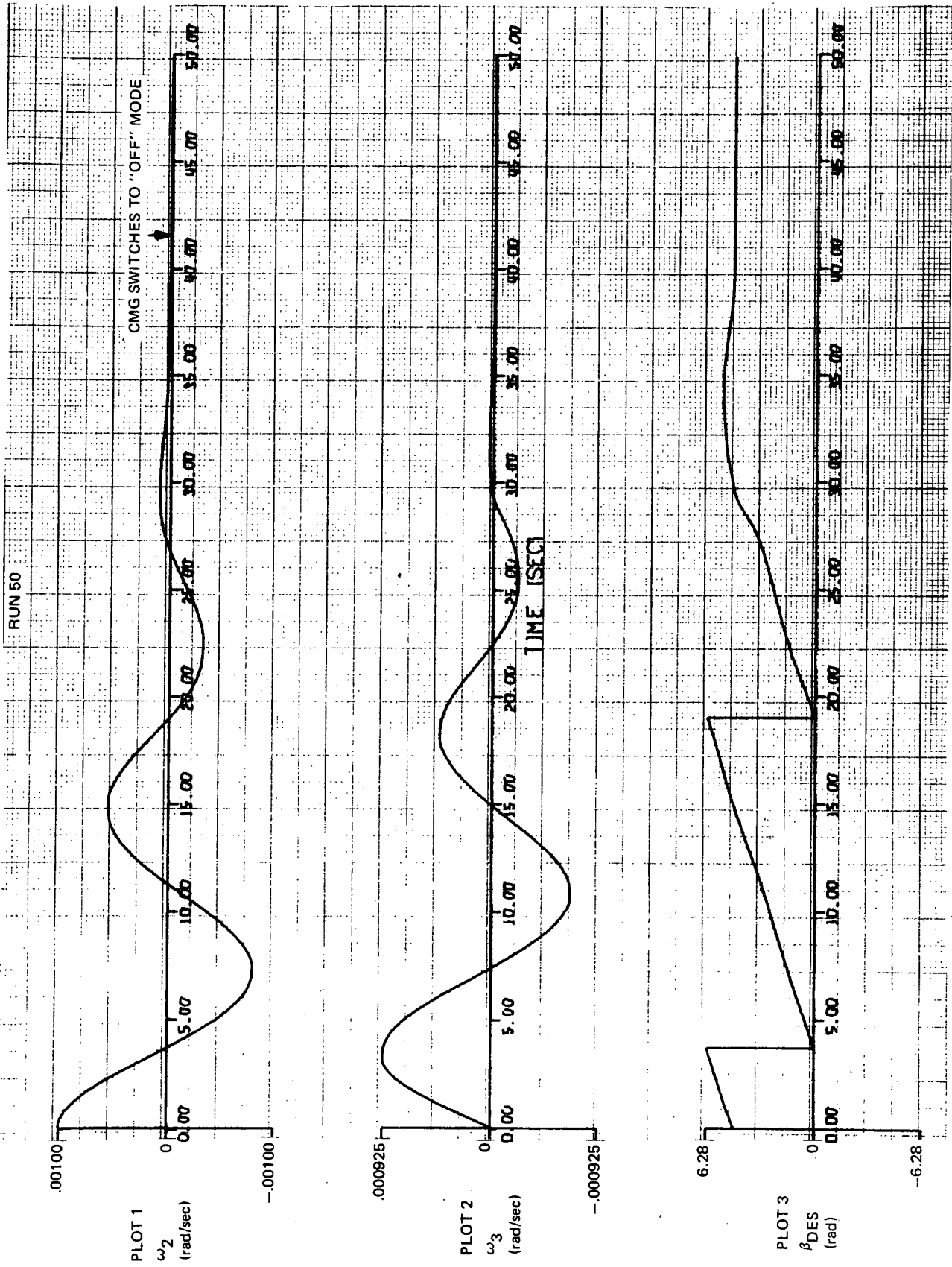


Fig. 5.21 Wobble Damping: Transverse Angular Rates and CMG Gimbal Angle Command

0.348×10^{-6} rad/sec, respectively. The decrease in magnitude is approximately straight-line, because the level of the CMG torque applied remains approximately constant until the time is reached when the CMG torque is turned off.

Plot 3 shows the gimbal angle command. Initially, it is 4.71 rad (270°) and increasing at an average rate of 0.4112 rad/sec (close to the spin rate value of 0.4189 rad/sec). The desired gimbal angle is one for which the CMG momentum vector in the transverse plane is 90° less than the component of the Space Station angular velocity vector in the transverse plane. The gimbal angle command continues to rotate in a counterclockwise manner at about the same rate until the Space Station angular rates are relatively small (time \cong 30 seconds). At this point, the rate of the gimbal angle command begins to fall off, and at time = 33.75 seconds the gimbal angle command changes direction and starts to move clockwise! At time = 40.75 seconds, the gimbal angle command is no longer used; command is switched to the gimbal angle rate command mode. After time = 40.75 seconds, the gimbal angle command is constant and not used. The gimbal angle rate command is not plotted, but at time = 40.75 seconds, it becomes equal to the negative of the spin rate and remains at this value while the CMG is in the "off" mode.

Plot 4 of Figure 5.22 shows the CMG gimbal angle error. At time = 0, its value is -1.57 rad (-90 degrees) since the gimbal angle command = 4.71 rad (270°) and the gimbal angle = 0. The gimbal angle is rotating at the negative of the spin rate. Initially, the gimbal angle is 90° from the gimbal angle command; thus, subsequently the gimbal angle is driven towards the value of the gimbal angle command. At time = approximately 3 seconds, the gimbal angle has been approximately matched to its command. Hypothetical improvement could result by altering the formula for establishing the initial conditions of the lead-lag integrator when switching to the gimbal angle control system. The gimbal angle follows its command until the time = 40.75 seconds, when the gimbal angle command is removed and replaced by the gimbal angle rate command. After time = 40.75 seconds, the gimbal angle rate is driven to the commanded value (negative spin rate = -0.4189 rad/sec).

Plot 6 shows the torque applied by the CMG on the Space Station about axis 2. From time = 0. to 1.5 seconds, when the gimbal angle is not yet close enough to its commanded value, the torques generated by the CMG on the station

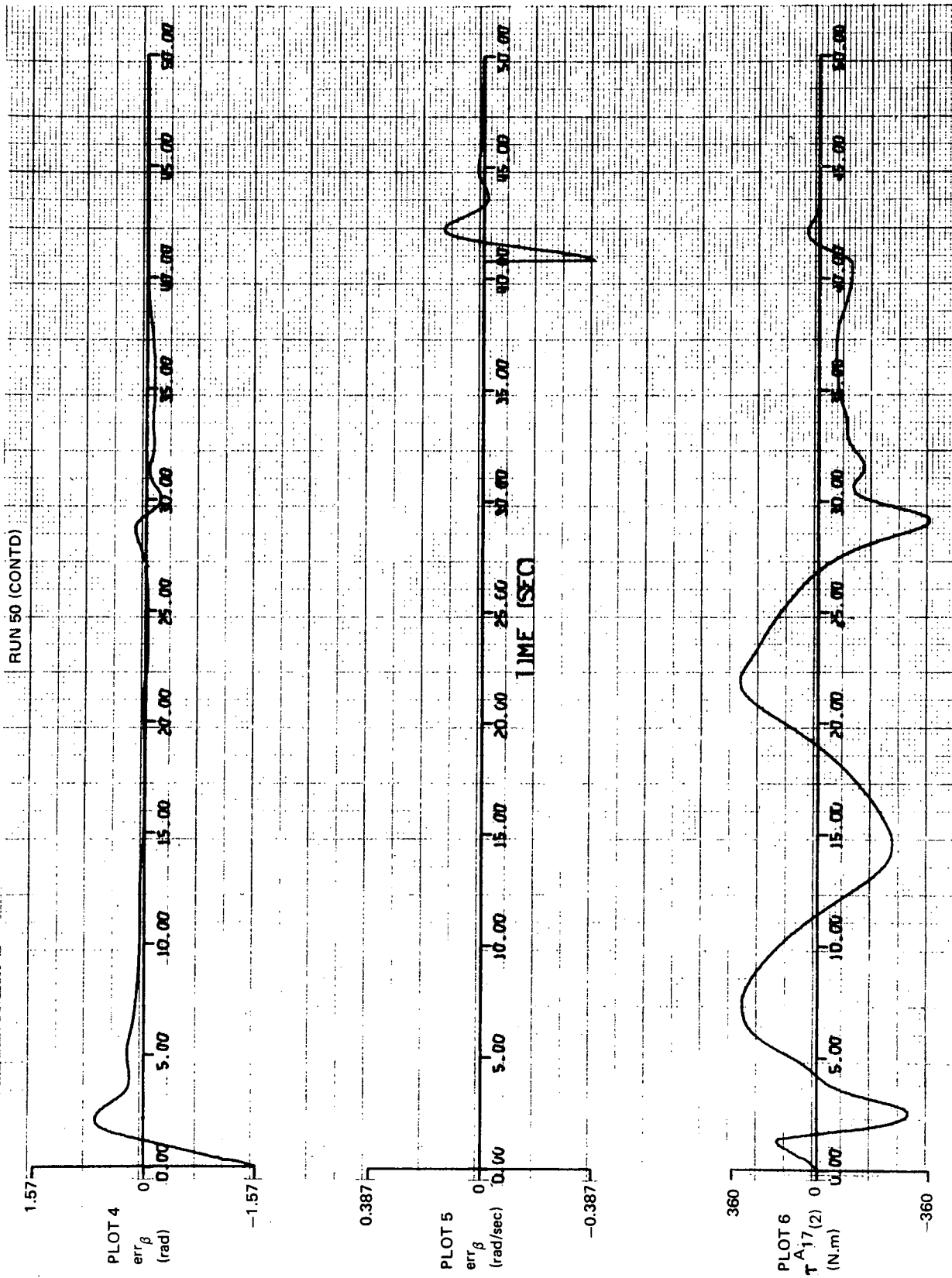


Fig. 5.22 Wobble Damping: Gimbal Angle Error, Gimbal Angle Rate Error, and Torque Applied to Vehicle by CMG about Axis 2

are of the wrong polarity. But after time = 1.5 seconds, the torques generated by the CMG on the station oppose the Space Station angular rates as desired, until time = 40.75 seconds. At this time, the torques generated by the CMG on the station decay toward zero.

Plot 5 shows the gimbal angle rate error which is applicable only when the gimbal angle rate control system is in operation. This occurs at time = 40.75 seconds; at this time the error is -0.391 rad/sec (the gimbal angle rate = -0.0279 rad/sec and the gimbal angle rate command = -0.4189 rad/sec, which is the negative of the spin rate). The gimbal angle rate error is well on the way to being nulled after only approximately 2.5 seconds.

5.5.6 Simultaneous Mass Balancing and Wobble Damping

Run 60

Run 60 demonstrates simultaneous control of the Space Station center of mass location and Space Station wobble, for a station spin rate of 4 RPM, and initial angular rates of 0.001 and 0 rad/sec about Laboratory axes 2 and 3, respectively. The Counterweight is fully deployed at -66.81 m. Initially, the location of the Space Station center of mass is at its desired position. Beginning at time = 5 seconds, the elevator is moved from 0 to 5 feet. The elevator weighs 4536 kg and the balance mass weighs 2268 kg. The CMG is initially set to give no control torque. The initial gimbal angle is zero and initial gimbal angle rate is equal to the negative of the spin rate.

Description of Run 60

Comparisons of Run 60 with Runs 40 and 50 show that mass balancing and wobble damping when performed simultaneously are the same as when performed individually.

5.6 CONCLUSIONS BASED ON RIGID-BODY DEMONSTRATION RUNS

The control systems perform their respective functions as generally intended for the rigid-body Space Station. The control system models can now be incorporated in the digital computer program for simulating the dynamics of the flexible Space Station.

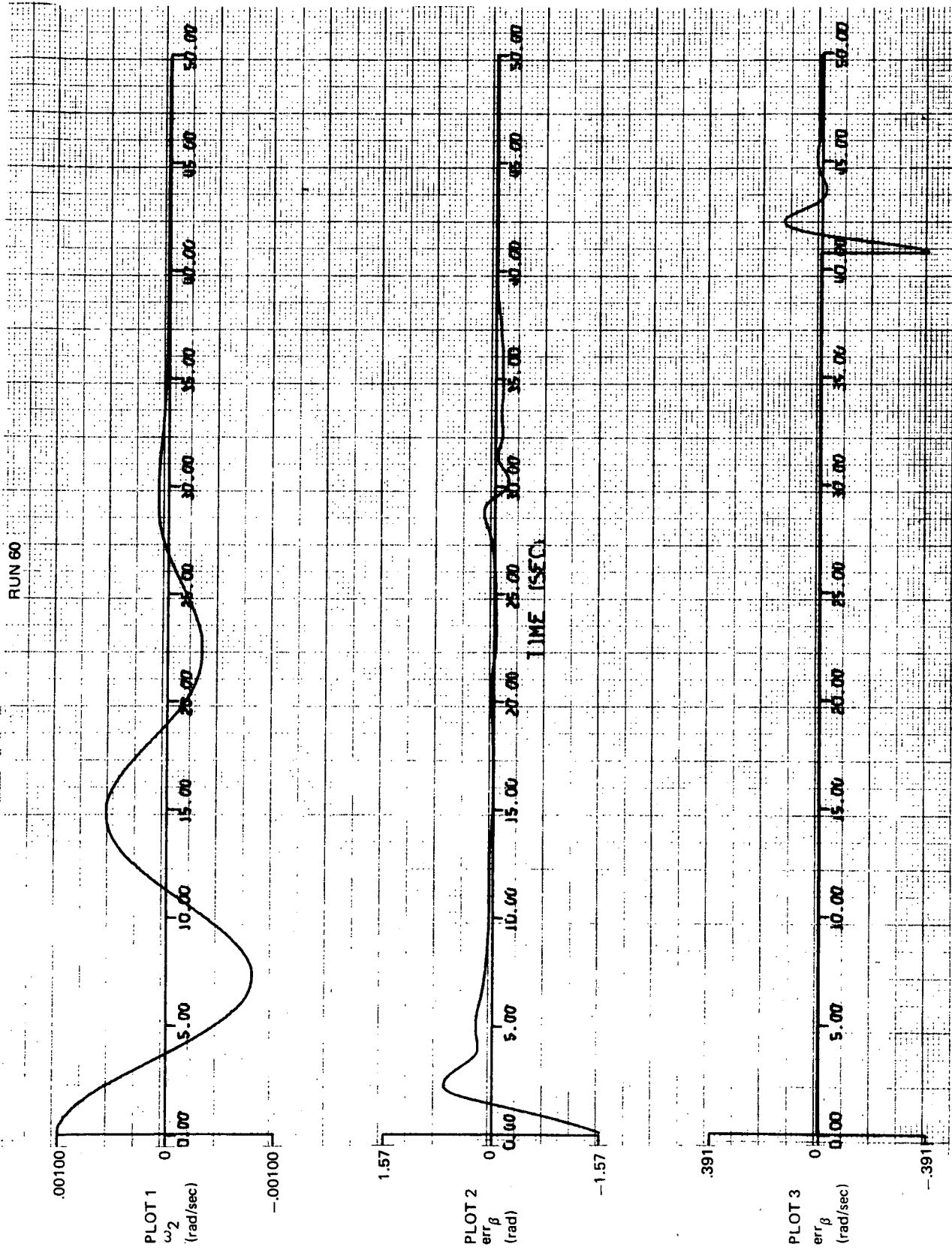


Fig. 5.23 Mass Balancing & Wobble Damping: Transverse Angular Rate (axis 2), Gimbal Angle Error, and Gimbal Angle Rate Error

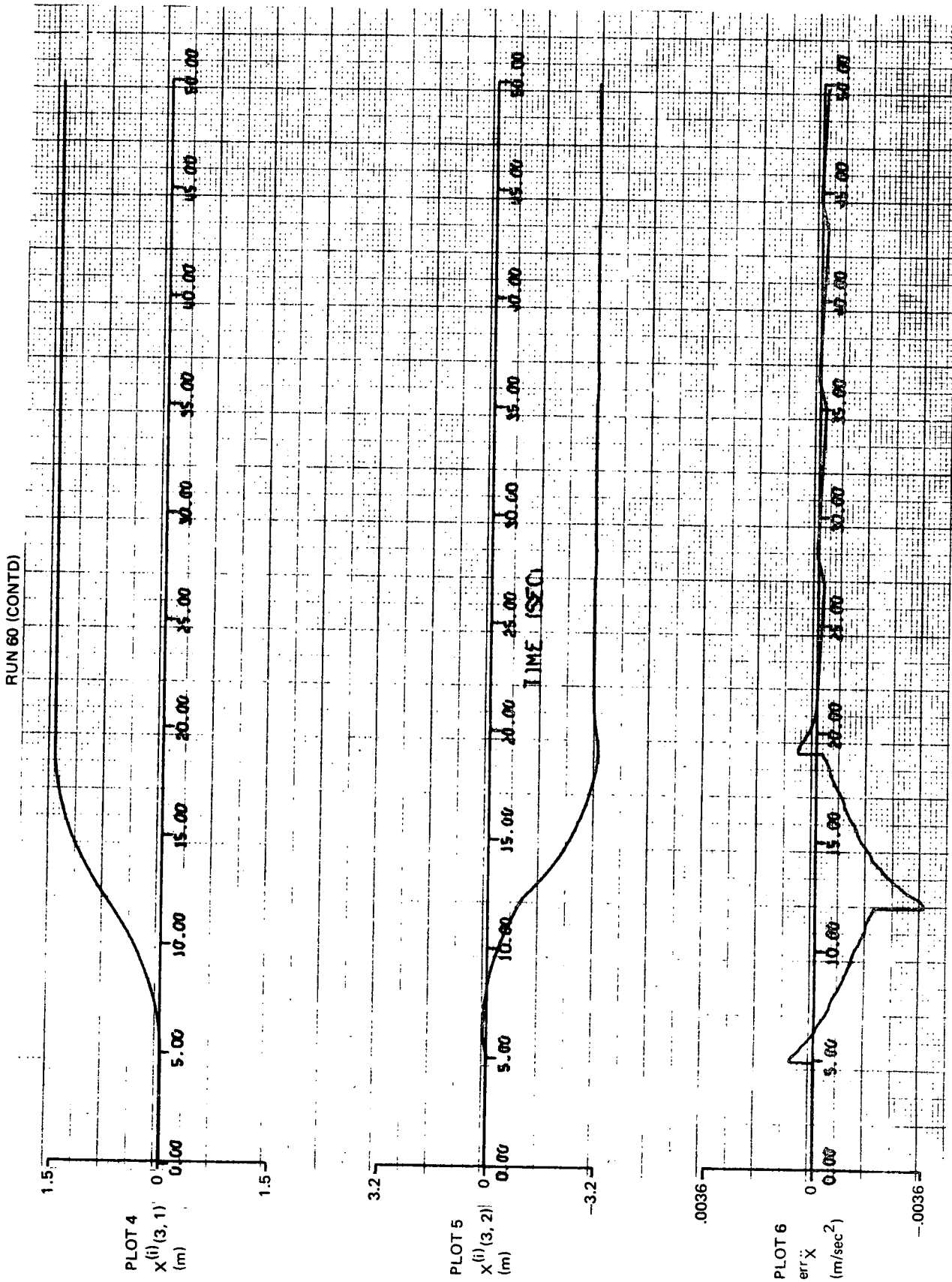


Fig. 5.24 Mass Balancing & Wobble Damping: Positions of Elevator and Balance Mass and Acceleration Commanded Minus Acceleration Sensed

To obtain sufficient control authority for holding constant spin rate during Counterweight deployment without going to higher levels of jet thrust, or using jets of different sizes, extra jets are required beyond those required for attitude control. Also the thrust level of each jet must exceed 100 N, when there are 4 jets per polarity with average jet arm = 4.57 m, so that the jet torque is capable of coping with the disturbance torque resulting from a Counterweight velocity of .06 m/sec. A time of 11.78 minutes is taken in moving the Counterweight from its fully retracted position (-23.99 m from the Laboratory center of mass) to its fully extended position (-66.81 m) at a maximum velocity of .06 m/sec relative to the Laboratory.

For the set of values used, spin-up from 0.2 RPM to 4 RPM requires 2.58 hours, using four 222.4 N thrust jets per polarity, each with an average arm of 4.57 m. (The computer machine time required to simulate the complete operation would be about 5.16 hours, since the ratio of machine time to real time is approximately 2.25.) A more efficient method would be to locate jets on the Counterweight as well as the Laboratory; however, this would involve other penalties. In the demonstration runs, it was assumed that all control-system components must be mounted on the Laboratory.

In the control of the Space Station center of mass location, the estimate for the elevator weight does not have to be accurate to achieve satisfactory operation. Estimate errors 50 percent low and 100 percent high were tested.

In wobble damping, the vehicle dynamic response is basically one of an unforced vehicle for large wobble and one of a forced vehicle for small wobble. The criterion for CMG torque shut-off (a measure of wobble similar to wobble energy) could be replaced by the CMG gimbal angle command, which changes in its basic nature as the wobble decays to small levels. (The type of CMG used for wobble damping is single-gimbal, with the gimbal axis parallel to the nominal spin axis.)

No interaction was observed between wobble damping and mass balancing when performed simultaneously.

6.0 NUMERICAL RESULTS DEMONSTRATING THE COMPUTER PROGRAMS

The NASA Langley Research Center provided Grumman with the configuration shown in Figure 6.1 for demonstrating the computer program. The physical properties of the structural components are presented in Appendix F. First, the modes of each module were computed. Then the free-free modes of the Laboratory and the Counterweight were synthesized using the Phase I computer program with the modes of the modules used as input data. The Counterweight was relatively rigid. The lowest flexible Counterweight frequency was 6.851 Hz whereas the sixth Laboratory frequency was .382 Hz. It was therefore decided to idealize the Counterweight as a rigid body in the Phase II Computer program which develops the time history. As shown in Figure 6.2, the Laboratory was idealized using seventy-two mass points. Six flexible Laboratory modes were used. These are tabulated in Appendix I. Because of the relatively large flexibility of the solar panels, most of the motion in these modes is solar-panel motion. A total of 18 coordinates are used in the time-history runs. These are the six Laboratory modes, six rigid-body coordinates locating the mean axes for the Laboratory, and six rigid-body coordinates for the Counterweight.

The Connecting Structure used in the examples is the telescopic tubular beam described in Section 4.4.2.1. The fully deployed undeformed length is 42.822 m and the retracted length is zero. Data for the demonstration runs is listed in Appendix J.

6.1 TESTING OF THE PROGRAMS

The check problems run on the Phase I computer program were discussed in Section 3.4. To test the Phase II computer program, a separate program was prepared by an independent programmer. In the test program only the equations for the configuration shown in Figure 6.1 were programmed. Unlike the problem used to demonstrate the program, the Counterweight was flexible and all appendages, including solar panels, were rigid. Test runs included free vibration with very general initial conditions, vibration with externally applied loads, vibration with fluid being pumped, vibration with two rigid masses in motion, and a Connecting-Structure retraction maneuver. In all

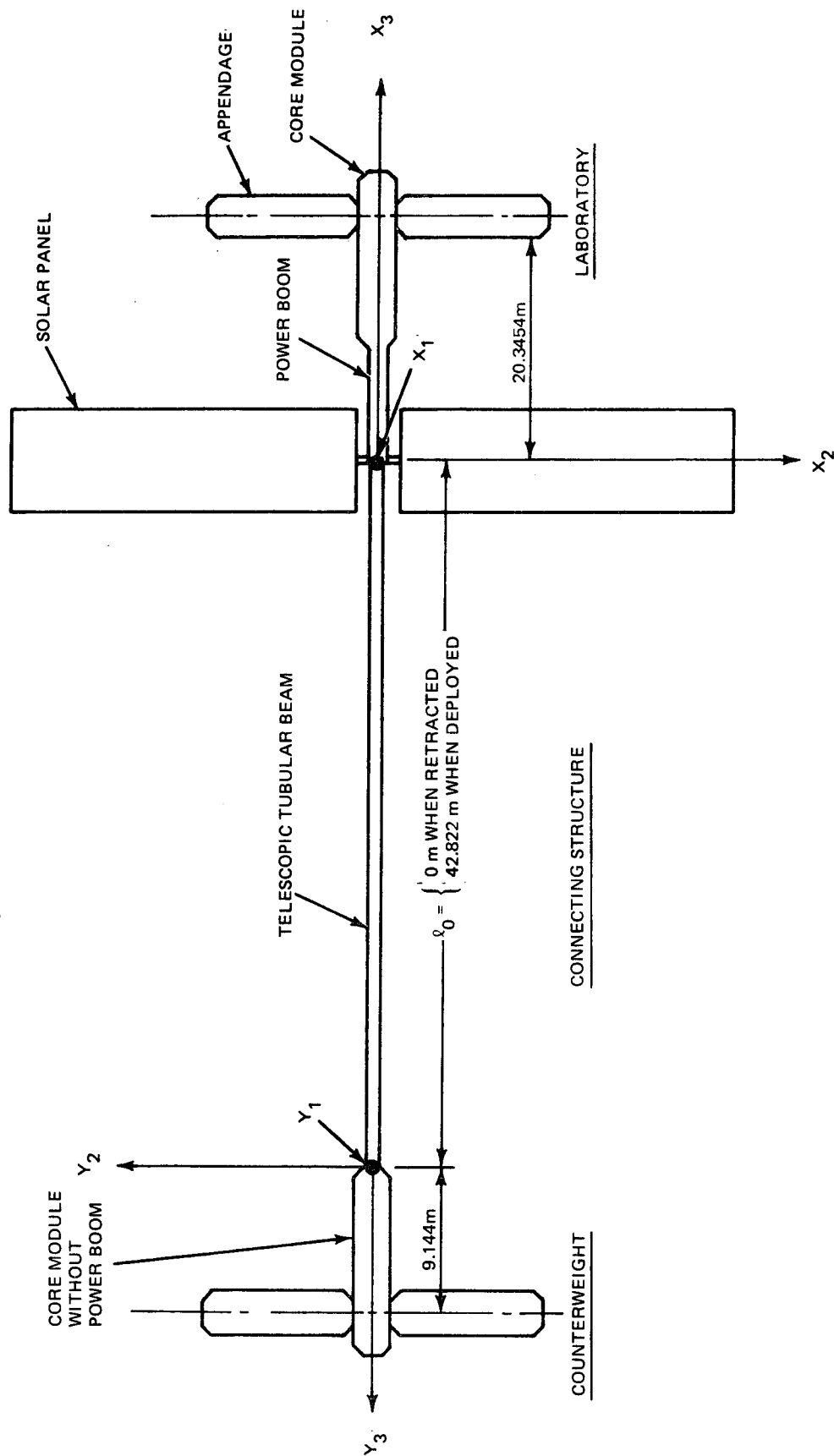


Fig. 6.1 Configuration for Demonstrating Computer Program

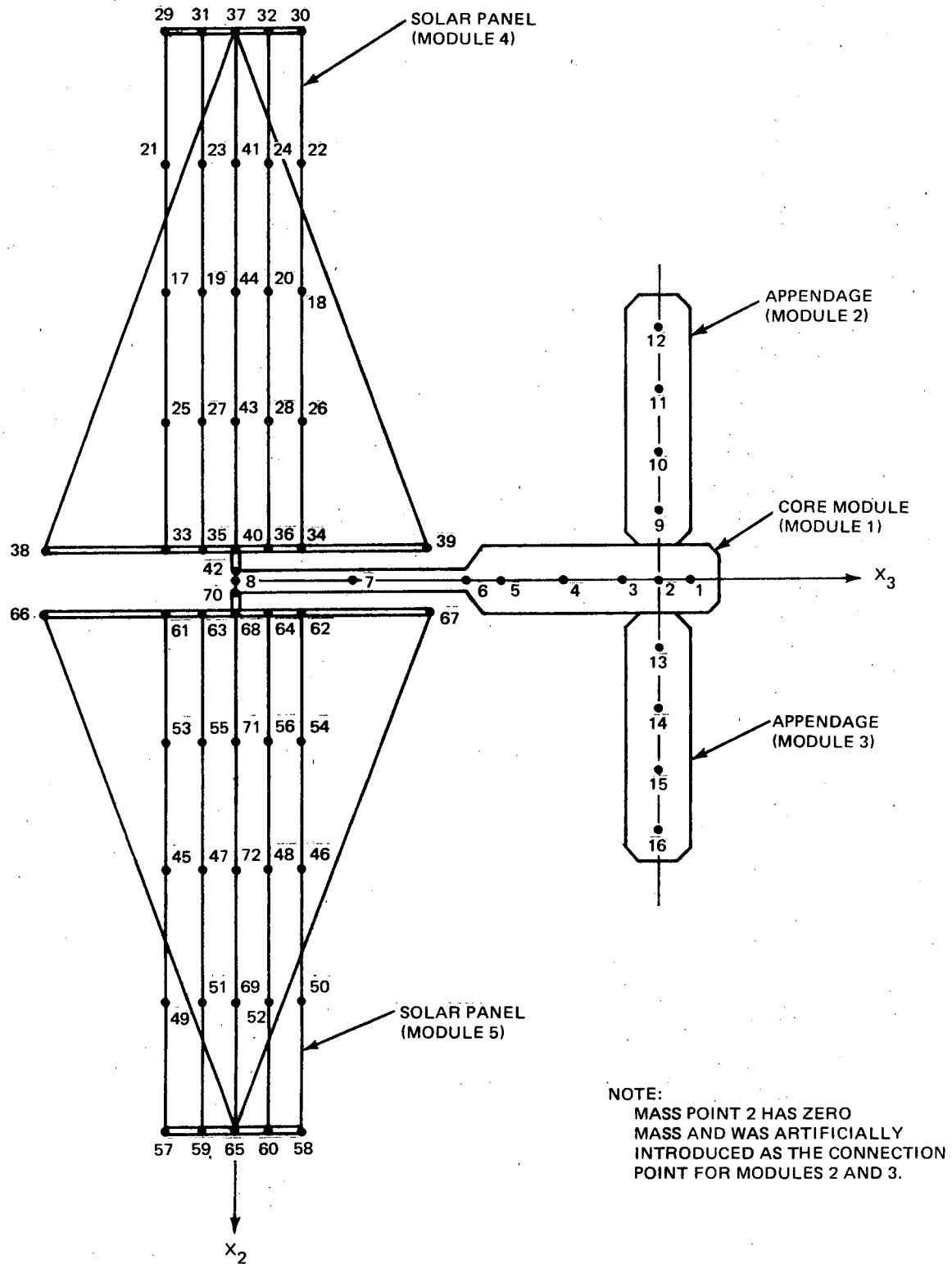


Fig. 6.2 Idealization of Manned Laboratory

cases, the angular velocity was 4 RPM. Also, the Space Station was run as a rigid body using the Phase II program, and the results were compared with those obtained on an existing rigid-body program. All results obtained from the Phase II program agreed with the results obtained from the above-described programs.

6.2 DEMONSTRATION RUNS

The following runs will be described in this section:

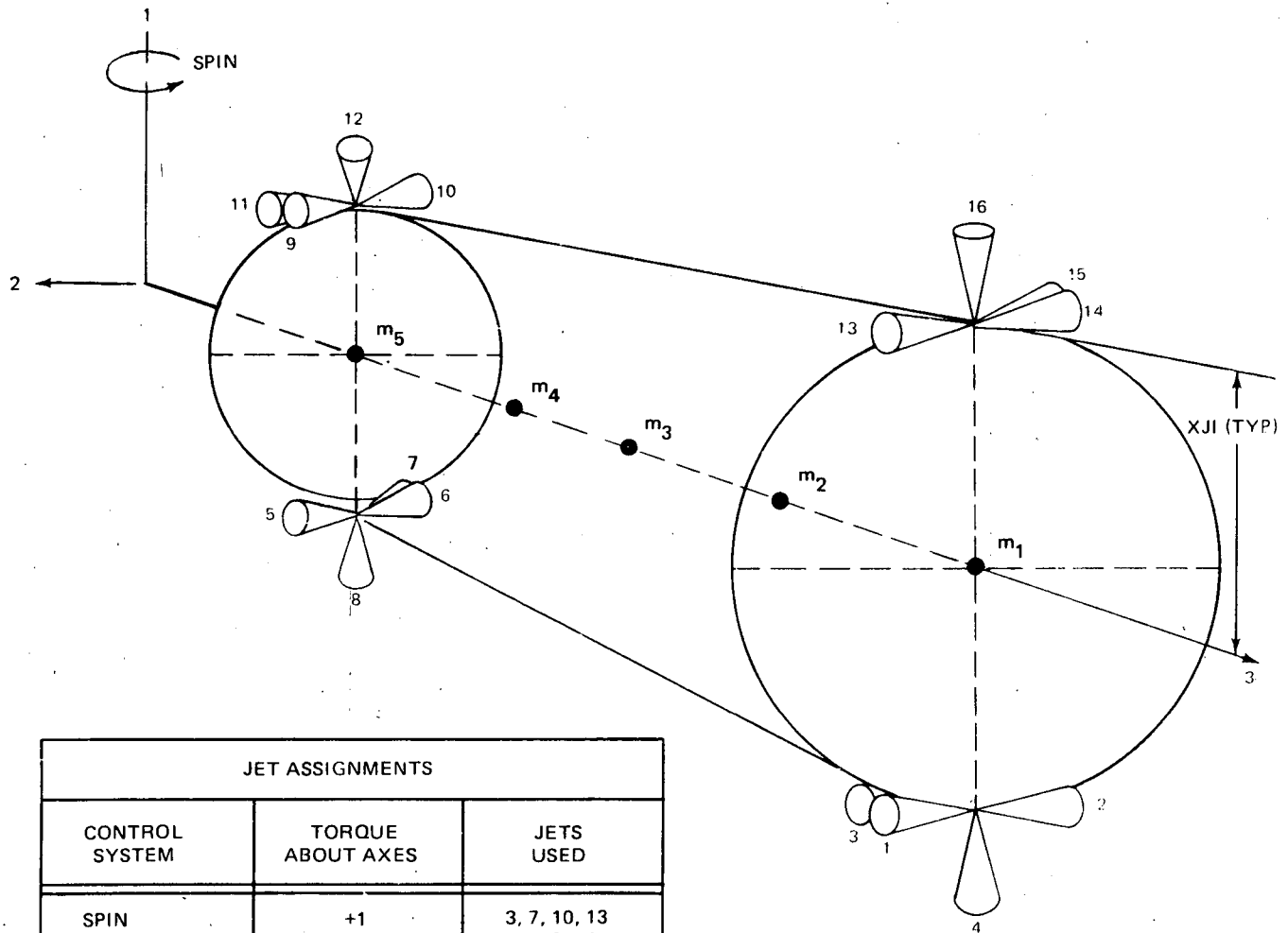
- Attitude control
- Deployment
- Spin up
- Wobble control
- Elevator motion with mass balancing
- Fluid pumped between reservoirs

All control-system jets were mounted on the Laboratory core module as shown in Figure 6.3. The control system sensor was mounted at the cm of mass point 4. The CMG was also mounted at mass point 4.

The runs were selected to demonstrate the capability of the computer program. There was no attempt to optimize any of the operation parameters such as control-system gains. Also, in the case of the deployment and spin-up maneuvers, the jet thrusts were increased to unrealistic values in order to complete the maneuvers within 45 sec., thereby saving computer time.

6.2.1 Attitude Control

During the attitude-control maneuver, the system was not rotating, and the Connecting Structure was fully retracted. The attitude control system developed in Section 5 required no modification for use on the flexible-system idealization. The three components of the main Euler-angle vector $\{\gamma\}$ are shown in Figure 6.4. Curves for a rigid-body run were overlaid with the flexible body curves of Figure 6.4 and no difference could be discerned. The Space Station was initially tilted so that each Euler angle was .01745 rad (1.0 degree). The control system then reduces each angle to the commanded value of zero. Similar behavior occurs along the three axes. The jets first apply a torque to begin correcting the attitude



JET ASSIGNMENTS		
CONTROL SYSTEM	TORQUE ABOUT AXES	JETS USED
SPIN	+1	3, 7, 10, 13
	-1	2, 5, 9, 14
ATTITUDE	+1	10, 13
	-1	9, 14
	+2	4, 12
	-2	8, 16
	+3	1, 15
	-3	6, 11

NOTE: THE POWER BOOM IS NOT SHOWN

Fig. 6.3 Jet Configuration on Laboratory Core Module

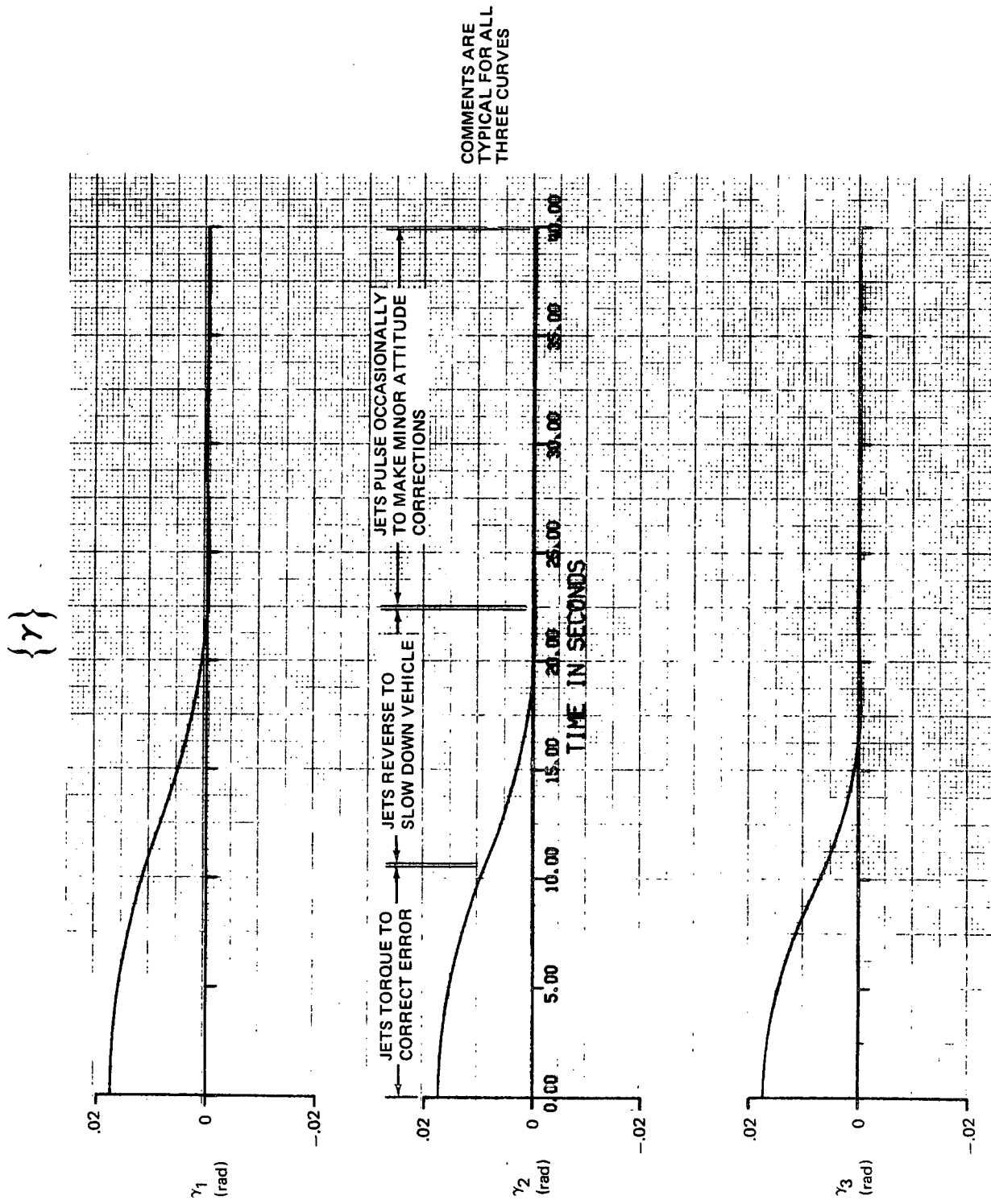


Fig. 6.4 Main-System Euler Angles During Attitude Control Maneuver

angle. Then a torque is applied in the negative direction to slow down the Space Station's angular rate. Figure 6.5 shows the components of the angular velocity vector during this run. Linear deformation in the Connecting Structure is shown in Figure 6.6. Since the Connecting Structure is fully retracted, the illustrated deformation actually represents the very small deflections of the relatively stiff Connecting-Structure docking hatch. This connection is only approximately represented as discussed in Section 4.4.2.1. Figure 6.7 illustrates the vibration at mass point 17 which is located at a very flexible strip on a solar panel. Examination of the two bending motions of the strip shows that the frequency in the 1 direction is seen to be roughly 50% of the frequency in the three direction. It can be seen from the solar-panel modes in Appendix F, that this difference in frequency is inherent in the solar-panel structure.

6.2.2 Deployment with Spin-Rate Hold

Figures 6.8 - 6.11 illustrate a deployment maneuver at .02094 rad/sec (.2 RPM). All motion in this run is in the spin plane. Figure 6.8 shows the prespecified motion of the undeformed Connecting Structure (i.e., the third component of $\{\dot{l}_0\}$). The Connecting Structure deploys from an undeformed length of zero to 42.822m. If the spin control system were not operational, the spin rate would decrease to maintain constant momentum; however, the command to maintain a constant spin rate was given during this run. To accomplish the deployment within 40 seconds, the jet thrust was increased from a nominal value of 222.4N (50 lbs) to 4448.2N (1000 lbs). Figure 6.9 shows the spin rate and the axial deformation in the beam during deployment. The deployment command is given at $t = 1$ sec, and as the Laboratory and Counterweight begin to separate, there is compression in the beam. During this phase $\dot{l}_{03} > 0$ (see Figure 6.8). When the maximum velocity $\dot{l}_{03} = 1.270$ m/sec (50 in/sec) is reached, and deployment proceeds at constant velocity, the beam is expanded slightly by the centrifugal force. At approximately 35 seconds, the deceleration begins ($\dot{l}_{03} < 0$) and the expansion in the beam is increased significantly. Deployment ends at about 40 seconds. The final expansion is much larger than the initial compression mainly because the Connecting Structure is more flexible when more of it is deployed. For the same reason the transient vibration occurs at a lower frequency when deployment is near

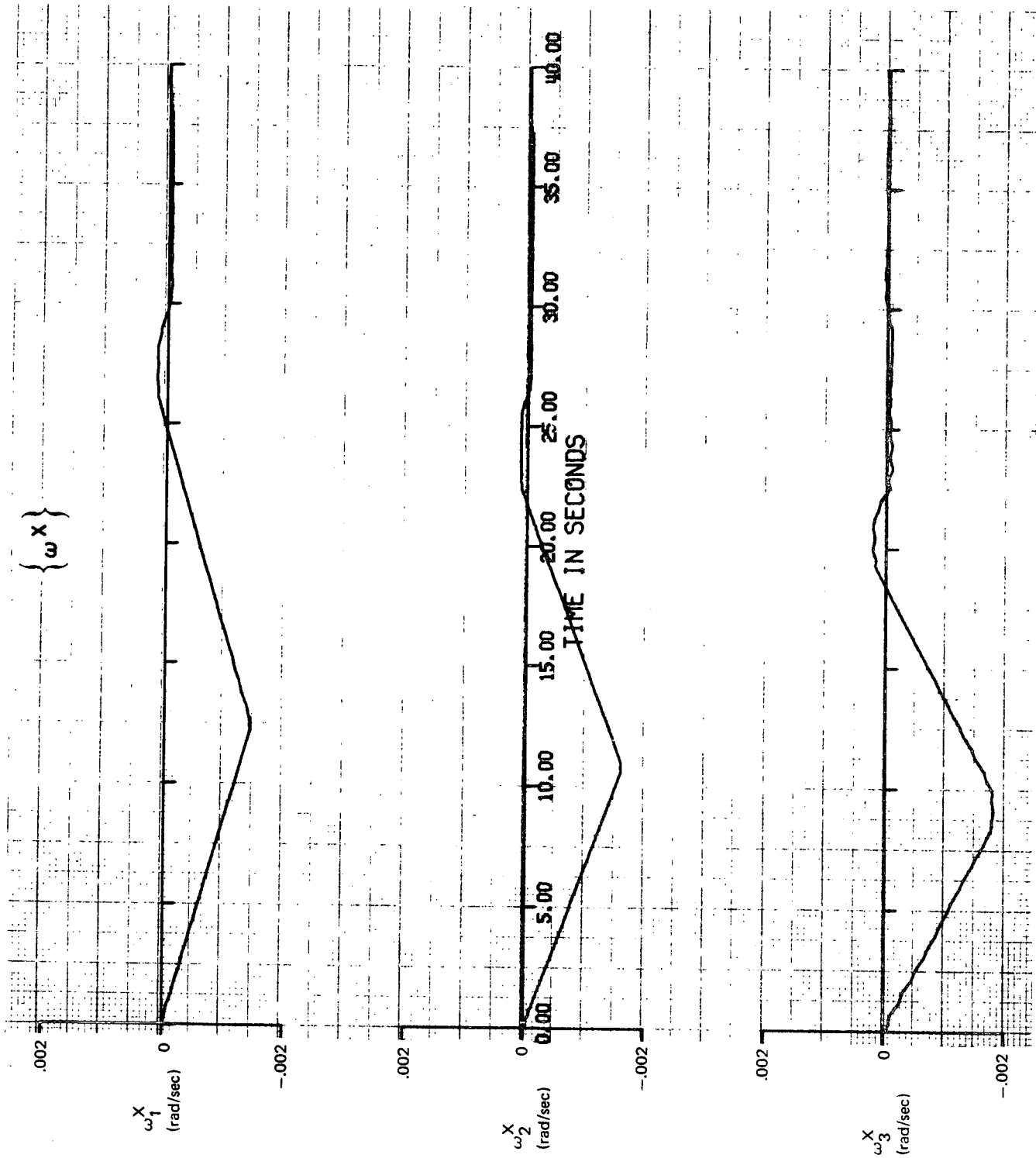


Fig. 6.5 Components of Main System Angular-Velocity Vector During Attitude Control Maneuver

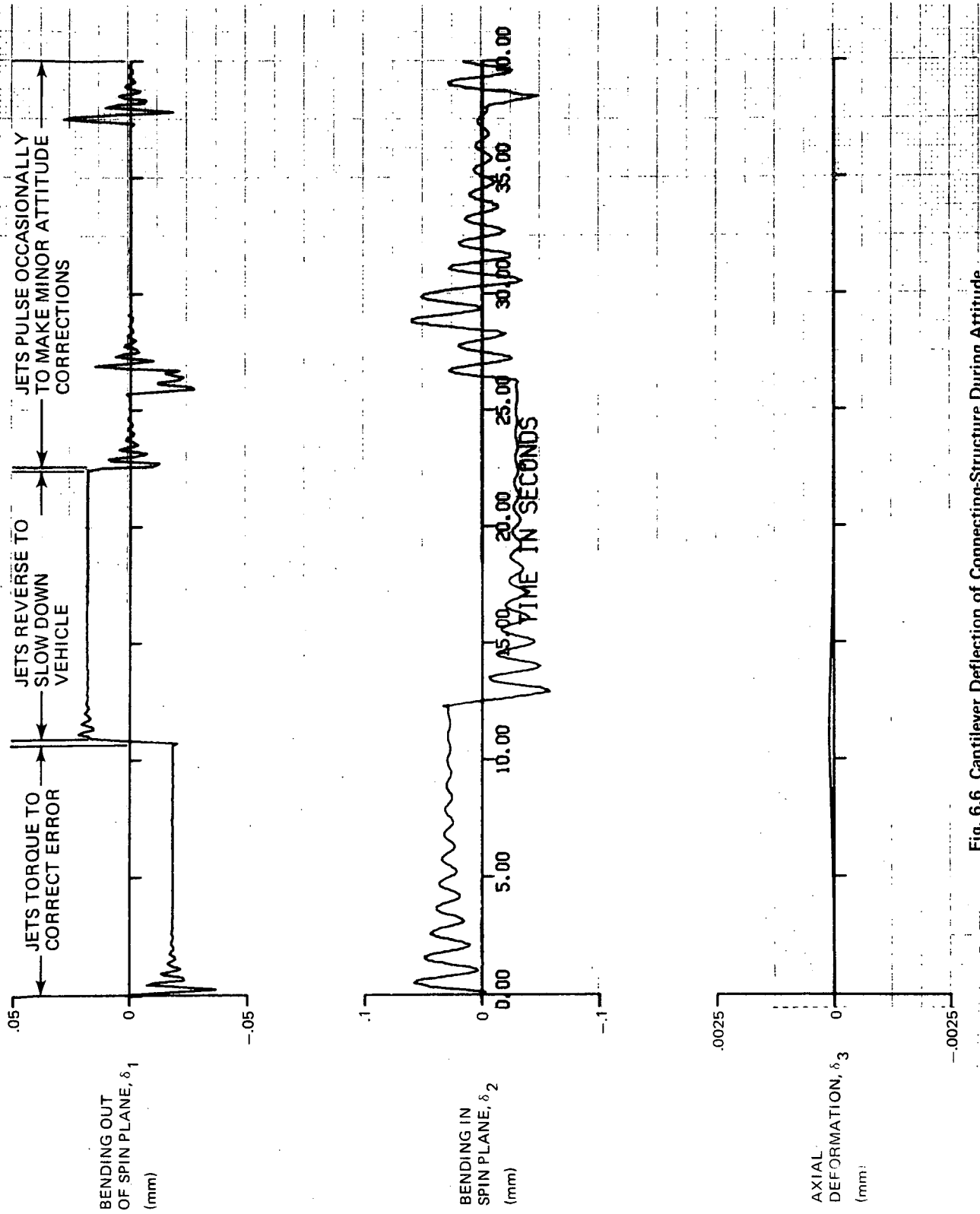


Fig. 6.6 Cantilever Deflection of Connecting Structure During Attitude Control Maneuver

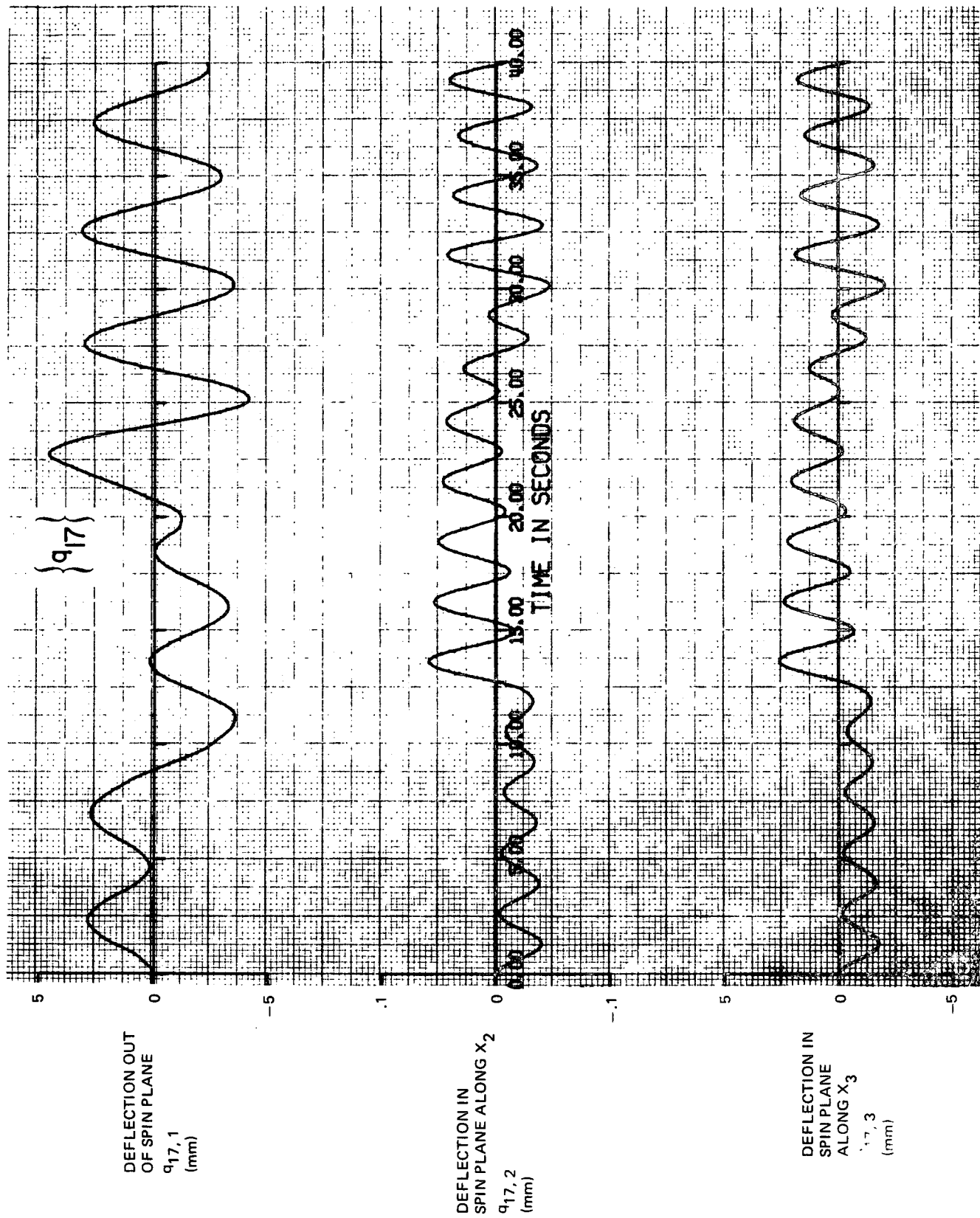


Fig. 6.7 Deflection of Point on Solar Panel (Mass Point 17) During Attitude Control Maneuver

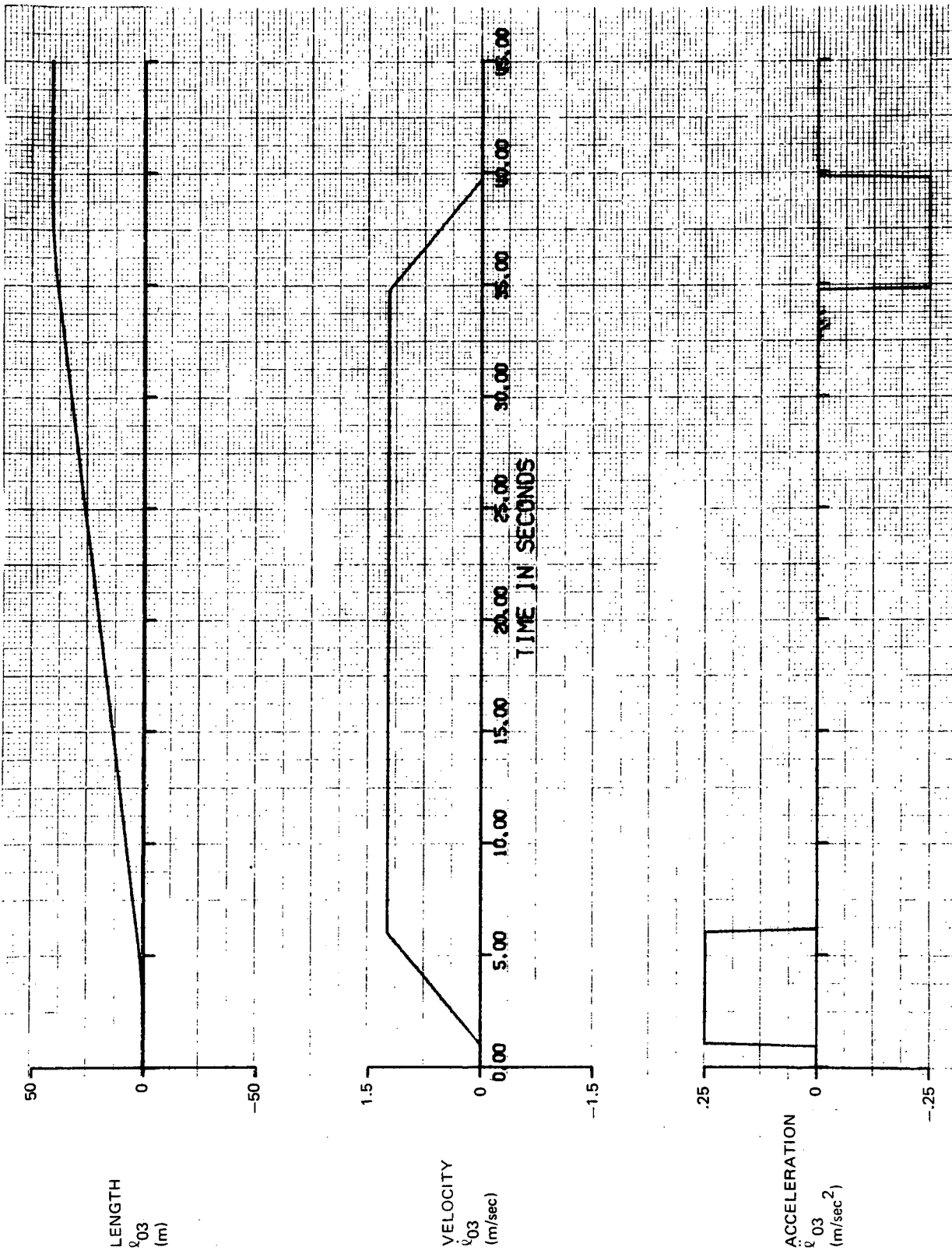


Fig. 6.8 Prespecified Undeformed Motion of Connecting Structure During Deployment Maneuver

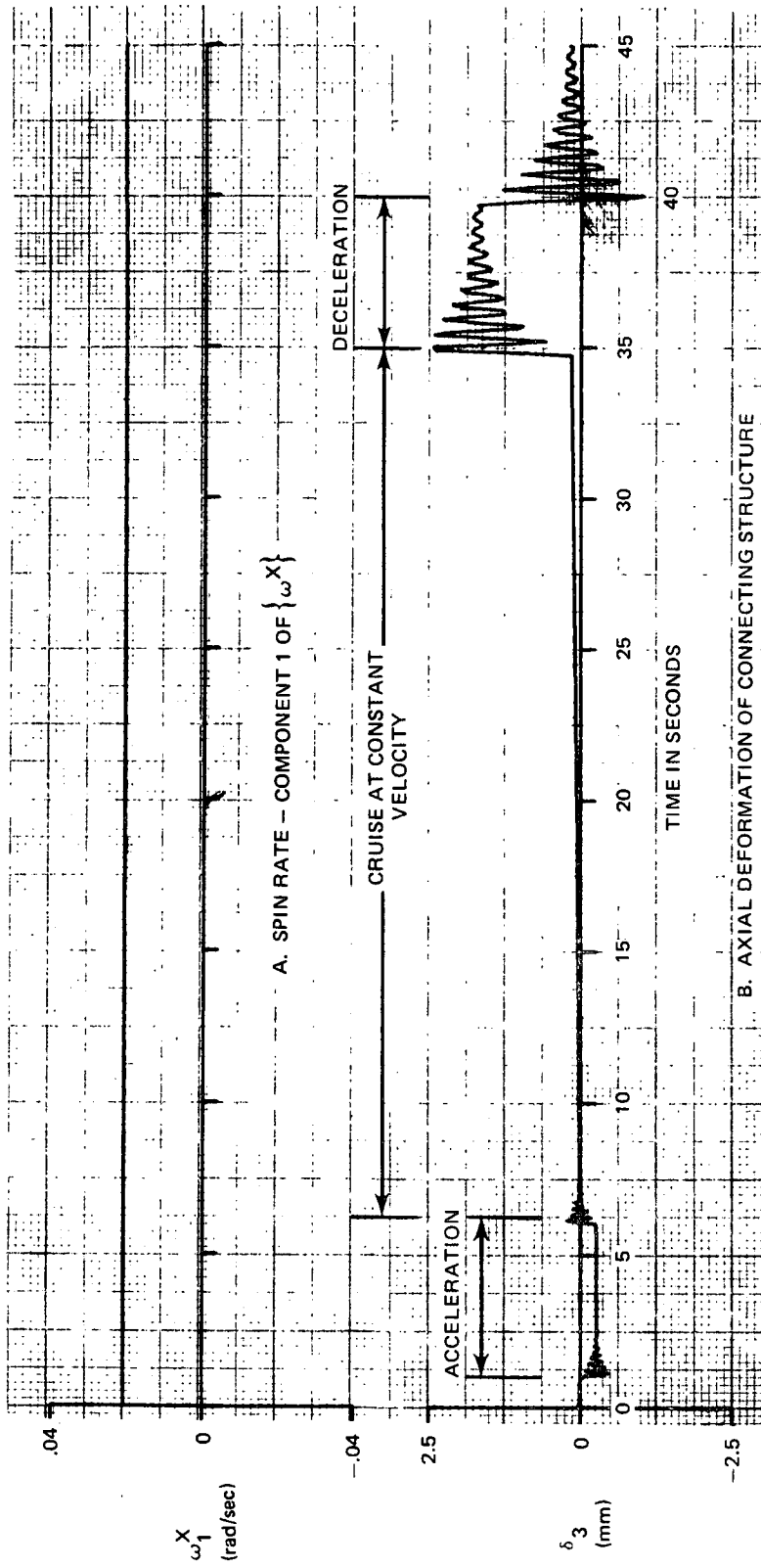


Fig. 6.9 Spin Rate and Axial Deformation of Connecting Structure During Deployment Maneuver

completion. Figure 6.10 illustrates the bending of the Connecting Structure during deployment. This bending occurs partially as a result of the Coriolis forces but primarily it is due to the spin jets torquing the Laboratory to maintain a constant angular velocity. The deformation at mass point 17 and the internal torque exerted by the solar panel on the core module are shown in Figure 6.11.

6.2.3 Spin Up

Figures 6.12-6.14 illustrate a spin up maneuver. The Space Station is initially rotating at $.02094 \text{ rad/s}$ (.2 RPM) and, at 5 seconds, the command is given to increase the spin speed to $.4189 \text{ rad/s}$ (4 RPM). All motion in this run is in the spin plane. In order to accomplish the maneuver in 40 sec, the jets on the Laboratory were increased from 222.4N (50 lbs) to 66.7kN (15,000 lbs). Figure 6.12A illustrates the increase of the spin speed, and Figure 6.12B illustrates the corresponding increase in the axial extension of the Connecting Structure due primarily to the centrifugal force. Figure 6.13 shows the bending in the Connecting Structure during the spin up maneuver. Unusually high deformations occur as a result of the large torques on the Laboratory generated by the increased jet thrusts. Figure 6.14 shows the largest component of the deformation at mass point 17 and the largest component of the force exerted by the solar panel on the core module at the root of the panel.

6.2.4 Quiescent State

When the Space Station is rotating in its nominal state of pure spin (i.e., it is in a state of pure rotation about the X_1 axis with no vibration), constant elastic deformations occur due to the centrifugal force. This state is known as the quiescent state. During the runs which were made when the Space Station was rotating at its nominal spin speed of $.4189 \text{ rad/sec}$ (4 RPM), the initial conditions are a variation from the quiescent state. Before making these runs, the quiescent state deformations were determined by setting all of the damping coefficients (for both the Laboratory and the Connecting Structure) to 80% of their critical values. A short run was made,

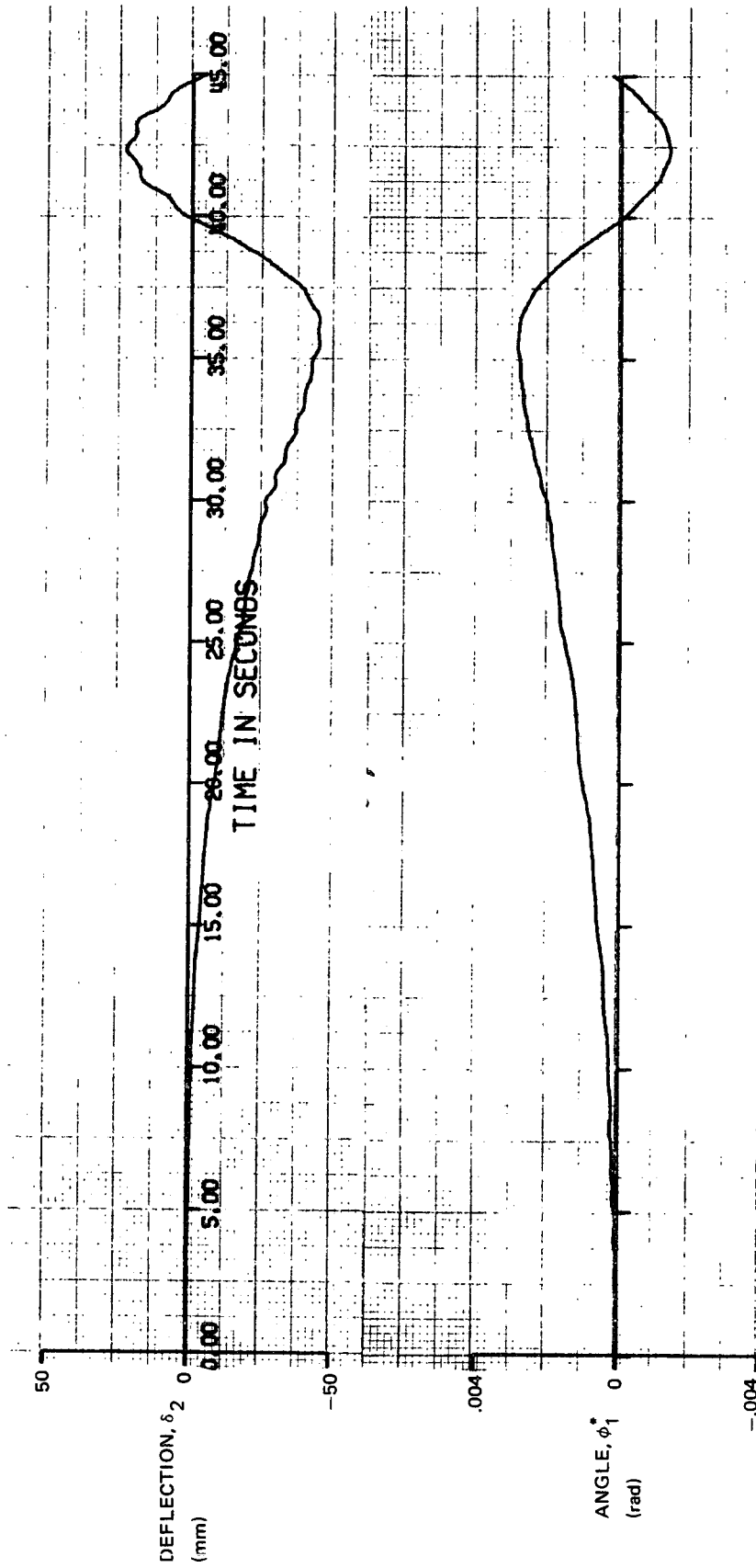


Fig. 6.10 Cantilever Bending in Spin Plane During Deployment Maneuver

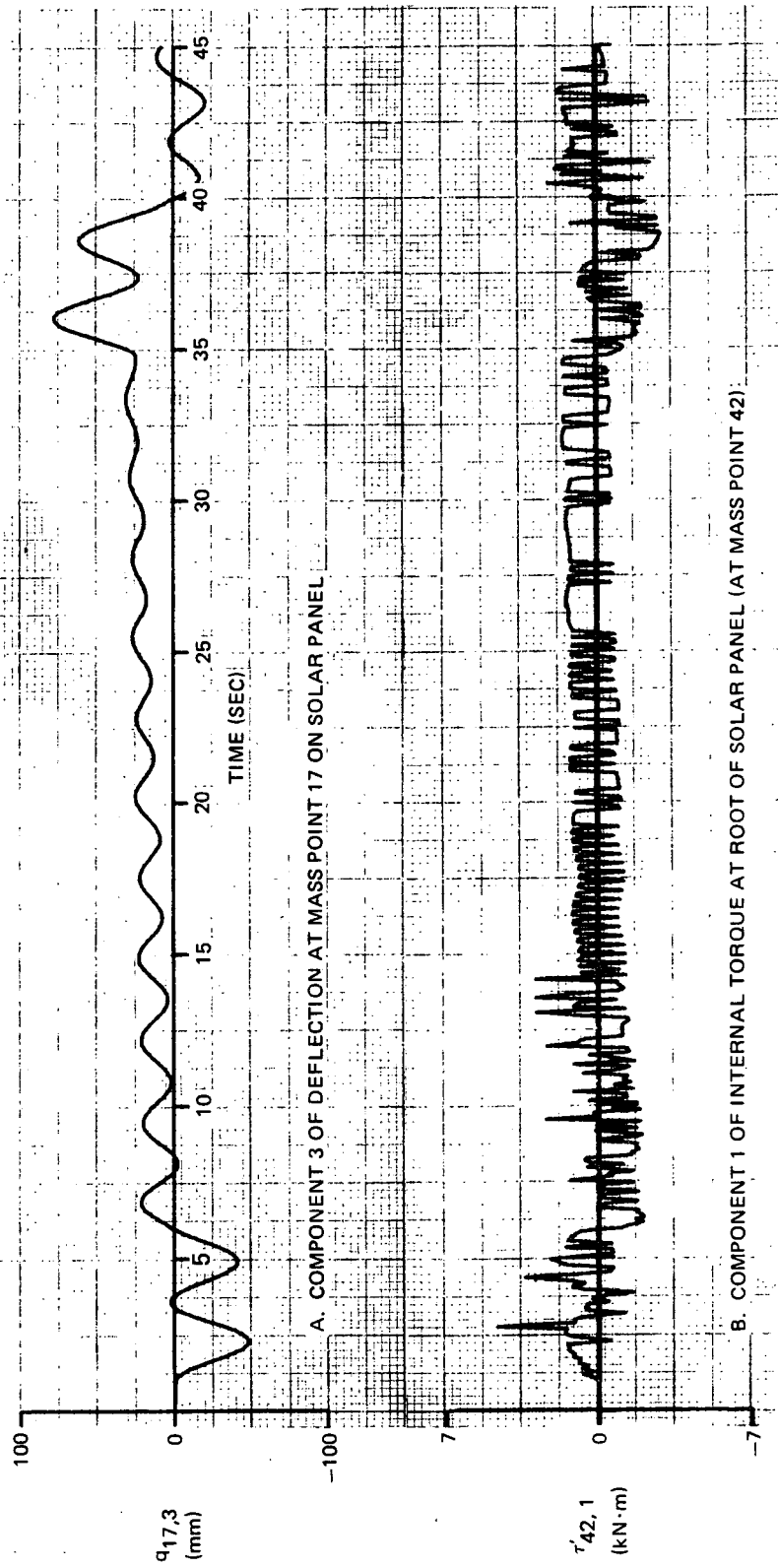


Fig. 6.11 Selected Deflection and Internal Torque Components During Deployment

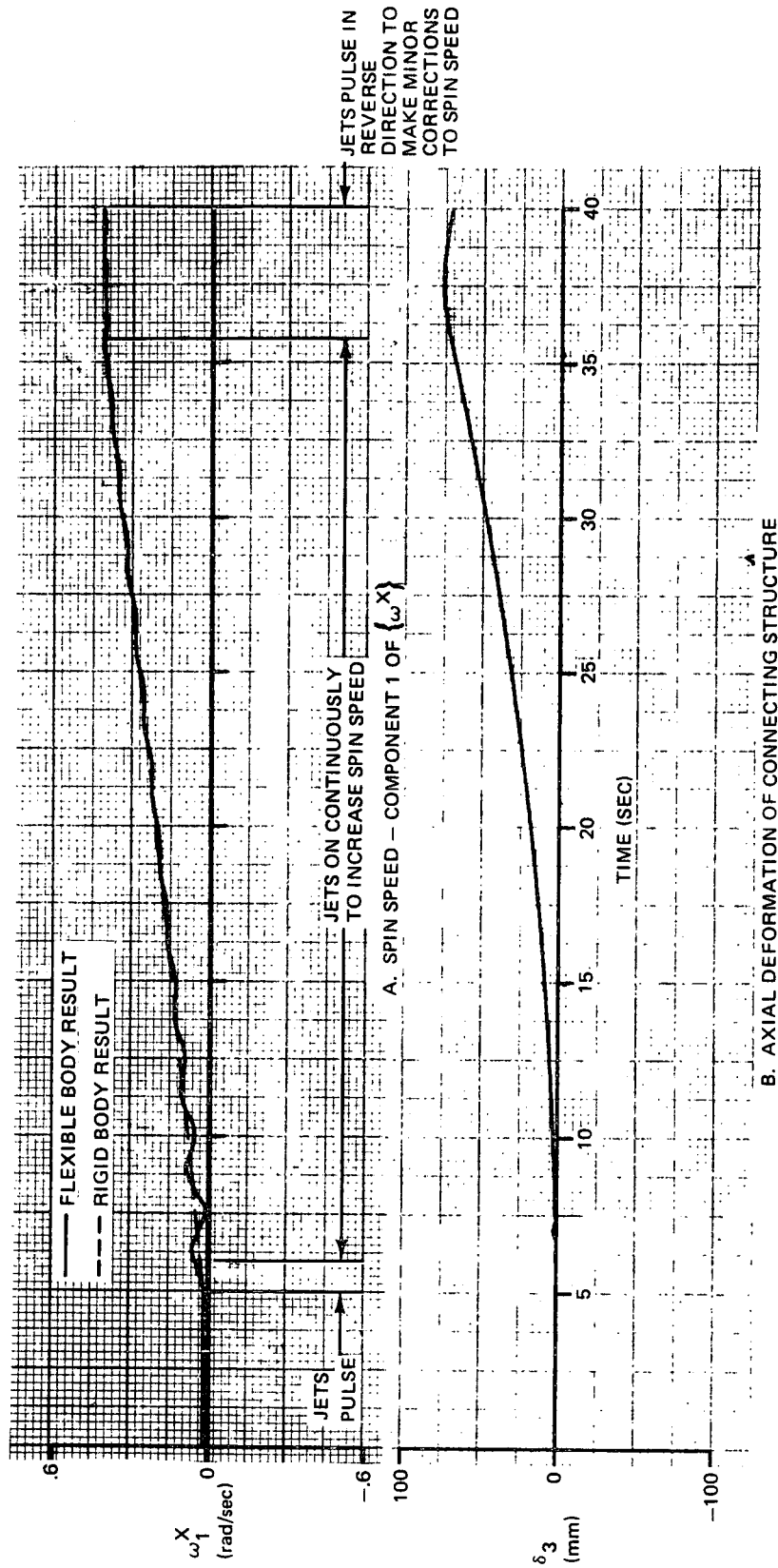


Fig. 6.12 Spin Speed and Axial Deflection of Connecting Structure During Spin Up Maneuver

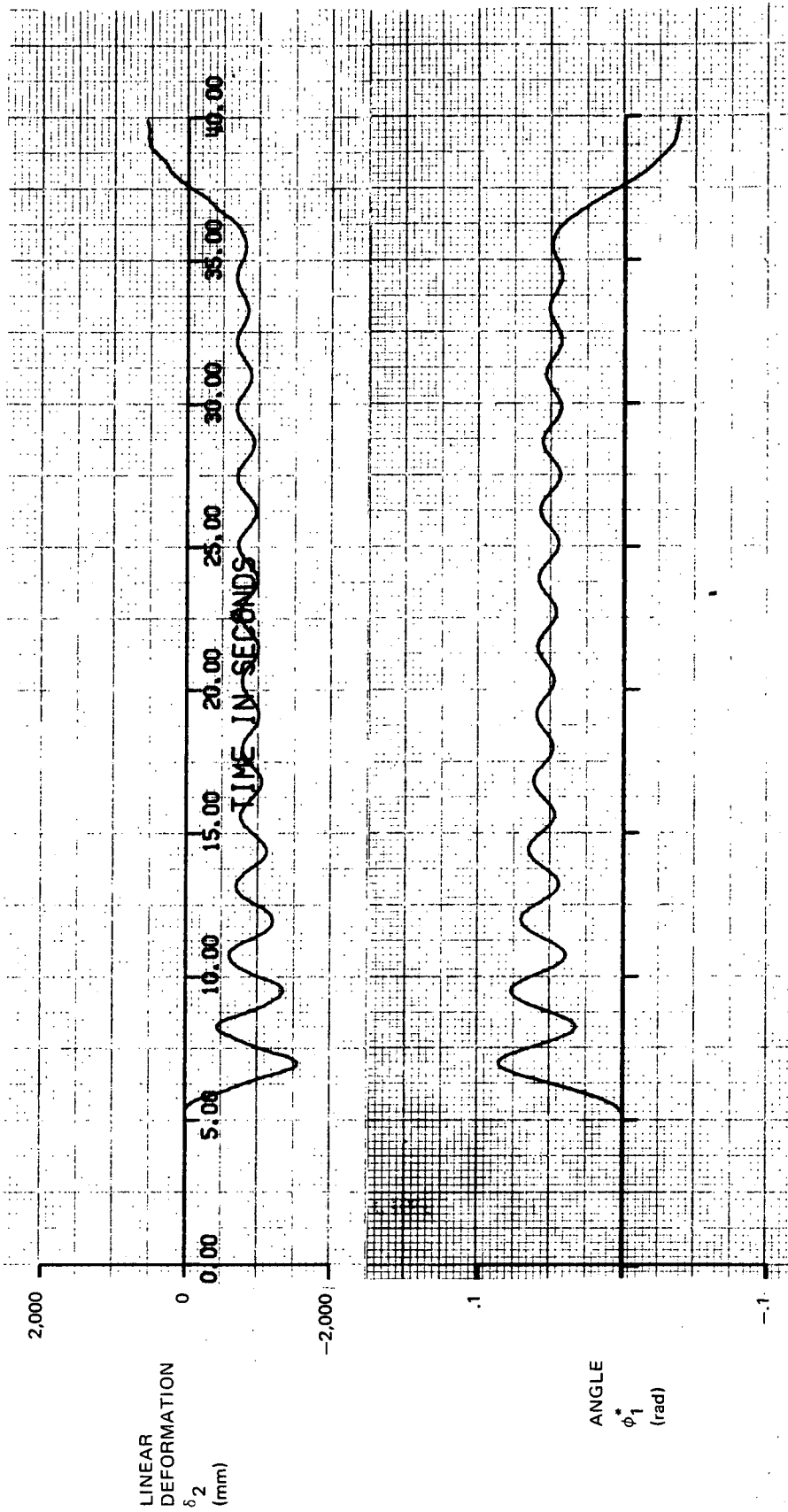


Fig. 6.13 Cantilever Bending of Connecting Structure in Spin Plane During Spin-Up Maneuver

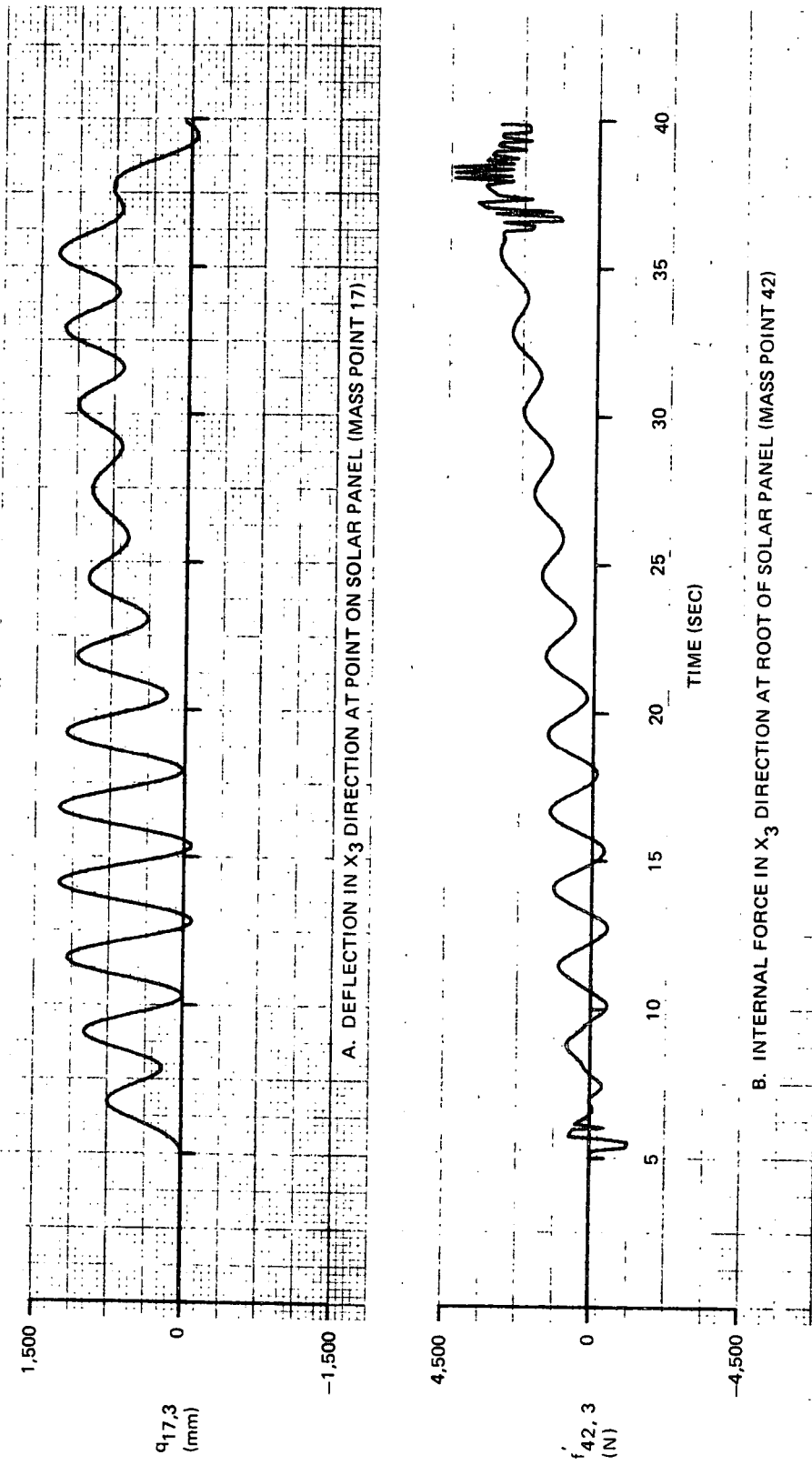


Fig. 6.14 Selected Deflection and Load Components During Spin-Up Maneuver

and the deformations rapidly damped to their quiescent values. The quiescent deformations were highest at certain points on the solar panels. As an example, the deformation in the X_3 direction at mass point 17 ($q_{17,3}$) was approximately 544 mm (21.4 in).

6.2.5 Wobble Control

Figures 6.15 - 6.17 illustrate time histories during wobble control. Initially, the deformations were set to their quiescent values, and the second component of $\{\omega^X\}$ was given a wobble component of .001 rad/sec. Figure 6.15 illustrates the performance of the wobble control system. Up to approximately 27 seconds the curves are essentially identical to a run made for a rigid Space Station. This indicates the usefulness of the mean axes; one reason that they were used was that they move at the average motion of the deformed system. After 27 seconds, some small higher-frequency oscillations predominate due to elastic vibration. The only modification required to the CMG control system was to decrease the amount of wobble at which the CMG stops trying to control wobble (see Section 5). Before this modification was made, the CMG sensor reacted to the residual vibration and the CMG continued to operate in the wobble-damping (gimbal angle-rate) mode throughout the entire run. Figures 6.16 and 6.17 illustrate some of the deformations occurring during this run. δ_3 , $q_{17,2}$, and $q_{17,3}$ have nonzero quiescent deformations, and the oscillations about these values are very small so that their deformations appear to be constant at the quiescent values. Figures 6.18 and 6.19 illustrate the same deformations for the same initial conditions; however, in this case there is no wobble control system present. As in the previous case, δ_3 , $q_{17,2}$, and $q_{17,3}$ are nearly constant at their quiescent values. When comparing the curves with the previous run, note the difference in scales. There is considerably less vibration out of the spin plane (δ_1 and $q_{17,1}$) without the control system since the control moment gyroscope induces primarily out-of-plane vibration in addition to some in-plane vibration. The in-plane vibration (δ_2) is somewhat smaller with no wobble control.

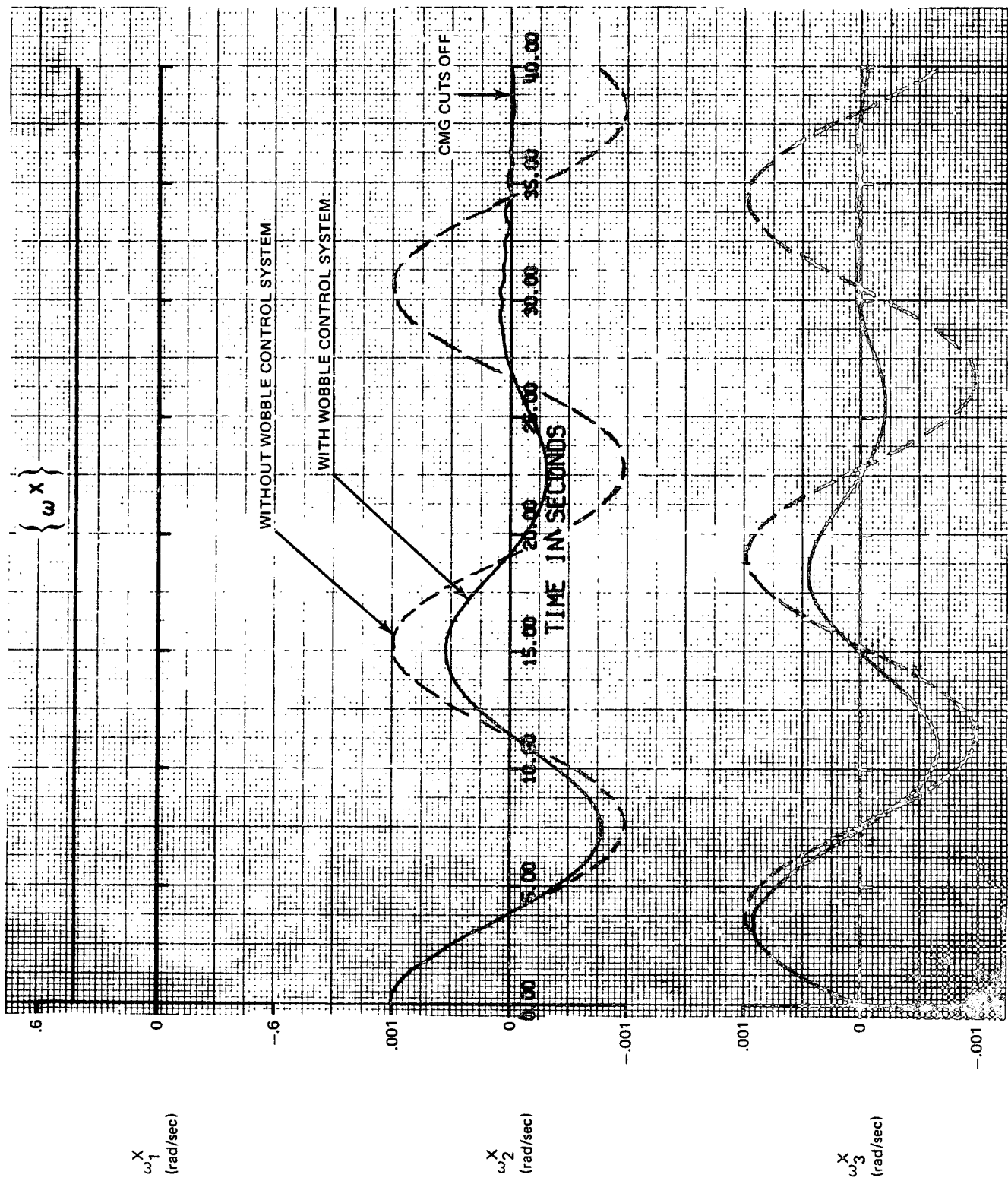


Fig. 6.15 Angular Velocity Illustrating Wobble Control System

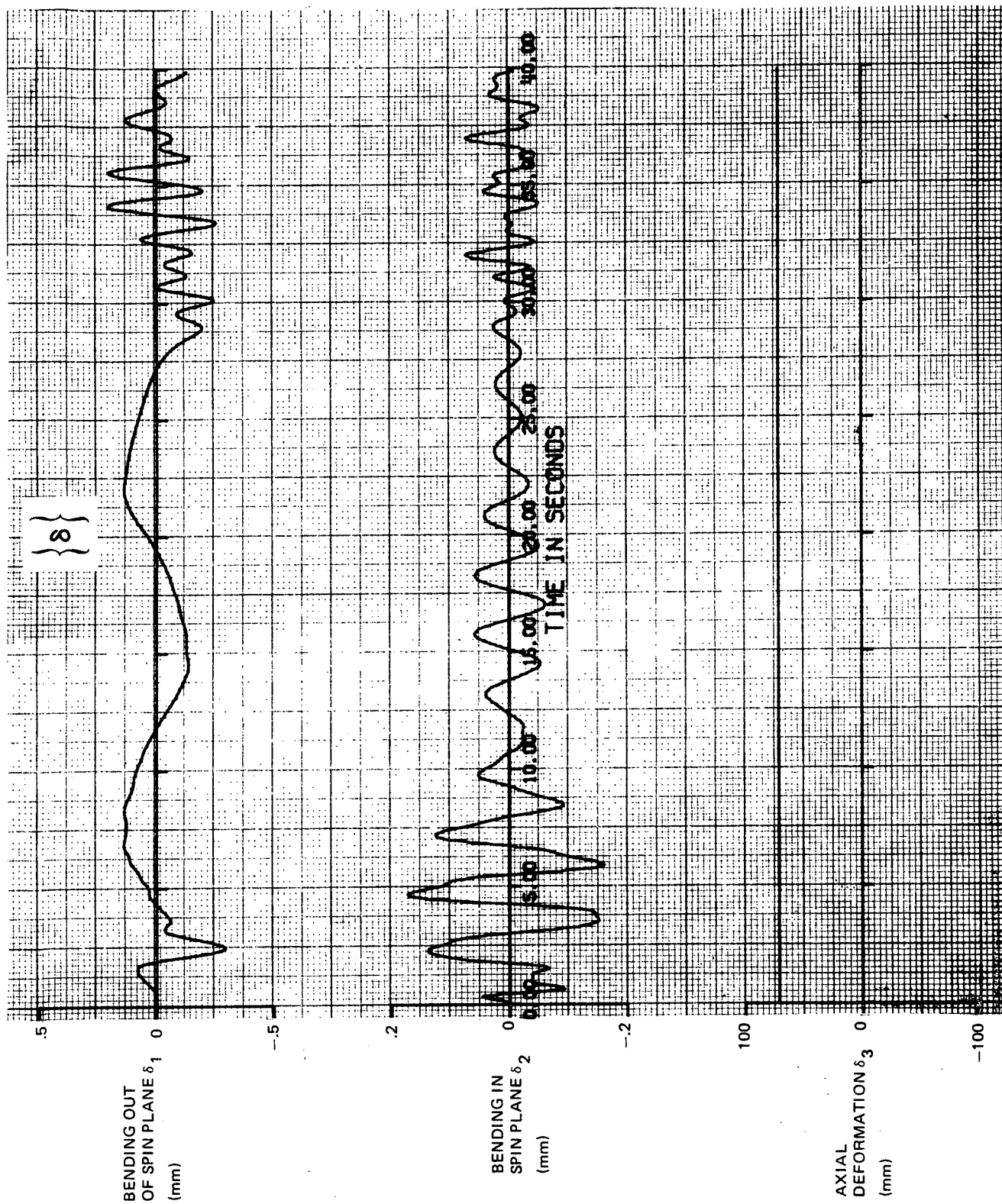


Fig. 6.16 Cantilever Deflection of Connecting Structure During Wobble Control

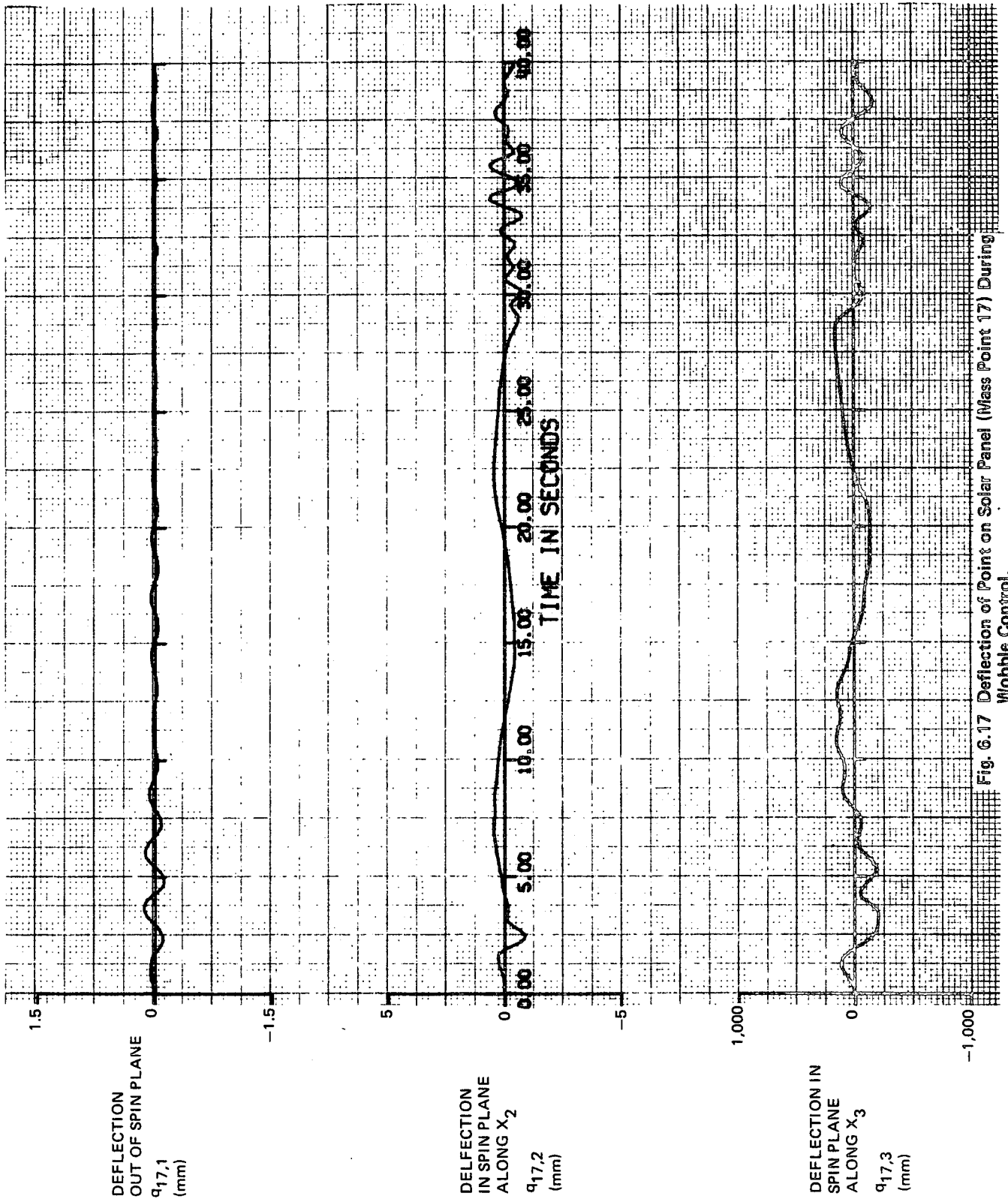


Fig. 6.17 Deflection of Point on Solar Panel (Mass Point 17) During Wobble Control.

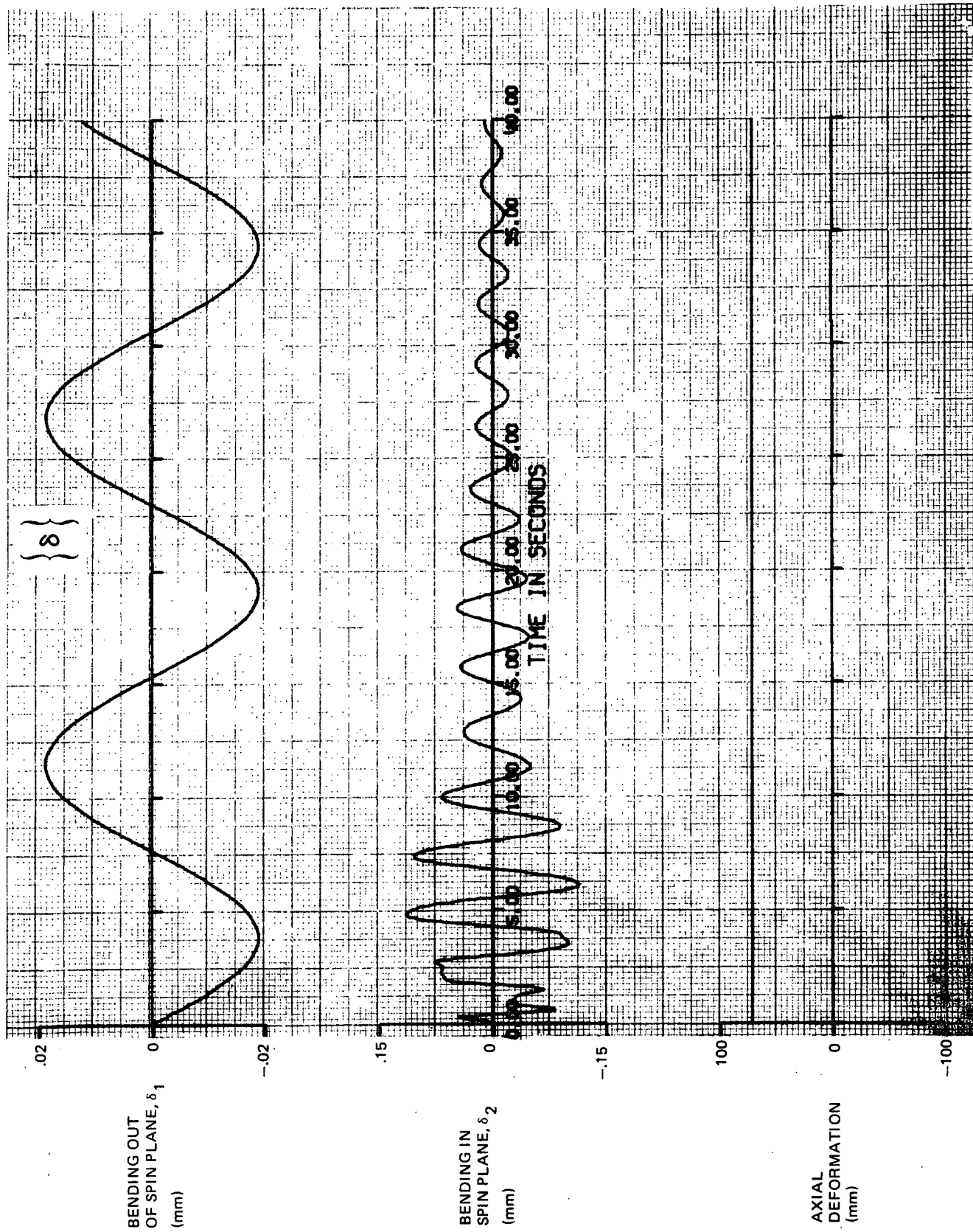


Fig. 6.18 Cantilever Deflection of Connecting Structure With Initial Wobble
But No Wobble Control

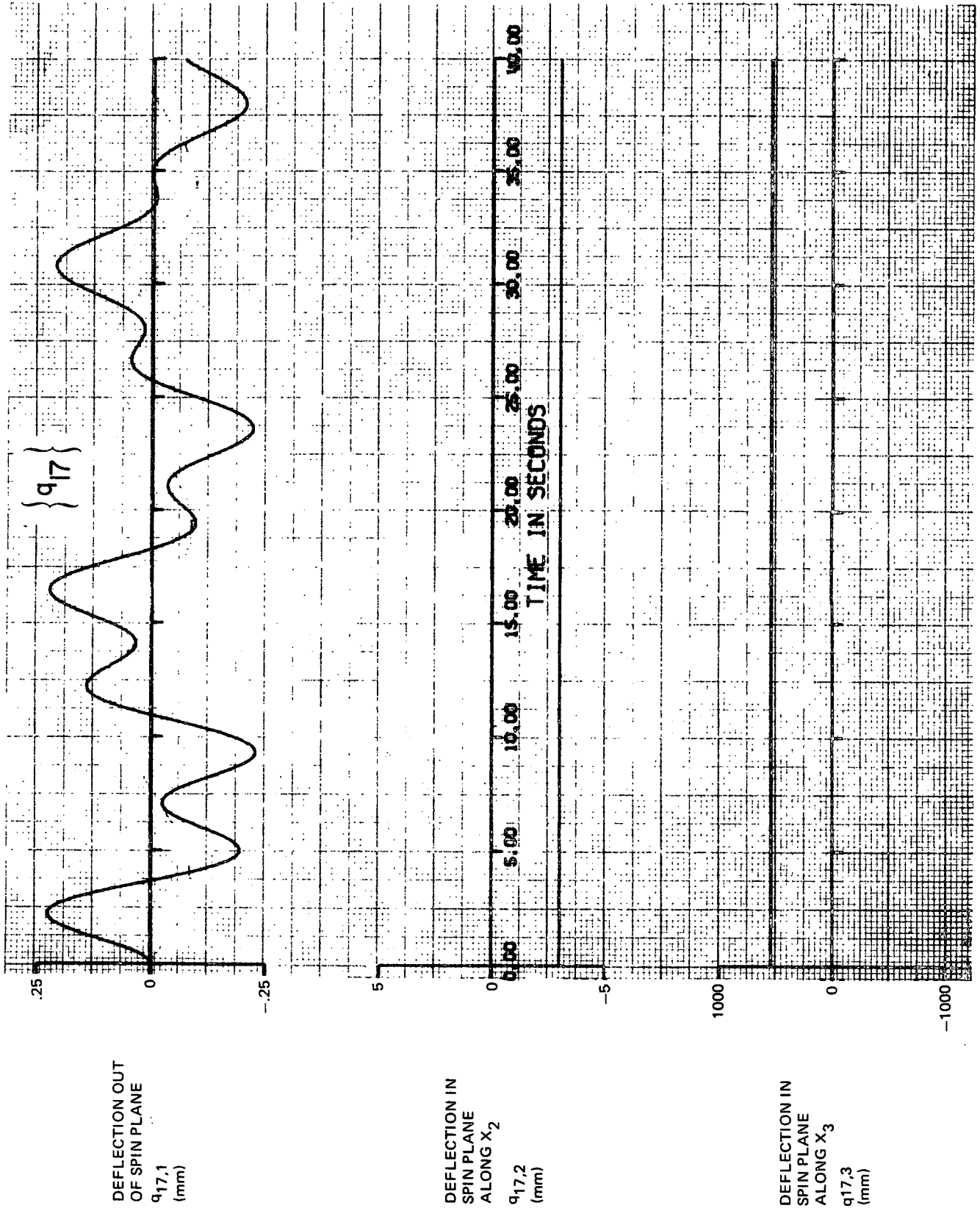


Fig. 6.19 Deflection of Point on Solar Panel (Mass Point 17) With Initial Wobble But No Wobble Control

6.2.6 Elevator Motion With Balance Mass Control

Moving rigid masses were present only in the runs described in this subsection. In these runs a 4,530 kg (10,000 lb) elevator and a 2,270 kg (5,000 lb) balance mass are initially located on the X_3 axis near the Laboratory cm. Both masses move along the X_3 axis. All rigid-body and flexible motion is in the spin plane. Initially the Space Station is rotating in the quiescent state. Figure 6.20 illustrates the performance of the control system which operated properly on a rigid idealization of the Space Station. The short 1.524 m (60 in) motion of the elevator should have resulted in a 3.048 m (120 in) motion of the balance mass in the opposite direction, thus nulling the error in the position of the Space-Station center of mass. The curves show that the balance mass overshoots and the error oscillates; thus this attempt at mass balancing is unsuccessful. To understand the reason for this problem, it is helpful to reexamine the the control concept. An accelerometer located at mass point 4 on the Laboratory senses the acceleration. When the centrifugal portion of the acceleration is unequal to the commanded value, it is known that the center of mass of the Space Station has shifted since the vehicle rotates about its center of mass. It is desired to move the balance mass in the proper direction to null the error in the measured acceleration. Compensation for rigid-body acceleration effects such as wobble has been provided in the control law in order to separate the centrifugal acceleration from the other components of acceleration; however, no compensation for vibration of the accelerometer support was provided. The original control system incorporated an on-off actuator where the balance mass was either moved at constant acceleration or at zero acceleration, depending on the magnitude of the error. Whenever the balance mass was moved, an equal and opposite reaction on the Laboratory caused elastic motion of the Laboratory relative to the Counterweight. Periodically, the generated acceleration at the sensor due to this vibration overwhelmed the centrifugal acceleration and caused the balance mass to reverse its direction at a relatively high frequency. The accompanying high frequency limit cycle vibration in the axial direction is evident in the plot of δ_3

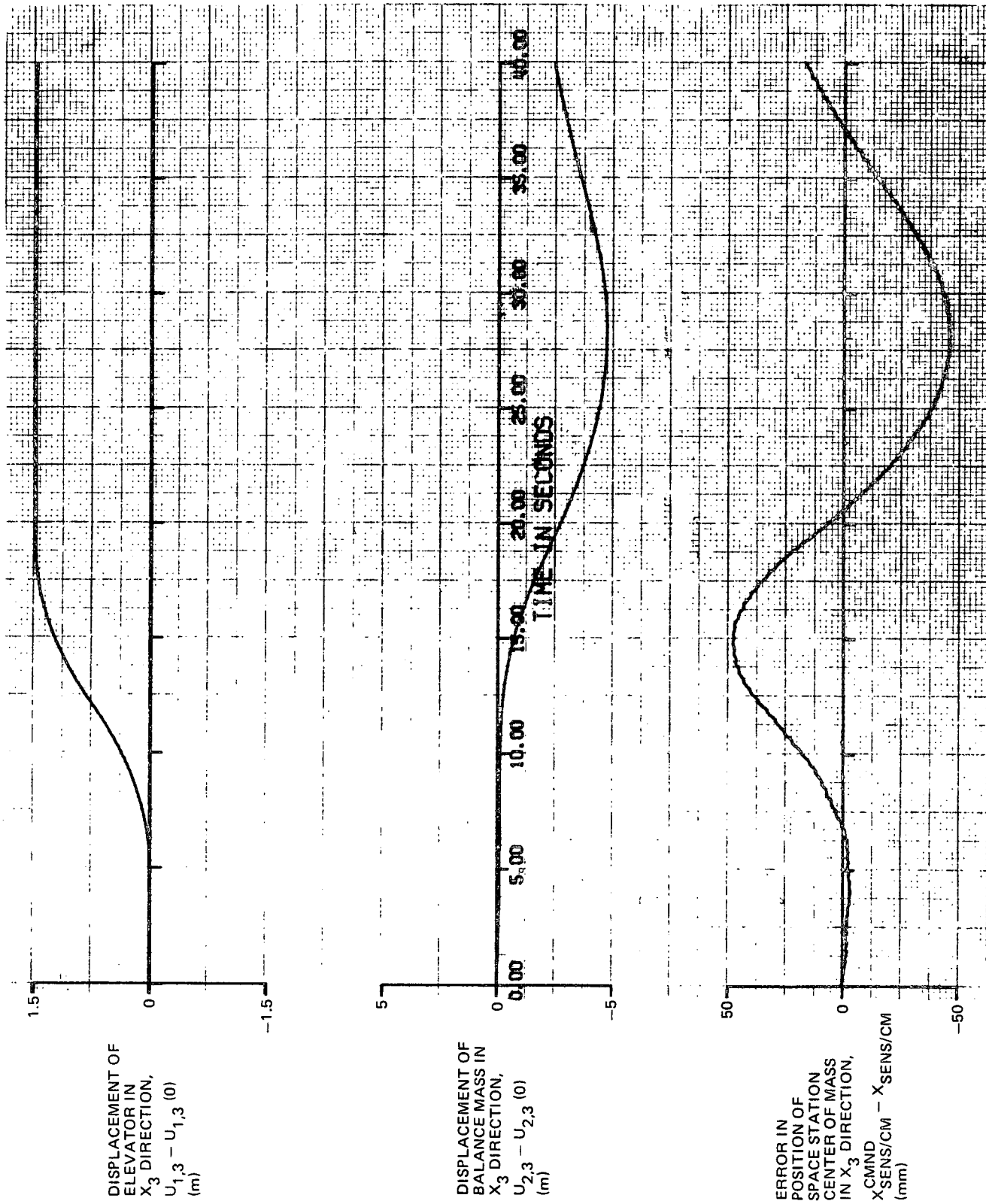


Fig. 6.20 Unsuccessful Attempt at Mass Balance Control

in Figure 6.21. The chattering of the balance mass caused the sluggish motion indicated in Figure 6.20 because it had short spurts of motion in the wrong direction for a large proportion of the time. Acceptable control could not be achieved by either varying the control-system parameters or filtering the error signal; therefore the on-off control law was replaced by the proportional control described in Section 5.

The new control law provided satisfactory control as shown in Figure 6.22. The elevator and balance mass are initially located at $X_3 = 19.4$ and 8.9 m, respectively, and the elevator moves towards the balance mass at $t = 5$ seconds. The control system is required to balance a longer elevator motion of 7.00 m. The curve showing the error in the position of the Space-Station center of mass indicates that there is a lag in the response of the balance mass, however by the end of the run the Space Station is balanced. The deformations in the Connecting Structure during this run are shown in Figure 6.23. Note that there is an initial vibration although the elevator does not begin its motion until 5 seconds. This initial vibration results because the initial quiescent deformations are inaccurate for this case since they were obtained in a run where moving masses were not present. The main Connecting-Structure bending effects are caused by the Coriolis forces exerted by the moving masses on the Laboratory and by the spin jets which torque the Laboratory to maintain the commanded constant spin speed. The deformation at mass point 17, which is on a solar panel, and the internal force exerted by the solar panel at its root (mass point 42) are shown in Figures 6.24 and 6.25.

6.2.7 Fluid Pumped Through Laboratory

Fluid was present only during this run. The fluid is pumped along the long axis of the Laboratory as shown in Figure J1 of Appendix J. Pumping begins at 2 seconds. The fluid velocity and height of the fluid in the emptying reservoir, located on mass point 8, are shown in Figure 6.26. Pumping proceeds until the emptying reservoir is empty at $t = 35.7$ seconds when the pump suddenly shuts down. After shut down, fluid remains in the pipe line. All motion during this run occurs in the spin plane. Figure 6.27 shows the deformations of the Connecting Structure. When the fluid is being pumped, the bending is illustrated in Figure 6.28.

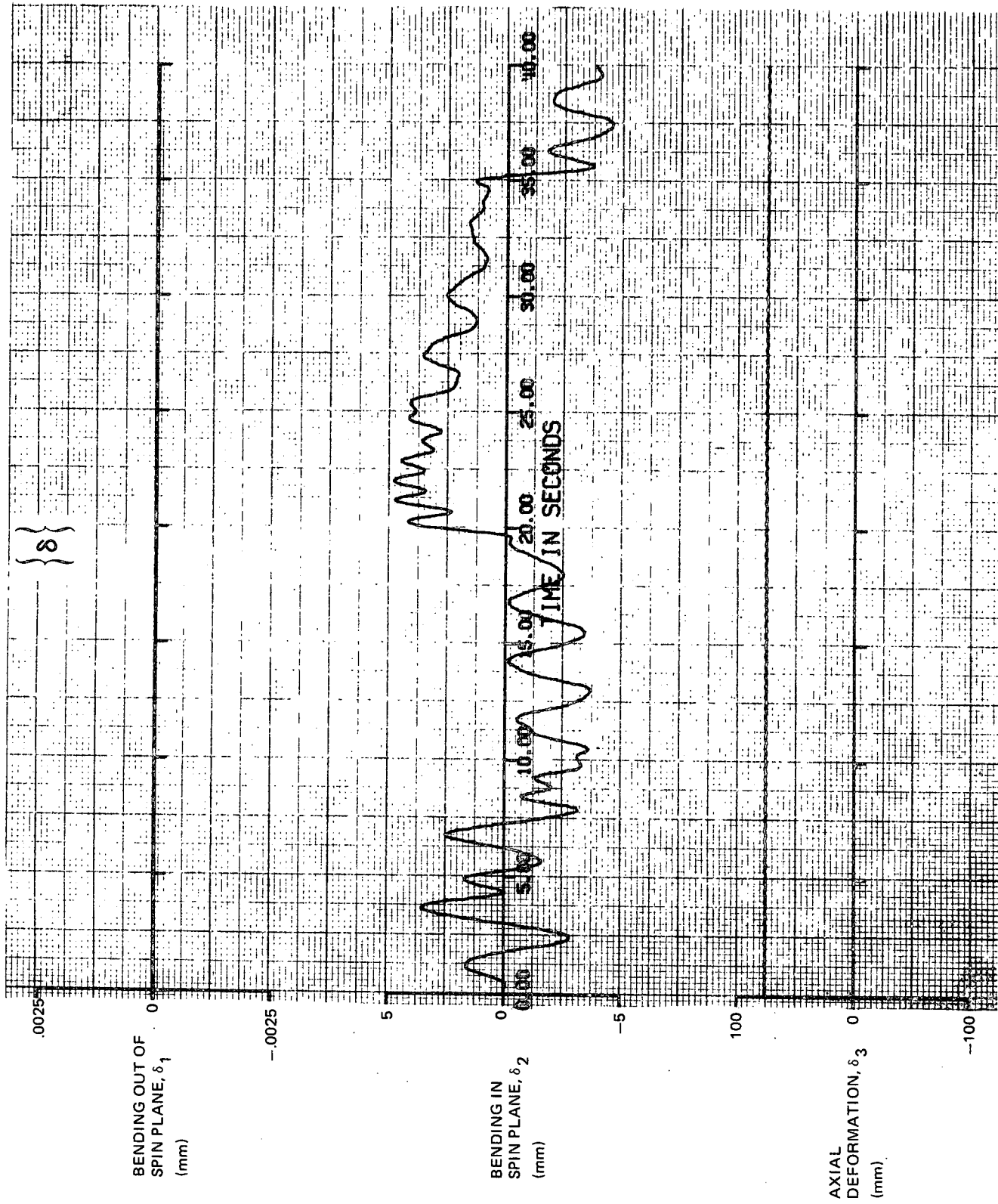


Fig. 6.21 Cantilever Deflection of Connecting Structure During Unsuccessful Attempt at Mass Balance Control

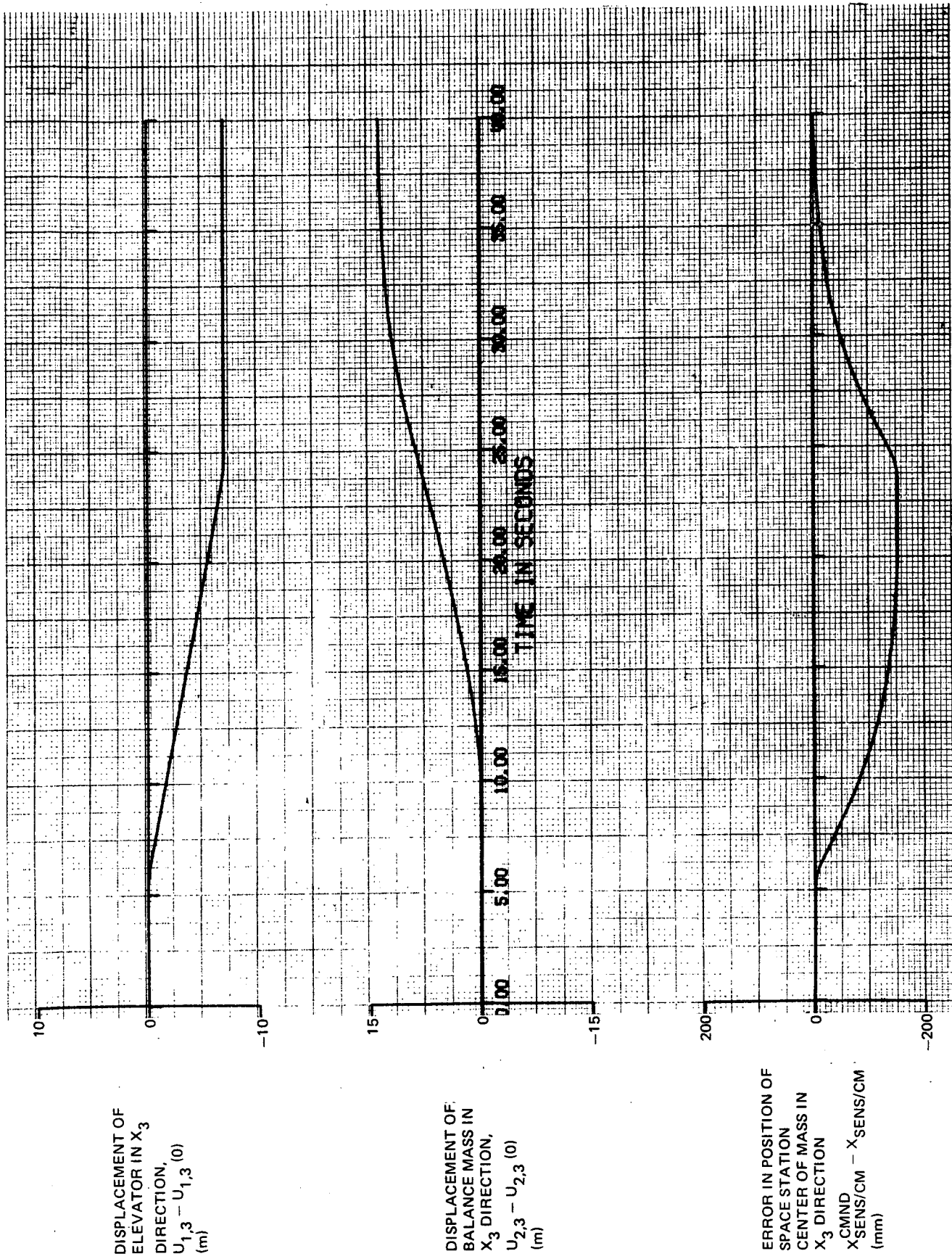


Fig. 6.22 Satisfactory Performance of Balance Mass Control System

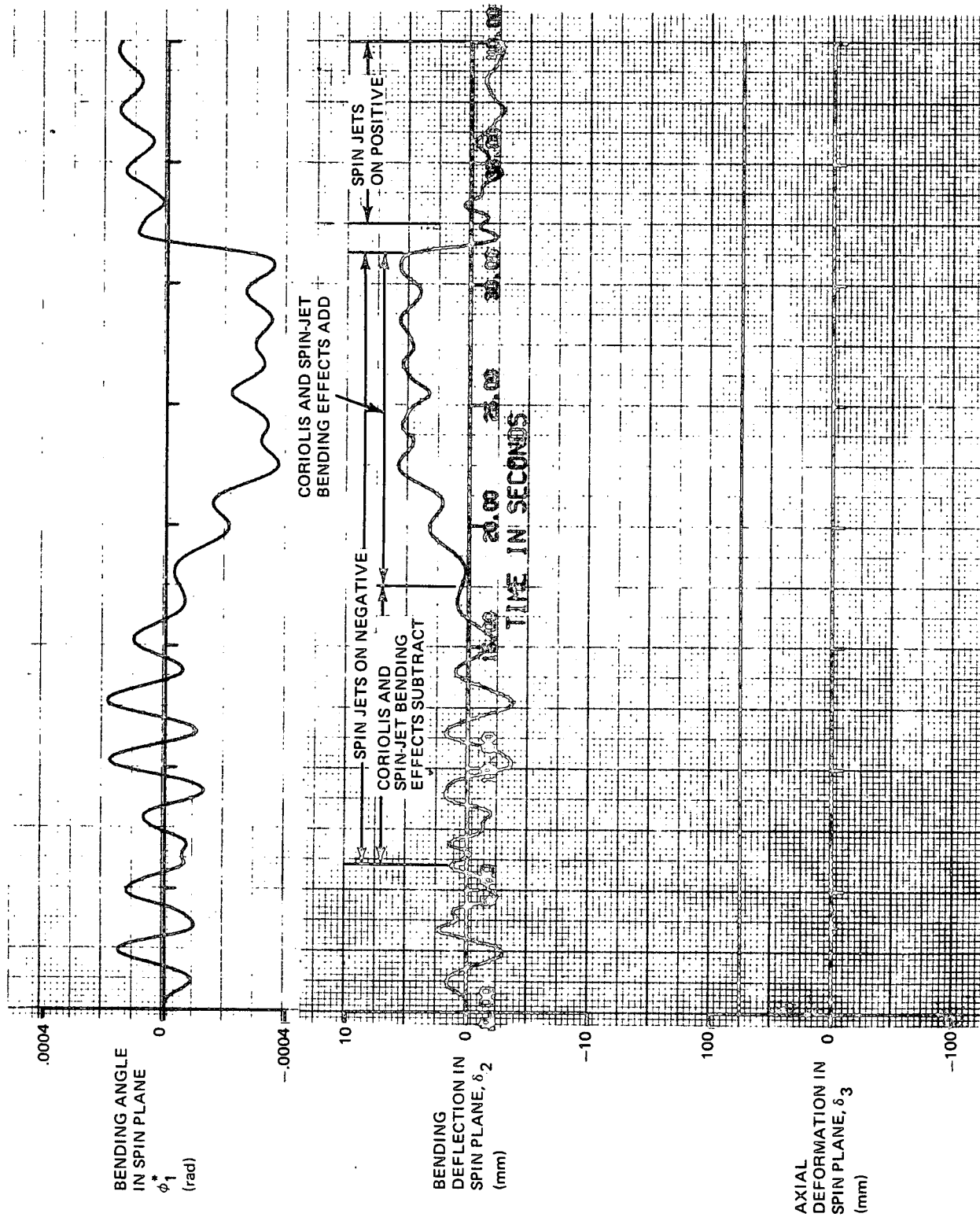


Fig. 6.23 Cantilever Deflection of Connecting Structure During Mass Balancing

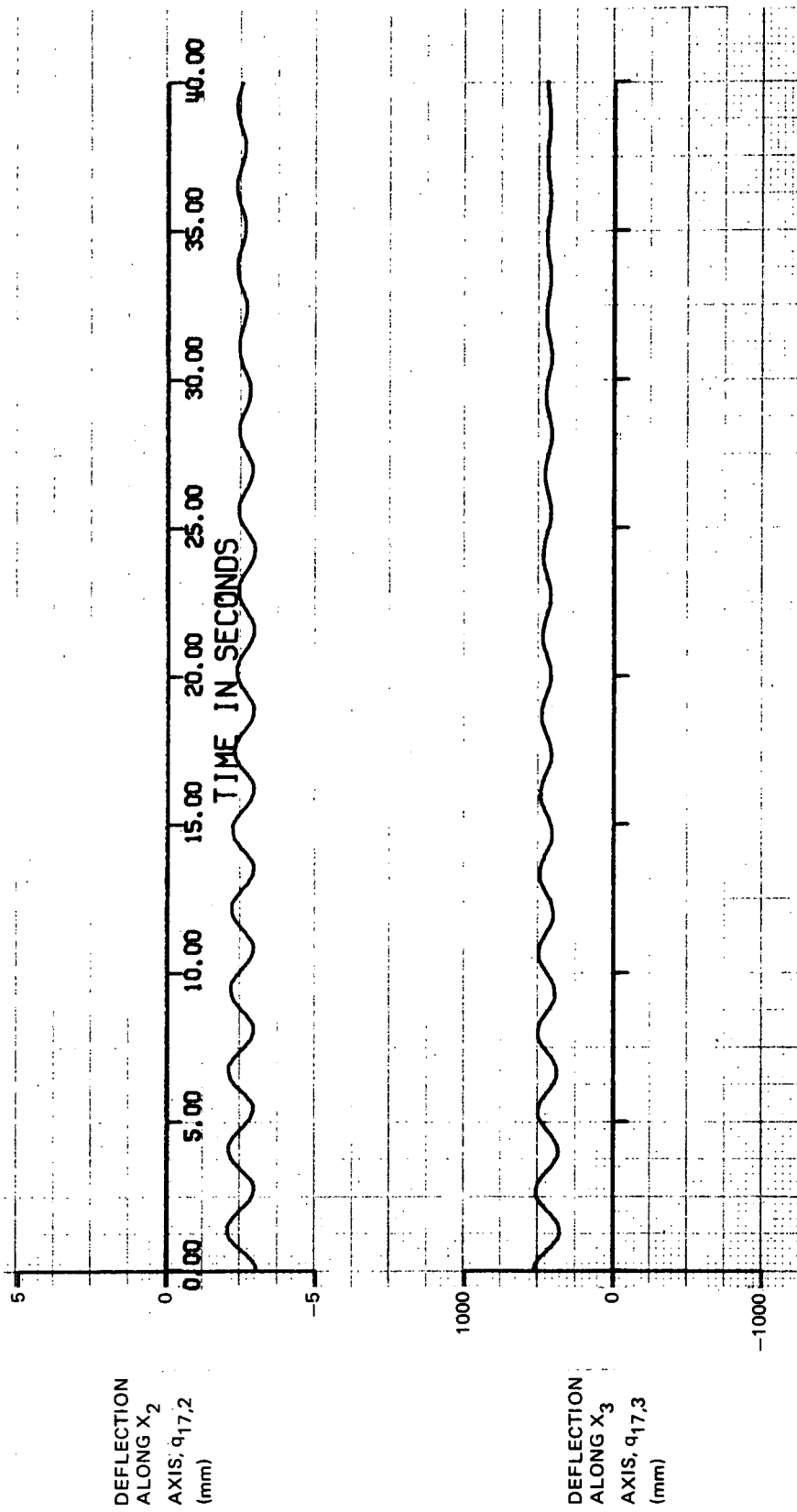


Fig. 6.24 Deflection of Point on Solar Panel (Mass Point 17) During Mass Balancing

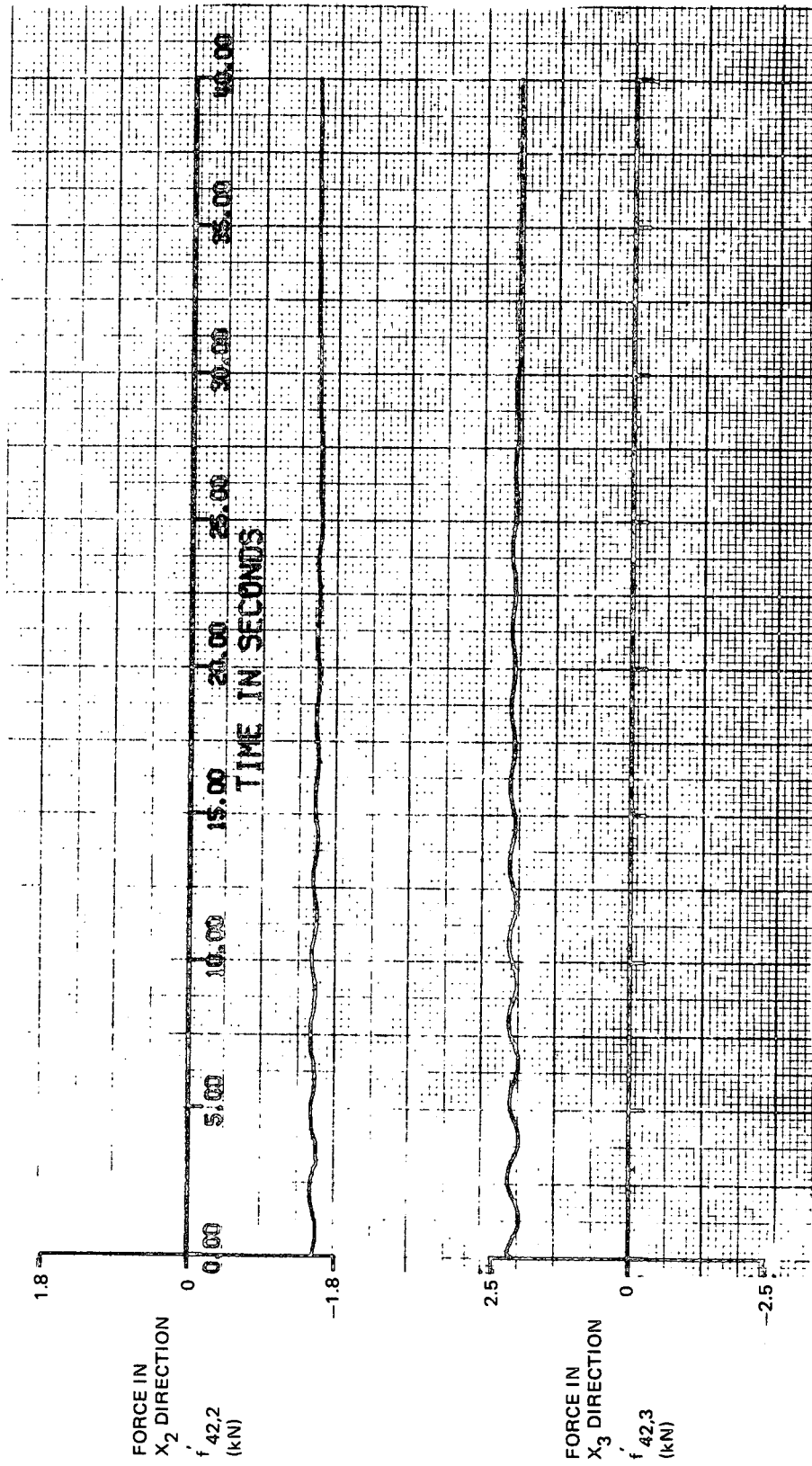


Fig. 6.25 Force at Root of Solar Panel (Mass Point 42) During Mass Balancing

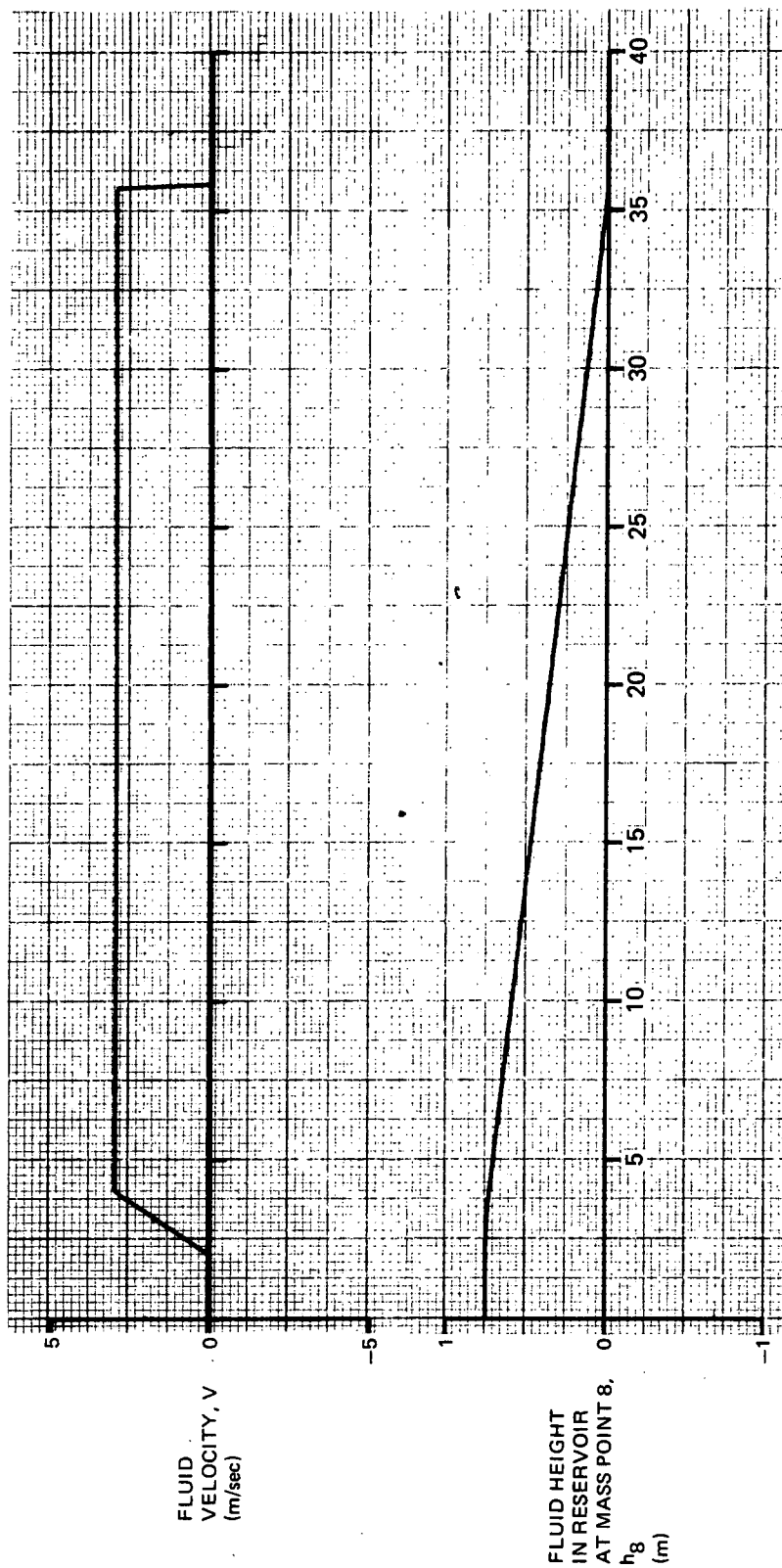


Fig. 6.26 Fluid Motion on the Laboratory

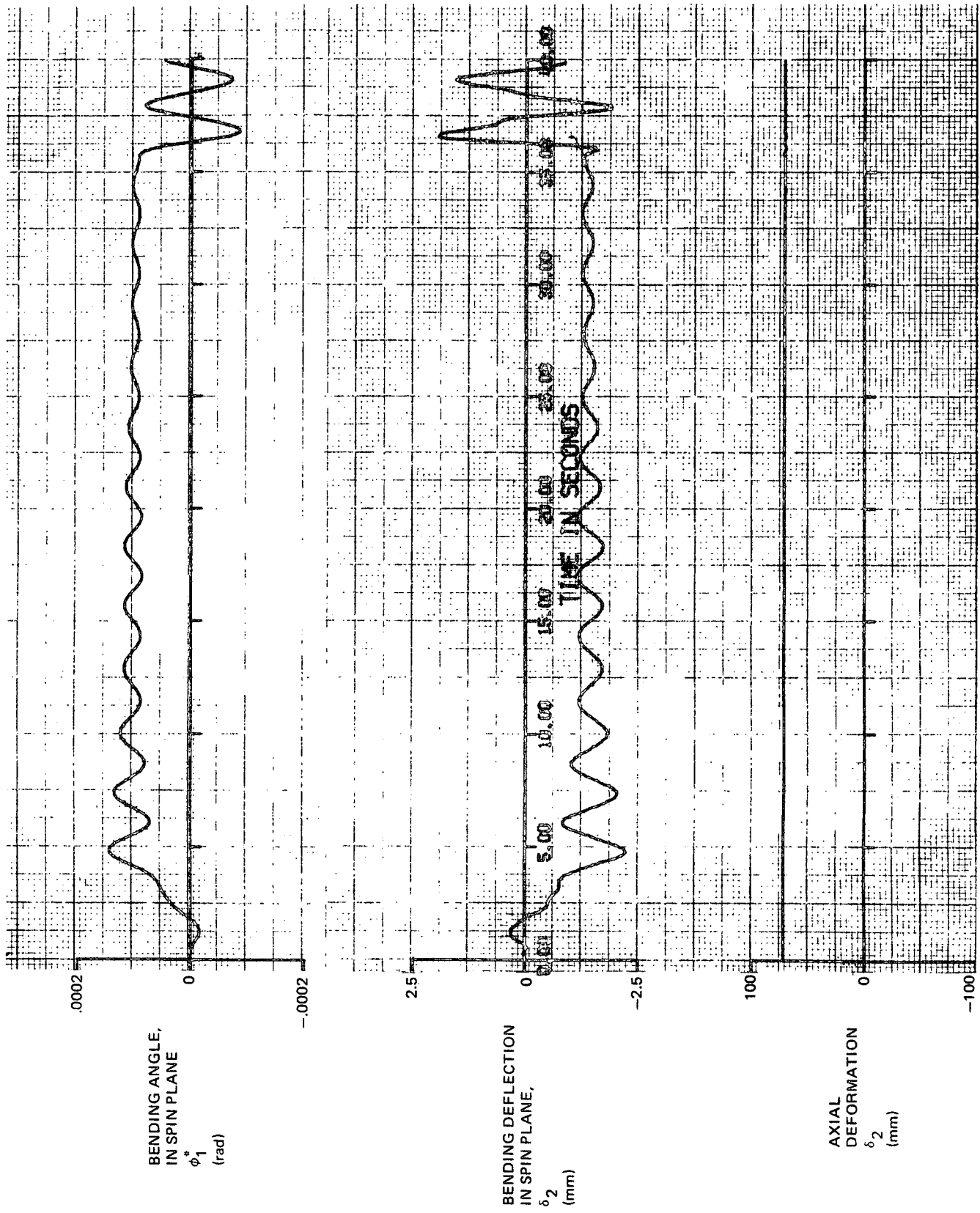


Fig. 6.27 Cantilever Deflection of Connecting Structure During Fluid Motion

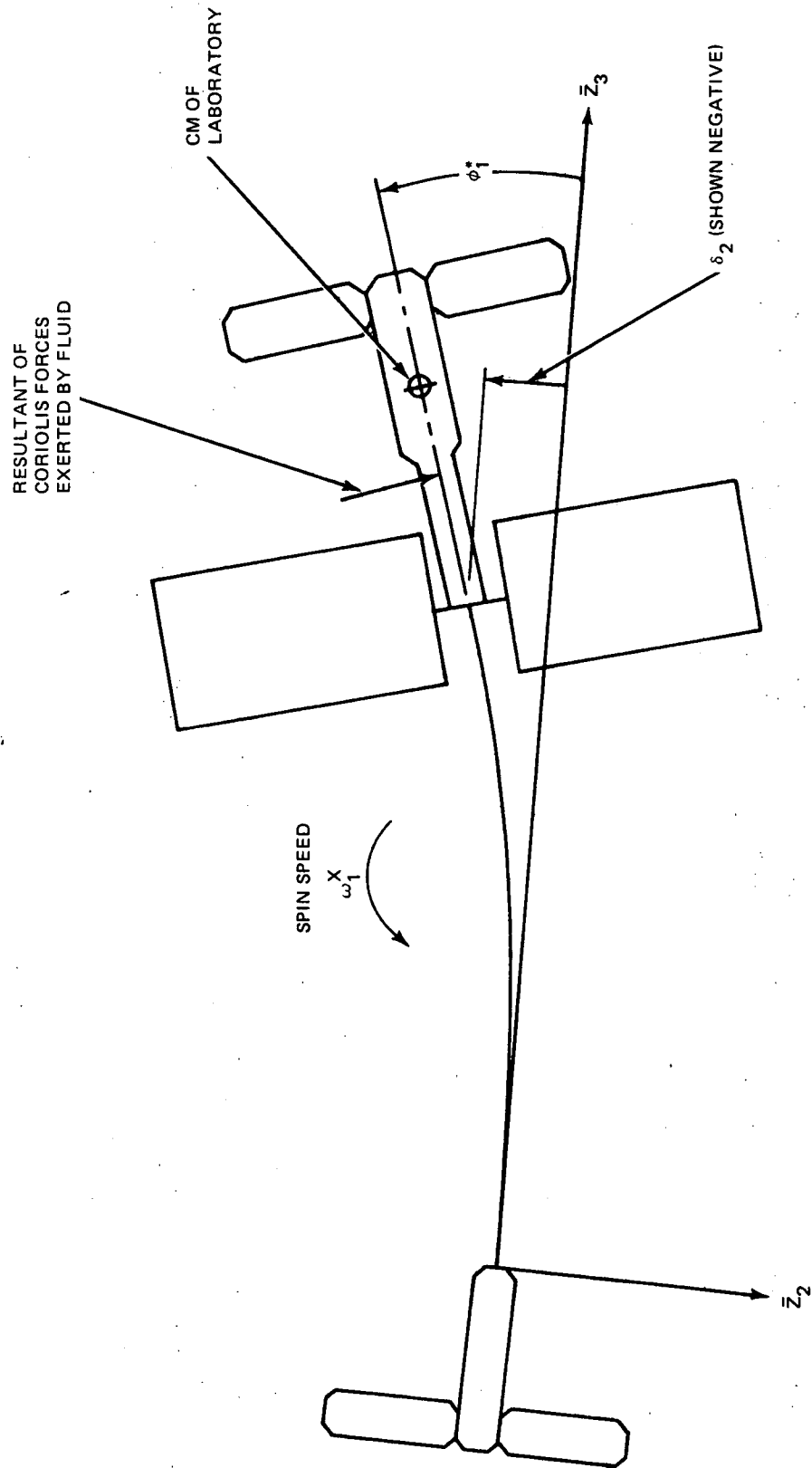


Fig. 6.28 Sketch Illustrating Bending in Connecting Structure (Exaggerated) During Fluid Motion

The primary reason for this bending is that the resultant of the Coriolis forces exerted by the fluid acts to the left of the cm of the Laboratory as illustrated in the figure. This force also tends to slow the spin speed of the Laboratory slightly (from .4189 to .4149 rad/sec). The control system is not operational; therefore the spin jets do not turn on to correct the spin speed.

7.0 CONCEPTS FOR A SCALE MODEL

7.1 INTRODUCTION

This section contains a discussion of concepts for the design of a working scale model of the Space Station which can be operated and observed in a small test facility. Because of gravitational effects it is felt that it is beyond the state-of-the-art to properly simulate the elastic properties of the Laboratory and the Counterweight; therefore these structures will be modeled as rigid bodies. The Connecting-Structure flexibility will, however, be taken into account.

A scale model has already been successfully constructed to demonstrate the unforced dynamic behavior of a system of this type.* It was possible to apply torques to this model; however the model could not simulate the motion if the externally applied forces were unbalanced (i.e., the resultant force had to be zero). Also, this model was not capable of illustrating deployment and retraction maneuvers. To correct these deficiencies, an advanced model is proposed. This new model will be capable of demonstrating the dynamics when unbalanced forces are applied.

It will also be capable of demonstrating deployment and retraction maneuvers. Thus, it will be possible to fit this model with a set of scaled control systems (e.g., a CMG, gas jets, deployment-retraction motor).

* Austin, F. and Bauer, E. "Scaled Dynamic Model of a Free Rotating Cable-Connected Space Station," Journal of Spacecraft and Rockets, Vol. 7, No. 10, October 1970, pp. 1272-1274 (also published as Grumman Aerospace Corporation Note No. ADN 06-03-70.1, June 1970).

7.2 SUSPENSION-SYSTEM DESIGN

The suspension system which supports the model must be able to effectively eliminate the influence of gravity forces and torques without interfering with the vehicle's natural motion. Gravity torques are eliminated by suspending both the Laboratory and the Counterweight at their centers of mass. At each of these two support points, the suspension system must apply an upward force, precisely equal to the weight of the member being supported. In addition, the ideal suspension system will accomplish these tasks without restraining any of the motions of the vehicle which would occur naturally as it moves in space.

The recommended suspension-system design is shown in Figures 7.2 and 7.5. This system, and alternative design concepts, will now be discussed. To understand the design requirements it is beneficial to first examine the degrees of freedom of the model.

The proposed model has 12 degrees of freedom; i.e., its position can be completely described by 12 independent coordinates. The coordinates illustrated in Figure 7.1 have been selected because they will facilitate the explanation of the model suspension system. These coordinates are the locations of the Space-Station center of mass, X , Y , and Z ; the Space-Station yaw and pitch angles ψ and η ; the deployment length l ; the roll, pitch, and yaw angles of the Laboratory θ_x , θ_y , and θ_z , and of the Counterweight ϕ_x , ϕ_y , and ϕ_z . If the suspension system allows independent movement of the model, in each of these 12 coordinate directions without providing any resisting loads (other than the weight-cancellation loads previously discussed), then Lagrange's equations for the model will be analogous to those for the Space Station.* As a result the motion of the model will duplicate the scaled motion of the Space Station.

The proposed model with the recommended suspension-system design is shown in Figure 7.2. Masses at each end of the model represent the Laboratory and the Counterweight. The two blocks representing each body provide correct scaling of the masses and moments of inertia. It is not necessary to scale the actual shapes.

* The ideal suspension system would have to be weightless and frictionless for the analogy to hold exactly.

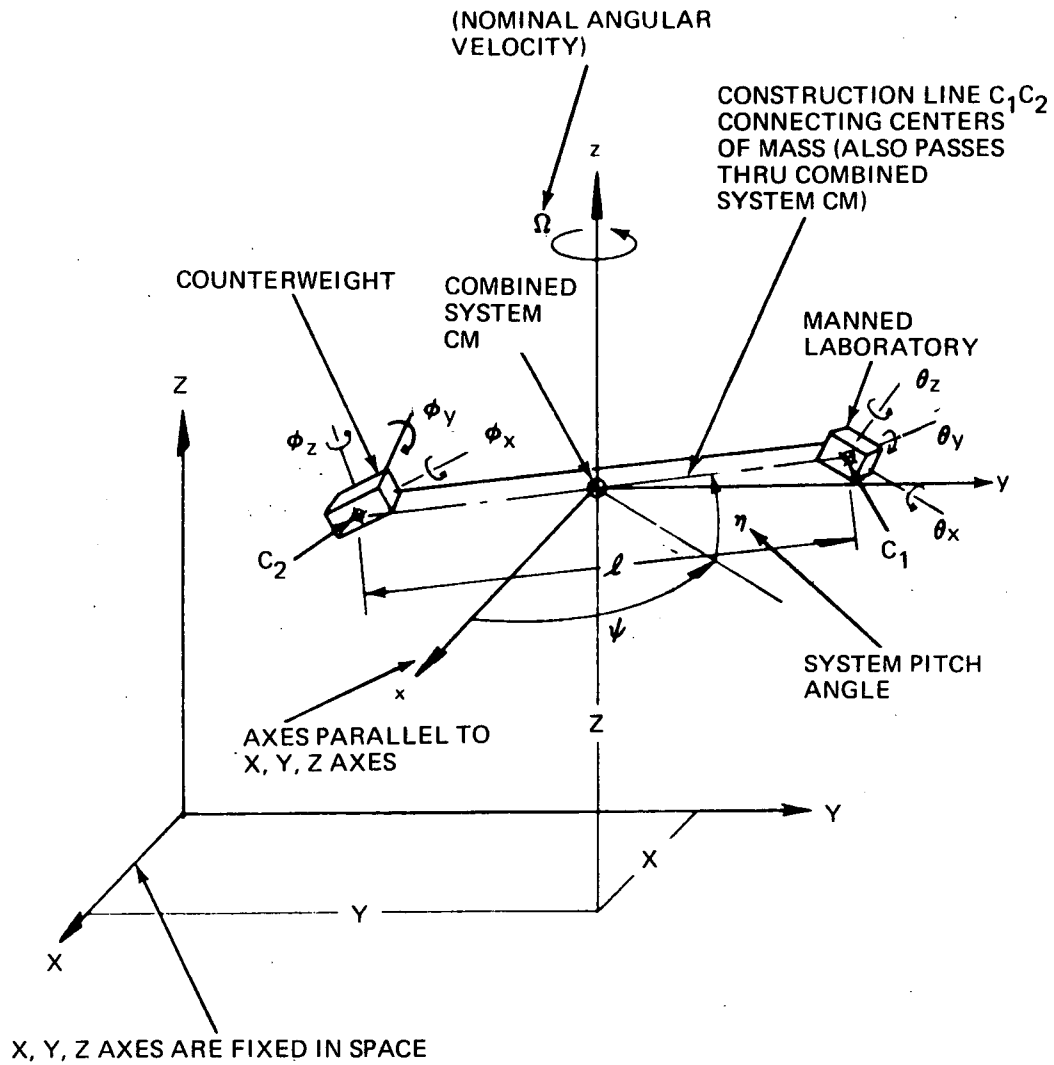


Fig. 7.1 Basic Coordinates For Space-Station Model

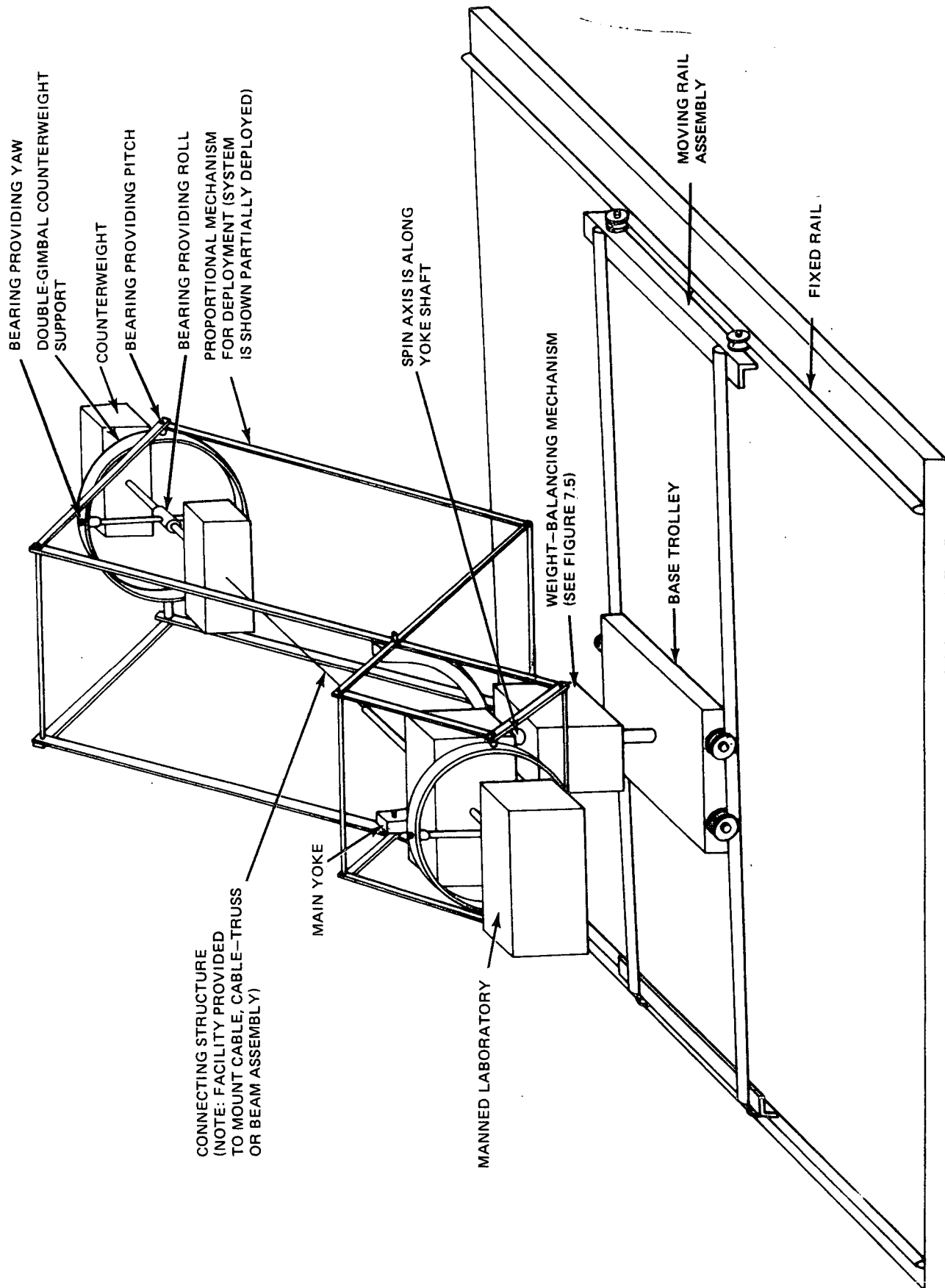


Fig. 7.2 Sketch of Space-Station Model and Recommended Suspension System

7.2.1 The Gimbaled Supports

The Laboratory is supported at its center of mass by the type of double-gimbal mechanism used to support gyroscopes. This device has bearings which provide yaw, pitch, and roll angles (θ_x , θ_y , and θ_z), respectively. The device supports the Laboratory at its center of mass as required. The Counterweight is supported by a similar device.

7.2.2 Proportional Mechanism

The proportional mechanism shown in Figure 7.2 is required to maintain the proper dimensions between the end-mass support points during normal Space-Station operation as well as deployment and retraction maneuvers. This is accomplished by the geometry of the pantograph-type proportional mechanism. As shown in Figure 7.3, the loads exerted on this mechanism are F_1 by the Laboratory, F_2 by the Counterweight, and $w_L + w_C$ by the main-yoke, where w_L and w_C are the weights of the Laboratory and Counterweight, respectively. The method for applying the constant load $w_L + w_C$ will be discussed later. The structure is balanced at the main-yoke support point; therefore the proportional mechanism must be in equilibrium. It follows that

$$\left. \begin{aligned} F_1 + F_2 &= w_L + w_C \\ F_1 a_1 \cos \eta &= F_2 a_2 \cos \eta \end{aligned} \right\} \quad (7.1)$$

For reasons that will become apparent shortly, it is also required that the proportional mechanism maintain the following value of a_1/a_2 for all possible values of the deployment length ℓ :

$$\frac{a_1}{a_2} = \frac{w_C}{w_L} \quad (7.2)$$

If a_1/a_2 is eliminated from the second of Equations (7.1) by substituting Equation (7.2) and the resulting equations are solved for F_1 and F_2 , the solutions obtained would be $F_1 = w_L$ and $F_2 = w_C$. Thus, the condition stipulated by Equation (7.2) guarantees that the vertical loads applied to

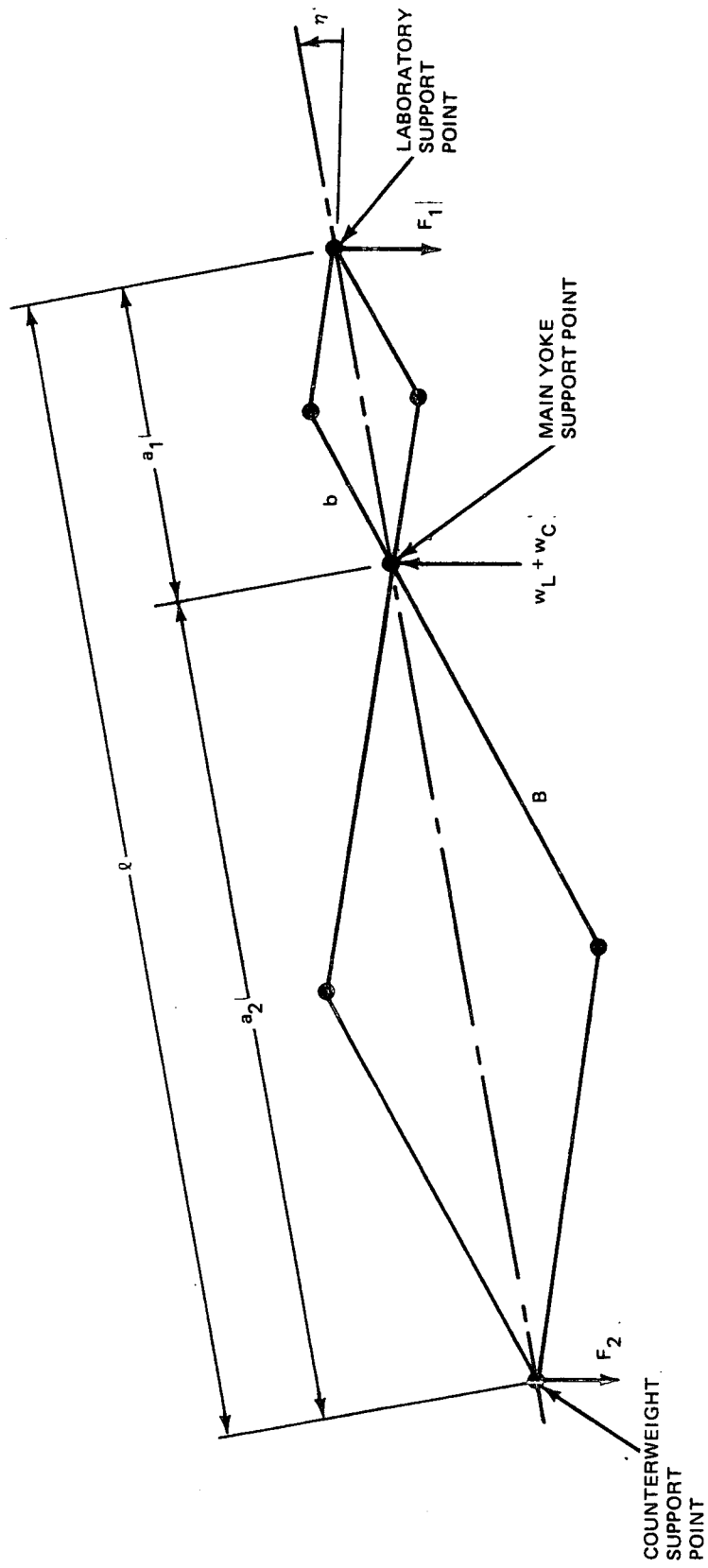


Fig. 7.3 Geometry of Proportional Mechanism

the Laboratory and the Counterweight by the suspension system are always equal to the weights of these bodies. A massless proportional mechanism has been assumed so that inertia loads did not enter into the above argument. The condition that a_1/a_2 is the constant weight ratio given by Equation (7.2) can always be met by the mechanism shown in Figure 7.3 by selecting the length of the links b and B such that

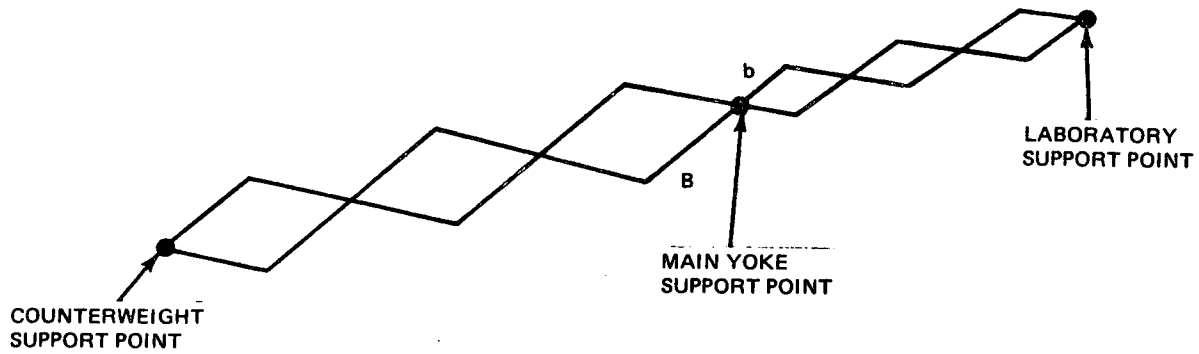
$$\frac{b}{B} = \frac{w_C}{w_L} \quad (7.3)$$

By the geometry of Figure 7.3, $a_1/a_2 = b/B$ regardless of ℓ , and substitution of Equation (7.3) into this relation yields Equation (7.2); thus, the proportional mechanism shown provides the proper value of a_1/a_2 for all possible values of the deployment length ℓ .

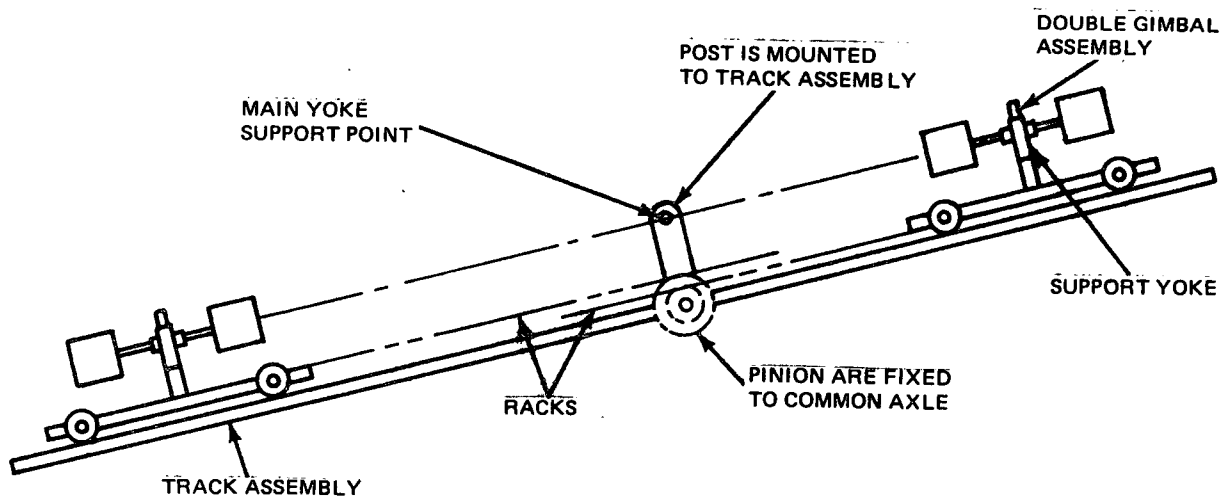
Actually, any proportional mechanism that maintains the constant ratio of a_1/a_2 given by Equation (7.2) may be used. Alternative mechanisms are shown in Figure 7.4. The extended pantograph shown in Figure 7.4A may have any number of diamonds; however the number to the right of the main yoke must be equal to the number to the left of the main yoke. While this mechanism takes up less space when it is retracted, it is more complex, has more bearings, and is likely to have more play than the simple pantograph of Figure 7.3. In Figure 7.4B, the ratio of Equation (7.2) is maintained by a set of racks and pinions. In this design each double-gimbal assembly of Figure 7.2 would be mounted to a support yoke which, in turn, is mounted to a trolley. Both trolleys ride on the track shown. Because of the complexity of this mechanism and additional mass it is considered less desirable than the design of Figure 7.3. In particular, when the Space Station is retracted, the moment of inertia of the track about the spin axis becomes relatively large. For the reasons cited above, the design of Figure 7.3 is recommended.

7.2.3 Main Yoke

The proportional mechanism tilts about a horizontal axis through the main yoke is shown on Figure 7.2. In this way, the degree of freedom η shown in Figure 7.1 is achieved. To obtain ψ , the yoke can rotate about a vertical axis. The bearing is located at the top of the weight-balancing device as shown in Figure 7.5.



A EXTENDED PANTOGRAPH



B RACK AND PINION MECHANISM

Fig. 7.4 Alternative Proportional-Mechanism Concepts

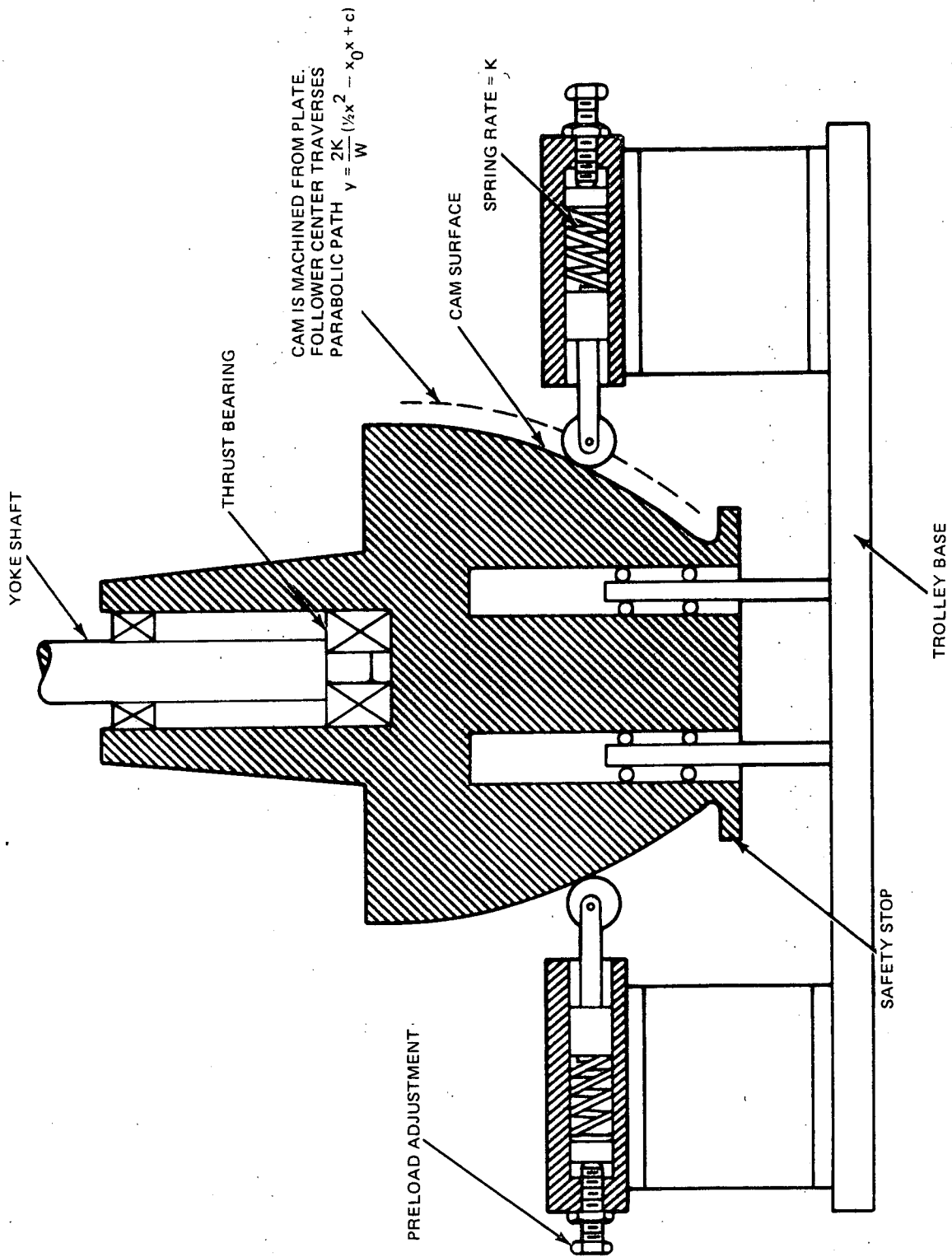


Fig. 7.5 Detail of Weight-Balancing Mechanism

7.2.4 Horizontal Freedom of Space Station Mass Center

The degrees of freedom X and Y shown in Figure 7.1 are achieved by the trolley and rail assemblies shown on Figure 7.2. The trolley moves in one direction along a moving rail assembly which, in turn, has freedom to move in the perpendicular direction by rolling along a fixed rail assembly. Alternative methods of achieving freedom of the base in the X and Y directions include removing the wheels of the base and simply allowing it to slide on a lubricated surface. However, the spurious friction forces would probably be too high. Casters could be mounted to the base; however, the friction forces would then be erratic. Finally, the base could ride on air bearings; however flexible tubing would then have to be mounted to the base, the air pressure would have to be carefully maintained, and the flexibility of the air cushion in the vertical direction might cause problems. For these reasons, the design illustrated in Figure 7.2 is recommended.

7.2.5 Weight-Balancing Mechanism

The remaining degree of freedom which has not been discussed is Z in Figure 7.1. In addition supplying this freedom in the vertical direction, a vertical force equal to the weight W of the entire structure must be applied. This force must remain constant as the structure moves up and down. Counter-balances are not acceptable for this purpose because the applied force would vary with the acceleration. Also, gas-type hydraulic mechanisms were considered and discarded since they would apply forces which are to a large extent proportional to relative velocity and displacement. Constant rate (negator-type) springs are not considered sufficiently accurate and have too much friction.

The final design shown in Figure 7.5 is recommended since it is believed to be far superior to the concepts discussed above. In this design, a cam compresses two springs as Z decreases. The cam surface is designed so that the vertical component of the load applied by the cam followers is always constant and equal to the required weight W . The equation for the cam-follower curve can be obtained from the geometry of Figure 7.6. Since the device is

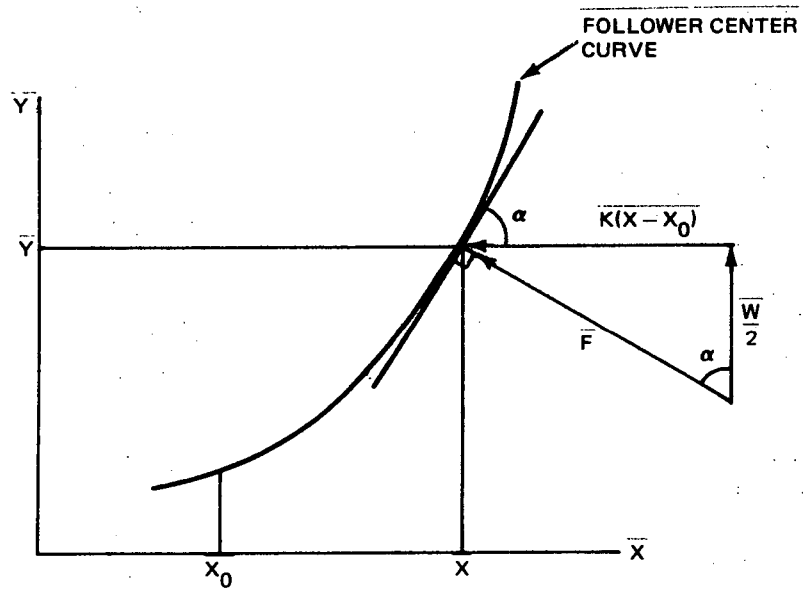


Fig. 7.6 Geometry for Obtaining Curve Traversed by Cam-Follower Center.

assumed frictionless, the resultant load F applied to the cam follower by its bearing is normal to the curve as shown. The horizontal component is $K(X-X_0)$, where X_0 is the value of X when the spring is undeformed, and the required vertical component is $W/2$ since there are two springs. From the geometry of the curves

$$\tan \theta = \frac{dY}{dX} = \frac{K(X-X_0)}{W/2}$$

Integrating,

$$Y = \frac{2K}{W} \left(\frac{1}{2} X^2 - X_0 X + C \right) \quad (7.4)$$

where C is a constant of integration which is determined by locating the curve in the X, Y plane. For example, one way of obtaining C would be to specify the value of Y when $X = X_0$.

7.3 SPURIOUS EFFECTS

In order to avoid spurious loads on the model, the ideal suspension system would be massless, frictionless, have perfectly rigid members, and no play in its bearings. Then the suspension system would not apply any inertia or friction loads on the model, nor would suspension-system vibration influence the model's motion. Thus, all bearings and other wear surfaces should be as friction-free as possible and should have a minimum of play. While light weight and high rigidity are to some extent contradictory requirements, the designer should make use of light rigid materials and cross sections such as I beams and tubes. Simple trade-off approximations between weight and rigidity can be made so that the lowest frequency associated with suspension-system vibration is at least ten times the highest model frequency.

APPENDIX A

FLUID MOTION DERIVATIVES

The following derivation is an extension of the derivation presented by Shapiro*. The main difference between the two derivations is that in the reference the control volume is fixed in space, whereas in this report the control volume is fixed to a structural mass of the vibrating rotating Space Station and therefore moves in space. Consider any vector quantity \vec{Q} that is a quantity per unit mass of the fluid. For example \vec{Q} may be the linear momentum of a particle of mass dm . The total contribution of \vec{Q} to the mass present within the control volume at a fixed time is

$$\vec{G} = \int_{S_Y} \vec{Q} dm = \int_{S_Y} \vec{Q} \rho dV \quad (A1)$$

where the S_Y indicates that the integral is taken over a system of fixed fluid mass particles. As time varies, the boundary of this system of particles changes, so that it will no longer coincide with the control-volume boundary at time t . Referring to Figure A1, the mass contained in the control volume shifts position and has the indicated boundary at time $t + \Delta t$. At time t , the fluid occupies the volume designated by I_t and III_t , and at time $t + \Delta t$ the fluid occupies the volume designated by $I_{t+\Delta t}$ and $II_{t+\Delta t}$. Then, the inertial derivative of \vec{G} is

$$\left(\frac{d\vec{G}}{dt} \right)_S = \lim_{\Delta t \rightarrow 0} \left[\frac{(\vec{G}_{I_{t+\Delta t}} + \vec{G}_{II_{t+\Delta t}}) - (\vec{G}_{I_t} + \vec{G}_{III_t})}{\Delta t} \right]$$

* Shapiro, Ascher H., "The Dynamics and Thermodynamics of Compressible Fluid Flow," VI, Ronald Press, N. Y. 1953, P. 12-20

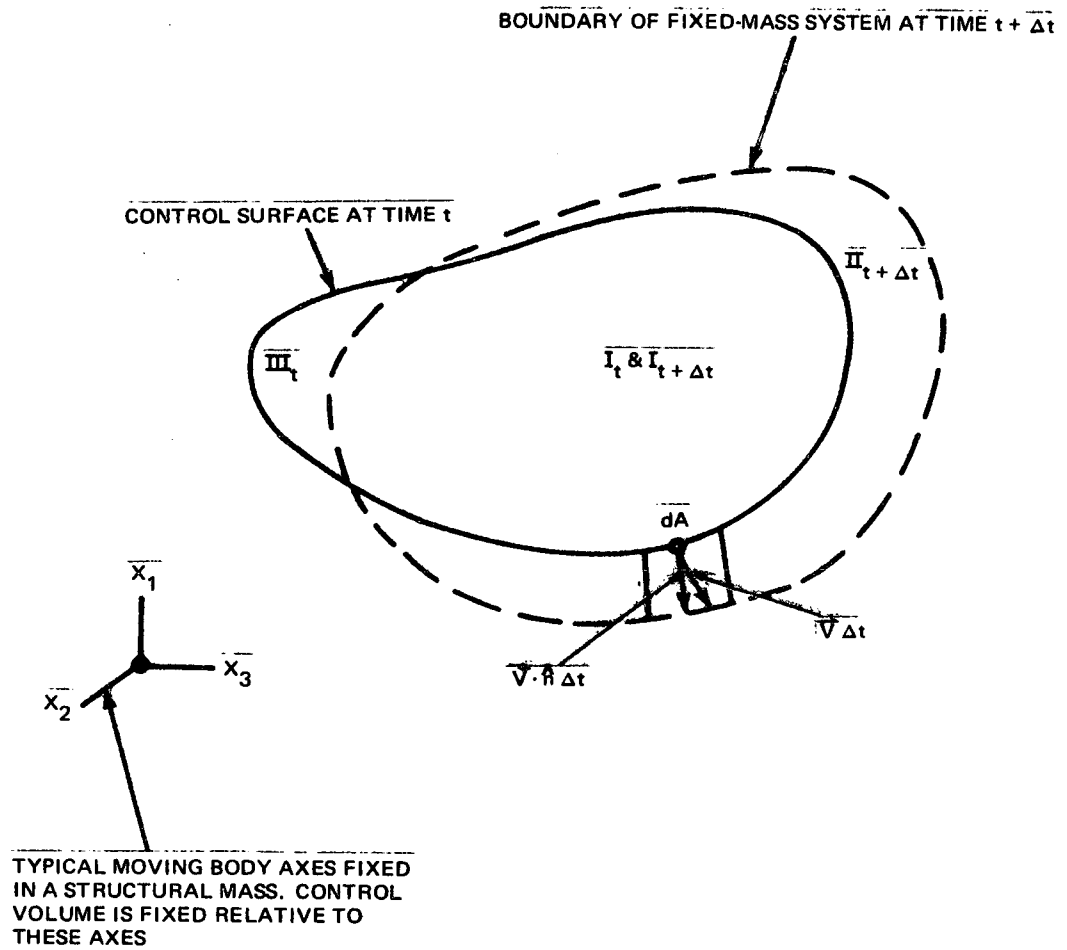


Fig. A1 Motion of Fixed Mass of Fluid Relative to Body Axes

where the subscripts on \vec{G} designate the associated volumes. Rearranging terms,

$$\left(\frac{d\vec{G}}{dt}\right)_S = \lim_{\Delta t \rightarrow 0} \left(\frac{\vec{G}_{I_{t+\Delta t}} - \vec{G}_{I_t}}{\Delta t} \right) + \lim_{\Delta t \rightarrow 0} \frac{\vec{G}_{II_{t+\Delta t}}}{\Delta t} - \lim_{\Delta t \rightarrow 0} \frac{\vec{G}_{III_t}}{\Delta t} \quad (A2)$$

The first term on the right may be evaluated as follows:

$$\begin{aligned} \lim_{\Delta t \rightarrow 0} \left(\frac{\vec{G}_{I_{t+\Delta t}} - \vec{G}_{I_t}}{\Delta t} \right) &= \lim_{\Delta t \rightarrow 0} \frac{\int_{I_{t+\Delta t}} \vec{\phi} \rho dV - \int_{I_t} \vec{\phi} \rho dV}{\Delta t} \\ &= \frac{d}{dt} \left(\int_{CV} \vec{\phi} \rho dV \right)_S \end{aligned} \quad (A3)$$

where CV indicates that the integral is evaluated over the control volume. The final limiting process shows that the above derivative is computed for the variable-mass system within the control volume. The second term on the right of Equation (A2) is

$$\lim_{\Delta t \rightarrow 0} \frac{\vec{G}_{II_{t+\Delta t}}}{\Delta t} = \lim_{\Delta t \rightarrow 0} \frac{1}{\Delta t} \int_{II_{t+\Delta t}} \vec{\phi} \rho dV$$

If \vec{V} is the fluid velocity measured by an observer fixed in the body axes, as indicated in Figure 4.4, that observer would measure the amount of mass passing through dA as being equal to $\rho \vec{V} \cdot \hat{n} \Delta t dA$; i.e., in the above equation, $\rho dV = \rho \Delta t \vec{V} \cdot d\vec{A}$ where $d\vec{A} = \hat{n} dA$. Thus,

$$\begin{aligned} \lim_{\Delta t \rightarrow 0} \frac{\vec{G}_{II_{t+\Delta t}}}{\Delta t} &= \lim_{\Delta t \rightarrow 0} \frac{1}{\Delta t} \int_{II_{t+\Delta t}} \vec{\phi} \rho \Delta t \vec{V} \cdot d\vec{A} \\ &= \int_{\substack{CS \\ \text{mass} \\ \text{out}}} \vec{\phi} \rho \vec{V} \cdot d\vec{A} \end{aligned} \quad (A4)$$

where "CS out" indicates that section of the control surface where mass is moving out at time t . The last term in Equation A2 is evaluated similarly, and the result is

$$\lim_{\Delta t \rightarrow 0} \frac{\vec{G}_{III}}{\Delta t} = - \int_{\substack{CS \\ \text{mass in}}} \vec{\phi} \rho \vec{V} \cdot d\vec{A} \quad (A5)$$

Substitution of Equations (A3-A5) into (A2) yields

$$\left(\frac{d\vec{G}}{dt}\right)_S = \frac{d}{dt} \left(\int_{CV} \vec{\phi} \rho dV \right)_S + \oint_{CS} \vec{\phi} \rho \vec{V} \cdot d\vec{A} \quad (A6)$$

Equation (A6) is the desired result and is nearly identical to the result for control volumes that are fixed in space. The only difference is that here \vec{V} is the velocity of the fluid relative to the moving control volume and \vec{V} is measured in a rotating coordinate system which is fixed relative to the control volume.

APPENDIX B

RELATIONS REQUIRED TO CONVERT THE EQUATIONS OF MOTION
FROM VECTOR TO MATRIX FORM

The equations developed in Section 4.2 are in vector form. In order to facilitate the conversion of these equations to the matrix form required for computation, certain notation and relationships are used. These mathematical tools are presented below:

B1. Coordinate Transformations and Angular Velocities

The axes of the coordinate systems used herein are always denoted as the 1, 2, and 3, axes; for example, the \underline{Z} coordinate-system axes are Z_1 , Z_2 , and Z_3 . All Euler angles are similarly denoted; for example, the set of angles used for the coordinate transformation from the \underline{Z} to \underline{X} axes of Figure 4.1 are called γ and the specific angles are γ_1 , γ_2 , and γ_3 . The order of rotation is always as follows: the number 1 angle about the 1 axis, the number 2 angle about the carried number 2 axis, and the number 3 angle about the twice carried number 3 axis. This is illustrated in Figure B1 for the angles γ . The \underline{X} axes have been translated so that their origin coincides with that of the \underline{Z} axes for the purpose of determining the coordinate transformation from vector components in the \underline{Z} axes to components in the \underline{X} axes. The matrix function $[\pi(\gamma)]$ is always used to denote a transformation between coordinate systems; for example, Figure B1, the transformation of the components of a vector $\{V\}$ from \underline{Z} coordinates to \underline{X} coordinates is written

$$\{V_X\} = [\pi(\gamma)] \{V_Z\} \quad (B1)$$

and, since the coordinate transformations are orthogonal,

$$\{V_Z\} = [\pi(\gamma)]^T \{V_X\}; \text{ i.e., } [\pi(\gamma)]^{-1} = [\pi(\gamma)]^T \quad (B1a)$$

From Figure B1

$$[\pi(\gamma)] \equiv [C(\gamma)][B(\gamma)][A(\gamma)] \quad (B2)$$

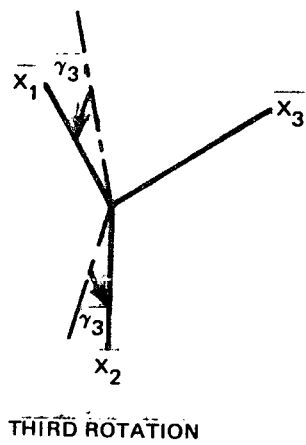
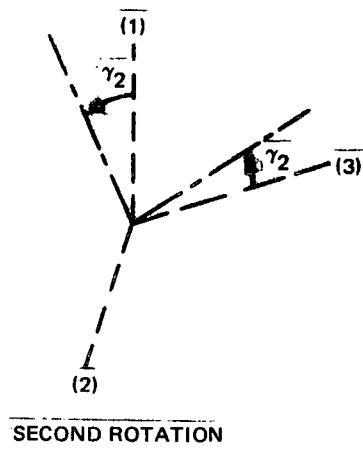
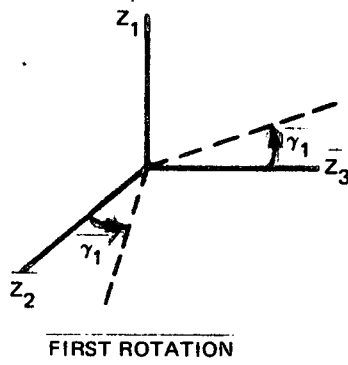


Fig. B1 Typical Set of Euler Angles

where $[A(\gamma)]$, $[B(\gamma)]$, and $[C(\gamma)]$ denote the first, second, and third intermediate transformations, respectively. From geometry,

$$[A(\gamma)] \equiv \begin{bmatrix} 1 & 0 & 0 \\ 0 & \cos \gamma_1 & \sin \gamma_1 \\ 0 & -\sin \gamma_1 & \cos \gamma_1 \end{bmatrix} \quad (B3)$$

$$[B(\gamma)] \equiv \begin{bmatrix} \cos \gamma_2 & 0 & -\sin \gamma_2 \\ 0 & 1 & 0 \\ \sin \gamma_2 & 0 & \cos \gamma_2 \end{bmatrix} \quad (B4)$$

$$[C(\gamma)] \equiv \begin{bmatrix} \cos \gamma_3 & \sin \gamma_3 & 0 \\ -\sin \gamma_3 & \cos \gamma_3 & 0 \\ 0 & 0 & 1 \end{bmatrix} \quad (B5)$$

The above notation is used throughout for all of the coordinate systems; for example, the angles η locate the \underline{Y} coordinates with respect to the \underline{X} coordinates, and the notation for the corresponding transformation would be $[\pi(\eta)] = [C(\eta)][B(\eta)][A(\eta)]$.

Similarly, the functional notation $[S(\)]$ is used to convert Euler-angle rates to angular velocities; for example, if $\{\omega^X\}$ is the angular velocity of the \underline{X} axes with respect to the \underline{Z} axes, projected onto the \underline{X} axes, we would write

$$\{\omega^X\} = [S(\gamma)]\{\dot{\gamma}\} \quad (B6)$$

where $\{\gamma\} = [\gamma_1 \ \gamma_2 \ \gamma_3]^T$ and, from kinematics,

$$[S(\gamma)] \equiv \begin{bmatrix} \cos \gamma_2 \cos \gamma_3 & \sin \gamma_3 & 0 \\ -\cos \gamma_2 \sin \gamma_3 & \cos \gamma_3 & 0 \\ \sin \gamma_2 & 0 & 1 \end{bmatrix} \quad (B7)$$

B2. Cross Products

The functional notation $[\Gamma(\)]$ is used to convert vector cross products to matrix form. For example, the expression $\vec{x} \times \vec{y}$ would be written as $[\Gamma(x)]\{y\}$ in matrix form, where $[\Gamma(x)]$ is defined so that the components of the products in the vector and matrix forms would be identical. This definition yields

$$[\Gamma(x)] \equiv \begin{bmatrix} 0 & -x_3 & x_2 \\ x_3 & 0 & -x_1 \\ -x_2 & x_1 & 0 \end{bmatrix} \quad (B8)$$

B3. Useful Identities

Certain identities which were employed in the analysis can be developed using the notations introduced in Equations (B1) and (B8). These identities are first listed below, and then their proofs will be presented.

$$[\Gamma(x)]^T = -[\Gamma(x)] \quad (B9)$$

For any scalar α and vectors $\{x\}$ and $\{y\}$,

$$[\Gamma(\alpha\{x\})] = \alpha [\Gamma(x)] \quad (B10)$$

$$[\Gamma(\{x\} + \{y\})] = [\Gamma(x)] + [\Gamma(y)] \quad (B11)$$

$$[\Gamma(x)]\{y\} = -[\Gamma(y)]\{x\} \quad (B12)$$

$$[\Gamma(x)][\Gamma(y)]\{z\} = (\{x\}\{z\}^T)\{y\} - (\{x\}\{y\}^T)\{z\} \quad (B13)$$

$$[\Gamma(\pi(\gamma))\{\chi\}] = [\pi(\gamma)][\Gamma(\chi)][\pi(\gamma)]^T \quad (\text{B14})$$

If $\{\omega_x\}$ is the angular velocity of the \underline{X} axes with respect to the \underline{Z} axes projected onto the \underline{X} axes and $\underline{\gamma}$ is a set of Euler angles used to locate the \underline{X} axes with respect to the \underline{Z} axes, then

$$\frac{d}{dt} [\pi(\gamma)] = -[\Gamma(\omega_x)][\pi(\gamma)] \quad (\text{B15})$$

Another identity involving derivatives of the transformation matrix is

$$\frac{d}{dt} ([\pi(\gamma)][\pi(\gamma)]^T) = -[\pi(\gamma)] \frac{d}{dt} ([\pi(\gamma)]^T) \quad (\text{B16})$$

The following identity applies only when γ can be linearized:

$$[\pi(\gamma)] = [1] - [\Gamma(\gamma)] \quad (\text{within linear terms}) \quad (\text{B17})$$

where $[1]$ is the identity matrix.

The following relationships apply to moment-of-inertia calculations. If $\{X\}$ is the vector (expressed in \underline{X} axes) to a differential mass dm of a mass system (see Figure B2), then the moment-of-inertia matrix of the mass system about the \underline{X} axes is

$$[I] = - \int [\Gamma(X)]^2 dm \quad (\text{B18})$$

where the diagonal terms of Equation (B18) are the moments of inertia and the off-diagonal terms are the negatives of the cross products of inertia. To compute the moment-of-inertia matrix ($[I_X]$) about the \underline{X}

axes when the matrix $[I_Y]$ about the \underline{Y} axes is known and the origins of these axes are coincident, the following equation may be applied:

$$[I_X] = [\pi(\eta)]^T [I_Y] [\pi(\eta)] \quad (B19)$$

where η is the set of Euler angles locating the \underline{Y} axes with respect to the \underline{X} axes. To transfer moments of inertia and cross products of inertia to a coordinate system which is both translated and rotated with respect to a coordinate system with its origin at the center of mass, a generalization of the well-known parallel-axis formula may be used. This formula is

$$[I] = [\pi(\eta)]^T [I_c] [\pi(\eta)] - m [\Gamma(X_c)]^2 \quad (B20)$$

where, referring to Figure B2, $[I_c]$ is the moment of inertia matrix about any axes \underline{Y} through the center of mass, $[I]$ is the moment of inertia matrix about the \underline{X} axes, η is a set of Euler angles defining the orientation of the \underline{Y} with respect to the \underline{X} axes, m is the total system mass, and $\{X_c\}$ is the vector from the origin of the \underline{X} axes to the origin of the $\{Y\}$ axes expressed in \underline{X} axes.

The proofs of Equations (B9-B20) are as follows. Equation (B9) follows immediately by forming the transpose of Equation (B8) which is skew-symmetric.

Equations (B10) and (B11) are also rapidly proved by direct substitution of the argument into the definition of $[\Gamma(\)]$, Equation (B8).

Equation (B12) is proved by writing the relation $\vec{x} \times \vec{y} = -\vec{y} \times \vec{x}$ in matrix form.

Equation (B13) is proved by writing in vector form the relation for the vector triple product: $\vec{x} \times (\vec{y} \times \vec{z}) = (\vec{x} \cdot \vec{z}) \vec{y} - (\vec{x} \cdot \vec{y}) \vec{z}$.

To prove Equation (B14), as previously let γ denote the set of Euler angles orienting the \underline{X} axes with respect to the \underline{Z} axes. Also, let primes denote vectors projected onto the \underline{X} axes, whereas the same symbol without the prime represents the same vector projected onto the

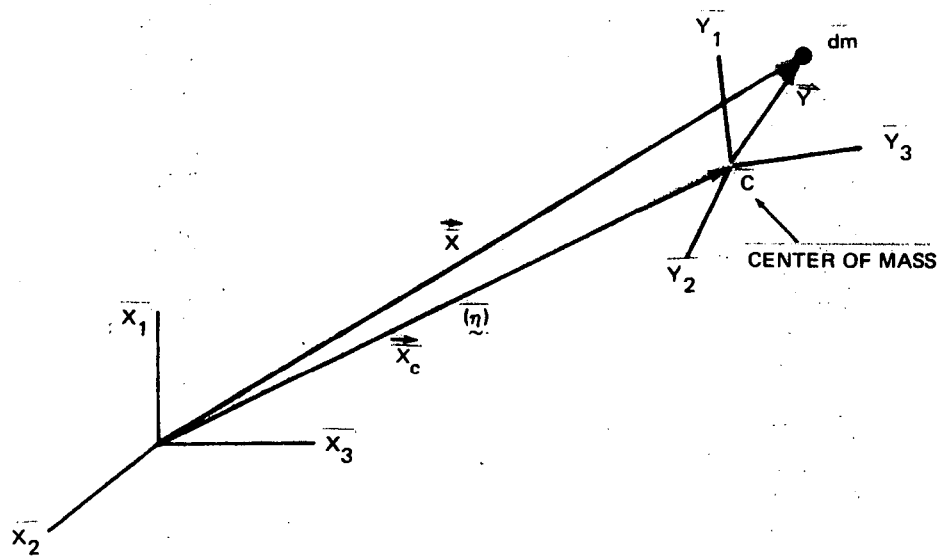


Fig. B2 Coordinates Used to Express Transfer-of-Axes Relation for Moment-of-Inertia Matrix

\underline{Z} axes. Then $\{u'\} = [\Pi(\gamma)]\{u\}$, and, since $[\Pi(\gamma)]$ is orthogonal, $\{v\} = [\Pi(\gamma)]^T \{v'\}$. Since the cross product of \vec{u} and \vec{v} formed in the \underline{X} axes is equal to the transformed cross product written in the \underline{Z} axes

$$[\Gamma(\pi(\gamma))\{u\}]\{v'\} = [\pi(\gamma)][\Gamma(u)][\pi(\gamma)]^T \{v'\}$$

This relation can be written for any vector $\{v'\}$ (in particular for $\{v'\} = [1 \ 0 \ 0]^T$, $[0 \ 1 \ 0]^T$, and $[0 \ 0 \ 1]^T$); therefore Equation (B14) follows.

In proving Equation (B15), the primes have the same meaning as in the above proof. In addition, $\{\omega_x\}$ is the angular velocity of the \underline{X} axes relative to the \underline{Z} axes. If $\{u'\}$ is any vector in the \underline{X} axes which is a constant in this coordinate system, and we differentiate the relation $\{u'\} = [\Pi(\gamma)]\{u\}$,

$$0 = \left(\frac{d}{dt} [\pi(\gamma)]\right)\{u\} + [\pi(\gamma)] \frac{d}{dt} \{u\} \quad (a)$$

But $d\vec{u}/dt = \vec{\omega}_x \times \vec{u}$ when \vec{u} has constant components in the \underline{X} axes, or in matrix form

$$[\pi(\gamma)] \frac{d\{u\}}{dt} = [\Gamma(\omega_x)]\{u'\} \quad (b)$$

Combining Equation (a) and (b) yield,

$$\left(\frac{d}{dt} [\pi(\gamma)]\right)\{u\} = -[\Gamma(\omega_x)]\{u'\}$$

or

$$\left(\frac{d}{dt} [\pi(\gamma)]\right) [\pi(\gamma)]^T \{u'\} = -[\Gamma(\omega_x)]\{u'\}$$

This relation can be written for any constant vector $\{u'\}$; therefore Equation (B15) follows:

Equation (B16) may be verified by substituting Equation (B15) into Equation (B16) and using Equation (B9).

Equation (B17) is easily proved by linearizing Equation (B2).

Equation (B18) may be verified by substitution of $\{X\} = [X_1 \ X_2 \ X_3]^T$ into the equation and carrying out the matrix multiplication. Equation (B19) may be proved by substitution of the relation

$$\{X\} = [\pi(\eta)]^T \{Y\}$$

into Equation (B18) and subsequent application of Equation (B14). Equation (B20) may be proved by substituting the following expression, obtained from the geometry of Figure B2, into Equation (B18):

$$\{X\} = \{X_c\} + [\pi(\varphi)]^T \{Y\}$$

where $\{Y\}$ has been expressed in the $\{Y\}$ axes. Then

$$\begin{aligned} [I] = & - \left([\Gamma(X_c)]^2_m + [\Gamma(X_c)][\pi(\varphi)]^T \left(\int [\Gamma(Y)] dm \right) [\pi(\varphi)] \right. \\ & + [\pi(\varphi)]^T \left(\int [\Gamma(Y)] dm \right) [\pi(\varphi)] [\Gamma(X_c)] \\ & \left. + [\pi(\varphi)]^T \left(\int [\Gamma(Y)][\Gamma(Y)] dm \right) [\pi(\varphi)] \right) \end{aligned}$$

Since the origin of the \underline{Y} axes is the center of mass,

$$\int [\Gamma(Y)] dm = 0$$

Using the above relation with Equation (B18), Equation (B20) is obtained.

APPENDIX C

PHASE II COMPUTATION PROCEDURE AND SUMMARY OF EQUATIONS

This appendix contains the computational scheme for the Phase II computer program and is followed by a summary of all required equations. The equation numbers referred to in the procedure pertain to equations of this appendix and not of the body of the report. The appendix begins with a list of required input data, including all data that will be automatically transmitted from the Phase I to the Phase II program. Section 4.0 contains the definitions of the symbols used.

INPUT DATA FOR PHASE III. BASIC MASS DISTRIBUTION AND FLEXIBILITY DATA TRANSMITTED FROM PHASE I

Specify if any of the following constraint options are to be used:

- Laboratory is rigid
- Counterweight is rigid
- Space Station is rigid

A. Laboratory

This data is obtained in either of the following two ways at the user's option:

- Phase I is run for the Laboratory, and the data is automatically transmitted to Phase II
- The data is supplied by the user

The data is as follows:

Item	Notation	
	Phase I	Phase II
Number of mass points		n
Undeformed mass-point locations	$(\bar{X}_i, \bar{Y}_i, \bar{Z}_i)$	\tilde{r}_i
Mass at each mass point. (If data is being transferred from Phase I, $[m_X^*]$ is block diagonal with 6 x 6 blocks. m_i is the 1, 1 element of the i^{th} block)		m_i
Moment of inertia matrix for each mass point. ($[I_i]$ is lower right 3 x 3 of i^{th} block described above)		$[I_i]$

If the Laboratory is rigid, the modal quantities listed below

$(p, [\Phi], [\mu], \omega_1^2)$ are not required and will be ignored if supplied.

Item	Notation	
	Phase I	Phase II
Modal matrix	$[\Phi_X]$	$[\Phi]$
Modal mass matrix corresponding to no. of modes used (max dimension is 20 x 20; matrix is diagonal)	$[1]$	$[\mu]$
Frequencies corresponding to modes used	Ω_i	$\omega_i, i=1, \dots, p$

B. Counterweight

If the Counterweight is rigid, the modal quantities $(\bar{p}, [\bar{\Phi}], [\bar{\mu}], \bar{\omega}_a^2)$ are not required and will be ignored if supplied.

This data is obtained in either of the following two ways at the user's option:

- Phase I is run for the Counterweight, and the data is automatically transmitted to Phase II
- The data is supplied by the user

All data is the same as listed in Section IA for the Laboratory. The Phase II notation for the Counterweight is the same as that listed in Section IA for the Laboratory except that a bar is placed over each symbol.

II. ADDITIONAL BASIC DATA

Initial Laboratory displacements and velocities:

Rigid Body: $\{R\}, \{\dot{R}\}, \{\gamma\}, \{\omega^X\}$

Elastic:* $\{q_i\}, \{\dot{q}_i\}, \{\theta_i\}, \{\dot{\theta}_i\} (i = 1, \dots, n)$

Initial Counterweight elastic displacements and velocities:*

$\{\bar{q}_a\}, \{\dot{\bar{q}}_a\}, \{\bar{\theta}_a\}, \{\dot{\bar{\theta}}_a\}$

* These quantities are not required if the structure is rigid, and will be ignored if supplied.

Percentage of critical damping for each mode:

For Laboratory: v_k ($k = 1, \dots, p$); v_k is constant on default

The v_k are not required if the Laboratory is rigid and will be ignored if supplied.

For Counterweight: \bar{v}_k ($k = 1, \dots, \bar{p}$); \bar{v}_k is constant on default

The \bar{v}_k are not required if the Counterweight is rigid and will be ignored if supplied.

Connecting structure data: *

\underline{i} , $\{s\}$, \underline{a} , $\{\bar{s}\}$, $\{\delta\}$, $\{\dot{\delta}\}$, $\{\phi^*\}$, $\{\dot{\phi}^*\}$, $\{\tilde{Y}^{a'}\}_{(a)}$, $\{\tilde{Y}^{a'}\}_{(b)}$, $\{\ell_0\}$

A subroutine is required for Connecting Structure loads when the Space Station is not rigid. The input data for this subroutine is described in Appendix G for the case of a beam.

III. ACCESSORY DATA PACKAGES

The following data packages may or may not be present.

A. Fluid Package

Clue stating whether fluid is present. If present, the following additional data will be supplied:

Subroutine of V and \dot{V} versus t . Input data for this subroutine is described in Appendix H7

ρ and A

Reservoirs:

Mass point number containing emptying reservoir

Mass point number containing filling reservoir

* $\{\delta\}$, $\{\dot{\delta}\}$, $\{\phi^*\}$, and $\{\dot{\phi}^*\}$ are not required if the Space Station is rigid and will be ignored if supplied.

The following data must be specified for each reservoir:

$$m_i^P, [I_i^P], \{S_i^P\}, \{e_i^R\}, \{u_i^R\}, \{u_i^B\}, \{e_i^B\}, [J_i^B], b_i, h_{i0}, \\ h_{i \max}, h_{i \min}, \{G_i^P\}$$

Through pipes:

Data specifying which masses contain through pipes (30 max).

For each such mass: $m_i^f, [I_i^f], \{S_i\}, \{\Delta u_i\}, \{\Delta e_i\}, \{G_i\}, [\Delta J_i], \{\Delta H_i\}$

B. Moving Mass Package

Clue whether moving masses are present. If present, specify μ_j ($j = 1, \dots, 8$ max). A subroutine is required to obtain the following for each moving mass:

Motion data: $\{U_j(t)\}, \{\dot{U}_j(t)\}, \{\ddot{U}_j(t)\}$

Values of k denoting the masses m_k which influence μ_j .

In the subroutines provided with the program, μ_2 is a balance mass and its motion is determined by a control system. The input data for this subroutine is described in Appendix H13.

The undeformed motion of the remaining masses is commanded by Subroutine MUCOM. The required input data is described in Appendix H5.

Subroutine LOOK determines the values of k denoting the masses m_k that influence the motion of μ_j . (A maximum of 16 m_k 's can influence each μ_j .) This subroutine is a table of k 's versus time, and must be provided for the particular structure. The subroutine requires no input data.

C. Control Systems Package

Clue whether control forces $\{f_c^i\}$, $\{\tau_c^i\}$, $\{\bar{f}_c^{a'}\}$, $\{\bar{\tau}_c^{a'}\}$ are present. If present a subroutine or subroutines are required. The input data for the subroutines supplied with the Phase II program is described in Appendix H.

D. Supplementary Forces

Clue whether supplementary forces are present: $\{f_s^i\}$, $\{\tau_s^i\}$, $\{\bar{f}_s^{a'}\}$, $\{\bar{\tau}_s^{a'}\}$. If present, a subroutine is required.

E. Print Out of Structural Loads

1. Connecting Structure:

Clue whether structural loads applied by Connecting Structure are required.

2. Laboratory:

Clue whether internal structural loads in Laboratory are required. If required, the following data is supplied. For each load-computation point: ℓ' , $\{t_{\ell'}\}$, index numbers of mass points comprising free body.

3. Counterweight:

Clue whether internal structural loads in Counterweight are required. If required, the following data is supplied. For each load-computation point: $\bar{\ell}'$, $\{\bar{t}_{\bar{\ell}'}\}$, index numbers of mass points comprising free body.

COMPUTATION PROCEDURE

Step No.	Operation	Required Equation
<u>Orientation of Connecting-Structure Axes in Counterweight</u>		
G1	Set up $\{\alpha_{3i}^*\}$	Eq. 28
G2	Compute C_k	Eq. 29
G3	Compute $\alpha_{31}, \alpha_{32}, \alpha_{33}$	Eq. 30
G4	Compute $\{\alpha_{2i}^*\}$	Eq. 31
G5	Compute C_j	Eq. 32
G6	Compute $\alpha_{21}, \alpha_{22}, \alpha_{23}$	Eq. 33
G7	Compute $\alpha_{11}, \alpha_{12}, \alpha_{13}$	Eq. 34
G8	Set up $[\pi(\rho)]$	Eq. 35

3

Initial Set-Up Procedure

- A1 (a) If Laboratory is rigid, set all $\{q_i\} = \{\theta\} = \{\dot{q}_i\} = \{\dot{\theta}_i\} = 0$
- (b) If Counterweight is rigid, set all $\{\bar{q}_a\} = \{\theta_a\} = \{\dot{q}_a\} = \{\dot{\theta}_a\} = 0$
- (c) If entire vehicle is rigid, also set $\{\delta\} = \{\dot{\phi}^*\} = \{\ddot{\delta}\} = \{\ddot{\phi}^*\} = 0$
- A2 Test all frequencies (w_i and \bar{w}_i) to see if any are zero ($\leq 10^{-5}$). If any are zero, print message and stop
- A3 Set up $[\pi(\rho)]$ (constant)

Eq. A1

Step No.	Operation	Required Equation
A4	Set up $[\pi(\phi^*)]$	Eq. 8
A5	Set up $[\Gamma(\bar{\sigma}_2)], [\Gamma(\theta_2)]$	Eq. A4
A6	Compute $[\pi(q)]$ and save for step A35	Eq. A3
A7	Compute $[\pi(q^*)]$	Eq. A5
A8	Compute $\{q^*\}, \{q\}$	Eq. A6, A6a
A9	Set up $[S(\phi^*)], [S(q)]$	Eq. A7
A10	Compute $[S(q)]^{-1}$	Eq. A8
A11	Compute $\{q^*\}$	Eq. A9
A12	Compute $\{\omega, \gamma\}$	Eq. A10
A13	Set $t = 0$	
A14	Read clue indicating whether or not there is deployment in this run. (a) If there is no deployment in the run, data card will contain elements of $\{l_0\}$; set $\{l_0\} = \{l_0\} = 0$; $\{l_0\}$ and $\{l_0\}$ are then constant in time. (b) If there is deployment, go to deployment subroutine in controls section and read in $\{l_0\}$, $\{l_0\}$ and $\{l_0\}$	
A15	Compute $\{l\}, \{l\}$	Eq. A11

Step No.	Operation	Required Equation
A16	Compute $\{\bar{R}\}$	Eq. A12
A17	(Step deleted)	
A18	Set up $[\Gamma(\dot{\sigma}_i)], [\Gamma(\dot{\sigma}_g)]$	Eq. A4
A19	Compute $\{\dot{R}\}$	Eq. A13
A20	Compute $\{\bar{R}_o\}$ (This is constant in time if there is no deployment)	Eq. A14
A21	Compute $\{\dot{R}_o\}$ and $\{\ddot{P}_o\}$ (These are zero if there is no deployment)	Eq. A15

Realignment of Initial Conditions

The initial conditions $\{\bar{R}\}, \{R\}, \{w\}, \{w^X\}, \{q_1\}, \{\dot{q}_1\}, \{\theta_1\}, \{\dot{\theta}_1\}, \{\bar{q}_g\}, \{\dot{q}_g\}, \{\theta_g\}, \{\dot{\theta}_g\}$ are now recomputed in terms of the mean axes. The above old values are designated by primes in steps A22 - A59 below.

A22	Set up $[\Gamma(r_i)]$ ($i = 1, \dots, n$)	Eq. A4
A23	Compute $M_L, [I_L],$ and $[D_L]$	Eq. A29
A24	Compute $\{g_o\}$ and $\{\sigma_o\}$. Save inverse for Step A40.	Eq. A28
A25	Compute $\{\sigma_i\}$ and $\{g_i\}$ ($i = 1, \dots, n$)	Eq. A30 & A31
A26	Set up $[\Gamma(\sigma_o)]$	Eq. A4

Step No.	Operation	Required Equation
A27	Set up $[\pi(\gamma')]$	Eq. 8
A28	Compute $[\pi(\gamma)]$	Eq. A32
A29	Compute $\{\gamma\}$	Eq. A33
A30	Compute $\{R\}$	Eq. A34
A31	Set up $[\Gamma(\bar{\gamma}_a)]$ ($a = 1, \dots, \bar{n}$)	Eq. A4
A32	Compute $M_c, [I_c], [D_c]$	Eq. A36
A33	Compute $\{\bar{\gamma}_0\}$ and $\{\bar{\sigma}_0\}$	Eq. A35
A34	Compute $\{\bar{\sigma}_a\}$ and $\{\bar{\gamma}_a\}$ ($a = 1, \dots, \bar{n}$)	Eq. A37 & A38
A34-a.	Set up $[\Gamma(\bar{\sigma}_0)]$	Eq. A4
A35	Recompute $[\Pi(\eta^*)]$. Use the $[\Pi(\eta)]$ computed in Step A6 for $[\Pi(\eta')]$	Eq. A39
A36	Compute a new value of η^*	Eq. A6
A37	Compute η	Eq. A6a
A38	Compute $[\pi(\eta)]$	Eq. A41
A39	Compute $\{\bar{R}\}$	Eq. A40
A40	Compute $\{\bar{\gamma}_0\}$ and $\{\bar{\sigma}_0\}$	Eq. A42

Use inverse from Step A24.

Step No.	Operation		Required Equation
A41	Compute $\{\dot{\sigma}_i\}$	and $\{\dot{f}_i\}$ ($i = 1, \dots, n$)	Eq A43 & 44
A42	Compute $\{\omega^x\}$		Eq. A45
A43	(Step deleted)		
A44	(Step deleted)		
A45	Compute $\{\dot{r}\}$		Eq. A47
A46	Compute $\{\dot{f}_0\}$	and $\{\dot{\sigma}_0\}$. Use inverse from Step A33.	Eq. A48
A47	Compute $\{\dot{\sigma}_a\}, \{\dot{f}_a\}$ ($a = 1, \dots, n$)		Eq. A49 & A50
A51	Compute $\{\omega^y\}$ in Step A12.	where $\{\omega^{y'}\}$ is the value of $\{\omega^y\}$ computed	Eq. A51
A52	(Step deleted)		
A53	(Step deleted)		
A54	Compute $\{\omega^{y/x}\}$		Eq. A53
A55	(Step deleted)		
A56	Compute $\{\dot{r}\}$		Eq. A54
A57	Compute $\{\Delta \bar{r}\}, \{\Delta \bar{r}\}$		Eq. A16
A58	Compute $[s(r)]^{-1}, [s(q)]^{-1}$		Eq. A8

Step No.	Operation	Required Equation
A59	Compute $\{\delta\}, \{\dot{\delta}\}$	Eq. A17
All initial conditions are now known in terms of the mean axes.		
Print the old and new values of the terms listed above step A22.		
<u>Initial Conditions in Best-Fit Modal Coordinates</u>		
A60	Set up $\{\delta\}, \{\ddot{\delta}\}, [M], [\bar{M}]$	Eq. A55-A57
A60A	If Laboratory is rigid, go to Step A62a	
A61	Compute $[\Phi']$	Eq. A58
A62	Compute $\{\delta\}, \{\ddot{\delta}\}$	Eq. A59
A62a	If Counterweight is rigid, go to Step A64a	
A63	Compute $[\bar{\Phi}']$	Eq. A60
A64	Compute $\{\ddot{\delta}\}, \{\ddot{\bar{\delta}}\}$	Eq. A61
A64a	All initial conditions for the numerical integration are now known. They are $\{\delta\}, \{\dot{\delta}\}, \{\ddot{\delta}\}, \{\omega^x\}, \{\Delta\ddot{R}\}, \{\dot{\gamma}^*\}, \{\omega^y\}, \{\dot{\delta}\}, \{\ddot{\delta}\}, \{\ddot{\bar{\delta}}\}$ Modal coordinates $\{\xi\}, \{\ddot{\xi}\}$ are not present if Laboratory is rigid. Also, $\{\bar{\xi}\}$ and $\{\ddot{\bar{\xi}}\}$ are not present if Counterweight is rigid.	
A65	Set up total modal matrix $[\phi]$	Eq. A62

Step No.	Operation	Required Equation
<u>Initialization of Parameters</u>		
1	If fluid is present set $k_i = 1$ for value of i corresponding to the m_i which contains the emptying reservoir. Set $k_i = -1$ for value of i corresponding to the m_i which contains the filling reservoir.	
2	Set all $\{f_c^i\}$, $\{\tau_c^i\}$, $\{\bar{f}_c^a\}$, $\{\bar{\tau}_c^a\}$ to zero if controls are not present.	
3	Set all $\{f_s^i\}$, $\{\tau_s^i\}$, $\{\bar{f}_s^a\}$, $\{\bar{\tau}_s^a\}$ to zero if supplementary forces are not present.	
<u>Enter Numerical-Integration Cycle</u>		
<u>Dynamic Terms for Structural Masses</u>		
4a	Set $\{L\} = 0$, $K = 0$	
4b	Set $i = 1$	
5	Compute $\{R_i\}$, $\{\dot{R}_i\}$, $\{\dot{R}_i^s\}$	Eq. 3
6	Compute $\{\omega x^i\}$	Eq. 4
7	Compute $[\lambda_1^i]$, $[\lambda_2^i]$, $\{\delta_1^i\}$ (Note: $[\lambda_1^i]$ is constant in time)	Tables
(These coefficients are associated with Newton's equations for the i^{th} laboratory node point.)		
7a	$[\Lambda_1^i] = [\lambda_1^i]$; $[\Lambda_2^i] = [\lambda_2^i]$; $[\Lambda_3^i] = [\lambda_3^i]$; $[\Lambda_4^i] = 0$; $\{\nabla_1^i\} = -\{\delta_1^i\}$	

Step No.	Operation	Required Equation
8	Compute $[\lambda_3^i], [\lambda_4^i], \{s_2^i\}$ (Note: $[\lambda_4^i]$ is constant in time). (These coefficients are associated with Euler's equations for the i^{th} laboratory node point)	Tables
8a	$[\Lambda_5^i] = 0 ; [\Lambda_6^i] = [\lambda_3^i] ; [\Lambda_7^i] = 0 ; [\Lambda_8^i] = [\lambda_4^i] ;$ $\{\nabla_2^i\} = -\{s_2^i\}$	
8b	Compute $\{L_i^m\}, K_i^m$ $\{L\} = \{L\} + \{L_i^m\} ; K = K + K_i^m$	Eq. A18 & A19
9	$i = i + 1$; if i is now greater than n proceed to Step 10. Otherwise return to Step 5.	
<u>Dynamic Terms for Fluid</u>		
10	Is fluid present in laboratory? If not, go to Step 34, skipping Steps 11 through 33 in every cycle. If fluid is present, obtain V and V from subroutine.	
11	Compute Q	Eq. 5a
12	Compute \dot{Q}	Eq. 5b

Step No.	Operation	Required Equation
<u>Reservoirs</u>		
13	Compute A_i^R for each reservoir (Note: A_i^R is constant in time)	Eq. 6
14	Compute h_i for each reservoir: If, for either reservoir, $h_i > h_{i \max}$ or $h_i < h_{i \min}$, disregard subroutine and set $V = Q = 0$ for all calculations in remainder of run. Also, reset $\dot{V} = -V/\Delta t$ and $\dot{Q} = \rho A \dot{V}$ at this time, and then $\dot{V} = 0$ at all future time steps.	Eq. 7
15	Do Steps 16 through 30 for each of the two reservoirs.	
16	Compute $[\pi(\gamma_i)]$; (Note: $[\pi(\gamma_i)]$ is constant in time)	Eqs. A64, A33, 8
17	Compute m_i^R	Eq. 9
18	Compute m_i^f	Eq. 10
19	Compute $\{\Delta u_i\}$	Eq. 11
20	Compute $\{S_i\}$	Eq. 12
21	Compute $\{G_i\}$	Eq. 13
22	Compute $[L_i]$	Eq. 14
23	Compute $\{u_i^c\}$	Eq. 15
24	Compute $[I_i^f]$	Eq. 16
25	Compute $[I_i]$	Eq. 17

Step No.	Operation	Required Equation
26	Compute $\{\dot{u}_i^c\}$	Eq. 18
27	Compute $[I_i^R]$	Eq. 19
28	Compute $[\lambda_{11}^c], [\lambda_{12}^c], [\lambda_{13}^c], \{\xi_5^c\}$	Tables
(These coefficients are associated with Newton's equations for the laboratory node containing the reservoir)		
28a	$[\Lambda_1^c] = [\Lambda_1^c] + [\lambda_{11}^c]; \quad [\Lambda_2^c] = [\Lambda_2^c] + [\lambda_{12}^c];$ $[\Lambda_3^c] = [\Lambda_3^c] + [\lambda_{11}^c]; \quad [\Lambda_4^c] = [\Lambda_4^c] + [\lambda_{13}^c]; \quad \{\nabla_1^c\} = \{\nabla_1^c\} - \{\xi_5^c\}$	Tables
29	Compute $[\lambda_{14}^i], [\lambda_{15}^i], [\lambda_{16}^i], \{\xi_6^i\}$ (These coefficients are associated with Euler's equations for the laboratory node containing the reservoir)	
29a	$[\Lambda_5^c] = [\Lambda_5^c] + [\lambda_{14}^c]; \quad [\Lambda_6^c] = [\Lambda_6^c] + [\lambda_{15}^c]; \quad [\Lambda_7^c] = [\Lambda_7^c] + [\lambda_{14}^c];$ $[\Lambda_8^c] = [\Lambda_8^c] + [\lambda_{16}^c]; \quad \{\nabla_2^c\} = \{\nabla_2^c\} - \{\xi_6^c\}$	
30	Compute $\{L_i^R\}, K_i^R$	Eq. A20, A21
	$\{L\} = \{L\} + \{L_2^R\}; \quad K = K + K_2^R$	

Step No.	Operation	Required Equation
<u>Through Pipes</u>		
31	<p>Compute $[\lambda'_5], [\lambda'_6], [\lambda'_7], \{\xi'_3\}$</p> <p>(Note: $[\lambda'_5]$ is constant in time)</p> <p>(These coefficients are associated with Newton's equations for laboratory node containing this pipe)</p>	Tables
31a	$[\Lambda'_1] = [\Lambda'_1] + [\lambda'_5]; [\Lambda'_2] = [\Lambda'_2] + [\lambda'_6]; [\Lambda'_3] = [\Lambda'_3] + [\lambda'_7];$ $[\Lambda'_4] = [\Lambda'_4] + [\lambda'_7]; \{\nabla'_1\} = \{\nabla'_1\} - \{\xi'_3\}$	
32	<p>Compute $[\lambda^i_8], [\lambda^i_9], [\lambda^i_{10}], \{\xi^i_4\}$ (Note: $[\lambda^i_{10}]$ is constant in time)</p> <p>These coefficients are associated with Euler's equations for laboratory node containing this pipe</p>	Tables
32a	$[\Lambda'_5] = [\Lambda'_5] + [\lambda^i_8]; [\Lambda'_6] = [\Lambda'_6] + [\lambda^i_9]; [\Lambda'_7] = [\Lambda'_7] + [\lambda^i_{10}];$ $[\Lambda'_8] = [\Lambda'_8] + [\lambda^i_{10}]; \{\nabla'_2\} = \{\nabla'_2\} - \{\xi^i_4\}$	
32b	<p>Compute $\{L^p_2\}, K^p_2$; $\{L\} = \{L\} + \{L^p_2\}$; $K = K + K^p_2$</p>	Eq. A22, A23
33	Repeat Steps 31 to 32b for each through pipe. Then go to Step 34.	

Step No.	Operation	Required Equation
	<u>Moving Masses:</u>	
34	Let $j = 0$	
35	Let $j = j + 1$ (if $j > j \text{ max}$, go to Step 49)	
36	(Step deleted)	
37	Obtain $\{U_j(t)\}$, $\{\dot{U}_j(t)\}$, $\{\ddot{U}_j(t)\}$ and values of k which influence μ_j from moving-mass subroutine	
38	(Step deleted)	
39	Compute all $\{d_k^j\}$	Eq. 20
40	If there is only one k , set $\lambda_k^j = 1$; denote this k by k^* and go to Step 44	
41	For more than one k , calculate each Π_k^j	Eq. 21
42	Note which k has largest Π_k^j and denote it by k^*	
43	Compute all λ_k^j	Eq. 22
44	Compute $\{W_j\}$ and $\{\dot{W}_j\}$	Eq. 23
45	Compute $[(\alpha_1)^j]$, $[(\alpha_2)^j]$, $[(\alpha_4)^j]$, $\{(\beta_1)^j\}$	Tables
	(Note: $[(\alpha_1)^j]$ is constant in time)	

Step No.	Operation	Required Equation
45 a	$\{\nabla_1^{k*}\} = \{\nabla_1^{k*}\} - \{(P_1)^{\dagger}\}$	
46	Compute $\{D_k^{\dagger}\}$	Eq. 24
47	Compute $[(\alpha 5)^{\dagger}], [(\alpha 7)^{\dagger}], [(\alpha 8)^{\dagger}], [(P_2)^{\dagger}]$	Tables
47a	$\{\nabla_2^{k*}\} = \{\nabla_2^{k*}\} - \{(P_2)^{\dagger}\}$ $[\lambda_1^{k*}] = [\lambda_1^{k*}] + [(\alpha 1)^{\dagger}], [\lambda_2^{k*}] = [\lambda_2^{k*}] + [(\alpha 3)^{\dagger}]$ $[\lambda_5^{k*}] = [\lambda_5^{k*}] + [(\alpha 5)^{\dagger}], [\lambda_6^{k*}] = [\lambda_6^{k*}] + [(\alpha 7)^{\dagger}]$ $[\lambda_3^{k*}] = [\lambda_3^{k*}] + [(\alpha 1)^{\dagger}], [\lambda_4^{k*}] = [\lambda_4^{k*}] + [(\alpha 4)^{\dagger}]$ $[\lambda_7^{k*}] = [\lambda_7^{k*}] + [(\alpha 5)^{\dagger}], [\lambda_8^{k*}] = [\lambda_8^{k*}] + [(\alpha 8)^{\dagger}]$	
47b	Compute $\{L^{u_i}\}, K^{u_i}; \{L\} = \{L\} + \{L^{u_i}\}; K = K + K^{u_i}$	Eq. A24, A25
48	Return to Step 35	
	<u>Counterweight</u>	
49	(Step deleted)	
50	Let $a = 0$	
51	Let $a = a + 1$ (If $a > a_{\max}$, go to Step 58a)	

Step No.	Operation	Required Equation
52	Compute $[\pi(q)]$	Eq. A41
53	(Step deleted)	
54	(Step deleted)	
55	Compute $[\lambda_{17}^a], [\lambda_{18}^a], [\lambda_{19}^a], [\lambda_{20}^a], \{\xi_7^a\}$	Tables
	(Note: $[\lambda_{19}^a]$ is constant in time)	
	(These coefficients are associated with Newton's equations for the a^{th} mass point of the counterweight)	
55a	$[\Delta_9^a] = [\lambda_{17}^a]; [\Delta_{10}^a] = [\lambda_{18}^a]; [\Delta_{11}^a] = [\lambda_{19}^a];$ $[\Delta_{12}^a] = [\lambda_{20}^a]; [\Delta_{13}^a] = [\lambda_{19}^a]; \{\nabla_3^a\} = -\{\xi_7^a\} - [\lambda_{19}^a]\{\ddot{R}_0\}$	
56	Compute $\{\omega^a\}$	Eq 27
57	Compute $[\lambda_{21}^a], [\lambda_{22}^a], \{\xi_8^a\}$	Tables
	(Note: $[\lambda_{22}^a]$ is constant in time)	
	(These coefficients are associated with Euler's equations for the a^{th} mass point of the counterweight)	
57a	$[\Delta_{14}^a] = [\lambda_{21}^a]; [\Delta_{15}^a] = [\lambda_{22}^a]; \{\nabla_4^a\} = -\{\xi_8^a\}$	

Step No.	Operation	Required Equation
57b	Compute $\{\bar{L}_a\}$, \bar{K}_a ; $\{L\} = \{L\} + \{\bar{L}_a\}$; $K = K + \bar{K}_a$	Eq. A26, A27
58	Return to step 51	
58a	Compute $\{ZFX\}$, $\{ZLX\}$, $\{ZMX\}$, $\{ZCY\}$	Eq. A27a
58b	Compute $\{ZCM\}$	Eq. A27b
58c	Compute $\{P_z\}$	Eq. A27c
	<u>Formation of Equations of Motion</u>	
59	Set up $[A]$ matrix	Eq. 36
60	$\{l_0\}$, $\{\delta\}$, $\{\dot{\delta}\}$, $\{\phi^*\}$, $\{\dot{\phi}^*\}$ are known - go to Connecting-Structure subroutine* to obtain $\{f_E^*\}$ and $\{\tau_E^*\}$. If the Space Station is rigid, bypass the subroutine and set $\{f_E^*\} = \{\tau_E^*\} = 0$.	
61	Compute $\{f_E\}$, $\{\tau_E\}$, $\{\bar{f}_E\}$, $\{\bar{\tau}_E\}$	Eq. 37
62	If controls are present, obtain $\{f_c^i\}$, $\{\tau_c^i\}$, $\{\bar{f}_c^a\}$ and $\{\bar{\tau}_c^a\}$ for all m_i and \bar{m}_a from controls subroutine	
63	If supplementary forces are present, obtain $\{f_s^i\}$, $\{\tau_s^i\}$, $\{\bar{f}_s^a\}$, $\{\bar{\tau}_s^a\}$, for all m_i and \bar{m}_a from supplementary loads subroutine	
64	Compute all $\{f^i\}$, $\{\bar{f}^a\}$	Eq. 38, 39
65	Compute all $\{\tau^i\}$, $\{\bar{\tau}^a\}$	Eq. 40, 41
66	Compute $\{\nabla_5^i\}$, $\{\nabla_6^i\}$, $\{\nabla_7^a\}$, and $\{\nabla_8^a\}$ for all i and a	Eq. 42
67	Assembly total $\{\nabla\}$	Eq. 43

* See Appendix G.

Step No.	Operation	Required Equation
67a	<p>If structural loads applied by Connecting Structure are to be printed, print loads on Laboratory in \tilde{X} axes, $([1] + [\Gamma(\theta_i)])\{\bar{f}_E\}$, $([1] + [\Gamma(\theta_i)])\{\tau_E\}$; and loads on Counterweight in \tilde{Y} axes $([1] + [\Gamma(\theta_a)])\{\bar{f}_E\}$, $([1] + [\Gamma(\theta_a)])\{\tau_E\}$.</p> <p>If internal Structural loads in Laboratory are required, compute and print $\{f'_\ell\}$ and $\{\tau'_\ell\}$. Summation in Equations (65) and (69) is over all mass points comprising free body.</p> <p>If internal structural loads in Counterweight are required, compute and print $\{f'_\ell\}$ and $\{\tau'_\ell\}$. Summation in Equations (71) and (75) is over all mass points comprising free body.</p>	<p>Eqs. 64 - 69</p> <p>Eqs. 70 - 75</p> <p>Eq. 44</p>
68	<p>Compute all $[Q^i]$, $[P^i]$, $[R^a]$, $[S^a]$, $[\bar{R}^a]$, $[S(\theta_i)]_\ell$, $[S(\bar{\theta}_a)]_\ell$</p>	C-22

Step No.	Operation	Required Equation
69	Set up total $[Q]$ matrix	Eq. 45-45e
70	Compute $[K]$ and $[C_M]$ if Laboratory is flexible; $[K]$ and $[C_M]$ if C.W. is flexible	Eq 46
71	Compute $[\Delta_R]$	Eq 47
72	Compute $\{f_M\}, \{\bar{f}_M\}$	Eq 48
73	Set up $\{F_M\}$	Eq 49
74	Compute $\{\nabla_R\}$	Eq 50
75	Compute $\{\ddot{x}_T\}$ by solving Equation 51	Eq 51
<u>Begin Numerical Integration Cycle</u>		
76	Integrate $\{\ddot{x}_T\}$ and $\{\dot{x}_T\}$ to obtain $\{\dot{x}_T\}$ and $\{x_T\}$ at $t + \Delta t$ (see Equation A63)	
76a	Compute $\{X\}$	Eq. 53
77	Set $t = t + \Delta t$	
78	Compute physical variables $\{\dot{x}\}, \{x\}$ at $t + \Delta t$	Eq 52, 53
79	Compute $\{q\}$	Eq A6a
80	Compute $[s(x)]', [s(q)]'$	Eq A8
81	Compute $[\pi(q^*)]$	Eq 8
82	Compute $[\pi(q)]$	Eq A41

Step No.	Operation	Required Equation
83	Compute $\{\dot{x}\}$	Eq. A17
84	Compute $\{\dot{q}^*\}$	Eq. A17
The following quantities are now known at $t + \Delta t$:		
	$\{R\}, \{\ddot{R}\}, \{\dot{x}\}, \{\ddot{x}\}, \{\omega^x\}, \{\dot{p}_i\}, \{\ddot{p}_i\}, \{\dot{\theta}_i\}, \{\ddot{\theta}_i\},$ $\{\Delta \ddot{R}\}, \{\Delta \dot{R}\}, \{\dot{q}^*\}, \{\ddot{q}^*\}, \{\omega^y\}, \{\ddot{p}_a\}, \{\dot{p}_a\}, \{\ddot{\theta}_a\}, \{\dot{\theta}_a\},$ $(i = 1, \dots, n; a = 1, \dots, n)$	
84a	If there is no deployment, go to 87	
85	If there is deployment in the run, go to deployment subroutine to obtain $\{\dot{l}_0\}$	
	$\{\dot{l}_0\}, \{\ddot{l}_0\}$	
86	Compute $\{\ddot{R}_0\}, \{\dot{R}_0\}, \{\ddot{R}_0\}$	Eq A14, A15
87	Compute $\{\ddot{R}\}, \{\dot{R}\}$	Eq 25
88	Set up $[\Gamma(\dot{\theta}_i)], [\Gamma(\ddot{\theta}_i)], [\Gamma(\dot{\theta}_a)], [\Gamma(\ddot{\theta}_a)]$	Eq A4
89	Compute $[\ddot{\eta}(\eta^*)]$	Eq 57
90	Compute $\{\delta\}$	Eq 58

Step No.	Operation	Required Equation
91	Set up $[s(q)], [s(r)]$	Eq. A7
92	Compute $\{i\}$	Eq. 59
93	Compute $\{i\}$	Eq. 60
94	Compute $\{s\}$	Eq. 61
95	Compute $[\pi(\phi^*)]$	Eq. 62
96	Compute $\{\phi^*\}$	Eq. A6
97	Compute $[s(\phi^*)]^{-1}$	Eq. A8
98	Compute $\{\phi^*\}$	Eq. 63
99	Go to step 4a	

Subsidiary Equations

$$[\pi(\varphi_0)] = \begin{bmatrix} 1 & 0 & 0 \\ 0 & -1 & 0 \\ 0 & 0 & -1 \end{bmatrix} \quad (A1)$$

(equation was deleted) (A2)

$$[\pi(\rho)] = [\pi(\bar{\theta}_2)]^T [\pi(\rho)]^T [\pi(\phi^*)]^T [\pi(\rho)] [\pi(\varphi_0)] [\pi(\theta_z)] \quad (A3)$$

$$[\Gamma(\lambda)] = \begin{bmatrix} 0 & -\lambda_3 & \lambda_2 \\ \lambda_3 & 0 & -\lambda_1 \\ -\lambda_2 & \lambda_1 & 0 \end{bmatrix} \quad (\text{typical}) \quad (A4)$$

$$[\pi(\varphi^*)] = [\pi(\varphi)] [\pi(\varphi_0)]^T = [\pi(\varphi)] [\pi(\varphi_0)] \quad (A5)$$

$$\left. \begin{aligned} \sin \phi_2^* &= \pi_{31}(\varphi^*) \\ \sin \phi_1^* &= \frac{1}{\cos \phi_2^*} \pi_{32}(\varphi^*) \\ \sin \phi_3^* &= -\frac{1}{\cos \phi_2^*} \pi_{31}(\varphi^*) \end{aligned} \right\} \begin{array}{l} \text{take arc sines} \\ -\frac{\pi}{2} \leq \phi_i^* \leq \frac{\pi}{2} \\ (\text{typical}) \end{array} \quad (A6)$$

$$\left. \begin{aligned} \phi^* &= \phi^* + \phi^* \\ [\pi(\phi^*)] &= \begin{bmatrix} \cos \phi_3^* \cos \phi_2^* & \sin \phi_3^* & 0 \\ -\sin \phi_3^* \cos \phi_2^* & \cos \phi_3^* & 0 \\ \sin \phi_2^* & 0 & 1 \end{bmatrix} \end{aligned} \right\} \begin{array}{l} (\text{typical}) \\ (A7) \end{array}$$

$$[\pi(\phi^*)]^{-1} = \frac{1}{\cos \phi_2^*} \begin{bmatrix} \cos \phi_3^* & -\sin \phi_3^* & 0 \\ \sin \phi_3^* \cos \phi_2^* & \cos \phi_3^* \cos \phi_2^* & 0 \\ -\cos \phi_3^* \sin \phi_2^* & \sin \phi_3^* \sin \phi_2^* & \cos \phi_2^* \end{bmatrix} \quad (\text{typical}) \quad (A8)$$

$$\{\dot{\rho}^*\} = [\pi(\varphi)]^T [\pi(\bar{\theta}_2)]^T (-[\pi(\rho)]^T [\pi(\phi^*)]^T ([\pi(\phi^*)] \{\dot{\phi}^*\} - [\pi(\rho)] [\pi(\varphi_0)] \{\dot{\theta}_z\}) - \{\dot{\bar{\theta}}_2\}) \quad (A9)$$

$$\{\omega\}^* = [\pi(\varphi)] \{\omega\}^* + [\pi(\varphi)] \{\dot{\rho}^*\} \quad (A10)$$

$$\left. \begin{aligned} \{\dot{\rho}\} &= \{\dot{\rho}_0\} + \{\dot{\rho}\} \\ \{\dot{\rho}\} &= \{\dot{\rho}_0\} + \{\dot{\rho}\} \end{aligned} \right\} \quad (A11)$$

$$\{\dot{R}\} = -[\pi(\bar{\theta}_2)]^T ([\pi(\rho)]^T \{\dot{\rho}\} + \{\dot{\bar{\theta}}_2\}) - \{\dot{\bar{\theta}}_2\} + [\pi(\varphi)] (\{\dot{\rho}_z\} + \{\dot{\rho}_z\} + [\pi(\theta_z)]^T \{\dot{\rho}\}) \quad (A12)$$

$$\left. \begin{aligned} \{\dot{R}\} &= -[\pi(\bar{\theta}_2)]^T [\pi(\rho)]^T \{\dot{\rho}\} - [\Gamma(\bar{\theta}_2)] ([\pi(\rho)]^T \{\dot{\rho}\} + \{\dot{\bar{\theta}}_2\}) - \{\dot{\bar{\theta}}_2\} \\ &\quad - [\Gamma([\pi(\varphi)] \{\dot{\rho}^*\})] [\pi(\varphi)] (\{\dot{\rho}_z\} + \{\dot{\rho}_z\} + [\pi(\theta_z)]^T \{\dot{\rho}\}) \\ &\quad + [\pi(\varphi)] (\{\dot{\rho}_z\} + [\Gamma(\theta_z)] \{\dot{\rho}\}) \end{aligned} \right\} \quad (A13)$$

$$\{\dot{\bar{R}}_0\} = -[\pi(\rho)]^T \{\dot{\bar{L}}_0\} - \{\dot{\bar{A}}\} - \{\dot{\bar{B}}\} + [\pi(\rho)] (\{\dot{v}_2\} + \{\dot{\bar{A}}\}) \quad (A14)$$

$$\begin{aligned} \{\dot{\bar{R}}_0\} &= -[\pi(\rho)]^T \{\dot{\bar{L}}_0\} \\ \{\dot{\bar{R}}_0\} &= [\pi(\rho)]^T \{\dot{\bar{L}}_0\} \end{aligned} \quad (A15)$$

$$\begin{aligned} \{\Delta \bar{E}\} &= \{\dot{\bar{E}}\} - \{\dot{\bar{R}}_0\} \\ \{\Delta \dot{\bar{E}}\} &= \{\dot{\bar{E}}\} - \{\dot{\bar{R}}_0\} \end{aligned} \quad (A16)$$

$$\{\dot{\gamma}\} = [S(\gamma)]^{-1} \{\omega^{x'}\} ; \quad \{\dot{\gamma}^{x'}\} = [S(\gamma)]^{-1} \{\omega^{x'/x}\} = [S(\gamma)]^{-1} (\{\omega^{x'}\} - [\pi(\gamma)] \{\omega^{x'}\}) \quad (A17)$$

$$\{\dot{L}_i^m\} = [\pi(\sigma)]^T ([\square] + [\Gamma(\theta_i)]) [\Xi_i] \{\omega^{x'}\} + m_i [\Gamma(\theta_i)] \{\dot{\bar{R}}_i^s\} \quad (A18)$$

$$K_i^m = \frac{1}{2} m_i \{\dot{\bar{R}}_i^s\}^2 + \frac{1}{2} \{\omega^{x'}\}^T [\Xi_i] \{\omega^{x'}\} \quad (A19)$$

$$\begin{aligned} \{\dot{L}_i^p\} &= [\pi(\sigma)]^T ([\Gamma(\theta_i)] (m_i^f \{\dot{\bar{R}}_i^s\} + ([\square] + [\Gamma(\theta_i)]) (k_i \phi \Delta u_i \{\dot{\gamma}\} + [\Gamma(\omega^{x'})] \{\dot{S}_i\})) \\ &\quad + ([\square] + [\Gamma(\theta_i)]) ([\Gamma(\sigma)] ([\square] - [\Gamma(\theta_i)]) \{\dot{\bar{R}}_i^s\} + k_i Q \Delta u_i \{\dot{\gamma}\} + [\Gamma_i^f] \{\omega^{x'}\})) \end{aligned} \quad (A20)$$

$$\begin{aligned} K_i^p &= \frac{1}{2} m_i^f \{\dot{\bar{R}}_i^s\}^2 \\ &\quad + \frac{1}{2} (m_i^p + m_i^f \left(\frac{A}{A_R}\right)^2) v^2 \\ &\quad + \frac{1}{2} \{\omega^{x'}\}^T [\Xi_i^f] \{\omega^{x'}\} + k_i \phi \{\omega^{x'}\}^T \{\dot{S}_i\} \\ &\quad + \{\dot{\bar{R}}_i^s\}^T ([\square] + [\Gamma(\theta_i)]) ([\Gamma(\omega^{x'})] \{\dot{S}_i\} + k_i \phi \Delta u_i \{\dot{\gamma}\}) \end{aligned} \quad (A21)$$

$$\{\dot{L}_i^p\} = \text{same expression as (A20) but with } k_i = 1 \quad (A22)$$

$$\begin{aligned} K_i^p &= \frac{1}{2} m_i^f (\{\dot{\bar{R}}_i^s\}^2 + v^2) \\ &\quad + \frac{1}{2} \{\omega^{x'}\}^T [\Xi_i^f] \{\omega^{x'}\} + \phi \{\omega^{x'}\}^T \{\dot{S}_i\} \\ &\quad + \{\dot{\bar{R}}_i^s\}^T ([\square] + [\Gamma(\theta_i)]) ([\Gamma(\omega^{x'})] \{\dot{S}_i\} + \phi \Delta u_i \{\dot{\gamma}\}) \end{aligned} \quad (A23)$$

$$\{\dot{L}_i^q\} = \frac{1}{2} [\pi(\sigma)]^T [\Gamma(\{\dot{R}\} + \{\dot{W}_p\})] (\{\dot{R}\} + \{\dot{W}_p\} + [\Gamma(\omega^{x'})] (\{\dot{R}\} + \{\dot{W}_p\})) \quad (A24)$$

$$K_i^q = \frac{1}{2} \frac{1}{m_i} (\{\dot{R}\} + \{\dot{W}_p\} + [\Gamma(\omega^{x'})] (\{\dot{R}\} + \{\dot{W}_p\}))^2 \quad (A25)$$

$$\begin{aligned} \{\dot{L}_a\} &= [\pi(\sigma)]^T [\pi(\gamma)]^T ([\square] + [\Gamma(\theta_a)]) [\Xi_a] \{\omega^{x'}\} \\ &\quad + m_a [\pi(\sigma)]^T [\pi(\gamma)]^T [\Gamma(\pi(\gamma))] \{\dot{R}\} + \{\dot{E}\} + \{\dot{\bar{A}}\} + \{\dot{\bar{B}}\} \} \{\dot{\bar{R}}_a^s\} \end{aligned} \quad (A26)$$

where $\{\dot{\bar{R}}_a^s\} = [\pi(\gamma)] (\{\dot{E}\} + [\Gamma(\omega^{x'})] \{\dot{R}\}) + \{\dot{R}\} + \{\dot{\bar{A}}\} + [\Gamma(\omega^{x'})] (\{\dot{R}\} + \{\dot{\bar{A}}\} + \{\dot{\bar{B}}\})$

$$K_a = \frac{1}{2} \{\omega^{x'}\}^T [\Xi_a] \{\omega^{x'}\} + \frac{1}{2} m_a \{\dot{\bar{R}}_a^s\}^2 \quad (A27)$$

$$\left. \begin{aligned}
 \{z_{FX}\} &= \sum (m_i^f \{R_i\} + ([I] + [\Gamma(\theta_i)]) \{S_i\}) \\
 \{z_{LX}\} &= \sum_{i=1}^n m_i \{R_i\} \\
 \{z_{MX}\} &= \sum_f \mu_f (\{R\} + \{W_f\}) \\
 \{z_{CY}\} &= M_c ([\pi(\gamma)] \{R\} + \{\bar{R}\}) + \sum_{a=1}^{\pi} \bar{m}_a (\{\bar{p}_a\} + \{\bar{f}_a\})
 \end{aligned} \right\} \quad (A27a)$$

$$\{z_{CM}\} = \frac{[\pi(r)]^T (\{z_{FX}\} + \{z_{LX}\} + \{z_{MX}\} + [\pi(\gamma)] \{z_{CY}\})}{M_L + M_c + \sum_f \mu_f + \sum m_i^f} \quad (A27b)$$

$$\{P_z\} = M_c [\pi(\beta)] ([I] - [\Gamma(\theta_z)]) [\Gamma(\omega\gamma)]^2 \left(\frac{1}{M_c} \{z_{CY}\} - [\pi(\gamma)] [\pi(r)] \{z_{CM}\} \right) \quad (A27c)$$

Initial Condition Procedure

Mean Axes

Lab Displacements:



$$\left. \begin{aligned} M_L \{ \varphi_0 \} - [D_L] \{ \theta_0 \} &= - \sum_{i=1}^n m_i \{ \varphi_i' \} \\ [D_L] \{ \varphi_0 \} + [I_L] \{ \theta_0 \} &= - \sum_{i=1}^n m_i [\Gamma(r_i)] \{ \varphi_i' \} - \sum_{i=1}^n [I_i] \{ \theta_i \} \end{aligned} \right\} \begin{array}{l} \text{invert \&} \\ \text{solve} \end{array} \quad (A28)$$

where:

$$M_L = \sum_{i=1}^n m_i ; [I_L] = \sum_{i=1}^n ([I_i] - m_i [\Gamma(r_i)]^2) ; [D_L] = \sum_{i=1}^n m_i [\Gamma(r_i)] \quad (A29)$$

$$\{ \theta_i \} = \{ \theta_i' \} + \{ \theta_0 \} \quad (i = 1, \dots, n) \quad (A30)$$

$$\{ \varphi_i \} = \{ \varphi_i' \} + \{ \varphi_0 \} - [\Gamma(r_i)] \{ \theta_0 \} \quad (i = 1, \dots, n) \quad (A31)$$

$$[\pi(r)] = [\pi(\theta_0)]^T [\pi(r')] \quad (A32)$$

$$\left. \begin{aligned} \sin \gamma_2 &= \pi_{31}(r) ; & |\gamma_2| &< \frac{\pi}{2} \\ \sin \gamma_3 &= -\pi_{21}(r) / \cos \gamma_2 ; & |\gamma_3| &< \frac{\pi}{2} \\ \sin \gamma_1 &= -\pi_{32}(r) / \cos \gamma_2 \\ \cos \gamma_1 &= \pi_{33}(r) / \cos \gamma_2 \end{aligned} \right\} \begin{array}{l} \text{use inverse} \\ \text{trig functions} \\ \text{(typical)} \end{array} \quad (A33)$$

$$0 \leq \gamma_i \leq 2\pi \quad (\text{note quadrant})$$

$$\{ R \} = [\pi(\theta_0)]^T \{ R' \} - \{ \varphi_0 \} \quad (A34)$$

Counterweight Displacements:

$$\left. \begin{aligned} M_c \{ \bar{\varphi}_0 \} - [D_c] \{ \bar{\theta}_0 \} &= - \sum_{a=1}^{\bar{n}} \bar{m}_a \{ \bar{\varphi}_a' \} \\ [D_c] \{ \bar{\varphi}_0 \} + [I_c] \{ \bar{\theta}_0 \} &= - \sum_{a=1}^{\bar{n}} \bar{m}_a [\Gamma(\bar{r}_a)] \{ \bar{\varphi}_a' \} - \sum_{a=1}^{\bar{n}} [\bar{I}_a] \{ \bar{\theta}_a' \} \end{aligned} \right\} \begin{array}{l} \text{invert \&} \\ \text{solve} \end{array} \quad (A35)$$

where:

$$M_c = \sum_{a=1}^{\bar{n}} \bar{m}_a ; [I_c] = \sum_{a=1}^{\bar{n}} ([\bar{I}_a] - \bar{m}_a [\Gamma(\bar{r}_a)]^2) ; [D_c] = \sum_{a=1}^{\bar{n}} \bar{m}_a [\Gamma(\bar{r}_a)] \quad (A36)$$

$$\{ \bar{\theta}_a \} = \{ \bar{\theta}_a' \} + \{ \bar{\theta}_0 \} \quad (a = 1, \dots, \bar{n}) \quad (A37)$$

$$\{ \bar{\varphi}_a \} = \{ \bar{\varphi}_a' \} + \{ \bar{\varphi}_0 \} - [\Gamma(\bar{r}_a)] \{ \bar{\theta}_0 \} \quad (a = 1, \dots, \bar{n}) \quad (A38)$$

$$[\pi(\varphi^*)] = [\pi(\bar{\theta}_0)]^T [\pi(\varphi')] [\pi(\bar{\theta}_0)] [\pi(\varphi_0)] \quad (A39)$$

$$\{ \bar{R} \} = [\pi(\varphi)] \{ \varphi_0 \} + [\pi(\bar{\theta}_0)]^T \{ \bar{R}' \} - \{ \bar{\varphi}_0 \} \quad (A40)$$

$$[\pi(\gamma)] = [\pi(\gamma^*)] [\pi(\gamma_0)] \quad (A41)$$

Lab Velocities:

$$\begin{aligned} M_L \{\dot{\bar{q}}_0\} - [D_L] \{\dot{\theta}_0\} &= - \sum_{i=1}^n m_i \{\dot{\bar{q}}_i'\} \\ [D_L] \{\dot{\bar{q}}_0\} + [I_L] \{\dot{\theta}_0\} &= - \sum_{i=1}^n m_i [\Gamma(r_i)] \{\dot{\bar{q}}_i'\} - \sum_{i=1}^n [I_i] \{\dot{\theta}_i'\} \end{aligned} \quad \left. \vphantom{\sum_{i=1}^n} \right\} \begin{array}{l} \text{invert \&} \\ \text{solve} \end{array} \quad (A42)$$

$$\{\dot{\theta}_i\} = \{\dot{\theta}_i'\} + \{\dot{\theta}_0\} \quad (i=1, \dots, n) \quad (A43)$$

$$\{\dot{\bar{q}}_i\} = \{\dot{\bar{q}}_i'\} + \{\dot{\bar{q}}_0\} - [\Gamma(r_i)] \{\dot{\theta}_0\} \quad (i=1, \dots, n) \quad (A44)$$

$$\{\omega^x\} = [\pi(\theta_0)]^T \{\omega^{x'}\} - \{\dot{\theta}_0\} \quad (A45)$$

$$(\text{Equation deleted}) \quad (A46)$$

$$\{\dot{R}\} = [\pi(\theta_0)]^T \{\dot{R}'\} + [\Gamma(\theta_0)] \{\dot{R}'\} - \{\dot{\bar{q}}_0\} \quad (A47)$$

Counterweight Velocities:

$$\begin{aligned} M_c \{\dot{\bar{q}}_0\} - [D_c] \{\dot{\theta}_0\} &= - \sum_{a=1}^{\bar{n}} \bar{m}_a \{\dot{\bar{q}}_a'\} \\ [D_c] \{\dot{\bar{q}}_0\} + [I_c] \{\dot{\theta}_0\} &= - \sum_{a=1}^{\bar{n}} \bar{m}_a [\Gamma(\bar{r}_a)] \{\dot{\bar{q}}_a'\} - \sum_{a=1}^{\bar{n}} [\bar{I}_a] \{\dot{\theta}_a'\} \end{aligned} \quad \left. \vphantom{\sum_{a=1}^{\bar{n}}} \right\} \begin{array}{l} \text{invert \&} \\ \text{solve} \end{array} \quad (A48)$$

$$\{\dot{\theta}_a\} = \{\dot{\theta}_a'\} + \{\dot{\theta}_0\} \quad (a=1, \dots, \bar{n}) \quad (A49)$$

$$\{\dot{\bar{q}}_a\} = \{\dot{\bar{q}}_a'\} + \{\dot{\bar{q}}_0\} - [\Gamma(\bar{r}_a)] \{\dot{\theta}_0\} \quad (a=1, \dots, \bar{n}) \quad (A50)$$

$$\{\omega^y\} = [\pi(\theta_0)]^T \{\omega^{y'}\} - \{\dot{\theta}_0\} \quad (A51)$$

$$(\text{Equation deleted}) \quad (A52)$$

$$\{\omega^{y/x}\} = \{\omega^y\} - [\pi(\eta)] \{\omega^x\} \quad (A53)$$

$$\{\dot{R}\} = - [\Gamma(\omega^{y/x})] [\pi(\eta)] \{\dot{\bar{q}}_0\} + [\pi(\eta)] \{\dot{\bar{q}}_0\} + [\Gamma(\theta_0)] \{\dot{R}'\} + [\pi(\theta_0)]^T \{\dot{R}'\} - \{\dot{\bar{q}}_0\} \quad (A54)$$

Physical and Modal Matrices

$$\{f\} = \begin{Bmatrix} f_1 \\ \theta_1 \\ f_2 \\ \theta_2 \\ \vdots \\ f_n \\ \theta_n \end{Bmatrix} \quad \{ \bar{f} \} = \begin{Bmatrix} \bar{f}_1 \\ \bar{\theta}_1 \\ \bar{f}_2 \\ \bar{\theta}_2 \\ \vdots \\ \bar{f}_n \\ \bar{\theta}_n \end{Bmatrix} \quad (A55)$$

$$[M] = \begin{bmatrix} m_1 [I_3] & & & \\ & [I_1] & & \\ & & m_2 [I_3] & \\ & & & [I_2] \\ & & & & \ddots \\ & & & & & m_n [I_3] \\ & & & & & & [I_n] \end{bmatrix} \quad (A56)$$

$$[\bar{M}] = \begin{bmatrix} \bar{m}_1 [I_3] & & & \\ & [\bar{I}_1] & & \\ & & \bar{m}_2 [I_3] & \\ & & & [\bar{I}_2] \\ & & & & \ddots \\ & & & & & \bar{m}_n [I_3] \\ & & & & & & [\bar{I}_n] \end{bmatrix} \quad (A57)$$

Initial Values of Generalized Coordinates

$$[\Phi'] = [\mu]^{-1} [\Phi]^T [M] \quad ([\mu] \text{ is diagonal}) \quad (A58)$$

$$\{\xi\} = [\Phi'] \{\rho\} \quad ; \quad \{\dot{\xi}\} = [\Phi'] \{\dot{\rho}\} \quad (A59)$$

$$[\bar{\Phi}'] = [\bar{\mu}]^{-1} [\bar{\Phi}]^T [\bar{M}] \quad ([\bar{\mu}] \text{ is diagonal}) \quad (A60)$$

$$\{\bar{\xi}\} = [\bar{\Phi}'] \{\bar{\rho}\} \quad ; \quad \{\dot{\bar{\xi}}\} = [\bar{\Phi}'] \{\dot{\bar{\rho}}\} \quad (A61)$$

Modal - Constraint Matrices

Flexible Connecting Structure:

$$[\phi] = [\phi] = \begin{bmatrix} |_6 & & & \\ & \Phi & & \\ & & |_6 & \\ & & & \bar{\Phi} \end{bmatrix} \quad \begin{array}{l} \text{Rigid Lab:} \\ \text{Width of } \Phi \text{ shrinks} \\ \text{to zero} \\ \text{Rigid Counterweight:} \\ \text{Width of } \bar{\Phi} \text{ shrinks} \\ \text{to zero} \end{array} \quad (A62a)$$

Rigid Space Station

$$[\phi] = \begin{bmatrix} |_6 & 6^* \\ 0 & 6(n+\bar{n})+6 \end{bmatrix} \quad [\phi] = \begin{bmatrix} |_6 & 6 \\ 0 & 6n+3 \\ 0 & [7\phi] & 3 \\ 0 & 6\bar{n} \end{bmatrix} \quad (A62b)$$

Integration Coordinates

$$\left\{ \begin{array}{c} \xi \\ \xi_T \end{array} \right\} = \left\{ \begin{array}{c} R \\ \gamma \\ \xi \\ \Delta R \\ \gamma^* \\ \xi \end{array} \right\} \quad \left\{ \begin{array}{c} \dot{\xi} \\ \dot{\xi}_T \end{array} \right\} = \left\{ \begin{array}{c} \dot{R} \\ \omega^x \\ \dot{\xi} \\ \Delta \dot{R} \\ \omega_y \\ \dot{\xi} \end{array} \right\} \quad (A63)$$

* These numbers are submatrix dimensions.

The height p of $\{\xi\}$ and $\{\dot{\xi}\}$ shrinks to zero if the Laboratory is rigid.

The height \bar{p} of $\{\bar{\xi}\}$ and $\{\dot{\bar{\xi}}\}$ shrinks to zero if the Counterweight is rigid.

The heights of $\{\xi\}$, $\{\dot{\xi}\}$, $\{\Delta\bar{R}\}$, $\{\Delta\dot{\bar{R}}\}$, $\{\eta^*\}$, $\{\omega^Y\}$, $\{\bar{\xi}\}$, $\{\dot{\bar{\xi}}\}$ all shrink to zero if the entire vehicle is rigid.

Euler Angles Orienting Reservoirs

$$\begin{cases} \pi_{31}(\gamma_i) \\ \pi_{32}(\gamma_i) \\ \pi_{33}(\gamma_i) \end{cases} = \{e_i^R\}, \quad \pi_{21}(\gamma_i) = 0 \quad (A64)$$

Main Equations

$$\left. \begin{array}{l} \\ \\ \\ \end{array} \right\} \begin{array}{l} \text{(Equations deleted)} \end{array} \left. \begin{array}{l} \\ \\ \\ \end{array} \right\} \begin{array}{l} (1a) \\ (1b) \\ (2a) \\ (2b) \end{array}$$

$$\{R_i\} = \{R\} + \{r_i\} + \{g_i\} \quad (3a)$$

$$\{\dot{R}_i\} = \{\dot{R}\} + \{\dot{g}_i\} \quad (3b)$$

$$\{\dot{R}_i^s\} = \{\dot{R}_i\} + [\tau \omega \times] \{R_i\} \quad (3c)$$

$$\{\omega^s\} = ([I] - [\Gamma(\theta_i)]) \{\omega\} + \{g_i\} \quad (4)$$

$$Q = \rho A V \quad (5a)$$

$$\dot{Q} = \rho A \dot{V} \quad (5b)$$

Reservoirs

$$A_i^R = \pi b_i^2 \quad (6)$$

$$h_i = h_{i0} - k_i \frac{A}{A_i^R} \int_0^t V dt \quad (7)$$

$$[\pi(\beta_i)] = \begin{bmatrix} \cos(\beta_i)_2 & \sin(\beta_i)_2 & 0 \\ -\sin(\beta_i)_3 & \cos(\beta_i)_3 & 0 \\ 0 & 0 & 1 \end{bmatrix} \begin{bmatrix} \cos(\beta_i)_2 & 0 & -\sin(\beta_i)_2 \\ 0 & 1 & 0 \\ \sin(\beta_i)_2 & 0 & \cos(\beta_i)_2 \end{bmatrix} \begin{bmatrix} 1 & 0 & 0 \\ 0 & \cos(\beta_i)_1 & \sin(\beta_i)_1 \\ 0 & -\sin(\beta_i)_1 & \cos(\beta_i)_1 \end{bmatrix} \quad (8)$$

(typical)

$$m_i^R = \rho A_i^R h_i \quad (9)$$

$$m_i^f = m_i^p + m_i^R \quad (10)$$

$$\{u_i\} = \{u_i^p\} - \{u_i^R\} + h_i \{c_i^f\} \quad (11)$$

$$\{s_i\} = \{s_i^p\} + m_i^R (\{u_i^R\} - \frac{1}{2} h_i \{c_i^f\}) \quad (12)$$

$$\{g_i\} = \{g_i^p\} + h_i [\Gamma(u_i^R)] \{c_i^f\} \quad (13)$$

$$[L_i] = \frac{m_i^R}{12} \begin{bmatrix} (3b_i^2 + h_i^2) & 0 & 0 \\ 0 & (3b_i^2 + h_i^2) & 0 \\ 0 & 0 & (6b_i^2) \end{bmatrix} \quad (14)$$

$$\{u_i^c\} = \{u_i^R\} - \frac{1}{2} h_i [\pi(\beta_i)]^T \begin{Bmatrix} 0 \\ 0 \\ 0 \end{Bmatrix} \quad (15)$$

$$[I_i^f] = [I_i^p] + [\pi(\beta_i)]^T [L_i] [\pi(\beta_i)] - m_i^R [\Gamma(u_i^c)]^2 \quad (16)$$

$$[I_i] = -\frac{k_i Q}{4} \begin{bmatrix} (b_i^2 + h_i^2) & 0 & 0 \\ 0 & (b_i^2 + h_i^2) & 0 \\ 0 & 0 & (2b_i^2) \end{bmatrix} \quad (17)$$

$$\{\dot{u}_i^c\} = \frac{L_i}{2} \sqrt{\frac{A}{A_i^R}} [\pi(\beta_i)]^T \begin{Bmatrix} 0 \\ 0 \end{Bmatrix} \quad (18)$$

$$[\ddot{x}_i^R] = [\pi(\beta_i)]^T [\ddot{L}_i] [\pi(\beta_i)] + k_i \phi [\Gamma(u_i^c)]^2 - m_i^R [\Gamma(\ddot{u}_i^c)] [\Gamma(u_i^c)] - m_i^R [\Gamma(u_i^c)] [\Gamma(\ddot{u}_i^c)] \quad (19)$$

Moving Masses

$$\{\dot{d}_k^s\} = \{\dot{u}_g(t)\} - \{\dot{d}_k\} \quad (20)$$

$$\pi_k^s = \frac{\pi_{m_1}^s}{(1+k)} (d_k^s)^2 \quad (21)$$

$$\lambda_k^s = \frac{\pi_k^s}{\sum_{m_1}^4 \pi_k^s} \quad (22)$$

$$\{\dot{W}_g\} = \{\dot{u}_g\} + \sum_k^4 \lambda_k^s (\{\dot{f}_k\} + [\Gamma(\theta_k)] \{\dot{d}_k^s\}) \quad (23a)$$

$$\{\dot{W}_g\} = \{\dot{u}_g\} + \sum_k^4 \lambda_k^s (\{\dot{f}_k\} + [\Gamma(\theta_k)] \{\dot{d}_k^s\} + [\Gamma(\omega_k)] \{\dot{u}_g\}) \quad (23b)$$

$$\{\dot{D}_{k^*}^s\} = \{\dot{W}_g\} - \{\dot{d}_k^s\} - \{\dot{f}_{k^*}\} \quad (24)$$

$$\{\dot{R}\} = \{\dot{R}_0\} + \{\Delta \dot{R}\} \quad (25a)$$

$$\{\dot{R}\} = \{\dot{R}_0\} + \{\Delta \dot{R}\} \quad (25b)$$

$$\text{(Equation deleted)} \quad (26)$$

$$\{\omega^{r^a}\} = ([I] - [r(\bar{\theta}_a)]) \{\omega^r\} + \{\bar{\theta}_a\} \quad (27)$$

Orientation of Connecting - Structure Axes in Counterweight

$$\{\alpha_{3i}^*\} = \begin{Bmatrix} \alpha_{31}^* \\ \alpha_{32}^* \\ \alpha_{33}^* \end{Bmatrix} = \{y^{z'}\}_{\odot} \quad (28)$$

$$C_k = (\alpha_{31}^{*2} + \alpha_{32}^{*2} + \alpha_{33}^{*2})^{1/2} \quad (29)$$

$$\{\alpha_{3i}^*\} = \begin{Bmatrix} \alpha_{31}^* \\ \alpha_{32}^* \\ \alpha_{33}^* \end{Bmatrix} = \frac{1}{C_k} \{\alpha_{3i}^*\} \quad (30)$$

$$\{\alpha_{2i}^*\} = \begin{Bmatrix} \alpha_{21}^* \\ \alpha_{22}^* \\ \alpha_{23}^* \end{Bmatrix} = [\Gamma(\{y^{z'}\}_{\odot})] \{y^{z'}\}_{\odot} \quad (31)$$

$$C_f = (\alpha_{21}^{*2} + \alpha_{22}^{*2} + \alpha_{23}^{*2})^{1/2} \quad (32)$$

$$\{\alpha_{2i}^*\} = \begin{Bmatrix} \alpha_{21}^* \\ \alpha_{22}^* \\ \alpha_{23}^* \end{Bmatrix} = \frac{1}{C_f} \{\alpha_{2i}^*\} \quad (33)$$

$$\{x_{1i}\} = \begin{Bmatrix} \alpha_{11} \\ \alpha_{12} \\ \alpha_{13} \end{Bmatrix} = [\Gamma(\alpha_{2i})] \{x_{2i}\} \quad (34)$$

$$[\pi(\beta)] = \begin{bmatrix} \alpha_{11} & \alpha_{12} & \alpha_{13} \\ \alpha_{21} & \alpha_{22} & \alpha_{23} \\ \alpha_{31} & \alpha_{32} & \alpha_{33} \end{bmatrix} \quad (35)$$

Reproduced from
best available copy.

Equation (36) appears on next page. (36)

Accumulation of Loads

$$\left. \begin{aligned} \{f_E\} &= - [\pi(\phi_0)] [\pi(\beta)]^T [\pi(\phi^*)] \{f_E^*\} \\ \{t_E\} &= - [\pi(\phi_0)] [\pi(\beta)]^T [\pi(\phi^*)] \{t_E^*\} \\ \{F_E\} &= [\pi(\beta)]^T \{f_E^*\} \\ \{T_E\} &= [\pi(\beta)]^T (\{t_E^*\} + [U] \{f_E^*\}) \end{aligned} \right\} \quad (37)$$

$$\{f^i\} = ([I] + [\Gamma(\theta_i)]) (\{f_c^i\} + \{f_a^i\}) \quad \text{for } i \neq \underline{a} \quad (38a)$$

$$\{f^i\} = ([I] + [\Gamma(\theta_i)]) (\{f_c^i\} + \{f_a^i\} + \{f_E\}) \quad \text{for } i = \underline{a} \quad (38b)$$

$$\{F^a\} = ([I] + [\Gamma(\theta_a)]) (\{F_c^a\} + \{F_a^a\}) \quad \text{for } a \neq \underline{a} \quad (39a)$$

$$\{F^a\} = ([I] + [\Gamma(\theta_a)]) (\{F_c^a\} + \{F_a^a\} + \{F_E\}) \quad \text{for } a = \underline{a} \quad (39b)$$

$$\{t^i\} = \{t_c^i\} + \{t_a^i\} \quad \text{for } i \neq \underline{a} \quad (40a)$$

$$\{t^i\} = \{t_c^i\} + \{t_a^i\} + \{t_E\} + [\Gamma(\alpha)] \{f_E\} \quad \text{for } i = \underline{a} \quad (40b)$$

$$\{T^a\} = \{T_c^a\} + \{T_a^a\} \quad \text{for } a \neq \underline{a} \quad (41a)$$

$$\{T^a\} = \{T_c^a\} + \{T_a^a\} + \{T_E\} + [\Gamma(\alpha)] \{f_E\} \quad (41b)$$

Right-Hand Side of Equations of Motion

$$\left. \begin{aligned} \{\nabla_6^i\} &= \{\nabla_1^i\} + \{f^i\} \\ \{\nabla_6^i\} &= \{\nabla_2^i\} + \{t^i\} \\ \{\nabla_7^a\} &= \{\nabla_3^a\} + \{F^a\} \\ \{\nabla_8^a\} &= \{\nabla_4^a\} + \{T^a\} \end{aligned} \right\} \quad (42)$$

$$\{\nabla\} = \begin{bmatrix} \nabla'_5 \\ \nabla'_6 \\ \nabla'^2_5 \\ \nabla'^2_6 \\ \vdots \\ \vdots \\ \vdots \\ \vdots \\ \vdots \\ \nabla''_5 \\ \nabla''_6 \\ \nabla'_7 \\ \nabla'_8 \\ \nabla'_7 \\ \nabla'_8 \\ \vdots \\ \vdots \\ \vdots \\ \vdots \\ \vdots \\ \nabla''_7 \\ \nabla''_8 \end{bmatrix} \quad (43)$$

$$\left. \begin{aligned} [\varphi^i] &= [\Gamma(R_i)] \\ [P^i] &= [1] + [\Gamma(\theta_i)] \\ [R^a] &= [\Gamma(R)] [\mathcal{T}(\varphi)]^T \\ [\bar{R}^a] &= [\Gamma(\{\bar{R}\} + \{\bar{\alpha}_a\} + \{\bar{\beta}_a\})] \\ [\bar{S}^a] &= [1] + [\Gamma(\bar{\theta}_a)] \end{aligned} \right\} \quad (44)$$

[Q] Matrix

$$[\Phi] = \begin{bmatrix} D_1 & D_2 \\ I_{6n} & D_3 \\ & I_{6n} \end{bmatrix} \quad (45)$$

where:

$$[D_1] = \begin{bmatrix} I_3 & 0 & I_3 & 0 & \cdot & \cdot & \cdot & I_3 & 0 \\ Q' & P' & Q^2 & P^2 & \cdot & \cdot & \cdot & Q'' & P'' \end{bmatrix} \quad (45a)$$

$$[D_2] = \begin{bmatrix} [\Pi(\eta)]^T & 0 & [\Pi(\eta)]^T & 0 & \cdot & \cdot & \cdot & [\Pi(\eta)]^T & 0 \\ R' & 0 & R^2 & 0 & \cdot & \cdot & \cdot & R'' & 0 \end{bmatrix} \quad (45b)$$

$$[D_3] = \begin{bmatrix} I_3 & 0 & I_3 & 0 & \cdot & \cdot & \cdot & I_3 & 0 \\ \bar{R}' & \bar{S}' & \bar{R}^2 & \bar{S}^2 & \cdot & \cdot & \cdot & \bar{R}'' & \bar{S}'' \end{bmatrix} \quad (45c)$$

Laboratory and Counterweight Modal Stiffness and Damping Matrices

$$[C_M] = \begin{bmatrix} c_{11}^M & & & \\ & c_{22}^M & & \\ & & \ddots & \\ & & & c_{pp}^M \end{bmatrix} \quad \text{with } c_{i,i}^M = 2 \gamma_i \omega_i \mu_{i,i} \quad (46a)$$

$$[\bar{C}_M] = \begin{bmatrix} \bar{c}_{11}^M & & & \\ & \bar{c}_{22}^M & & \\ & & \ddots & \\ & & & \bar{c}_{\bar{p}\bar{p}}^M \end{bmatrix} \quad \text{with } \bar{c}_{i,i}^M = 2 \bar{\gamma}_i \bar{\omega}_i \bar{\mu}_{i,i} \quad (46b)$$

$$[K] = \begin{bmatrix} k_{11} & & & \\ & k_{22} & & \\ & & \ddots & \\ & & & k_{pp} \end{bmatrix} \quad \text{with } k_{i,i} = \omega_i^2 \mu_{i,i} \quad (46c)$$

$$[\bar{K}] = \begin{bmatrix} \bar{k}_{11} & & & \\ & \bar{k}_{22} & & \\ & & \ddots & \\ & & & \bar{k}_{\bar{p}\bar{p}} \end{bmatrix} \quad \text{with } \bar{k}_{i,i} = \bar{\omega}_i^2 \bar{\mu}_{i,i} \quad (46d)$$

Modal-Constraint Reduction of Problem Size

$$[\Lambda_F] = [\phi]^T [\varphi] [\Lambda] [\phi] \quad (47)$$

$$\{f_M\} = -[K]\{\xi\} - [C_M]\{\dot{\xi}\} \quad (48a)$$

$$\{\bar{F}_M\} = -[R]\{\bar{\xi}\} - [C_M]\{\dot{\bar{\xi}}\} \quad (48b)$$

$$\{F_M\} = \begin{Bmatrix} \{O_6\} \\ \{f_M\} \\ \{O_6\} \\ \{\bar{F}_M\} \end{Bmatrix}, \text{ where } \{O_6\} = \begin{Bmatrix} 0 \\ 0 \\ 0 \\ 0 \\ 0 \\ 0 \end{Bmatrix} \quad (49)$$

Height p of $\{f_M\}$ shrinks to zero if Lab is rigid

Height \bar{p} of $\{\bar{F}_M\}$ shrinks to zero if CW is rigid

$\{F_m\} = \{O_6\}$ if entire vehicle is rigid

$$\{\nabla_R\} = [\phi]^T [\varphi] \{\nabla\} + \{F_M\} \quad (50)$$

$$[\Lambda_R]\{\ddot{\xi}\} = \{\nabla_R\} \quad (51)$$

Transformation to Physical Coordinates

$$\left. \begin{aligned} \{\dot{x}\} &= [\phi] \{\dot{\xi}_T\} \\ \{x\} &= [\phi] \{\xi_T\} \\ \{\ddot{x}\} &= [\phi] \{\ddot{\xi}_T\} \end{aligned} \right\} \quad (52)$$

where:

$$\{x\} = \begin{Bmatrix} R \\ y \\ \vdots \\ \bar{p}_i \\ \theta_i \\ \vdots \\ \Delta \bar{R} \\ \gamma^* \\ \vdots \\ \bar{p}_a \\ \bar{\theta}_a \\ \vdots \end{Bmatrix} \quad \{\dot{x}\} = \begin{Bmatrix} \dot{R} \\ \omega^x \\ \vdots \\ \dot{\bar{p}}_i \\ \dot{\theta}_i \\ \vdots \\ \Delta \dot{\bar{R}} \\ \omega^y \\ \vdots \\ \dot{\bar{p}}_a \\ \dot{\theta}_a \\ \vdots \end{Bmatrix} \quad (53)$$

$$(\text{Equation Deleted}) \quad (54)$$

$$(\text{Equation Deleted}) \quad (55)$$

Connecting - Structure Deformations

(Equation deleted)

(56)

$$\begin{aligned}
 \pi_{11}(\psi^*) &= 2(2\sin^2\theta_2^* \sin^2\theta_3^* - \sin^2\theta_2^* - \sin^2\theta_3^*) \\
 \pi_{12}(\psi^*) &= \sin\theta_3^* \cos\theta_1^* + \cos\theta_3^* \sin\theta_2^* \sin\theta_1^* \\
 \pi_{13}(\psi^*) &= \sin\theta_3^* \sin\theta_1^* - \cos\theta_3^* \sin\theta_2^* \cos\theta_1^* \\
 \pi_{21}(\psi^*) &= -\sin\theta_3^* \cos\theta_1^* \\
 \pi_{22}(\psi^*) &= 2(2\sin^2\theta_2^* \sin^2\theta_3^* - \sin^2\theta_2^* - \sin^2\theta_3^*) - \sin\theta_1^* \sin\theta_2^* \sin\theta_3^* \\
 \pi_{23}(\psi^*) &= \cos\theta_3^* \sin\theta_1^* + \sin\theta_3^* \sin\theta_2^* \cos\theta_1^* \\
 \pi_{31}(\psi^*) &= \sin\theta_3^* \\
 \pi_{32}(\psi^*) &= -\cos\theta_2^* \sin\theta_1^* \\
 \pi_{33}(\psi^*) &= 2(2\sin^2\theta_2^* \sin^2\theta_3^* - \sin^2\theta_2^* - \sin^2\theta_3^*)
 \end{aligned} \tag{57}$$

$$\begin{aligned}
 \{\delta\} &= [\pi(\rho)] \left(-\{\delta\bar{e}\} + [\pi(\psi^*)] [\pi(\psi)] \{\delta\dot{e}\} + \{\delta a\} \right. \\
 &\quad - \{\delta\dot{e}\} + [\pi(\psi)] \{\delta\dot{e}\} + [\Gamma(\theta_2)] \{\delta a\} \\
 &\quad \left. - [\Gamma(\theta_2)] \{-\{\bar{e}\} - \{\delta\dot{e}\} - \{\delta\dot{e}\} + [\pi(\psi)] \{\delta\dot{e}\} + \{\delta\dot{e}\} + ([\Gamma] + [\Gamma(\theta_2)]) \{\delta a\} \} \right) \tag{58}
 \end{aligned}$$

$$\{\delta\dot{e}\} = \{\delta\dot{e}_0\} + \{\delta\delta\} \tag{59}$$

$$\begin{aligned}
 \{\delta\dot{e}\} &= [\pi(\rho)] ([\Gamma] - [\Gamma(\theta_2)]) ([\Gamma(\theta_2)] (-[\pi(\rho)] \{\delta\dot{e}\} - \{\delta\dot{e}\} - \{\delta\dot{e}\} \\
 &\quad - [\Gamma(\theta_2)] \{\delta\dot{e}\}) [\pi(\psi)] \{\delta\dot{e}\} + \{\delta\dot{e}\} + ([\Gamma] + [\Gamma(\theta_2)]) \{\delta a\} \\
 &\quad + [\pi(\psi)] \{\delta\dot{e}\} + [\Gamma(\theta_2)] \{\delta a\} \} \tag{60}
 \end{aligned}$$

$$\{\delta\dot{e}\} = \{\delta\dot{e}\} - \{\delta\dot{e}_0\} \tag{61}$$

$$[\pi(\psi^*)] = [\pi(\rho)] [\pi(\psi)] ([\Gamma] - [\Gamma(\theta_2)]) [\pi(\psi)]^T ([\Gamma] + [\Gamma(\theta_2)]) [\pi(\rho)]^T \tag{62}$$

$$\{\delta\dot{e}^*\} = [\pi(\rho^*)]^T ([\pi(\rho)] [\pi(\psi)] \{\delta\dot{e}\} - [\pi(\rho^*)] [\pi(\rho)] ([\Gamma] - [\Gamma(\theta_2)]) [\pi(\psi)] \{\delta\dot{e}\} + \{\delta\dot{e}\}) \tag{63}$$

Loads Between ModulesLaboratory:

$$\{w_F^i\} = \{\nabla_5^i\} - [\Lambda_1^i]\{\ddot{R}\} - [\Lambda_2^i]\{\dot{\omega}^x\} - [\Lambda_3^i]\{\ddot{f}_2\} - [\Lambda_4^i]\{\ddot{\theta}_2\} \quad (64)$$

$$\{f_{f'}^i\} = \sum_i \{w_F^i\} \quad (65)$$

$$\{X_{f'}^i\} = \{r_{f'}^i\} + \{f_{f'}^i\} + ([I] + [\Gamma(\theta_{f'})])\{t_{f'}^i\} \quad (66)$$

$$\{X_{f'}^i\} = \{r_{f'}^i\} + \{f_{f'}^i\} - \{X_{f'}^i\} \quad (67)$$

$$\{w_T^i\} = [\Gamma(X_{f'}^i)]\{w_F^i\} + ([I] + [\Gamma(\theta_{f'})])(\{\nabla_6^i\} - [\Lambda_5^i]\{\ddot{R}\} - [\Lambda_6^i]\{\dot{\omega}^x\} - [\Lambda_7^i]\{\ddot{f}_2\} - [\Lambda_8^i]\{\ddot{\theta}_2\}) \quad (68)$$

$$\{T_{f'}^i\} = \sum_i \{w_T^i\} \quad (69)$$

Counterweight:

$$\{\bar{w}_F^a\} = \{\nabla_7^a\} - [\Lambda_9^a]\{\ddot{R}\} - [\Lambda_{10}^a]\{\dot{\omega}^x\} - [\Lambda_{11}^a]\{\ddot{4R}\} - [\Lambda_{12}^a]\{\dot{\omega}^y\} - [\Lambda_{13}^a]\{\ddot{f}_2\} \quad (70)$$

$$\{\bar{f}_{f'}^a\} = \sum_a \{\bar{w}_F^a\} \quad (71)$$

$$\{Y_{f'}^a\} = \{\bar{r}_{f'}^a\} + \{\bar{f}_{f'}^a\} + ([I] + [\Gamma(\theta_{f'})])\{\bar{t}_{f'}^a\} \quad (72)$$

$$\{Y_{f'}^a\} = \{\bar{r}_{f'}^a\} + \{\bar{f}_{f'}^a\} - \{Y_{f'}^a\} \quad (73)$$

$$\{\bar{w}_T^a\} = [\Gamma(Y_{f'}^a)]\{\bar{w}_F^a\} + ([I] + [\Gamma(\theta_{f'})])(\{\nabla_8^a\} - [\Lambda_{14}^a]\{\dot{\omega}^y\} - [\Lambda_{15}^a]\{\ddot{\theta}_2\}) \quad (74)$$

$$\{\bar{T}_{f'}^a\} = \sum_a \{\bar{w}_T^a\} \quad (75)$$

TABLESNewton - Laboratory Mass

$$[\lambda'_1] = m_i [\dot{\Gamma}]$$

$$[\lambda'_2] = -m_i [\Gamma(R_i)]$$

$$\{\xi'_i\} = m_i (2 [\Gamma(\omega^*)] \dot{\xi}_i + [\Gamma(\omega^*)]^2 \xi_i)$$

Euler - Laboratory Mass

$$[\lambda'_3] = [\Gamma_i] ([\dot{\Gamma}] - [\Gamma(\theta_i)])$$

$$[\lambda'_4] = [\Gamma_i]$$

$$\{\xi'_i\} = -[\Gamma_i] [\Gamma(\theta_i)] \dot{\omega}^* + [\Gamma(\omega^*)] [\Gamma_i] \dot{\omega}^*$$

Newton - Pipe

$$[\lambda'_5] = m_i^f [\dot{\Gamma}]$$

$$[\lambda'_6] = -(m_i^f [\Gamma(R_i)] + ([\dot{\Gamma}] + [\Gamma(\theta_i)]) [\Gamma(s_i)] ([\dot{\Gamma}] - [\Gamma(\theta_i)]))$$

$$[\lambda'_7] = -([\dot{\Gamma}] + [\Gamma(\theta_i)]) [\Gamma(s_i)]$$

$$\begin{aligned} \{\xi'_i\} = m_i^f (2 [\Gamma(\omega^*)] \dot{\xi}_i + [\Gamma(\omega^*)]^2 \xi_i) \\ + ([\dot{\Gamma}] + [\Gamma(\theta_i)]) (\dot{\phi} \dot{\Delta} u_i + 2\phi [\Gamma(\omega^*)] \dot{\Delta} u_i + [\Gamma(\omega^*)]^2 \xi_i + \phi \dot{\Delta} e_i + [\Gamma(s_i)] [\Gamma(\theta_i)] \dot{\omega}^*) \end{aligned}$$

Euler - Pipe

$$[\lambda'_8] = [\Gamma(s_i)] ([\dot{\Gamma}] - [\Gamma(\theta_i)])$$

$$[\lambda'_9] = [\Gamma_i^f] ([\dot{\Gamma}] - [\Gamma(\theta_i)]) - [\Gamma(s_i)] ([\dot{\Gamma}] - [\Gamma(\theta_i)]) [\Gamma(R_i)]$$

$$[\lambda'_{10}] = [\Gamma_i^f]$$

$$\begin{aligned} \{\xi'_i\} = [\Gamma(\omega^*)] (\dot{\phi} \dot{\xi}_i + [\Gamma_i^f] \dot{\omega}^*) - [\Gamma_i^f] [\Gamma(\theta_i)] \dot{\omega}^* \\ + \rho V [\Delta T_i] \dot{\omega}^* + \dot{\phi} \dot{\xi}_i + \phi V \dot{\Delta} H_i \\ + [\Gamma(s_i)] ([\dot{\Gamma}] - [\Gamma(\theta_i)]) (2 [\Gamma(\omega^*)] \dot{\xi}_i + [\Gamma(\omega^*)]^2 \xi_i) \end{aligned}$$

Newton - Reservoir

$$[\lambda'_{11}] = m_i^f [\dot{\Gamma}]$$

$$[\lambda'_{12}] = -(m_i^f [\Gamma(R_i)] + ([\dot{\Gamma}] + [\Gamma(\theta_i)]) [\Gamma(s_i)] ([\dot{\Gamma}] - [\Gamma(\theta_i)]))$$

$$[\lambda'_{13}] = -([\dot{\Gamma}] + [\Gamma(\theta_i)]) [\Gamma(s_i)]$$

$$\begin{aligned} \{\xi'_i\} = m_i^f (2 [\Gamma(\omega^*)] \dot{\xi}_i + [\Gamma(\omega^*)]^2 \xi_i) \\ + ([\dot{\Gamma}] + [\Gamma(\theta_i)]) (k_i \dot{\phi} \dot{\Delta} u_i + \phi V (\dot{\xi} e_i^f - \frac{A}{A^f} \dot{\xi} e_i^f) + k_i 2\phi [\Gamma(\omega^*)] \dot{\Delta} u_i + [\Gamma(\omega^*)]^2 \xi_i \\ + [\Gamma(s_i)] [\Gamma(\theta_i)] \dot{\omega}^*) \end{aligned}$$

Euler - Reservoir

$$[\lambda'_{14}] = [\Gamma(s_i)] ([\dot{\Gamma}] - [\Gamma(\theta_i)])$$

$$[\lambda'_{15}] = [\Gamma_i^f] ([\dot{\Gamma}] - [\Gamma(\theta_i)]) - [\Gamma(s_i)] ([\dot{\Gamma}] - [\Gamma(\theta_i)]) [\Gamma(R_i)]$$

$$[\lambda'_{16}] = [\Gamma_i^f]$$

$$\begin{aligned} \{\xi'_i\} = [\Gamma(s_i)] ([\dot{\Gamma}] - [\Gamma(\theta_i)]) (2 [\Gamma(\omega^*)] \dot{\xi}_i + [\Gamma(\omega^*)]^2 \xi_i) - [\Gamma_i^f] [\Gamma(\theta_i)] \dot{\omega}^* \\ + ([\Gamma_i^f] + k_i \rho V [\Gamma_i^f]) \dot{\omega}^* + [\Gamma(\omega^*)] ([\Gamma_i^f] \dot{\omega}^* + k_i \dot{\phi} \dot{\xi}_i + k_i \dot{\phi} \dot{\xi}_i) \\ + \phi V ([\Gamma(u_i^f)] \dot{\xi} e_i^f - \frac{A}{A^f} [\Gamma(u_i^f)] \dot{\xi} e_i^f) \end{aligned}$$

TABLES (Continued)Moving Point Mass

$$[\alpha_1]^{\dot{}} = \mu_f [1]$$

$$[\alpha_3]^{\dot{}} = -\mu_f [\Gamma(R+W_f)]$$

$$[\alpha_4]^{\dot{}} = -\mu_f [\Gamma(d_{k^*}^{\dot{}})]$$

$$[\alpha_{k^*}] = ([1] - [\Gamma(\theta_{k^*})]) [\Gamma(D_{k^*}^{\dot{}})]$$

$$[\alpha_5]^{\dot{}} = [\alpha_{k^*}] [\alpha_1]^{\dot{}}$$

$$[\alpha_7]^{\dot{}} = [\alpha_{k^*}] [\alpha_3]^{\dot{}}$$

$$[\alpha_8]^{\dot{}} = [\alpha_{k^*}] [\alpha_4]^{\dot{}}$$

$$\{\beta_1\}^{\dot{}} = \mu_f (2 [\Gamma(\omega^x)] \{\dot{R} + \dot{W}_f\} + [\Gamma(\omega^x)]^2 \{R + W_f\} + \{\ddot{U}_f\} \\ + \sum_{k^*} \lambda_{k^*}^+ (2 [\Gamma(\dot{\theta}_{k^*})] \{\dot{U}_f\} + [\Gamma(\theta_{k^*})] \{\ddot{U}_f\}))$$

$$\{\beta_2\}^{\dot{}} = [\alpha_{k^*}] \{\beta_1\}^{\dot{}}$$

Newton - Counterweight

$$[\lambda_{17}^a] = m_a [\pi_f]$$

$$[\lambda_{18}^a] = -m_a [\pi_f] [\Gamma(R)]$$

$$[\lambda_{19}^a] = m_a [1]$$

$$[\lambda_{20}^a] = -m_a [\Gamma(\bar{R} + \bar{r}_a + \bar{\theta}_a)]$$

$$\{\delta_7^a\} = m_a (\pi_f) (2 [\Gamma(\omega^x)] \{\dot{R}\} + [\Gamma(\omega^x)]^2 \{R\} + 2 [\Gamma(\omega^x)] \{\dot{R} + \dot{\bar{r}}_a\} + [\Gamma(\omega^x)]^2 \{\bar{R} + \bar{r}_a + \bar{\theta}_a\})$$

Euler - Counterweight

$$[\lambda_{21}^a] = [\bar{F}_a] ([1] - [\Gamma(\bar{\theta}_a)])$$

$$[\lambda_{22}^a] = [\bar{F}_a]$$

$$\{\delta_8^a\} = [\Gamma(\omega^x)] [\bar{F}_a] \{\omega^x\} - [\bar{F}_a] [\Gamma(\dot{\bar{\theta}}_a)] \{\omega^x\}$$

APPENDIX D

REDUCTION OF THE SIZE OF THE NUMERICAL-INTEGRATION PROBLEM

The size of the numerical-integration problem will be reduced by using modes, constraint relations, or a combination of these methods. The justification of the procedure is complicated by the fact that:

- Two basic elastic structures are involved, the Laboratory and the Counterweight
- Free-free elastic modes are used together with nonlinear physical rigid-body coordinates for each structure
- Angular velocities are used and these quantities are not the derivatives of true coordinates

To facilitate the explanation, the procedure will first be justified for a simpler case and then will be extended to encompass the space-station type of structure.

D1. Nonrotating Elastic Structure

Consider any nonrotating elastic structure that is fixed to the ground and is idealized by using lumped masses which may have rotatory inertia. The equations of motion may be obtained by a variety of methods (Newton's laws, Lagrange's equations, etc.) and typically have the following form:

$$[M]\{\ddot{x}\} + \dots = \{f\} \quad \left(\begin{array}{l} n \text{ equations,} \\ n \text{ unknowns} \end{array} \right) \quad (D1)$$

where the dots indicate lower-derivative, possibly nonlinear, dynamic terms.

D1.1. The Lagrangian Form

Before proceeding, it is advantageous to reduce Equations (D1) to the Lagrangian form if they are not already in this form. This is accomplished by first giving all coordinates $\{q\}$ an arbitrary virtual displacement $\{\delta q\}$ and computing the virtual work δW done by $\{f\}$. δW , in general, has the following form:

$$\delta W = \{\delta q\}^T [Q] \{f\} \quad (D2)$$

where $[Q]$ is defined by Equation (D2); i.e., $[Q]$ may be obtained by calculating δW and writing it in the form (D2). The generalized forces associated with $\{\delta q\}$ are therefore $[Q]\{f\}$. Multiplying Equation (D1) by $[Q]$ yields

$$[M^*]\{\ddot{q}\} + \dots = [Q]\{f\} \quad \begin{pmatrix} n \text{ equations,} \\ n \text{ unknowns} \end{pmatrix} \quad (D3)$$

where

$$[M^*] \equiv [Q][M] \quad (D4)$$

Equations (D3) and (D1) are equivalent sets of equations of motion. In the form (D3) the forces on the right are generalized forces, and these equations are therefore identical to Lagrange's equations for the system. Accordingly, the new mass matrix $[M^*]$ is a symmetric matrix. If Equations (D1) were Lagrange's equations to begin with, then $[Q]$ would have turned out to be the identity matrix.

D1.2. The Constraint Reduction Method

Next, suppose that some linear constraint relations are introduced; for example, it may be desirable to evaluate the response with one portion of the structure rigidized. Then a new set of variables $\{q_1\}$, may be related to the old set of variables in terms of a constraint matrix $[T]$ as follows:

$$\{q\} = [T]\{q_1\} \quad \begin{pmatrix} \text{Dimensions:} \\ \{q\} \quad \text{is } n \times 1 \\ \{q_1\} \quad \text{is } r \times 1 \text{ (} r < n \text{)} \\ [T] \quad \text{is } n \times r \end{pmatrix} \quad (D5)$$

The procedure will be restricted to the case where $[T]$ is constant or a function of time only. Substitution of Equation (D5) into Equation (D3) yields

$$[M^*][T]\{\ddot{q}_1\} + \dots = [Q]\{f\} + [Q]\{f_1'\} \quad (D6)$$

(n equations, r unknowns in $\{q_1\}$)

where $\{f\}$ has been decomposed as follows. As a result of the constraints which have been imposed, forces of constraint have appeared; for example, if a portion of a structure is to be rigidized, an imaginary rigid weightless mechanism could be attached in the idealization in order to hold that part of the structure rigidly. The forces introduced by that mechanism are the forces of constraint. $\{f\}$ has been decomposed into these forces of constraint $\{f'_1\}$ and the balance of the forces $\{f_1\}$. Equation (D6) now appears to contain less unknowns (r) than equations (n); however, the additional $n-r$ unknowns are actually the forces of constraint appearing in $\{f'_1\}$.

In order to automatically eliminate the forces of constraint from the formulation, the virtual work of the constrained system is computed by substituting Equation (D5) into Equation (D2) and decomposing $\{f\}$ into $\{f_1\}$ and $\{f'_1\}$. The result is

$$\delta W = \{\delta q_1\}^T [T]^T [Q] \{f_1\} + \{\delta q_1\}^T [T]^T [Q] \{f'_1\}$$

$\{\delta q_1\}$ is now the arbitrary virtual displacement whereas $\{\delta q\}$ must satisfy Equation (D5). In accordance with the theory used to derive Lagrange's equations, the virtual work of the forces of constraint vanishes; i.e., $\{\delta q_1\}^T [T]^T [Q] \{f'_1\} = 0$. Since $\{\delta q_1\}$ is arbitrary, we have

$$[T]^T [Q] \{f'_1\} = 0 \quad (D7)$$

From Equation (D7), it is clear that premultiplication of Equation (D6) by $[T]^T$ would have the desired effect of eliminating the forces of constraint from the formulation. The final result is

$$[T]^T [M^*] [T] \{\ddot{x}\} + \dots = [T]^T [Q] \{f_1\} \quad (D8)$$

(r equations, r unknowns)

Equations (D8) are the new set of equations of motion that have been reduced from n to r equations. Since $\delta W = \{\delta q_1\}^T [T]^T [Q] \{f_1\}$, the generalized forces corresponding to $\{\delta q_1\}$ are $[T]^T [Q] \{f_1\}$; therefore Equations (D8) are of the Lagrangian form.

While the above explanation was somewhat lengthy, the procedure is straightforward and may be summarized as follows:

1. Compute the virtual work and write it in the form of Equation (D2) to obtain $[Q]$.
2. Premultiply the equations of motion by $[Q]$ to obtain Equations (D3), the Lagrangian form of Equations (D1).
3. Substitute the constraint equations of the form (D5) into the equations of motion (D3) and premultiply by $[T]^T$, the transpose of the constraint matrix.

The result, Equation (D8), is the desired reduced set of equations of motion.

D.1.3. The Modal Reduction Method

Suppose that it is desired to approximate the solution by using a reduced number of modes of some related eigenvalue problem. Then, instead of Equation (D5), the following similar equation holds:

$$\{\xi\} = [\phi] \{\xi\} \quad (D9)$$

where $[\phi]$ now takes on the role of $[T]$ and $\{\xi\}$ takes on the role of $\{q_1\}$. In fact, the entire theory of the previous section is applicable. Substitution of Equation (D9) into the equations of motion (D3) would give rise to forces of constraint. These are forces which must be present to suppress the appearance of any mode shapes that are not included in $[\phi]$ and therefore to constrain all solutions to be of the form (D9). After substitution of Equation (D9) into the Lagrangian form of the Equations of motion, Equation (D3), the resulting set of equations is reduced in number by premultiplication by the rectangular matrix $[\phi]^T$. The logic for this premultiplication is that it eliminates the above-mentioned forces of constraint. Note that reduction of the equations of motion by premultiplication using any rectangular matrix other than $[\phi]^T$ would usually provide a different solution since the reduction process cannot be reversed to obtain the original set of equations.

It is emphasized that Equation (D1) must first be premultiplied by $[Q]$ to obtain the Lagrangian form, otherwise the forces of constraint will not be properly eliminated from the equation and inaccuracies will result. The final result is

$$[\phi]^T [M^*] [\phi] \{\ddot{\xi}\} + \dots = [\phi]^T [Q] \{f\} \quad (D10)$$

The modal- and constraint-reduction procedures have even a stronger relation than that indicated above. The mode shapes may be computed so that they satisfy certain constraints; for example, elastic motion in a particular direction may have been set to zero in computing the mode shapes. The the solution $\{\xi\}$ to the numerical integration problem Equation (D10), yields a solution of $\{q\}$ which will also satisfy these constraints since $\{q\}$ is obtained by substituting $\{\xi\}$ into Equation (D9).

The next step in the solution is to solve Equation (D10) for $\{\ddot{\xi}\}$ and numerically integrate. This solution is particularly simple to carry out if the modes are orthogonal with respect to $[M^*]$.

Converting the initial conditions to modal coordinates requires special attention. From Equation (D9), at $t = 0$

$$\{q\} = [\phi] \{\xi\} , \quad \{\dot{q}\} = [\phi] \{\dot{\xi}\} \quad (\text{at } t = 0) \quad (D11)$$

Since $[\phi]$ is rectangular, the above equations can not be inverted; however an inverse in a limited (best fit) sense will be obtained. The procedure is first illustrated and will then be proved. The equation for $\{q\}$ is premultiplied by $[\phi]^T [M^*]$ yielding

$$[\phi]^T [M^*] [\phi] \{\xi\} = [\phi]^T [M^*] \{q\} \quad (\text{at } t = 0)$$

The coefficient matrix for $\{\xi\}$ is square and may now be inverted; therefore

$$\{\xi\} = ([\phi]^T [M^*] [\phi])^{-1} [\phi]^T [M^*] \{q\} \quad (D12)$$

(at $t = 0$)

Similarly

$$\{\dot{\xi}\} = ([\phi]^T [M^*] [\phi])^{-1} [\phi]^T [M^*] \{\dot{x}\} \quad (D13)$$

(at $t = 0$)

The proof of this procedure is as follows. Given any equation of the form $\{q\} = [\phi]\{\xi\}$, where $\{q\}$ is given, different values of $\{\xi\}$ may be selected in an attempt to approximate $\{q\}$. The error vector is then defined as

$$\{e\} = \{q\} - [\phi]\{\xi\} \quad (D14)$$

A scalar measure of the error is

$$E = \{e\}^T [M^*] \{e\} \quad (D15)$$

where the symmetric weighting matrix $[M^*]$ has been used since we wish to give more weight to errors in the coordinates associated with heavy masses than light masses. Note that Equation (D15) has the same form as twice the kinetic energy function with the coordinate errors replacing the velocities. Substituting Equation (D14) into Equation (D15) yields

$$E = (\{q\} - [\phi]\{\xi\})^T [M^*] (\{q\} - [\phi]\{\xi\})$$

To determine the $\{\xi\}$ which minimizes the error E , set the partial of E with respect to each component of $\{\xi\}$ to zero. Since $[M^*]$ is symmetric,

$$\frac{\partial E}{\partial \xi_i} = 0 = -2\{e_i\}^T [\phi]^T [M^*] (\{q\} - [\phi]\{\xi\})$$

$$i = 1, 2, \dots$$

where $\{e_i\} = [0 \dots 0 \ 1 \ 0 \dots 0]^T$ with the 1 in the i th position. Since the above equation is true for each i ,

$$[\phi]^T [M^*] (\{q\} - [\phi] \{\xi\}) = 0$$

or

$$[\phi]^T [M^*] [\phi] \{\xi\} = [\phi]^T [M^*] \{q\}$$

Solving for $\{\xi\}$ yields

$$\{\xi\} = ([\phi]^T [M^*] [\phi])^{-1} [\phi]^T [M^*] \{q\} \quad (D16)$$

This is the value of $\{\xi\}$ which will minimize the error (D14) as measured by Equation (D15)*; i.e., the value of $\{\xi\}$ which produces the best-fit of $[\phi] \{\xi\}$ to $\{q\}$. However, Equation (D16) is identical to Equation (D12); thus the procedure described to obtain Equation (D12) does produce the best-fit solution. Similarly, Equation (D13) yields the best-fit solution for $\{\ddot{q}\}$.

A procedure analogous to that described above provides further justification for the steps leading to Equation (D10). In addition to eliminating the forces of constraint it is now evident that these steps lead to a best-fit solution of $[\phi] \{\ddot{\xi}\}$ to $\{\ddot{q}\}$.

* By direct computation $\partial^2 E / \partial \xi_i^2 > 0$; therefore the value of $\{\xi\}$ which was obtained does not maximize E .

D2. Rotating Space Station

The previous procedure will now be extended for the case of the rotating space station. The equations of motion were developed using angular velocities ($\{\omega^X\}$ and $\{\omega^Y\}$) instead of Euler-angle rates because the use of angular velocities led to a simpler formulation. The velocity vector is

$$\{\dot{x}\} = \left\{ \begin{array}{l} \dot{\bar{q}} \\ \omega^X \\ \hline \dot{\bar{q}} \\ \Delta \bar{R} \\ \omega^Y \\ \hline \dot{\bar{q}} \end{array} \right\} \begin{array}{l} \text{Rigid-body motion of Laboratory} \\ \text{(6 coordinates)} \\ \hline \text{elastic motion of Laboratory} \\ \text{(6 n coordinates)} \\ \hline \text{rigid-body motion of Counterweight} \\ \text{(6 coordinates)} \\ \hline \text{elastic motion of Counterweight} \\ \text{(6 } \bar{n} \text{ coordinates)} \end{array} \quad (D17)$$

where $\{q\}$ and $\{\bar{q}\}$ contain both elastic displacements and rotations (see Equation 4.105). Since the angular velocities are not the derivatives of physical quantities, it is pointless to speak about the integral $\{x\}$ of Equation (D17). To circumvent this difficulty, the virtual displacements $(\delta\pi^X)$ and $(\delta\pi^Y)$ are introduced. These vectors contain the differential variational rotations about each of the \underline{X} and \underline{Y} axes, respectively. They may be contrasted with variations in Euler angles which are differential rotations about intermediate axes. By analogy to Equation (B6), $\{\delta\pi^X\}$ and $\{\delta\pi^Y\}$ are related to the variation in the Euler angles as follows:

$$\left. \begin{array}{l} \{\delta\pi^X\} = [S(\gamma)] \{\delta\gamma\} \\ \{\delta\pi^Y\} = [S(\eta)] \{\delta\eta\} + [\pi(\eta)] [S(\gamma)] \{\delta\gamma\} \end{array} \right\} \quad (D18)$$

Since the non-differential quantities $\{\pi^X\}$ and $\{\pi^Y\}$ have no physical meaning, they are not true coordinates and are called Quasi Coordinates.* We may now write:

* Whittaker, E. T., "A Treatise on the Analytical Dynamics of Particles and Rigid Bodies, "Fourth Edition, Cambridge University Press, 1937 (reprinted 1964), pp. 41-44.

$$\{\delta x\} = \begin{Bmatrix} \delta R \\ \delta \pi^x \\ \delta q \\ \delta \bar{R} \\ \delta \pi^y \\ \delta \bar{q} \end{Bmatrix} \quad (D19)$$

Since there are $n + \bar{n}$ masses and $12 + 6 (n + \bar{n})$ coordinates in both $\{\delta x\}$ and $\{\dot{x}\}$, 12 coordinates are dependent, and an appropriate dependency relationship among the coordinates will be introduced below. These 12 additional coordinates determine the motion of the \underline{X} and \underline{Y} axes, and the dependency relationships which will be introduced actually set the motion of these axes.

When the elastic free-free modes for both the Laboratory and Counterweight are used to represent the flexible motion of the respective bodies we may write

$$\{\delta\} = [\Phi]\{\varepsilon\}, \quad \{\bar{\delta}\} = [\bar{\Phi}]\{\bar{\varepsilon}\} \quad (D20)$$

Since the six rigid-body modes of the Laboratory have been eliminated from $[\Phi]$, if all elastic modes are used, $\{\varepsilon\}$ would contain 6 fewer coordinates than $\{q\}$. Under the same circumstances, $\{\bar{\varepsilon}\}$ would also contain 6 fewer coordinates than $\{\bar{q}\}$. As discussed in Appendix E, elimination of the rigid-body modes locates the mean or "rigid-body" axes (the \underline{X} and \underline{Y} axes in Figure 4.1) relative to the deformed Laboratory and Counterweight. If fewer than the total number of elastic modes are

used, $\{\xi\}$ and/or $\{\bar{\xi}\}$ would contain even less coordinates. Equations (D20) are the aforementioned dependency relations among the coordinates in $\{\delta x\}$.

Using Equations (D20), the following relations may be written:

$$\{\delta x\} = [\phi] \{\delta \xi_T\}, \quad \{\dot{x}\} = [\phi] \{\dot{\xi}_T\} \quad (D21)$$

where

$$\{\delta \xi_T\} = \begin{Bmatrix} \delta R \\ \delta \pi^x \\ \delta \xi \\ \delta \bar{R} \\ \delta \pi^y \\ \delta \bar{\xi} \end{Bmatrix}, \quad \{\dot{\xi}_T\} = \begin{Bmatrix} \dot{R} \\ \omega^x \\ \dot{\xi} \\ \Delta \dot{\bar{R}} \\ \omega^y \\ \dot{\bar{\xi}} \end{Bmatrix} \quad (D22)$$

all structures
are flexible

and $[\phi]$ is the appropriate constraint matrix that relates the coordinates $\{\delta x\}$ to the reduced coordinates $\{\delta \xi_T\}$. When the modes given by Equation (D20) are used to represent the Laboratory and Counterweight and when the Connecting Structure is flexible, $[\phi]$ has the following value:

$$[\phi] = \begin{bmatrix} [1_6] & & & \\ & [\Phi] & & \\ & & [1_6] & \\ & & & [\bar{\Phi}] \end{bmatrix} \quad (D23)$$

all structures
are flexible

where $[1_6]$ is the 6 x 6 identity matrix. Equations (D21) now have the effect of substituting modal coordinates for the elastic motion while duplicating the rigid-body coordinates. Unlike the coordinates of $\{\delta x\}$, the coordinates of $\{\delta \xi_T\}$ are linearly independent; thus $\{\delta \xi_T\}$ can be an arbitrary virtual displacement.

As previously, the virtual work done by the forces $\{f\}$ may be written in the form

$$\delta W = \{\delta x\}^T [Q] \{f\} \quad (D24)$$

Substitution of the first of Equations (D21) into Equation (D24) yields

$$\delta W = \{\delta \xi_T\}^T [\phi]^T \{f_1\} + \{\delta \xi_T\}^T [\phi]^T [Q] \{f_1'\} \quad (D24a)$$

where, as in the previous section, $\{f\}$ has been decomposed into constraint forces $\{f_1'\}$ and nonconstraint forces $\{f_1\}$. Since $\{\delta \xi\}$ is arbitrary we may proceed as previously and obtain

$$[\phi]^T [\phi] \{f_1'\} = 0 \quad (D25)$$

Also, for future reference we note that

$$\delta W = \{\delta \xi_T\}^T [\phi]^T [\phi] \{f_1\}$$

Therefore the generalized forces associated with $\{\xi_T\}$ are

$$\{f\}_{gen} = [\phi]^T [\phi] \{f_1\} \quad (D25a)$$

The second of Equations (D21) is substituted into the equations of motion, Equations (4.101) and the result is

$$[\Lambda] [\phi] \{\ddot{\xi}_T\} = \{f_1\} + \{f_1'\} + \{c\} \quad (D26)$$

The forces of constraint are now eliminated by premultiplying by $[\phi]^T [Q]$ and applying Equation (D25). The result is the desired reduced set of equations of motion.

$$[\Lambda_R] \{\ddot{\xi}_T\} = \{\nabla_R\} \quad (D27)$$

where the reduced mass matrix is

$$[\Lambda_R] \equiv [\phi]^T [\phi] [\Lambda] [\phi] \quad (D28)$$

and the reduced right-side vector is

$$\{\nabla_R\} \equiv [\phi]^T [\phi] (\{f\} + \{\sigma\}) \quad (D29)$$

The subscript 1 has been dropped from $\{f\}$ for convenience in notation; however it is clear that it is not necessary to include the forces of constraint in the $\{f\}$ of Equations (D29).

The above procedure could be used to handle a problem with a combination of modes and conventional constraints. For example, the Counterweight could be rigidized by shrinking $[\bar{\phi}]$ to zero in width while the Laboratory is represented by its elastic modes $[\phi]$ in Equation (D23).

Since the forces appearing on the right side of Equations (D27) (the elements of $[\phi]^T [Q] \{f\}$) are the generalized forces corresponding to $\{\xi_T\}$, Equations (D27) are the associated Lagrange equations in quasi coordinates.* Accordingly, the reduced mass matrix $[\Lambda_R]$ is symmetric.

As in the previous section, it is necessary to obtain a best-fit solution for the initial conditions in modal coordinates. This is done separately for the Laboratory and the Counterweight, and in each case, the mass matrix that is used to obtain the modes is also used as the weighting matrix in the error function, Equation (D15). These mass matrices are denoted by $[M]$ and $[\bar{M}]$, respectively, and are already in the Lagrangian ($[M^*]$) form.

The results for the Laboratory are

* Ibid

$$\{\xi\} = [\mu]^{-1} [\Phi]^T [M] \{\dot{x}\} \quad \text{at } t = 0 \quad (D30)$$

$$\{\dot{\xi}\} = [\mu]^{-1} [\Phi]^T [M] \{\ddot{x}\} \quad \text{at } t = 0 \quad (D31)$$

where $[\mu]$ is the modal mass matrix which is diagonal since the modes are required to be orthogonal with respect to $[M]$. Similarly, for the counterweight,

$$\{\bar{\xi}\} = [\bar{\mu}]^{-1} [\bar{\Phi}]^T [\bar{M}] \{\bar{\dot{x}}\} \quad \text{at } t = 0 \quad (D32)$$

$$\{\dot{\bar{\xi}}\} = [\bar{\mu}]^{-1} [\bar{\Phi}]^T [\bar{M}] \{\bar{\ddot{x}}\} \quad \text{at } t = 0 \quad (D33)$$

APPENDIX E

INITIAL ALIGNMENT OF RIGID-BODY AXES

E1. LABORATORY

As described in Section 4.3.5, the elements of $\{q\}$ and $\{\dot{q}\}$ must satisfy Equations (4.117), (4.118), and their derivatives with respect to t . However, at $t = 0$, the user will be permitted to specify these quantities relative to any convenient \tilde{X} coordinate system*; therefore, the input values of $\{q\}$ and $\{\dot{q}\}$ may not satisfy the above equations. It will be demonstrated, by direct computation, that a neighboring set of axes exist such that, when $\{q\}$ and $\{\dot{q}\}$ are specified relative to these axes, the required equations will be satisfied. Equations (4.117) and (4.118) therefore serve to locate the \tilde{X} axes (also known as mean axes or rigid-body axes) relative to the deformed structure.

We will denote the user-supplied input data with primes, and the adjusted initial conditions which satisfy the required equation will be unprimed. In Figure E1, the reference axes used in supplying the initial conditions is denoted \tilde{X}' . The origin of the \tilde{X}' axes is located at $\{q_0\}$ relative to \tilde{X} axes, and the orientation of the \tilde{X}' axes is $\{\theta_0\}$ relative to \tilde{X} . The first step will be to determine these unknown values. The user-supplied input data is as follows:

γ' locates the orientation of the \tilde{X}' axes relative to the \tilde{Z} axes
 $\{\omega^{\tilde{X}'}\}$ is the angular velocity of the \tilde{X}' axes relative to the \tilde{Z} axes expressed in \tilde{X}'

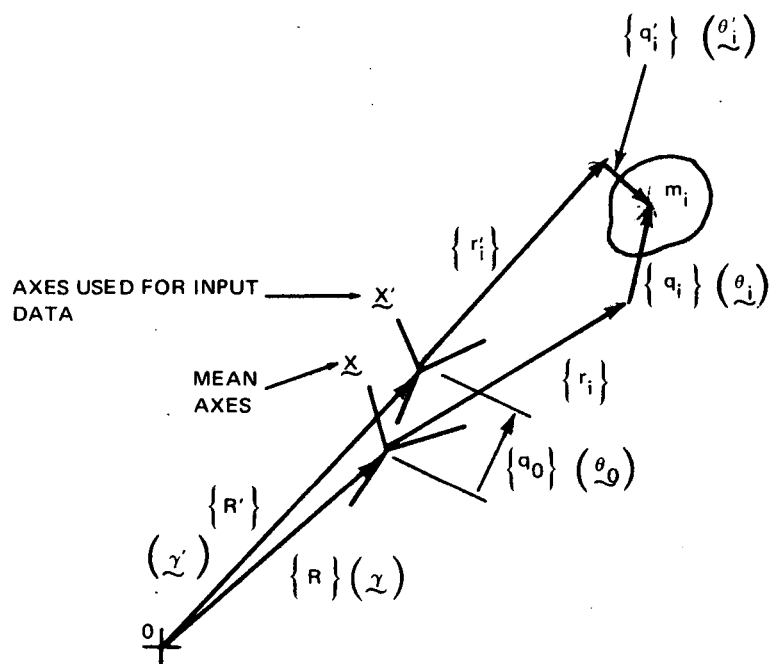
$\{R'\}$ locates origin of the \tilde{X}' axes and is expressed in \tilde{X}'

$\{\dot{R}'\}$ is expressed in \tilde{X}'

$\{q_i'\}$, $\{\theta_i'\}$ and their derivatives are expressed in

\tilde{X}' for $i = 1, \dots, n$.

* The $\{q_i\}$ and $\{\theta_i\}$ supplied by the user at $t = 0$ must however be small so that linearity is not violated; thus, the \tilde{X} coordinate system selected by the user will be near the mean axes defined in this appendix.



NOTE: COMPONENTS OF $\{r'_i\}$ IN X' AXES ARE EQUAL
TO COMPONENTS OF $\{r_i\}$ IN X AXES

Fig. E1 Rigid-Body Axes at $t = 0$ for Laboratory

C4

The first step will be to locate the mean axes. From geometry, using linearized relationships (e.g., $[\pi(\theta_0)] = [1] - [\Gamma(\theta_0)]$),

$$\{\theta_i\} = \{\theta_i'\} + \{\theta_0\} ; \quad i = 1, \dots, n \quad (E1)$$

$$\{f_i\} = \{f_i'\} + \{f_0\} - [\Gamma(\theta_0)]\{\theta_0\} ; \quad i = 1, \dots, n \quad (E2)$$

$$[\pi(\gamma)] = ([1] + [\Gamma(\theta_0)])[\pi(\gamma')] \quad (E3)$$

$$\{R\} = ([1] + [\Gamma(\theta_0)])\{R'\} - \{f_0\} \quad (E4)$$

Equations (E1) and (E2) are substituted into Equations (4.117) and (4.118) and the resulting relations are Equations (A28) of Appendix C. These equations are solved simultaneously for $\{q_0\}$ and $\{\theta_0\}$. These values locate the \tilde{X} , or mean, axes; thus we have demonstrated that Equations (4.117) and (4.118) do locate these axes.

Next the values of $\{q_0\}$ and $\{\theta_0\}$ are substituted into Equations (E1) and (E2) and $\{\theta_i\}$ and $\{q_i\}$ are determined for each value of i . Then $[\pi(\gamma)]$ is computed using Equations (E3), and the value of γ may be extracted from $[\pi(\gamma)]$ by using the definition of the π matrix which yields

$$\left. \begin{aligned} \sin \gamma_2 &= \pi_{31}(\gamma) ; \quad |\gamma_2| < \frac{\pi}{2} \\ \sin \gamma_3 &= -\pi_{21}(\gamma)/\cos \gamma_2 ; \quad |\gamma_3| < \frac{\pi}{2} \\ \sin \gamma_1 &= -\pi_{32}(\gamma)/\cos \gamma_2 \\ \cos \gamma_1 &= \pi_{33}(\gamma)/\cos \gamma_2 \end{aligned} \right\} \quad 0 \leq \gamma_1 \leq 2\pi \quad (E5)$$

where $\pi_{ij}(\gamma)$ is the ij^{th} element of $[\pi(\gamma)]$. Finally, Equation (E4) is used to obtain $\{R\}$. All position data is now known.

The procedure for converting the velocity data is nearly identical to the above described data for displacements, except that the derivatives of Equations (4.117), (4.118), (E1), (E2), and (E4) are used. In place of the derivative of Equation (E3), it is simpler to use the following relation which may be obtained from Figure E1:

$$\{\omega^x\} = ([I] + [I(\theta_o)])\{\omega^{x'}\} - \{\dot{\theta}_o\} \quad (\text{E6})$$

All of the equations required to convert the velocity data are presented as Equations (A42 - A47) of Appendix C.

E2. COUNTERWEIGHT

The derivation for adjusting the input data is nearly identical to that used for the Laboratory except for some differences due to geometry which will be discussed below. The geometry for this case is shown in Figure E2. The user supplied input data is as follows:

η' locates the orientation of the \tilde{Y}' axes relative to the \tilde{X}' axes.

$\{\omega^{Y'}\}$ is the angular velocity of the \tilde{Y}' axes relative to the \tilde{Z} axes (shown in Figure E1) expressed in \tilde{Y}' .

$\{\bar{R}'\}$ is expressed in \tilde{Y}'

$\{\bar{q}_a'\}$, $\{\bar{\theta}_a'\}$ and their derivatives are expressed in \tilde{Y}'

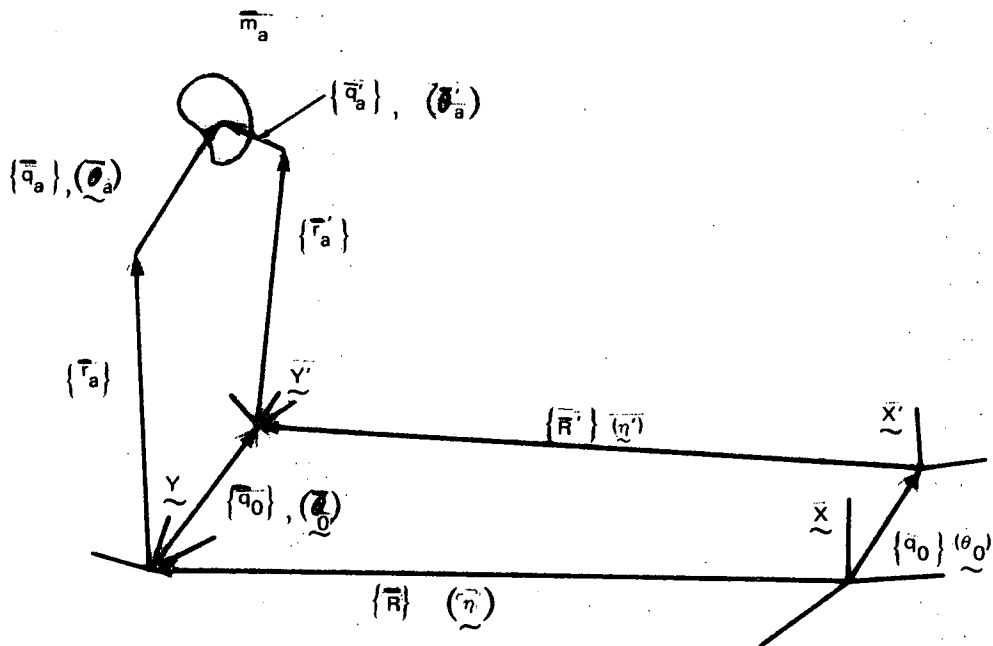
From the geometry of Figure E2,

$$\{\bar{\theta}_a\} = \{\bar{\theta}_a'\} + \{\bar{\theta}_o\} \quad (a = 1, \dots, \bar{n}) \quad (\text{E7})$$

$$\{\bar{f}_a\} = \{\bar{f}_a'\} + \{\bar{f}_o\} - [I(\bar{f}_a)]\{\bar{\theta}_o\} \quad (a = 1, \dots, \bar{n}) \quad (\text{E8})$$

$$[\pi(\gamma)] = ([I] + [I(\bar{\theta}_o)])[\pi(\gamma')]([I] - [I(\theta_o)]) \quad (\text{E9})$$

$$\{\bar{R}\} = [\pi(\gamma)]\{\bar{f}_o\} + ([I] + [I(\bar{\theta}_o)])\{\bar{R}'\} - \{\bar{f}_o\} \quad (\text{E10})$$



NOTE: THE COMPONENTS OF $\{\underline{r}_a'\}$ IN THE \underline{y}' AXES ARE EQUAL TO THE COMPONENTS OF $\{\underline{r}_a\}$ IN THE \underline{y} AXES.

Fig. E2 Rigid-Body Axes at $t = 0$ for Counterweight

Equations identical to Equations (4.117) and (4.118) are also used; however, a bar is placed over each symbol to denote that the application is for the Counterweight. The balance of the computation procedure is identical to that used for the Laboratory, and the results are Equations (A35-A41) of Appendix C.

The derivation for the velocities is also analagous to that used for the Laboratory; however, in place of Equation (E6), the following relation is used:

$$\{\omega^Y\} = ([I] + [I(\bar{\theta}_0)])\{\omega^{Y'}\} - \{\dot{\bar{\theta}}_0\} \quad (E11)$$

The Equations needed to adjust the counterweight-velocity input data are presented as Equations (A48 - A54) of Appendix C.

APPENDIX FPHYSICAL PROPERTIES OF SPACE STATION MODEL
USED TO DEMONSTRATE THE COMPUTER PROGRAMS

The assembled Space Station is shown in Figure 6.1. Figure 6.2 is a detailed view of the Laboratory.

F1. LABORATORY AND COUNTERWEIGHT

In the demonstration problems the Laboratory and Counterweight are made up of the following types of structures:

- core module
- appended module (also referred to as appendage)
- solar panel

The physical properties of the above structures were supplied to Grumman by NASA. The core and appended module properties are based on North American Aviation studies and the solar panel properties are based on a study conducted by Fairchild Industries and Wolf Research and Development Corporation.*

A typical core and an appended module are shown in Figures F1 and F2. These modules were idealized as beams with the stiffness properties listed in Table F1. The mass properties are shown in Table F2.

A typical solar panel is shown in Figure F3. The mass at each node is listed in Table F3. The rotatory inertia at each solar-panel node was assumed to be zero. The solar-panel elastic properties are described in terms of their normal modes of vibration. These modes were computed in the previously referenced investigation* and were used as input data in the Phase I computer program. The following 12 solar-panel modes were used because these modes were determined to have the most significant participations in the Space-Station dynamics problem* These are modes 1, 2, 3, 9, 10, 11, 17, 18, 19, 20, 28, and 32. They are presented in Table F4.

Damping in the Laboratory was assumed to be 2% of critical for each mode of the assembled Laboratory.

* Heindrichs, J.A. and Fee, J.J., "Integrated Dynamic Analysis Simulation of Space Stations with Controllable Solar Arrays (Supplemental Data and Analyses), NASA CR-112145, September 1972.

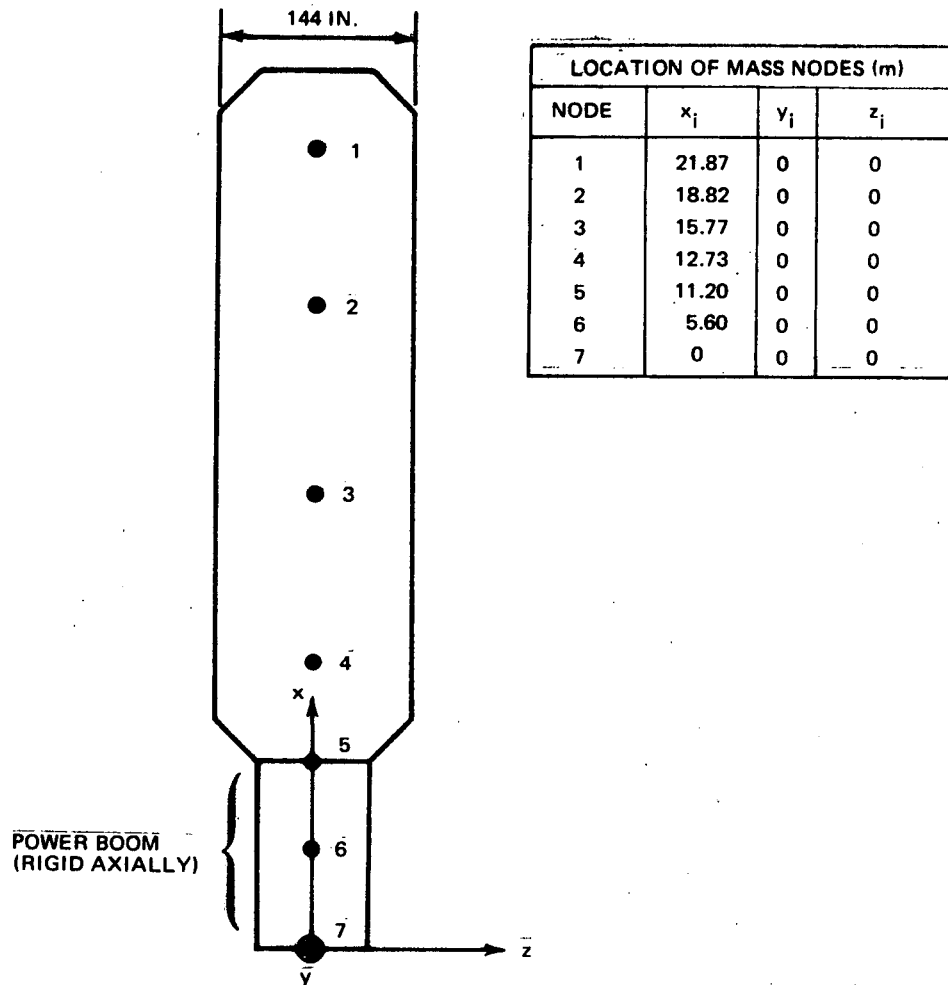


Fig. F1 Typical Core Module

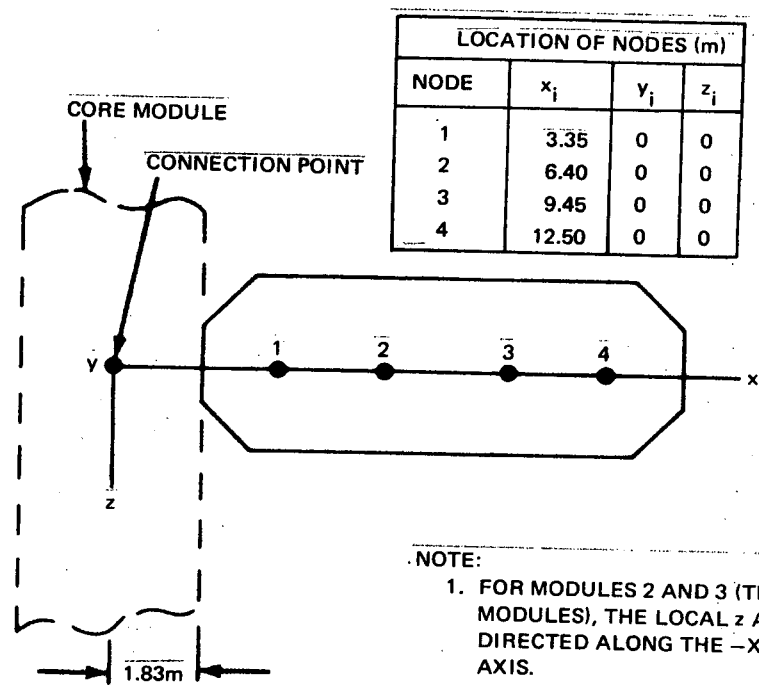


Fig. F2 Typical Appended Module

Table F1

STIFFNESS PROPERTIES OF CORE AND
APPENDED MODULES

STRUCTURE	BENDING EI (N.m ²)	TORSION GJ (N.m ²)	SHEAR kAG (N)	AXIAL EXTENSION AE (N)
Core Module:				
Main Section	2210 X 10 ⁶	1062 X 10 ⁶	32.2 X 10 ⁷	133.0 X 10 ⁷
Power Boom	413 X 10 ⁶	231 X 10 ⁶	22.4 X 10 ⁷	rigid
Appended Module	7749 X 10 ⁶	6199 X 10 ⁶	136.1 X 10 ⁷	340.3 X 10 ⁷

Table F2

MASS PROPERTIES OF CORE AND APPENDED MODULES

MODULE	NODE	MASS (kg)	MOMENT OF INERTIA (kg.m ²)		
			I _x	I _y	I _z
Core Module	1 - 4	2833	4942	4561	4503
	5	1530	921	1442	1427
	6	3059	1843	8919	8831
	7	2889	921	1442	1427
Appended Module	1 - 4	2833	5643	5498	5439

NOTES:

1. ALL DIMENSIONS ARE IN METERS.
2. $z = 0$ AT ALL POINTS.
3. FOR MODULES 4 AND 5 (THE SOLAR PANELS), THE LOCAL y AXIS IS DIRECTED ALONG THE $+X_3$ LABORATORY AXIS.

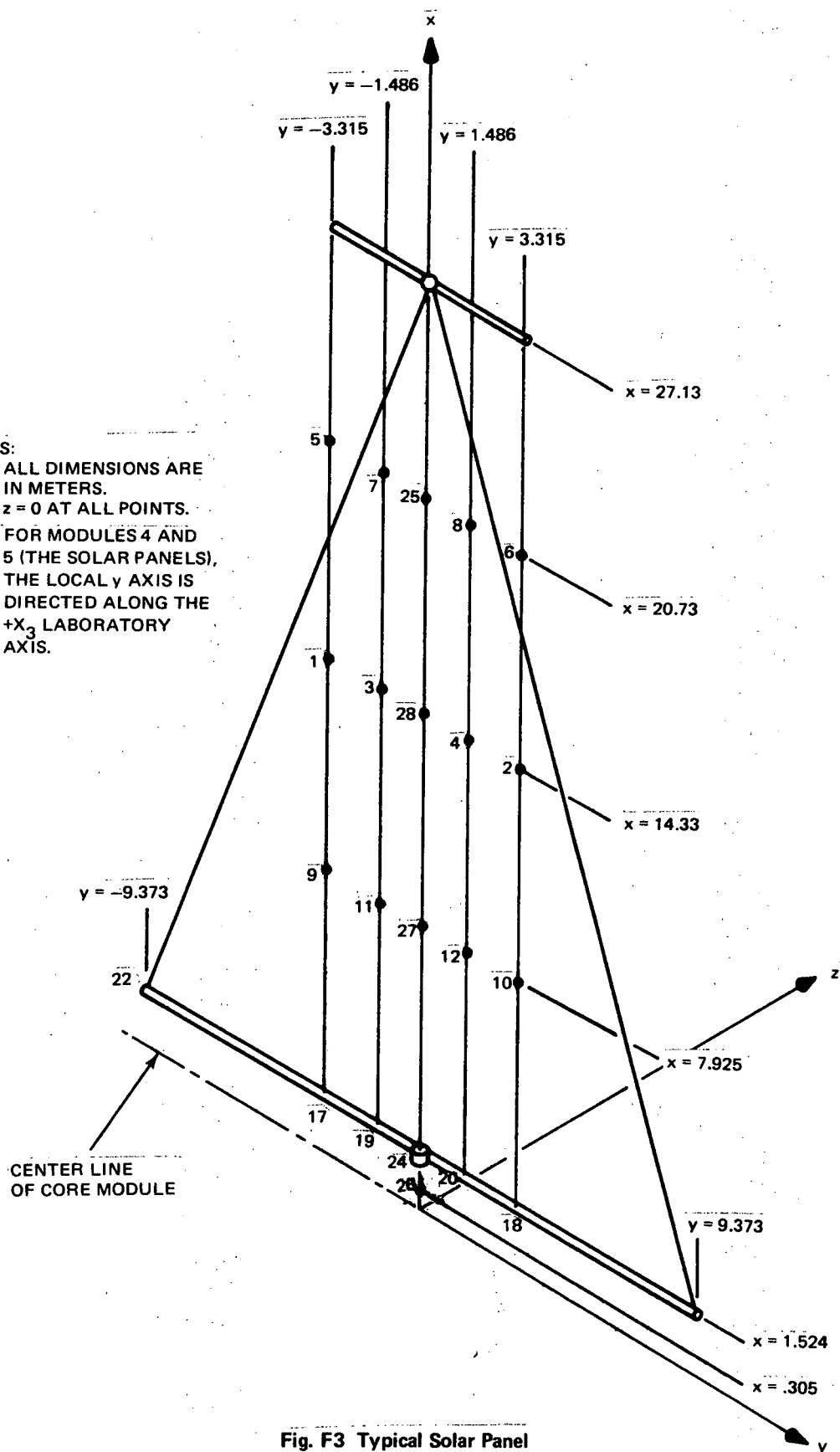


Fig. F3 Typical Solar Panel

Table F3MASS PROPERTIES OF SOLAR PANEL

Node	Mass (kg)
1-12	21.93
13-14	24.41
15-16	15.71
17-18	150.8
19-20	14.40
21	14.83
22-23	137.9
24	17.44
25	24.22
26	0
27-28	24.22

TABLE F4 - SOLAR PANEL MODES

MODE 1

Frequency = .19889690 Hz

NODE	X	Y	Z	θ_X	θ_Y	θ_Z
1	0.0	0.0	-0.69848102E 00	0.0	0.0	0.0
2	0.0	0.0	0.65839708E 00	0.0	0.0	0.0
3	0.0	0.0	-0.32379495E 00	0.0	0.0	0.0
4	0.0	0.0	0.28456396E 00	0.0	0.0	0.0
5	0.0	0.0	-0.91623098E 00	0.0	0.0	0.0
6	0.0	0.0	0.86455804E 00	0.0	0.0	0.0
7	0.0	0.0	-0.42476696E 00	0.0	0.0	0.0
8	0.0	0.0	0.37355596E 00	0.0	0.0	0.0
9	0.0	0.0	-0.37859094E 00	0.0	0.0	0.0
10	0.0	0.0	0.35595900E 00	0.0	0.0	0.0
11	0.0	0.0	-0.17547399E 00	0.0	0.0	0.0
12	0.0	0.0	0.15395893E 00	0.0	0.0	0.0
13	0.0	0.0	-0.10000000E 01	0.0	0.0	0.0
14	0.0	0.0	0.94429296E 00	0.74497499E-02	0.0	0.0
15	0.0	0.0	-0.46362495E 00	0.74496791E-02	0.0	0.0
16	0.0	0.0	0.40792203E 00	0.74494481E-02	0.0	0.0
17	0.0	0.0	-0.33388201E-02	0.74494071E-02	0.0	0.0
18	0.0	0.0	0.14678799E-02	0.26228590E-04	0.0	0.0
19	0.0	0.0	-0.14929299E-02	0.40531695E-05	0.0	0.0
20	0.0	0.0	0.84160687E-03	0.24564390E-04	0.0	0.0
21	0.0	0.0	-0.27850699E-01	0.13366001E-04	0.0	0.0
22	0.0	0.0	-0.96520670E-02	0.74487478E-02	0.37561389E-04	0.0
23	0.0	0.0	0.0	0.26591690E-04	0.0	0.0
24	0.0	0.0	-0.15676301E-03	-0.11258499E-04	0.0	0.0
25	0.0	0.0	-0.19535299E-01	0.20655600E-04	0.57191792E-05	0.0
26	0.0	0.0	0.0	0.55917278E-02	0.35893798E-04	0.0
27	0.0	0.0	-0.35622802E-02	0.0	0.0	0.0
28	0.0	0.0	-0.10078598E-01	0.18776800E-02	0.20490086E-04	0.0
				0.37347001E-02	0.30436888E-04	0.0

F-7

TABLE F4 - SOLAR PANEL MODES (Continued)

MODE 2

Frequency = .2031515 Hz

NODE	X	Y	Z	θ_X	θ_Y	θ_Z
1	0.0	0.0	-0.53773501E 00	0.0	0.0	0.0
2	0.0	0.0	-0.70919198E 00	0.0	0.0	0.0
3	0.0	0.0	-0.65713996E 00	0.0	0.0	0.0
4	0.0	0.0	-0.68917900E 00	0.0	0.0	0.0
5	0.0	0.0	-0.82998109E 00	0.0	0.0	0.0
6	0.0	0.0	-0.92518598E 00	0.0	0.0	0.0
7	0.0	0.0	-0.85603601E 00	0.0	0.0	0.0
8	0.0	0.0	-0.89871699E 00	0.0	0.0	0.0
9	0.0	0.0	-0.34817398E 00	0.0	0.0	0.0
10	0.0	0.0	-0.33497800E 00	0.0	0.0	0.0
11	0.0	0.0	-0.35796595E 00	0.0	0.0	0.0
12	0.0	0.0	-0.37447399E 00	0.0	0.0	0.0
13	0.0	0.0	-0.89557302E 00	-0.39892504E-03	0.0	0.0
14	0.0	0.0	-0.10000000E 01	-0.40131388E-03	0.0	0.0
15	0.0	0.0	-0.92430395E 00	-0.39924798E-03	0.0	0.0
16	0.0	0.0	-0.97111404E 00	-0.40095882E-03	0.0	0.0
17	0.0	0.0	-0.54819696E-02	0.18813094E-04	0.0	0.0
18	0.0	0.0	-0.20166200E-02	0.81430398E-05	0.0	0.0
19	0.0	0.0	-0.41680299E-02	0.17240091E-04	0.0	0.0
20	0.0	0.0	-0.26261702E-02	0.92534292E-05	0.0	0.0
21	0.0	0.0	-0.94759107E 00	-0.40006591E-03	0.13119099E-02	0.0
22	0.0	0.0	-0.10031499E-01	0.1920698E-04	0.0	0.0
23	0.0	0.0	C.C	0.86116097E-05	0.0	0.0
24	0.0	0.0	-0.32627999E-02	0.13123500E-04	0.13218999E-03	0.0
25	0.0	0.0	-0.62232906E 00	-0.29676897E-03	0.12494100E-02	0.0
26	0.0	0.0	0.0	0.0	0.0	0.0
27	0.0	0.0	-0.10902697E 00	-0.90173807E-04	0.67733089E-03	0.0
28	0.0	0.0	-0.32991394E 00	-0.19347099E-03	0.10459998E-02	0.0

F-8

TABLE F4 - SOLAR PANEL MODES (Continued)

MODE 3

Frequency = .3784189 Hz

MODE	X	Y	Z	θ_X	θ_Y	θ_Z
1	-0.56071207E-02	-0.1000000E 01	0.0	0.0	0.0	0.0
2	0.56034774E-02	-0.99854702E 00	0.0	0.0	0.0	0.0
3	-0.27825602E-02	-0.99973005E 00	0.0	0.0	0.0	0.0
4	0.27787101E-02	-0.99907905E 00	0.0	0.0	0.0	0.0
5	-0.70650764E-02	-0.79015410E 00	0.0	0.0	0.0	0.0
6	0.70602074E-02	-0.78916603E 00	0.0	0.0	0.0	0.0
7	-0.34305600E-02	-0.78996295E 00	0.0	0.0	0.0	0.0
8	0.34251201E-02	-0.78952104E 00	0.0	0.0	0.0	0.0
9	-0.41370876E-02	-0.68041295E 00	0.0	0.0	0.0	0.0
10	0.41346774E-02	-0.67926496E 00	0.0	0.0	0.0	0.0
11	-0.21285799E-02	-0.68020695E 00	0.0	0.0	0.0	0.0
12	0.21263098E-02	-0.67969203E 00	0.0	0.0	0.0	0.0
13	-0.85078180E-02	-0.16197497E 00	0.0	0.0	0.0	0.0
14	0.85017383E-02	-0.16197497E 00	0.0	0.0	0.0	0.0
15	-0.40711686E-02	-0.16196400E 00	0.0	0.0	0.0	0.0
16	0.40641464E-02	-0.16196400E 00	0.0	0.0	0.0	0.0
17	-0.26581499E-02	-0.59382408E-03	0.0	0.0	0.0	0.0
18	0.26569802E-02	-0.35763183E-03	0.0	0.0	0.0	0.0
19	-0.14700098E-02	-0.56039100E-03	0.0	0.0	0.0	0.0
20	0.14693399E-02	-0.45450693E-03	0.0	0.0	0.0	0.0
21	-0.36721294E-05	-0.16195399E 00	0.0	0.0	0.0	0.0
22	0.0	-0.66774595E-03	0.0	0.0	0.0	0.0
23	0.0	0.0	0.0	0.0	0.0	0.0
24	-0.17397497E-06	-0.52422378E-03	0.0	0.0	0.0	0.0
25	-0.27977049E-05	-0.12881595E 00	0.0	0.0	0.0	0.0
26	0.0	0.0	0.0	0.0	0.0	0.0
27	-0.10486001E-05	-0.27020600E-01	0.0	0.0	0.0	0.0
28	-0.19231893E-05	-0.77389598E-01	0.0	0.0	0.0	0.0

F.9

TABLE F4 - SOLAR PANEL MODES (Continued)

MODE 9

Frequency = .5036502 Hz

NODE	X	Y	Z	θ_x	θ_y	θ_z
1	0.0	0.0	0.1000000E 01	0.0	0.0	0.0
2	0.0	0.0	0.99332601E 00	0.0	0.0	0.0
3	0.0	0.0	0.99946004E 00	0.0	0.0	0.0
4	0.0	0.0	0.99647003E 00	0.0	0.0	0.0
5	0.0	0.0	0.12124294E 00	0.0	0.0	0.0
6	0.0	0.0	0.12231297E 00	0.0	0.0	0.0
7	0.0	0.0	0.12256995E 00	0.0	0.0	0.0
8	0.0	0.0	0.12289697E 00	0.0	0.0	0.0
9	0.0	0.0	0.94086701E 00	0.0	0.0	0.0
10	0.0	0.0	0.93300903E 00	0.0	0.0	0.0
11	0.0	0.0	0.93898600E 00	0.0	0.0	0.0
12	0.0	0.0	0.93546396E 00	0.0	0.0	0.0
13	0.0	0.0	-0.87122601E 00	0.26680995E-04	0.0	0.0
14	0.0	0.0	-0.86373508E 00	0.30731098E-04	0.0	0.0
15	0.0	0.0	-0.86929804E 00	0.26990092E-04	0.0	0.0
16	0.0	0.0	-0.86594003E 00	0.30417898E-04	0.0	0.0
17	0.0	0.0	-0.69493498E-03	-0.21783591E-04	0.0	0.0
18	0.0	0.0	-0.23677398E-02	0.90326494E-05	0.0	0.0
19	0.0	0.0	-0.21524702E-02	-0.17504397E-04	0.0	0.0
20	0.0	0.0	-0.29036298E-02	0.46685309E-05	0.0	0.0
21	0.0	0.0	-0.56759097E 00	0.28700189E-04	0.10582898E-02	0.0
22	0.0	0.0	0.46799965E-02	-0.22912791E-04	0.0	0.0
23	0.0	0.0	0.0	0.10375100E-04	0.0	0.0
24	0.0	0.0	-0.28979598E-02	-0.64161695E-05	0.12581500E-03	0.0
25	0.0	0.0	-0.60022706E 00	0.19921092E-04	0.10673902E-02	0.0
26	0.0	0.0	0.0	0.0	0.0	0.0
27	0.0	0.0	-0.11479394E 00	0.23629300E-05	0.71014580E-03	0.0
28	0.0	0.0	-0.33610797E 00	0.11142000E-04	0.10003899E-02	0.0

TABLE F4 - SOLAR PANEL MODES (Continued)

MODE 10

Frequency = .5214531 Hz

NODE	X	Y	Z	θ_X	θ_Y	θ_Z
1	0.0	0.0	0.97737604E 00	0.0	0.0	0.0
2	0.0	0.0	-0.98543304E 00	0.0	0.0	0.0
3	0.0	0.0	0.43754697E 00	0.0	0.0	0.0
4	0.0	0.0	-0.44198799E 00	0.0	0.0	0.0
5	0.0	0.0	-0.13650999E-01	0.0	0.0	0.43999968E-03
6	0.0	0.0	0.14645499E-01	0.0	0.0	0.0
7	0.0	0.0	-0.85177384E-02	0.0	0.0	0.0
8	0.0	0.0	0.71534067E-02	0.0	0.0	0.0
9	0.0	0.0	0.99175602E 00	0.0	0.0	0.0
10	0.0	0.0	-0.99476409E 00	0.0	0.0	0.0
11	0.0	0.0	0.44370496E 00	0.0	0.0	0.0
12	0.0	0.0	-0.44675797E 00	0.0	0.0	0.0
13	0.0	0.0	-0.99692100E 00	0.76515786E-02	0.0	0.0
14	0.0	0.0	0.10000000E 01	0.76515190E-02	0.0	0.0
15	0.0	0.0	-0.44601899E 00	0.76510571E-02	0.0	0.0
16	0.0	0.0	0.44910300E 00	0.76510198E-02	0.0	0.0
17	0.0	0.0	0.90312101E-02	-0.76893499E-04	0.0	0.0
18	0.0	0.0	-0.39660893E-02	-0.10197699E-04	0.0	0.0
19	0.0	0.0	0.37650501E-02	-0.67865491E-04	0.0	0.0
20	0.0	0.0	-0.23603102E-02	-0.34364086E-04	0.0	0.0
21	0.0	0.0	0.15424399E-02	0.76501667E-02	0.18256997E-05	0.0
22	0.0	0.0	0.29544190E-01	-0.84276486E-04	0.0	0.0
23	0.0	0.0	0.0	0.30042793E-04	0.0	0.0
24	0.0	0.0	0.19816101E-03	-0.52710486E-04	-0.60762595E-05	0.0
25	0.0	0.0	0.19373999E-02	0.57244487E-02	0.10504791E-05	0.0
26	0.0	0.0	0.0	0.0	0.0	0.0
27	0.0	0.0	0.14116298E-02	0.18730098E-02	-0.35142393E-05	0.0
28	0.0	0.0	0.19690499E-02	0.37987300E-02	-0.94884302E-06	0.0

TABLE P4 - SOLAR PANEL MODES (Continued)

MODE 11

Frequency = 7044816 Hz

NODE	X	Y	Z	θ_X	θ_Y	θ_Z
1	0.93393996E-02	-0.16557699E 00	0.0	0.0	0.0	0.0
2	-0.93342066E-02	-0.16541100E 00	0.0	0.0	0.0	0.0
3	0.46294965E-02	-0.16555297E 00	0.0	0.0	0.0	0.0
4	-0.46240576E-02	-0.16547894E 00	0.0	0.0	0.0	0.0
5	0.11575099E-01	0.97170806E 00	0.0	0.0	0.0	0.0
6	-0.11568200E-01	0.97271305E 00	0.0	0.0	0.0	0.0
7	0.55956692E-02	0.97174102E 00	0.0	0.0	0.0	0.0
8	-0.55880398E-02	0.97219104E 00	0.0	0.0	0.0	0.0
9	0.70340373E-02	-0.99902195E 00	0.0	0.0	0.0	0.0
10	-0.70305876E-02	-0.10000000E 01	0.0	0.0	0.0	0.0
11	0.36287799E-02	-0.99905103E 00	0.0	0.0	0.0	0.0
12	-0.36255799E-02	-0.99848907E 00	0.0	0.0	0.0	0.0
13	0.13724398E-01	0.32587296E 00	0.0	0.0	0.0	0.97355893E-04
14	-0.13715800E-01	0.32587296E 00	0.0	0.0	0.0	0.97375014E-04
15	0.65200664E-02	0.32585496E 00	0.0	0.0	0.0	0.10546700E-03
16	-0.65103099E-02	0.32585496E 00	0.0	0.0	0.0	0.10547899E-03
17	0.46761669E-02	0.77517494E-03	0.0	0.0	0.0	0.15349302E-04
18	-0.46744869E-02	0.44814085E-03	0.0	0.0	0.0	0.15342899E-04
19	0.26009802E-02	0.74625690E-03	0.0	0.0	0.0	0.39938895E-04
20	-0.26000298E-02	0.5965579E-03	0.0	0.0	0.0	0.39926890E-04
21	0.50977096E-05	0.32583696E 00	0.0	0.0	0.0	0.11892099E-03
22	0.0	0.62442287E-03	0.0	0.0	0.0	-0.37084596E-04
23	0.0	0.0	0.0	0.0	0.0	-0.37070786E-04
24	0.24192298E-06	0.73599094E-03	0.0	0.0	0.0	0.46375499E-04
25	0.38843300E-05	0.27135897E 00	0.0	0.0	0.0	0.31668996E-03
26	0.0	0.0	0.0	0.0	0.0	0.0
27	0.14562893E-05	0.61097402E-01	0.0	0.0	0.0	0.38427883E-03
28	0.26704793E-05	0.17159396E 00	0.0	0.0	0.0	0.45053684E-03

TABLE F4 - SOLAR PANEL MODES (Continued)

MODE 17

Frequency = .7781657 Hz

NODE	X	Y	Z	θ_X	θ_Y	θ_Z
1	0.0	0.0	-0.26005596E 00	0.0	0.0	0.0
2	0.0	0.0	-0.21145999E 00	0.0	0.0	0.0
3	0.0	0.0	-0.24466002E 00	0.0	0.0	0.0
4	0.0	0.0	-0.22285098E 00	0.0	0.0	0.0
5	0.0	0.0	-0.93785304E 00	0.0	0.0	0.0
6	0.0	0.0	-0.84633499E 00	0.0	0.0	0.0
7	0.0	0.0	-0.92213696E 00	0.0	0.0	0.0
8	0.0	0.0	-0.88122201E 00	0.0	0.0	0.0
9	0.0	0.0	0.10000000E 01	0.0	0.0	0.0
10	0.0	0.0	0.89686900E 00	0.0	0.0	0.0
11	0.0	0.0	0.98060495E 00	0.0	0.0	0.0
12	0.0	0.0	0.93447795E 00	0.0	0.0	0.0
13	0.0	0.0	0.48417997E 00	-0.26573800E-03	0.0	0.0
14	0.0	0.0	0.41371298E 00	-0.27428288E-03	0.0	0.0
15	0.0	0.0	0.46502799E 00	-0.26653986E-03	0.0	0.0
16	0.0	0.0	0.43344098E 00	-0.27342886E-03	0.0	0.0
17	0.0	0.0	0.21081198E-01	-0.16375900E-03	0.0	0.0
18	0.0	0.0	-0.28692002E-02	-0.17565297E-04	0.0	0.0
19	0.0	0.0	0.10319397E-01	-0.13240000E-03	0.0	0.0
20	0.0	0.0	-0.46589482E-03	-0.51605195E-04	0.0	0.0
21	0.0	0.0	0.44935602E 00	-0.26995386E-03	-0.34460099E-03	0.0
22	0.0	0.0	0.66200674E-01	-0.20189099E-03	0.0	0.0
23	0.0	0.0	0.0	0.26827896E-04	0.0	0.0
24	0.0	0.0	0.36719602E-02	-0.92219096E-04	-0.13977401E-03	0.0
25	0.0	0.0	0.35530901E 00	-0.22552001E-03	-0.43040095E-03	0.0
26	0.0	0.0	0.0	0.0	0.0	0.0
27	0.0	0.0	0.91031611E-01	-0.13665301E-03	-0.49768598E-03	0.0
28	0.0	0.0	0.22921497E 00	-0.18108600E-03	-0.55451784E-03	0.0

TABLE F4 - SOLAR PANEL MODES (Continued)

MODE 18

Frequency = .7941298 Hz

MODE	X	Y	Z	θ_X	θ_Y	θ_Z
1	0.0	0.0	-0.32917798E 00	0.0	0.0	0.0
2	0.0	0.0	0.34152997E 00	0.0	0.0	0.0
3	0.0	0.0	-0.14123499E 00	0.0	0.0	0.0
4	0.0	0.0	0.15962398E 00	0.0	0.0	0.0
5	0.0	0.0	-0.80677997E 00	0.0	0.0	0.0
6	0.0	0.0	0.88668603E 00	0.0	0.0	0.0
7	0.0	0.0	-0.34931697E 00	0.0	0.0	0.0
8	0.0	0.0	0.41009098E 00	0.0	0.0	0.0
9	0.0	0.0	0.91599494E 00	0.0	0.0	0.0
10	0.0	0.0	-0.10000000E 01	0.0	0.0	0.0
11	0.0	0.0	0.39517695E 00	0.0	0.0	0.0
12	0.0	0.0	-0.46305197E 00	0.0	0.0	0.0
13	0.0	0.0	0.59685403E 00	-0.47231391E-02	0.0	0.0
14	0.0	0.0	-0.63571805E 00	-0.47228299E-02	0.0	0.0
15	0.0	0.0	0.25680095E 00	-0.47225878E-02	0.0	0.0
16	0.0	0.0	-0.29568499E 00	-0.47223493E-02	0.0	0.0
17	0.0	0.0	0.25265197E-01	-0.22957700E-03	0.0	0.0
18	0.0	0.0	-0.97465478E-02	-0.22169799E-04	0.0	0.0
19	0.0	0.0	0.10122098E-01	-0.18787001E-03	0.0	0.0
20	0.0	0.0	-0.59009187E-02	-0.83600593E-04	0.0	0.0
21	0.0	0.0	-0.19446298E-01	-0.47217868E-02	0.29655287E-04	0.0
22	0.0	0.0	0.89457465E-01	-0.28264080E-03	0.0	0.0
23	0.0	0.0	0.0	0.72383991E-04	0.0	0.0
24	0.0	0.0	0.49635093E-03	-0.13875899E-03	-0.13978200E-04	0.0
25	0.0	0.0	-0.11942100E-01	-0.35760298E-02	0.30005496E-04	0.0
26	0.0	0.0	0.0	0.0	0.0	0.0
27	0.0	0.0	0.46418980E-03	-0.12845199E-02	0.12245599E-04	0.0
28	0.0	0.0	-0.45582493E-02	-0.24302702E-02	0.26360693E-04	0.0

TABLE F4 - SOLAR PANEL MODES (Continued)

MODE 19

Frequency = .9051450 Hz

MODE	X	Y	Z	θ_X	θ_Y	θ_Z
1	0.0	0.0	0.1423609E 00	0.0	0.0	0.0
2	0.0	0.0	-0.45958001E-01	0.0	0.0	0.0
3	0.0	0.0	0.22363996E-01	0.0	0.0	0.0
4	0.0	0.0	-0.62861691E-01	0.0	0.0	0.0
5	0.0	0.0	-0.27063400E 00	0.0	0.0	0.0
6	0.0	0.0	0.91394792E-01	0.0	0.0	0.0
7	0.0	0.0	-0.10453397E 00	0.0	0.0	0.0
8	0.0	0.0	0.59428798E-01	0.0	0.0	0.0
9	0.0	0.0	0.12410396E 00	0.0	0.0	0.0
10	0.0	0.0	-0.44090699E-01	0.0	0.0	0.0
11	0.0	0.0	0.81617475E-01	0.0	0.0	0.0
12	0.0	0.0	0.62740184E-02	0.0	0.0	0.0
13	0.0	0.0	0.13619995E 00	-0.70657698E-03	0.0	0.0
14	0.0	0.0	-0.48113700E-01	-0.70607290E-03	0.0	0.0
15	0.0	0.0	0.85331261E-01	-0.70638093E-03	0.0	0.0
16	0.0	0.0	0.27214701E-02	-0.70598791E-03	0.0	0.0
17	0.0	0.0	-0.27010000E 00	0.25408298E-02	0.0	0.0
18	0.0	0.0	0.91340065E-01	0.19790900E-03	0.0	0.0
19	0.0	0.0	-0.10627194E 00	0.19797601E-02	0.0	0.0
20	0.0	0.0	0.56403901E-01	0.79681491E-03	0.0	0.0
21	0.0	0.0	0.44019599E-01	-0.70594577E-03	-0.21800799E-03	0.0
22	0.0	0.0	-0.10000000E 01	0.33201498E-02	0.0	0.0
23	0.0	0.0	0.0	-0.67342096E-03	0.0	0.0
24	0.0	0.0	-0.71082438E-02	0.13905098E-02	0.21569700E-03	0.0
25	0.0	0.0	-0.78891292E-02	-0.18183100E-03	-0.18194599E-03	0.0
26	0.0	0.0	0.0	0.0	0.0	0.0
27	0.0	0.0	-0.41495101E-01	0.86639798E-03	0.59238988E-04	0.0
28	0.0	0.0	-0.41953002E-01	0.34228293E-03	-0.77763689E-04	0.0

TABLE F4 - SOLAR PANEL MODES (Continued)

MODE 20

Frequency = .9348565 Hz

MODE	X	Y	Z	θ_X	θ_Y	θ_Z
1	0.11285998E-01	-0.1000000E 01	0.0	0.0	0.0	0.0
2	-0.11274297E-01	-0.99852794E 00	0.0	0.0	0.0	0.0
3	0.57366379E-02	-0.99978304E 00	0.0	0.0	0.0	0.0
4	-0.57245865E-02	-0.999912304E 00	0.0	0.0	0.0	0.0
5	0.12971897E-01	0.42082494E 00	0.0	0.0	0.0	0.0
6	-0.12956495E-01	0.41962898E 00	0.0	0.0	0.0	0.0
7	0.62750392E-02	0.42066795E 00	0.0	0.0	0.0	0.0
8	-0.62582195E-02	0.42013198E 00	0.0	0.0	0.0	0.0
9	0.94517097E-02	0.81060803E 00	0.0	0.0	0.0	0.0
10	-0.94439164E-02	0.80999094E 00	0.0	0.0	0.0	0.0
11	0.51228479E-02	0.81049812E 00	0.0	0.0	0.0	0.0
12	-0.51157176E-02	0.81022102E 00	0.0	0.0	0.0	0.0
13	0.14487296E-01	0.48178196E 00	0.0	0.0	0.0	0.10599599E-03
14	-0.14468499E-01	0.48178196E 00	0.0	0.0	0.0	0.10603499E-03
15	0.67309774E-02	0.48175800E 00	0.0	0.0	0.0	0.11118999E-03
16	-0.67096092E-02	0.48175800E 00	0.0	0.0	0.0	0.11121700E-03
17	0.74932453E-02	0.17902199E-02	0.0	0.0	0.0	0.20508494E-04
18	-0.74894279E-02	0.10783698E-02	0.0	0.0	0.0	0.20493491E-04
19	0.44417270E-02	0.17094498E-02	0.0	0.0	0.0	0.62615698E-04
20	-0.44396184E-02	0.13903398E-02	0.0	0.0	0.0	0.62588195E-04
21	0.11128400E-04	0.48173797E 00	0.0	0.0	0.0	0.11950699E-03
22	0.0	0.20119401E-02	0.0	0.0	0.0	-0.57381592E-04
23	0.0	0.0	0.0	0.0	0.0	-0.57350102E-04
24	0.52912003E-06	0.16330699E-02	0.0	0.0	0.0	0.87415494E-04
25	0.84807807E-05	0.42534095E 00	0.0	0.0	0.0	0.37530879E-03
26	0.0	0.0	0.0	0.0	0.0	0.0
27	0.31805594E-05	0.10851896E 00	0.0	0.0	0.0	0.65976777E-03
28	0.58313090E-05	0.28812695E 00	0.0	0.0	0.0	0.68415189E-03

F-16

TABLE P4 - SOLAR PANEL MODES (Continued)

MODE 28

Frequency = 1.065360 Hz

MODE	X	Y	Z	θ_x	θ_y	θ_z
1	-0.1695279E-01	-0.3552339E 00	0.0	0.0	0.0	0.0
2	0.1692889E-01	-0.3547290E 00	0.0	0.0	0.0	0.0
3	-0.8890219E-02	-0.3551695E 00	0.0	0.0	0.0	0.0
4	0.8865729E-02	-0.3549429E 00	0.0	0.0	0.0	0.0
5	-0.1774148E-01	0.6169601E 00	0.0	0.0	0.0	0.0
6	0.1771019E-01	0.6167359E 00	0.0	0.0	0.0	0.0
7	-0.8617509E-02	0.6169169E 00	0.0	0.0	0.0	0.0
8	0.8583453E-02	0.6168139E 00	0.0	0.0	0.0	0.0
9	-0.1587459E-01	0.1633459E 00	0.0	0.0	0.0	0.0
10	0.1585859E-01	0.1624659E 00	0.0	0.0	0.0	0.0
11	-0.9011209E-02	0.1632539E 00	0.0	0.0	0.0	0.0
12	0.8996680E-02	0.1628589E 00	0.0	0.0	0.0	0.0
13	-0.1822749E-01	-0.1000000E 01	0.0	0.0	0.0	0.0
14	0.1818930E-01	-0.1000000E 01	0.0	0.0	0.0	0.0
15	-0.8197709E-02	-0.9999559E 00	0.0	0.0	0.0	0.0
16	0.8154697E-02	-0.9999559E 00	0.0	0.0	0.0	0.0
17	-0.1452569E-01	-0.3573079E-02	0.0	0.0	0.0	0.0
18	0.1451769E-01	-0.2145489E-02	0.0	0.0	0.0	0.0
19	-0.8978407E-02	-0.3434819E-02	0.0	0.0	0.0	0.0
20	0.8974086E-02	-0.2794860E-02	0.0	0.0	0.0	0.0
21	-0.2236339E-04	-0.9999230E 00	0.0	0.0	0.0	0.0
22	0.0	-0.4034526E-02	0.0	0.0	0.0	0.0
23	0.0	0.0	0.0	0.0	0.0	0.0
24	-0.1064750E-05	-0.3324560E-02	0.0	0.0	0.0	0.0
25	-0.1704449E-04	-0.9239999E 00	0.0	0.0	0.0	0.0
26	0.0	0.0	0.0	0.0	0.0	0.0
27	-0.6393649E-05	-0.2523539E 00	0.0	0.0	0.0	0.0
28	-0.1172069E-04	-0.6543730E 00	0.0	0.0	0.0	0.0

F-17

TABLE P4 - SOLAR PANEL MODES (Continued)

MODE 32

Frequency = 3.842224 Hz

MODE	X	Y	Z	θ_x	θ_y	θ_z
1	-0.99932498E-07	-0.91379263E-07	0.0	0.0	0.0	0.0
2	-0.10000000E-01	-0.58137598E-07	0.0	0.0	0.0	0.0
3	-0.35324299E-07	-0.78970004E-07	0.0	0.0	0.0	0.0
4	-0.35345399E-07	-0.64064693E-07	0.0	0.0	0.0	0.0
5	-0.83663899E-07	0.19979097E-05	0.0	0.0	0.0	0.0
6	-0.83747405E-07	0.19972795E-05	0.0	0.0	0.0	0.0
7	-0.30126095E-07	0.19959598E-05	0.0	0.0	0.0	0.0
8	-0.30156195E-07	0.19956797E-05	0.0	0.0	0.0	0.0
9	-0.94017202E-07	0.28072300E-05	0.0	0.0	0.0	0.0
10	-0.94053805E-07	0.10598596E-05	0.0	0.0	0.0	0.0
11	-0.32680899E-07	0.21566393E-05	0.0	0.0	0.0	0.0
12	-0.32688397E-07	0.13731396E-05	0.0	0.0	0.0	0.0
13	-0.48822898E-07	-0.10496800E-03	0.0	0.0	0.0	-0.48706681E-02
14	-0.48903799E-07	-0.10496800E-03	0.0	0.0	0.0	0.48777089E-02
15	-0.18240196E-07	-0.10487800E-03	0.0	0.0	0.0	-0.30014298E-02
16	-0.18272597E-07	-0.10487800E-03	0.0	0.0	0.0	0.30075798E-02
17	-0.67231196E-07	-0.14752599E-03	0.0	0.0	0.0	-0.44951588E-02
18	-0.67228705E-07	-0.155674289E-04	0.0	0.0	0.0	0.44960380E-02
19	-0.22782655E-07	-0.11332700E-03	0.0	0.0	0.0	-0.62178671E-02
20	-0.22774899E-07	-0.72141993E-04	0.0	0.0	0.0	0.62179491E-02
21	-0.84481299E-01	-0.10480099E-03	0.0	0.0	0.0	0.23861794E-05
22	0.0	-0.25782688E-03	0.0	0.0	0.0	0.64759590E-02
23	0.0	0.0	0.0	0.0	0.0	-0.64762394E-02
24	-0.10479999E-01	-0.85488704E-04	0.0	0.0	0.0	-0.16038894E-05
25	-0.66278875E-01	0.10579199E-03	0.0	0.0	0.0	-0.26707194E-05
26	0.0	0.0	0.0	0.0	0.0	0.0
27	-0.29209998E-01	0.23712900E-03	0.0	0.0	0.0	0.26048992E-05
28	-0.47832504E-01	0.62357495E-03	0.0	0.0	0.0	-0.3745795E-06

F-18

The Counterweight shown in Figure 6.1 was assumed to be rigid. It's properties are given below in the notation of Section 4.0.

Vector to cm:

$$\{\bar{r}_1\} = [0 \ 0 \ 8.128]^T \text{ m}$$

mass:

$$\bar{m}_1 = 33,992.013 \text{ kg}$$

moment of inertia matrix:

$$[\bar{I}_1] = \begin{bmatrix} 1.950100 & & \\ & .2649178 & \\ & & 1.750095 \end{bmatrix} \times 10^6 \text{ kg.m}^2$$

F.2 CONNECTING STRUCTURE

The Connecting Structure used for demonstrating the program was the telescopic beam described in Section 4.4.2.1. Its physical properties are listed below. The notation of Appendix G is used

$$M_L = 43,598.5 \text{ kg}$$

$$M_C = 33,991.9 \text{ kg}$$

$$I_L = 4.36150 \times 10^6 \text{ kg.m}^2$$

$$I_C = 1.94967 \times 10^6 \text{ kg.m}^2$$

$$J_L = 2.06698 \times 10^6 \text{ kg.m}^2$$

$$J_C = 1.74963 \times 10^6 \text{ kg.m}^2$$

$$a = 15.8562 \text{ m}$$

$$b = 8.12800 \text{ m}$$

$$l_{\text{Omin}} = 7.62000 \text{ m}$$

$$AE = 133.447 \times 10^6 \text{ N}$$

$$EI = 389.434 \times 10^6 \text{ N}$$

$$JG = 311.662 \times 10^6 \text{ N.m}^2$$

$$\gamma_A = .05$$

$$\gamma_B = .05$$

$$\gamma_T = .05$$

Except for the value of AE, the above data was based on a uniform aluminum beam with a diameter of .6096 m and a wall thickness of approximately .0635 m. AE was reduced to lower the axial extension frequency in order to reduce the computer time required for the numerical demonstrations. Because of the end connections and joints between the telescopic sections, the equivalent AE of a realistic structure would actually be lower than that computed for a uniform beam; thus the artificial lowering of this quantity might be realistic.

APPENDIX G

CONNECTING-STRUCTURE SUBROUTINE COMPUTATIONPROCEDURE AND SUMMARY OF EQUATIONS

As discussed in Section 4.4.2, the theory for two types of connecting structures has been developed, the circular beam and the cable truss. The computation procedure and a summary of the equations used is presented in this appendix.

G1. Circular Beam

The main program must supply six vectors to the Connecting-Structure subroutine, viz. $\{P_z\}$, $\{\ell_o\}$, $\{\delta\}$, $\{\phi^*\}$, $\{\dot{\delta}\}$, and $\{\dot{\phi}^*\}$ (See Nomenclature of Section 4.) The required input data are as follows:

M_L	mass of entire Laboratory
M_C	mass of entire Counterweight
I_L	transverse moment of inertia (average of yaw and pitch) of the Laboratory
I_C	transverse moment of inertia (average of yaw and pitch) of the Counterweight
J_L	axial moment of inertia (roll) of the Laboratory
J_C	axial moment of inertia (roll) of the Counterweight
a	distance from Laboratory mass center to beam attachment point
b	distance from Counterweight mass center to beam attachment point
$\ell_o \min$	minimum value of ℓ_o on which stiffness coefficients are based
AE, EI, JG	axial, bending and torsional stiffness, respectively, of the beam
$\gamma_A, \gamma_B, \gamma_T$	ratios of damping coefficients to critical damping for axial, bending, and torsional beam modes, respectively

The computation procedure is outlined below. Step 1 should be done once; if there is no deployment in the run, Steps 2 through 23 should be done once.

Step No.	Operation	Required Equations
1	Compute \bar{M}, \bar{J}	Eqns 1
2	Compute ℓ_o and \bar{I}_o	Eq. 2
3	Compute K_1, K_2, K_3, K_A, K_T	Eqns. 3
4	(Step deleted)	
5	Compute \bar{I}	Eq. 5
6	Compute M_1, M_2, M_3	Eqns. 6
7	(Step deleted)	
8	Compute A, B, C	Eqns. 8
9	Compute ω_1^2, ω_2^2	Eqns. 9
10	If $(K_1 - \omega_1^2 M_1) = 0$, set $\bar{\delta}_1=1, \bar{\phi}_1=0$ and go to step 14	
11	If $(K_2 - \omega_1^2 M_2) = 0$, set $\bar{\delta}_1=0, \bar{\phi}_1=1$ and go to step 14	
12	Compute R_1	Eq. 10
13	Compute $\bar{\delta}_1, \bar{\phi}_1$	Eqns. 11
14	If $(K_1 - \omega_2^2 M_1) = 0$, set $\bar{\delta}_2=1, \bar{\phi}_2=0$ and go to step 18	
15	If $(K_2 - \omega_2^2 M_2) = 0$, set $\bar{\delta}_2=0, \bar{\phi}_2=1$ and go to step 18	
16	Compute R_2	Eq. 12
17	Compute $\bar{\delta}_2, \bar{\phi}_2$	Eqns. 13
18	Compute $[M_G]$	Eq. 14
19	Compute $[K_G]$	Eq. 15
20	Compute $[C_G]$	Eq. 16
21	Compute C_1, C_2, C_3	Eq. 17
22	Compute C_A	Eq. 18
23	Compute C_T	Eq. 19
23a	Compute P	Eq. 4
24	Compute $\{f_E^*\}, \{\tau_E^*\}$	Eqns. 20

Subsidiary Equations for Beam Connecting Structure

$$\bar{M} = \frac{M_c M_L}{M_c + M_L}, \quad \bar{J} = \frac{J_c J_L}{J_c + J_L} \quad (1)$$

$$l_0 = (\{l_0\}^T \{l_0\})^{1/2}, \quad \tilde{l}_0 = \text{larger of } (l_0, l_{\min}) \quad (2)$$

$$\left. \begin{aligned} K_1 &= 12EI/\tilde{l}_0^3, \quad K_2 = -6EI/\tilde{l}_0^2, \quad K_3 = 4EI/\tilde{l}_0 \\ K_A &= AE/\tilde{l}_0, \quad K_T = GJ/\tilde{l}_0 \end{aligned} \right\} \quad (3)$$

$$P = [0, 0, 1] \{P_{\bar{z}}\} \quad (4)$$

$$\bar{I} = I_c + I_L + \bar{M} (a + b + l_0)^2 \quad (5)$$

$$\left. \begin{aligned} M_1 &= \bar{M} (I_c + I_L) / \bar{I} \\ M_2 &= \bar{M} (I_c a - I_L (b + l_0)) / \bar{I} \\ M_3 &= (\bar{M} (I_L (b + l_0)^2 + I_c a^2) + I_c I_L) / \bar{I} \end{aligned} \right\} \quad (6)$$

$$\text{Equation Deleted} \quad (7)$$

$$\left. \begin{aligned} A &= M_1 M_3 - M_2^2 \\ B &= 2K_2 M_2 - K_1 M_3 - K_3 M_1 \\ C &= K_1 K_3 - K_2^2 \end{aligned} \right\} \quad (8)$$

$$\left. \begin{aligned} \omega_1^2 &= (-B - (B^2 - 4AC)^{1/2}) / 2A \\ \omega_2^2 &= (-B + (B^2 - 4AC)^{1/2}) / 2A \end{aligned} \right\} \quad (9)$$

$$R_1 = -(\kappa_1 - \omega_1^2 M_1) / (\kappa_2 - \omega_1^2 M_2) \quad (10)$$

$$\left. \begin{aligned} \text{If } |R_1| > 1, \text{ set } \bar{\phi}_1 = 1, \bar{\delta}_1 = 1/R_1 \\ \text{If } |R_1| \leq 1, \text{ set } \bar{\delta}_1 = 1, \bar{\phi}_1 = R_1 \end{aligned} \right\} \quad (11)$$

$$R_2 = -(\kappa_1 - \omega_2^2 M_1) / (\kappa_2 - \omega_2^2 M_2) \quad (12)$$

$$\left. \begin{aligned} \text{If } |R_2| > 1, \text{ set } \bar{\phi}_2 = 1, \bar{\delta}_2 = 1/R_2 \\ \text{If } |R_2| \leq 1, \text{ set } \bar{\delta}_2 = 1, \bar{\phi}_2 = R_2 \end{aligned} \right\} \quad (13)$$

$$[M_G] = \begin{bmatrix} \bar{\delta}_1 & \bar{\phi}_1 \\ \bar{\delta}_2 & \bar{\phi}_2 \end{bmatrix} \begin{bmatrix} M_1 & M_2 \\ M_2 & M_3 \end{bmatrix} \begin{bmatrix} \bar{\delta}_1 & \bar{\delta}_2 \\ \bar{\phi}_1 & \bar{\phi}_2 \end{bmatrix} = \begin{bmatrix} M_{11} & 0 \\ 0 & M_{22} \end{bmatrix} \quad (14)$$

$$[K_G] = \begin{bmatrix} \bar{\delta}_1 & \bar{\phi}_1 \\ \bar{\delta}_2 & \bar{\phi}_2 \end{bmatrix} \begin{bmatrix} \kappa_1 & \kappa_2 \\ \kappa_2 & \kappa_3 \end{bmatrix} \begin{bmatrix} \bar{\delta}_1 & \bar{\delta}_2 \\ \bar{\phi}_1 & \bar{\phi}_2 \end{bmatrix} = \begin{bmatrix} K_{11} & 0 \\ 0 & K_{22} \end{bmatrix} \quad (15)$$

$$[C_G] = 2\gamma_B \begin{bmatrix} (K_{11}M_{11})^{1/2} & 0 \\ 0 & (K_{22}M_{22})^{1/2} \end{bmatrix} \quad (16)$$

$$\begin{bmatrix} C_1 & C_2 \\ C_2 & C_3 \end{bmatrix} = (\bar{\delta}_1 \bar{\phi}_2 - \bar{\delta}_2 \bar{\phi}_1)^{-2} \begin{bmatrix} \bar{\phi}_2 & -\bar{\phi}_1 \\ -\bar{\delta}_2 & \bar{\delta}_1 \end{bmatrix} [C_G] \begin{bmatrix} \bar{\phi}_2 & -\bar{\delta}_2 \\ -\bar{\phi}_1 & \bar{\delta}_1 \end{bmatrix} \quad (17)$$

$$C_A = 2\gamma_A (\bar{M} K_A)^{1/2} \quad (18)$$

$$C_T = 2\gamma_T (\bar{J} K_T)^{1/2} \quad (19)$$

$$\{f_E^*\} = \left(\begin{bmatrix} K_1 & 0 & 0 & 0 & K_2 & 0 \\ 0 & K_1 & 0 & -K_2 & 0 & 0 \\ 0 & 0 & K_A & 0 & 0 & 0 \end{bmatrix} + \frac{P}{10\tilde{\ell}_0} \begin{bmatrix} 12 & 0 & 0 & 0 & -\tilde{\ell}_0 & 0 \\ 0 & 12 & 0 & \tilde{\ell}_0 & 0 & 0 \\ 0 & 0 & 0 & 0 & 0 & 0 \end{bmatrix} \right) \begin{Bmatrix} \delta \\ - \\ \phi^* \end{Bmatrix} \quad (20a)$$

$$+ \begin{bmatrix} C_1 & 0 & 0 & 0 & C_2 & 0 \\ 0 & C_1 & 0 & -C_2 & 0 & 0 \\ 0 & 0 & C_A & 0 & 0 & 0 \end{bmatrix} \begin{Bmatrix} \dot{\delta} \\ - \\ \dot{\phi}^* \end{Bmatrix}$$

$$\{f_E^*\} = \left(\begin{bmatrix} 0 & -K_2 & 0 & K_3 & 0 & 0 \\ K_2 & 0 & 0 & 0 & K_3 & 0 \\ 0 & 0 & 0 & 0 & 0 & K_T \end{bmatrix} + \frac{P}{10\tilde{\ell}_0} \begin{bmatrix} 0 & \tilde{\ell}_0 & 0 & \frac{4}{3}\tilde{\ell}_0^2 & 0 & 0 \\ -\tilde{\ell}_0 & 0 & 0 & 0 & \frac{4}{3}\tilde{\ell}_0^2 & 0 \\ 0 & 0 & 0 & 0 & 0 & 0 \end{bmatrix} \right) \begin{Bmatrix} \delta \\ - \\ \phi^* \end{Bmatrix} \quad (20b)$$

$$+ \begin{bmatrix} 0 & -C_2 & 0 & C_3 & 0 & 0 \\ C_2 & 0 & 0 & 0 & C_3 & 0 \\ 0 & 0 & 0 & 0 & 0 & C_T \end{bmatrix} \begin{Bmatrix} \dot{\delta} \\ - \\ \dot{\phi}^* \end{Bmatrix}$$

G2. Cable Truss

The main program must supply the following previously used terms to the Connecting-Structure Subroutine: $\{s\}$, $\{\bar{s}\}$, $[\Pi(\theta)]$, $\{\ell_0\}$, $\{\dot{\ell}_0\}$, $\{\ell\}$, $\{\dot{\ell}\}$.

The required new input data is as follows:

NCAB	number of cables
$\{x_j\}$, $j = 1, 2, \dots, \text{NCAB}$	position vector (expressed in \underline{x}^i) which specifies the Laboratory attachment point of the j th cable
$\{\bar{x}_j\}$, $j = 1, 2, \dots, \text{NCAB}$	position vector (expressed in \underline{x}^a) which specifies the Counterweight attachment point of the j th cable
$(AE)_j$, $j = 1, 2, \dots, \text{NCAB}$	spring constant per unit length of the j th cable
γ_j , $j = 1, 2, \dots, \text{NCAB}$	viscous damping coefficient per unit length of the j th cable

The computation procedure is outlined below. Do Step 1 the first time through only. If there is no deployment in the run, do Steps 2-5 the first time through only.

Step No.	Operation	Required Equation
1	Set up $[\Pi(\eta_0)]$	Eq. 1
2	Compute $\{\ell_{j0}\}$, $j = 1, \dots, \text{NCAB}$	Eq. 2
3	Compute $\{\dot{\ell}_{j0}\}$, $j = 1, \dots, \text{NCAB}$	Eq. 3
4	Compute ℓ_{j0} , $j = 1, \dots, \text{NCAB}$	Eq. 4
5	Compute n_{j0} , $j = 1, \dots, \text{NCAB}$	Eq. 5
6	Compute $\{\ell_j\}$, $j = 1, \dots, \text{NCAB}$	Eq. 6
7	Compute $\{\dot{\ell}_j\}$, $j = 1, \dots, \text{NCAB}$	Eq. 7
8	Compute ℓ_j , $j = 1, \dots, \text{NCAB}$	Eq. 8
9	Compute n_j , $j = 1, \dots, \text{NCAB}$	Eq. 9
10	Compute ϵ_j , $j = 1, \dots, \text{NCAB}$	Eq. 10
11	If $\epsilon_j < 0$, set $\epsilon_j = \dot{\epsilon}_j = 0$ } $j = 1, \dots, \text{NCAB}$ otherwise, compute $\dot{\epsilon}_j$	Eq. 11
12	Compute $\{P_j\}$, $j = 1, \dots, \text{NCAB}$	Eq. 12
13	Compute $\{T_j\}$, $j = 1, \dots, \text{NCAB}$	Eq. 13
14	Compute $\{f_E\}$, $\{T_E^*\}$	Eq. 14

$$[\pi(\phi)] = \begin{bmatrix} 1 & 0 & 0 \\ 0 & -1 & 0 \\ 0 & 0 & -1 \end{bmatrix} \quad (1)$$

$$\{x_{j0}\} = [\pi(\beta)](\{\bar{x}\} - \{\bar{x}_f\}) + \{x_0\} + [\pi(\beta)] [\pi(\phi)] (\{\bar{x}_f\} - \{\bar{x}\}) \quad (2)$$

$$\{\dot{x}_{j0}\} = \{\dot{x}_0\} \quad (3)$$

$$x_{j0} = (\{x_f\}^T \{x_{j0}\})^{1/2} \quad (4)$$

$$\{n_{j0}\} = \frac{\{x_{j0}\}}{x_{j0}} \quad (5)$$

$$\{x_j\} = [\pi(\beta)](\{\bar{x}\} - \{\bar{x}_f\}) + \{x\} + [\pi(\phi^*)]^T [\pi(\beta)] [\pi(\phi)] (\{\bar{x}_f\} - \{\bar{x}\}) \quad (6)$$

$$\{\dot{x}_j\} = \{\dot{x}\} + [\pi(\phi^*)]^T [\pi(\phi)] (\{\bar{x}_f\} - \{\bar{x}\}) \quad (7)$$

$$x_f = (\{x_f\}^T \{x_f\})^{1/2} \quad (8)$$

$$\{n_f\} = \{x_f\} / x_f \quad (9)$$

$$\epsilon_j = x_j - x_{jc} \quad (10)$$

$$\dot{\epsilon}_j = \{x_j\}^T \{n_j\} - \{x_{jc}\}^T \{n_{jc}\} \quad (11)$$

$$\{P_j\} = \left(\frac{(AE)_j}{x_{jc}} \epsilon_j + \frac{\delta_j \dot{\epsilon}_j}{x_{jc}} \right) \{n_j\} \quad (12)$$

$$\{T_j\} = [\Gamma([\pi(\phi^*)])^T [\pi(\phi)] (\{x_j\} - \{x_{jc}\})] \{P_j\} \quad (13)$$

$$\{f_E^*\} = \sum_{j=1}^{N_{CAB}} \{P_j\} \quad , \quad \{T_E^*\} = \sum_{j=1}^{N_{CAB}} \{T_j\} \quad (14)$$

APPENDIX H

COMPUTATION PROCEDURE FOR CONTROL-SYSTEM SUBROUTINES

This appendix outlines the computation procedure used in the control-system subroutines and the method of using these subroutines in the Phase II (flexible-body) computer program. The hierarchy of the subroutines as used in the Phase II program is indicated in Figure H1. Subroutine CONTROL was written to interface most of the control-system routines with the Phase II program. It contains the additional computations required to generate the input to the control-system subroutines and to generate the output in the form required by the Phase II program. CONTROL also reads the input data and writes the output for the subroutines that it services, thus, this facilitates replacing the controls subroutines. Subroutine BMCON is a similar interface routine; however, it services only the balance-mass control routine BMCTR. MUCOM and POSCOM utilize the service command routines, POSCOM and VELCOM, to command the motion of moving rigid masses and the fluid velocity, respectively.

In the flexible vehicle idealization it is assumed that mass point i_s contains a controls package which includes all sensor elements and the CMG used to eliminate wobble. The 16 jets are assumed to be located on mass points 1 and 5 as shown in Figure 6.3. Each jet is assumed to have the same thrust f_{JET} . i_s and f_{JET} are read in by subroutine CONTROL.

The symbols used in the models of the control systems described in the following sections are defined in Table H1. The previously used Phase II (flexible-body analysis) symbols used in the interface programs are defined in Section 4.0.

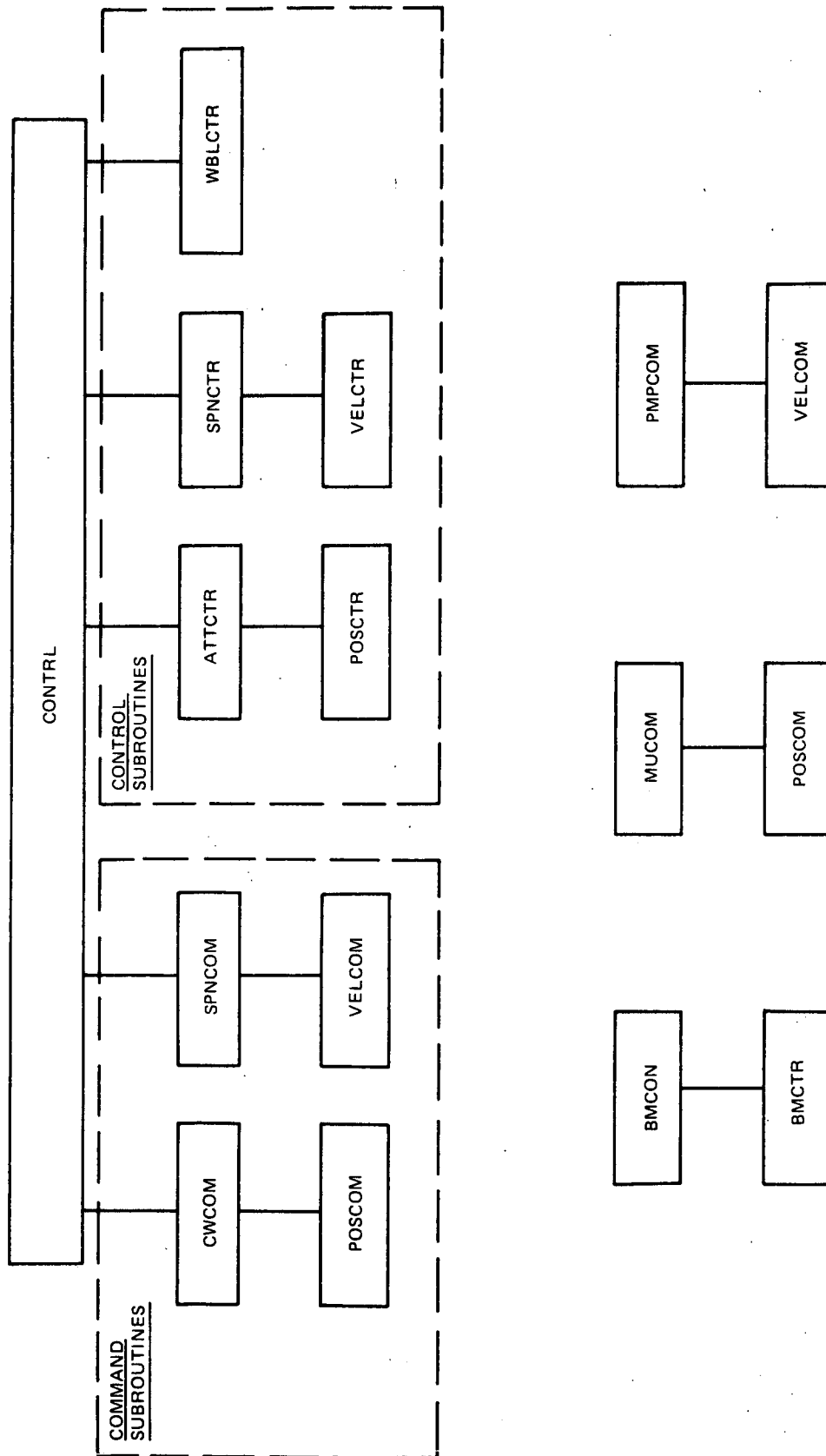


Fig. H1 Hierarchy of Control Subroutines in Phase II Computer Program

Table H1 Definitions of Symbols Used in the
Models of the Command and Control
System Subroutines

<u>Mode</u>	<u>Symbol</u>	<u>Definition</u>
	time	time increment of integration in main program
	time	time at which run ends
Attitude and Spin Rate Control	f_{JET}	force exerted by jet (each jet is the same)
Attitude Control	$\{acc_{\theta S}\}$	magnitude of acceleration, used to compute parabolic switching curves in POSCTR (value for each of three axes)
Attitude Control	$e_{\theta MAX}$	error rate θ , maximum magnitude, used for straight-line switching curves in Policy 1
Attitude Control	$e_{\theta DB}$	error in θ , dead band (same value for each of 3 axes)
Spin Rate Command	ω_{1CU}	spin rate command update
Spin Rate Command	$t_{\omega 1CU}$	time for spin rate command to be updated
Spin Rate Command	$acc_{\omega 1C}$	magnitude of spin acceleration command
Spin Rate Command	ω_{1C}	spin rate command
Spin Rate Control	$e_{\omega 1}$	error in spin rate, $\omega_1 - \omega_{1C}$
Spin Rate Control	$e_{\omega 1 DB}$	error in spin rate, dead band
Counter-weight Command	x_{B3CU}	position of counterweight center of mass relative to laboratory, along axis 3, command update
Counter-weight Command	t_{XB3CU}	time for updating commanded position of counterweight center of mass relative to laboratory, along axis 3

<u>Mode</u>	<u>Symbol</u>	<u>Definition</u>
Counter-weight Command	acc_{B3C}	magnitude of acceleration, counter-weight, along axis 3
Counter-weight Command	vel_{MBC}	velocity, maximum magnitude, counter-weight command
Counter-weight Command	X_{B3C}	position of counterweight center of mass relative to laboratory, along axis 3, command
Elevator Command	X_{13CU}	position of elevator center of mass relative to laboratory, along axis 3, command update
Elevator Command	t_{X13CU}	time for updating commanded position of elevator center of mass relative to laboratory, along axis 3
Elevator Command	acc_{13C}	magnitude of acceleration, elevator, along axis 3
Elevator Command	vel_{MLC}	velocity, maximum magnitude, elevator command
Elevator Command	X_{13C}	position of elevator center of mass relative to laboratory, along axis 3, command
Mass Balancing	$\{X_{SENS}\}$	position of accelerometer sensor relative to laboratory (projections along X_1 , X_2 , X_3)
Mass Balancing	m_{1EST}	estimate of mass in mass 1
Mass Balancing	$\text{err}_{\ddot{X}}$	acceleration command - acceleration sensed, $\ddot{X}_3^{CMND} - \ddot{X}_3^{SENS}$
Mass Balancing	K_{eXSE}	constant multiplying error between acceleration commanded and acceleration sensed
Mass Balancing	$e_{\dot{X}DB}$	error in mass 2 (balance mass) velocity (actual minus commanded velocity), dead band
Mass Balancing	acc_{23C}	magnitude of acceleration for mass 2 (balance mass)
CMG Control	β	gimbal angle, CMG, reference coordinate is laboratory axis 3, positive counterclockwise

<u>Mode</u>	<u>Symbol</u>	<u>Definition</u>
CMG Control	K_T	constant, multiplies error err_β to give torque $t_{KGIM} + t_{PASS}$ in gimbal angle control (in gimbal angle rate control, K_T multiplies err_β to give err_{KT})
CMG Control	t_{LIM}	torque limit of torque motor
CMG Control	K_β	constant, multiplies $\dot{\beta}$ to give t_{FDBK}
CMG Control	mom_{CMG}	momentum of the CMG
CMG Control	$I_{\beta GIM}$	inertia of CMG gimbal about the vehicle spin axis, which is axis of gimbal freedom

H1. COMMAND ROUTINE POSCOM (POSITION COMMAND)

This service routine is used by routines which command the positions of the Counterweight, the elevator and other moving masses, except the balance mass.

Inputs

time	time
poscu	position command update
timcu	time of position command update (commencement of update)
acc _{MAG}	magnitude of non-zero acceleration
vel _{MAX}	magnitude of maximum velocity

Outputs

out	control: 0 update data not yet computed 1 update data computed
time0	commencement of update, acceleration is applied
time1	time acceleration is ended and coast is commenced
time2	time coast is ended and deceleration is commenced
time3	time deceleration is ended and position command is updated
acc01	acceleration from time0 to time1
acc12	acceleration from time1 to time2
acc23	acceleration from time2 to time3
posc0	position command at time0
posc1	position command at time1
posc2	position command at time2
velc1	velocity command at time1
velc2	velocity command at time2
acc _{CMN}	acceleration command
vel _{CMN}	velocity command
pos _{CMN}	position command

COMPUTATION PROCEDURE

If time = 0. \rightarrow out = 0.
 $\text{acc}_{\text{CMN}} = 0.$
 $\text{vel}_{\text{CMN}} = 0.$

$\neq 0.$ \rightarrow continue

If time < timcu \rightarrow go to End
 $\geq \text{timcu} \rightarrow$ continue

If out $\leq 0.$ \rightarrow continue
 $> 0.$ \rightarrow go to (1)

$$\text{error} = \text{poscu} - \text{pos}_{\text{CMN}}$$

$$t_{1/2} = \sqrt{|\text{error}| / \text{acc}_{\text{MAG}}}$$

$$\text{vel}_{1/2} = \sqrt{|\text{error}| \text{acc}_{\text{MAG}}}$$

If $\text{vel}_{1/2} \leq \text{vel}_{\text{MAX}}$ \rightarrow continue
 $> \text{vel}_{\text{MAX}}$ \rightarrow go to (2)

$$\text{time0} = \text{timcu}$$

$$\text{time1} = \text{time0} + t_{1/2}$$

$$\text{time2} = \text{time1}$$

$$\text{time3} = \text{time2} + t_{1/2}$$

$$\text{acc01} = (\text{error} / |\text{error}|) \text{acc}_{\text{MAG}}$$

$$\text{acc12} = 0.$$

$$\text{acc23} = (-\text{error} / |\text{error}|) \text{acc}_{\text{MAG}}$$

$$\text{out} = 1.$$

go to ①

$$\textcircled{2} \quad t_1 = \text{vel}_{\text{MAX}} / \text{acc}_{\text{MAG}}$$

$$t_2 = |\text{error}| / \text{vel}_{\text{MAX}}$$

$$\text{time0} = \text{timcu}$$

$$\text{time1} = \text{time0} + t_1$$

$$\text{time2} = \text{time0} + t_2$$

$$\text{time3} = \text{time2} + t_1$$

$$\text{acc01} = (\text{error} / |\text{error}|) \text{acc}_{\text{MAG}}$$

$$\text{acc12} = 0.$$

$$\text{acc23} = (-\text{error} / |\text{error}|) \text{acc}_{\text{MAG}}$$

$$\text{out} = 1.$$

③ If $acc_{cmn} = 0.$ \rightarrow go to End
 $\neq 0.$ \rightarrow continue

$$vel_{cmn} = 0.$$

$$pos_{cmn} = pos_{c2} + vel_{c2} (time_3 - time_2) + (1/2) acc_{c2} (time_3 - time_2)^2$$

$$acc_{cmn} = 0.$$

End

① If $time < time_3 \rightarrow \text{continue}$
 $\geq time_3 \rightarrow \text{go to } \textcircled{3}$

If $time < time_2 \rightarrow \text{go to } \textcircled{7}$
 $\geq time_2 \rightarrow \text{continue}$

If $acc_{CMN} = acc_{23} \rightarrow \text{go to } \textcircled{4}$

If $acc_{CMN} = acc_{01} \rightarrow \text{go to } \textcircled{5}$

$$pos_{CMN} = pos_{c1} + vel_{c1} (time_2 - time_1)$$

go to $\textcircled{6}$

⑤ $vel_{CMN} = acc_{01} (time_1 - time_0)$

$$pos_{CMN} = pos_{c0} + (1/2) acc_{01} (time_1 - time_0)^2$$

$$pos_{CMN} = pos_{CMN} + vel_{CMN} (time_2 - time_1)$$

⑥ $vel_{c2} = vel_{CMN}$

$$pos_{c2} = pos_{CMN}$$

$$acc_{CMN} = acc_{23}$$

④ $vel_{CMN} = vel_{c2} + acc_{23} (time - time_2)$

$$pos_{CMN} = pos_{c2} + vel_{c2} (time - time_2) + (1/2) acc_{23} (time - time_2)^2$$

go to End

⑦ If $time < time_1 \rightarrow \text{go to } \textcircled{9}$

$\geq time_1 \rightarrow \text{continue}$

If $acc_{CMN} = acc_{12} \rightarrow \text{go to } \textcircled{8}$
 $\neq acc_{12} \rightarrow \text{continue}$

$$vel_{CMN} = acc_{01} (time_1 - time_0)$$

$$pos_{CMN} = pos_{00} + (1/2) acc_{01} (time_1 - time_0)^2$$

$$vel_{C1} = vel_{CMN}$$

$$pos_{C1} = pos_{CMN}$$

$$acc_{CMN} = acc_{12}$$

$$vel_{CMN} = vel_{C1}$$

$$\textcircled{8} \quad pos_{CMN} = pos_{C1} + vel_{C1} (time - time_1)$$

go to End

$$\textcircled{9} \quad \text{If } time < time_0 \rightarrow \text{go to } \textcircled{3}$$

$$\geq time_0 \rightarrow \text{continue}$$

$$\text{If } acc_{CMN} = acc_{01} \rightarrow \text{go to } \textcircled{10}$$

$$\neq acc_{01} \rightarrow \text{continue}$$

$$acc_{CMN} = acc_{01}$$

$$pos_{00} = pos_{CMN}$$

$$\textcircled{10} \quad vel_{CMN} = acc_{01} (time - time_0)$$

$$pos_{CMN} = pos_{00} + (1/2) acc_{01} (time - time_0)^2$$

go to End

H2 COMMAND ROUTINE VELCOM (VELOCITY COMMAND)

This service routine is used by subroutines which command the spin rate and the fluid velocity.

Input to Subroutine

time	time
velcu	velocity command update
timcu	time of velocity command update (commencement of update)
out	control: 0 update data not yet computed 1 update data computed
time0	time at which update is commenced; acceleration is applied.
timel	time at which update process is complete; acceleration is removed
acc0l	acceleration from time0 to timel
velco	velocity command at time0
acc _{MAG}	magnitude of non-zero acceleration command

Output of Subroutine

acc _{CMN}	acceleration command
vel _{CMN}	velocity command

Computation Procedure

If $\text{time} = 0. \rightarrow \text{acc}_{\text{CMN}} = 0.$
 $\text{out} = 0.$
 $\neq 0. \rightarrow \text{continue}$

If $\text{time} < \text{timeu} \rightarrow \text{go to End}$
 $\geq \text{timeu} \rightarrow \text{continue}$

If $\text{out} \leq 0. \rightarrow \text{continue}$
 $> 0. \rightarrow \text{go to } \textcircled{1}$

$$\text{error} = \text{velcu} - \text{vel}_{\text{CMN}}$$

$$t_1 = |\text{error}| / \text{acc}_{\text{MAG}}$$

$$\text{timeo} = \text{timecu}$$

$$\text{time1} = \text{timeo} + t_1$$

$$\text{acco1} = (\text{error} / |\text{error}|) \text{acc}_{\text{MAG}}$$

$$\text{out} = 1.$$

① If $\text{time} < \text{time1} \rightarrow \text{continue}$
 $\geq \text{time1} \rightarrow \text{go to } \textcircled{3}$

If $\text{time} < \text{timeo} \rightarrow \text{go to End}$
 $\geq \text{timeo} \rightarrow \text{continue}$

If $\text{acc}_{\text{CMN}} = \text{acco1} \rightarrow \text{go to } \textcircled{2}$
 $\neq \text{acco1} \rightarrow \text{continue}$

$$\text{velco} = \text{vel}_{\text{CMN}}$$

$$\text{acc}_{\text{CMN}} = \text{acco1}$$

② $\text{vel}_{\text{CMN}} = \text{velco} + \text{acco1} (\text{time} - \text{timeo})$

go to End

③ If $\text{acc}_{\text{CMN}} = 0. \rightarrow \text{go to End}$
 $\neq 0. \rightarrow \text{continue}$

$$\text{vel}_{\text{CMN}} = \text{velco} + \text{acco1} (\text{time1} - \text{timeo})$$

$$\text{acc}_{\text{CMN}} = 0.$$

End

H.3 COMMAND ROUTINE CWCMD (COUNTERWEIGHT COMMAND)

This subroutine is used to command the position of the Counterweight.

Input Data Read in by Subroutine CONTROL (Phase II Symbols Used)

l_{03U} , t_{l03U} , $acc_{l03\ mag}$, $vel_{l03\ max}$, initial value of l_{03} (which is 3rd component of $\{l_0\}$)

These symbols are defined below.

Input to Subroutine CWCMD

<u>Symbol</u>		
Phase II	Control	
<u>Analysis</u>	<u>Analysis</u>	
t	$time$	$time$
l_{03U}	X_{B3CU}	position of counterweight relative to lab along axis 3, command update
t_{l03U}	t_{XB3CU}	time for updating commanded position of counterweight relative to lab along axis 3
acc_{l03mag}	acc_{B3C}	magnitude of acceleration, counterweight, along lab axis 3
vel_{l03max}	vel_{MBC}	magnitude of maximum commanded velocity of counterweight relative to lab

Output of Subroutine CWCMD

<u>Symbol</u>		
Phase II	Control	
<u>Analysis</u>	<u>Analysis</u>	
\ddot{l}_{03}	\ddot{X}_{B3C}	acceleration of counterweight along lab axis 3, command
\dot{l}_{03}	\dot{X}_{B3C}	velocity of counterweight along lab axis 3, command
l_{03}	X_{B3C}	position of counterweight along lab axis 3, command

Computation Procedure (control analysis symbols used)

Call Subroutine POSCOM

(Arguments:

time, x_{B3CU} , t_{XB3CU} ,

out_{XB}, time 0_B, time 1_B, time 2_B, time 3_B,

acc01_B, acc12_B, acc23_B,

posc0_B, posc1_B, posc2_B,

velc1_B, velc2_B,

acc_{B3C}, vel_{MBC},

\ddot{x}_{B3C} , \dot{x}_{B3C} , x_{B3C})

H4. COMMAND ROUTINE ELCOM (ELEVATOR COMMAND)*

This subroutine is used to command the position of the elevator. It is used only with the rigid-body control-systems development program. Subroutine MUCOM performs this task in the Phase II program.

Inputs to Subroutine

time	time
X_{13CU}	position of elevator c.m. relative to lab along axis 3, command update
t_{X13CU}	time for updating commanded position of elevator c.m. relative to lab along axis 3
acc_{13C}	magnitude of acceleration, elevator, along lab axis 3
vel_{MLC}	velocity, maximum magnitude, elevator, command

Output of Subroutine

\ddot{X}_{13C}	acceleration of elevator along lab axis 3, command
\dot{X}_{13C}	velocity of elevator along lab axis 3, command
X_{13C}	position of elevator along lab axis 3, command

Computation Procedure

Call Subroutine POSCOM

(Arguments:

time, X_{13CU} , t_{X13CU} ,
 out $_{X1}$, time 0 $_1$, time 1 $_1$, time 2 $_1$, time 3 $_1$,
 acc01 $_1$, acc12 $_1$, acc23 $_1$,
 posC0 $_1$, posC1 $_1$, posC2 $_1$,
 velC1 $_1$, velC2 $_1$,
 acc $_{13C}$, vel $_{MLC}$,
 \ddot{X}_{13C} , \dot{X}_{13C} , X_{13C})

* Control-system analysis symbols are used (see Table H1)

H5 COMMAND ROUTINE MUCOM (COMMANDS POSITIONS OF MOVING MASSES) *

This subroutine is used in the Phase II program to command the position of each moving rigid mass on the Laboratory, except the balance mass. The motion of the balance mass is controlled by the balance mass control subroutine BMCTR.

For each mass μ_j controlled by MUCOM, each axis of the position vector $\{U_j\}$ may be controlled independently. Ideal control is assumed; i.e., the commanded and controlled positions are assumed to be identical.

Input Data Read in by Subroutine MUCOM

i axis along which motion occurs

$\{U_j\}$ initial value

For the i th component of $\{U_j\}$ specify the following:

U_U update value of position coordinate

t_U time of update

acc_{mag} magnitude of acceleration

vel_{max} magnitude of maximum velocity

Input to Subroutine

t time

j moving mass (μ_j) subscript

Output of Subroutine

$\{U_j\}$ position of μ_j \sim axes

$\{\dot{U}\}$

$\{\ddot{U}\}$

Computation Procedure

If no motion of μ_j is specified, keep $\{U_j\}$ constant. If motion is specified, call Subroutine POSCOM to obtain motion $\{U_j(t)\}$ for each axis i along which motion occurs. All POSCOM arguments (except t) must be stored as a function of the mass index j and the axis i .

* The Phase II symbols are used (See Section 4.0)

H6. COMMAND ROUTINE SPNCOM (SPIN COMMAND) †

This subroutine commands the spin rate of the Space Station. In the version of SPNCOM used for the rigid-body control-system development program the spin acceleration command was set equal to the system's capability (i.e., equal to the jet torque divided by the spin inertia). In the version of SPNCOM used with the Phase II program, the acceleration command was not computed; instead it was input data.

Input Data Read in by CONTROL in Phase II Version of Subroutine

initial value of ω_{1C} ,

ω_{1CU} , $t_{\omega 1CU}$, $acc_{\omega 1C}$

These symbols are defined below

Input to Subroutine SPNCOM

Inputs

time	time
ω_{1CU}	spin rate command
$t_{\omega 1CU}$	time for spin rate command to be updated
$acc_{\omega 1C}$	magnitude of non-zero spin acceleration command
f_{JET}	force exerted by jet (each jet is the same)
$\{X^A_j\}$	locations of points A_j in X axes
$[M_{11}]$	moment of inertia matrix for vehicle (lab + counterweight + 2 masses in lab)*

Output of Subroutine SPNCOM

$\dot{\omega}_{1C}$	spin acceleration command *
ω_{1C}	spin rate command
ω_{1CMAG}	magnitude of spin rate command

Computation Procedure

$$acc_{\omega 1C} = 2 f_{JET} (X^{A_j}(3,13) - X^{A_j}(3,10)) / M_{11}(1,1) \quad (1)**$$

* Not used in Phase II version of subroutine.

** Equation deleted from Phase II version of subroutine.

† Control-system analysis symbols are used. See Table H1.

Call Subroutine VELCOM

(2)

(Arguments:

time, ω_{1cu} , $t_{\omega_{1cu}}$,out _{ω} , timeo _{ω} , time1 _{ω} ,acco1 _{ω} , velco _{ω} , acco1 _{c} , $\dot{\omega}_{1c}$, ω_{1c})

$$\omega_{1cMAG} = |\omega_{1c}|$$

(3)

H7. COMMAND ROUTINE PMPCOM (PUMP COMMAND)

This subroutine is used in the Phase II program to command the velocity of the fluid in the pipe line. PMPCOM calls subroutine VELCOM to perform this task.

Input Data Read in by Subroutine PMPCOM

V velocity of fluid in pipe (initial value read in)
 V_U update velocity of fluid in pipe
 t_{fU} time of velocity update
 acc_{fMAG} magnitude of acceleration (must be > 0)

Input to Subroutine

t time

Output of Subroutine

\dot{V} acceleration of fluid in pipe
 V velocity of fluid in pipe

Computation Procedure

Call Subroutine VELCOM

Arguments:

t , V_U , t_{fU} , out, time 0, time 1, acc 01, vel00, acc_{fMAG} ,
 \dot{V} , V

H8. CONTROL ROUTINE POSCTR (Position Control)

This service routine is used by the subroutine which controls the attitude of the nonrotating Space Station.

Input to Subroutine

e error, attitude - attitude command, one axis
 e_{DB} error dead band
 \dot{e} error rate, rate - rate command
 \dot{e}_{MAX} error rate maximum (for switching)
 acc_S non-zero acceleration magnitude (for switching)

Output of Subroutine

acc_{NOW} acceleration now (+1., 0., -1.)

Computation Procedure

$$e_1 = 1.$$

If $\dot{e} < 0.$ → go to ⑤
 $\geq 0.$ → continue

⑥ If $e < e_{DB}$ → continue
 $\geq e_{DB}$ → go to ①

$$e_2 = \sqrt{-2 acc_S (e + e_{DB})}$$

If $\dot{e} \leq e_2$ → continue
 $> e_2$ → go to ⑦

If $\dot{e} \leq \dot{e}_{MAX}$ → go to ②
 $> \dot{e}_{MAX}$ → go to ③

① If $e < e_{DB} \rightarrow \text{continue}$
 $\geq e_{DB} \rightarrow \text{go to } \textcircled{4}$

$$\textcircled{7} \quad e_3 = \sqrt{-2 \text{acc}_S (e - e_{DB})}$$

If $\dot{e} < e_3 \rightarrow \text{go to } \textcircled{3}$
 $\geq e_3 \rightarrow \text{go to } \textcircled{4}$

$$\textcircled{2} \quad \text{acc}_{\text{now}} = e_1$$

go to End

$$\textcircled{3} \quad \text{acc}_{\text{now}} = 0.$$

go to End

$$\textcircled{4} \quad \text{acc}_{\text{now}} = -e_1$$

go to End

$$\textcircled{5} \quad e = -e$$

$$\dot{e} = -\dot{e}$$

$$e_1 = -1.$$

go to $\textcircled{6}$

 End

H9. CONTROL ROUTINE VELCTR (VELOCITY CONTROL)

This service routine is used by subroutines which control the spin rate and (in the rigid-body control-system development program only) the position of the balance mass.

Input to Subroutine

\dot{e} error rate (rate - rate command)

\dot{e}_{DB} error rate dead band

Output of Subroutine

acc_{NOW} acceleration now (+1., 0., or -1.)

Computation Procedure

If $\dot{e} < \dot{e}_{DB}$ → go to ①
 $> \dot{e}_{DB}$ → continue

④ $acc_{NOW} = -1.$
 go to End

① If $\dot{e} \leq \dot{e}_{DB}$ → continue
 $> \dot{e}_{DB}$ → go to ②

⑤ $acc_{now} = +1.$

go to End

② If $e < 0.$ → go to ③
 $\geq 0.$ → continue

If $acc_{now} = -1.$ → go to ④

$acc_{now} = 0.$

go to End

③ If $acc_{now} = +1.$ → go to ⑤

$acc_{now} = 0.$

 End

H10 CONTROL ROUTINE ATTCTR (ATTITUDE CONTROL)

This subroutine is used to control the attitude of the nonrotating Space Station. In order to include the flexible body effects, i.e., the vibration of the sensor and the jets, the required equations (presented below) have been included in interface subroutine CONTROL. CONTROL also is used to read the following input data for ATTCTR. The terms are defined in the table describing the input to ATTCTR which appears on a subsequent page.

Input Data Read in by Subroutine CONTROL

$$e_{0PB}, e_{0MAX}, XJ1$$

where XJ1 is the jet momentum (see Figure 6.3) and the other symbols are defined in the table of subroutine input which appears on a subsequent page.

Computation Procedure for Subroutine CONTROL to Interface Phase II

Simulation with Subroutine ATTCTR *

1. Compute sensor attitude expressed in the Z axes $\{\delta_{is}\}$ and attitude rate for nonrotating state assuming linear deformations. i_s is index number of mass point containing sensor.

$$\{\gamma_{i_s}\} = \{\gamma\} + \{\theta_{i_s}\}$$

$$\{\dot{\gamma}_{i_s}\} = \{\dot{\gamma}\} + \{\dot{\theta}_{i_s}\}$$

2. Compute control forces and torques (on mass points 1 and 5).

$$\{f_c'\} = \begin{Bmatrix} f_4 + f_{16} \\ f_1 + f_2 + f_3 + f_{13} + f_{14} + f_{16} \\ 0 \end{Bmatrix}$$

$$\{\tau_c'\} = \begin{Bmatrix} 0 \\ 0 \\ XJ1(-f_1 - f_2 - f_3 + f_{13} + f_{14} + f_{15}) \end{Bmatrix}$$

* The Phase II analysis symbols are used.

$$\{f_c^5\} = \begin{Bmatrix} f_8 + f_{12} \\ f_5 + f_6 + f_7 + f_9 + f_{10} + f_{11} \\ 0 \end{Bmatrix}$$

$$\{\tau_c^5\} = \begin{Bmatrix} 0 \\ 0 \\ XJ1(-f_5 - f_6 - f_7 + f_9 + f_{10} + f_{11}) \end{Bmatrix}$$

where f_j is the thrust of jet number j in Figure 6.3. Its value is determined in ATTCTR or SPNCTR (see Appendix H10). It is given the value zero when turned off or $\pm f_{JET}$ when on depending on its direction in the figure.

3. Compute $\{X_j^A\}$, the vector to the j th jet in the control analysis notation. If $r_{i,k}$ is the k th component of $\{r_i\}$, $\{X_j^A\}$ is given by the following table:

	$\{X_j^A\}$		
	Component 1	Component 2	Component 3
1-4	-XJ1	0	$r_{1,3}$
5-8	-XJ1	0	$r_{5,3}$
9-12	XJ1	0	$r_{5,3}$
13-16	XJ1	0	$r_{1,3}$

4. Compute the moment of inertia $[I]$ of the entire undeformed Space Station about its center of mass. This is done by evaluating the following equations in succession. The Phase II notation is used; in particular, the quantities computed in Equations (A29) and (A36) of Appendix C are used. D_{Lij} and D_{Cij} are the ij components of $[D_L]$ and $[D_C]$, respectively.

$$\{\mathbf{r}_c\} = \frac{1}{M_L} \begin{Bmatrix} D_{L32} \\ D_{L13} \\ D_{L21} \end{Bmatrix}, \quad \{\bar{\mathbf{r}}_c\} = \frac{1}{M_c} \begin{Bmatrix} D_{c32} \\ D_{c13} \\ D_{c21} \end{Bmatrix}$$

$$\{\mathbf{r}_{ss}\} = \frac{1}{M_L + M_c} (M_L \{\mathbf{r}_c\} + M_c [\pi(\eta_0)] (\{\bar{\mathbf{r}}_0\} + \{\bar{\mathbf{r}}_c\}))$$

$$[I] = [I_L] + [I_c] + M_L ([\Gamma(\mathbf{r}_c)]^2 - [\Gamma(\mathbf{r}_c - \mathbf{r}_{ss})]^2) \\ + M_c ([\Gamma(\bar{\mathbf{r}}_c)]^2 - [\Gamma(\{\bar{\mathbf{r}}_0\} + \{\bar{\mathbf{r}}_c\} - [\pi(\eta_0)]\{\mathbf{r}_{ss}\})]^2)$$

All of the required input for Subroutine ATTCTR is now available.

Input to Subroutine ATTCTR

<u>Symbol</u>		
Phase II	Control	
<u>Analysis</u>	<u>Analysis</u>	
$\{\gamma_{is}\}$	$\{\theta\}$	Euler angles of sensor
$\{\dot{\gamma}_{is}\}$	$\{\dot{\theta}\}$	
	$e_{\theta DB}$	error in θ_1 , dead band
	$\dot{e}_{\theta MAX}$	error rate, $\dot{\theta}_1$, maximum magnitude (used for switching curves)
	$\{X^A_j\}$	locations of points A_j in X axes
$[I]$	$[M_{11}]$	moment of inertia matrix for vehicle (lab + counter-weight + 2 masses in lab)
	f_{JET}	force exerted by jet (each jet is the same)
	ω_{1CMAG}	magnitude of spin rate command

Output of Subroutine ATTCTR

$\{f^A_j\}$	forces exerted at points A^j in lab (due to jets)
-------------	---

Computation Procedure in ATTCTR

Control analysis symbols are used.

If $\omega_{1CMAG} \neq 0.$, go to END

$$\{f^{A_j}\} = [0 \quad 0 \quad 0]^T \text{ for all points } A_j$$

$$acc_{\theta_s}(1) = f_{JET} (X^{A_j}(3,13) - X^{A_j}(3,10)) / M_{11}(1,1)$$

$$acc_{\theta_s}(2) = f_{JET} (X^{A_j}(3,4) - X^{A_j}(3,12)) / M_{11}(2,2)$$

$$acc_{\theta_s}(3) = f_{JET} (X^{A_j}(1,15) - X^{A_j}(1,1)) / M_{11}(3,3)$$

$$\{e_{\theta}\} = \{0\}$$

$$\{\dot{e}_{\theta}\} = \{\dot{0}\}$$

Call Subroutine POSCTR

(Arguments:

$$e_{\theta}(j), e_{\theta DB}, \dot{e}_{\theta}(j),$$

$$\dot{e}_{\theta MAX}, acc_{\theta_s}(j), acc_{\theta}(j))$$

Axis 1

$$\text{If } acc_{\theta}(1) < 0. \rightarrow f^{A_j}(2, 14) = f_{JET}$$

$$f^{A_j}(2, 9) = -f_{JET}$$

$$= 0. \rightarrow \text{go to next axis}$$

$$> 0. \rightarrow f^{A_j}(2, 13) = -f_{JET}$$

$$f^{A_j}(2, 10) = f_{JET}$$

Axis 2

$$\text{If } acc_{\theta}(2) < 0. \rightarrow f^{A_j}(1, 16) = -f_{JET}$$

$$f^{A_j}(1, 8) = f_{JET}$$

$$= 0. \rightarrow \text{go to next axis}$$

$$> 0. \rightarrow f^{A_j}(1, 4) = f_{JET}$$

$$f^{A_j}(1, 12) = -f_{JET}$$

Axis 3

$$\text{If } acc_{\theta}(3) < 0. \rightarrow f^{A_j}(2, 11) = -f_{JET}$$

$$f^{A_j}(2, 6) = f_{JET}$$

$$= 0. \rightarrow \text{go to End}$$

$$> 0. \rightarrow f^{A_j}(2, 15) = f_{JET}$$

$$f^{A_j}(2, 1) = -f_{JET}$$

End

H11 CONTROL ROUTINE SPNCTR (Spin Control)

This subroutine is used to control the spin speed of the Space Station. The spin speed of the sensor mass $\{\omega^{is}\}$ is computed in the main program along with the angular velocity of every other mass point. (See Equation (4) of Appendix C). Based on the actual and commanded spin speeds, subroutine SPNCTR computes the jet thrusts. The resulting jet loads on the Space Station $\{f_C^1\}$, $\{\tau_C^1\}$, $\{f_C^5\}$, and $\{\tau_C^5\}$ are computed in Subroutine CONTROL using the equations listed in Appendix H9.

Input Data Read in by Subroutine CONTROL

$e_{\omega LDB}$ (defined below)

Input to Subroutine SPNCTR (1)

ω_{1C} spin rate command (lab axis 1)
 $\{\omega\}$ angular velocity vector of lab (2)
 $e_{\omega LDB}$ error in spin rate, dead band
 f_{JET} thrust of each jet (each jet is the same)
 ω_{1CMAG} magnitude of spin rate command

Output of Subroutine (1)

$e_{\omega 1}$ error, spin rate - spin rate command (3)
 $\{f_{Aj}^A\}$ forces exerted at points A^j in lab (due to jets)

Computation Procedure (1)

If $\omega_{1CMAG} = 0.$, go to End
 $\neq 0.$, continue

$$e_{\omega 1} = \omega_1 - \omega_{1C}$$

Call Subroutine VELCTR

(arguments $e_{\omega 1}$, $e_{\omega LDB}$, acc_{N01})

-
- (1) Control analysis symbols are used.
 - (2) $\{\omega^{is}\}$ is input in the flexible body analysis
 - (3) Output only in control analysis version of subroutine

If $acc_{NO1} < 0.$

$$\rightarrow f^{A_j}(2,14) = f_{JET}$$

$$f^{A_j}(2,9) = -f_{JET}$$

$$f^{A_j}(2,2) = f_{JET}$$

$$f^{A_j}(2,5) = -f_{JET}$$

$= 0.$

\rightarrow go to End

$> 0.$

$$\rightarrow f^{A_j}(2,13) = -f_{JET}$$

$$f^{A_j}(2,10) = f_{JET}$$

$$f^{A_j}(2,3) = -f_{JET}$$

$$f^{A_j}(2,7) = f_{JET}$$

End

H12 CONTROL ROUTINE WBLCTR (Wobble Control)

This subroutine is used to control wobble in the rotating Space Station. It is assumed that the CMG is located on mass number i_s , the same mass which contains the sensor package. The output of the subroutine is the torque on this mass. Intermediate terms required to interface the Phase II program with subroutine WBLCTR are computed in subroutine CONTROL. The procedure for computing [I] has already been documented in Appendix H9. CONTROL also reads the following data used in WBLCTR. The terms are defined in the table describing the input to WBLCTR which appears on a subsequent page.

Input Data Read in by Subroutine CONTROL

β_G and $\dot{\beta}_G$ at $t = 0$, K_t , tq_{LIM} , K_β , mom_{CMG} , $I_{\beta GIM}$

Additional Integration Required in Main Program

$\dot{\beta}_G$, $\ddot{\beta}_G$, err_{KT} , and err_{LL} are parameters generated in WBLCTR that require integration. This integration is performed in the Phase II program together with all other quantities that are integrated. The initial conditions for $\dot{\beta}_G$ and $\ddot{\beta}_G$ are input data whereas the initial conditions for err_{KT} and err_{LL} are established in WBLCTR.

Computation Procedure for Subroutine CONTROL to Interface Phase II

Simulation with WBLCTR

Compute angular acceleration of sensor mass.

$$\{\ddot{\omega}^{X_i s}\} = ([1] - [\Gamma(\theta_{i_s})])\{\dot{\omega}^X\} + \{\ddot{\theta}_{i_s}\} - [\Gamma(\dot{\theta}_{i_s})]\{\omega^X\}$$

Input to Subroutine WBLCTR

<u>Symbol</u>		
Phase II	Control	
<u>Analysis</u>	<u>Analysis</u>	
$\{\omega^{X^i}_s\}$	$\{\omega\}$	angular velocity of sensor projected onto \tilde{X} axes
$[I]$	$[M_{11}]$	moment of inertia for vehicle (lab + counterweight + 2 masses in lab)
β_G	β	gimbal angle, CMG, reference axis is lab axis 3, positive counterclockwise
$\dot{\beta}_G$	$\dot{\beta}$	gimbal angle rate, CMG
	K_T	constant, multiplies error err_β or $\text{err}_{\dot{\beta}}$
	tg_{LIM}	torque limit of CMG torquer motor
	$K_{\dot{\beta}}$	constant, multiplies $\dot{\beta}$ to give tg_{FDBK}
	err_{KT}	error err_β or $\text{err}_{\dot{\beta}}$ multiplied by K_T
	err_{KTI}	integral of err_{KT}
	err_{LL}	output of lead-lag, $\frac{1 + as}{s}$, gimbal-angle or gimbal-angle rate-control loop
	err_{LLI}	integral of err_{LL}
$\{\dot{\omega}^{X^i}_s\}$	$\{\dot{\omega}\}$	angular acceleration of sensor
t	time	time
	mom_{CMG}	momentum of CMG
	$I_{\beta\text{GIM}}$	inertia of CMG gimbal about vehicle spin axis
	ω_{ICMAG}	magnitude of spin rate command
	i_s	index number of mass containing sensor

Output of Subroutine WBLCTR

<u>Symbol</u>	
Phase II	Control
<u>Analysis</u>	<u>Analysis</u>
n_{CMG}	1 - indicates CMG torque is being applied to vehicle 0 - indicates CMG torque is not being applied to vehicle
$\ddot{\beta}_G$	$\ddot{\beta}$ acceleration of CMG gimbal relative to vehicle
$\{\tau_{CMG}^i\}$	$\{t_j^A\}$ torque applied at point A_j in lab (from CMG)

Computation Procedure for Subroutine WBLCTR

Control analysis symbols are used.

time1 = time

If time = 0. $\rightarrow \dot{\beta}_{MAX} = t_{g_LIM} / K_{\dot{\beta}}$

LEAD = $10 I_{\beta GIM} / K_{\dot{\beta}}$

$\beta_{DES} = 0.$

$n_{CMG} = 0$

$err_{KTI} = 0.$

$err_{LLI} = K_{\dot{\beta}} \ddot{\beta}$

time1 = -0.025

$\neq 0. \rightarrow$ continue

$$\text{If } \omega_{\text{CMG}} < 0.02 \text{ rad/sec} \rightarrow \ddot{\beta} = 0.$$

$$\{t^{Aj}\} = [0 \ 0 \ 0]^T$$

go to End

$$> 0.02 \text{ rad/sec} \rightarrow \text{continue}$$

$$\mu = \sqrt{(M_{11}(1,1) - M_{11}(3,3))(M_{11}(1,1) - M_{11}(2,2)) / M_{11}(2,2) M_{11}(3,3)}$$

$$\text{SWITCH} = \pi \left(1 - (\mu \omega_1 / \dot{\beta}_{\text{MAX}}) \right)$$

$$\text{If } (\omega_3 = 0. \text{ and } \omega_2 = 0.) \rightarrow \omega_{23} = 0.$$

$$\text{otherwise} \rightarrow \omega_{23} = \tan^{-1}(\omega_3 / \omega_2)$$

$$e_1 = (1/2) \left[M_{11}(2,2) \omega_2^2 + \frac{(M_{11}(1,1) - M_{11}(3,3)) M_{11}(3,3) \omega_3^2}{(M_{11}(1,1) - M_{11}(2,2))} \right]$$

$$e_2 = \text{mom}_{\text{CMG}} \omega_1$$

$$e_3 = 10 e_1 / e_2$$

$$\text{If } \beta < 0. \rightarrow \beta = \beta + 2\pi$$

$$> 0. \rightarrow \text{continue}$$

$$\beta_{DE} = \omega_{23} - (\pi/2)$$

$$\text{If } \beta_{DE} < 0. \rightarrow \beta_{DE} = \beta_{DE} + 2\pi$$

$$> 0. \rightarrow \text{continue}$$

If $n_{CMG} = 1 \rightarrow$ go to ①
 $= 0 \rightarrow$ go to ②

① If $e_3 < 0.0001^*$ $\rightarrow n_{CMG} = 0$

$$err_{KTI} = 0.$$

$$err_{LLI} = K_{\dot{\beta}} \dot{\beta}$$

$$③ \quad err_{\dot{\beta}} = -\omega_1 - \dot{\beta}$$

$$err_{KT} = K_T err_{\dot{\beta}}$$

$$err_{LL} = err_{KTI} + (LEAD) err_{KT}$$

$$tq_{PASS} = mom_{CMG} (\omega_3 \cos \beta - \omega_2 \sin \beta)$$

$$tq_{KGIM} = err_{LLI} - tq_{PASS}$$

$$④ \quad \text{If } |tq_{KGIM}| \leq tq_{LIM} \rightarrow tq_{LGIM} = tq_{KGIM}$$

$$> tq_{LIM} \rightarrow tq_{LGIM} = \text{SIGN}(tq_{KGIM}) \cdot tq_{LIM}$$

$$tq_{FDBK} = K_{\dot{\beta}} \dot{\beta}$$

$$tq_{TGIM} = tq_{LGIM} - tq_{FDBK}$$

$$tq_{GIM} = tq_{TGIM} + tq_{PASS}$$

$$\ddot{\beta}_p = tq_{GIM} / I_{\beta GIM}$$

$$\ddot{\beta} = \ddot{\beta}_p - \ddot{\omega}_1$$

* This limit was changed to 0.001 for use with the Phase II program.
 The rigid-body runs of Section 5 were obtained using the smaller limit.

$$t^{Aj}(1) = \text{mom}_{\text{CMG}} (-\dot{\omega}_2 \sin \beta + \dot{\omega}_3 \cos \beta - \dot{I}_{\beta \text{GIM} 1} (\dot{\omega}_1 + \ddot{\beta}))$$

$$t^{Aj}(2) = \text{mom}_{\text{CMG}} (\sin \beta) (\dot{\beta} + \dot{\omega}_1) - \dot{I}_{\beta \text{GIM} 2} (\dot{\omega}_2 + \dot{\omega}_3 \dot{\beta})$$

$$t^{Aj}(3) = -\text{mom}_{\text{CMG}} (\cos \beta) (\dot{\beta} + \dot{\omega}_1) - \dot{I}_{\beta \text{GIM} 3} (\dot{\omega}_3 - \dot{\omega}_2 \dot{\beta})$$

End

$$> 0.0001^* \rightarrow (5) \beta_{\text{DES}} = \beta_{\text{DE}}$$

$$\text{err}_{\beta} = \beta_{\text{DES}} - \beta$$

$$\text{If } \text{err}_{\beta} < 0. \rightarrow \text{err}_{\beta} = \text{err}_{\beta} + 2\pi$$

$$= 0. \rightarrow \text{go to } (6)$$

$$> 0. \rightarrow \text{continue}$$

$$\text{If } \text{err}_{\beta} \leq \text{SWITCH} \rightarrow \text{continue}$$

$$> \text{SWITCH} \rightarrow \text{err}_{\beta} = \text{err}_{\beta} - 2\pi$$

$$(6) \text{err}_F = \text{err}_{\beta}$$

$$t_{\text{PASS}} = \text{mom}_{\text{CMG}} (\dot{\omega}_3 \cos \beta - \dot{\omega}_2 \sin \beta)$$

$$\text{err}_{\text{KT}} = k_T \text{err}_F$$

$$\text{err}_{\text{LL}} = \text{err}_{\text{KTI}} + (\text{LEAD}) \text{err}_{\text{KT}}$$

$$t_{\text{KGIM}} = \text{err}_{\text{LL}} - t_{\text{PASS}}$$

$$\text{go to } (4)$$

* This limit was changed to 0.001 for use with the Phase II Program. The rigid-body runs of Section 5 were obtained using the smaller limit.

(2) If $e_3 < 0.001^*$ \rightarrow go to (3)

$> 0.001^*$ \rightarrow $SPCASE = 2\mu\omega_1(\text{time} - \text{time}_1)$

If $\beta_{DE} \leq SPCASE \rightarrow \beta_{DE} = \beta_{DE} + 2\pi$

$> SPCASE \rightarrow$ continue

If $\beta_{DE} \leq \beta \rightarrow$ go to (3)

$> \beta \rightarrow$ continue

$$n_{CMG} = 1$$

$$err_{KTI} = K_{\beta} \dot{\beta}$$

go to (5)

* This limit was changed to 0.01 for use with the Phase II program.
The rigid-body runs of Section 5 were obtained using the smaller limit.

H13 CONTROL ROUTINE BMCTR (Balance Mass Control)

This subroutine is used to control the motion of the balance mass. Since the original control system did not function on the flexible idealization, the final control system developed for the Phase II program differs from the control system for the rigid-body runs of Section 5. For completeness, both control systems are treated herein. For the flexible-body work, subroutine BMCON was prepared to interface the Phase II program with BMCTR. The input data is listed below. The definition of the symbols used (except for $\{X_A^{is}\}$) is given in the table of subroutine input which appears on a subsequent page. $\{X_A^{is}\}$ is the location of the accelerometer in the local \underline{X} axes.

Input Data Read in by Subroutine BMCON for Phase II Control System

$\{U_2\}$ and \dot{U}_{23} the third component of $\{U_2\}$ at $t = 0$, μ_{1EST} , K_{eXSE} , K_{DESE} , τ_{BAL} , ω_{1CBAL} , $\{X_A^{is}\}$, $\{X_{SENS/CM}^{CMND}\}$

Additional Integration Required in Main Program

\dot{U}_{23} and \ddot{U}_{23} must be integrated. This integration is performed in the Phase II program together with all other quantities that are integrated.

Computation Procedure for Subroutine BMCON

Phase II symbols are used. First compute the inertial acceleration of the accelerometer in the local axes of the mass containing the sensor, the \underline{X}^{is} axes.

$$\begin{aligned} \{\ddot{X}^{SENS}\} = & ([I] - [\Gamma(\theta_{is})]) \left(\{\ddot{R}\}^* + \{\ddot{q}_{is}\}^* + 2[\Gamma(\omega^X)] \{\dot{R}_{is}\} \right. \\ & + [\Gamma(\omega^X)]^2 \{R_{is}\} - [\Gamma(R_{is})] \{\dot{\omega}^X\}^* \left. \right) + [\Gamma(\omega^{X^{is}})]^2 \{X_A^{is}\} \\ & - [\Gamma(X_A^{is})] \{\dot{\omega}^{X^{is}}\}^* \end{aligned}$$

* Terms marked with an asterisk are evaluated one numerical-integration cycle back. At $t=0$, these terms are zero.

Next compute the vector from the center of mass of the Space Station to the accelerometer in the \underline{X} axis system.

$$\{X_{\text{SENS/CM}}\} = \{R_{i_s}\} + [I] + [\Gamma(\theta_{i_s})] \{X_A^i\} - [\Pi(\gamma)] \{ZCM\}$$

where $\{ZCM\}$ is given by Equation (A27b) of Appendix C. In order to evaluate the performance of the control system, compute and plot the third component of

$$\{X_{\text{SENS/CM}}^{\text{CMND}}\} - \{X_{\text{SENS/CM}}\}$$

The total mass of the system is

$$M = M_L + M_C + \sum_{\substack{\text{moving} \\ \text{masses}}} \mu_j + \sum_{\text{fluid}} m_i^f$$

M was already computed as the denominator for Equation (A27b) of Appendix C. The first two components of $\{U_2\}$ are constant and are maintained at their initial values. The position and velocity of the balance mass vector are

$$\{U_2\} = \begin{Bmatrix} U_{21} \\ U_{22} \\ U_{23} \end{Bmatrix}, \quad \{\dot{U}_2\} = \begin{Bmatrix} 0 \\ 0 \\ \dot{U}_{23} \end{Bmatrix}$$

where U_{23} and \dot{U}_{23} are obtained from integration.

Input to Subroutine BMCTR

<u>Symbol</u>		
Phase II	Control	
<u>Analysis</u>	<u>Analysis</u>	
	$\{X^B\}$	position of counterweight relative to the lab ⁽¹⁾
$\{\dot{l}_o\}$	$\{\dot{X}^B\}$	velocity of counterweight relative to the lab
$\{\omega^{X^i s}\}$	$\{\dot{\omega}\}$	angular acceleration of lab about lab X axes
	$\{X^{SENS}\}$	position of acclerometer sensor relative to lab ⁽¹⁾
	M	mass of system
	M_B	mass of counterweight ⁽¹⁾
μ_i	m_i	mass of i^{th} moving point mass in lab ($i=1, 2$)
	$\{X^{(i)}\}$	position of i^{th} moving mass in lab ($i=1,2$) ⁽¹⁾
$[\Gamma(\omega^{X^i s})]$	$[\Gamma(\dot{\omega})]$	$\begin{bmatrix} 0 & -\dot{\omega}_3 & \dot{\omega}_2 \\ \dot{\omega}_3 & 0 & -\dot{\omega}_1 \\ -\dot{\omega}_2 & \dot{\omega}_1 & 0 \end{bmatrix}, \begin{bmatrix} 0 & -\omega_3 & \omega_2 \\ \omega_3 & 0 & -\omega_1 \\ -\omega_2 & \omega_1 & 0 \end{bmatrix}$
$[\Gamma(\omega^{X^i s})]$	$[\Gamma(\omega)]$	
$\{\dot{U}_i\}$	$\{\dot{X}^{(i)}\}$	velocity of i^{th} mass relative to lab
μ_{LEST}	m_{LEST}	estimate of mass in mass 1
	K_{eXSE}	constant multiplying error between accelerations commanded and sensed
K_{DESE}		constant multiplying balance mass velocity ⁽²⁾

(1) Used only in rigid-body (control analysis) version of subroutine.

(2) Used only in flexible-body (Phase II analysis) version of subroutine.

Input to Subroutine BMCTR (Continued)

<u>Symbol</u>		
Phase II	Control	
<u>Analysis</u>	<u>Analysis</u>	
τ_{BAL}		time constant of filter used to filter accelerometer error; set to zero to bypass filter(2)
ω_{LMAG}		magnitude of spin speed
ω_{LCBAL}		magnitude of minimum commanded spin speed at which balance mass control system will operate(2)
	e_{XDB}	error tolerance in mass 2 (balance mass) velocity (actual minus commanded velocity) (1)
	acc_{X23}	magnitude of non-zero acceleration for mass 2 (balance mass) (1)
	ω_{LCMAG}	magnitude of spin rate command
$\{X_{SENS/CM}^{CMND}\}$		commanded vector from center of mass of Space Station to sensor in \underline{X} axes (2)
$\{\ddot{X}^{SENS}\}$		inertial acceleration of sensor in \underline{X} axes
$\{\ddot{U}_1\}$	$\{\ddot{X}^{(1)}\}$	acceleration of elevator

(1) Used only in rigid-body (control analysis) version of subroutine.

(2) Used only in flexible-body (Phase II analysis) version of subroutine

Output of Subroutine BMCTR

<u>Symbol</u>	
Phase II	Control
<u>Analysis</u>	<u>Analysis</u>
$\{X^C\}$	position of vehicle center of mass (lab + counterweight + 2 moving parts) (1)
$\{\ddot{X}^{SENS}\}$	acceleration at sensor (accelerometer) location (1)
$\{X^{CMND}\}$	position of vehicle c.m., commanded (1)
$\{\ddot{X}^{CMND}\}$	acceleration commanded at sensor (accelerometer) location (1)
$err_{\ddot{X}}$	error in acceleration, $err_{\ddot{X}} = \ddot{X}^{CMND}(3) - \ddot{X}^{SENS}(3)$
$\{\ddot{U}_2\}$	$\{\ddot{X}^{(2)}\}$ acceleration of mass 2

 (1) Used only in rigid-body (control analysis) version of subroutine.

Computation Procedure for Subroutine BMCTR

If time = 0. $\rightarrow \ddot{X}^{CMD}(3) = 0.$

$$\ddot{X}^{SENS}(3) = 0.$$

$$\dot{e}_{FILT} = 0$$

$$err_{\ddot{X}} = 0.$$

$$\{X^{CMD}\} = [0 \ 0 \ 0]^T$$

$$\{X^C\} = [0 \ 0 \ 0]^T$$

$\neq 0. \rightarrow \text{continue}$

If $\ddot{X}^B(3) \neq 0. \rightarrow \ddot{X}(3,2) = 0., \dot{X}(3,2)=0,$

$$\dot{e}_{FILT} = 0, \text{ go to end}$$

$= 0. \rightarrow \text{continue}$

$> 0. \rightarrow \ddot{X}(3,2) = 0., \text{ go to End}$

If $\omega_{1CMAG} < \omega_{1CBAL} \rightarrow \ddot{X}(3,2) = 0., \text{ go to End}$

$\geq \omega_{1CBAL} \rightarrow \text{continue}$

The following equations are used only in the control analysis version of the subroutine:

$$\{X^C\} = (1/M)(M_B \{X^B\} + \sum_{i=1}^2 m_i \{X^{(i)}\})$$

$$\begin{aligned} \{\ddot{X}^{SENS}\} = & \{\dot{\omega}\} X(\{X^{SENS}\} - \{X^C\}) \\ & + \{\omega\} X[\{\omega\} X(\{X^{SENS}\} - \{X^C\})] \\ & - (1/M) \sum_{j=1}^2 m_j \{\ddot{X}^{(j)}\} \end{aligned}$$

$$\{X^{CMND}\} = (1/M)(M_B \{X^B\})$$

$$\begin{aligned} \{\ddot{X}^{CMND}\} &= \{\dot{\omega}\}X(\{X^{SENS}\} - \{X^{CMND}\}) \\ &\quad + \{\omega\}X[\{\omega\}X(\{X^{SENS}\} - \{X^{CMND}\})] \\ &\quad - (1/M)(m_{1EST}\{\ddot{X}^{(1)}\} + m_2\{\ddot{X}^{(2)}\}) \end{aligned}$$

$$err_{\ddot{X}} = \ddot{X}^{CMND}(3) - \ddot{X}^{SENS}(3)$$

$$\dot{X}_{23C} = k_{exse} err_{\ddot{X}}$$

$$e_{\dot{X}_{23}} = \dot{X}(3,2) - \dot{X}_{23C}$$

Call Subroutine VELCTR

(arguments $e_{\dot{X}_{23}}$, $e_{\dot{X}_{DB}}$, acc_{NX2})

$$\ddot{X}^{(i)}(3,2) = acc_{NX2} acc_{X23}$$

End

End of control analysis version of subroutine.

The following equations are used only in the Phase II analysis version of the subroutine:

$$\{\ddot{X}^{CMND}\} = ([\Gamma(\dot{\omega}^{i_A})]^* + [\Gamma(\omega^{i_A})]^2) \{X_{SENS/CM}^{CMND}\} \\ - \frac{1}{M} (\mu_{1EST} \{\ddot{U}_1\} + \mu_2 \{\ddot{U}_2\}^*)$$

$$err_{\ddot{X}} = \ddot{X}^{CMND}(3) - \ddot{X}^{SENS}(3)$$

$$\text{if } \tau_{BAL} = 0, \quad e_{FILT} = err_{\ddot{X}}$$

$$\text{if } \tau_{BAL} \neq 0,$$

$$\dot{e}_{FILT} = \frac{err_{\ddot{X}} - e_{FILT}}{\tau_{BAL}} \quad (\text{initially } e_{FILT} = 0)$$

$$\ddot{X}^{(u)}(3, 2) = -K_{DESE} \dot{X}^{(u)}(3, 2) + K_{EXSE} e_{FILT}$$

End

* Terms marked with an asterisk are evaluated at the previous numerical-integration cycle. At $t = 0$, these terms are set to zero.

APPENDIX I
SYNTHESIZED MODES OF THE LABORATORY

The modes of the Laboratory were synthesized using the Phase I Computer program. The configuration is shown in Figure 6.1, and the properties of each substructure are presented in Appendix F. Table I1 presents the correspondence between the mass-point numbers used for the total structure with the numbers for the substructures. The number of substructure modes used in the synthesis were as follows:

- 30 modes were used for the core module
- 10 modes were used for each appendage
- 12 modes were used for each solar panel

Table I2 presents the synthesized modes of the Laboratory. These modes have been normalized so that each modal mass is unity.

TABLE II
CORRESPONDENCE BETWEEN MASS POINT NUMBERS

Module 1 Core Module		Module 4 Solar Panel		Module 5 Solar Panel	
Substructure	Total Structure	Substructure	Total Structure	Substructure	Total Structure
1	1 2*	1	17	1	45
2	3	2	18	2	46
3	4	3	19	3	47
4	5	4	20	4	48
5	6	5	21	5	49
6	7	6	22	6	50
7	8	7	23	7	51
Module 2 Appendage		8	24	8	52
		9	25	9	53
		10	26	10	54
		11	27	11	55
Substructure	Total Structure	12	28	12	56
		13	29	13	57
1	9	14	30	14	58
2	10	15	31	15	59
3	11	16	32	16	60
4	12	17	33	17	61
Module 3 Appendage		18	34	18	62
		19	35	19	63
		20	36	20	64
		21	37	21	65
Substructure	Total Structure	22	38	22	66
		23	39	23	67
1	13	24	40	24	68
2	14	25	41	25	69
3	15	26	42	26	70
4	16	27	43	27	71
		28	44	28	72

* Mass-point 2 of the total structure was artificially introduced to serve as the connection point for Modules 2 and 3.

TABLE I2
SYNTHESIZED LABORATORY MODES

MODE 1 Frequency = .198874 Hz

MASS NO.	Q(1)	Q(2)	Q(3)	THETA(1)	THETA(2)	THETA(3)
1	0.1121169E-05	0.1954213E-09	0.4337425E-12	0.7004969E-15	0.3147705E-08	0.9416044E-06
2	0.9322054E-06	0.2018765E-09	0.4339812E-12	0.3386863E-13	0.3147599E-08	0.9415951E-06
3	0.7426529E-06	0.2130753E-09	0.5264435E-12	-0.4956326E-13	0.3147065E-08	0.9379352E-06
4	0.3637018E-06	0.2325329E-09	-0.5973097E-13	-0.4635154E-12	0.3143456E-08	0.9305915E-06
5	-0.1478269E-07	0.1208256E-09	0.1350842E-11	-0.8471206E-12	0.3135952E-08	0.9232268E-06
6	-0.2036755E-06	0.1190724E-10	0.2783560E-12	-0.1100793E-11	0.3127211E-08	0.9171530E-06
7	-0.8817460E-06	-0.6813434E-09	0.2783560E-12	-0.1513308E-11	0.2969388E-08	0.8546469E-06
8	-0.1515587E-05	-0.7928840E-09	0.2783560E-12	0.3852099E-11	0.2727572E-08	0.7920815E-06
9	0.1252471E-03	0.2018723E-09	-0.3595260E-11	0.3035956E-13	0.3147638E-08	0.9418990E-06
10	0.2383125E-03	0.2018663E-09	-0.7601153E-11	0.2641633E-13	0.3147679E-08	0.9421519E-06
11	0.3513941E-03	0.2018615E-09	-0.9462971E-11	0.2465237E-13	0.3147710E-08	0.9422759E-06
12	0.4644787E-03	0.2018589E-09	-0.1237754E-10	0.2407537E-13	0.3147727E-08	0.9423104E-06
13	-0.1233825E-03	0.2018735E-09	0.4433343E-11	0.3001926E-13	0.3147638E-08	0.9418974E-06
14	-0.2364476E-03	0.2018694E-09	0.9545384E-11	0.2766902E-13	0.3147679E-08	0.9421493E-06
15	-0.3495289E-03	0.2018665E-09	0.1042751E-10	0.2623732E-13	0.3147710E-08	0.9422728E-06
16	-0.4626138E-03	0.2018650E-09	0.1245567E-10	0.2589607E-13	0.3147727E-08	0.9423072E-06
17	-0.5705474E 00	-0.2610889E-09	-0.1111123E-07	0.3852099E-11	0.2727572E-08	0.7920815E-06
18	0.5628632E 00	-0.1387681E-08	-0.1109822E-07	0.3852099E-11	0.2727572E-08	0.7920815E-06
19	-0.2575750E 00	-0.5501979E-09	-0.1110880E-07	0.3852099E-11	0.2727572E-08	0.7920815E-06
20	0.2505915E 00	-0.1060013E-08	-0.1110297E-07	0.3852786E-11	0.2727572E-08	0.7920815E-06
21	-0.7484553E 00	-0.2413478E-09	-0.1079089E-07	0.3852099E-11	0.2727572E-08	0.7920815E-06
22	0.7390767E 00	-0.1397707E-08	-0.1078178E-07	0.3852099E-11	0.2727572E-08	0.7920815E-06
23	-0.3374288E 00	-0.5422165E-09	-0.1078909E-07	0.3852099E-11	0.2727572E-08	0.7920815E-06
24	0.3289275E 00	-0.1064877E-08	-0.1078502E-07	0.3852099E-11	0.2727572E-08	0.7920815E-06
25	-0.3092003E 00	-0.2744458E-09	-0.7364395E-08	0.3852099E-11	0.2727572E-08	0.7920815E-06
26	0.3043393E 00	-0.1370801E-08	-0.7353421E-08	0.3852099E-11	0.2727572E-08	0.7920815E-06
27	-0.1395519E 00	-0.5559579E-09	-0.7362459E-08	0.3852099E-11	0.2727572E-08	0.7920815E-06
28	0.1356097E 00	-0.1052690E-08	-0.7357542E-08	0.3852099E-11	0.2727572E-08	0.7920815E-06
29	-0.8169122E 00	-0.2163440E-09	-0.6046765E-08	0.4349314E-11	0.6222934E-02	0.7920815E-06
30	0.8072077E 00	-0.1401911E-08	-0.6046765E-08	0.4640258E-11	0.6222919E-02	0.7920815E-06
31	-0.3688650E 00	-0.5323748E-09	-0.6046641E-08	0.4461886E-11	0.6222680E-02	0.7920815E-06
32	0.3591609E 00	-0.1067610E-08	-0.6046641E-08	0.4641235E-11	0.6222680E-02	0.7920815E-06
33	-0.2638019E-02	-0.2817644E-09	-0.2377443E-09	0.3817426E-11	0.2153270E-04	0.7920815E-06
34	0.1308196E-02	-0.1347505E-08	-0.2349780E-09	0.4085564E-11	0.3233210E-05	0.7920815E-06
35	-0.1122383E-02	-0.5596537E-09	-0.2373768E-09	0.3931231E-11	0.2017448E-04	0.7920815E-06
36	0.7968415E-03	-0.1043104E-08	-0.2361369E-09	0.4302072E-11	0.1098139E-04	0.7920815E-06
37	-0.4851837E-02	-0.7953604E-09	-0.6046530E-08	0.4645661E-11	0.6222118E-02	-0.6268554E-05
38	-0.7820301E-02	0.6253285E-09	-0.2386258E-09	0.3800192E-11	0.2182665E-04	0.7920815E-06
39	0.4701565E-04	-0.2215364E-08	-0.2308061E-09	0.3413964E-11	-0.9548537E-05	0.7920815E-06
40	-0.2437137E-04	-0.7931944E-09	-0.2339969E-09	0.4167668E-11	0.1699060E-04	-0.1532101E-05
41	-0.3292012E-02	-0.7948278E-09	-0.4722377E-08	0.5841124E-11	0.4670851E-02	-0.6032360E-05
42	0.7989381E-05	-0.7928840E-09	-0.4605577E-10	0.3852099E-11	0.2727572E-08	0.7920815E-06
43	-0.7080385E-03	-0.7937426E-09	-0.1549498E-08	0.6014625E-11	0.1568278E-02	-0.3764398E-05
44	-0.1858219E-02	-0.7942880E-09	-0.3150762E-08	0.6475461E-11	0.3119563E-02	-0.5241245E-05
45	0.5712085E 00	-0.2595075E-09	0.1115218E-07	0.3852099E-11	0.2727572E-08	0.7920815E-06
46	-0.5636138E 00	-0.1387680E-08	0.1113911E-07	0.3852099E-11	0.2727572E-08	0.7920815E-06
47	0.2578463E 00	-0.5494942E-09	0.1114974E-07	0.3852099E-11	0.2727572E-08	0.7920815E-06
48	-0.2509531E 00	-0.1060156E-08	0.1114389E-07	0.3851116E-11	0.2727572E-08	0.7920815E-06
49	0.7493244E 00	-0.2399239E-09	0.1071216E-07	0.3852099E-11	0.2727572E-08	0.7920815E-06
50	-0.7400609E 00	-0.1397805E-08	0.1070315E-07	0.3852099E-11	0.2727572E-08	0.7920815E-06
51	0.3382864E 00	-0.5416072E-09	0.1071038E-07	0.3852099E-11	0.2727572E-08	0.7920815E-06
52	-0.3294007E 00	-0.1065008E-08	0.1070635E-07	0.3852099E-11	0.2727572E-08	0.7920815E-06
53	0.3095565E 00	-0.2728995E-09	0.7291728E-08	0.3852099E-11	0.2727572E-08	0.7920815E-06
54	-0.3047465E 00	-0.1370859E-08	0.7280875E-08	0.3852099E-11	0.2727572E-08	0.7920815E-06
55	0.1396971E 00	-0.5552308E-09	0.7289810E-08	0.3852099E-11	0.2727572E-08	0.7920815E-06
56	-0.1358069E 00	-0.1052900E-08	0.7284946E-08	0.3852099E-11	0.2727572E-08	0.7920815E-06
57	0.8178622E 00	-0.2152410E-09	0.6104191E-08	0.4358906E-11	-0.6230686E-02	0.7920815E-06
58	-0.8082812E 00	-0.1402239E-08	0.6104191E-08	0.4642143E-11	-0.6230575E-02	0.7920815E-06
59	0.3692568E 00	-0.5319205E-09	0.6104067E-08	0.4469742E-11	-0.6230436E-02	0.7920815E-06
60	-0.3596764E 00	-0.1067773E-08	0.6104067E-08	0.4644342E-11	-0.6230436E-02	0.7920815E-06
61	0.2637165E-02	-0.2804343E-09	0.2384752E-09	0.3822711E-11	-0.2155211E-04	0.7920815E-06
62	-0.1312202E-02	-0.1347771E-08	0.2356300E-09	0.4083739E-11	-0.3231158E-05	0.7920815E-06
63	0.1120169E-02	-0.5589700E-09	0.2381009E-09	0.3942666E-11	-0.2019241E-04	0.7920815E-06
64	-0.8006557E-03	-0.1043427E-08	0.2368254E-09	0.4303667E-11	-0.1098875E-04	0.7920815E-06
65	0.4790053E-02	-0.7952925E-09	0.6103953E-08	0.4650649E-11	-0.6229874E-02	-0.6186246E-05
66	0.7824093E-02	0.6253285E-09	0.2393832E-09	0.3789184E-11	-0.2184621E-04	0.7920815E-06
67	-0.4803389E-04	-0.2215364E-08	0.2313400E-09	0.3413205E-11	0.9566300E-05	0.7920815E-06
68	0.2119922E-04	-0.7931862E-09	0.2377163E-09	0.4178433E-11	-0.1700500E-04	-0.1525756E-05
69	0.3250645E-02	-0.7947745E-09	0.4776613E-08	0.5872768E-11	-0.4676670E-02	-0.5954093E-05
70	-0.1102054E-04	-0.7928840E-09	0.4659419E-10	0.3852099E-11	0.2727572E-08	0.7920815E-06
71	0.6986093E-03	-0.7937193E-09	0.1565075E-08	0.6105845E-11	-0.1570227E-02	-0.3723002E-05
72	0.1835133E-02	-0.7942496E-09	0.3190050E-08	0.6559795E-11	-0.3123446E-02	-0.5176122E-05

TABLE I2 - SYNTHESIZED LABORATORY MODES (Continued)

MODE 2 Frequency = .198979 Hz

MASS NO.	Q(1)	Q(2)	Q(3)	THETA(1)	THETA(2)	THETA(3)
1	0.1791825E-02	-0.4205827E-09	-0.1008118E-09	0.1939374E-11	0.5034464E-05	-0.6207665E-09
2	0.1489587E-02	0.4246712E-09	-0.1007485E-09	-0.7436377E-12	0.5034334E-05	-0.6203356E-09
3	0.1186227E-02	0.1973176E-08	-0.1095788E-09	-0.3785834E-11	0.5033049E-05	-0.6186383E-09
4	0.5797613E-03	0.8989287E-09	-0.9045707E-10	-0.1145151E-10	0.5025281E-05	-0.6137493E-09
5	-0.2545207E-04	-0.5202700E-08	-0.9933553E-10	-0.1277346E-10	0.5010280E-05	-0.6090948E-09
6	-0.3272020E-03	-0.6474366E-08	-0.1085990E-09	-0.8142181E-11	0.4993463E-05	-0.6054106E-09
7	-0.1406009E-02	-0.1543033E-09	-0.1085990E-09	0.2109161E-10	0.4708405E-05	-0.5661152E-09
8	-0.2407280E-02	0.2278895E-08	-0.1085990E-09	0.2858368E-12	0.4298497E-05	-0.5255891E-09
9	0.1489617E-02	0.4246825E-09	-0.1592293E-11	-0.7421111E-12	0.5034398E-05	-0.5497010E-09
10	0.1489832E-02	0.4246989E-09	0.8834171E-10	-0.7437545E-12	0.5034466E-05	0.1451968E-08
11	0.1490093E-02	0.4247087E-09	0.1801703E-09	-0.7445744E-12	0.5034517E-05	0.1852621E-08
12	0.1490354E-02	0.4247134E-09	0.2648817E-09	-0.7461042E-12	0.5034544E-05	0.1952082E-08
13	0.1489780E-02	0.4246834E-09	-0.1999531E-09	-0.7427129E-12	0.5034398E-05	-0.1790684E-08
14	0.1490144E-02	0.4247012E-09	0.4290176E-09	-0.7448572E-12	0.5034466E-05	-0.2693235E-08
15	0.1490555E-02	0.4247114E-09	-0.3810479E-09	-0.7459193E-12	0.5034517E-05	-0.3094039E-08
16	0.1490964E-02	0.4247167E-09	-0.4693554E-09	-0.7475141E-12	0.5034544E-05	-0.3193546E-08
17	0.5293770E 00	0.2359543E-08	-0.1098767E-07	0.2858368E-12	0.4298497E-05	-0.5255891E-09
18	-0.6009079E 00	0.2174257E-08	-0.1097211E-07	0.2858368E-12	0.4298497E-05	-0.5255891E-09
19	0.2172709E 00	0.2317642E-08	-0.1098477E-07	0.2858368E-12	0.4298497E-05	-0.5255891E-09
20	-0.2894946E 00	0.2230276E-08	-0.1097780E-07	0.7185675E-13	0.4298497E-05	-0.5255891E-09
21	0.6959722E 00	0.2376330E-08	-0.8754920E-08	0.2858368E-12	0.4298497E-05	-0.5255891E-09
22	-0.7879210E 00	0.2160961E-08	-0.8744102E-08	0.2858368E-12	0.4298497E-05	-0.5255891E-09
23	0.2864765E 00	0.2325012E-08	-0.8752853E-08	0.2858368E-12	0.4298497E-05	-0.5255891E-09
24	-0.3787484E 00	0.2224032E-08	-0.8748017E-08	0.2858368E-12	0.4298497E-05	-0.5255891E-09
25	0.2852181E 00	0.2345070E-08	-0.7703747E-08	0.2858368E-12	0.4298497E-05	-0.5255891E-09
26	-0.3258844E 00	0.2189987E-08	-0.7691462E-08	0.2858368E-12	0.4298497E-05	-0.5255891E-09
27	0.1162641E 00	0.2311083E-08	-0.7701530E-08	0.2858368E-12	0.4298497E-05	-0.5255891E-09
28	-0.1578049E 00	0.2237387E-08	-0.7696013E-08	0.2858368E-12	0.4298497E-05	-0.5255891E-09
29	0.7607378E 00	0.2395018E-08	-0.1900517E-08	0.8283076E-12	-0.6208487E-02	-0.5255891E-09
30	-0.8596284E 00	0.2149741E-08	-0.1900517E-08	0.9327582E-12	-0.6208602E-02	-0.5255891E-09
31	0.3137305E 00	0.2333055E-08	-0.1900411E-08	0.9074131E-12	-0.6208260E-02	-0.5255891E-09
32	-0.4126130E 00	0.2218547E-08	-0.1900411E-08	0.9718042E-12	-0.6208353E-02	-0.5255891E-09
33	-0.6629308E-03	0.2332798E-08	-0.1316601E-09	0.3229650E-12	-0.1551583E-04	-0.5255891E-09
34	-0.3193425E-02	0.2207985E-08	-0.1294694E-09	0.4191374E-12	0.1581077E-05	-0.5255891E-09
35	-0.1751917E-02	0.2305287E-08	-0.1313346E-09	0.4324218E-12	-0.1437377E-04	-0.5255891E-09
36	-0.3036375E-02	0.2245289E-08	-0.1303525E-09	0.5654184E-12	-0.5933633E-05	-0.5255891E-09
37	-0.4943981E-01	0.2278025E-08	-0.1900314E-08	0.1038019E-11	-0.6207738E-02	-0.6589838E-04
38	0.3054013E-02	0.2386421E-08	-0.1323333E-09	0.1566842E-12	-0.1561908E-04	-0.5255891E-09
39	-0.8211650E-03	0.2172224E-08	-0.1261396E-09	0.1817519E-13	0.1413182E-04	-0.5255891E-09
40	-0.2520416E-02	0.2278784E-08	-0.1309708E-09	0.5183174E-12	-0.1156513E-04	-0.5090366E-05
41	-0.3310515E-01	0.2278212E-08	-0.1499605E-08	0.2021398E-11	-0.4658710E-02	-0.6266292E-04
42	-0.2407287E-02	0.2278895E-08	-0.1118514E-09	0.2858368E-12	0.4298497E-05	-0.5255891E-09
43	-0.7532164E-02	0.2278592E-08	-0.4273177E-09	0.1720137E-11	-0.1560613E-02	-0.3315254E-04
44	-0.1846834E-01	0.2278401E-08	-0.9433794E-09	0.2233758E-11	-0.3109660E-02	-0.5215603E-04
45	0.5286627E 00	0.2366935E-08	0.1216598E-07	0.2858368E-12	0.4298497E-05	-0.5255891E-09
46	-0.6002035E 00	0.2163122E-08	0.1214840E-07	0.2858368E-12	0.4298497E-05	-0.5255891E-09
47	0.2169484E 00	0.2321638E-08	0.1216271E-07	0.2858368E-12	0.4298497E-05	-0.5255891E-09
48	-0.2891810E 00	0.2224962E-08	0.1215484E-07	0.7188244E-13	0.4298497E-05	-0.5255891E-09
49	0.6950352E 00	0.2385991E-08	0.9474785E-08	0.2858368E-12	0.4298497E-05	-0.5255891E-09
50	-0.7869958E 00	0.2148171E-08	0.9462717E-08	0.2858368E-12	0.4298497E-05	-0.5255891E-09
51	0.2860534E 00	0.2329901E-08	0.9472487E-08	0.2858368E-12	0.4298497E-05	-0.5255891E-09
52	-0.3783368E 00	0.2218024E-08	0.9467083E-08	0.2858368E-12	0.4298497E-05	-0.5255891E-09
53	0.2848309E 00	0.2350561E-08	0.8351634E-08	0.2858368E-12	0.4298497E-05	-0.5255891E-09
54	-0.3255036E 00	0.2180975E-08	0.8337970E-08	0.2858368E-12	0.4298497E-05	-0.5255891E-09
55	0.1160892E 00	0.2314308E-08	0.8349151E-08	0.2858368E-12	0.4298497E-05	-0.5255891E-09
56	-0.1576354E 00	0.2232941E-08	0.8343026E-08	0.2858368E-12	0.4298497E-05	-0.5255891E-09
57	0.7597149E 00	0.2407239E-08	0.2013365E-08	0.9127647E-12	-0.6200697E-02	-0.5255891E-09
58	-0.8586180E 00	0.2135699E-08	0.2013365E-08	0.1035526E-11	-0.6200813E-02	-0.5255891E-09
59	0.3132687E 00	0.2338936E-08	0.2013240E-08	0.1002714E-11	-0.6200466E-02	-0.5255891E-09
60	-0.4121636E 00	0.2211996E-08	0.2013240E-08	0.1078394E-11	-0.6200559E-02	-0.5255891E-09
61	-0.6662414E-03	0.2336735E-08	-0.8440429E-10	0.3300766E-12	-0.1548977E-04	-0.5255891E-09
62	-0.3192178E-02	0.2201529E-08	-0.8707457E-10	0.4431018E-12	0.1585133E-05	-0.5255891E-09
63	-0.1753324E-02	0.2307852E-08	-0.8478984E-10	0.4646600E-12	-0.1434842E-04	-0.5255891E-09
64	-0.3035371E-02	0.2241871E-08	-0.8598690E-10	0.6209615E-12	-0.5919852E-05	-0.5255891E-09
65	-0.4944605E-01	0.2277874E-08	0.2013126E-08	0.1151031E-11	-0.6199952E-02	0.6590648E-04
66	0.3044174E-02	0.2386421E-08	-0.8357966E-10	0.1283704E-12	-0.1559158E-04	-0.5255891E-09
67	-0.8211017E-03	0.2172224E-08	-0.9112902E-10	-0.3440898E-13	0.1411984E-04	-0.5255891E-09
68	-0.2520443E-02	0.2278765E-08	-0.8521388E-10	0.5746317E-12	-0.1154379E-04	0.5092267E-05
69	-0.3310936E-01	0.2278093E-08	-0.1558329E-08	0.2328140E-11	-0.4652862E-02	0.6267072E-04
70	-0.2407273E-02	0.2278895E-08	-0.1052044E-09	0.2858368E-12	0.4298497E-05	-0.5255891E-09
71	-0.7533055E-02	0.2278539E-08	0.2750371E-09	0.2123991E-11	-0.1558650E-02	0.3315738E-04
72	-0.1847071E-01	0.2278315E-08	0.9063712E-09	0.2690861E-11	-0.3105754E-02	0.5216278E-04

TABLE I2 - SYNTHESIZED LABORATORY MODES (Continued)

MODE 3 Frequency = .214268 Hz

MASS NO.	Q(1)	Q(2)	Q(3)	THETA(1)	THETA(2)	THETA(3)
1	0.6959897E-02	-0.9774679E-09	-0.3635972E-09	0.1607973E-10	0.6690304E-04	0.2236561E-08
2	0.2944958E-02	-0.1045180E-08	-0.3623744E-09	0.3691026E-11	0.6690220E-04	0.2243278E-08
3	-0.1072409E-02	0.7947041E-09	-0.3995129E-09	0.3551903E-11	0.6689505E-04	0.2221858E-08
4	-0.9104963E-02	0.2136588E-08	-0.2965326E-09	0.2054895E-11	0.6686772E-04	0.2209323E-08
5	-0.1713134E-01	0.2062362E-08	-0.3614964E-09	-0.2261580E-12	0.6682603E-04	0.2194855E-08
6	-0.2114012E-01	0.1727217E-08	-0.3768761E-09	-0.1959156E-11	0.6678641E-04	0.2180266E-08
7	-0.3581216E-01	-0.9460952E-09	-0.3768761E-09	-0.3290731E-11	0.6634383E-04	0.2030135E-08
8	-0.5038800E-01	0.5823597E-09	-0.3768761E-09	-0.1670057E-10	0.6615877E-04	0.1807530E-08
9	0.2945515E-02	-0.1045192E-08	-0.8300589E-09	0.3678080E-11	0.6690319E-04	0.4924235E-08
10	0.2946451E-02	-0.1045211E-08	-0.1266202E-08	0.3661275E-11	0.6690423E-04	0.6991584E-08
11	0.2947483E-02	-0.1045233E-08	-0.1797031E-08	0.3653477E-11	0.6690502E-04	0.7909538E-08
12	0.2948524E-02	-0.1045241E-08	-0.2137372E-08	0.3648716E-11	0.6690544E-04	0.8137413E-08
13	0.294917E-02	-0.1045191E-08	0.1093406E-09	0.3682695E-11	0.6690319E-04	-0.4415073E-09
14	0.2945318E-02	-0.1045209E-08	0.5466070E-09	0.3669742E-11	0.6690423E-04	-0.2512045E-08
15	0.2945825E-02	-0.1045230E-08	0.1012714E-08	0.3663814E-11	0.6690502E-04	-0.3431572E-08
16	0.2946320E-02	-0.1045239E-08	0.1382634E-08	0.3659555E-11	0.6690544E-04	-0.3659872E-08
17	0.4299585E 00	-0.8719743E-09	-0.4089504E-08	-0.1670057E-10	0.6615877E-04	0.1807530E-08
18	0.3458992E 00	0.2845044E-08	-0.4070529E-08	-0.1670057E-10	0.6615877E-04	0.1807530E-08
19	0.4062031E 00	0.3929733E-10	-0.4085972E-08	-0.1670057E-10	0.6615877E-04	0.1807530E-08
20	0.3645105E 00	0.1637080E-08	-0.4077471E-08	-0.2096330E-10	0.6615877E-04	0.1807530E-08
21	0.5817696E 00	-0.8657006E-09	0.2464893E-08	-0.1670057E-10	0.6615877E-04	0.1807530E-08
22	0.4665489E 00	0.2811275E-08	0.2477677E-08	-0.1670057E-10	0.6615877E-04	0.1807530E-08
23	0.5501484E 00	0.4375508E-10	0.2467408E-08	-0.1670057E-10	0.6615877E-04	0.1807530E-08
24	0.4984989E 00	0.1623858E-08	0.2473124E-08	-0.1670057E-10	0.6615877E-04	0.1807530E-08
25	0.2037380E 00	-0.8972187E-09	-0.3943466E-08	-0.1670057E-10	0.6615877E-04	0.1807530E-08
26	0.1675519E 00	0.2860236E-08	-0.3928044E-08	-0.1670057E-10	0.6615877E-04	0.1807530E-08
27	0.1934657E 00	0.2810445E-10	-0.3940741E-08	-0.1670057E-10	0.6615877E-04	0.1807530E-08
28	0.1772336E 00	0.1643767E-08	-0.3933817E-08	-0.1670057E-10	0.6615877E-04	0.1807530E-08
29	0.6359744E 00	-0.8753909E-09	0.1505169E-07	-0.1545868E-10	-0.4948387E-03	0.1807530E-08
30	0.5070322E 00	0.2762030E-08	0.1505169E-07	-0.1628316E-10	-0.4932727E-03	0.1807530E-08
31	0.6003522E 00	0.4243274E-10	0.1505185E-07	-0.1553929E-10	-0.4945938E-03	0.1807530E-08
32	0.5425528E 00	0.1605094E-08	0.1505185E-07	-0.1604751E-10	-0.4934741E-03	0.1807530E-08
33	-0.5639643E-01	-0.9402734E-09	0.6163441E-09	-0.1619618E-10	0.6336246E-04	0.1807530E-08
34	-0.4015701E-01	0.2857919E-08	0.6196739E-09	-0.1695688E-10	0.6135984E-04	0.1807530E-08
35	-0.5189484E-01	0.1069400E-10	0.6168077E-09	-0.1585304E-10	0.6187233E-04	0.1807530E-08
36	-0.4462350E-01	0.1644395E-08	0.6183005E-09	-0.1690520E-10	0.6252497E-04	0.1807530E-08
37	0.5714343E 00	0.5895580E-09	0.1505198E-07	-0.1566461E-10	-0.4939828E-03	0.8614466E-03
38	-0.7205188E-01	-0.5601539E-08	0.6152803E-09	-0.1754691E-10	0.6678059E-04	0.1807530E-08
39	-0.2597528E-01	0.6874007E-08	0.6246945E-09	-0.1645103E-10	0.5851334E-04	0.1807530E-08
40	-0.4827795E-01	0.5832488E-09	0.6172998E-09	-0.1633089E-10	0.6210874E-04	0.8579255E-04
41	0.3578038E 00	0.5880059E-09	0.1132090E-07	-0.1419370E-10	-0.3549599E-03	0.8203161E-03
42	-0.5038797E-01	0.5823597E-09	-0.1776952E-09	-0.1670057E-10	0.6615877E-04	0.1807530E-08
43	0.2094520E-01	0.5848453E-09	0.4373362E-08	-0.1425556E-10	-0.7691450E-04	0.4440146E-03
44	0.1657814E 00	0.5864333E-09	0.7838949E-08	-0.1360506E-10	-0.2159375E-03	0.6864716E-03
45	0.4299760E 00	-0.7623298E-09	0.2146455E-07	-0.1670057E-10	0.6615877E-04	0.1807530E-08
46	0.3459172E 00	0.2754601E-08	0.2141924E-07	-0.1670057E-10	0.6615877E-04	0.1807530E-08
47	0.4062208E 00	0.9235725E-10	0.2145613E-07	-0.1670057E-10	0.6615877E-04	0.1807530E-08
48	0.3685285E 00	0.1590854E-08	0.2143583E-07	-0.2096329E-10	0.6615877E-04	0.1807530E-08
49	0.5817922E 00	-0.7316501E-09	0.1084666E-07	-0.1670057E-10	0.6615877E-04	0.1807530E-08
50	0.4665720E 00	0.2693336E-08	0.1081580E-07	-0.1670057E-10	0.6615877E-04	0.1807530E-08
51	0.5501711E 00	0.1078455E-09	0.1084068E-07	-0.1670057E-10	0.6615877E-04	0.1807530E-08
52	0.4985218E 00	0.1565635E-08	0.1082688E-07	-0.1670057E-10	0.6615877E-04	0.1807530E-08
53	0.2037475E 00	-0.8143162E-09	0.1571910E-07	-0.1670057E-10	0.6615877E-04	0.1807530E-08
54	0.1675615E 00	0.2795378E-08	0.1568312E-07	-0.1670057E-10	0.6615877E-04	0.1807530E-08
55	0.1934754E 00	0.6927781E-10	0.1571265E-07	-0.1670057E-10	0.6615877E-04	0.1807530E-08
56	0.1772431E 00	0.1608891E-08	0.1569652E-07	-0.1670057E-10	0.6615877E-04	0.1807530E-08
57	0.6359978E 00	-0.7189791E-09	-0.1291668E-07	-0.1434665E-10	-0.4948359E-03	0.1807530E-08
58	0.5070563E 00	0.2615081E-08	-0.1291668E-07	-0.1526418E-10	-0.4932694E-03	0.1807530E-08
59	0.6003757E 00	0.1167839E-09	-0.1291703E-07	-0.1434417E-10	-0.4945914E-03	0.1807530E-08
60	0.5425767E 00	0.1534364E-08	-0.1291703E-07	-0.1490973E-10	-0.4934710E-03	0.1807530E-08
61	-0.5639646E-01	-0.8862682E-09	-0.1365992E-08	-0.1599518E-10	0.6336166E-04	0.1807530E-08
62	-0.4015718E-01	0.2816805E-08	-0.1373570E-08	-0.1684201E-10	0.6135956E-04	0.1807530E-08
63	-0.5189493E-01	0.3920446E-10	-0.1367058E-08	-0.1538632E-10	0.6187163E-04	0.1807530E-08
64	-0.4462365E-01	0.1620257E-08	-0.1370456E-08	-0.1655764E-10	0.6252462E-04	0.1807530E-08
65	0.5714579E 00	0.5904328E-09	-0.1291735E-07	-0.1433037E-10	-0.4939791E-03	-0.8614811E-03
66	-0.7205170E-01	-0.5601539E-08	-0.1363606E-08	-0.1798707E-10	0.6677968E-04	0.1807530E-08
67	-0.2597550E-01	0.6874007E-08	-0.1385033E-08	-0.1676706E-10	0.5851316E-04	0.1807530E-08
68	-0.4827808E-01	0.5833523E-09	-0.1386206E-08	-0.1586821E-10	0.6210821E-04	-0.8579278E-04
69	0.3578188E 00	0.5886904E-09	-0.9796796E-08	-0.1100137E-10	-0.3549578E-03	-0.8203494E-03
70	-0.5038801E-01	0.5823597E-09	-0.5772804E-09	-0.1670057E-10	0.6615877E-04	0.1807530E-08
71	0.2094723E-01	0.5851439E-09	-0.4621345E-08	-0.1124577E-10	-0.7691415E-04	-0.4440309E-03
72	0.1657889E 00	0.5869256E-09	-0.7213416E-08	-0.9742910E-11	-0.2159362E-03	-0.6864988E-03

TABLE I2 - SYNTHESIZED LABORATORY MODES (Continued)

MODE 4 Frequency = .216833 Hz

MASS NO.	Q(1)	Q(2)	Q(3)	THETA(1)	THETA(2)	THETA(3)
1	-0.1785249E-06	-0.2232897E-08	0.2288768E-10	0.8535017E-11	-0.1529546E-08	0.9688784E-04
2	-0.8974405E-07	-0.1472247E-08	0.2290208E-10	0.1237201E-10	-0.1535451E-08	0.9688670E-04
3	-0.6829985E-09	-0.1892689E-08	0.3302761E-10	0.1806080E-10	-0.1538098E-08	0.9643887E-04
4	0.1858547E-06	0.1056306E-08	-0.2873686E-10	0.1268558E-10	-0.1529451E-08	0.9554047E-04
5	0.3683983E-06	0.3052520E-09	0.1174864E-09	0.1372250E-10	-0.1523554E-08	0.9463947E-04
6	0.4589751E-06	0.4785732E-09	0.7285028E-11	0.1560230E-10	-0.1519873E-08	0.9389647E-04
7	0.7881909E-06	-0.2259997E-08	0.7285028E-11	0.7749053E-13	-0.1514981E-08	0.8625026E-04
8	0.1124106E-05	-0.2000527E-09	0.7285028E-11	0.1685910E-10	-0.1514553E-08	0.7859700E-04
9	0.1279192E-01	-0.1472232E-08	-0.1646285E-08	0.1238791E-10	-0.1535474E-08	0.9692377E-04
10	0.2442737E-01	-0.1472209E-08	-0.3129694E-08	0.1228628E-10	-0.1535500E-08	0.9695467E-04
11	0.3606496E-01	-0.1472229E-08	-0.4336879E-08	0.1226371E-10	-0.1535518E-08	0.9696979E-04
12	0.4770282E-01	-0.1472242E-08	-0.6390643E-08	0.1224855E-10	-0.1535528E-08	0.9697401E-04
13	-0.1279211E-01	-0.1472267E-08	0.1687085E-08	0.1234432E-10	-0.1535474E-08	0.9692377E-04
14	-0.2442754E-01	-0.1472296E-08	0.3192346E-08	0.1243638E-10	-0.1535499E-08	0.9695467E-04
15	-0.3606514E-01	-0.1472281E-08	0.4477528E-08	0.1245459E-10	-0.1535518E-08	0.9696979E-04
16	-0.4770299E-01	-0.1472271E-08	0.6561717E-08	0.1246870E-10	-0.1535528E-08	0.9697401E-04
17	-0.3942336E 00	0.2213554E-08	-0.2686635E-07	0.1685910E-10	-0.1514553E-08	0.7859700E-04
18	-0.4041547E 00	-0.2892292E-08	-0.2684152E-07	0.1685910E-10	-0.1514553E-08	0.7859700E-04
19	-0.3967437E 00	0.8257379E-09	-0.2686165E-07	0.1685910E-10	-0.1514553E-08	0.7859700E-04
20	-0.4011922E 00	-0.1528054E-08	-0.2685052E-07	0.1696090E-10	-0.1514553E-08	0.7859700E-04
21	-0.5044679E 00	0.2256886E-08	-0.3454685E-07	0.1685910E-10	-0.1514553E-08	0.7859700E-04
22	-0.5185112E 00	-0.2951456E-08	-0.3453176E-07	0.1685910E-10	-0.1514553E-08	0.7859700E-04
23	-0.5082234E 00	0.8426189E-09	-0.3454311E-07	0.1685910E-10	-0.1514553E-08	0.7859700E-04
24	-0.5145198E 00	-0.1549918E-08	-0.3453635E-07	0.1685910E-10	-0.1514553E-08	0.7859700E-04
25	-0.2151651E 00	0.2157045E-08	0.1335884E-07	0.1685910E-10	-0.1514553E-08	0.7859700E-04
26	-0.2193940E 00	-0.2841664E-08	-0.1333191E-07	0.1685910E-10	-0.1514553E-08	0.7859700E-04
27	-0.2160801E 00	0.8038286E-09	-0.1335470E-07	0.1685910E-10	-0.1514553E-08	0.7859700E-04
28	-0.2179778E 00	-0.1508839E-08	-0.1334264E-07	0.1685910E-10	-0.1514553E-08	0.7859700E-04
29	-0.5271875E 00	0.2288516E-08	-0.2930494E-07	0.1978587E-10	-0.5894763E-04	0.7859700E-04
30	-0.5427784E 00	-0.3017102E-08	0.2930494E-07	0.1930980E-10	-0.6052546E-04	0.7859700E-04
31	-0.5314374E 00	0.8549592E-09	-0.2930435E-07	0.1987562E-10	-0.5916820E-04	0.7859700E-04
32	-0.5384260E 00	-0.1573791E-08	-0.2930435E-07	0.1958222E-10	-0.6029944E-04	0.7859700E-04
33	0.1119760E-02	0.2088323E-08	-0.1055929E-08	0.1755379E-10	0.1234002E-04	0.7859700E-04
34	0.3417103E-02	-0.279249E-08	-0.1041197E-08	0.1711364E-10	0.5358688E-05	0.7859700E-04
35	0.1985649E-02	0.7772700E-09	-0.1054280E-08	0.1854621E-10	0.1141457E-04	0.7859700E-04
36	0.3012593E-02	-0.1492075E-08	-0.1047676E-08	0.1793729E-10	0.6177463E-05	0.7859700E-04
37	-0.5349132E 00	-0.1956899E-09	0.2930384E-07	0.2002473E-10	-0.5972774E-04	-0.7785524E-03
38	-0.1831705E-02	0.6328417E-08	-0.1060911E-08	0.1527059E-10	0.1239277E-04	0.7859700E-04
39	0.4716381E-02	-0.6564981E-08	-0.1019271E-08	0.1590485E-10	0.5492193E-05	0.7859700E-04
40	0.2587236E-02	-0.1995291E-09	-0.1052829E-08	0.1869713E-10	0.8760438E-05	-0.7673799E-05
41	-0.3421621E 00	-0.1966351E-09	-0.2344997E-07	0.2612151E-10	-0.4260587E-04	-0.7375402E-03
42	0.9442873E-03	-0.2000527E-09	-0.1988978E-09	0.1685910E-10	-0.1514553E-08	0.7859700E-04
43	-0.4662099E-01	-0.1985580E-09	-0.7342031E-08	0.3089838E-10	-0.8361606E-05	-0.3634307E-03
44	-0.1709351E 00	-0.1975922E-09	-0.1622249E-07	0.3206878E-10	-0.2548355E-04	-0.6043431E-03
45	0.3942141E 00	0.2179352E-08	0.2846585E-07	0.1685910E-10	-0.1514553E-08	0.7859700E-04
46	0.4041386E 00	-0.2858143E-08	0.2843892E-07	0.1685910E-10	-0.1514553E-08	0.7859700E-04
47	0.3967251E 00	0.8086198E-09	0.2846084E-07	0.1685910E-10	-0.1514553E-08	0.7859700E-04
48	0.4011753E 00	-0.1510972E-08	0.2844877E-07	0.1675748E-10	-0.1514553E-08	0.7859700E-04
49	0.5044417E 00	0.2215685E-08	0.3224383E-07	0.1685910E-10	-0.1514553E-08	0.7859700E-04
50	0.5184894E 00	-0.2910313E-08	0.3222797E-07	0.1685910E-10	-0.1514553E-08	0.7859700E-04
51	0.5081985E 00	0.8226977E-09	0.3224020E-07	0.1685910E-10	-0.1514553E-08	0.7859700E-04
52	0.5144967E 00	-0.1530042E-08	0.3223311E-07	0.1685910E-10	-0.1514553E-08	0.7859700E-04
53	0.2151561E 00	0.2130174E-08	0.1464971E-07	0.1685910E-10	-0.1514553E-08	0.7859700E-04
54	0.2193860E 00	-0.2814836E-08	0.1462572E-07	0.1685910E-10	-0.1514553E-08	0.7859700E-04
55	0.2160711E 00	0.7896805E-09	0.1464579E-07	0.1685910E-10	-0.1514553E-08	0.7859700E-04
56	0.2179695E 00	-0.1494715E-08	0.1463503E-07	0.1685910E-10	-0.1514553E-08	0.7859700E-04
57	0.5271588E 00	0.2240712E-08	0.2807323E-07	0.1944299E-10	0.5896701E-04	0.7859700E-04
58	0.5427547E 00	-0.2969353E-08	0.2807323E-07	0.1896697E-10	0.6054474E-04	0.7859700E-04
59	0.5314102E 00	0.8324259E-09	0.2807272E-07	0.1950845E-10	0.5918754E-04	0.7859700E-04
60	0.5384010E 00	-0.1551310E-08	0.2807272E-07	0.1921507E-10	0.6031875E-04	0.7859700E-04
61	-0.1117234E-02	0.2069049E-08	0.1054586E-08	0.1749526E-10	-0.1234294E-04	0.7859700E-04
62	-0.3415324E-02	-0.2780002E-08	0.1041423E-08	0.1705526E-10	-0.5361504E-05	0.7859700E-04
63	-0.1983329E-02	0.7662322E-09	0.1053096E-08	0.1838320E-10	-0.1141742E-04	0.7859700E-04
64	-0.3010611E-02	-0.1481048E-08	0.1047196E-08	0.1777450E-10	-0.6180336E-05	0.7859700E-04
65	0.5348870E 00	-0.1957156E-09	0.2807227E-07	0.1961760E-10	0.5974711E-04	-0.7785130E-03
66	0.1834959E-02	0.6328417E-08	0.1058974E-08	0.1542108E-10	-0.1239585E-04	0.7859700E-04
67	-0.4715245E-02	-0.6564981E-08	0.1021770E-08	0.1605509E-10	-0.5494866E-05	0.7859700E-04
68	-0.2585082E-02	-0.1995304E-09	0.1051760E-08	0.1849079E-10	-0.8763296E-05	-0.7669873E-05
69	0.3421456E 00	-0.1966547E-09	0.2272396E-07	0.2497177E-10	0.4261966E-04	-0.7375027E-03
70	-0.9420398E-03	-0.2000527E-09	0.2137729E-09	0.1685910E-10	-0.1514553E-08	0.7859700E-04
71	0.4661997E-01	-0.1985654E-09	0.7140287E-08	0.2926671E-10	0.8364307E-05	-0.3634107E-03
72	0.1709275E 00	-0.1976058E-09	0.1556327E-07	0.3025931E-10	0.2549177E-04	-0.6043117E-03

TABLE I2 - SYNTHESIZED LABORATORY MODES (Continued)

MODE 5 Frequency = .381114 Hz

MASS NO.	Q(1)	Q(2)	Q(3)	THETA(1)	THETA(2)	THETA(3)
1	0.7536634E-09	-0.1644374E-05	0.7573929E-02	0.7574670E-08	-0.1122535E-10	-0.9198209E-13
2	-0.1268183E-08	-0.1188847E-05	0.7573757E-02	0.7573838E-08	-0.1095985E-10	-0.9653319E-13
3	-0.3005620E-08	-0.7293478E-06	0.7572249E-02	0.7516658E-08	-0.1266852E-10	-0.4049590E-11
4	0.3170859E-08	0.1685530E-06	0.7569078E-02	0.7389811E-08	-0.1355387E-10	-0.1044029E-10
5	0.3609640E-08	0.1057960E-05	0.7566117E-02	0.7245049E-08	-0.100971E-10	-0.1297249E-10
6	0.2425026E-08	0.1492128E-05	0.7564589E-02	0.7111588E-08	-0.9964279E-11	-0.1143153E-10
7	0.6130620E-08	0.2882251E-05	0.7564589E-02	0.5370605E-08	-0.5031423E-10	0.7613380E-11
8	0.5925624E-08	0.3842233E-05	0.7564589E-02	0.3257806E-08	0.2738687E-11	-0.1535515E-12
9	-0.1284191E-08	-0.1188882E-05	0.7574853E-02	-0.1427651E-07	-0.1095404E-10	-0.4405602E-12
10	-0.1398388E-08	-0.1188933E-05	0.7579345E-02	-0.3112807E-07	-0.1094960E-10	-0.7351357E-12
11	-0.1512251E-08	-0.1188972E-05	0.7584710E-02	-0.3861264E-07	-0.1094630E-10	-0.7806429E-12
12	-0.1600292E-08	-0.1188992E-05	0.7590055E-02	-0.4047074E-07	-0.1094365E-10	-0.7572253E-12
13	-0.1274920E-08	-0.1188883E-05	0.7576849E-02	0.2944244E-07	-0.1096407E-10	-0.9790931E-13
14	-0.1247919E-08	-0.1188936E-05	0.7583167E-02	0.4630921E-07	-0.1096683E-10	-0.1123166E-12
15	-0.1229556E-08	-0.1188976E-05	0.7590357E-02	0.5380123E-07	-0.1096886E-10	-0.1876884E-13
16	-0.1247970E-08	-0.1188997E-05	0.7597525E-02	0.5566143E-07	-0.1097083E-10	0.5756029E-13
17	0.2551696E-06	0.3850199E-02	-0.6832372E 00	0.3257806E-08	0.2738687E-11	-0.1535515E-12
18	-0.1618914E-06	-0.3839950E-02	-0.6822334E 00	0.3257806E-08	0.2738687E-11	-0.1535515E-12
19	0.1314427E-06	0.1912167E-02	-0.6830508E 00	0.3257806E-08	0.2738687E-11	-0.1535515E-12
20	-0.5552737E-07	-0.1901826E-02	-0.6826009E 00	0.3257806E-08	0.2738687E-11	-0.1535515E-12
21	-0.5483287E-08	0.4853662E-02	-0.5374672E 00	0.3257806E-08	0.2738687E-11	-0.1535515E-12
22	0.1235873E-06	-0.4842587E-02	-0.5367855E 00	0.3257806E-08	0.2738687E-11	-0.1535515E-12
23	0.3936242E-07	0.2358758E-02	-0.5373355E 00	0.3257806E-08	0.2738687E-11	-0.1535515E-12
24	0.9734316E-07	-0.2347333E-02	-0.5370303E 00	0.3257806E-08	0.2738687E-11	-0.1535515E-12
25	0.2454894E-06	0.2838729E-02	-0.4621130E 00	0.3257806E-08	0.2738687E-11	-0.1535515E-12
26	-0.2974292E-06	-0.2829326E-02	-0.4613209E 00	0.3257806E-08	0.2738687E-11	-0.1535515E-12
27	0.9613859E-07	0.1461621E-02	-0.4619709E 00	0.3257806E-08	0.2738687E-11	-0.1535515E-12
28	-0.1471919E-06	-0.1452361E-02	-0.4616154E 00	0.3257806E-08	0.2738687E-11	-0.1535515E-12
29	-0.1719297E-06	0.5846992E-02	-0.1030480E 00	0.4101200E-04	0.1255260E-08	-0.1535515E-12
30	0.1557539E-06	-0.5835116E-02	-0.1030480E 00	0.4102154E-04	0.1255876E-08	-0.1535515E-12
31	-0.8155376E-07	0.2800423E-02	-0.1030405E 00	0.4491619E-04	0.1255258E-08	-0.1535515E-12
32	0.6533458E-07	-0.2787927E-02	-0.1030405E 00	0.4492258E-04	0.1255753E-08	-0.1535515E-12
33	-0.2820174E-07	0.1821404E-02	0.7158626E-02	0.6063668E-05	0.3208527E-09	-0.1535515E-12
34	0.1723264E-07	-0.1812870E-02	0.7320002E-02	0.6060366E-05	0.2666208E-10	-0.1535515E-12
35	-0.7572755E-08	0.1008073E-02	0.7181533E-02	0.1556712E-04	0.2486309E-09	-0.1535515E-12
36	0.1279935E-07	-0.9999126E-03	0.7253878E-02	0.1556105E-04	0.9977255E-10	-0.1535515E-12
37	-0.8118047E-08	0.6354343E-05	-0.1030336E 00	0.5140828E-04	0.1255390E-08	0.1718274E-10
38	-0.1208599E-06	0.5044369E-05	0.7108148E-02	-0.1445551E-04	0.4223217E-09	-0.1535515E-12
39	0.6927312E-08	0.2640109E-05	0.7564388E-02	-0.1444845E-04	-0.7815454E-10	-0.1535515E-12
40	0.4858400E-08	0.3561497E-05	0.7206362E-02	0.1766994E-04	0.1740024E-09	-0.3371872E-10
41	-0.1157482E-07	0.5756222E-05	-0.8027923E-01	0.1226511E-03	0.9850436E-09	0.6789311E-11
42	0.5923447E-08	0.3842233E-05	0.7564548E-02	0.3257806E-08	0.2738687E-11	-0.1535515E-12
43	-0.4075154E-08	0.4559774E-05	-0.1080614E-01	0.1144258E-03	0.4443499E-09	-0.3344691E-10
44	-0.1052692E-07	0.5158024E-05	-0.4511463E-01	0.1474968E-03	0.7146963E-09	-0.1565716E-10
45	0.2830990E-06	-0.3843260E-02	-0.6835421E 00	0.3257806E-08	0.2738687E-11	-0.1535515E-12
46	-0.1906868E-06	0.3848596E-02	-0.6825380E 00	0.3257806E-08	0.2738687E-11	-0.1535515E-12
47	0.1432633E-06	-0.1904908E-02	-0.6833555E 00	0.3257806E-08	0.2738687E-11	-0.1535515E-12
48	-0.6916207E-07	0.1910012E-02	-0.6829057E 00	0.3257806E-08	0.2738687E-11	-0.1535515E-12
49	0.8537342E-07	-0.4847188E-02	-0.5377052E 00	0.3257806E-08	0.2738687E-11	-0.1535515E-12
50	0.1769317E-07	0.4851662E-02	-0.5370233E 00	0.3257806E-08	0.2738687E-11	-0.1535515E-12
51	0.7700959E-07	-0.2351702E-02	-0.5375734E 00	0.3257806E-08	0.2738687E-11	-0.1535515E-12
52	0.4697403E-07	0.2355712E-02	-0.5372682E 00	0.3257806E-08	0.2738687E-11	-0.1535515E-12
53	0.1327293E-06	-0.2831346E-02	-0.4623213E 00	0.3257806E-08	0.2738687E-11	-0.1535515E-12
54	-0.1656088E-06	0.2837515E-02	-0.4615288E 00	0.3257806E-08	0.2738687E-11	-0.1535515E-12
55	0.4999060E-07	-0.1454165E-02	-0.4621792E 00	0.3257806E-08	0.2738687E-11	-0.1535515E-12
56	-0.8377896E-07	0.1460344E-02	-0.4618236E 00	0.3257806E-08	0.2738687E-11	-0.1535515E-12
57	-0.2283129E-06	-0.5840998E-02	-0.1030897E 00	-0.4102316E-04	0.1720962E-08	-0.1535515E-12
58	0.2208998E-06	0.5844597E-02	-0.1030897E 00	-0.4103378E-04	0.1721514E-08	-0.1535515E-12
59	-0.1044056E-06	-0.2793579E-02	-0.1030822E 00	-0.4492930E-04	0.1720899E-08	-0.1535515E-12
60	0.9695526E-07	0.2796489E-02	-0.1030822E 00	-0.4493637E-04	0.1721344E-08	-0.1535515E-12
61	-0.3157725E-07	-0.1813598E-02	0.7158834E-02	-0.6059342E-05	0.3518799E-09	-0.1535515E-12
62	0.1856649E-07	0.1820578E-02	0.7320285E-02	-0.6057016E-05	0.2960907E-10	-0.1535515E-12
63	-0.8904834E-08	-0.1000424E-02	0.7181756E-02	-0.1556679E-04	0.2739218E-09	-0.1535515E-12
64	0.1363124E-07	0.1007682E-02	0.7254131E-02	-0.1556207E-04	0.1109728E-09	-0.1535515E-12
65	-0.3732502E-08	0.1338217E-05	-0.1030753E 00	-0.5142455E-04	0.1720937E-08	-0.2271490E-10
66	-0.1328070E-06	0.5044369E-05	0.7108338E-02	0.1446770E-04	0.4607177E-09	-0.1535515E-12
67	0.6945680E-08	0.2640109E-05	0.7564779E-02	0.1446205E-04	-0.8789881E-10	-0.1535515E-12
68	0.4820222E-08	0.3724057E-05	0.7206596E-02	-0.1767119E-04	0.1926209E-09	0.3491228E-10
69	-0.8606655E-08	0.1934618E-05	-0.8031249E-01	-0.1226988E-03	0.1338857E-08	-0.1259517E-10
70	0.5926985E-08	0.3842233E-05	0.7564623E-02	0.3257806E-08	0.2738687E-11	-0.1535515E-12
71	-0.3772470E-08	0.3127557E-05	-0.1081213E-01	-0.1144694E-03	0.5747005E-09	0.2997988E-10
72	-0.9029613E-08	0.2531070E-05	-0.4513404E-01	-0.1475552E-03	0.9567780E-09	0.1004093E-10

TABLE I2 - SYNTHESIZED LABORATORY MODES (Continued)

MODE 6

Frequency = .381605 Hz

MASS NO.	Q(1)	Q(2)	Q(3)	THETA(1)	THETA(2)	THETA(3)
1	-0.2519131E-08	0.7330623E-02	0.1702252E-05	-0.3355520E-04	0.1055995E-10	0.4809150E-11
2	-0.1104486E-08	0.5308751E-02	0.1702292E-05	-0.3365302E-04	0.1155339E-10	-0.1144607E-10
3	0.3089580E-08	0.3279069E-02	0.1702626E-05	-0.3340705E-04	0.1384913E-10	-0.1262153E-10
4	0.4585694E-08	-0.7349586E-03	0.1703344E-05	-0.3284613E-04	0.1415044E-10	-0.1797634E-10
5	0.2871856E-09	-0.4675575E-02	0.1703974E-05	-0.3219243E-04	0.1771418E-10	-0.1343980E-10
6	-0.1455005E-08	-0.6607983E-02	0.1704339E-05	-0.3160175E-04	0.1641744E-10	-0.1536066E-10
7	-0.2002630E-08	-0.1279315E-01	0.1704339E-05	-0.2361673E-04	-0.3706081E-11	-0.6611588E-11
8	-0.1327272E-09	-0.1705660E-01	0.1704339E-05	-0.1444727E-04	0.1245948E-10	-0.1551449E-10
9	-0.2518991E-08	0.5308919E-02	0.4447103E-02	-0.3369298E-04	0.1155720E-10	-0.1148739E-10
10	-0.3884306E-08	0.5309157E-02	0.8495212E-02	-0.3372628E-04	0.1155881E-10	-0.1207238E-10
11	-0.5412449E-08	0.5309340E-02	0.1254557E-01	-0.3374259E-04	0.1156046E-10	-0.1279691E-10
12	-0.7031520E-08	0.5309436E-02	0.1659626E-01	-0.3374713E-04	0.1156174E-10	-0.1313705E-10
13	0.3308804E-09	0.5308919E-02	-0.4443698E-02	-0.3369298E-04	0.1155696E-10	-0.1165180E-10
14	0.1825068E-08	0.5309157E-02	-0.8491803E-02	-0.3372625E-04	0.1155833E-10	-0.1199321E-10
15	0.3307303E-08	0.5309340E-02	-0.1254217E-01	-0.3374257E-04	0.1155980E-10	-0.1229213E-10
16	0.4777657E-08	0.5309436E-02	-0.1659286E-01	-0.3374711E-04	0.1156098E-10	-0.1240774E-10
17	-0.8940714E-07	-0.1540823E-01	-0.6778843E 00	-0.1444727E-04	0.1245948E-10	-0.1551449E-10
18	0.7376627E-07	-0.1920190E-01	-0.6768875E 00	-0.1444727E-04	0.1245948E-10	-0.1551449E-10
19	-0.4324619E-07	-0.1611323E-01	-0.6776993E 00	-0.1444727E-04	0.1245948E-10	-0.1551449E-10
20	0.2997849E-07	-0.1817390E-01	-0.6772525E 00	-0.1444727E-04	0.1245948E-10	-0.1551449E-10
21	-0.1627184E-06	-0.1437739E-01	-0.5273737E 00	-0.1444727E-04	0.1245948E-10	-0.1551449E-10
22	0.1509167E-06	-0.2015069E-01	-0.5266593E 00	-0.1444727E-04	0.1245948E-10	-0.1551449E-10
23	-0.7880067E-07	-0.1565904E-01	-0.5272068E 00	-0.1444727E-04	0.1245948E-10	-0.1551449E-10
24	0.6164078E-07	-0.1860107E-01	-0.5269035E 00	-0.1444727E-04	0.1245948E-10	-0.1551449E-10
25	0.1728652E-06	-0.1639122E-01	-0.4634662E 00	-0.1444727E-04	0.1245948E-10	-0.1551449E-10
26	-0.1420352E-06	-0.1819010E-01	-0.4626816E 00	-0.1444727E-04	0.1245948E-10	-0.1551449E-10
27	0.8756621E-07	-0.1655155E-01	-0.4633251E 00	-0.1444727E-04	0.1245948E-10	-0.1551449E-10
28	-0.5346915E-07	-0.1772339E-01	-0.4629733E 00	-0.1444727E-04	0.1245948E-10	-0.1551449E-10
29	0.1628151E-06	-0.1330978E-01	-0.9289616E-01	0.2471270E-04	-0.9705350E-09	-0.1551449E-10
30	-0.9056419E-07	-0.2104342E-01	-0.9289616E-01	0.2715728E-04	-0.9707304E-09	-0.1551449E-10
31	0.9285344E-07	-0.1519284E-01	-0.9288877E-01	0.2903544E-04	-0.9704473E-09	-0.1551449E-10
32	-0.2070011E-07	-0.1900684E-01	-0.9288877E-01	0.3054284E-04	-0.9706154E-09	-0.1551449E-10
33	0.5286008E-08	-0.1732758E-01	0.4702681E-03	-0.9615173E-05	-0.5777531E-10	-0.1551449E-10
34	-0.1974152E-08	-0.1712067E-01	0.6286150E-03	-0.7372310E-05	0.5758744E-11	-0.1551449E-10
35	0.1537890E-08	-0.1697457E-01	0.4928242E-03	-0.7309683E-06	-0.4400530E-10	-0.1551449E-10
36	-0.1768333E-08	-0.1725196E-01	0.5638092E-03	0.2369680E-05	-0.1179721E-10	-0.1551449E-10
37	0.3606118E-07	-0.1707523E-01	-0.9288204E-01	0.3619812E-04	-0.9703944E-09	-0.4467532E-10
38	0.2185822E-07	-0.2238763E-01	0.4208670E-03	-0.2701674E-04	-0.7593656E-10	-0.1551449E-10
39	0.3512796E-08	-0.1172557E-01	0.8685379E-03	-0.3024541E-04	0.3200690E-10	-0.1551449E-10
40	-0.6253100E-09	-0.1705909E-01	0.5173429E-03	0.2846022E-05	-0.2845241E-10	-0.6376646E-12
41	0.2471936E-07	-0.1707127E-01	-0.7411921E-01	0.1061081E-03	-0.7349079E-09	0.4575462E-10
42	-0.3142524E-09	-0.1705660E-01	0.1750715E-03	-0.1444727E-04	0.1245948E-10	-0.1551449E-10
43	0.3504114E-08	-0.1706319E-01	-0.1340506E-01	0.9716494E-04	-0.2639386E-09	0.3008242E-10
44	0.1316435E-07	-0.1706725E-01	-0.4327897E-01	0.1298796E-03	-0.4994232E-09	0.4380768E-10
45	-0.2300435E-07	-0.1540997E-01	0.6775756E 00	-0.1444727E-04	0.1245948E-10	-0.1551449E-10
46	-0.3225119E-07	-0.1920016E-01	0.6765794E 00	-0.1444727E-04	0.1245948E-10	-0.1551449E-10
47	-0.2639063E-07	-0.1611409E-01	0.6773905E 00	-0.1444727E-04	0.1245948E-10	-0.1551449E-10
48	-0.3055906E-07	-0.1817304E-01	0.6769441E 00	-0.1444727E-04	0.1245948E-10	-0.1551449E-10
49	-0.8660962E-08	-0.1437958E-01	0.5270953E 00	-0.1444727E-04	0.1245948E-10	-0.1551449E-10
50	-0.9712096E-07	-0.2014850E-01	0.5264169E 00	-0.1444727E-04	0.1245948E-10	-0.1551449E-10
51	-0.3085351E-07	-0.1566010E-01	0.5269642E 00	-0.1444727E-04	0.1245948E-10	-0.1551449E-10
52	-0.7029564E-07	-0.1860001E-01	0.5266610E 00	-0.1444727E-04	0.1245948E-10	-0.1551449E-10
53	-0.2142757E-06	-0.1639250E-01	0.4632576E 00	-0.1444727E-04	0.1245948E-10	-0.1551449E-10
54	0.1529876E-06	-0.1818882E-01	0.4624734E 00	-0.1444727E-04	0.1245948E-10	-0.1551449E-10
55	-0.1144466E-06	-0.1655221E-01	0.4631166E 00	-0.1444727E-04	0.1245948E-10	-0.1551449E-10
56	0.5011299E-07	-0.1772273E-01	0.4627649E 00	-0.1444727E-04	0.1245948E-10	-0.1551449E-10
57	-0.3501295E-06	-0.1331243E-01	0.9284961E-01	0.2469415E-04	0.1824861E-08	-0.1551449E-10
58	0.1260770E-06	-0.2104078E-01	0.9284961E-01	0.2713878E-04	0.1824937E-08	-0.1551449E-10
59	-0.2187583E-06	-0.1519410E-01	0.9284228E-01	0.2901509E-04	0.1824721E-08	-0.1551449E-10
60	-0.5306870E-08	-0.1900558E-01	0.9284228E-01	0.3052253E-04	0.1824813E-08	-0.1551449E-10
61	-0.8067104E-08	-0.1732840E-01	-0.4670424E-03	-0.9617907E-05	0.7359133E-10	-0.1551449E-10
62	0.4469644E-08	-0.1711985E-01	-0.6253163E-03	-0.7375049E-05	0.1916231E-10	-0.1551449E-10
63	-0.3160054E-08	-0.1697503E-01	-0.4895884E-03	-0.7379945E-05	0.6230558E-10	-0.1551449E-10
64	0.2580129E-08	-0.1725150E-01	-0.5605407E-03	0.2362654E-05	0.3459513E-10	-0.1551449E-10
65	-0.1121239E-06	-0.1707523E-01	0.9283549E-01	0.3617496E-04	0.1824555E-08	0.1483672E-09
66	-0.2791745E-07	-0.2238763E-01	-0.4176642E-03	-0.2701022E-04	0.8811110E-10	-0.1551449E-10
67	0.5314970E-08	-0.1172557E-01	-0.8651293E-03	-0.3023889E-04	-0.4024672E-11	-0.1551449E-10
68	0.1299967E-09	-0.1705910E-01	-0.5140959E-03	0.2838043E-05	0.4913193E-10	0.9066517E-11
69	-0.7489916E-07	-0.1707127E-01	0.7408297E-01	0.1060527E-03	0.1380699E-08	0.1450980E-09
70	0.1390774E-10	-0.1705660E-01	-0.1716629E-03	-0.1444727E-04	0.1245948E-10	-0.1551449E-10
71	-0.1251788E-07	-0.1706319E-01	0.1340017E-01	0.9711327E-04	0.4929892E-09	0.8478308E-10
72	-0.3998930E-07	-0.1706725E-01	0.4325856E-01	0.1298130E-03	0.9368435E-09	0.1279185E-09

APPENDIX J

DATA FOR DEMONSTRATION RUNS

The physical properties of the structure illustrated in Figures 6.1 and 6.2 are presented in Appendix F. The same properties were used in all demonstration runs. The synthesized modes of the Laboratory are presented in Appendix I. Additional data (including initial conditions, control-system parameters, and fluid parameters) are specified in this appendix.

J1. BASIC DATA

The symbols of Section 4 are used in describing the basic data. In each run

$$\{\dot{\phi}^*\} = \{\dot{R}\} = \{\dot{S}\} = \{\dot{\phi}^*\} = 0$$

and

$$\{\dot{\varphi}_i\} = \{\dot{\theta}_i\} = 0$$

Additional basic data is given in Table J1. Where the word "quiescent" is listed for initial elastic displacements, quiescent initial displacements were obtained by introducing 80% of critical damping into the structure, and rotating the fully extended undeformed Space Station at .4189 rad/sec.* A preliminary computer run was made and the displacements resulting when the vibrations damped out are the quiescent displacements which were used as initial conditions in the indicated runs. In the preliminary computer run, no fluid or moving masses were present on the Laboratory.

J2. CONTROL-SYSTEMS DATA

Control-systems data is presented in Table J2 using the notation of Appendix H. Additional Data for the Mass Balancing run is given in Table J3. Both moving masses move along axis X_3 .

J3. FLUID MOTION

The fluid system is shown in Figure J1. The emptying reservoir is located on mass 8, and the filling reservoir is located on mass 2. The fluid is assumed to be water at room temperature. Except for the pump command system, the controls were not operating during the fluid run. The fluid-run data is given in Table J4. In this Table the notation of Section 4 is used except for the pump command data which is presented using the notation of Appendix H.

* The quiescent initial conditions are among the input data printed for Example 2 of Appendix B2 in Volume II.

Fig. J1 Location of Fluid System on Laboratory

Table J1 - BASIC DATA

Property	Run					
	Attitude Control	Deployment	Spin Up	Wobble Damping	Mass Balancing	Fluid Motion
Component 3 of $\{R\}$ (m)*	-5.34890	-5.34890	13.4112	13.4455	11.0867	13.4457
$\{v\}$ (rad) component 1	.0174533	0	0	0	0	0
component 2	.0174533	0	0	0	0	0
component 3	.0174533	0	0	0	0	0
component 1 of $\{w^x\}$ (rad/sec)*	0	.02094	.02094	.4189	.4189	.4189
component 3 of $\{\delta\}$ (m)	0	0	0	.071628	.0764396	.0726440
$\{q_i\}$ (m)	0	0	0	quiescent	quiescent	quiescent
$\{\theta_i\}$ (rad)	0	0	0	quiescent	quiescent	quiescent
component 3 of $\{l_o\}$ (m)*	0	0	42.8223	42.8223	42.8223	42.8223
moving masses present	No	No	No	No	Yes	No
integration step size (sec)	variable	.03	.06	variable	.05	.06

* The other two components are zero.

Table J2 - CONTROL-SYSTEMS DATA

Property	Run				
	Attitude Control	Deployment	Spin Up	Wobble Damping	Mass Balancing
<u>General Data</u>					
i_s	4	4	4	4	4
f_{JET} (N)	222.411	4448.22	66723.3	222.411	222.411
<u>Counterweight Command</u>					
l_{03U} (m)	42.8223	42.8223	42.8223	42.8223	42.8223
t_{03U} (sec)	950	1	950	950	950
acc_{03MAG} (m/sec ²)	.03048	.254	.03048	.03048	.03048
vel_{03MAX} (m/sec)	.06096	1.27	.06096	.06096	.06096
<u>Spin Command</u>					
ω_{LC} (rad/sec)	0	.02094	.02094	.4189	.4189
ω_{LCU} (rad/sec)	0	.02094	.4189	.4189	.4189
$acc_{\omega_{LC}}$ (rad/sec ²)	.04	.04	.04	.04	.04
$t_{\omega_{LC}}$ (sec)	950	950	5	950	950
<u>Attitude Control</u>					
$e_{\theta DB}$ (rad)	.0001745	.0001745	.0001745	.0001745	.0001745
$\dot{e}_{\theta MAX}$ (rad/sec)	.001745	.001745	.001745	.001745	.001745
XJ1 (m)	1.8288	1.8288	1.8288	1.8288	1.8288
<u>Spin Control</u>					
$e_{\omega_{LDB}}$ (rad/sec)	.0002094	.0002094	.004	.0002094	.0002094
<u>Wobble Control</u>					
β_G (rad)	0	0	0	0	0
$\dot{\beta}_G$ (rad/sec)	0	-.02094	-.02094	-.4189	-.4189
K_T (N.m/sec)	325.396	325.396	325.396	325.396	325.396
tq_{LIM} (N.m)	40.6745	40.6745	40.6745	40.6745	40.6745
K_{β} (N.m.sec)	40.6745	40.6745	40.6745	40.6745	40.6745
mom_{CMG} (kg.m ² /sec)	271.164	271.164	271.164	271.164	271.164
$I_{\beta GIM}$ (kg.m ²)	20.3373	20.3373	20.3373	20.3373	20.3373

Table J3 - ADDITIONAL DATA FOR MASS BALANCING RUN

Property	Value
<u>Balance Mass Control</u>	
μ_2 (kg)	2266.13
component 3 of $\{U_2\}$ (m)*	8.85236
\dot{U}_{23} (m/sec)	0
μ_{1EST} (kg)	2266.13
K_{exSE} (none)	10
K_{DESE} (1/sec)	.364
τ_{BAL} (sec)	0
ω_{1CBAL} (rad/sec)	.4
$\{X_A^{is}\}$ (m)	0
component 3 of $\{X_{SENS/CM}^{CMND}\}$ (m)*	26.8551
<u>Moving Mass Command</u>	
μ_1 (kg)	4532.27
component 3 of $\{U_1\}$ (m)	19.3581
U_U (m)	12.3543
t_U (sec)	5
acc_{MAG} (m/sec ²)	.254
vel_{MAX} (m/sec)	.381

* The other two components are zero.

Table J4 - FLUID RUN DATA

Property	Value
<u>General Data</u>	
ρ (kg/m ³)	998.797
A (m ²)	.00967740
<u>Emptying Reservoir</u>	
b_8 (m)	.635
$h_{8,0}$ (m)	.762
h_{8max} (m)	1.524
h_{8min} (m)	0
<u>Filling Reservoir</u>	
b_2 (m)	.635
$h_{2,0}$ (m)	.508
h_{2max} (m)	1.524
h_{2min} (m)	0
<u>Pump Command</u>	
V (m/sec)	0
V_U (m/sec)	3.048
t_{fU} (sec)	2
acc_{MAG} (m/sec ²)	1.524

APPENDIX KDATA FOR RIGID-BODY RUNS USING CONTROL-SYSTEMS DEVELOPMENT PROGRAM

The Space-Station parameter values used are given in Table K1 below. These values were the same in each run. The input data that varied from run to run is presented in Table K2. The symbols used in the model of the rigid-body vehicle are defined in Table K3, and the symbols used in the models of the command and control systems are defined in Table H1 of Appendix H.

Computed Control Parameters

The following parameter values are computed rather than being brought in as input.*

$$\{acc_{\theta_s}\} = f_{JET} \begin{Bmatrix} (x_{J(3,13)}^A - x_{J(3,10)}^A) / M_{11} (1,1) \\ (x_{J(3,4)}^A - x_{J(3,12)}^A) / M_{11} (2,2) \\ (x_{J(1,15)}^A - x_{J(1,1)}^A) / M_{11} (3,3) \end{Bmatrix}$$

$$acc_{\omega_{1C}} = 2f_{JET} (x_{J(3,13)}^A - x_{J(3,10)}^A) / M_{11} (1,1)$$

Common Initial Conditions

The following initial values of space station variables were used for all the runs.

$$\{Z^C\} = [0 \quad 0 \quad 0]^T \quad m$$

$$\{\dot{Z}^C\} = [0 \quad 0 \quad 0]^T \quad m/sec$$

* In the flexible-body idealization, $acc_{\omega_{1C}}$ is input data.

Table K1 SPACE STATION PARAMETER VALUES USED IN
RIGID-BODY DEMONSTRATION RUNS*

$$M_A = 43639.25 \text{ kg}$$

$$[I_A] = \begin{bmatrix} 4365563. & 0 & 0 \\ 0 & 2365321. & 0 \\ 0 & 0 & 2068901. \end{bmatrix} \text{ kg. m}^2$$

$$\{X^A_j\} = \begin{bmatrix} -1.829 & 0 & 6.014 \end{bmatrix}^T \text{ m} \quad \begin{array}{l} j=1 \text{ through } 4 \\ =5 \text{ through } 8 \\ =9 \text{ through } 12 \\ =13 \text{ through } 16 \\ =17 \end{array}$$

$$\begin{bmatrix} -1.829 & 0 & -3.130 \end{bmatrix}^T$$

$$\begin{bmatrix} 1.829 & 0 & -3.130 \end{bmatrix}^T$$

$$\begin{bmatrix} 1.829 & 0 & 6.014 \end{bmatrix}^T$$

$$\begin{bmatrix} 0 & 0 & 5.182 \end{bmatrix}^T$$

$$M_B = 34023.71 \text{ kg}$$

$$[I_B] = \begin{bmatrix} 1951484. & 0 & 0 \\ 0 & 265201 & 0 \\ 0 & 0 & 1751259. \end{bmatrix} \text{ kg. m}^2$$

$$\{\alpha\} = \begin{bmatrix} 0 & 0 & 0 \end{bmatrix}^T \text{ rad}$$

$$\{Y^B_j\} = \begin{bmatrix} -1.829 & 0 & 6.61 \end{bmatrix}^T \text{ m} \quad \begin{array}{l} j=1 \text{ through } 4 \\ =5 \text{ through } 8 \\ =9 \text{ through } 12 \\ =13 \text{ through } 16 \end{array}$$

$$\begin{bmatrix} -1.829 & 0 & -2.54 \end{bmatrix}^T$$

$$\begin{bmatrix} +1.829 & 0 & -2.54 \end{bmatrix}^T$$

$$\begin{bmatrix} +1.829 & 0 & 6.61 \end{bmatrix}^T$$

* The symbols are defined in Table K3

Table K2INPUT DATA FOR RIGID-BODY RUNSKEY TO RUNSRun No. - Maneuver

- 10 - Attitude Control
- 21 - Counterweight Deployment
- 31 - Spin-Up
- 40 - Mass Balancing
- 50 - Wobble Damping
- 60 - Simultaneous Mass Balancing and Wobble Damping

	Run Number					
	10	21	31	40	50	60
<u>Variables</u>						
$\{\omega\}$ (rad/sec) {	0	0.02094	0.02094	0.4189	0.4189	0.4189
	0	0	0	0	0.001	0.001
	0	0	0	0	0	0
$\{\theta\}$ (rad) {	0.017453291	0	0	0	0	0
	0.017453291	0	0	0	0	0
	0.017453291	0	0	0	0	0
m_1 (kg)	2268.24	2268.24	2268.24	4536.5	2268.24	4536.5
m_2 (kg)	2268.24	2268.24	2268.24	2268.24	2268.24	2268.24
$\{X^{(1)}\}$ (m) {	0	0	0	0	0	0
	0	0	0	0	0	0
	0	0	0	0	0	0
$\{X^{(2)}\}$ (m) {	0	0	0	0	0	0
	0	0	0	0	0	0
	0	0	0	0	0	0
$\{X^B\}$ (m) {	0	0	0	0	0	0
	0	0	0	0	0	0
	-23.99	-23.99	-66.81	-66.81	-66.81	-66.81
β (rad)	0	0	0	0	0	0
$\dot{\beta}$ (rad/sec)	0	-0.02094	-0.02094	-0.4189	-0.4189	-0.4189

Table K2 (Continued)

	Run Number					
	10	21	31	40	50	60
<u>Commands</u>						
ω_{1C} (rad/sec)	0	0.02094	0.02094	0.4189	0.4189	0.4189
ω_{1CU} (rad/sec)	0	0.02094	0.4189	0.4189	0.4189	0.4189
$t_{\omega 1CU}$ (sec)	300	950	5	300	300	300
X_{13C} (m)	0	0	0	0	0	0
X_{13CU} (m)	0	0	0	1.524	0	1.524
t_{X13CU} (sec)	300	950	300	5	300	5
X_{B3C} (m)	-23.99	-23.99	-66.81	-66.81	-66.81	-66.81
X_{B3CU} (m)	-23.99	-66.81	-66.81	-66.81	-66.81	-66.81
t_{XB3CU} (sec)	300	5	300	300	300	300
<u>Parameters</u>						
Δ time (sec)	0.025	0.025	0.025	0.025	0.025	0.025
time e (sec)	100	800	50	50	50	50
$e_{\theta DB}$ (rad)	0.0001745					
$\dot{e}_{\theta MAX}$ (rad/sec)	0.001745					
f_{JET} (N)	222.4	222.4	22241.1	222.4	222.4	222.4
$e_{\omega 1DB}$ (rad/sec)		0.0002094	0.0002094	0.0002094	0.0002094	0.0002094
acc_{B3C} (m/sec ²)		0.03048				
vel_{MBC} (m/sec)		0.06096				
K_{eXSE} (sec)				200		200
\dot{e}_{XDB} (m/sec)				0.0003048		0.0003048
acc_{X23} (m/sec ²)				0.6096		0.6096

Table K2 (Continued)

	Run Number					
	10	21	31	40	50	60
<u>Parameters</u> (Continued)						
$\{X_{SENS}\}$ (m) }				0 0 4.654		0 0 4.654
m_{LEST} (kg)				2268.24		2268.24
K_T (N.m/sec)					325.4	24.405
tq_{LIM} (N.m)					40.67	40.67
K_p (N.m.sec)					40.67	40.67
mom_{CMG} (kg.m ² /sec)					271.164	271.164
$I_{\beta GIM}$ (kg.m ²)					20.3373	20.3373
acc_{13C} (m/sec ²)				.03048		0.03048
vel_{MLC} (m/sec)				.3048		0.3048

Table K3

DEFINITION OF SYMBOLS USED FOR THE MATHEMATICAL
MODEL OF THE RIGID-BODY VEHICLE

<u>Symbol</u>	<u>Definition</u>	<u>Matrix Dimension</u>
$[I_A]$	moment-of-inertia matrix of Laboratory (not including m_i) about X axes (off- diagonal terms are negatives of cross- products of inertia)	3, 3
$[I_B]$	moment-of-inertia matrix of Counter- weight about Y axes (off-diagonal terms are negatives of cross-products of inertia)	3, 3
M_A	mass of Laboratory	1
M_B	mass of Counterweight	1
$[M_{11}]$	moment-of-inertia matrix of Space Station about axes parallel to X axes with origin at cm of Space Station	3, 3
$\{m_i\}$	mass of i^{th} moving point mass in Laboratory	2
X	axes fixed in Laboratory with origin at cm of Laboratory (not including the m_i)	-
$\{X^A_j\}$	location of A_j in X axes	3, 17
$\{X^B\}$	location of center of mass of Counterweight in X axes	3
$\{X^{(i)}\}$	location of i^{th} mass in X axes	3, 2
Y	axes fixed in Counterweight with origin at cm of Counterweight	-
$\{Y^B_j\}$	location of B_j in Y axes	3, 16